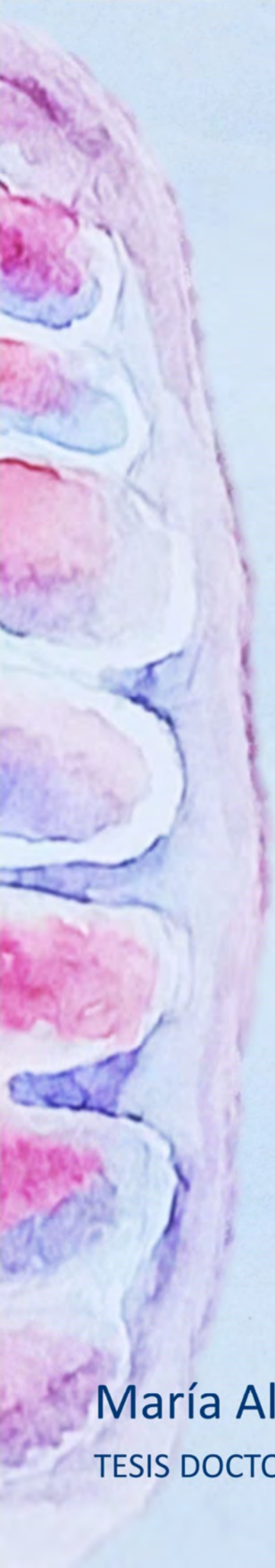

UNIVERSIDAD PABLO DE OLAVIDE SEVILLA

Pathophysiology of Primary Coenzyme Q_{10} Deficiencies

Molecular Characterisation of *COQ4* gene

María Alcázar Fabra

TESIS DOCTORAL. Sevilla, 2021

UNIVERSIDAD PABLO DE OLAVIDE SEVILLA

TESIS DOCTORAL

Pathophysiology of Primary Coenzyme Q_{10} Deficiencies. Molecular Characterisation of *COQ4* gene.

María Alcázar Fabra

Sevilla, 2021

Pathophysiology of Primary Coenzyme Q_{10} Deficiencies. Molecular Characterisation of *COQ4* gene.

TESIS DOCTORAL

Universidad Pablo de Olavide

Dpto. Fisiología, Anatomía y Biología Celular

Área de Biología Celular

Memoria presentada por

María Alcázar Fabra

para optar al título de

Doctor en Biotecnología, Ingeniería y Tecnología Química

Programa de Doctorado en Biotecnología, Ingeniería y Tecnología Química

(RD: 99/2011)

Sevilla, 2021

La directora de la tesis

Dra. Gloria Brea Calvo

Profesora contratada doctora

Dpto. Fisiología, Anatomía y Biología Celular

Área de Biología Celular

Universidad Pablo de Olavide

El director de la tesis

Dr. Plácido Navas Lloret

Catedrático

Dpto. Fisiología, Anatomía y Biología Celular

Área de Biología Celular

Universidad Pablo de Olavide

Dña. GLORIA BREA CALVO, Doctora en Biología Celular por la Universidad Pablo de Olavide y Profesora Contratada Doctora del Área de Biología Celular en el Departamento de Fisiología, Anatomía y Biología Celular de la Universidad Pablo de Olavide de Sevilla

INFORMA

Que DÑA. MARÍA ALCÁZAR FABRA, graduada en Biotecnología por la Universidad Pablo de Olavide de Sevilla, ha realizado bajo su dirección la tesis doctoral titulada "PATHOPHYSIOLOGY OF PRIMARY COENZYME Q_{10} DEFICIENCIES. MOLECULAR CHARACTERISATION OF *COQ4* GENE", y que a su juicio reúne los méritos suficientes para superar el programa de Doctorado en Biotecnología, Ingeniería y Tecnología Química.

Y para que conste, firmo el presente en Sevilla, 2021

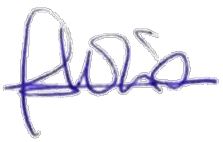

Fdo.: Gloria Brea Calvo

D. PLÁCIDO NAVAS LLORET, Doctor en Ciencias por la Universidad de Sevilla y Catedrático del Área de Biología Celular en el Departamento de Fisiología, Anatomía y Biología Celular de la Universidad Pablo de Olavide de Sevilla

INFORMA

Que DÑA. MARÍA ALCÁZAR FABRA, graduada en Biotecnología por la Universidad Pablo de Olavide de Sevilla, ha realizado bajo su dirección la tesis doctoral titulada "PATHOPHYSIOLOGY OF PRIMARY COENZYME Q_{10} DEFICIENCIES. MOLECULAR CHARACTERISATION OF *COQ4* GENE", y que a su juicio reúne los méritos suficientes para superar el programa de Doctorado en Biotecnología, Ingeniería y Tecnología Química.

Y para que conste, firmo el presente en Sevilla, 2021

Fdo.: Plácido Navas

INFORME EXPERTO EXTERNO / EXTERNAL REFEREE REPORT

Nombre y apellidos del experto / Name of the referee	
Cristiane Beninca, PhD	
Categoría académica o profesional / Academic or professional position	
Project Scientist	
Departamento / Department	**Universidad u organismo y país / University or institution and country**
David Geffen School of Medicine	University of California – Los Angeles
Doctor por la Universidad de / Doctor by the University of	**Año de defensa de la tesis doctoral / Year of the Doctoral Thesis Defence**
Barcelona	2012

Título de la tesis presentada / Title of the thesis
Pathophysiology of Primary CoQ_{10} Deficiencies. Molecular Characterization of *COQ4* gene.
Nombre y apellidos del doctorando / Name of the candidate
María Alcázar Fabra
Nombre del director(s) de la tesis / Name of the thesis director(s)
Gloria Brea Calvo and Plácido Navas Lloret

INFORME RAZONADO / REASONED REPORT

SOBRE LA CALIDAD CIENTÍFICA DE LA TESIS DOCTORAL
ABOUT THE SCIENTIFIC QUALITY OF THE PhD

María Alcázar Fabra shows in her thesis the molecular characterization of *COQ4* and *COQ7* genes in the pathophysiology of CoQ_{10} deficiencies. She presents a great revision of the literature in her introduction, with a comprehensive compilation of genes and phenotypes in CoQ_{10} deficiencies, as well as mitochondria physiology in health and diseases. The revision of the literature in CoQ_{10} deficiencies is even better covered in her results section, highly recommended for publication as a clinical review as per the great quality presented. The project aims are well defined and approached with well-designed experiments, concluded successfully in several chapters, showing her capacity to perform several techniques asking scientifically interesting questions as well as writing in a well-organized way. She reports new mutations in COQ4 and COQ7,

expanding the genotype/phenotype correlations with her own data and including evaluation of possible treatments in a more translational approach. For the molecular characterization in vitro, she generates a *COQ4* knockout using CRISPR/Cas9 system, performing respirometry and biochemical assays in addition to several sophisticated techniques like in vivo mitochondrial translation and proteomics. Specifically, for proteomic analyses, she explores CoQ biosynthesis and composition, using not only conventional proteomics, but advanced techniques like SILAC and lipidomics alongside with developing new methods of crosslinking proteins. She presents all her results with clear figures, tables, and statistics, and likewise, she shows protein structure models and knowledge to use important bioinformatic tools. Importantly, she also shows a new relationship to be explored further, in how CoQ biosynthesis impact in mtDNA replication and metabolism, an interesting observation with impactful conclusions. María Alcázar Fabra shows her ability to plan, perform and conclude experiments as showed in this thesis, an important collaboration to the mitochondria field.

Informo favorablemente que la calidad científica de esta tesis doctoral es merecedora de obtener la mención Doctor Internacional.

I inform that the scientific quality of this thesis is worthy of obtaining the International Doctor Mention.

FECHA / DATE

25/01/2021

FIRMA / SIGNATURE

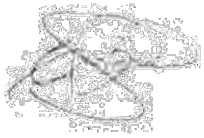

Fdo.: Cristiane Beninca, PhD

INFORME EXPERTO EXTERNO / EXTERNAL REFEREE REPORT

Nombre y apellidos del experto / Name of the referee	
Carlo Viscomi, PhD	
Categoría académica o profesional / Academic or professional position	
Associate Professor of Genetics	
Departamento / Department	**Universidad u organismo y país / University or institution and country**
Biomedical Sciences	University of Padova, Italy
Doctor por la Universidad de / Doctor by the University of	**Año de defensa de la tesis doctoral / Year of the Doctoral Thesis Defence**
Milan, Italy	2002

Título de la tesis presentada / Title of the thesis
Pathophysiology of Primary CoQ_{10} Deficiencies. Molecular Characterization of *COQ4* gene.
Nombre y apellidos del doctorando / Name of the candidate
María Alcázar Fabra
Nombre del director(s) de la tesis / Name of the thesis director(s)
Gloria Brea Calvo and Plácido Navas Lloret

INFORME RAZONADO / REASONED REPORT

SOBRE LA CALIDAD CIENTÍFICA DE LA TESIS DOCTORAL
ABOUT THE SCIENTIFIC QUALITY OF THE PhD

The PhD thesis presented by the candidate, María Alcázar Fabra, reflects an outstanding scientific quality. The candidate presented a massive amount of new data, which will have a profound impact on the field of coenzyme Q biology and medicine. The candidate has studied several aspects of Coenzyme Q (CoQ) biology, providing new insight into several mechanisms of both basic processes and medical/translational aspects. The data warrant future investigations but are highly intriguing and have the potential to open novel scenarios in CoQ biology.

The thesis opens with a detailed and accurate introduction on mitochondrial and CoQ biology and related medical aspects. The aims of the thesis are clearly stated and appropriately discussed in the different chapters. The material and methods are very detailed and accurate, with a thorough description of the methodologies used in each of the experiments presented in the thesis.

Chapters 1 and 2 are dedicated to an extensive revision of the literature of all the known manifestations of the highly complex and heterogeneous syndromes related to CoQ deficiencies. In this part, the candidate first gives a general overview of the clinical manifestations of these diseases and relates them to all the genes that have been associated to every clinical sign. Then, she revises the biochemical features, the pathogenetic mechanisms, the phenotype-genotype correlation, the diagnostic workout and management of both primary and secondary CoQ deficiencies. In the results of this part of her thesis, the candidate enters into the details and describes all the patients, mutations and genes so far involved in CoQ deficiencies. This massive effort unravels the impressive complexity intrinsic to primary and secondary CoQ-related syndromes and has a great value in itself for clinicians and scientist in the field or those who approach this fascinating field.

Chapter 3 is dedicated to the study of the role of COQ4, one of the proteins taking part to the biosynthesis of CoQ and forming a supramolecular complex with the other enzymes participating to this pathway. Importantly, very little is known about the exact role of COQ4 in CoQ biosynthesis. To unravel the role of COQ4, the candidate initially uses in-silico and cellular models of COQ4. The in-silico analysis suggests that COQ4 forms homodimers, with a hydrophobic pocket where lipids can bind. In addition, the homodimers appear to have a domain able to chelate divalent cations. The analysis also identifies some residues potentially important for the regulation of the protein activity by phosphorylation. The in-silico analysis also reveals that the vast majority of the known mutations in COQ4 reside on the surface, suggesting that they may act by disrupting important interactions. In a second experimental setup, the candidate takes a cell biology approach to investigate the subcellular and submitochondrial localization of COQ4, by using elegant immunofluorescence and sub-fractionation techniques. These experiments convincingly demonstrate that COQ4 localized in the mitochondrial matrix but is also detected in the mitochondrial associated membranes.

Chapter 4 is dedicated to investigating the role of COQ4 in CoQ biosynthesis, a yet not completely elucidated process. After an extensive revision of this process in both yeast, the main organism used to discover the major steps in CoQ biosynthesis, and mammalian cells, the candidate uses *COQ4* KO cells, generated by CRISPR/Cas9, to detect CoQ intermediates by using ^{14}C labelling followed by HPLC/mass spectrometry analysis to identify biosynthetic intermediates. This experiment revealed a peak, previously described in patients' fibroblasts carrying COQ4 mutations, and corresponding to an uncharacterized CoQ intermediate, whose full determination warrant further investigations.

A highly relevant part of the thesis is dedicated to the development of new treatments for CoQ-related diseases, especially based on by-passing therapy. Several CoQ patients respond to the treatment with CoQ. Yet, this is not true for all of them and more effective treatments are needed. To this end, the candidate uses several precursors of

analogues of 4hydroxybenzoate to investigate if they could rescue CoQ defect in the *COQ4* KO cells, but no one had a significant impact on CoQ levels. In contrast, re-expression of tagged or untagged wildtype COQ4 was able to fully rescue CoQ biosynthesis, independently of the expression levels, as expected in the case of an enzymatic role for the protein. The candidate also uses site-directed mutagenesis to investigate the role of the putative phosphorylation sites identified by in silico analysis. Mutations in any of the considered sites could rescue CoQ biosynthesis, so that more work is warranted to understand their true meaning.

Interestingly, the expression of different mutations found in the patients, revealed that most of the mutations in COQ4 were able to restore normal levels of CoQ and the disappearance of the uncharacterized CoQ peak mentioned above. This suggests that most of the mutations are hypomorphic and the defect is likely compensated by high expression levels of the mutated protein in the cells. Additional experiments showed that shorter predicted isoforms were inactive in CoQ biosynthesis and unable to restore CoQ levels in KO cells. Not surprisingly, *COQ4* KO cells had severely impaired respiration, which was corrected by COQ4 re-expression or CoQ_{10} supplementation.

An important piece of information comes from BNGE and SILAC-based proteomic analysis of COQ4-containing complexes. Although these experiments were unsuccessful in identifying stable interactors of COQ4, the results are rather robust and suggest that the CoQ biosynthetic complex is probably unstable and other techniques, such as BioID, will be required to identify additional components of this complex. As a first approach, the candidate immunoprecipitated COQ4-Flag under native conditions and analyzed the immunoprecipitate by mass-spectrometry. All the COQ proteins were identified, as well as several proteins of the respiratory chain, TCA cycle, FAO, and amino acids biosynthesis. Most importantly, an enrichment of proteins belonging to the nucleoids and other compartments, including ER, Golgi, lysosomes etc…were also identified. Although the meaning of several of the potential interactors warrants additional studies, this result confirms that COQ4 interacts with the other components of the CoQ biosynthetic pathway forming a supramolecular complex. Moreover, *COQ4* KO cells showed increased levels of COQ5 and 7, while *COQ6* KO showed increase of COQ4. These results indicate that several COQ proteins are needed for the complex stability and the absence of one component can destabilize or is tentatively compensated by the increase of others. The candidate then investigates if CoQ supplementation could impact on COQ complex stability. Indeed, she found that at least in COQ6 KO cells CoQ10 was able to normalize the increased levels of COQ4, 5 and 7.

Overall, this part of the thesis is highly original and uses cutting-edge methodologies to explore COQ4 role at an unprecedented level. Future studies will be needed to better define which are COQ4 transient interactors identify the steps of the complex biogenesis.

Finally, in chapter 5 the candidate investigates a very intriguing and novel aspect which relates COQ4 to mtDNA maintenance. In particular, since CoQ shares part of the biosynthetic pathway with cholesterol, this study opens the question of the role of cholesterol in mtDNA replication and maintenance. As the candidate recalls in the introduction, compelling data present in the literature link mtDNA and mitochondria-ER contacts. Importantly, this submitochondrial compartment is critical for colesterol and COQ biosynthesis. The data presented show that mtDNA copy number is decreased in COQ4 KO cells. Notably, also mutants in the putative phosphorylation loop were able to at least partially rescue mtDNA depletion, whilst they had no effect on CoQ biosynthesis. In contrast, no effect on mitochondrial transcripts is reported in *COQ4* KO cells. A rather surprising result, however, is that ethidium bromide-induced mtDNA depletion recovered faster in *COQ4* KO cells than in control cells. In parallel, several proteins of the respiratory chain followed a similar kinetics, as a consequence of depletion/repletion of mtDNA. This effect was not corrected by supplementation of CoQ, ruling out an indirect effect of CoQ deficiency. *COQ6* KO cells behaved in the same way. These results prompted the candidate to explore in more detail the relationship between cholesterol and nucleoids. No major differences were detected in total or mitochondrial cholesterol. However, local differences cannot be excluded at this stage. Importantly, *COQ4* KO cells showed some differences vs. WT cells in the distribution of nucleoid proteins on an iodixanol density gradient, supporting a role of COQ4 in nucleoids assembly/stability.

This is an excellent thesis with many interesting data on both the clinical aspects of CoQ-related diseases, and several original observations on basic aspects of CoQ biology. The data presented warrant future investigations and can open new avenues to our understanding of a highly complex and challenging area of mitochondrial biology and medicine.

Informo favorablemente que la calidad científica de esta tesis doctoral es merecedora de obtener la mención Doctor Internacional.

I inform that the scientific quality of this thesis is worthy of obtaining the International Doctor Mention.

FECHA / DATE

29/01/2021

FIRMA / SIGNATURE

Fdo.: Carlo Viscomi, PhD

Esta Tesis Doctoral ha sido realizada dentro del Programa de Doctorado en Biotecnología, Ingeniería y Tecnología Química (RD: 99/2011), en el grupo de investigación del CIBERER U729, en el Centro Andaluz de Biología del Desarrollo, Área de Biología Celular del Departamento de Fisiología, Anatomía y Biología Celular de la Universidad Pablo de Olavide y bajo la dirección de la Dra. Gloria Brea Calvo y el Dr. Plácido Navas Lloret. El trabajo ha sido financiado por una ayuda FPU (Ayudas para la formación de profesorado Universitario), referencia FPU14/04873 y, en parte, por el proyecto de investigación del FIS PI17-01286.

A mis padres y a mis hermanas

A Hugo y mi pequeño Lynx

Acknowledgements / Agradecimientos

Tras nada más y nada menos que 5 años de trabajo, llegó el momento de finalizar esta etapa. Un trabajo que he realizado con mucho esfuerzo, y durante el que me he podido sentir muy afortunada por contar con mucho apoyo. Por eso me gustaría plasmar en estas líneas mi agradecimiento a todas esas personitas que me han ayudado, de una u otra manera, a llegar a donde estoy hoy.

Como no podría ser de otra manera, quiero comenzar agradeciendo a Gloria por ser mi guía y mentora durante todo este viaje. Estoy muy contenta de haber sido tu primera doctoranda a tiempo completo, no puedo ser más afortunada. Juntas hemos recorrido un camino nuevo y emocionante, lleno de subidas y bajadas. Ahora, mirando hacia atrás, pienso que no podría haber tenido mejor compañía. Admiro tu forma de ver la vida y la ciencia, tu pasión y dedicación, y te agradezco todo lo que me has enseñado y ayudado científica y personalmente. Eres, sin duda alguna, mi modelo a seguir.

Por supuesto, me gustaría agradecer a Plácido todo su apoyo durante este periodo. Gracias por confiar en mí y por siempre estar dispuesto a ayudarme tanto en lo profesional como en lo personal. No solo durante estos años de tesis, sino desde que llegué al laboratorio hace nada más y nada menos que 7 años.

Me siento afortunada de haber llegado al laboratorio de BioCel hace tantos años, y de haberme podido rodear de tantas buenas personas y amigos.

Fue en ese momento en el que llegué, hace 7 años *y pico*, cuando tuve la suerte de empezar a trabajar con Ana, *la Q*. Y después de eso, hemos vivido muchísimas aventuras más, tanto en el laboratorio como fuera de él. Muchas gracias por todo el Q que has medido para la presente tesis, pero, sobre todo, por contagiarme tu optimismo y tu fuerza en el trabajo y en la vida, y por ser una gran amiga. Mi otro compañero de aventuras ha sido sin duda JuanDi. Muchas gracias, amigo, por estar siempre ahí para todo lo que necesitara, incluso para comer a las 5 de la tarde si el día era complicado en el laboratorio. Y por los buenos ratos y por tus bromitas, que, en el fondo, puede que fueran graciosas. Lo hemos pasado muy bien tanto en el laboratorio como fuera, en nuestros viajes y congresos.

Otro gran apoyo en el laboratorio ha sido Mariví. Gracias por mostrarme tu manera de ver la vida, y ayudarme siempre en todo lo que he necesitado (tanto que hasta colonicé tu buhardilla con mis trastos durante mi estancia). Y por supuesto, a Anita. Muchas gracias por todo tu trabajo en el laboratorio, haces que todo funcione mejor. Y, sobre todo, por ser mi competencia dulcera. Ya echo de menos nuestros desayunos en el Dulce Marie, que empezaron tarde, pero fueron bien aprovechados. También quería mencionar y agradecer a mi querida compi Aída, siempre enérgica y dispuesta a ayudar y a compartir buenos momentos.

Muchas gracias a todos los doctores, profesores e investigadores del grupo. Muchas gracias, Guille, por tu ayuda con el citómetro y por estar siempre dispuesto a una charla científica. Carlos, gracias por tus consejos y por hacerme ver los problemas como un reto con solución. Dani, te agradezco mucho tu ayuda con el pHB, los análisis de secuencias y cualquier otra cosa que haya necesitado. Juan Carlos, gracias por tu ayuda con el HPLC y por transmitir tu forma metódica de trabajar. A Manu y Antonio, por estar siempre dispuestos a aportar consejos en las reuniones. Claudio, gracias por presentarme el laboratorio y por inspirarme a tener pensamiento crítico y motivación por la ciencia. Emilio, muchas gracias por transmitirme tu tesón, y siempre estar dispuesto a ayudar con consejos.

No me puedo olvidar de las personas que estaban en el laboratorio cuando llegué y fueron partiendo. O aquellas con las que el tiempo compartido ha sido demasiado breve, pero de verdadera calidad. Elena, Ángela, Cristiane, Cathe. Con vosotras he pasado grandes momentos. Muchas gracias, amigas. Mi querido amigo Matías, qué suerte tuve al conocerte. Muchas gracias por enseñarme otra manera de ver la vida.

Y por supuesto, muchas gracias a todos los *peques* que han pasado o siguen por el lab. Al principio era yo la *peque*, pero durante los últimos años han pasado por el laboratorio pequeñas grandes personitas que me han hecho crecer. Andrés, Verónica, Manu, Carmine, Pablo, Ana Belén, Simone, Valentina, Alessandra… Valle y Lucía, con las que he compartido mis últimos meses en el laboratorio, y me han hecho sentir orgullosa de todo lo que han aprendido. Además, me gustaría agradecer a todos los estudiantes que han pasado por el laboratorio y han confiado en mí para resolver sus dudas o para aprender. En esos momentos yo también he aprendido mucho.

Por otro lado, estos años he podido involucrarme en las tareas de docencia en la Universidad, y ha sido una tarea muy gratificante. Os agradezco a todos los profesores doctores que me habéis guiado y tutorizado en este emocionante camino: Gloria, Emilio, Dani y Manu.

Me gustaría dar las gracias a todas las personas con las que he coincidido por el CABD, que han hecho que la vida durante el doctorado fuera más amena y entretenida. Muchas gracias Laura Tomás por toda tu ayuda y consejos con los experimentos de proteómica. También a Kathy, por tu ayuda con la microscopía y con la citometría. Muchísimas gracias a todo el personal de cocinas por todas las facilidades que ofrecéis para trabajar; a todos los grupos de investigación de la Universidad y del CSIC por vuestra disposición a compartir recursos, conocimientos y también buenos ratos; a todo el personal de administración, conserjes, mantenimiento y servicio de limpieza, que hacéis del CABD un lugar acogedor.

Unos periodos muy importantes durante mi tesis han sido mis dos estancias en el laboratorio del profesor Massimo Zeviani, a quien agradezco su acogida. Erika, me faltan palabras para agradecerte todo lo que me has enseñado durante la estancia, tanto de ciencia como de la vida. A Marta, por contagiarme tu alegría y locura; a Noor, por ofrecerme tu valiosa amistad; a *the crêpes group* y *the leftover crêpes* (Teresa, Pedro, Elisa, Angela, Kai, Pascal, Elena, Adrien) por nuestras cenas y nuestras risas. A todos los amigos y compañeros de la MBU y de Cambridge, os agradezco que hayáis hecho de esta experiencia una de las mejores de mi vida.

El CABD y la UPO, durante estos años, me ha dado amistades de las que he aprendido mucho. Amalia, encontré un tesoro al tenerte como amiga. Javi, gracias por ser tan tú, eso hace que nos entendamos tan bien. Agradezco a mis queridos Aventureros de la Escama, Juan, Inma, Ana, Félix y Hugo, por todas nuestras hazañas vividas y por vivir, por hacer del mundo un lugar mejor. Raquel, compartimos el inicio de este camino y me alegro muchísimo de que nos pudiéramos conocer y vivir juntas una gran experiencia.

Hugo, mi compañero de vida, muchas gracias por tu comprensión, por ser mi apoyo todos los días. Por aguantarme, quererme y conocerme tan bien. Y tú sabes que por muchas cosas más.

Y para terminar, me gustaría agradecer con todo mi corazón a mis padres. Mi ejemplo a seguir. Sin vuestro apoyo incondicional todos y cada uno de los días de mi vida, sin duda, no habría conseguido todo lo que hoy he conseguido. No podría haber tenido más suerte. Queridas hermanas, gracias por estar siempre ahí también. Os quiero.

Muchas gracias a todos, de todo corazón

Funding

I am grateful to all the institutions and people that have made possible this PhD project. The research contained in this dissertation has been mostly held in the Centro Andaluz del Biología del Desarrollo (CABD-CSIC-UPO-JA), in the Department of Phisiology, Anatomy and Cell Biology at Pablo de Olavide University. I have been working in Prof. Plácido Navas Lloret's laboratory, which also belongs to the CIBERER (Unit 729).

This PhD project has been funded by the FPU grant "Ayudas para la formación de profesorado Universitario" (Reference FPU14/04873) awarded by the Spanish Government (Ministerio de Educación, Cultura y Deporte), from 2015 until 2019. The last year has been funded by the Decision Making in Cell Collectives María de Maeztu Unit of Excellence, which accorded Dr. Gloria Brea Calvo a research award.

During my PhD, I was able to work for nine months in Prof. Massimo Zeviani's laboratory at the Medical Research Council – Mitochondrial Biology Unit, University of Cambridge (United Kingdom), thanks to the grants "Ayudas a la movilidad para estancias breves y traslados temporales FPU" (References EST16/00630 and EST17/00627) awarded by the Spanish Government (Ministerio de Educación, Cultura y Deporte).

I have also been able to present some data of my PhD project in several international and national conferences thanks to several grants: "Ayudas destinadas a cubrir gastos para la mejora cualitativa en el desarrollo de sus tesis doctorales" from Pablo de Olavide University, funding from the Department of Phisiology, Anatomy and Cell Biology at Pablo de Olavide University and several grants from the organising committees of the conferences (Mitochondrial Medicine 2016 and 2019 conferences, Wellcome Genome Campus, Cambridge and II National Congress of Young Researchers in Biomedicine, Valencia).

Finally, some of the work in this PhD has been funded by the project "Diagnóstico molecular y patogénesis de las enfermedades mitocondriales con deficiencia de coenzima Q_{10}" awarded by the Instituto de Salud Carlos III (ISCIII) (Ministerio de Salud, Spanish Government) in 2017 (Reference FIS PI17-01286), whose PI is Dr. Plácido Navas Lloret. The group is also funded by the Junta de Andalucía BIO-177, and the FEDER

Funding Program from the European Union and CIBERER (U729)-ISCIII. Some of the work has been also funded by the project “Papel de la síntesis de Coenzima Q en el mantenimiento del ADN mitochondrial”, co-awarded by the FEDER Funding Program from the European Union and the Junta de Andalucía within the framework of the Andalusian FEDER operational program 2014-2020 (Reference UPO-1265673), whose PI is Dr. Gloria Brea Calvo.

Abstract / Resumen

Pathophysiology of Primary Coenzyme Q_{10} Deficiencies. Molecular Characterisation of *COQ4* gene.

Primary Coenzyme Q_{10} (CoQ_{10}) deficiencies are a group of rare conditions genetically caused by autosomal recessive biallelic mutations in one of the *COQ* genes required in CoQ_{10} biosynthesis pathway. The associated clinical manifestations are highly heterogeneous and mainly affect central and peripheral nervous system, kidney, skeletal muscle and heart.

The first part of this thesis is focused on studying the primary CoQ_{10} deficiency syndrome.

Firstly, we present an updated and comprehensive review of all the clinical manifestations associated to each of the pathogenic variants in the *COQ* genes described in the literature. With this, we describe patterns of symptoms related with the age of onset of the disease for each *COQ* gene and even, when possible, for each mutation involved in primary CoQ_{10} deficiency, as an attempt to establish genotype-phenotype correlations.

Secondly, we report new cases of primary CoQ_{10} deficiency due to mutations in *COQ4* and *COQ7*, expanding phenotypes and genotypes associated to these disorders. We worked with different *in vitro* cellular models with mutations in *COQ4*, *COQ6* or *COQ7*, which accumulate diagnostic intermediates, specific for each *COQ* defect. Moreover, we demonstrate that treatment with 4-hydroxybenzoate (4-HB) analogues is effective in some of the cases. 2,4-dihydroxybenzoic acid (2,4-dHB) decreases DMQ_{10} accumulation, increases CoQ_{10} levels and ameliorate respiratory function in *COQ7* mutant fibroblasts. Vanillic acid (VA) restores CoQ_{10} biosynthesis and respiration in *COQ6* KO cells.

In the second part of the thesis, we focused on human COQ4 protein, which has an essential role in CoQ_{10} biosynthesis.

In our work, we demonstrate that human COQ4 protein is essential for CoQ_{10} biosynthesis in cells. We have generated a human *COQ4* KO cell line, which has a

profound deficiency in CoQ_{10} levels and a great respiratory defect, rescued with CoQ_{10} treatment or WT *COQ4* expression. Moreover, the lack of COQ4 protein produces the accumulation of a specific intermediate. We also found that most of the mutations described in patients are hypomorphic, fully recovering CoQ_{10} biosynthesis in the *COQ4* KO cells when overexpressed.

With proteomics studies, we identified all the COQ proteins (except for COQ8A) copurifying with COQ4 after immunocapture. This fact provides evidence for the mammalian CoQ biosynthesis complex and its composition. Moreover, we observed that the lack of COQ4 or COQ6 proteins alters the levels of other COQs proteins, probably modifying the stability of the biosynthetic complex.

In this context, yeast CoQ head-modifying enzymes have been resolved in discrete *loci*, so-called CoQ domains, adjacent to ER-mitochondria contact sites [1,2]. Mitochondrial DNA (mtDNA) maintenance and distribution seems to depend on endoplasmic reticulum (ER) -mitochondria contacts [3], and cholesterol levels in these sites are reported to be key for this issue [4]. We explored these relationships with our *COQ4* KO model. We found that the lack of COQ4 led to a slight decrease of mtDNA copy number, with no effect on mtDNA transcription and a very subtle effect on mtDNA-encoded translation. Regarding mtDNA replication, the lack of COQ4 or COQ6 induced a faster mtDNA recovery rate after an induced depletion. In order to find the molecular mechanism explaining this surprising phenotype, we studied cholesterol content and distribution of nucleoid proteins in density gradients. We found that total cholesterol levels were not altered in mitochondria, but we found subtle differences between *COQ4* KO and control cells in terms of nucleoid proteins (TFAM and ATAD3) distribution in these gradients. This fact may be behind the fast mtDNA recovery after induced depletion. However, there is still a lot of work to be done to better understand the relationship between CoQ biosynthesis and mtDNA metabolism.

Fisiopatología de las Deficiencias Primarias de Coenzima Q_{10}. Caracterización Molecular del Gen *COQ4*.

Las deficiencias primarias de coenzima Q_{10} (CoQ_{10}) son un grupo de enfermedades raras genéticas causadas por mutaciones bialélicas recesivas en uno de los genes *COQ* requeridos en la ruta de biosíntesis de CoQ_{10}, a nivel enzimático o regulador. Las manifestaciones clínicas asociadas son muy heterogéneas y afectan principalmente al sistema nervioso central y periférico, a los riñones, al músculo esquelético y al corazón.

La primera parte de esta tesis se centra en el estudio del síndrome de la deficiencia primaria en CoQ_{10}.

En primer lugar, hemos realizado una revisión actualizada y exhaustiva de todas las manifestaciones clínicas asociadas a cada una de las variantes patogénicas en los genes *COQ* descritas en la literatura. En ella, describimos patrones de síntomas relacionados con la edad de aparición de la enfermedad para cada gen *COQ* e incluso, para cada mutación, cuando es posible. Con estos patrones, hemos intentado establecer correlaciones genotipo-fenotipo para la deficiencia primaria en CoQ_{10}.

En segundo lugar, hemos descrito nuevos casos de deficiencia primaria de CoQ_{10} debido a mutaciones en los genes *COQ4* y *COQ7*, ampliando los fenotipos y genotipos asociados a estos trastornos. Hemos trabajado con diferentes modelos celulares *in vitro* con mutaciones en *COQ4*, *COQ6* y *COQ7*, que acumulan intermediarios diagnósticos, específicos para cada defecto *COQ*. Además, demostramos que el tratamiento con análogos del 4-hidroxibenzoato (4-HB) es eficaz para mejorar la deficiencia de CoQ_{10} y el defecto respiratorio en nuestros modelos celulares humanos: el ácido 2,4-dihidroxibenzoico (2,4-dHB) para la deficiencia en *COQ7* y el ácido vainillínico (VA) para los defectos en *COQ6*.

En la segunda parte de la tesis, nos hemos centrado en la proteína COQ4 humana, que tiene un papel esencial en la biosíntesis de CoQ_{10}.

En nuestro trabajo, demostramos que la proteína COQ4 humana es esencial para la biosíntesis de CoQ_{10} en las células. Hemos generado una línea celular humana KO en *COQ4*, que tiene una gran deficiencia en CoQ_{10} y en la respiración mitocondrial. Estos defectos son rescatados con un tratamiento con CoQ_{10} o con la expresión del gen *COQ4*

WT. Además, la falta de proteína COQ4 produce la acumulación de un intermediario específico de la ruta de síntesis. También encontramos que la mayoría de las mutaciones descritas en pacientes son hipomórficas, capaces de recuperar completamente la biosíntesis de CoQ_{10} en las células *COQ4* KO cuando son sobreexpresadas.

Con estudios de proteómica, hemos podido identificar todas las proteínas COQ (excepto COQ8A) copurificando con COQ4, lo que es una evidencia más de la existencia del complejo de síntesis de CoQ en mamíferos. Además, observamos que la falta de proteínas COQ4 o COQ6 altera los niveles de otras proteínas COQs, probablemente modificando la estabilidad del complejo biosintético.

Se ha descrito que las enzimas modificadoras de la cabeza de CoQ en levadura resuelven en *loci* discretos, denominados dominios CoQ, que se encuentran adyacentes a los sitios de contacto entre el retículo endoplásmico (ER) y las mitocondrias [1,2]. Además, el mantenimiento y la distribución del ADN mitocondrial (mtDNA) depende de estos contactos ER-mitocondria [3], y los niveles de colesterol en estos sitios parecen ser clave para ello [4]. En la última parte de la tesis, hemos explorado estas relaciones en nuestro modelo *COQ4* KO. La falta de COQ4 produce una ligera disminución del número de copias de mtDNA, sin efecto sobre la transcripción de mtDNA y un efecto muy sutil sobre la traducción de proteínas codificadas por el mtDNA. Con respecto a la replicación del mtDNA, la falta de COQ4 o COQ6 induce una tasa de recuperación más rápida del mtDNA después de una depleción inducida. Para encontrar el mecanismo molecular de este sorprendente fenotipo, hemos estudiado el contenido de colesterol y la distribución de proteínas de los nucleoides en gradientes de densidad. Los niveles de colesterol total parecen no estar alterados en las mitocondrias de las células *COQ4* KO. Sin embargo, hemos encontrado diferencias sutiles entre COQ4 KO y las células control en la distribución de proteínas de los nucleoides (TFAM y ATAD3) en estos gradientes. Este hecho podría estar detrás de la rápida recuperación del mtDNA después de la depleción inducida. Sin embargo, todavía queda mucho trabajo por hacer para comprender mejor la relación entre la biosíntesis de CoQ y el metabolismo del mtDNA.

Contents

Table of contents

List of Figures

List of Tables

Abbreviations

1D	first dimension
2,4-dHB	2,4-dihydroxy benzoic acid
2D	second dimension
2-moHQ	2-Methoxy-hydroquinone
3,4-dHB	3,4-dihydroxybenzoate
3D	three dimensions
4-AP$_6$	3-hexaprenyl-4-aminophenol
4-HB	4-hydroxybenzoate
4-HBz	4-hydroxybenzaldehyde
4-HP$_n$	3-(hexa/octa/deca)prenyl-1,4-benzoquinone/quinol
4-HPP	4-hydroxyphenylpyruvate
aa	amino acid
AAA	ATPases Associated with diverse cellular Activities
AAVs	adeno-associated viral vectors
Ab	Antibiotic-Antimycotic
ADCK	AarF Domain Containing Kinases
ADP	adenosine diphosphate
AE-MS	affinity enrichment mass spectrometry
AICAR	5-aminoimidazole-4-carboxamide 1-β-D-ribofuranoside
AntA	antimycin A
APcI	Atmospheric Pressure Chemical Ionization
ARCA2	Autosomal recessive cerebellar ataxia 2
ARS	aminoacyl synthetase
ATI	alternative translation initiation
ATP	adenosine triphosphate
b5R	NADH-cytochrome *b*$_5$ reductase
BGL	Basal ganglia lesions
BN	Blue Native
bp	base pair
BSA	bovine serum albumin
Cas	CRISPR-associated
Cas9D10A	Cas9 nickase
CAt	Cerebellar atrophy
CD	Crohn's Disease
cDNA	complementary DNA
CDS	coding sequence
CHyp	Cerebellar hypoplasia
CI	Complex I
CII	Complex II
CIII	Complex III
CIV	Complex IV
CKD	Chronic kidney disease
CLD	Chronic Lung Disease
CMV	Cytomegalovirus
CNS	central nervous system
CoA	coenzyme A
CoQH·	semi-ubiquinone
CoQ$_n$	Coenzyme Q, ubiquinone
CoQ$_n$H$_2$	ubiquinol
COX	Cytochrome c oxidase complex
CRISPR	Clustered regularly interspaced short palindromic repeats
crRNA	CRISPR RNA
cryo-EM	cryo-electron microscopy
CS	Citrate synthase
CuZn-SOD	copper-zinc superoxide dismutase
CV	ComplexV, ATP synthase
CytC	cytochrome C
DAmb	Deteriorated ambulation
DAPI	4',6-diamidino-2-phenylindole dihydrochloride
DBH$_2$	decilubiquinone
DCPIP	2,6-dichlorophenolindophenol
DD	Developmental delay
DDA	Data-dependent acquisition
DDM	n-dodecyl-β-D-maltoside
DDMQ$_n$	2-demethyl-6-demethoxy-coenzyme Q
del	deletion
DHHB /DOHB /DDHB	3-(hexa/octa/deca)prenyl-4,5-dihydroxybenzoate
DHHP /DHOP /DHDP	3-(hexa/octa/deca)prenyl-5-hydroxy-1,4-benzoquinone/quinol
DHODH	dihydroorotate dehydrogenase
D-loop	displacement loop
DM	Diabetes Mellitus
DMAPP	dimethylallyl diphosphate

DMEM	Dulbecco's Modified Eagle Medium
$DMeQ_n$	6-demethyl-coenzyme Q
DMQ_n	6-demethoxy-coenzyme Q
dNTP	Deoxynucleotide triphosphate
DOX	doxycycline
Drp1	dynamin-like protein 1
DSB	double-strand breaks
DSS	disuccinimidyl suberate
DTNB	5,5'-dithiobis (2-nitrobenzoic acid)
DTT	dithiothreitol
Dy	Dysarthria
E4P	erythrose-4-phosphate
ECD	electrochemical detector
EDTA	ethylenediaminetetraacetic acid
EEG	electroencephalogram
EI	Exercise intolerance
EMA	European Medicine Agency
Ep	Epilepsy
ER	endoplasmic reticulum
ERMES	endoplasmic reticulum-mitochondria encounter structure
ESRD	End-stage Renal Disease
EtBr	Ethidium Bromide
ETC	electron transport chain
ETFDH	electron transport flavoprotein dehydrogenase
EUCOMM	European Conditional Mouse Mutagenesis Program
F_o	membrane-intrinsic proton-translocating domain of the ATP synthase
F_oF_1-ATPase	ATP synthase
F_1	membrane-extrinsic matrix-facing catalytic domain of the ATP synthase
FACS	fluorescence activated cell sorting
FAD+	flavin adenine dinucleotide
$FADH_2$	reduced flavin adenine dinucleotide
FBS	Fetal bovine Serum
FCCP	carbonyl cyanide-4-trifluoromethoxy-phenylhydrazone
FDR	False Discovery Rate
Fe-S	iron-sulphur
FGF-21	fibroblast growth factor-21
Flp	flippase
FMN	flavin mononucleotide
FMO	flavin-dependent monooxygenase
FPP	farnesyl diphosphate
FRT	*flippase recognition target*
fs	frame shift
FS	FLAG-Strep tag
FSP1	Ferroptosis Suppressor Protein 1
Fw	forward
GDF-15	growth differentiation factor-15
GFP	Green fluorescent protein
GGPP	geranylgeranyl diphosphate
GI	Gait instability
GO	Gene Ontology
GPDH	glycerol-3-phosphate dehydrogenase
GPP	geranyl diphosphate
GPX4	glutathione peroxidase 4
gRNA	guide RNA
GTP	guanosine triphosphate
H	Heavy
HA	Human influenza hemagglutinin
HAB	3-hexaprenyl-4-aminobenzoic acid
HB	hypotonic buffer
HCM	Hypertrophic Cardiomyopathy
HDF Neo	Human Dermal Fibroblasts, neonatal
HDR	homologous directed repair
HEK	Human embrionic Kidney
HEPES	4-(2-hydroxyethyl)-1-piperazineethanesulfonic acid
HF	Heart Failure
HHAB	3-hexaprenyl-4-amino-5-hydroxybenzoic acid
HHB /OHB /DHB	3-(hexa/octa/deca)prenyl-4-hydroxybenzoate
HHMB /OHMB /DHMB	3-(hexa/octa/deca)prenyl-4-hydroxy-5-methoxybenzoate
HHyp	Heart hypoplasia
HL	Hearing Loss
HMG-CoA	3-hydroxy-3-methylglutaryl-CoA
HMP /OMP /DMP	2-(hexa/octa/deca)prenyl-6-methoxyphenol
HPLC	high-performance liquid chromatography
HPP /OPP /DPP	2-(hexa/octa/deca)prenyl-phenol
HQ	1,4- dihydroxy benzene or hydroquinone
HRP	horseradish peroxidase
HSP	heavy-strand promoter

Ht Hypotonia
HT Hypertension
ID Intellectual deficiency
$IDMQ_n$ 4-imino-6-demethoxyCoQ
IH Impaired Handwriting
IMM inner mitochondrial membrane
IMPC International Mouse Phenotyping Consortium
IMS intermembrane space
IOD iodixanol
IP_3Rs inositol-triphosphate receptors
IPP isopentenyl diphosphate
iPSCs Induced pluripotent stem cells
IVNC Isolated ventricular non-compactation
KCN potassium cyanide
KD knock-down
KD Kidney dysfunction
KI knock-in
KO knock-out
KP potassium phosphate
L Light
LAM Lipid accumulation in muscle
LBS lipid binding site
LC-MS liquid chromatography mass spectrometry
LDH-A lactate dehydrogenase A
LF Liver failure
LFA Lipofectamine 3000 reagent
LHON Leber hereditary optic neuropathy
LHyp Lung Hypoplasia
LR Livedo Reticularis
LS Leigh-like Syndrome
LSP light-strand promoter
m/z mass-to-charge ratio
MADD multiple acyl-CoA dehydrogenation deficiency
MAMs mitochondrial associated membranes
MCU mitochondrial calcium uniporter
MELAS Mitochondrial encephalomyopathy, lactic acidosis, and stroke- like episodes
MERRF Myoclonic epilepsy with ragged red fibres
MF Muscle fatigue
MFN mitofusin
MGIE Multifocal global ischemic events
MIA mitochondrial intermembrane space assembly
MNC Medullary nephrocalcinosis
MnSOD manganese superoxide dismutase
MOMP outer membrane permeabilisation
MOPS 3-(N-morpholino)propanesulfonic acid
MPP mitochondrial processing peptidase
MPTP mitochondrial permeability transition pore
MRC mitochondrial respiratory chain
MRG mitochondrial RNA granules
MRI magnetic resonance imaging
MRP mitoribosomal proteins
MS mass spectrometry
MS Muscle stiffness
MSA multisystem atrophy
MSH Mannitol-sucrose-HEPES buffer
mtDNA mitochondrial DNA
mtPAP mitochondrial poly(A) polymerase
mt-rRNA mitochondrial ribosomal RNA
MTS mitochondrial targeting signal
mtSSB mitochondrial single-stranded DNA-binding protein
mt-tRNA mitochondrial transfer RNA
MW Muscle weakness
My Myoclonus
NAD^+ nicotinamide adenine dinucleotide
NADH reduced nicotinamide adenine dinucleotide
NaN_3 sodium azide
NARP Neuropathy, ataxia, and retinitis pigmentosa
NCR non-coding region
nDNA nuclear DNA
NGS next-generation sequencing
NHEJ non-homologous end joining
NHS amine-reactive
NMD nonsense-mediated mRNA decay
NMR nuclear magnetic resonance
NQO1 NAD(P)H:quinone reductase 1
nt nucleotide
NTS nuclear localisation signal
nVP Non-visual pursuit
Ny Nystagmus
o.n. overnight

OA	Optic Nerve Atrophy
OAB	4-amino-3-octaprenyl-benzoate
OAP	2-amino-3-octaprenylphenol
OCR	Oxygen consumption rate
OE	overexpression
O_H	origin of mtDNA replication of the strand H
OHP	2-hydroxy-3-(hexa/octa/deca)prenylphenol
O_L	origin of mtDNA replication of the strand L
OL	oligomycin
OMM	outer mitochondrial membrane
OPA	2-octaprenyl-aniline
OPA1	optic atrophy 1
ORF	open reading frame
OXPHOS	oxidative phosphorylation
P	phosphorylation
pABA	para-amino benzoic acid / para-aminobenzoate
PAGE	polyacrylamide gel electrophoresis
PAM	Protospacer Adjacent Motif
PARL	Presenilin Associated Rhomboid Like
PBS	phosphate-buffered saline
PBSi	PBS with PIC
PBSS	PBS, 5% FBS
PBSST	PBSS buffer with 0.3 % Triton X-100
PCR	Polymerase chain reaction
PDB	Protein Data Bank
PEP	phosphoenolpyruvate
PFA	paraformaldehyde
PGC1α	peroxisome proliferator-activated receptor γ coactivator 1 α
Pi	inorganic phosphate
PIC	protease inhibitors cocktail
PKL	protein kinase-like
PMF	proton-motive force
PMSF	phenylmethylsulfonyl fluoride
PNS	peripheral nervous system
PNSN	Peripheral Neuropathy
POLG	mtDNA polymerase gamma
POLRMT	mitochondrial RNA polymerase
poly-PDS	poly-prenyl diphosphate synthases
POPC	1-palmitoyl-2-oleoyl-glycero-3-phosphocholine
POPE	1-hexadecanoyl-2-(9Z-octadecenoyl)-sn-glycero-3-phosphoethanolamine
POPG	1-palmitoyl-2-oleoyl-sn-glycero-3-phospho-(1'-rac-glycerol)
PPARs	peroxisome proliferator-activated receptors
PPI	Protein-protein interaction
ppm	parts per million
pre-crRNA	pre-CRISPR RNA
ProDH	proline dehydrogenase 1
Pt	Ptosis
PVDF	polyvinylidene difluoride
Rad	radio-flow detector
RBPs	RNA binding proteins
RD	Respiratory distress
RET	retrograde electron transport
RF	Respiratory failure
RIs	replication intermediates
RITOLS	Ribonucleotides are Incorporated ThroughOut the Lagging Strand
RNA-Seq	RNA sequencing
ROS	reactive oxygen species
Rot	rotenone
RP	Retinitis Pigmentosa
Rp	Retinopathy
RT	room temperature
rt	retention time
RT-PCR	Reverse Transcription-PCR
RT-qPCR	Real-time quantitative PCR
Rv	reverse
RXR	retinoid X receptor
SAM	S-adenosylmethionine
SAM-Mtases	S-adenosylmethionine-dependent methyltransferases
SB	Laemmli Sample Buffer
SCP2	sterol carrier protein 2
SCR	Strand coupled replication
SCs	mitochondrial supercomplexes
SD	standard deviation
SDM	site-directed mutagenesis
SDR	Strand displacement replication
SDS	sodium dodecyl sulphate
SEM	Saccadic eye movements
SILAC	stable isotope labelling by amino acids in cell culture
SLL	Stroke-like lessions
SN	supernatant
SNHL	Sensorineural hearing loss

SO sensory organs
Sp Spasticity
SQOR sulphide-quinone oxidoreductase
SRNS steroid-resistant nephrotic syndrome
SSB single-strand break
START steroidogenic acute regulatory protein-related lipid transfer
Sz Seizures
TALENs transcription activator-like effector nucleases
TBE Tris-Borate-EDTA
TBS Tris-buffered saline
TCA tricarboxylic acid
TCEP tris(2-carboxyethyl)phosphine
TEFM mitochondrial transcription elongation factor
Tet-FBS Tetracycline Free FBS
TetR Tet Repressor gene
TFAM mitochondrial transcription factor A
TFB2M mitochondrial transcription factor B2
TFR TetR family of transcriptional regulator
TGS Tris-Glycine-SDS buffer
THyp Thalamic hypoplasia
TIM translocase of the inner membrane
TIS translation initiation sites
TNB thionitrobenzoic acid
TOF time of flight
TOM translocase of the outer membrane
Tp Tubulopathy
Tr Tremor
tracrRNA trans-activating crRNA
TSS transcription start sites
TTBS TBS with 0.05% Tween-20
UbiC chorismate lyase
UCPs Uncoupling proteins
UTR untranslated region
VA Vanillic acid
VDAC voltage-dependent anion channel
Vp Valvulopathy
WB western blot
WBC white blood cells
WES Whole exome sequencing
WGS Whole genome sequencing
WT wild type
ZBM zinc binding motif
ZNFs zinc-fingers nucleases
µg microgram
µl microlitre
µM micromolar

Introduction

Introduction

I1. Mitochondria

The term *mitochondria* was first coined in 1898 by the German microbiologist Dr Carl Benda. By using a light microscope, he observed long granulated chains during spermatogenesis and named them *mitochondrion*. This word derives from the Greek *mitos*, meaning thread, and *chondrion*, meaning grain [5]. It is widely accepted that, together with chloroplasts, mitochondria originated from a facultative anaerobic α-proteobacterium that was endocytosed by a primitive methanogenic archaebacterium during eukaryotic evolution [6]. This endosymbiotic event provided the bioenergetic means for large variations in the shape, size and function of eukaryotic cells to evolve, leading to the creation of multicellular organisms with specialised cell types. Mitochondria contain their own DNA, the mitochondrial DNA (mtDNA), which over the course of evolution was reduced through horizontal gene transfer into nuclear DNA (nDNA), but still encodes for a subset of the mitochondrial proteins (See Chapter 5).

Mitochondria are membrane-enclosed organelles of eukaryotic cells, vital for producing the energy needed for all biological processes. Commonly known as "the powerhouse of the cell", mitochondria are specialised in adenosine triphosphate (ATP) production by a process called oxidative phosphorylation (OXPHOS), for which oxygen is required[7]. These organelles are in the centre of the cellular energy metabolism, as they also host essential biochemical processes such as the tricarboxylic acid (TCA) cycle or Krebs cycle, urea cycle and β-oxidation of fatty acids, which are intimately linked to OXPHOS. In addition, mitochondria play a critical role in other cellular pathways, such as the regulation of calcium homeostasis, the production of reactive oxygen species (ROS), autophagy and apoptosis or programmed cell death.

I1.1. Mitochondrial architecture and dynamics

Mitochondria have an extremely developed membrane system, composed by two membranes known as mitochondrial inner and outer membranes, fact that is considered evidence of the endosymbiotic theory. Both the outer and the inner membranes,

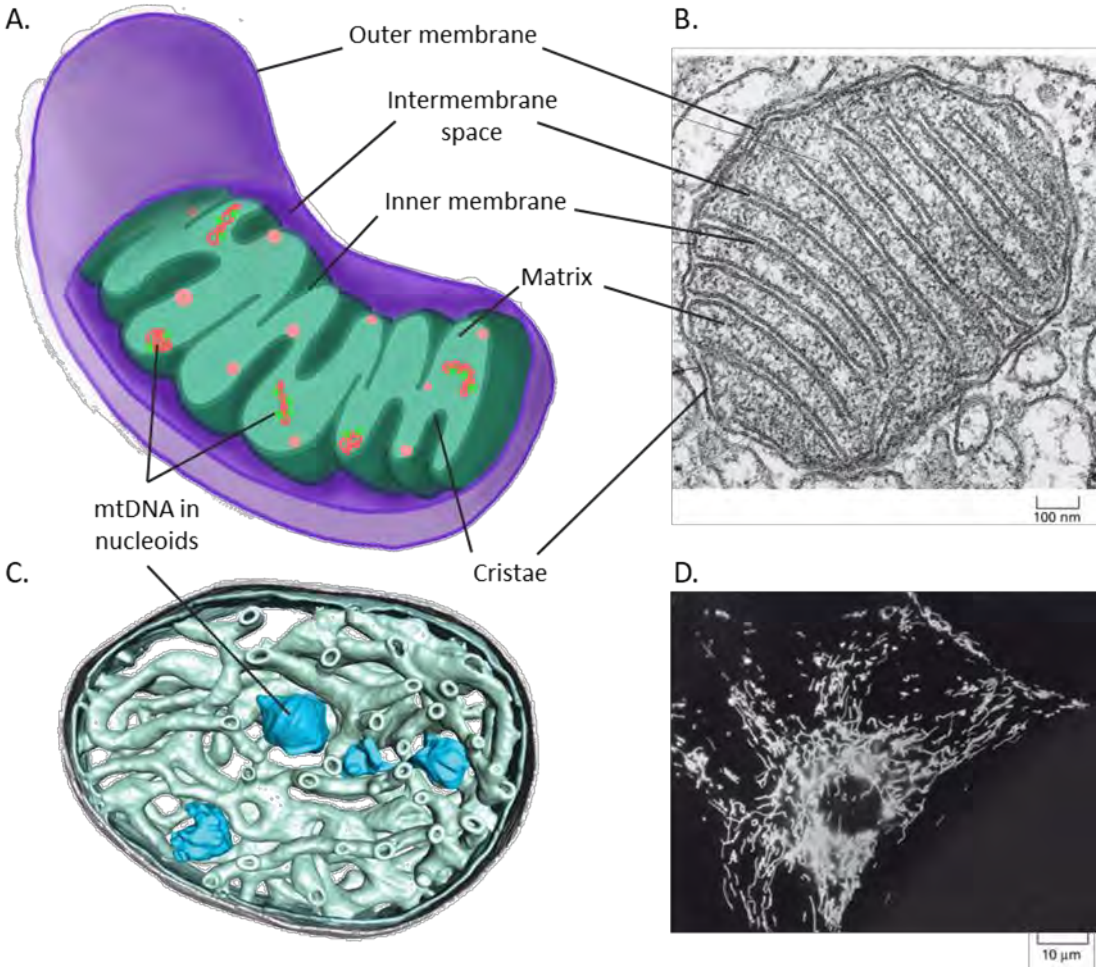

Figure I.1. Mitochondrial architecture and dynamics.
(A) Cartoon representation of mitochondrion. (B) Electron micrograph of a mitochondrion (Taken from Alberts et al., 2015[8]). (C) Computer model generated from segmented tomograms of bovine heart mitochondrion (Taken from Gustafsson et al., 2016[9]). (D) Mitochondrial network shown in a light micrograph of chains of living mammalian cell in culture (stained with rhodamine 123) (Taken from Alberts et al., 2015[8]).

together with membrane protein complexes, work to transform biomolecules, such as sugars, lipids and proteins, into chemical energy in the form of ATP. These two membranes have distinct biochemical properties and functions, and they divide the organelle into two separate compartments: the matrix (inside the inner membrane) and the intermembrane space (IMS), between the two membranes (Figure I.1.A, B and C) [8].

The outer mitochondrial membrane (OMM) has a similar composition to the cell plasma membrane. It contains a large number of integral proteins called porins or voltage-dependent anion channels (VDAC), that make it permeable to small molecules (< 5 kDa) and ions. Therefore, the IMS has the same ionic composition and pH than the cytoplasm, and there is no electrochemical gradient across the OMM. A dedicated translocase of the outer membrane (TOM) complex is in charge of the import of bigger proteins [10–13].

Moreover, mitochondria can interact with other cellular structures through contacts that are established on the OMM, such as the endoplasmic reticulum (ER)-mitochondria contact sites. Mitochondria-ER contacts are specific and specialised domains in which many processes occur, such as the exchange of lipids between the two membrane systems or the induction of mitochondrial fission (see Chapter 5).

The inner mitochondrial membrane (IMM) is more complex and shares many characteristics with the bacterial cell membrane, such as the presence of cardiolipin[14], among others. It has a high protein concentration and low permeability, being only permeable to O_2, carbon dioxide (CO_2), and water (H_2O). Specific mitochondrial carriers exist to transport proteins and other molecules through the IMM. This controlled permeability allows the generation and maintenance of an electrochemical gradient across the IMM, known as the proton-motive force (PMF), which is essential for ATP synthesis [7] and other mitochondrial functions such as Ca^{2+} uptake through the mitochondrial calcium uniporter (MCU) [15]. IMM is forming highly folded invaginations called cristae, enhancing the surface in which the OXPHOS machinery is installed [16,17]. Continuous with the cristae membrane, there is the boundary membrane region, which is thought to contain the machinery for protein import (translocase of the inner membrane, TIM), new membrane insertion and respiratory complexes assembly.

The IMS is crucial for several mitochondrial functions, such as the exchange of proteins, lipids and metal ions between the matrix and the cytosol [18–20]. It contains the mitochondrial intermembrane space assembly (MIA) for oxidative protein folding [21]. Cytochrome c, a protein involved in electron transfer on the IMM, is also located in the IMS, and its release into the cytoplasm triggers apoptosis. The IMS also contains other proteins such as Cu/Zn superoxide dismutase, which detoxifies superoxide ($O^{2\cdot-}$), a potentially harmful by-product of oxygen metabolism.

Mitochondrial matrix is a viscous, protein-rich compartment. It contains multiple copies of the mtDNA genome packed with specific proteins in the so-called nucleoids, as well as the replication, transcription and translation machineries for expression and maintenance of the mtDNA. It also contains pools of ions and proteins involved in many different processes, such as the catabolism of pyruvate, fatty acids and amino acids, the

TCA cycle, the biosynthesis of coenzyme Q (CoQ) and steroids, the biosynthesis of haem moieties and iron-sulphur (Fe-S) clusters, etc [22].

Mitochondria form a markedly dynamic tubular network, constantly dividing, fusing and changing shape or position, for what they are often associated to the microtubules of the cytoskeleton (Figure I.1.D) [23]. Mitochondrial fusion produces elongated tubular mitochondria, optimising mitochondrial function by spreading metabolites, protein and mtDNA throughout the entire mitochondrial compartment. Fission produces small spherical mitochondria, allowing the segregation and isolation of dysfunctional mitochondria. Fusion and fission are both driven by membrane remodelling enzymes which are part of the dynamin family of large GTPases, including Dynamin-related/-like protein 1 (Drp1), mitofusin (MFN) and optic atrophy 1 (OPA1) proteins. Fusion and fission events in the mitochondrial network are balanced, in order to adapt mitochondrial morphology to the metabolic needs of the cell. The regulation of mitochondrial dynamics is crucial for mitochondrial function and quality control [23–26].

I1.2. Energy transduction in mitochondria: the OXPHOS system

Energy transduction in mitochondria starts with the catabolism of pyruvate (from carbohydrates), fatty acids (from fats) and amino acid (from proteins), which are imported to mitochondria by specialised mitochondrial carriers, and are degraded to acetyl-coenzyme A (CoA) (Figure I.2) [27]. The pyruvate dehydrogenase complex decarboxylates pyruvate to acetyl-CoA, also producing a molecule of CO_2 and a molecule of reduced nicotinamide adenine dinucleotide (NADH). Fatty acids are activated as fatty acyl-CoA, and broken down completely by a cycle of reactions (beta-oxidation of fatty acids) that trims two carbons at a time from its carboxyl end, generating a molecule of acetyl-CoA, a molecule of NADH and a molecule of reduced flavin adenine dinucleotide ($FADH_2$) for each turn of the cycle [8].

The acetyl groups are incorporated to the TCA cycle to form citric acid, which is gradually oxidised. The energy of these oxidations is stored in the form of three molecules of NADH, a molecule of $FADH_2$ and a molecule of guanosine triphosphate (GTP) for each turn of the cycle, and two molecules of CO_2 are produced as the result of the total

oxidation of the acetyl-CoA. NADH and $FADH_2$ produced during this oxidative process feed electrons into de electron transport chain (ETC) in the IMM (Figure I.2) [8].

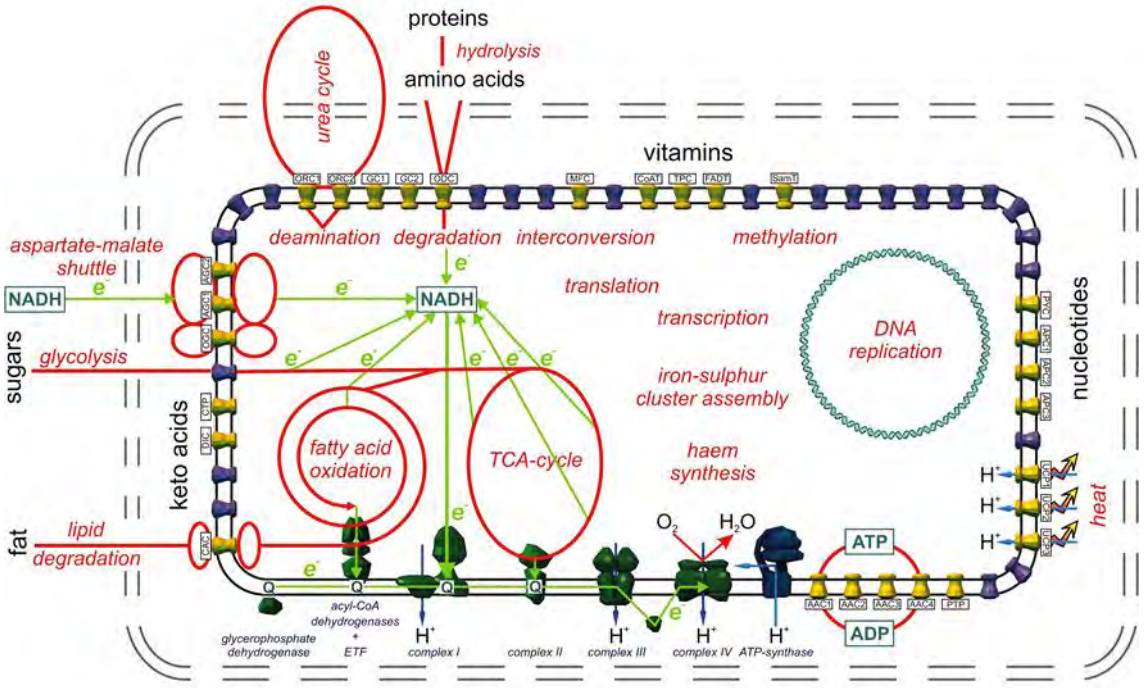

Figure I.2. General overview of mitochondrial metabolism.
Main metabolic pathways are shown in red. The outer and inner membranes are indicated with dashed and continuous lines, respectively. The ATP synthase and the complexes of the respiratory chain are blue and green, respectively. Known and unknown carrier proteins are shown in yellow and purple, respectively. Green arrows indicate electron flux, blue arrows indicate proton pumping and the curly red arrow indicates oxygen conversion to water (Taken from Kunji and Robinson, 2010[27]).

In the process of electron transport, subsequent redox reactions occur spontaneously from a pair with lower or more negative redox potential ($NADH/NAD^+$), to a pair with a higher or more positive redox potential (Figure I.3). Each complex of the system has a higher affinity for electrons (or higher redox potential) than the previous one, being the molecular oxygen the acceptor with the highest electron affinity of all. The electrons finally combine with O_2 to form H_2O, a low energy molecule. The energy released during the electron transport results in pumping H^+ out of the matrix, across the IMM [8].

This process generates an electrochemical gradient across the IMM, which causes a PMF. Two components define the PMF: an electrical membrane potential ($\Delta\Psi$) and a chemical pH gradient (ΔpH), which tends to drive H^+ back to the matrix. The ATP synthase or complex V uses this force to rotate and generate ATP from adenosine diphosphate (ADP) and inorganic phosphate (Pi). The whole process is called oxidative phosphorylation (OXPHOS) (Figure I.4) [8].

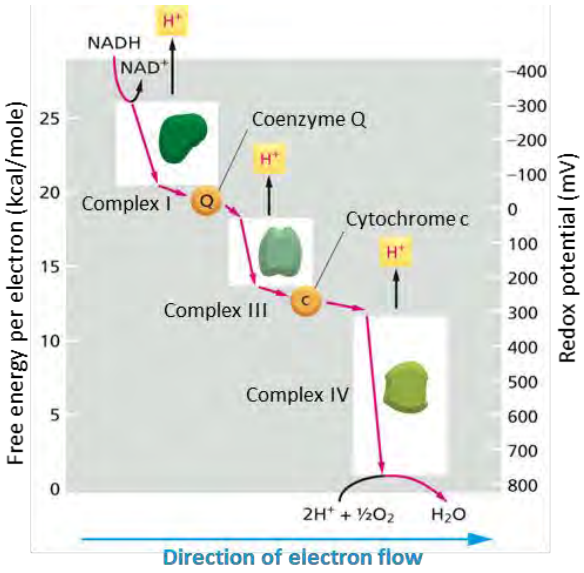

Figure I.3. Standard free-energy change for the transfer of each of the two electrons donated by an NADH molecule. NADH dehydrogenase (complex I) and cytochrome b-c_1 (complex III) complexes each pump two H^+ per electron. Cytochrome oxidase (complex IV) pumps one H^+ per electron. Pink arrows indicate electron flux, black arrows indicate proton flux. (Taken from Alberts et al., 2015[8]).

The mitochondrial respiratory chain (MRC) is composed by three large enzymatic complexes embedded in the IMM, which pump electrons to the IMS and contribute to the PMF: Complex I, Complex III and Complex IV; the ATP synthase or Complex V, which uses this force to generate ATP; two small mobile electron carriers, to support electron transfer between complexes: coenzyme Q or ubiquinone (CoQ) and cytochrome C (CytC) (Figure I.4); and other protein complexes or enzymes that feed the chain with electrons: Complex II and other enzymes giving electrons to CoQ (dihydroorotate dehydrogenase, mitochondrial glycerol-3-phosphate dehydrogenase, electron transport flavoprotein dehydrogenase (ETFDH), proline dehydrogenase 1 and 2, sulphide-quinone oxidoreductase, see Introduction, Section I2.3) [28].

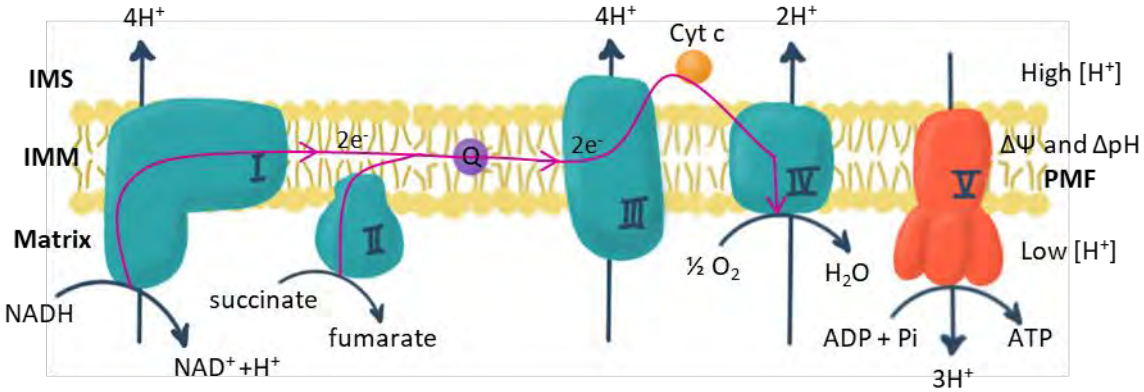

Figure I.4. Schematic representation of mitochondrial respiratory chain and OXPHOS.
Electrons are donated to CI or CII by the electron carriers NADH and $FADH_2$ respectively, and then flow to CIII and CIV, with the help of CoQ and CytC (pink arrows). Finally, electrons reach Complex IV and are passed onto the terminal electron acceptor O_2, which is reduced to H_2O. Electron transport provides energy to complexes I, III and IV to pump protons across the IMM, generating the PMF. The PMF drives H^+ back down its gradient through CV (F_oF_1-ATP synthase), which harnesses the energy of this movement to phosphorylate ADP to ATP.

Complex I

Complex I is also known as NADH dehydrogenase complex or NADH:ubiquinone oxidorreductase (Complex I, CI, EC1.6.5.3). It is the largest complex, with 45 subunits constituting a L-shaped enzyme, with a hydrophilic arm, facing the matrix, and a membrane embedded hydrophobic arm. CI catalyses the electron transfer from NADH to the lipid-soluble electron carrier CoQ through the matrix arm, through a non-covalently bound flavin mononucleotide (FMN), one 2Fe-2S cluster and six 4Fe-4S clusters (Figure I.5) [29]. The energy derived from the transfer of two electrons from NADH to ubiquinone is used to pump 4 H^+ to the IMS, through the membrane arm. Ubiquinone receives 2 electrons, and also takes up 2 H^+ from the matrix to be fully reduced. This reduced ubiquinol ($CoQH_2$) diffuses in the IMM to transfer its electrons to Complex III (CIII)[8].

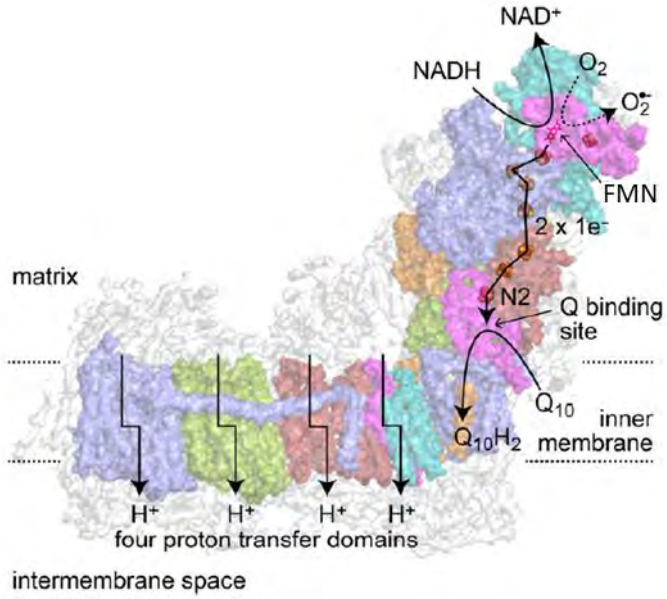

Figure I.5. Structure and reactions catalyzed by mammalian complex I.
NADH is oxidized by a FMN at the top of the hydrophilic domain. Electrons are then passed along a chain of iron–sulfur clusters (ending in cluster N2) to reduce CoQ in the Q-binding site. Four protons are transferred from the matrix to the IMS for each NADH oxidized. The reduced FMN also reacts with O_2 to form ROS. The fourteen subunits of the core enzyme are shown in color. (Taken from Hirst & Roessler, 2016[29]).

Complex II

Complex II is also named succinate dehydrogenase or succinate:ubiquinone reductase (Complex II, CII, EC1.3.5.1): CII is a component of the TCA cycle that catalyses the electron transfer from succinate to ubiquinone, through a flavin adenine dinucleotide (FAD), the 2Fe-4S, 4Fe-2S and 3Fe-4S clusters and one haem (Figure I.6) [30,31]. CII contains the dimeric TCA enzyme succinate dehydrogenase, and three other small hydrophobic subunits embedded in the crista membrane. CII does not pump H^+, so it does not contribute to the PMF [8]. That is why sometimes it is not considered as a part of the MRC, but as one of the many dehydrogenases that donate electrons to CoQ in the IMM, which afterwards transfers electrons to CIII (See Introduction, Section I2.3).

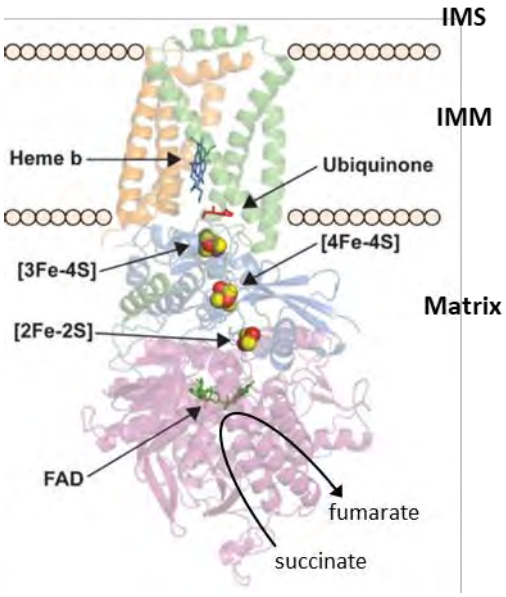

Figure I.6. Structure and reactions catalyzed by porcine complex II.
Electron transfer occurs from succinate to ubiquinone via a FAD, three iron-sulphur clusters (2Fe-4S, 4Fe-2S and 3Fe-4S) and one haem (heme b). (Adapted from Van Vranken et al., 2015[31]).

Complex III

Cytochrome c reductase, cytochrome b-c1 complex or ubiquinol:cytochrome c oxidoreductase (Complex III, CIII, EC1.10.2.2) are other names for CIII. It is a dimeric complex, and each of the monomers contains three cytochrome haems and one 2Fe-2S cluster. CIII catalyses the electron transfer from a two-electron carrier ($CoQH_2$) to a one-electron carrier (CytC) by the Q cycle (Figure I.7). In the process of electron transfer, protons are vectorially translocated to the IMS [32–35]. Each $CoQH_2$ in the intermembrane side of the IMM passes two electrons to CIII, one to reduce one CytC and the other one to a molecule of oxidised CoQ in the matrix side of the IMM, reducing it to semiubiquinone. This semiubiquinone will be fully reduced to ubiquinol when another $CoQH_2$ molecule transfers again a pair of electrons to CIII, one to reduce a second CytC molecule, and the other one to the semiubiquinone on the matrix side. Thus, two $CoQH_2$ molecules (IMS side) are required to eventually reduce two CytC and one CoQ (matrix side). Simultaneously, 2 H^+ are transported to the intermembrane space per cycle, so 4 H^+ are translocated per pair of electrons transported through CIII to CytC. The net effect of the electron pair transfer is that one molecule of $CoQH_2$ is oxidised to CoQ, and two molecules of oxidised CytC are reduced. CytC is a small soluble protein, located in the IMS, which carries electrons, one at a time, to Complex IV [8].

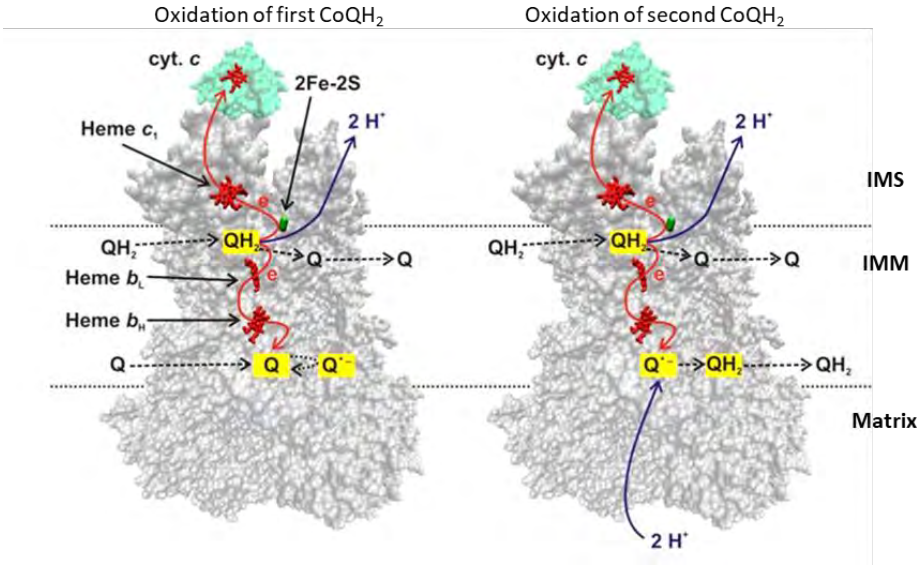

Figure I.7. The Q-cycle through complex III.
Successive oxidation of two $CoQH_2$ (IMS side), resulting in the reduction of one CoQ and two cytochrome c(matrix side). The electron transfer pathways through the co-factors are represented with red arrows, and the proton transfer with blue arrows. (Adapted from Wikström et al., 2015[35]).

Complex IV

Complex IV is the cytochrome c oxidase complex (COX) or succinate:cytochrome c oxidoreductase (Complex IV, CIV, EC1.9.31). It contains two cytochrome haems and three copper atoms. CIV accepts electrons, one at a time, from reduced CytC and transfers them to O_2, producing H_2O (Figure I.8). Coupled with the reduction by four electrons of O_2 to two molecules of H_2O, 4 H^+ are pumped to the IMS [8,36].

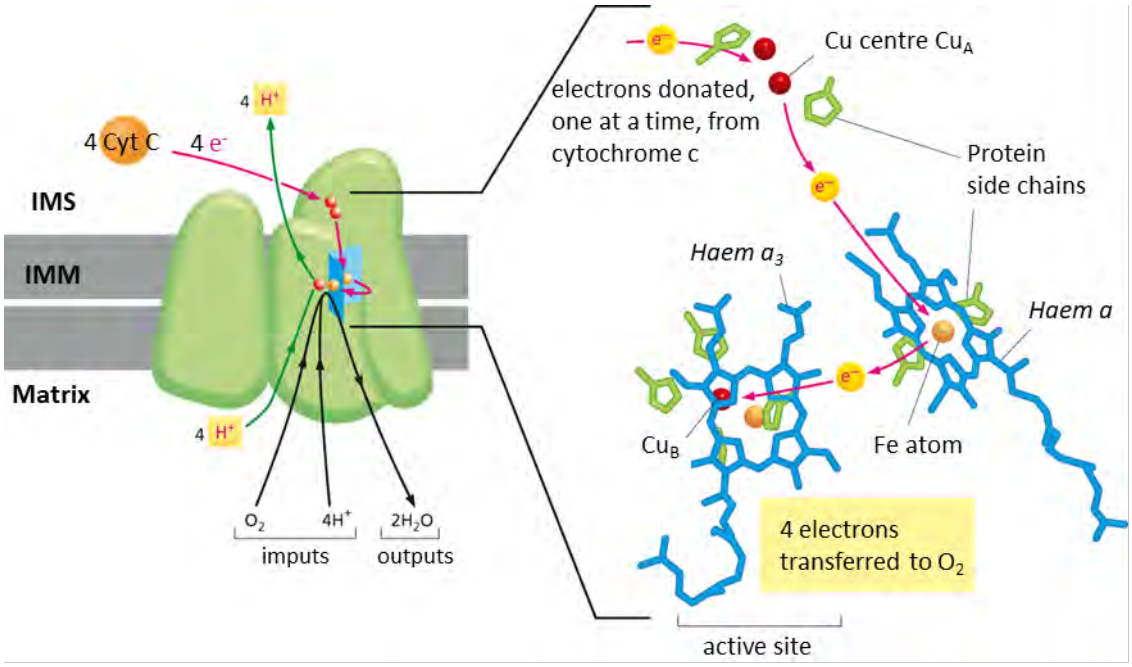

Figure I.8. Reactions catalyzed by complex IV.
Electron transfer occurs from cytochrome c to O_2 via copper centre Cu_A, then haem *a* and finally to haem-a_3-Cu_B centre-haem (pink arrows). Proton pumping is represented with green arrows. (Adapted from Alberts et al., 2015[8]).

Complex V

Complex V is the ATP synthase, H^+-transporting two-sector ATPase or F_oF_1-ATPase (Complex V, CV, EC 3.6.14). This complex uses the PMF generated by the respiratory complexes CI, III and IV to produce ATP from ADP and Pi. It is composed of two distinct domains: the membrane-intrinsic proton-translocating domain (F_o) and the membrane-extrinsic matrix-protruding catalytic domain (F_1), and both are connected through central and peripheral stalks. In the IMM, dimers of the ATP synthase are formed by the association of their membrane domains. These dimers are localized at the region of highest curvature along the edges of the cristae[37].

H^+ from the IMS pass through the F_0 region, driven by the PMF. This leads to conformational changes that cause the clock-wise rotation of the central stalk. The central stalk transmits the rotational energy of the motor to the catalytic domain of F_1, producing conformational changes that allow the catalysis and release of one molecule of ATP per 3 H^+ translocated, approximatively (Figure I.9) [37–39]. F_1 contains five types of subunits: α_3, β_3, γ, δ and ε. The conversion of ADP+Pi to ATP occurs at the catalytic sites of β subunits, which can exist in three different conformations: the open form, which does not bind neither substrate nor product; the loose form that binds ADP and Pi weakly; and the tight form, which binds a molecule of ATP. Most of the ATP produced by the OXPHOS system is translocated by ADP/ATP carrier proteins into the cytosol, where it is used as the chemical energy supply in a myriad of other cellular reactions.

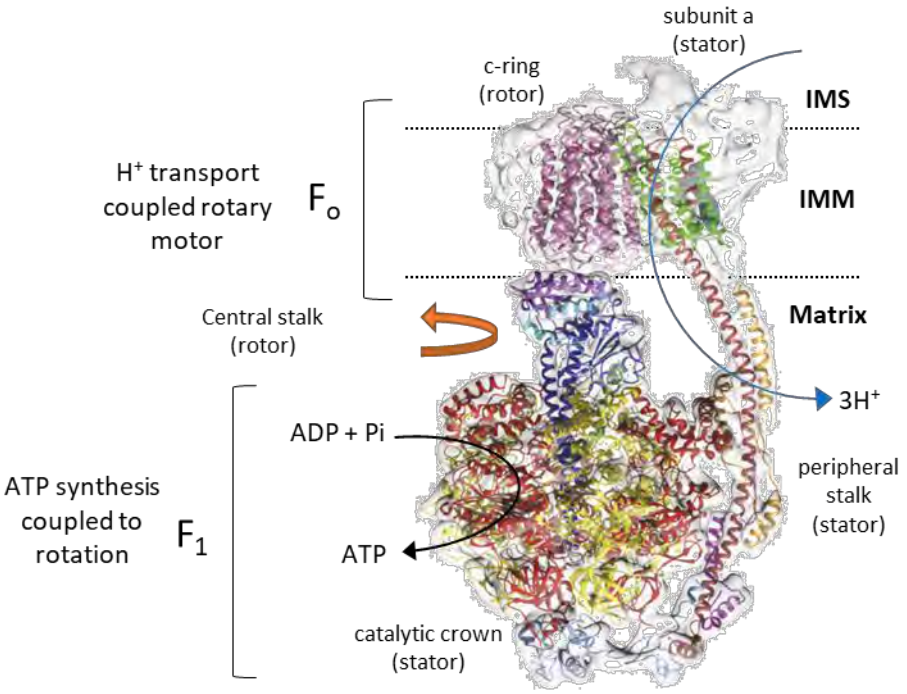

Figure I.9. Structure and ATP synthesis function of bovine ATP synthase.
The ATP synthase is found in the IMM, with the F_1 region in the mitochondrial matrix and the F_O region accessible from the IMS. The PMF drives protons across the c-ring (blue arrow), inducing a clockwise rotation of this subunit that is transferred to the central stalk (orange arrow). The rotation induced conformational changes in the catalytic crown of F_1 region, that catalyses the conversion of ADP+Pi to ATP (black arrow) (Adapted from Zhou et al., 2015[38] and Mukherjee et al., 2017[39]).

Supercomplexes

MRC complexes interact with each other forming higher order structures with different stoichiometries, called supercomplexes (SCs). Blue Native Gel Electrophoresis (BN-PAGE) of digitonin treated mitochondria has revealed SCs with different molecular size and subunit composition, including III_2IV_1, I_1III_2, $I_1III_2IV_1$, and $I_2III_2IV_{1–2}$ [40–42]. The supercomplex $I_1III_2IV_1$ has been called the respirasome, and the supercomplex $I_2III_2IV_2$ has been named as respiratory megacomplex. High-resolution cryo-electron microscopy (cryo-EM) structures of the respirasome of several mammalian species, including human, have been resolved in the last years [43–46]. However, their mode of assembly and specific roles are not known yet [36,41–44,47].

It has been proposed that CoQ is organised in different pools, being each of them specific and essential for each respiratory-active super assembly [48,49]. However, this fact is controversial, since CoQ can be experimentally reoxidised more rapidly by alternative quinol oxidases outside the SCs than by CIII inside these SCs [50,51]. This would indicate substrate channelling does not occur, but instead CoQ diffuses freely, constituting one single pool [50,51].

I1.3. Other mitochondrial functions

Besides their function in ATP production metabolism, mitochondria also have a plethora of other functions, including many metabolic pathways. Mitochondria participate in amino acid metabolism. Some anabolic and catabolic pathways of all the 20 amino acids are associated with mitochondria [52]. Additionally, some steps of the synthesis and degradation of nucleotides [53] and fatty acids [54] also occur inside mitochondria. The biosynthesis of CoQ [28], steroids [55] and cardiolipin [14] take place inside this organelle as well. Moreover, mitochondria play a pivotal role in iron metabolism[56]. The incorporation of iron into haems [57] and Fe-S clusters [58,59] also takes part in the mitochondria.

Mitochondria have an important role in calcium storage and signalling. Mitochondrial Ca^{2+} uptake is performed through the mitochondrial calcium uniporter (MCU) [15]. Movement of calcium into the mitochondria modulates mitochondrial ATP production.

Mitochondria are key players in both programmed cell death by apoptosis and necrotic cell death. Apoptosis occurs in response to stress, such as DNA damage, growth factor withdrawal or oxidative stress. During apoptosis, the OMM is permeabilised and several IMS proapoptotic proteins, such as CytC, are released to the cytosol [60]. Necrosis is triggered by excessive production of ROS, and Ca^{2+} overload of the mitochondrial matrix. Necrosis death is characterised by permeabilisation of the IMM, by opening the mitochondrial permeability transition pore (MPTP). This leads to the dissipation of the IMM potential, ion deregulation, mitochondrial and cellular swelling, activation of degradative enzymes, failure of the plasmatic membrane and cell lysis [61–63].

I1.4. Mitochondrial diseases: an overview

Mitochondrial diseases are a group of rare genetic disorders with very heterogeneous origins, leading to a total or partial mitochondrial dysfunction of the OXPHOS system, the main source of ATP in cells. Therefore, clinical manifestations typically involve organs with high energetic demands, such as brain, muscle, eye, heart or kidney. They are highly heterogenous, both genetically and clinically, and they can affect virtually any organ and may present at any age [64,65]. Genetically, they are further complicated by the involvement of both nuclear and mitochondrial genomes coding for essential mitochondrial proteins.

Their estimated prevalence is 1 out of 5,000 people, being as a whole, the most frequent cause of inherited metabolic disease [66,67]. Several studies have shown that nuclear genetic defects are the main cause of childhood mitochondrial disease whereas mtDNA mutations are more prevalent in adult cases [64].

Genetics of mitochondrial diseases and molecular diagnosis

Mitochondria are under the control of two different genetic programmes, the nuclear and the mitochondrial genome. Thus, mitochondrial diseases can be due to mutations in nDNA, with autosomal and X-linked inheritance, or in the mtDNA, maternally inherited. Some rare sporadic cases of diseases caused by *de novo* mutations in either mtDNA or nDNA genes have also been found [65].

The nuclear genome encodes around 1,500 proteins that are involved in mitochondrial structure and function [69]. Around 300 nuclear genes encoding mitochondrial proteins have been associated with mitochondrial diseases to date (Figure I.10) [64,68,70]. These proteins can be classified as: MRC subunits, MRC assembly factors, proteins involved in mtDNA maintenance, replication and transcription, factors involved in mitochondrial protein synthesis, protein import machinery, proteins involved in mitochondrial dynamics, motility, membrane integrity and protein quality control, or other proteins participating in mitochondrial metabolism, such as the biosynthesis of lipids and cofactors, the iron metabolism, etc. [64,65,68,70–72].

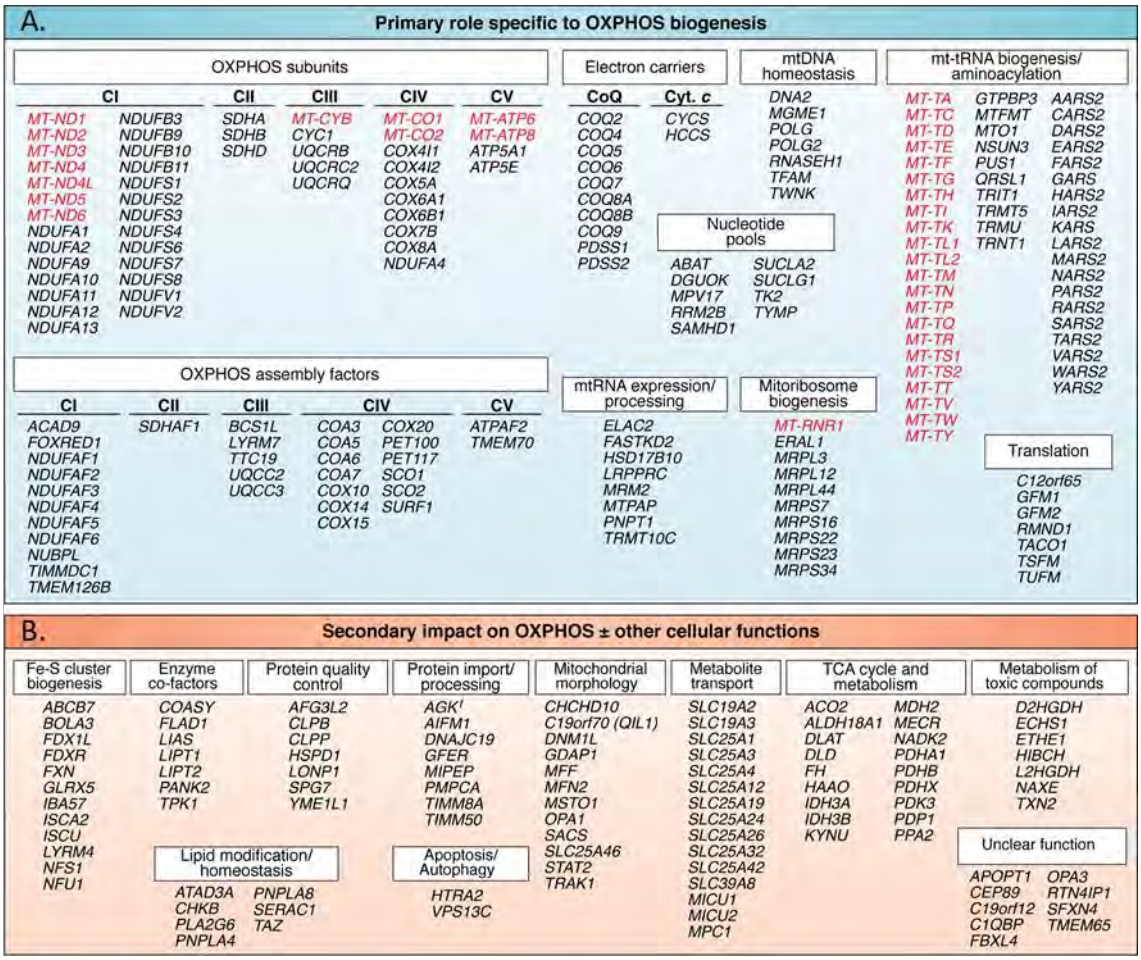

Figure I.10. Genes linked to mitochondrial disease.
All of the genes reported to date in which mutations have been shown to cause mitochondrial diseases. They are classified by their specific function in (A) genes directly involved in OXPHOS biogenesis or (B) genes with a secondary impact on OXPHOS is secondary, likely involving additional cellular functions. Genes listed in red are encoded by mtDNA and in black by nuclear DNA (Extracted from Frazier et al., 2019[68]).

The mitochondrial genome only has 37 genes, but the mtDNA can exist in multiple copies in each cell, and different populations of mtDNA molecules can coexist in the same cell (heteroplasmy) (See Chapter 5, section 5.1.2). Therefore, in patients with mutations in the mitochondrial genome (Figure I.10), the pathological variant can be in homoplasmy or different levels of heteroplasmy, which complicates the inheritance pattern and the clinical outcome.

In general, the higher the percentage of heteroplasmy is, the more severe the disease is, and critical threshold level above 60-80% of heteroplasmy is required to trigger the OXPHOS defects in specific tissues. However, it depends widely on the patient's background, the mutation, the disease, the tissues or organs affected, etc. Moreover, the percentage of heteroplasmy can vary among tissues, and the mutation load increases with age, complicating even more the picture. Currently, more than 250 pathogenic mtDNA mutations have been identified (Mito-MAP database, www.mitomap.org) and can be classified as: large-scale rearrangements (partial deletions or duplications), that are usually sporadic; and point mutations, that are usually maternally inherited [65,73].

The development of next-generation sequencing (NGS) technologies has revolutionised the diagnosis of genetic disorders in general, and mitochondrial diseases in particular. Mitochondrial disorders are particularly amenable to such strategies, as they are very heterogeneous [72]. Over the past decade, different NGS approaches have been successfully implemented [70]:

i. Whole mtDNA sequencing allows the identification of any mtDNA variant and its accurate heteroplasmy levels.

ii. Targeted gene panels sequence a specific list of genes encoding respiratory chain components or known disease-associated genes, or even more expansive panels, known as the MitoExome which included all genes listed in the MitoCarta database.

iii. Whole exome sequencing (WES) analyses only the exons (around 1.6 % of the total genome) and allows the identification of pathogenic variants in the protein-coding region of any gene, which is the most common case (85%).

iv. Whole genome sequencing (WGS) extends the analysis to the whole genome, being helpful to detect variations outside the exons.

v. RNA sequencing (RNA-Seq) transcriptomics is sometimes implemented to complement WGS and aid in variant prioritisation, when no clear variants are initially identified.

Clinical and biochemical features of mitochondrial diseases

From the clinical point of view, mitochondrial diseases are characterised by a wide range of symptoms, severity, age of onset and outcome, which hinders the diagnosis. Typically, organs and tissues with a high metabolic demand are the most affected. The most common clinical presentations affect the central nervous system (CNS) (encephalopathy, migraine, epilepsy, dementia, ataxia, dysphagia, etc.), the cardiac muscle (heart muscle weakness), the respiratory system (hypoventilation, apnea, pneumonia) and the skeletal muscle, although ophthalmoplegia, optic atrophy, blindness, deafness and diabetes are also usual (Figure I.11). The broad spectrum of clinical symptoms can be classified as particular syndromes, such as MELAS (Mitochondrial encephalomyopathy, lactic acidosis, and stroke- like episodes), MERRF (Myoclonic epilepsy with ragged red fibres), LHON (Leber hereditary optic neuropathy), NARP (Neuropathy, ataxia, and retinitis pigmentosa), Leigh Syndrome (progressive neurodegenerative disorder with basal ganglia lesions) and Pearson Syndrome (refractory sideroblastic anaemia, vacuolisation of bone marrow precursors and exocrine pancreatic dysfunction). Nonetheless, many patients do not fit into this syndromic classification [70]. Patients with adult-onset disease usually display myopathy with a variable involvement of the CNS, while early-onset patients mostly present Leigh syndrome, which can be caused by mutations in over 75 different genes [74].

Patients with mitochondrial diseases often manifest a deficiency in one or more OXPHOS complexes, which can be measured biochemically or histochemically from patients' tissue biopsy or cell culture. ATP levels are usually decreased as result of an impaired OXPHOS function. Also, lactic acid is commonly increased in blood and/or cerebrospinal fluid, due to the impaired pyruvate aerobic oxidation.

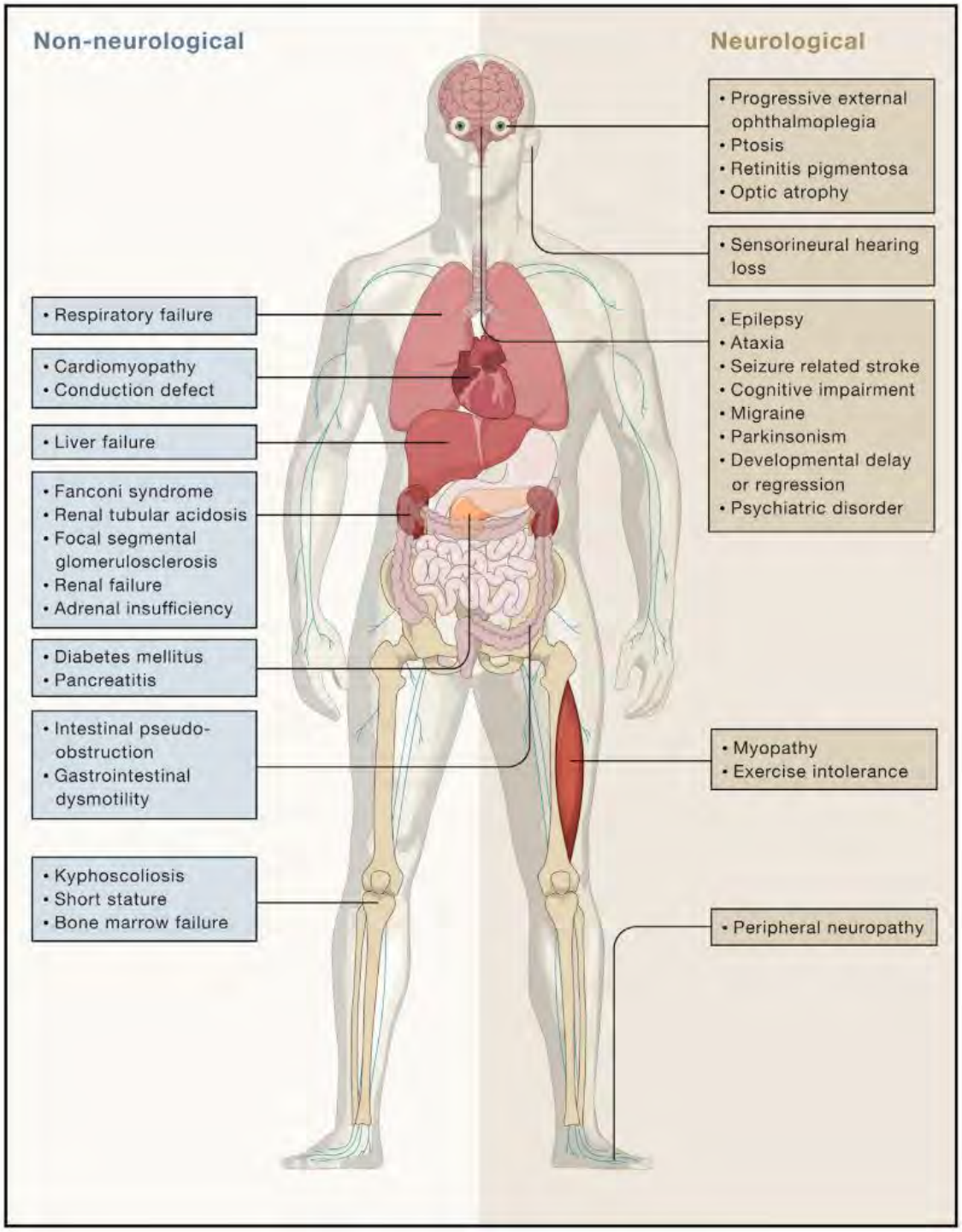

Figure I.11. Clinical Features of Mitochondrial Disease.
Mitochondrial dysfunction can cause a range of neurological and non-neurological symptoms. The spectrum of tissues involved varies between the mutation (mtDNA or nDNA), heteroplasmy, and age of onset and thus makes it difficult to predict dis- ease progression. (Extracted from Russell et al., 2020[64]).

Treatments and therapies

Treatment of mitochondrial diseases is still very challenging, due to several characteristics of these kind of defects:

i. they are highly heterogeneous both clinical and genetically;

ii. they are very often multisystemic, so difficult to address all the dysfunctions at once;

iii. it is difficult for a drug to cross the blood brain barrier and reach the brain, which is very often affected;

iv. the double membrane surrounding mitochondria make it difficult to deliver bioactive molecules to the specific mitochondrial compartment;

v. mtDNA is present in multiple copies in each cell

vi. and it has no recombination systems;

vii. mitochondria cannot import nucleic acids, impeding the use of CRISPR/Cas9-based techniques, or equivalent technologies.

Nowadays, clinical treatments for mitochondrial diseases are mostly symptomatic, and, very often, they lack effectiveness. Therapies that are used today in clinical practices include some pharmacological and dietary supplementation, such as vitamins (thiamine, riboflavin, folinic acid, and others), CoQ, aminoacids (arginine), lipoic acid, and other components, taken in cocktails of three or four supplements [75]. These pharmacological agents are usually complemented with treatment of the symptomatic complications and supportive care, and exercise can also be beneficial [76,77].

Recent advancements in molecular genetics and biochemical methodologies, have provided better understanding of the aetiology and pathogenesis of mitochondrial diseases and substantially improved diagnosis. This knowledge has also helped to develop new promising therapies that target different pathological mechanisms of the mitochondrial dysfunction, aiming to change the course of the disease [64,73,75,78]. Some examples are described below.

i. Enhancing ETC function with treatments: Some mitochondrial treatments strengthen the function of the ETC by increasing the levels of its components (CoQ, idebenone) or utilisation rate of its substrate (thiamine). Among them, CoQ (in its ubiquinone or ubiquinol forms) is the most commonly used. It has a relatively high effectivity and little side effects, even when high doses are applied [79]. It has been proven especially effective in patients with primary CoQ deficiency (See Chapter 1) [80]. In fact, The European Medicine Agency (EMA) has recently approved ubiquinol ($CoQ10H_2$) as an orphan drug for the treatment of primary CoQ10 deficiency [79]. Idebenone, a CoQ_{10} analogue, was also defined by the EMA as an orphan drug for LHON (Leber hereditary optic neuropathy) treatment [75,81].

ii. Decreasing ROS: antioxidants have been proven useful to reduce the excess of ROS produced in a pathological context. For example, the redox modulator KH176 has been shown to reduce ROS levels and protect OXPHOS-deficient human cells against redox stress [82]. This drug has been approved by the EMA as an orphan drug for treatment of MELAS and Leigh Syndrome, and it is being tested on clinical trials for a range of mitochondrial diseases.

iii. Deoxynucleotide triphosphate (dNTP) bypass: supplementation of dNTPs has been shown to be successful in several *in vitro* and *in vivo* models of disorders characterised by defects in mtDNA replication and dNTP pool metabolism, which causes a decrease in the mtDNA copy number, multiple deletions or point mutations of mtDNA, consequently affecting OXPHOS activity [53,75,83–85].

iv. Mitochondrial biogenesis activation: The stimulation of mitochondrial biogenesis is considered one of the most promising approaches for mitochondrial disease. Increasing mitochondrial biogenesis is driven by the activation of peroxisome proliferator-activated receptor γ coactivator 1 α (PGC1α), which can be targeted by AMPK, SIRT1 or peroxisome proliferator-activated receptors (PPARs). Currently, PGC1α stimulators (benzafibrate, a PPAR agonist), epicatechin and RTA 408 (isoprenoid that activates NRF2)) are under clinical study to assess their effectivity in different mitochondrial disease patients [75,77]. Positive results have been reported on several mouse models of mitochondrial diseases using other compounds, such as the AMP analogue 5-

aminoimidazole-4-carboxamide 1-β-D-ribofuranoside (AICAR) (AMPK agonist) [86], NR (a NAD+ precursor) and PARP1 (an inhibitor of NAD+ consuming enzymes). These last two drugs act by increasing NAD^+ concentration, which activate SIRT1 and other sirtuins [87,88].

v. Manipulating mitochondrial dynamics: In mouse models, moderate overexpression of Opa1, the master regulator of mitochondrial cristae morphology, has been proven to significantly ameliorate mitochondrial damage induced by drugs, surgical denervation [89], OXPHOS dysfunction due to CI or CIV defects [90] and also mtDNA depletion [91].

vi. Inhibition of mTORC1: mTORC1 plays essential roles in a vast number of cellular metabolic (mainly anabolic) pathways, including activation of protein translation, immune response, nucleotide and lipid synthesis, and glucose metabolism, and, in parallel, inhibition of catabolic pathways, such as autophagy and lysosomal biogenesis [81,92]. Treatment with rapamycin, an inhibitor of mTORC1 was beneficial for fly and mouse models with mitochondrial dysfunction [93–95].

vii. Scavenging specific toxic compounds: Mitochondrial diseases are sometimes characterised by accumulation of different toxic metabolites. For example, hydrogen sulphide (H2S) is accumulated in patients with ethylmalonic encephalopathy, a fatal infant disease due to mutations in *ETHE1*, one of the enzymes involved in sulphide degradation [96]. Treatment with N-acetylcysteine and metronidazole partially corrected the pathogenic effects of H2S accumulation in patients with ethylmalonic encephalopathy and in an *Ethe1* knock-out (KO) mouse model [97].

viii. Heteroplasmy shift: the recent development of new techniques for genome editing have allowed the development of strategies that aim to modify heteroplasmy levels is by selectively cleaving mutated mtDNA [98]. Mitochondrially targeted endonucleases [99], TALENs (transcription activator-like effector nucleases) [100,101] and ZNFs (zinc-fingers nucleases) [102–104] have been shown to selectively eliminate pathogenic DNA, decreasing the heteroplasmy percentage in different cellular and mouse models with mtDNA mutations.

ix. Gene therapy: the expression of genes, such as the wild type (WT) form of a defective gene or other therapeutic genes, delivered by adeno-associated viral vectors (AAVs) targeted to specific tissues is a very promising strategy for some mitochondrial diseases [75,81]. In this context, AAVs have been used to deliver therapeutic genes in several mouse models and some clinical trials [81,105–107].

Many other strategies for mitochondrial disease therapy are being studied and developed, such as ketogenic diet, enzyme replacement therapies, hypoxia, bypass of electron chain defects by expression of xenogenes, mtDNA replacement or mitochondrial donation.

I2. Coenzyme Q

I2.1. Coenzyme Q structure and properties

Coenzyme Q (CoQ) or ubiquinone is the only endogenously synthetised redox-active lipid. It is especially abundant in mitochondrial membranes, but it is found in virtually all endomembranes, plasma membrane and serum lipoproteins. Its chemical structure is a benzoquinone ring as a redox-active head group, and a polyisoprenoid chain, which gives hydrophobicity to the molecule (Figure I.12.A). The length of the lipid tail varies depending on the species. CoQ has 6 isoprene units in *Saccharomyces cerevisiae* (CoQ_6), while in humans it has mainly 10 (CoQ_{10}), although a small subset of molecules has 9 units (CoQ_9). The main form found in mice is CoQ_9, but also low amounts of CoQ_{10} are present in their membranes.

CoQ was first described by Cain and Morton in 1955 [108]. Soon after, its main function in the mitochondrial ETC was proposed by Crane and cols., who also demonstrated its redox proprieties [109]. CoQ is in a permanent balance between a completely reduced form ($CoQH_2$ or ubiquinol) and a completely oxidised form (CoQ or ubiquinone), through oxidation-reduction cycles (Figure I.12.B). When this redox cycle occurs by a two-step transfer of one electron each, as it happens during the Q-cycle in the ETC, a semiquinone free radical (or semi-ubiquinone, $CoQ^{\cdot -}$) intermediate is produced [32,33]. This intermediate is particularly relevant also in the plasma membrane antioxidant system, generated by the reduction of CoQ by cytochrome b5 reductase. This semiquinone maintains vitamin C and α-tocopherol in a reduced state in the plasma membrane [110,111].

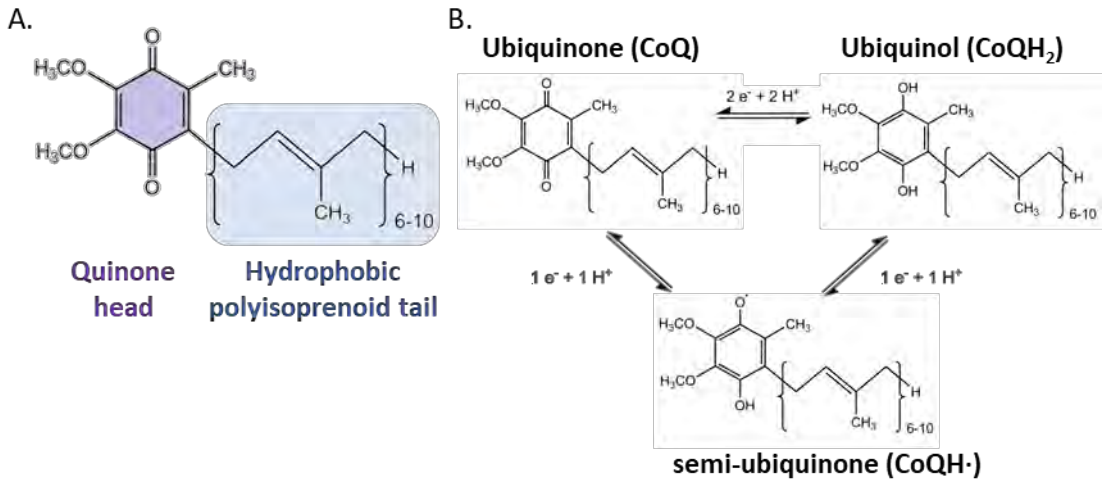

Figure I.12. Structure and redox forms of coenzyme Q.
(A) Chemical structure of CoQ. (B) Redox cycle of its head group, in CoQ oxidized form (ubiquinone) can be reduced to ubiquinol ($CoQH_2$) by two steps of one electron each, through semi-ubiquinone radical form, or by one reaction of two electrons, without the semi-ubiquinone intermediate (Adapted from Alcázar-Fabra et al., 2018[112]).

I2.2. Coenzyme Q biosynthesis and distribution

Most of the CoQ is endogenously synthesised by a set of nuclear-encoded proteins that reside in the mitochondria, through a pathway that is not completely understood yet. Most of the work on CoQ biosynthesis has been performed in the yeast model. The isoprenoid side chain comes from the mevalonate pathway in extramitochondrial membranes. Yeast Coq1p assembles the polyprenyl tail, determining the number of isoprene units. The quinone head is synthesised from tyrosine in the cytosol and linked to the polyprenylated tail by Coq2p in mitochondria. The rest of the reactions take place in a multiprotein biosynthetic complex localised in the matrix side of the IMM, consisting in sequential modifications of the aromatic ring. Coq6p and Coq7p are hydroxylases; Coq3p and Coq5p are methylases; Coq4p, Coq8p, Coq9p, and Coq10p are proteins with regulatory function (See Chapter 4, section 4.1)).

Levels of CoQ are quite stable in cells but its concentration varies among different tissues and organs, depending on the dietary conditions and age [113–116]. Although CoQ is mainly endogenously synthetised in mitochondria and then distributed to other cell membranes [117], cells can incorporate a certain amount from dietary sources.

Experimental biophysical studies and computational molecular dynamics prediction models have showed how, in the IMM, CoQ is mainly located either close to the membrane-water interface, with its relatively small head group being shadowed by the bigger polar heads of phospholipids, or stabilised in the middle of the bilayer. During the process of electron transfer, CoQ rapidly translocates from one side to the other of the inner membrane bilayer, with a rate that varies depending on the redox state of the molecule. This process enables the interaction with the reducing and oxidising sites in the proteins of the ETC complexes, located close to the membrane surfaces [118,119].

I2.3. Coenzyme Q functions in mitochondrial and extramitochondrial membranes

CoQ is an essential component of the MRC. In addition to this central role in the energy metabolism, CoQ is also involved in a big number of other cellular functions, and it is even probable that some of them are still unknown.

CoQ is a key node in the mitochondrial respiratory chain

The major function attributed to CoQ is the transport of electrons in the MRC, contributing to generate the membrane potential coupled to OXPHOS. CoQ is a unique compound that receives electrons from Complex I, Complex II and other dehydrogenases, and transfer them to Complex III in the MRC (Figure I.13) [49,120].

CoQ accepts electrons from NADH in CI, through a FMN, one 2Fe-2S cluster and six 4Fe-4S clusters. The CoQ binding site of CI is in the interface of both hydrophilic and hydrophobic arms of the L-shaped NADH dehydrogenase enzyme (Figure I.5). Very interestingly, CoQ bound to its specific site at CI may contribute to the proton translocation to the IMS [121]. Complex II or succinate dehydrogenase is a component of the TCA cycle that provides electrons from succinate to CoQ, through a FAD, the 4Fe-4S, 2Fe-2S and 3Fe-4S clusters and one haem [30]. CIII catalyses the electron transfer from $CoQH_2$ to CytC by the Q cycle [33], a mechanism that enables the sequential reduction of CytC by two reduction steps of one electron each (Figure I.7). The Q-cycle is an essential step for proton translocation and hence energy conservation (see section I1.2).

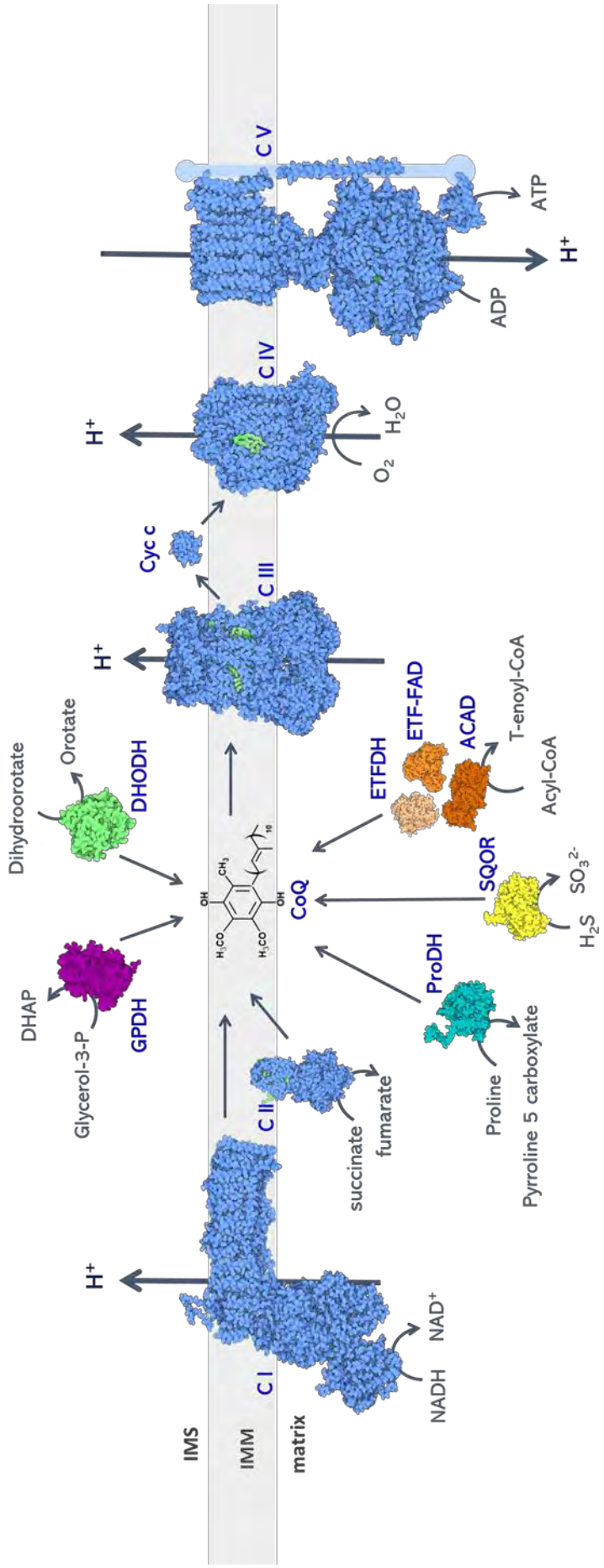

Figure I.13. Functional integration of CoQ in the mitochondrial inner membrane.
OXPHOS system showing complexes I and II, and other dehydrogenases that reduce CoQ in the inner mitochondrial membrane. Depicted using Illustrate (Goodsell et al., 2019[122]). CI: NADH:CoQ oxidoreductase; CII: succinate dehydrogenase; CIII: CoQ:cytochrome c oxidoreductase; CIV: Cytochrome c oxidase; CV: ATP synthetase; DHODH: Dihidroorotate dehydrogenase; GPDH: Glycerol 3 phosphate dehydrogenase; ProDH: Proline dehydrogenase; ACAD: Acyl-CoA dehydrogenase; ETF-FAD: Electron Transfer Flavoprotein; ETFDH: Electron Transfer Flavoprotein coenzyme Q reductase; SQOR: sulfide:quinone oxidoreductase; Cyt c: cytochrome c; IMS: inter membrane space; IMM: mitochondrial inner membrane (Adapted from Alcázar-Fabra et al., 2018[112]).

The NADH to O_2 pathway (catalysed by CI, CIII and CIV) and the succinate to O_2 pathway (catalysed by CII, CIII and CIV) are the two main electron flux pathways through the MRC that result in generation of the PMF that is utilised to produce ATP. However, there are many other dehydrogenases delivering electrons to the CoQ, producing $CoQH_2$ that can be efficiently reoxidised by CIII in the ETC (Figure I.13). Some of these dehydrogenases and the processes in which are involved are:

i. Dihydroorotate dehydrogenase (DHODH), a key enzyme for pyrimidine biosynthesis [123], which can influence the reactive oxygen species (ROS) production by $CoQH_2$ accumulation in skeletal muscle, thus partially contributing to ROS signalling in mitochondria [124].

ii. Mitochondrial glycerol-3-phosphate dehydrogenase (GPDH) [125], a tissue-specific component of mitochondria connecting glycolysis, OXPHOS and fatty acid metabolism[126].

iii. Electron transport flavoprotein dehydrogenase (ETFDH), a key enzyme involved in the fatty acid β-oxidation and branched-chain amino acid oxidation pathways[127]

iv. Proline dehydrogenase 1 (ProDH), an enzyme required for proline and arginine metabolism[128].

v. Probably, hydroxyproline dehydrogenase (or proline dehydrogenase 2), involved in the glyoxylate metabolism[129].

vi. Sulphide-quinone oxidoreductase (SQOR)[130] during hydrogen sulfide (H_2S) detoxification, a gas modulator of relevant cellular processes which is toxic in excess [131]. SQOR which oxidises H_2S in the first step of its catabolism in the mitochondria [131–133].

CoQ participates in reactive oxygen species production.

The MRC is the major source of reactive oxygen species (ROS) within the cell [134]. ROS are mainly produced in the form of superoxide ($O_2^{\cdot -}$) that is transformed to hydrogen peroxide (H_2O_2) by the manganese superoxide dismutase (MnSOD) in the mitochondrial

matrix or released to the IMS and the cytosol to be further detoxified by the copper-zinc superoxide dismutase (CuZn-SOD) [135,136].

Overall, uncontrolled and aberrant mitochondrial ROS production can cause damage to cellular components inducing the accumulation of lipid peroxides, carbonylated proteins and mtDNA mutations. This damage can lead to mitochondrial dysfunction. Also, mitochondrial ROS can produce the release of CytC via the mitochondrial outer membrane permeabilisation (MOMP), as well as opening of the MPTP of the IMM, leading to apoptotic and necrotic cell death, respectively. Very interestingly, ROS production, by inducing lipid peroxidation, has been even proposed to influence the organisation of the mitochondrial respiratory complexes in SCs [137].

However, mitochondria-derived ROS also have a beneficial redox signalling role, being physiologically produced at low concentrations in response to environmental stresses [138]. ROS signalling can regulate life- and health-span [139,140], enabling communication between the mitochondria, the cytosol and the nucleus.

There are at least ten different points of ROS production in the MRC, but the FMN site or the CoQ-binding site in Complex I and the CoQ_0 site in Complex III are the most important ones[141,142]. It is widely accepted that the accumulation of reduced CoQ generates superoxide through the retrograde electron transport (RET), driving electrons throughout Complex I to NAD^+, a mechanism that balances the $CoQ/CoQH_2$[143,144]. Complex III is also capable of producing ROS under certain conditions[134,145]. The $CoQ^{\cdot -}$/CoQ couple formed during the Q cycle is highly reducing, thus capable of donating an electron to O_2, forming $O_2^{\cdot -}$.

CoQ participates in the plasma membrane redox system.

CoQ is reduced at the plasma membrane by several NAD(P)H-oxidoreductases. These include the NADH-cytochrome b_5 reductase (b5R), the NAD(P)H:quinone reductase 1 (NQO1), the NADH-ferricyanide reductase [146] and the Ferroptosis Suppressor Protein 1 (FSP1)[147,148], amongst others [111,149]. There is also evidence for the existence of a NADH-dependent CoQ reductase involved in proton translocation to the lysosome [150].

b5R (EC 1.6.5.5, ascorbate free radical reductase) is a FAD-containing monomeric enzyme and is involved in the transfer of one electron from NADH to CoQ in the plasma

membrane, forming $CoQ^{\cdot -}$. NQO1 (EC 1.6.99.2) is a homodimeric enzyme with a non-covalently bound FAD that is involved in the transfer of two electron from NADH to CoQ, resulting in no $CoQ^{\cdot -}$ radical production [111,149]. Recently, the FSP1 CoQ oxidoreductase has been described to be recruited to the plasma membrane to reduce CoQ, which functions as a radical-trapping antioxidant that suppresses the propagation of lipid peroxides. This pathway prevents cell death by ferroptosis, in parallel to the traditional function of the glutathione peroxidase 4 (GPX4) [147,148].

The CoQ-dependent transport of electrons across plasma membrane is important for the regulation of cytosolic NAD^+/NADH ratio, the regeneration of other antioxidants such as α-tocopherol and ascorbate [151], the maintenance of the antioxidant capacity of membranes, the inhibition of the propagation of lipid peroxidation [147,148], among others.

CoQ is a potent endogenously synthesised, lipid-soluble antioxidant

In line with the previous section, the ability to sustain continuous oxidation/reduction cycles makes CoQ not only a great electron carrier for different cellular processes, but also a potent membrane antioxidant, which protects lipids, proteins and nucleic acids from harmful oxidative damage [120,152,153]. In membranes, $CoQH_2$ has been shown to prevent both initiation and propagation of lipid peroxidation [154,155] and, indirectly, to regenerate other antioxidants, such as α-tocopherol and ascorbate [151]. The high efficiency of CoQ against oxidative stress may be related to its ubiquitous distribution, its localization in the core of membranes and the availability of diverse dehydrogenases, able to efficiently regenerate the molecule.

CoQ participates in the regulation of the opening of the mitochondrial transition pore

The IMM has a low permeability to ions and solutes, which allows the electron and proton gradient to be maintained. MPTP is a protein complex located on the IMM that controls permeability of this membrane. However, its exact composition is still unknown [61–63]. The MPTP is involved in regulating cell death by apoptosis, since a prolonged opening of this pore results in a loss of membrane potential, a dramatic increase in ROS production and the release of pro-apoptotic proteins and CytC outside the mitochondria[156].

CoQ and analogues have been reported to inhibit apoptosis by preventing the opening of the MPTP [157–160], being this fact independent to the free radical scavenging property of CoQ [161].

CoQ is a cofactor of uncoupling proteins

Uncoupling proteins (UCPs) are a family of carriers with 5 different isoforms (UCP1-5), whose role is to produce a controlled dissipation of the electrochemical proton gradient by transporting H^+ across the IMM from the cytosol into the mitochondria. This phenomenon uncouples the mitochondria and produces a heat release, being important for thermogenesis [162,163]. CoQ acts as a cofactor for some of these UCPs, interacting with them in the lipid bilayer and regulating their function. CoQ would subtract H^+ from the fatty acids and move them to the H^+ acceptor group of the UCPs, in charge of directing them towards the mitochondrial matrix [164].

I2.4. Coenzyme Q_{10} deficiency: a mitochondrial disease

Since CoQ main function is the electron transport in the MRC, contributing to ATP generation in the OXPHOS system, CoQ_{10} deficiency mainly leads to different degrees of mitochondrial dysfunction, with energy deficiency. CoQ_{10} deficiency in humans manifests with a broad spectrum of clinical phenotypes, affecting different organs, tissues and systems, mainly central and peripheral nervous system, kidney, skeletal muscle and heart.

Patients with CoQ_{10} deficiency have reduced levels of CoQ_{10} in tissues, which can be primary or secondary. Primary CoQ_{10} deficiencies are caused by mutations in one of the genes participating in the CoQ_{10} biosynthesis pathway at the enzymatic or regulatory levels. Secondary CoQ_{10} deficiencies are caused by defects not directly linked to CoQ_{10} biosynthesis. These disorders will be described in depth in Chapter 1.

Project Aims

Project Aims

Primary CoQ_{10} deficiency syndrome is a rare condition, genetically caused by autosomal recessive biallelic mutations in one of the *COQ* genes participating in the CoQ_{10} biosynthesis pathway. The main aim in this project is the study of the pathophysiology of primary CoQ_{10} deficiency, with a special focus on the still poorly characterised *COQ4* gene. For this purpose, the following specific aims have been proposed:

i. Study of phenotypic or genetic patterns of all primary CoQ_{10} deficiency patients reported in the literature so far (described in Chapter 1).

ii. Determination of the pathophysiology of primary CoQ_{10} deficiency by using *in vitro* cell models with defects in *COQ7, COQ6* and *COQ4* (described in Chapter 2).

iii. Characterisation of human *COQ4* by studying its subcellular localization and its function in CoQ_{10} biosynthesis and mitochondrial respiration (described in Chapters 3 and 4).

iv. Study of the relationship between CoQ_{10} biosynthesis (or *COQ4* function) and mtDNA metabolism (described in Chapter 5).

Materials and Methods

Materials and Methods

M1. Literature review and patient classification

We performed an extensive review of all primary CoQ_{10} deficiency published cases, obtained by Pubmed search using search terms PDSS1, PDSS2, COQ2, COQ3, COQ4, COQ5, COQ6, COQ7, COQ8A, ADCK3, COQ8B, ADCK4 and Coenzyme Q_{10} deficiency. We compiled the information about clinical manifestations (classified by organ and tissue affected), age at onset, pathogenic variants found and functional validation. Information about CoQ_{10} treatment and response was also obtained.

The patterns and frequency of clinical manifestations were evaluated for each primary CoQ_{10} deficiency-causing gene, as a whole, and also stratified by age at onset.

M2. Cell culture methods

M2.1. Cell lines and maintenance

All cells were cultured at 37°C in an incubator with an atmosphere at 5% CO_2. They are described in Table M.1. Cell culture media are specified in next sections.

Patient Fibroblasts

Skin fibroblasts derived from skin biopsies from the patients with *COQ4* (P105, P108 and P109) and *COQ7* (P102 and P112) mutations were kindly provided by our collaborators from different hospitals (Table M.1). Informed consents for biological sample collection and genetic studies were obtained in origin from all the subjects involved in our studies in agreement with the Declaration of Helsinki. Two different controls were used, a neonatal control: HDF Neo (Human Dermal Fibroblasts, neonatal) (Sigma Aldrich) and an adult control (B003). Patient and control fibroblasts were cultured in Gibco™ 1g/L glucose DMEM (Dulbecco's Modified Eagle Medium) supplemented with 10% (v/v) Fetal bovine serum (FBS) and 1% (v/v) Gibco® Antibiotic-Antimycotic (Ab). P105 patient fibroblasts showed difficulty in growing, so they were grown in 1g/L glucose DMEM supplemented with 20% (v/v) of FBS, 1% Ab and 10 µM uridine (Sigma). All the experiments were performed with cells with passage numbers lower than 15.

Continuous cell lines

Human HEK293T-Rex/Flp-In ™ (Thermo Fisher Scientific) cells were cultured in Gibco™ 4.5g/L glucose DMEM supplemented with 10% (v/v) FBS and 1% (v/v) Ab (complete High glucose medium). These cells contain a single stably integrated *flippase recognition target* (FRT) site at a transcriptionally active genomic locus (Figure M.1.A). When they are co-transfected with pcDNA5 plasmid, carrying the gene of interest and an FRT site, together with pOG44, expressing the flippase, the flippase mediates the recombination between the genomic and the plasmid FRT sites, introducing the gene of interest in the genome of the transfected cell (Figure M.1.B).

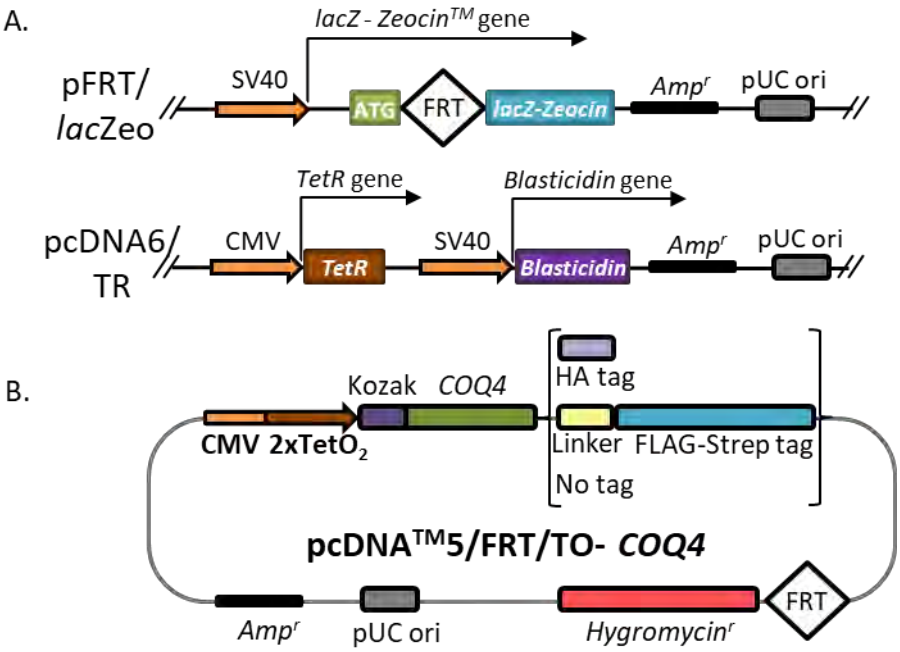

Figure M.1. HEK 293T-Rex/Flp-In cells genomic background and protein expression system.
(A) HEK 293T-Rex/Flp-In cells contain two stably, independently integrated plasmids. pFRT/*lacZeo* plasmid is in a transcriptionally active genomic locus and introduces a single FRT (Flp Recombination Target) site and stably expresses the *lacZ-Zeocin*™ fusion gene under the control of the SV40 promoter. pcDNA™6/TR plasmid stably expresses the *Tet repressor* (*TetR*) gene under the constitutive human cytomegalovirus (CMV) promoter. Parental HEK 293T-Rex/Flp-In cells are, thus, resistant to blasticidin and zeocin.
(B) The pcDNA™5/FRT/TO vector contains our gene of interest (*COQ4*) under a tetracycline/doxycycline inducible promoter (CMV fused to TetO2), a single FRT site for Flp recombinase-mediated integration and a hygromycin resistance gene for selection. The Flp recombinase is expressed from the pOG44 plasmid, which must be co-transfected with pcDNA5 into Flp-In™ T-REx™ mammalian host cells.

Uridine 10 µM (Sigma) was added to the medium for cells defective in *COQ4* and *COQ6* genes (and their controls), in order to compensate the reduced synthesis of pyrimidine derivatives due to a decrease in the activity of the dihydroorotate dehydrogenase, which is CoQ-dependent. For some experiments, cells were incubated in DMEM medium with 2mM glucose, to induce respiratory function.

Table M.1. List of cell lines used in this project.

Cell line	Description	Source
HDF Neo	Neonatal control skin fibroblasts	Sigma Aldrich
B003	Adult control skin fibroblasts	Laboratorio de Fisiopatología Celular y Bioenergética, UPO, Sevilla, Spain
P102 patient fibroblasts	Skin fibroblasts derived from a patient carrying biallelic mutations in *COQ7* (NM_016138.5): c.161_161delG and c.319C>T	Hospital Universitario la Fe de Valencia, Spain
P112 patient fibroblasts	Skin fibroblasts derived from a patient carrying a homozygous mutation in COQ7 (NM_016138.5): c.3G>T	Hospital Costa del Sol, Marbella, Spain
P105 patient fibroblasts	Skin fibroblasts derived from a patient carrying biallelic mutations in COQ4 (NM_016035.5): c.23_33delTCCTCCGTCGG and c.532+6 T>A	Center for Rare Diseases, Department of Paediatrics, University Hospital Copenhagen, Denmark
P108 and P109 patient fibroblasts	Skin fibroblasts derived from twin patients carrying a homozygous mutation in COQ4 (NM_016035.5): c.437T>G	The Azrieli Faculty of Medicine, Bar Ilan University, Safed, Israel
HEK293T-COQ6 KO	HEK293T knocked out in COQ6	Dr. Leonardo Salviati laboratory [165]
HEK293T-Rex/Flp-In ™	Parental HEK 293T cell line with FRT site	Thermo Fisher Scientific
HEK293T-COQ4 KO	HEK293T-Rex/Flp-In knocked out in COQ4	This study
Transfected HEK293T-COQ4 KO	COQ4 KO transfected with pcDNA5 plasmids described in Table M.12	This study

M2.2. Treatments

When required, supplemental molecules were added to the culture medium, prediluted in ethanol 100%. The conditions of the treatments are detailed in Table M.2. In the case of CoQ_{10}, the ethanol stock was prediluted in the FBS before preparing the complete medium. All these reagents were purchased from Sigma.

Table M.2. Reagents used for cell treatment and conditions.

Molecule	Name	Objective	Concen-tration factor of stocks	Final concentration	Duration of the treatment
CoQ_{10}	Coenzyme Q_{10}	CoQ supplementation	500X	5 µM	4 -10 days
^{14}C-4-HB	*^{14}C* 4-hydroxy-benzoate	*De novo* CoQ labelling	10000X	7.2 nM	3 days
VA	Vanillic acid	CoQ biosynthesis bypass	600X	500 µM	4 days
2,4-dHB	2,4-dihydroxy benzoic acid		333X	0.1-5mM	8-10 days
HQ	1,4- dihydroxy benzene or hydroquinone		1000X	5 and 25 µM	3 days
2-moHQ	2-Methoxy-hydroquinone		1000X	5 and 25 µM	3 days
pABA	Para amino benzoic acid	CoQ biosynthesis inhibition	1000X	100 µM	1-3 days
DOX	Doxycycline	Induction of the transgene expression	1000X	0.1-5 ng/ml	24h

M2.3. Co-transfection of HEK293T-Rex/Flp-In ™ cells with pCDNA5 and pOG44 plasmids

Before the transfection with pcDNA5/pOG44 plasmids, HEK293T-Rex/Flp-In ™ cells were grown in High glucose DMEM supplemented with 10% Tetracycline Free FBS (Tet-FBS), 1% Ab, 10µM uridine, 15 µg/mL of Blasticidin (Blasticidin S HCl, 10 mg/mL, Thermo Fischer Scientific) and 100 µg/mg Zeocin (Zeocin™ Selection Reagent, 100 mg/mL, Thermo Fischer Scientific).

Transfections were carried on 6-well plates, with 70-80% confluent cells and Lipofectamine 3000 reagent (Invitrogen) (LFA). For this purpose, cells were seeded 1 day before transfection at a confluency of 40% in High glucose medium without antibiotics. At least 3 wells were seeded per cell line and each of them would be transfected with pOG44+pcDNA5-gene+LFA (reaction of interest), pOG44+LFA and only LFA (negative controls), respectively.

On the day of transfection, a DNA-tube was prepared for each transfection reaction. In each tube, 300 µL of Gibco® Opti-MEM® (Thermo Fischer Scientific) were mixed with 1350ng of pOG44 and 150 ng of pcDNA5-gene plasmids (ratio pCDNA5-gene of

interest:pOG44 = 1:9). For the control reactions, no DNA or only pOG44 was mixed with Opti-MEM. 3 µL of P3000 reagent (included in the LFA 3000 kit) were added to the reactions tubes (2 µL / µg of DNA). Then, a LFA mix tube was prepared, with 300 µL of Opti-MEM and 3.6 µL of LFA per transfection reaction. Within the following 5 minutes, 300 µL of LFA mix were added to each DNA-tube and gently mixed. A 20 minutes incubation at room temperature (RT) was performed to allow the formation of LFA-DNA complexes. After that, wells were washed with warm sterile phosphate-buffered saline (PBS), and the 600 µL of each LFA-DNA tube were added to each well. This step was followed by a 4 hours incubation at 37°C, to let the complexes transfect the cells.

Then, 600 µL of DMEM 30% Tet-FBS 15 µg/mL Blasticidin were added to each well. 24h after transfection, the medium was removed, and 2 mL of DMEM 10% Tet-FBS, 1% Ab, 15 µg/mL Blasticidin were added to each well. 48h after transfection, the medium was changed to a selective one, to select transfected clones. The selective medium was a High glucose DMEM supplemented with 10% Tet-FBS, 1% Ab, 10 µM uridine, 15 µg/mL of Blasticidin and 100 µg/mg of Hygromycin B (Sigma).

M2.4. Generation of a *COQ4* KO cell model

Paired nickases 3-plasmid strategy was chosen to increase the specificity of the genomic DNA modifications. gRNAs target sequences were designed to target *COQ4* exon 2 (Table M.3), using the CRISPR-design tool from Zhang Lab (http://crispr.mit.edu), which is no longer available. Potential off-target sites of the different pairs of gRNAs were analysed with the same tool, using 4 different combinations of Forward and Reverse gRNA.

All plasmids were purchased from Sigma-CRISPR Products and are detailed in Table M.12. Each gRNA sequence was contained in a pU6-gRNA plasmid (Table M.3, Figure M.2.B). Cas9 nickase (Cas9D10A) and GFP (green fluorescent protein) sequences were both included in the pCMV-Cas9D10A-GFP plasmid (Table M.12, Figure M.2.A). CMV (cytomegalovirus) promoter would allow strong transient expression of Cas9-D10A, co-expressed with GFP from the same mRNA via a 2A peptide linkage. This would enable tracking of transfection efficiency and enrichment of genome editing activity in cell populations via fluorescence activated cell sorting (FACS).

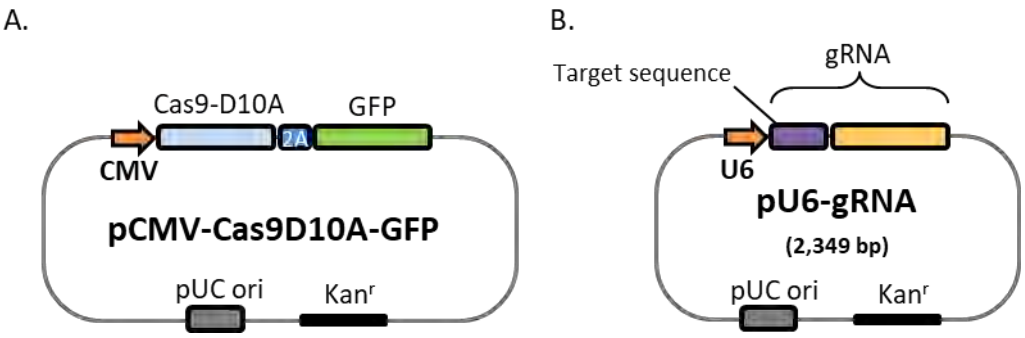

Figure M.2. CRISPR plasmids.
Paired nickases CRISPR/Cas9 3 plasmid strategy was used to generate the COQ4 KO in a HEK 293T-Rex/Flp-In wild type background, transfecting these cells with a pCMV-Cas9D10A-GFP, which expresses the nickase-GFP (A), and two pU6-gRNA plasmids (B), each one with a different target sequence (Table M.3).

Table M.3. gRNAs target sequences.

gRNA target sequence	Orientation	Target ID	Sequence 5'-3'
gRNA1	Fw	HSL0002175793	UGGUGCGAGUAUAGCGGGCCGG
gRNA2	Fw	HSL0002175797	CUUUCUGCAGCGGGGAGGUGGG
gRNA3	Rv	HSL0002175798	CUGUUGGCCGCCGGCUCCGCGG
gRNA4	Rv	HSL0002175799	GCCGCCGGCUCCGCGGCGAUGG

Transfection

CRISPR plasmids transfection protocol was adapted from Ran et al., 2013[166]. Transfections with the 4 combinations of plasmids containing the gRNAs were performed (named CRISPR 1-4 reactions), together with the pCMV-Cas9D10A-GFP plasmid. Two transfection controls were also performed. The negative control was transfected with no DNA, and served as GFP negative control for FACS; the positive control was only transfected with the pCMV-Cas9D10A-GFP plasmid, and served as GFP positive control for FACS. The genome editing activity was also tracked using CRISPR controls. The CRISPR negative control was transfected with the CRISPR/Cas9 negative control (pU6-gRNA/CMV-Cas9-GFP), and was used as a control for no genome editing activity; and the CRISPR positive control was transfected with the two CRISPR/Cas9 nickase EMX1 positive control plasmids (pU6-EMX1-s4 and pU6-EMX1-as4), together with the pCMV-Cas9D10A-GFP plasmid, and served as positive control for the genome edition.

Table M.4. Conditions for transfection with CRISPR plasmids.

Reaction	Plasmid	DNA ng	Number of reactions
Transfection - Control	-	-	3
Transfection + Control	pCMV-Cas9D10A-GFP	311.32	3
CRISPR Reaction 1	pU6-gRNA1	94.34	3
	pU6-gRNA3	94.34	
	pCMV-Cas9D10A-GFP	311.32	
CRISPR Reaction 2	pU6-gRNA1	94.34	3
	pU6-gRNA4	94.34	
	pCMV-Cas9D10A-GFP	311.32	
CRISPR Reaction 3	pU6-gRNA2	94.34	3
	pU6-gRNA3	94.34	
	pCMV-Cas9D10A-GFP	311.32	
CRISPR Reaction 4	pU6-gRNA2	94.34	3
	pU6-gRNA4	94.34	
	pCMV-Cas9D10A-GFP	311.32	
CRISPR + Control	pU6-EMX1-s4	94.34	3
	pU6-EMX1-as4	94.34	
	pCMV-Cas9D10A-GFP	311.32	
CRISPR – Control	pU6-gRNA/CMV-Cas9-GFP	311.32	3

Transfections were carried on 24 well plates, with 70-90% confluent HEK293T-Rex/Flp-In cells and LFA 3000. Cells were seeded 1 day before transfection at a density of $3 \cdot 10^5$ cells in 1 mL High glucose medium without antibiotics per well. On the day of transfection, a DNA-tube was prepared for each transfection reaction. In each tube, 100 µL of Opti-MEM were mixed with the amounts of plasmids specified on Table M.4 (plasmids were mixed at equimolar ratios and the maximal amount of DNA used was 500 ng). For transfection control reactions, no DNA or only pCMV-Cas9D10A-GFP were mixed with Opti-MEM. Then, a LFA mix tube was prepared, with 100 µL of Opti-MEM and 2 µl of LFA per transfection reaction. Within the following 5 minutes, 100 µL of LFA mix were added to each DNA-tube and gently mixed. After 20 minutes incubation at RT, cells were washed with warm sterile PBS and the 200 µL of each LFA-DNA tube were added to each well. Cells were incubated with the LFA-DNA complexes for 4 hours at 37°C. Then, 300 µL of DMEM 30% Tet-FBS per well were added. 24h after transfection, 500 µl of DMEM 10% Tet-FBS were added to each well.

Isolation of clonal cell lines by FACS and clone expansion

The transfected population was FACS sorted for GFP expression 48 h after transfection. Cells were resuspended in high glucose phenol red–free DMEM supplemented with 10%

Tet-FBS and 1% antibiotics, dissociated and filtered with a 70 µm cell strainer. GFP-positive single cells were sorted and collected in cytometer tubes with complete High glucose medium supplemented with 10 µM uridine. Then, they were diluted in order to get 100 cells/ml and seeded in 96 well plates (100 µL of complete DMEM with uridine + 10 µL of cell dilution per well), to get 1 single cell per well. 1 plate was seeded per transfection reaction, and the rest of the cell dilutions were also seeded into 24 well plates as pools. Single colonies could be isolated from these pools too. The isolated clones and pools were grown into populations over a period of 1 month. Populations were expanded, and DNA was harvested from the 80% of cells of confluent 12-well plates with a DNeasy Blood & Tissue Kit (Qiagen). The remaining 20% of cells was used to continue expanding the populations.

Genotyping of the clones

Genomic DNA was amplified with *COQ4* primers (*EMX1* primers for the positive controls) spanning the target cut site (Table M.11, primers #4, #5, #6 and #7). PCR was performed with KOD Hot Start Master Mix (Novagen), following the manufacturer's protocol. 2.5 µL of the PCR product were ran in a 1,8% agarose gel, and differences on the size of the products could be observed. Amplicons were gel-purified and A-tailed with Taq polymerase (HorsePower Taq polymerase, Canvax). They were then ligated into pGEMT Easy Vector (Promega) and transformed into DH5α bacteria using standard molecular biology techniques. A minimum of 5 bacterial clones were sequenced per each tested cell line (See sections M4.8, M4.10, M4.12-14).

M2.5. Assessment of mitochondrial respiratory function using Seahorse Extracellular Flux Analyzer

General protocol

Oxygen consumption rate (OCR) was determined using a Seahorse XF24 Extracellular Flux Analyzer (Agilent) following the manufacturer's instructions. The protocol was optimised for each cell line, detailed in Table M.5. Cells were seeded at an optimal density onto Seahorse 24-well plates, 1-3 days previous to the assay (depending on the experiment) (Table M.5). The day of the experiment and prior to the measurements,

medium was removed and cells were washed twice with Seahorse XF base medium (bicarbonate-free medium) supplemented with glucose (2 mM, 1g/l or 4.5 g/L), 2 mM glutamine and 1 mM sodium pyruvate. After the second wash, 500 µL/well of base medium were added and the plate was incubated for 1 hr at 37°C without CO_2.

The cartridge was pre-hydrated one day before the assay with Seahorse XF Calibrant Solution, and incubated overnight (o. n.) at 37°C. The day of the assay, while cells were incubating with the base medium, the injection cartridge was loaded with the respiratory modulators of choice. In our case, we wanted to measure the OCR, so we used the Mito-Stress Test, using inhibitors of the respiratory chain (oligomycin (OL), carbonyl cyanide-4-trifluoromethoxy-phenylhydrazone (FCCP), rotenone (Rot) and antimycin A (AntA)) at an optimised concentration (Table M.5). We loaded the four ports of the cartridge A, B, C and D with 56, 62, 69 and 76 µL of 10X stocks of OL, FCCP, Rot and AntA, respectively (volumes are optimised by taking into account the well volume increment after the addition of each compound). The cartridge was introduced into the Analyzer and calibrated. Finally, the cell plate was introduced into the Analyzer as well, and the Mito-Stress assay was run. OCR was measured under basal conditions, and after the sequential injection of oligomycin, FCCP, rotenone and antimycin A. To normalize respiration rates, cells were harvested and counted after the assay.

Table M.5. Optimal Seahorse parameters for each cell line

Optimised parameter	Fibroblasts	HEK cell lines
Seeding cell density (cells/well)	$50 \cdot 10^3$	$30 \cdot 10^3$
Number of days between seeding and the assay	1	2 (or 3, in experiments with 2mM glucose medium)
Glucose concentration in Seahorse XF base medium	1 g/L	4.5 g/L (or 2mM in specific experiments)
Oligomycin final concentration	4 µM	1 µM
FCCP final concentration	1 µM	0.2 µM
rotenone final concentration	1 µM	1 µM
antimycin A final concentration	2.5 µM	2.5 µM

i. Fibroblasts particularities

In some experiments, 9 days before seeding the Seahorse plate, cells were treated with 2,4-dHB or with CoQ_{10} (See Materials and Methods, Section M2.2).

ii. HEK cell lines particularities

Seahorse plates must be poly-D-lysine pre-coated before seeding, in order to ameliorate the attachment of the cells. For this purpose, they were incubated with 200 µL of a filter-sterile poly-D-lysine (Sigma) solution (50 µg/mL) for 30 min at 37°C. After incubation, the solution was removed and the plates were dried in the tissue culture hood. The solution can be used twice.

For Seahorse experiments with 2mM glucose medium, cells were seeded onto the Seahorse plates with high glucose DMEM medium, and 48h later, medium was replaced with 2mM glucose DMEM medium. Cells were incubated in these conditions for additional 24 hours. Prior to the measurements, medium was replaced with Seahorse XF base medium supplemented with 2mM glucose, and the washes were not performed because cells were very delicate at this time and detached easily.

Analysis of the results

The measurement of OCR after the sequential addition of inhibitors of the respiratory chain, like oligomycin (inhibitor of ATP synthase), FCCP (uncoupling agent), rotenone (inhibitor of CI) and antimycin A (inhibitor of CIII), allows to determine different important parameters of mitochondrial function (Figure M.3).

These parameters are:

i. Non-Mitochondrial respiration: Minimum rate measurement after injection of all ETC inhibitors.

ii. Basal respiration: Mitochondrial OCR under resting conditions. It is calculated as the value of the last rate measurement before oligomycin injection minus the non-mitochondrial respiration.

iii. Maximal respiration: Maximal utilization of mitochondrial respiration after the addition of an uncoupling agent (FCCP). Mitochondria are forced to respire more, trying to compensate the loss of mitochondrial membrane potential. It is calculated as the value of the maximum rate measurement after FCCP injection minus the non-mitochondrial respiration rate.

iv. Spare respiratory capacity: Measurement of the cells' ability to respond to an energetic demand. It is an indicator of cell fitness or flexibility. It is calculated as the value of the maximal respiration minus the basal respiration.

v. Coupled or ATP-linked respiration: OCR coupled to ATP production. It is calculated as the value of the last rate measurement before oligomycin injection minus the minimum rate measurement after oligomycin injection.

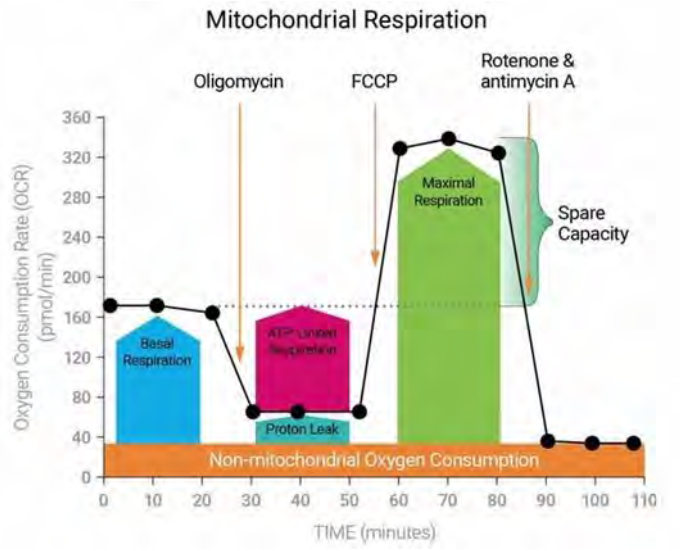

Figure M.3. Seahorse Mitostress test OCR profile. Example of an oxygen consumption rate assay with Seahorse, with serial injections of oligomycin, FCCP, and rotenone/antimycin A. The assay reports key parameters, including basal respiration, ATP-linked respiration, maximal respiration and spare respiratory capacity (taken from Seahorse Analyzer manufacturer's protocol).

M2.6. *In vivo* mitochondrial translation assay

The *in vivo* analysis of mitochondrial translation products was performed following protocols previously described (Figure M.4) [167–170]. Briefly, HEK cells were seeded two days before the experiment on 60 mm diameter culture dishes, being at least 80% confluent the day of the assay. They were washed three times with warm methionine (Met) and cysteine (Cys)-free DMEM (2 mL per plate), and incubated for 5 minutes with the third wash. Then, cells were incubated with 2 ml of labelling medium (Met and Cys-free DMEM, supplemented with 96 µg/ml Cys, 2mM GlutaMAX, 1mM sodium pyruvate, 10% of dialysed FBS and 1% of Ab) for 10 min at 37°C. Later, the cytosolic protein translation inhibitor emetine (Sigma, 25 mg/ml in PBS) was added to each plate to a final concentration of 100 µg/ml and plates were incubated for 30 min at 37°C. Then, 10 µL of 33 µCi/µL ^{35}S L-methionine (L-Methionine, [^{35}S]-Cell Labelling Grade, PerkinElmer)

were added to each plate, to get a final concentration of 166.6 µCi/mL per plate. Cells were incubated for 1h at 37°C and afterwards, harvested in 1 mL of cold PBS and washed 4 times by centrifuging at 10,000g for 30 s.

Cell pellets were lysed in 45 µL of PBS supplemented with 0.1% of n-dodecyl-β-D-maltoside (DDM), 1x protease inhibitors cocktail (PIC) (cOmplete™ Mini EDTA-free Protease Inhibitor Cocktail, Roche) and 50 units of benzonase for 1h on ice. Then, SDS (sodium dodecyl sulphate) was added to a final concentration of 1% and samples were vortexed and left 5 min at RT. 30 µg of protein of each sample were ran onto a Novex™ 18% Tris-Glycine precast SDS polyacrylamide gel (Invitrogen) for 2h at 100V. Gel was fixed with 20 % methanol, 10 % acetic acid solution and dried under vacuum at 80°C for 2h.

To visualise the bands corresponding to the radiolabelled mitochondrial translation products, the dried gel was exposed to a Storage Phosphor Screen (GE Healthcare) for at least 48h at RT. The screen was then developed with Amersham Typhoon (GE Healthcare), and the images analysed by using Fiji-ImageJ [171].

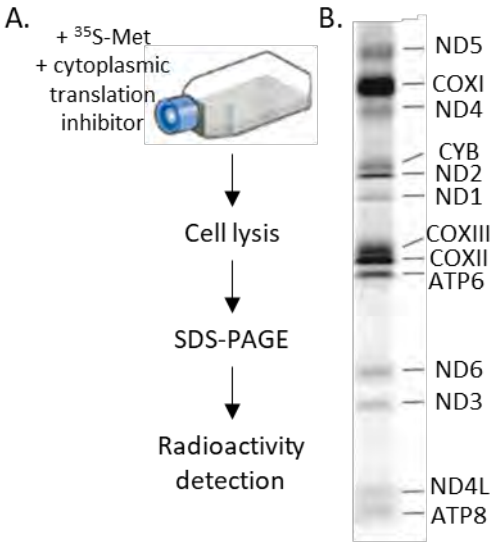

Figure M.4. In vivo analysis of mitochondrial translation.
(A) Cells are incubated with radiolabelled methionine and a cytoplasmic translation inhibitor. (B) Typical pattern of pulse-labeled mitochondrial translation products in human cultured cells, shown here for immortalized myoblasts. The 13 mitochondrially synthesized proteins are indicated at the left of the panel: ND subunits of Complex I, COX subunits of Complex IV, ATP subunits of Complex V, cyt b subunit of Complex III (Adapted from Sasarman et al., 2012[170]).

M2.7. mtDNA copy number depletion and recovery rate after ethidium bromide treatment and withdrawal

Cells were seeded at a confluency of 2.5% and 1 day after, ethidium bromide (EtBr) (Sigma) was added to the plate at a final concentration of 100 ng/mL. Treatment was extended for 4 days, when cells reached the 10% of their original mtDNA copy number before the treatment. After the treatment, 4 washes with fresh medium of 1 hour each were done and then, cells were collected and seeded in different percentages of confluency for each time point of the recovery assay. 5 μM CoQ_{10} was added to the recovery medium for some experimental conditions. Every 24h , cells were harvested in cold PBS and pellets stored at -20°C. These samples were used to determine the mtDNA copy number (See M4.7) and for protein extraction and quantification by western blot (See M3.3). The mtDNA copy number data was represented as a percentage, considering the mtDNA quantification of the cells before EtBr treatment as the 100%.

M3. Biochemical methods

M3.1. Total protein extraction and quantification

Cell lysates were prepared by adding to fresh or frozen cell pellets 50 to 500 µL of Lysis solution (2% DDM, 1x PIC in PBS), depending on the pellet volume. After 15 min rotating at 4˚C, the lysates were centrifuged at 20,000 x g at 4˚C for 20min and the cleared supernatants were kept (stored at -20˚C or used immediately).

Protein was measured in triplicates with Bradford Protein Assay (BioRad) in 96 well microplates, using a Pierce (bovine serum albumin) BSA Standards (2mg/ml, Thermo Fischer Scientific) curve. 10 µL of NaOH 1M, 2.5 µL of sample and 200 µL of 1X Bradford reagent were added per well, and after a 5 min incubation at RT, in the dark, absorbance at 595 nm was measured with a POLARstar Omega microPlate Reader Spectrophotometer (BMG LABTECH).

M3.2. Protein gel electrophoresis

SDS-PAGE

Total cell protein lysates were separated through polyacrylamide gel electrophoresis in denaturing conditions (SDS-PAGE). After protein quantification, 10-100 µg of each protein sample were mixed with 2x Laemmli Sample Buffer (2XSB), containing 4% SDS, 20% glycerol, 10% β-mercaptoethanol, 0.004% bromophenol blue and 125 mM Tris-HCl at pH 6.8, at a 1:1 ratio. Samples were incubated at 42°C for 45 minutes.

The samples were then resolved on 12% SDS-PAGE mini-gels using the Mini-PROTEAN Tetra cell (Bio-Rad) at 100 V for 2 hours in running buffer TGS (25 mM Tris, 192 mM glycine, 0.1% SDS, pH 8.3) (Bio-Rad). As a standard, 5 µl of Precision Plus Protein all blue or dual color standards (Bio-Rad) was loaded.

Blue Native-PAGE

Blue native polyacrylamide gel electrophoresis (BN-PAGE) was used for the separation of mitochondrial complexes in non-denaturing conditions after as the solubilisation of the mitochondrial membranes using neutral mild detergents such as DDM or digitonin[172–174].

Mitochondrial enriched fractions were obtained by resuspending the cell pellets in 200 µL of cold PBS and incubating at 4°C for 10’ with one volume of cold 8 mg/mL digitonin. Digitonin breaks the cell membrane and enriches the sample in mitochondria. After two washes with 1 mL of cold PBS and centrifugations at 10,000 x g for 10 min at 4˚C, the mitochondria-enriched samples were resuspended in 100 µL of a Solubilization Buffer, containing 1.5 M aminocaproic acid, 50 mM Bis-Tris/HCl at pH 7 and 1 % DDM (stronger detergent) or 2 % digitonin (milder detergent). After an incubation at 4°C for 5 min, samples were centrifuged at 18,000 x g at 4˚C for 30’, to remove the insoluble material. Cleared supernatants were mixed with 10 µL of sample buffer (750 mM aminocaproic acid, 50 mM Bis-Tris/HCl pH 7, 0.5 mM ethylenediaminetetraacetic acid (EDTA) and 5 % Serva Blue-G250). Samples were stored at -80˚C or loaded directly to run BN-PAGE.

Samples were run through a 3-12 % Native-PAGE gel (NativePAGE™ Novex™ Bis-Tris Gels, Thermo Fisher Scientific) at 150 V and 4˚C. The cathode buffer was 50 mM Tricine,

15 mM Bis-Tris, 0.02 % Serva Blue-G250, pH 7.4 and the anode buffer 50 mM Bis-Tris, pH 7.4. The cathode buffer requires a constant supply of negative charges (from the Serva Blue-G250) to keep the proteins negatively charged, which ensures their electrophoretic mobility and their separation in the gel according to molecular weight differences. After 1h of running, the cathode buffer was substituted by a similar buffer with lower amount of dye (0.002% Serva Blue-G250), to allow a better visualization of the samples during the electrophoresis.

After first dimension (1D), run in native conditions, a denaturing second dimension (2D) was performed to separate the different subunits from the native complexes. For that, each lane was cut, denatured with 1 % SDS and 1 % β-mercaptoethanol for 1 hour at RT and then run through a 4-12 % SDS-PAGE gel (NuPAGE® Novex® Bis-Tris Protein Gels, 1.0 mm, 2D-well, Thermo Fisher Scientific).

M3.3. Western blotting and immunodetection

Western blotting analysis was performed after electrophoresis. The gel was blotted onto a methanol-activated polyvinylidene difluoride (PVDF) membrane (Immobilon. Millipore). Semi-dry transfer was performed with a Trans-Blot® SD Semi-Dry Transfer Cell (Bio-Rad) at 25 V for 1 hour, in transfer buffer TG (25 mM Tris-HCl, 192 mM Glycine, 20 % methanol (v/v) and 0.025 % SDS) (Bio-Rad).

The membrane was blocked with 5% milk in TTBS (TBS (Tris-buffered saline) with 0.05% Tween-20) for 1h at RT, and subsequently washed three times in TTBS for 10 min. After the washes, it was incubated at 4˚C o.n. with different specific antibodies diluted at the appropriate concentrations in 5% milk in TTBS (Table M.6). After three washes in TTBS, the membrane was incubated for 1-2h at RT with the species-appropriate secondary antibody, diluted 1:5000 in 5% milk in TTBS (Table M.6), which is conjugated with horseradish peroxidase (HRP), essential for the following detection. After three more washes with TTBS, membranes were developed with Immobilon Crescendo Western HRP substrate (Millipore) and visualized with ChemiDocTM XRS+ Imaging System (Bio-Rad).

Table M.6. Antibodies used in this project.

Primary antibodies					
Antigen	**Mono/poly clonal**	**Host species**	**Incubation conditions**	**Company**	**Catalog number**
COQ4	Polyclonal	Rabbit	1/1000	Sigma	HPA042945
COQ5	Polyclonal	Rabbit	1/1000	Proteintech	17453-1-AP
COQ6	Polyclonal	Rabbit	1/1000	Proteintech	12481-1-AP
COQ7	Polyclonal	Rabbit	1/1000	Proteintech	15083-1-AP
β-actin	Monoclonal	Mouse	1/2000	Sigma	A2228
β-tubulin	Monoclonal	Mouse	1/10000	Sigma	T5201
TOM20	Monoclonal	Mouse	1/500	abcam	ab56783
ATAD3	Monoclonal	Mouse	1/1000	Santa Cruz	sc-376185
LDH-A	Polyclonal	Goat	1/1000	Santa Cruz	sc-27230
FLAG	Monoclonal	Mouse	1/1000	Sigma	F3165
HA	Monoclonal	Rat	1/1000	Roche	11 867 431 001
HSP60	Polyclonal	Rabbit	1/10000	abcam	ab46798
TIM23	Polyclonal	Rabbit	1/1000	Sigma	SAB1100941
Mitoprofile	Monoclonal (Cocktail)	Mouse	1/500	abcam	ab110412
COXI	Monoclonal	Mouse	1/1000	abcam	ab14705
COXII	Monoclonal	Mouse	1/10000	abcam	ab110258
TRUB2	Polyclonal	Rabbit	1/1000	Proteintech	19891-1-AP
TFAM	Monoclonal	Mouse	1/1000	Santa Cruz	sc-376672
LRPPRC	Polyclonal	Rabbit	1/1000	abcam	ab97505
TUFM	Polyclonal	Mouse	1/1000	Abnova	H0000728-4
NDUFS3	Monoclonal	Rabbit	1/1000	abcam	ab177471
NDUFA9	Monoclonal	Mouse	1/1000	abcam	ab14713
VDAC	Monoclonal	Mouse	1/2000	abcam	ab14734
MRPS18B	Polyclonal	Rabbit	1/1000	Proteintech	16139-1-AP
Secondary-HRP conjugated antibodies					
Antibody		**Host species**	**Incubation conditions**	**Company**	**Catalog number**
anti-Goat		Rabbit	1/5000	Sigma	401504
anti-Rabbit		Goat	1/5000	Cell Signaling	#7074
anti-Mouse		Horse	1/5000	Cell Signaling	#7076
anti-Rat		Goat	1/5000	Santa Cruz	sc-2032

M3.4. Immunostaining of fixed cells for fluorescence confocal analysis

Immunofluorescence labelling was used to study the subcellular localisation of COQ4 protein. Cells were seeded on poly-D-lysine-coated 24x24 mm glass coverslips in a 6-well plate. The next day, cells were washed with PBS three times, fixed with 4 % (w/v) paraformaldehyde (PFA) in DMEM-only for 15 minutes at 37 ˚C, washed again three times, and permeabilised for 5 minutes at RT in PBSS buffer (PBS, 5% FBS) with 0.3 % (v/v) Triton X-100 (Fisher Bioreagents) (PBSST). After three washes of 5 min with PBS, the coverslips were incubated with the anti-FLAG primary antibody (Anti-FLAG® M2 mouse antibody, Sigma) 1:1000 in PBSST, either for 1.5 hours at RT or overnight at 4 ˚C in a wet chamber. After washing, the coverslips were incubated with the secondary antibody Alexa fluor®488

anti-mouse (Invitrogen) 1:1000 in PBSS, for 1 hour at RT. At the same time, in order to visualise the mitochondrial network, an anti-TOMM20 Alexa Fluor®568 (ab210841, abcam) was also added at a 1:50 dilution. After the incubation, samples were washed again, protected from light. Slides were mounted using ProLong Gold antifade with 4',6-diamidino-2-phenylindole dihydrochloride (DAPI, Invitrogen). The fluorescence was detected with a confocal laser microscope (Confocal Microscope Leica SPE, Leica Microsystems).

M3.5. Cell subfractionation

Mitochondria and mitochondria associated membranes (MAMs) purification

The mitochondrial isolation procedure was adapted from the one described by Fernández-Vizarra et al. [168]. The starting material could vary depending on the final purpose for the mitochondria, but it was usually 5-10 T175 flasks (175 cm^2 flasks) at 80-90% confluency. All the process was performed on ice, and sometimes in the cold room. Cells were harvested by banging the flasks, pelleted at 1,000g for 5 min at 4°C and washed twice with cold PBS. Pellets were weighed and volume of cell pellet was estimated (1 g of cells = 0.8 ml wet volume).

Cells were resuspended in 9 volumes of hypotonic buffer (HB: 20 mM 4-(2-hydroxyethyl)-1-piperazineethanesulfonic acid (HEPES) pH 7.8, 5 mM KCl, 1.5 mM $MgCl_2$, 2 mM dithiothreitol (DTT), 1 mg/ml BSA, 1 mM phenylmethylsulfonyl fluoride (PMSF) and PIC), and homogenized by 20 strokes using a tight-fitting 15 ml Dounce homogenizer. The homogenate was immediately mixed with 2 ml of 2.5x MSH buffer for every 3ml of HB added previously (2.5XMSH: 525 mM Mannitol, 175 mM Sucrose, 20 mM HEPES pH 7.8, 5 mM EDTA, 1 mg/ml BSA, 2 mM DTT, 1 mM PMSF, PIC), in order to make the medium isotonic.

The homogenate was centrifuged at low speed (1,000 g for 10 min at 4°C) to remove cell debris, unbroken cells and nuclei. The supernatant was collected and centrifuged again at low speed. This second supernatant was then spun at 10,000 g for 10 min at 4°C with a Sorvall LYNX 6000 Superspeed Centrifuge (Thermo Scientific). The supernatant was kept as the cytosolic fraction, while the pellet, containing crude mitochondria, was washed 3 times with 1x MSH and kept on ice until used.

Further purification was sometimes performed in order to get pure mitochondria. For this purpose, crude mitochondria resuspended in 1x MSH were loaded onto a 1.5-1 M sucrose gradient (2 and 10 ml respectively) in 10 mM HEPES pH 7.8/ 5 mM EDTA/ 2 mM DTT. The gradients containing the mitochondria were spun in polypropylene tubes (14 x 95mm, Beckman 331374) at 40,000 g for 30 min at 4°C in SW 40 Ti Rotor (Beckman Coulter) in an Optima L-90K Ultracentrifuge (Beckman Coulter). After the spin, mitochondria were forming a neat band in the interphase between 1.5 and 1 M sucrose. Slightly above this band, there was another small band corresponding to the mitochondrial associated membranes (MAMs) fraction. Both fractions were transferred into clean tubes and washed with 1x MSH.

Mitochondria solubilization with DDM

Crude or pure mitochondria were resuspended in 2X Lysis buffer (40 mM HEPES pH 7.8, 150 mM NaCl, 10 mM EDTA, 4 mM DTT, 4x PIC) to get 10 mg/ml protein. 1 volume of 0.8% n-dodecyl-β-D-maltoside (DDM) was added and tubes were incubated in the roller at 4°C for 20 min. Samples were spun at 2,000g for 10 min at 4°C, and supernatant (SN) was ready for subsequent procedures.

Submitochondrial localisation by a mild trypsin treatment

Aliquots with 200 µg of fresh crude mitochondria were resuspended in 100 µL of a hypotonic buffer (20 mM HEPES, pH 7.6), and trypsin was added to a final concentration of 5 µg/mL. The reactions were incubated at 30°C during different times, 0, 1, 10, 20 and 60 min. After the incubation time, the reactions were stopped by the addition of 1 µL of 100 mg/mL of Pefabloc (Sigma), a trypsin inhibitor, and 2XSB. 15 µL per sample were run on an SDS-PAGE gel. This assay was adapted from the literature [175].

Iodixanol gradients

Top-down iodixanol (IOD) gradient centrifugation of pure mitochondria was carried out as described in the literature [4,176]. Sometimes, a digitonin pre-treatment was performed in order to separate membranes and soluble components, by using a digitonin (µg) to protein (µg) ratio of 2/1 in PBS supplemented with PIC. After a 10-minute incubation on

ice, digitonin pre-treated samples were centrifuged at 14,000 g for 10 min at 4°C to obtain a membrane enriched pellet and associated components and a supernatant containing soluble components.

Briefly, pure mitochondria or digitonin pre-treated membrane enriched fraction were lysed with 0.4% DDM. Samples (total DDM lysates, membrane enriched DDM lysates or digitonin-treated soluble components) were loaded on a 20–42.5% iodixanol gradient prepared in 20 mM HEPES pH 7.8, 1 mM EDTA, 50 mM NaCl, 2 mM DTT, 0.05% DDM and protease inhibitors) and centrifuged at 100,000 g for 14 h. Fractions (500 µL) were collected by punching a small hole into the bottom of the tube.

M3.6. Lipid compounds quantification

Lipids extraction

The extraction was performed following standard procedures of our laboratory [177]. Frozen pellets from cells or mitochondria were thawed on ice and resuspended in 200 µL of PBS. Protein was measured and 0.5 mg of total cell homogenate or 40 µg of mitochondrial protein were aliquoted for extraction into 1.5 mL polypropylene tubes in a total volume of 100 µL in PBS. When the starting material were iodixanol fractions, 100 µL of each fraction were used. To estimate the CoQ_{10} recovery of the extraction process, 50 pmol of CoQ_6 was added as an internal standard (5 µL of 10 µM CoQ_6 in ethanol). Disruption of membranes was performed by adding SDS (1% final concentration, 5 µL of 20% SDS) and 1 min of vortexing. Lipids were dispersed with an alcohol cocktail (ethanol-isopropanol 95:5) added to the disrupted biological sample (ratio 1:2 v/v, 220 µL of alcohol cocktail) and 1 min of vortexing. The samples underwent subsequent triplicated hexane extraction (dispersed sample:hexane ratio 3:5 v/v, 500 µL of hexane and 1 min of vortexing, followed by a 1,000 g 4°C 5min centrifugation). Hexane fractions were mixed and dried under vacuum, and then reconstituted in ethanol prior to high-performance liquid chromatography (HPLC) analysis.

Quinones HPLC detection

CoQ_{10} content was analysed by the injection of lipid extracts in HPLC as described by Rodríguez-Aguilera et al., 2017 [177]. These measurements were performed at the

Laboratory of Cellular Physiopathology and Bioenergetics (Pablo de Olavide University, Sevilla, Spain), mainly by Ana Cortés Rodríguez. A guard cell was installed before or after the injection valve, depending on the experiment (after the injection valve when oxidation of the whole sample was required before chromatographic separation). Separation was performed in C18 ReversePhase-HPLC columns (5 µm, 150 × 4.6 mm) with 20 mM $AcNH_4$ pH 4.4 in methanol (solvent A) and 20 mM $AcNH_4$ pH 4.4 in propanol (solvent B). A gradient method with an 85:15 solvent mixture (A:B ratio), and a flow rate of 1.2 mL/min, was used as starting conditions. The mobile phase turned to a 50:50 ratio, starting in minute 6 and completed in minute 8, as the flow rate decreased to 1.1 mL/min. After 20 min (run time) at 40 °C, the columns were re-equilibrated to the initial conditions for three additional minutes.

CoQ_{10} levels were analysed and detected by electrochemical detector (ECD) (channel 1 set to −700 mV and channel 2 set to +500 mV), UV-vis detector (set to 275 nm) and radio-flow detector (LB 509 with a solid cell YG 150 Al-U4D (Berthold Technologies)) when needed.

Analysis of CoQ_{10} Biosynthesis

CoQ_{10} biosynthesis rate was assessed by measuring the incorporation of ^{14}C-4-HB, precursor of the benzoquinone ring. ^{14}C-4-HB was chemically synthesized from ^{14}C-tyrosine by Fernández-Ayala et al., 2005 [117]. Cells were seeded on 100 mm diameter culture dishes in a density of $3{\cdot}10^5$ cells/dish ($5{\cdot}10^3$ cells/cm^2), 24 h before the addition of ^{14}C-4-HB. Cell cultures were incubated with 7.2 nM ^{14}C-4-HB for 72 hours (72 pmol of ^{14}C-4-HB in 10ml of medium). In some cases, cells were also grown with unlabelled 4-HB in the same conditions. Labelled-CoQ_{10} content was analysed by lipid extract injection in HPLC as described above.

CoQ_{10} biosynthesis Intermediates characterisation

These analyses were performed at the Mass Spectrometry Laboratory (Instituto de la Grasa, Sevilla, Spain), by Alicia Sánchez García and José Julián Ríos. Samples were analysed in an HPLC-APcI-MS system. This equipment is composed of a UHPLC Dionex Ultimate 3000RS (Thermo Fisher Scientific) coupled to a high-resolution mass

spectrometer with a Time-of-Flight (TOF) analyser, micrOTOF-QII (Bruker Daltonics), equipped with an APcI (Atmospheric Pressure Chemical Ionization) source.

Chromatographic separation was performed as described previously [177]. The injection volume was 30 µl and the flow rate was 1 ml / min. The reverse phase column used was a Mediterranea SEA18 (3 µm, 200 x 4 mm) (Teknokroma). A 0.4 ml / min post-column split was directly introduced into the APcI source. The parameters of the APcI source used were the following: 4000 V (capillary voltage), 6000nA (intensity of the corona), 2.5 bar of nebulization pressure, 4 l / min of drying gas flow, 220 ºC of drying temperature and 300 ºC source vaporization temperature. The mass spectrometer operated in positive mode, detecting the compounds in full scan in a mass range m / z of 50-1800.

A specific database with the compounds of interest was prepared for the occasion (see Table 4.7), including the elemental composition and the name of the compounds, and sometimes other data such as the retention time.

Data analysis was done by using the DataAnalysis 4.1 software (Bruker Daltonics), and the automatic detection from the database was carried out with the TargetAnalysis™ 1.2 (Bruker Daltonics). This program identifies a compound according to two aspects: the mass accuracy of the compound, and the SigmaFit™ criteria. The SigmaFit™ algorithm provides a numerical comparison between the experimental and theoretical isotopic pattern, with smaller values indicating a closer match between theoretical and measured isotopic patterns [178]. Only those results with mass accuracy error and mSigma values within the tolerance limits (5 ppm (parts per million) and 50, respectively) were considered as confident results.

Cholesterol quantification

Cholesterol was quantified using a fluorometric enzymatic kit, Amplex® Red Cholesterol Assay Kit (Invitrogen) according to the manufacturer's instructions. Briefly, the assay measures the production of hydrogen peroxide (H_2O_2) after the oxidation of cholesterol by the enzyme cholesterol oxidase. The production of H_2O_2 is measured by the appearance of fluorescence, since, in the presence of HRP, the non-fluorescent Amplex Red reagent reacts in a 1:1 stoichiometry with H_2O_2 to produce highly fluorescent resorufin. For measuring total cholesterol levels (and not only free-cholesterol), a

cholesterol esterase is also added to the reaction mix, so cholesterol esters are transformed in free-cholesterol and fatty acids, and this free-cholesterol can be quantified as well.

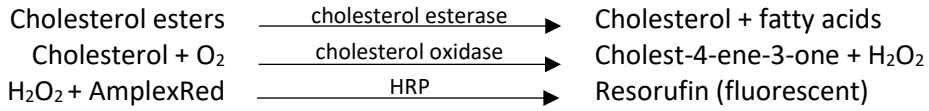

Lipid extracts from different origins were used to measure cholesterol levels:

i. Samples from IOD gradients: the 20% of this extract was used for each measurement of cholesterol.

ii. Samples from mitochondria: Lipid extract from 10 µg of crude mitochondria was used for each measurement.

iii. Samples from homogenates: Lipid extract from 20 µg of total homogenates was used for each measurement.

Cholesterol-containing samples were diluted 1:5 in the 1X Reaction Buffer from the kit. A volume of 40 µL of the diluted sample was used for each reaction. 10 µL of catalase 100U/mL (Sigma) were pipetted in each well. Catalase was utilised to consume endogenous peroxides of the solvent/sample, to reduce the background and increase sensitivity[179]. After this, 40 µL of the diluted samples, controls and STD curve were added to the catalase-containing wells, followed by incubation for 15 min at 37°C. Afterwards, 50 µL of a working solution (300 µM Amplex® Red reagent, 2 U/mL HRP, 2 U/mL cholesterol oxidase, 0.2 U/mL cholesterol esterase) were added to each microplate well, followed by incubation for 30 or longer min at 37°C, protected from light. The fluorescence was measured by using the scanner Amersham Typhoon (GE Healthcare), with the microplate tray and the Cy3 filter (excitation: 532 nm, emission: 570 nm) and quantified by ImageQuant TL v 5.2 (GE Healthcare).

M3.7. Mitochondrial respiratory function assessment

For respiratory complexes enzymatic activity measurements, cell samples were harvested and digitonised, in order to obtain a mitochondrial membranes-rich fraction. Then, enzymatic activities were measured spectrophotometrically in 96-well microplates, measuring the kinetics for 2 or 3 minutes. Complexes I, II, III and IV activities, and citrate synthase activity were measured by adapting the protocol

previously described [180]. CoQ-dependent activities (complexes I + III and II + III) were measured according to García-Corzo et al., 2014[181].

Digitonisation of cultured cells for enzymatic assays

Fresh pellets of $5 \cdot 10^6$ cells were harvested and washed twice with PBS. Pellets were resuspended in 400 µL of buffer A (20 mM MOPS (3-(N-morpholino)propanesulfonic acid) KOH pH 7.4, 250 mM sucrose) and the same volume of 0.2 mg/mL of digitonin in buffer A was added. After incubation at 4°C for 5 min, samples were microfuged at 5,000 g, for 3 min at 4°C. Resulting pellets were resuspended in 600 µL of buffer B (20 mM MOPS KOH pH 7.4, 250mM sucrose, 1 mM EDTA-Na_4) and, after incubation at 4°C for 5 min, microfuged at 10,000xg, for 3 min at 4°C. The mitochondria enriched fraction (pellet) was stored at -80°C. Right before starting the measurements, samples were thawed on ice and resuspended in 200 µL of potassium phosphate (KP) buffer (10 mM, pH 7.4). For lysis, samples were frozen in liquid nitrogen and thawed at 37°C, for 3 cycles. Protein concentration was measured as previously described (see M3.1).

Complex I activity measurement

Complex I activity (rotenone-sensitive NADH-CoQ oxidoreductase) was measured at 30°C, following the disappearance of NADH as a decrease in absorbance at 340 nm (extinction coefficient= 6.81 mL $\cdot nmol^{-1} \cdot cm^{-1}$). 20 µL of each sample were incubated with the reaction mixture (20 mM KP buffer pH 8, 0.2 mM NADH, 1 mM sodium azide (NaN_3), 1 mg/mL BSA) for 2 minutes at 30 ° C. The reaction was started with 50 µM of CoQ_1 and the kinetics was measured for 2 minutes. Then, 5 µM rotenone were added, and the variation in absorbance was measured. CI specific activity was represented as nmol of NADH consumed per min and per mg of protein, rotenone sensitive.

Complex II activity measurement

Complex II activity (succinate dehydrogenase) was measured at 30°C, following the disappearance of the oxidized artificial electron acceptor 2,6-dichlorophenolindophenol (DCPIP), as a decrease in absorbance at 600 nm (extinction coefficient= 19 $mL \cdot nmol^{-1} \cdot cm^{-1}$). 15 µL of each sample were incubated with 15 µL succinate (1.63

mg/mL in 10mM KP buffer pH 7.4) for 30 min at 4°C. Then, samples were incubated with the reaction mixture (50 mM KP buffer pH 7, 1.5 mM potassium cyanide (KCN), 0.1 mM DCPIP) for 2 minutes at 30°C. The kinetics was measured both before and after the addition of 50µM of CoQ_1. CII specific activity was represented as nmol of DCPIP consumed per min and per mg of protein.

Complex III activity measurement

Complex III activity (decilubiquinone (DBH_2):cytochrome c oxidoreductase) was measured at 30°C, following the reduction of cytochrome c, as a variation in absorbance at 550 nm (extinction coefficient= 21 $mL \cdot nmol^{-1} \cdot cm^{-1}$). 10 µL of each sample were added to the reaction mixture (50 mM KP buffer pH 7.4, 2 mM NaN_3, 1 mg/mL BSA, 50 µM cytochrome c, 50 µM reduced DBH_2) and the kinetics was measured for 2 minutes at 30°C. CIII specific activity was represented as nmol of cytochrome c reduced per min and per mg of protein.

Complex IV activity measurement

Complex IV activity (cytochrome c oxidase) was measured at 37°C, following the oxidation of cytochrome c, as a variation in absorbance at 550 nm (extinction coefficient= 18.5 $mL \cdot nmol^{-1} \cdot cm^{-1}$). 10 µL of each sample were added to the reaction mixture (50 mM KP buffer pH 7, 100 µM reduced cytochrome c) and the kinetics was measured for 3 minutes at 37°C. CIV specific activity was represented as nmol of cytochrome c oxidized per min and per mg of protein.

CoQ-dependent activities measurement

Complex I+III and II+III activities were measured at 30°C, following the reduction of cytochrome c, as a variation in absorbance at 550 nm (extinction coefficient= 21 $mL \cdot nmol^{-1} \cdot cm^{-1}$).

i. For CI+III activity measurement, 8 µL of sample were added to the reaction mixture (100 mM KP buffer pH 7.4, 5% BSA, 0.5 mM KCN, 0.1 mM cytochrome c) in the presence or absence of 25 µM rotenone, incubating 4 min at 30°C. The reaction began with the addition of 0.2 mM of NADH and the absorbance was

monitored for 3 min at 30°C. The activity was represented as the rotenone sensitive activity.

ii. For CII+III activity measurement, 8 µL of sample were added to the reaction mixture (75 mM KP buffer pH 7.4, BSA 1%, 0.5 mM KCN, 0.3 mM succinate, 25 µM rotenone), incubating 10 min at 30 ° C. The reaction began with the addition of 0.1 mM cytochrome c and the absorbance was monitored for 3 min at 30°C.

CI+III and II+III specific activities were represented as nmol of cytochrome c reduced per min and per mg of protein.

Citrate synthase activity measurement

Citrate synthase (CS) activity was measured at 30°C, following the appearance of thionitrobenzoic acid (TNB), proportional to the amount of liberated CoA, as a variation in absorbance at 412 nm (extinction coefficient= 13.8 ml $\cdot nmol^{-1} \cdot cm^{-1}$). 5 µL of sample were incubated with the reaction mixture (75 mM Tris-HCl pH 8, 100 µM DTNB (5,5'-dithiobis (2-nitrobenzoic acid)), 0.1 % Triton X-100 and 400 µM acetyl-CoA) for 2 min. The reaction began with the addition of 0.5 mM oxaloacetate and the absorbance was measured for 2 min at 30 ° C. CS specific activity was represented as nmol of CoA formed per min and per mg of protein. The specific activities of each complex (nmol/min/mg prot) were normalized by the specific activity of CS.

M3.8. Detection of COQ4 interaction partners

COQ4 protein affinity purification

For isolation of FLAG or HA-tagged COQ4 or untagged COQ4 with their interaction partners, immunocapture using an anti-FLAG, an anti-HA or an anti-COQ4 antibody was performed. Transfected cells with COQ4-FLAG-Strep tags (COQ4-FS), COQ4-HA or with untagged COQ4 were grown and doxycycline treated for the induction of the transgene (0.1 ng/mL, 24 h). Non-transfected *COQ4* KO cells were also used for all the procedure, as a negative control. Cells were collected, and 15 mg of cell protein were resuspended in PBS with PIC (PBSi) and treated with 0.5 mg/ml digitonin for 10 min at 4°C, in order to get a mitochondria-enriched fraction. Samples were centrifuged at 11,000 g for 5 min and pellets were washed with PBSi. Then, they were resuspended in 330 µL of

solubilisation buffer (PBSi with 10 % (w/v) glycerol, 1X lipid stock (10X stock: 0.9 mg/ml 1-palmitoyl-2-oleoyl-glycero-3-phosphocholine (POPC), 0.3 mg/ml 1-hexadecanoyl-2-(9Z-octadecenoyl)-sn-glycero-3-phosphoethanolamine (POPE), 0.3 mg/ml 1-palmitoyl-2-oleoyl-sn-glycero-3-phospho-(1'-rac-glycerol) (POPG), Avanti Polar Lipids) and 1.5 % (w/v) DDM), and incubated for 30 minutes at 4°C. Lysates were centrifuged at 16,900 x g for 10 min. Clear supernatants were filtered using spin-X-centrifuge filters, 0.22 µm cellulose acetate (Costar) or ultrafree -MC durapore 0.22 µm PVDF filters (Millipore). Samples were incubated with 40 µL of agarose beads crosslinked to the antibody of interest, o.n. at 4°C in rotation.

i. For FLAG-tagged protein purification, EZview red anti-FLAG M2 affinity gel (Sigma-Aldrich) was used.

ii. For HA-tagged protein purification, HA-Tag (C29F4) rabbit mAb sepharose bead conjugate (Cell Signaling Technology) was used.

iii. For untagged COQ4 purification, rabbit anti-COQ4 antibody (HPA042945, Atlas Antibodies) was crosslinked to agarose beads the day before the experiment by using the Pierce Crosslink Immunoprecipitation Kit (ThermoScientific), following the manufacturer's instructions.

The unbound material was collected and affinity resins were washed 5 times with wash buffer containing PBSi, 10% glycerol, 1 x lipid stock and 0.05 % (w/v) DDM. Bound material was eluted in different ways.

i. For FLAG-tagged proteins, a native elution was performed by using 30 µL of 150 µg/mL FLAG peptide (Sigma-Aldrich) in wash buffer, for 4h at 4°C.

ii. For HA-tagged proteins and untagged COQ4, a denaturing elution was performed by using 200 mM glycine at pH 2.5 with 0.05% (w/v) DDM, for 30 min at RT. The eluate was neutralised with Tris Base.

The presence of specific proteins in the eluates was analysed by SDS-PAGE, WB and immunodetection, and by mass spectrometry (MS).

Crosslinking of mitochondrial proteins

For crosslinking experiments, 0.5 - 2 mM disuccinimidyl suberate (DSS) were added to crude mitochondria, for 30-120 min at RT. Then, the reaction was quenched by using 200 mM ammonium bicarbonate 15 min at RT. Crosslinked mitochondria were washed twice with PBS. Then, immunoprecipitation was performed as described above, starting with the resuspension of crosslinked mitochondria with solubilization buffer.

Stable isotope labelling by amino acids in cell culture

SILAC (stable isotope labelling by amino acids in cell culture) is a simple and efficient approach of quantitative proteomics which allows an accurate relative quantification of the proteomes from two different cell populations (Figure M.5) [182–184]. Essential amino acids labelled with stable non-radioactive isotopes, ^{15}N- and ^{13}C- labelled arginine (R_{10}) and lysine (K_8), are added to an amino acid deficient cell culture medium. Through normal metabolic processes, the cells grown in this heavy (H) medium replace the natural (light, L) amino acids (^{14}N and ^{12}C arginine and lysine, R_0 and K_0) with the heavy ones, which are fully incorporated into the newly synthetized proteome after 8-10 doublings (Figure M.5.A). SILAC amino acids do not have effects on cell morphology, metabolism or growth rates and allow the two differentially labelled cell pools to be equally mixed in a single sample and then analysed by mass spectrometry (MS), remaining fully distinguishable.

In this study, SILAC was used to compare *COQ4*-defective cell line to the same cell overexpressing different tagged or untagged forms of COQ4, in order to identify COQ4 interactors. The two cell lines to be compared by SILAC MS were grown in H-DMEM containing R_{10} and K_8 and in L-DMEM containing R_0 and K_0 (Sigma-Aldrich), for at least 8 doublings. Both SILAC media also contained proline, to avoid the conversion of the excess of arginine to proline, and 10% dialyzed FBS, to prevent the dilution of heavy isotopes. Full incorporation of heavy amino acids was checked before the experiments.

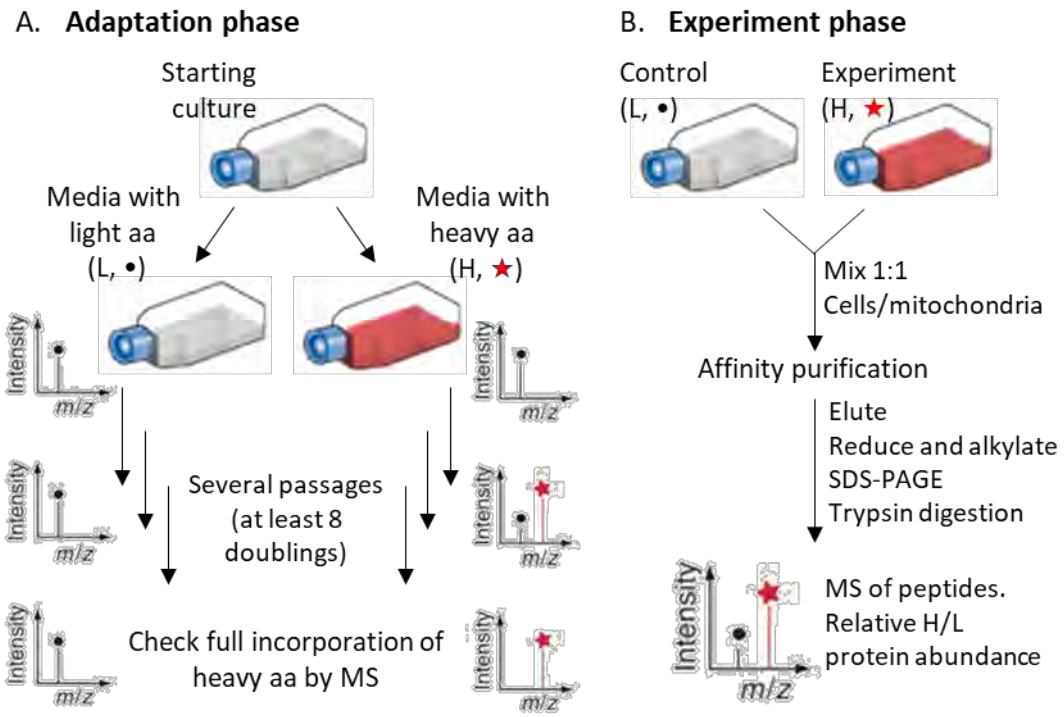

Figure M.5. Overview of SILAC protocol.
The SILAC experiment consists of two distinct phases—an adaptation (A) and an experimental (B) phase. (A) During the adaptation phase, cells are grown in light (L) and heavy (H) SILAC media until cells grown in the H medium have fully incorporated the heavy amino acids (red star). The two SILAC cell pools are then fully distinguishable by MS (black dot (L) and red star (H) peptides, respectively). (B) In the experiment phase, the two cell populations (control and experiment) that are differentially labelled are expanded and during the experiment, they can be mixed and processed as a single sample. In our case, we performed affinity purification of COQ4-FS protein, and analysed the eluted fraction. Samples were reduced and alkylated, resolved by SDS-PAGE and trypsin digested. Resulting peptides were as a single pool by MS for protein identification and quantification (Adapted from Ong et al., 2006[183]).

Quantitative proteomics with SILAC labelling

Each quantitative proteomics analysis was based on two SILAC experiments, namely exp. 1 and exp. 2, one in which the overexpressing cell line (COQ4-FS, COQ4-HA or COQ4) was H-labelled and the control cell line (*COQ4* KO) unlabelled, and the second one with reverse labelling, respectively. For each experiment, equal portions of the differentially labelled H and L cells were mixed (Figure M.5.B), and protein immunoprecipitation was performed as described above (with or without crosslinking, and with or without mitochondria purification).

Eluted samples were prepared for MS by reducing and alkylating the cysteine residues. Reduction was done by adding tris(2-carboxyethyl)phosphine (TCEP) (5 mM final concentration, Sigma-Aldrich) dissolved in gel sample buffer (40 % (w/v) glycerol, 200

mM Tris pH 9, 4 mM EDTA pH 8, 4 % (w/v) SDS), and incubating at 37 °C for 30 min. Samples were brought to RT and alkylation was performed by adding iodoacetamide (15 mM final concentration) and incubating in dark at RT for 30 minutes. Then DTT (25 mM final concentration) was added to quench the excess of iodoacetamide. Proteins were then resolved by SDS-PAGE in 10-20% acrylamide Novex Tris-Glycine Mini Gel, WedgeWell format (Invitrogen) electrophoresis. Next, the gel was stained with Coomassie Brilliant Blue R-250 [185] in order to visualize the protein bands. Each lane of the gel was cut in eleven 0.6 mm slices, which were sent to the mass spectrometry facility at the MRC-Mitochondrial Biology Unit (Cambridge, UK), where they performed all the following steps of proteins digestion, MS and protein identification and quantification.

Briefly, proteins were digested with trypsin and the resulting peptides analysed by liquid chromatography mass spectrometry (LC-MS) employing an LTQ XL-Orbitrap system (Thermo Fisher Scientific), as described previously [186]. Proteins were identified by Andromeda and quantification of heavy to light (H/L) ratio was calculated with MaxQuant [187]. Ratio was based on reciprocal labelling duplicate SILAC experiments. The median peptide ratio was taken to be the protein ratio, using at least two ratio counts for each peptide. The ratios from each experiment were plotted as the $\log_2$ value on a scatter plot, at the x and y axes, respectively, each protein represented by a point.

In the scatter plot, proteins unaffected by experimental conditions cluster around the origin. Proteins with a consistent increase or decrease in abundance occur in the top right or bottom left quadrants, respectively. Points in the two other quadrants represent proteins with irreproducible results within replicates. Those in the top left quadrant contain exogenous contaminants. A diagonal line from the top right to bottom left represents a perfect correlation between the two experiments.

Statistically significant proteins ($P < 0.05$) in one or both orientations of labelling were identified with Perseus [188]. The significance of the enriched proteins was calculated based on significance B with permutation-based False Discovery Rate (FDR) control [189], considering a Benjamini-Hochberg FDR<5%.

Mass spectrometry

Mitoplasts from *COQ4* KO and *COQ4* KO-overexpressing COQ4-FS (induced with doxycycline) were affinity purified using anti-FLAG beads, as described above. Protein eluates were methanol-chloroform precipitated, dried under vacuum (Speed Vac) and send to the proteomics facility of the Pablo de Olavide University (Seville, Spain), where they performed all the following steps of sample digestion, LC-MS and protein identification.

Briefly, protein pellets were resuspended in urea 6 M, 50 mM ammonium bicarbonate. Disulphide bonds were reduced adding DTT 10 Mm, 50 mM ammonium bicarbonate to protein solution and incubating for 60 min at RT. For carbamidometylation of cysteine –SH groups, iodoacetamide 30 mM, 50 mM ammonium bicarbonate was added to samples and incubated in the dark for 30min.

Samples were digested overnight at 37°C using trypsin bovine (Sequencing Grade Modified Trypsin, Promega) in a ratio 1:12 enzyme-substrate. Reaction was stopped using formic acid to 0.5%. OMIX C18 tips (Agilent Technologies) were used for concentrating and desalting peptide extracts. Samples were dried and resuspended in 0.1% trifluoroacetic acid and injected in a nano-HPLC system.

Protein digested samples were separated in a Thermo ScientificTM Easy nLC system using a 50 cm C18 Thermo Scientific™ EASY-Spray™ column. The following solvents were employed as mobile phases: Water 0.1% Formic Acid (phase A) and Acetonitrile, 20% H_2O, 0.1% Formic Acid (phase B). Separation was achieved with an acetonitrile gradient from 10% to 35% over 120 min, 35% to 100% over 1 min, and 100% B over 5 min at a flow rate of 200 nL/min.

A Thermo ScientificTM Q Exactive™ Plus Orbitrap™ mass spectrometer was used for acquiring the top 10 MS/MS spectra in DDA (Data-dependent acquisition) mode. LC-MS data were analysed using the SEQUEST® HT search engine in Thermo Scientific™ Proteome Discoverer™ 2.2 software using static carbamidomethylation (C), dynamic oxidation (M) and acetylation (C, H, K, S, T, Y) modifications. Data were searched against the Uniprot Human protein database and results were filtered using a 1% protein FDR threshold [189].

The list of identified proteins was analysed by gene name, to eliminate replicated results. Venn diagrams of the resulting lists were generated by using the Venny 2.1 tool [190]. We subjected the protein list (by gene names) to a Gene Ontology (GO) PANTHER overrepresentation analysis, by cellular component, biological process and molecular function, using a Homo sapiens reference list containing all genes in the GO database [191–193]. In order to simplify the results, similar GO terms were fused.

M4. Molecular biology methods

M4.1. Nucleic acid extraction and quantification

Total genomic DNA was extracted from cell pellets, by using the Promega Wizard Genomic DNA Purification kit (Promega), following the manufacturer's protocol. When the pellets were very small, all the volumes of the standard protocol were divided by 3. Dry DNA pellet was reconstituted in milliQ H_2O.

Total RNA was extracted from cell pellets, by using the TRIzol Plus RNA Purification System (Invitrogen-ThermoFisher Scientific), following the manufacturer's protocol. Dry RNA pellet was reconstituted in RNAase free milliQ H_2O.

DNA and RNA concentrations were measured using a NanoDrop One UV-Vis Spectrophotometer (Thermo Scientific). Good quality samples had a 260 nm / 280 nm ratio between 1.6-2.0 for DNA and between 1.8-2 for RNA. Additionally, to check RNA integrity, 0.5 µg of RNA was run on a 1% TBE-agarose gel to observe the 18S and 28S ribosomal RNA bands.

M4.2. Polymerase chain reaction (PCR) amplification

PCR was performed in order to amplify DNA fragments for different purposes (cloning, sequencing, checking ligations, etc.) and from different origins (genomic DNA, cDNA, plasmid, bacteria colony). DNA was amplified with HorsePower Taq polymerase kit (Canvax Biotech), using the manufacturer’s protocol. The PCR amplification set-up is detailed in Table M.7 and the thermocycler conditions were optimised for each specific reaction (Table M.8).

Table M.7. Standard PCR assay.

Reagent	Volume (µL) 20 µL/reaction	Final concentration
10x PCR buffer	2	1x
$MgCl_2$ 25mM	2	2.5 mM
dNTP 10mM mixture	1.6	0.8 mM
Primer Forward (Fw) 10 µM	1.5	0.75
Primer Reverse (Rv) 10 µM	1.5	0.75
DNA template	0.2-10	1.75-2.5 ng/µL
Horse-Power-Taq DNA polymerase (5 U/µL)	0.2	0.05 U/µL
milliQ H_2O	to 20	

Table M.8. Cycling conditions for PCR.

Step	Temperature (°C)	Time	Number of cycles
Initial denaturation	95	5 min	1x
Denaturation	95	30 s	2.5 mM
Annealing	Melting temperature (Tm)	30 s	0.8 mM
Elongation	72	1 min / Kb	0.75
Final elongation	72	10 min	0.75
Hold	4	∞	-

M4.3. Agarose gel electrophoresis

Agarose gel electrophoresis was used for the separation of DNA or RNA in fragments of varying sizes. 1 % agarose gels were used for general applications, 0.7-0.8 % when resolving large fragments (>5 kb) and 1.5 % for small fragments (<0.5 kb). Gels were cast with the appropriated percentage (w/v) of agarose low melting point (Sigma-Aldrich) dissolved in 50 mL / 100 mL of Tris/Borate/EDTA (TBE) buffer (89 mM Tris-borate, 100 mM boric acid, 2 mM EDTA) and 1x RedSafe™ dye (20,000X, iNtRON biotechnology). DNA samples were mixed with loading dye (6X) at a 5:1 volume ratio and were always run alongside the GeneRuler 1 kb DNA Ladder (Termo Scientific). Gel electrophoresis was performed at voltage of 80-100 V with TBE as running buffer, in a ReadySub-Cell GT Horizontal Electrophoresis System (Bio-Rad). Bands were visualized with a ChemiDocTM XRS+ Imaging System (Bio-Rad).

M4.4. Retrotranscription of RNA

Purified RNA (40 µL) was treated with DNase I Amplification Grade (Sigma-Aldrich), to remove any DNA traces. Briefly, 5 µL of 10x reaction buffer and 5 µL of DNase were added to the RNA and incubated at RT for 15 min. Then, 5 µL of stop solution were added

and samples were incubated for 10 min at 70°C. 1 µg of DNase-treated RNA was retrotranscribed with the iScript kits (Bio-Rad), to obtain the complementary DNA (cDNA).

iScript Reverse Transcription Supermix was used when cDNA was needed for subsequent gene expression analysis by Real-time quantitative PCR (RT-qPCR), while iScript Select cDNA Synthesis Kit was used when cDNA was needed for subsequent cloning (Tables M.9 and 10).

Table M.9. cDNA synthesis reaction.

iScript Reverse Transcription Supermix	
Reagent	**Volume (µL)**
5x iScript Reaction Mix	4
iScript Reverse Transcriptase	1
milliQ H_2O	To 20
RNA template (1 µg)	variable
iScript Select cDNA Synthesis Kit	
Reagent	**Volume (µL)**
5x iScript Select Reaction Mix	4
iScript Reverse Transcriptase	1
Oligo $(dT)_{20}$ primer	2
milliQ H_2O	To 20
RNA template (1 µg)	variable

Table M.10. cDNA synthesis reaction protocol.

Step	**Temperature (°C)**	**Time**
Priming	25	5 min
Reverse Transcription	46	20 min
RT inactivation	95	1 min
Hold	4	∞

M4.5. Real-time quantitative PCR

To perform a relative quantification of gene expression levels, RT-qPCR was performed by using the iTaq Universal SYBR Green Supermix, following the instructions and protocol provided by the manufacturer. Generally, an amount of first-strand cDNA equivalent to 50 ng of starting RNA was used. Samples were loaded in 96-Well Reaction Plates (Bio-Rad) and the RT-qPCR was performed in CFX Connect Real-Time PCR Detection System (Bio-Rad). The relative quantification was calculated by using the $2^{-\Delta\Delta Cp}$ method [194].

M4.6. In vitro studies of spliceogenicity of patients' variants

Reverse Transcription- Semi-quantitative PCR

Semi-quantitative PCR was performed by using an amount of first-strand cDNA equivalent to 150 ng of starting RNA. We used the standard PCR protocol, but with a 25-cycle amplification protocol, to ensure that the PCR amplification remained in the exponential phase.

The RT-PCR products were analysed by agarose gel electrophoresis. The relative amounts of the different forms were determined by densitometry, using the Fiji-Image J [171] and expressed as a percentage. After electrophoresis, bands were excised from the gel for cloning and sequencing.

Minigene constructs expression and analysis of the transcripts

Minigene constructs expression and analysis were performed by our collaborators from Dr Eva Trevisson's laboratory in Padova. Briefly, the ß-globin minigene was developed by Forzan et al., 2010 [195], by cloning the ß-globin gene in a pcDNA™3.1/Hygro(+) vector (Thermo Fischer Scientific), with a polylinker containing the restriction sites for enzymes XhoI, NotI and HindIII in the intron 2 of ß-globin gene. The patient's genomic DNA fragment carrying the c.532+6 T>A variant was amplified with primers with the same restriction sites and subsequently cloned inside the ß-globin minigene.

The *COQ4* fragment amplified consisted in the exon closest to the intronic variant to analyse and a portion of 100 bp of flanking intronic regions upstream and downstream. For comparison, the WT equivalent sequence was also cloned in the minigene vector. WT and mutant plasmids were used for transfection in HEK293 cells that do not express ß-globin, in addition with the empty ß-globin vector, as negative control. 24 hours after transfection, total RNA was extracted, retrotranscribed and the resulting cDNA was amplified with a semiquantitative-PCR, using specific primers for the ß-globin gene, designed on exon 2 (forward) and exon 3 (reverse).

RNAseq

RNA from control and patient fibroblasts pellets was extracted from 175 cm^2 of cells grown in 1g/L glucose DMEM supplemented with 20% (v/v) of FBS, 1% Ab and 10 µM uridine. Total RNA was extracted and quantified as described in section M4.1. Samples were submitted to Novogene Europe (Cambridge, United Kingdom) with a total RNA quantity of at least 2 µg.

Novogene prepared the libraries and performed the paired-end sequencing of the samples with Illumina NovaSeq 6000, with a read length of 150 nt. They analysed the results, mapping the obtained sequences to the human reference genome GRCh38 assembly. Data was visualised with the Integrative Genomics Viewer (IGV) software (Broad Institute and UC San Diego)[196], focusing on COQ4 transcript and counting the reads for each exon.

M4.7. mtDNA copy number determination

DNA from frozen cell pellets was extracted using the Promega Wizard Genomic DNA Purification kit. mtDNA copy number was measured by RT-qPCR, using Taqman probes for a nuclear (*APP*, probe: Hs02339796_cn, Applied Biosystems) and a mitochondrial gene (*COXI*, probe: Hs02596864_g1, Applied Biosystems), using the Mix qPCR TaqMan® Gene Expression Master Mix (Applied Biosystems), following the manufacturer's instructions.

20 ng of genomic DNA were used per reaction, and for each sample, three technical replicates were added to the plate. RT-qPCR was run in an ABI PRISM® 7900HT Sequence Detection System (Applied Biosystems). The relative quantification was calculated by using the $2^{-\Delta\Delta Cp}$ method [194], using the nuclear gene *APP* for normalisation.

M4.8. Purification of PCR products from agarose gels

Agarose-embedded DNA fragments were purified using the NucleoSpin® Gel and PCR Clean-up kit (Macherey-Nagel). Briefly, a high-salt binding buffer was added to the cut-out gel band, and it was heated to dissolve the agarose. The mixture was then applied to the spin column, where, in the presence of chaotropic salt, DNA binds to the silica membrane. Contaminations were removed by washing steps with ethanolic Wash Buffer

NT3. Finally, the pure DNA was eluted under low salt conditions with slightly alkaline Elution Buffer NE (5 mM Tris/HCl, pH 8.5).

M4.9. DNA digestion and plasmid dephosphorylation

DNA plasmids were digested at 37 °C for 1 h with the Anza Restriction Enzymes system (Thermo Scientific) according to manufacturer's instructions. After digestion, vectors were dephosphorylated (to avoid self-ligation) by adding 1 µL of the Anza™ Alkaline Phosphatase to the reaction and incubating at 37°C for 30 minutes. DNA fragments were then separated on 1 % (w/v) agarose gels, and the bands corresponding to the fragments of interest (the linearised vector or the insert) were excised from the gel and purified.

M4.10. DNA ligation

PCR products amplified with Taq polymerase, which leaves a A-overhang, were cloned directly into the pCR2.1 (Invitrogen) or the pGEM®-T Easy vector, following the manufacturer's protocol. In the case of blunt-end fragments, A-tailing was performed before ligation. For this, the purified DNA fragments were incubated at 72°C for 20 minutes with 0.2 mM of dATP (Sigma) and the HorsePower Taq polymerase kit (Canvax Biotech): 1X PCR Reaction Buffer, 2.5mM $MgCl_2$ and 0.5 u/ µL of HorsePower Taq polymerase, in nuclease-free water to a final volume of 10 µL.

The restriction enzyme -digested inserts and vectors, were ligated using Anza™ T4 DNA Ligase Master Mix (Thermo Scientific). Ligation reactions of 20 µL containing 5 µL of Anza™ T4 DNA Ligase Master Mix were set up at a 1:5 vector:insert ratio, with 50 ng of linearised vector, and incubated at RT for 1 h, or 4°C o.n. Ligation products were then transformed into DH5α chemically competent bacteria.

M4.11. Site directed mutagenesis

Site directed mutagenesis (SDM) was performed by using the QuikChange II XL Site-Directed Mutagenesis kit (Agilent), following the manufacturer's protocol. These oligonucleotides are specified in Table M.11.

M4.12. Transformation of *E. coli*

Chemically competent *E. coli* DH5α bacteria were used for plasmid transformation and maintenance. For transformation, they were taken from the stock at -80°C and thawed on ice. Plasmids or ligation products to be transformed were added to the cells (1-5 µL, 5-100 ng), with subsequent incubation on ice for 10 min. A heat shock was performed at 42°C for 45 seconds, and samples were returned to ice immediately after, for 10 min. 500 µL of LB (10 g/L tryptone, 5 g/L yeast extract, 5 g/L NaCl) were added and incubated 30 min at 37°C, with 200 rpm shaking. Different dilutions were plated in LB plates with 100 µg/ml ampicillin, and grown 24h at 37°C to visualize the results.

Table M.11. List of primers used in this project.

#	Primer name	Fw/ Rv	Sequence (5' → 3')	Purpose	
1	COQ4-HindIII	Fw	AACCAAGCTTGCCACCATGGCGACTCTGCTG	Cloning	COQ4 in pcDNA5
2	COQ4-FS-XhoI	Rv	GTACGCTCGAGGGCCAAGCCCTGGACGTGC		COQ4-FS in pcDNA5
3	COQ4-HA*-XhoI	Rv	AACCCTCGAGCTACTAAGCGTAATCTGGAACATCGTATGG GTAGGCCAAGCCCTGGACGTG		COQ4-HA in pcDNA5
4	COQ4 CRISPR	Fw	CTGACCTCGGCCTTTTTCTT	CRISPR geno-typing	COQ4 KO
5		Rv	TCGACCTCGGAGTTGACTTT		
6	EMX1 C+ CRISPR	Fw	ATGGGAGCAGCTGGTCAGAG		EMX1 C+
7		Rv	CAGCCCATTGCTTGTCCCT		
8	qPCR-MTND1	Fw	CAACATCGAATACGCCGCAG	RT-qPCR	CI-MTND1
9		Rv	TTCAGGGGAGAGTGCGTCAT		
10	qPCR-SDHB	Fw	GCTACTGGTGGAACGGAGAC		CII-SDHB
11		Rv	GCGCTCCTCTGTGAAGTCAT		
12	qPCR-MTCYB	Fw	CCCATCCAACATCTCCGCAT		CIII-MTCYB
13		Rv	GATGAAAAGGCGGTTGAGGC		
14	qPCR-MTCOX1	Fw	ATACCAAACGCCCCTCTTCG		CIV-MTCOX1
15		Rv	TGTTGAGGTTGCGGTCTGTT		
16	qPCR-MTATP6	Fw	GCCACAACTAACCTCCTCGG		CV-MTATP6
17		Rv	GGTAAGAAGTGGGCTAGGGC		
18	qPCR-hAct	Fw	CTCGCTGTCCACCTTCCA		Actin housekeeping
19		Rv	GCTGTCACCTTCACCGTTC		
20	hcoq4 stop	Fw	CCGGATCCCGTACGCTACTAGGCCAAGCCCTGGACG	SDM	untagged-COQ4 in pcDNA5
21		Rv	CGTCCAGGGCTTGGCCTAGTAGCGTACGGGATCCGG		
22	hcoq4106-107AA	Fw	TCCCCGGATTGCGGCATCCACCCTCGACCT		phospho mutant M1
23		Rv	AGGTCGAGGGTGGATGCCGCAATCCGGGGA		
24	hcoq4106-109AAAA	Fw	AGGTCGAGGGCGGCTGCCGCAATCCGGGGA		
25		Rv	TCCCCGGATTGCGGCAGCCGCCCTCGACCT		
26	hcoq4 mutSTET	Fw	AGGTCGAGGGTCTCTGTCGAAATCCGGGGACGCTC		phospho mutant M2
27		Rv	GAGCGTCCCCGGATTTCGACAGAGACCCTCGACCT		
28	hcoq4 mutAAEA	Fw	CCAGGTCGAGGGCCTCTGCCGCAATCCGGGGACGC		phospho mutant M3
29		Rv	GCGTCCCCGGATTGCGGCAGAGGCCCTCGACCTGG		

Table M.11. List of primers used in this project (Continued).

#	Primer name	Fw/ Rv	Sequence (5' → 3')	Purpose	
30	hCOQ4 mut V8ATer1	Fw	ATGGCGACTCTGCTGCGCCCTGCTCTGCGGGCTCCCGGGCCTACAGC	SDM for patients' mutation intro-duction	p.Val8Alafs*19
31		Rv	GCTGTAGGCCCGGGAGCCCGCAGAGCAGGGCGCAGCAGAGTCGCCAT		
32	hCOQ4 mutL52S	Fw	CCGGCGGCCGACAGCGCTTTCTGCAGC		p.Leu52Ser
33		Rv	GCTGCAGAAAGCGCTGTCGGCCGCCGG		
34	hCOQ4 mutG55V	Fw	TCGCCGCGGAGACGGCGGCCAAC		p.Gly55Val
35		Rv	GTTGGCCGCCGTCTCCGCGGCGA		
36	hCOQ4 mutP64S	Fw	GGCGATGGCGCTCTATAACAGCTACCGCCACGAC		p.Pro64Ser
37		Rv	GTCGTGGCGGTAGCTGTTATAGAGCGCCATCGCC		
38	hCOQ4 mutR66Q	Fw	CTGCGACCATGTCGTGCTGGTAGGGGTTATAGAG		p.Arg66Gln
39		Rv	CTCTATAACCCCTACCAGCACGACATGGTCGCAG		
40	hCOQ4 mutD68H	Fw	CTGCGACCATGTGGTGGCGGTAGGG		p.Asp68His
41		Rv	CCCTACCGCCACCACATGGTCGCAG		
42	hCOQ4 mutT77I	Fw	GGTGCGGTGTCCTATGGTCTCCCCTAGAAC		P.Thr77Ile
43		Rv	GTTCTAGGGGAGACCATAGGACACCGCACC		
44	hCOQ4 mutL82Q	Fw	CCTGAGGACCTTCTGGGTGCGGTGTCC		p.Leu82Gln
45		Rv	GGACACCGCACCCAGAAGGTCCTCAGG		
46	hCOQ mutD111Y	Fw	CTGGAGCTTGCCCAGATAGAGGGTGGATGTCGA		p.Asp111Tyr
47		Rv	TCGACATCCACCCTCTATCTGGGCAAGCTCCAG		
48	hCOQ4 mutP119L	Fw	GAGGGAGCCTTCCAGCAGGCTCTGGAG		p.Pro119Leu
49		Rv	CTCCAGAGCCTGCTGGAAGGCTCCCTC		
50	hCOQ4 mutG124S	Fw	GAGATACTCGCGACTGAGGGAGCCTTCCG		p.Gly124Ser
51		Rv	CGGAAGGCTCCCTCAGTCGCGAGTATCTC		
52	hCOQ4 mutR141*	Fw	GGGTGGGTGCTCAGGTGTCTGGGGA		p.Arg141*
53		Rv	TCCCCAGACACCTGAGCACCCACCC		
54	hCOQ4 mutR145G	Fw	CATCCACGAAGCCGGTGGGTGCTCG		p.Arg145Gly
55		Rv	CGAGCACCCACCGGCTTCGTGGATG		
56	hCOQ4 mutF146C	Fw	CTCATCATCCACGCAGCGGGTGGGTGCTC		p.Phe146Cys
57		Rv	GAGCACCCACCCGCTGCGTGGATGATGAG		
58	hCOQ4 mutQ157L	Fw	CCGGTACCGCTTAATCACATACGCTAGCTCCTC		p.Gln157Lys
59		Rv	GAGGAGCTAGCGTATGTGATTAAGCGGTACCGG		
60	hCOQ4 mutR158Q	Fw	TGCACCTCCCGGTACTGCTGAATCACATACG		p.Arg158Gln
61		Rv	CGTATGTGATTCAGCAGTACCGGGAGGTGCA		
62	hCOQ4 mutdel174	Fw	GCTGGGGATGCCCAACATTCTGGGGG		p.Thr174del
63		Rv	CCCCCAGAATGTTGGGCATCCCCAGC		
64	hCOQ4 mutR240C	Fw	GGACTGCTCCCAGCACCGCTCATAGTACA		p.Arg240Cys
65		Rv	TGTACTATGAGCGGTGCTGGGAGCAGTCC		

M4.13. Plasmid preparation

Bacteria colonies carrying a plasmid of interest were grown o.n. in 5 mL of LB medium supplemented with 100 µg/ml ampicillin or 50 µg/mL of kanamycin (depending on the plasmid resistance gene, see Table M.12), at 37 °C with shaking at 200 rpm. DNA plasmids from the overnight cultures were isolated using the QIAprep Spin Miniprep kit (Qiagen). Briefly, bacterial cultures were lysed and centrifugated. Cleared lysates were then applied to the spin columns, where DNA binds to the membrane. Impurities were washed and pure DNA was eluted in elution buffer.

M4.14. Sequencing

All the constructs were checked by DNA Sanger sequencing (STAB VIDA company).

M4.15. Plasmids, primers and tags used in this project

Primers and plasmids used in this project are listed in Table M.11 and Table M.12, respectively.

All primers for standard PCR were designed with Primer3 tool [197,198], and posterior manual optimisation. All primers for SDM were designed using the tool provided by Agilent (www.agilent.com/genomics/qcpd) [199]. All primers were synthesised by STAB VIDA company. Sequences used for protein tagging are detailed in Table M.13.

Table M.12. List of plasmids used in this project.

Plasmid name	Description	Source
pU6-gRNA1 (Forward)	U6-gRNAs plasmids expressing guide sequences to human COQ4 exon 2 under U6 promoter. pUC origin and Kan^R gene for multiplication and selection in bacteria	Sigma-CRISPR Products
pU6-gRNA2 (Forward)		
pU6-gRNA3 (Reverse)		
pU6-gRNA4 (Reverse)		
pCMV-Cas9D10A-GFP	Cas9-D10A nickase plasmid co-expressing GFP under CMV promoter. pUC origin and Kan^R gene for multiplication and selection in bacteria. (CAS9D10AGFPP-1EA)	
pU6- EMX1-s4	CRISPR/Cas9 nickase EMX1 positive control: 2 U6-gRNAs plasmids expressing guide sequences to human EMX1 under U6 promoter. pUC origin and Kan^R gene for multiplication and selection in bacteria. (CRISPR02-1SET)	
pU6- EMX1-as4		
pU6-gRNA/CMV-Cas9-GFP	CRISPR/Cas9 negative control: U6-gRNA/CMV-Cas9-GFP plasmid expressing a non-targeting guide sequence under U6 promoter and co-expressing Cas9 and GFP under CMV promoter. pUC origin and Kan^R gene for multiplication and selection in bacteria. (CRISPR06-1EA)	
pcDNA™5/ FRT/TO	Inducible expression vector designed for use with the Flp-In™ T-REx™ System (CMV/TetO2 promoter, for Tet/DOX-regulated expression of the gene of interest; FRT site for Flp recombinase-mediated integration; Hygromycin resistance gene for selection of stable cell lines; pUC origin and Amp^R gene for multiplication and selection in bacteria)	Invitrogen
pOG44	Flp recombinase gene under CMV promoter, pUC origin and Amp^R gene for multiplication and selection in bacteria	
pcDNA5-FS	Linker-FLAG-linker-Strep-STOP tag sequences cloned with XhoI and ApaI in pcDNA5 multicloning site (MCS), for C-terminal tagging of proteins. Genes of interest must be cloned with XhoI and no stop codon in 3'	Dr. Jiuya He, MRC-MBU, Cambridge, UK
pcDNA5-COQ4-FS	COQ4 WT gene sequence cloned in pcDNA5-FS. Amplified from cDNA with primers #1 and #2 and digested with HindIII and XhoI	This study. Dr. Gloria Brea Calvo, UPO, Seville, Spain
pcDNA5-COQ4-HA	COQ4-HA-stop sequence cloned in pcDNA5-FS. Amplified from pcDNA5-COQ4-FS with primers #1 and #3, to introduce HA tag, and digested with HindIII and XhoI	This study
pcDNA5-COQ4-stop	Untagged COQ4 sequence with two stop codons in pcDNA5-COQ4-FS. Obtained by SDM with primers #20 and #21	
pcDNA5-COQ4-FS-M1	COQ4-FS in pcDNA5 with M1 phospho-mutation introduced by SDM from pcDNA5-COQ4-FS in two rounds, with primers #22 and #23, and #24 and #25	
pcDNA5-COQ4-FS-M2	COQ4-FS in pcDNA5 with M2 phospho-mutation introduced by SDM from pcDNA5-COQ4-FS with primers #26 and #27	
pcDNA5-COQ4-FS-M3	COQ4-FS in pcDNA5 with M3 phospho-mutation introduced by SDM from pcDNA5-COQ4-FS-M1 with primers #28 and #29	
pcDNA5-COQ4-HA-Patient mutations	COQ4-HA in pcDNA5 with patients' mutations introduced by SDM from pcDNA5-COQ4-HA, with primers #30 to #65	

Table M.12. List of plasmids used in this project (Continued).

Plasmid name	Description	Source
pcDNA5-COQ4-HA *Iso b*	COQ4-HA Iso b splice variant (missing exon 3) sequence cloned in pcDNA5. Amplified from P105/HDF Neo cDNA with primers #1 and #3, and digested with HindIII and XhoI	This study
pcDNA5-COQ4-HA *Iso c*	COQ4-HA Iso c splice variant (missing exon 5) sequence cloned in pcDNA5. Amplified from P105/HDF Neo cDNA with primers #1 and #3, and digested with HindIII and XhoI	
pcDNA5-COQ4-HA *Iso d*	COQ4-HA Iso d splice variant (missing exons 3 and 5) sequence cloned in pcDNA5. Amplified from P105/HDF Neo cDNA with primers #1 and #3, and digested with HindIII and XhoI	
pcDNA5-COQ4-HA *Iso e*	COQ4-HA Iso e splice variant (missing exons 3 to 5) sequence cloned in pcDNA5. Amplified from P105/HDF Neo cDNA with primers #1 and #3, and digested with HindIII and XhoI	

Table M.13. Tag sequences used for fusion proteins generation.

Tag	Nucleotide sequence	Amino acid sequence
Flag-Streptavidin (FS) tag (Linker-FLAG-linker-Strep-STOP tag)	CTCGAG (XhoI) CGTACGGGATCCGGAGGAGGAGGAGAAAACCTGTATT TTCAGGGCGGATCCGGAGGAGGAGGAACCGGTGGAG CTGGC (linker 1) GATTACAAGGACGACGATGACAAG (Flag) GGCGGAGCCGCTGGA (linker 2) TGGAGCCACCCCCAGTTCGAGAAG (Strep) TGATGA (StopStop) GGGCCC (ApaI)	LERTGSGGGGENLYFQ GGSGGGGTGGAG (linker 1) DYKDDDDK (Flag) GGAAG (linker 2) WSHPQFEK (Strep) ** (StopStop)
Human influenza hemagglutinin (HA) tag	TACCCATACGATGTTCCAGATTACGCT (HA) TAGTAG (StopStop)	YPYDVPDYA (HA) ** (StopStop)

M5. In silico analysis of gene and protein sequences and protein structures

M5.1. Sequence analysis

Reference sequences were retrieved from NCBI Refseq [200] and UniprotKB [201] databases. Different tools were used for sequence analysis.

Multiple alignment

BioEdit [202] + Clustal W [203] were used for the multiple alignment of sequences and visualization.

Translation initiation site prediction

We predicted translation initiation sites (TIS) of mRNA sequences using NetStart1.0 [204] and ATGpr [205] tools.

RNA secondary structure prediction

We used the RNAfold server[206] to predict the secondary structure of the pre-mRNA that would contribute a state of minimum free energy. As input, we used a sequence containing the mutated nucleotide and 100 or 200 nucleotides flanking it upstream and downstream.

Protein secondary structures prediction

Secondary structures of proteins were predicted by JPred [207].

MTS prediction

Prediction of a mitochondrial targeting signal (MTS) and cleavage sites of proteases was performed using MitoMiner [208] and MitoFates [209].

Phosphorylation prediction

Human *COQ4* sequence and some *COQ4* ortholog sequences (mouse, zebra fish, yeast and worm) were aligned and subjected to different *in silico* analysis for phosphorylation prediction. Potentially phosphorylatable residues (Ser, Thr, Tyr) were analyzed in terms of conservation. Residues that were conserved in at least 2 of these species (human's, among these two) were analyzed by different in silico phosphorylation prediction tools or phosphorylation databases. The tools used were the following: GPS 3.0 (Group Based Prediction System [210], score>6, cut off>6, threshold medium, all the kinases), PHOSIDA (phosphorylation site database [211]), DISPHOS 1.3 (Disorder-Enhanced Phosphorylation Sites Predictor [212], score>0.5), NetPhos 2.0 (Generic phosphorylation sites in eukaryotic proteins [213]), NetPhosK 1.0 (kinase specific eukaryotic protein phosphorylation sites [214]), KinasePhos 2.0 [215] and PhosphositePlus [216]. For each selected residue, the number of tools for which the phosphorylation prediction was positive was counted and considered to be the score for that residue (tools score: 0-7). Phosphorylation at a site depends on many factors, including the structure and solvent accessibility of the phosphorylation site, and it is thought that it predominantly occurs in regions of intrinsic disorder. Information about 3D structure was also taken into account as a supplemental score for each residue. Protein structures for human, mouse and yeast were modelled using the

only COQ4 ortholog protein structure which is crystallized (PBD: 3KB4). The models with the highest coverage of the sequence were selected (Human: positions 38-256; mouse: positions 39-257; yeast: positions 85-303). We considered the position of the residue in the 3D structure of the models to give it an additional score. When the residue was on the surface of the protein, in a disordered region, the score was the highest, and when it was totally buried within a conformational ordered region of the protein structure, the score was zero (3D structure score: 0-2). We also considered the solvent accessibility predicted by JPred, giving the maximum score when the residue was exposed in a disordered region and the minimum score when it was buried and in an ordered region, calculated using different accessibility cut offs (solvent accessibility score: 0-4). The residues with the highest scores were selected for ulterior experimental studies.

Prediction of mutations' pathogenicity

Different complementary online software for pathogenicity prediction were employed: SIFT [217] (available at https://sift.bii.a-star.edu.sg/) and PolyPhen-2 [218] (available at http://genetics.bwh.harvard.edu/pph2/) for missense variants; SPiCEv2.1 [219] (available at https://sourceforge.net/projects/spicev2-1/) for splicing variants; and CADD v1.6 [220] (available at https://cadd.gs.washington.edu/). SIFT score <0.05 was considered pathogenic. PolyPhen-2 score >0.05 was considered probably damaging, using the HumVar data set. Spliceogenicity of the variants was predicted with a prediction tool called SPiCE. Splicing Prediction in Consensus Elements (SPiCE) has been developed by Leman et al., 2018 [219] as a protocol for variant spliceogenicity prediction. It combines *in silico* predictions from SpliceSiteFinder-like and MaxEntScan and uses logistic regression to define optimal decision thresholds. These thresholds were defined as two probability thresholds to set optimal sensitivity and specificity: optimal sensitivity threshold (ThSe=0.115) and optimal specificity threshold (ThSp=0.749). ThSe is designed to give the highest detection rate while allowing false positives, and ThSp is designed to minimize false positives while allowing false negatives. SPiCE gives a P probability for a given variant. When P is above the 2 optimal thresholds, the variant is classified as variant with high probability to alter splicing; the region in between the two thresholds is defined for variants with medium probability to alter splicing; and the variants with a

P under the two thresholds are predicted to have low probability to alter splicing. CADD score > 20 was considered pathogenic.

M5.2. Protein homology modelling

Human COQ4 structure was modelled using its sequence obtained from UniProt database (Q9Y3A0). SWISS-MODEL [221] server was used to construct a homology model of human COQ4, using the PDB (Protein Data Bank) structures 3KB4, 3MSQ and 6E12 as templates. The structures were visualised by using UCSF Chimera software [222]. For the visualization of the conservation mapped on the structure, we used the AL2CO method[223] through the UCSF Chimera software [222]

Human COQ7 structure was modelled from its sequence obtained from UniProt database (Q99807). SWISS-MODEL [221] server was used to generate a homology model of the human COQ7. As a template, we used a ferritin (PDB: 5HJH), which has a 15% sequence identity to COQ7. The model was generated using the same specifications than [224] and it was visualised by using UCSF Chimera software [222]

M6. Statistical analysis

All results were expressed as mean ± SD, unless otherwise specified. Data analysis was performed with GraphPad Prism 8.0. Samples were assumed to come from a normal distribution. In the case of comparison between two groups, we used unpaired two-tailed t-test with a Welch's correction. Multiple samples were compared using a one-way (1 group) or two-way ANOVA (2 or more groups), with Sidak's, Tukey's or Dunnett's multiple comparison post-hoc test (depending on the nature of the data and the comparisons). P-values < 0.05 were considered statistically significant.

Chapter 1

Chapter 1.

Clinico-Genetic aspects of primary CoQ_{10} deficiency: a literature review

1.1. Introduction

1.1.1. Primary CoQ_{10} deficiencies

Primary CoQ_{10} deficiency syndrome is a very rare condition, genetically caused by autosomal recessive biallelic mutations in one of the genes participating in the CoQ_{10} biosynthesis pathway. To date, ten genes encoding CoQ_{10} biosynthetic proteins have been shown to have pathogenic variants causing human CoQ_{10} deficiency: *PDSS1*, *PDSS2*, *COQ2*, *COQ4*, *COQ5*, *COQ6*, *COQ7*, *COQ8A*, *COQ8B* and *COQ9* [112,225].

Up to date, over 275 patients from 180 families have been described in the literature (Table 1.3). It has been estimated a worldwide total of 123,789 individuals (1 in 50,000) affected by primary CoQ_{10} deficiencies, being only 1,665 (less than 1 in 3,000,000) due to known pathogenic variants, taking into account the frequency of the different known or predicted pathogenic variants in given populations [226].

Clinical symptoms associated to primary CoQ_{10} deficiency

Primary CoQ_{10} deficiency patients manifest a broad spectrum of clinical phenotypes. Different organs, tissues and systems can be involved in a highly variable way, depending on the affected gene, the age of onset and the specific defect on the gene, among other causes that are still not entirely known. Genetic factors, including hypomorphic mutations or polymorphisms that affect the susceptibility to the disease; epigenetics; compensation mechanisms; maternal effect; aging and/or environmental factors, amongst others, could determine the moment and the tissues affected during development or during life, and thus, influence the outcome of each genetic defect in each individual.

While mutations in some *COQ* genes can affect different organs (e.g. *COQ2*, *COQ4*), pathogenic variants of other *COQ* genes show a more specific phenotype (e.g. *COQ8A*, *COQ8B*). Even more, mutations in the same *COQ* gene can cause very variable clinical phenotypes with different age of onset (e.g. *COQ2*, *COQ4*) (Figure 1.1). The age of onset may generally range from birth to early childhood (*PDSS1*, *PDSS2*, *COQ2*, *COQ4*, *COQ5*, *COQ6*, *COQ7*, *COQ9*), or from childhood to adolescence (*COQ8A*, *COQ8B*), but there are also some adult-onset cases (*COQ8A* [227,228]; *COQ8B* [229]).

The systems mainly affected are the central and peripheral nervous system, kidney, heart and skeletal muscle (Figure 1.1 and Table 1.1) [112]:

i. Central nervous system (CNS) manifestations: CNS is often affected in these patients, showing a wide range of clinical manifestations, including encephalopathy, developmental delay (DD), intellectual deficiency (ID), cerebellar ataxia (CAt), seizures (Sz), hypotonia (Ht), nystagmus (Ny), dysarthria (Dy), dystonia or epilepsy (Ep), among others. These symptoms have been reported in patients with mutations in any of the described *COQ* genes, being less frequent in patients with pathogenic variants of *COQ6* and *COQ8B*, in whom the renal involvement predominates[112,230].

ii. Peripheral nervous system (PNS) and sensory organs (SO) manifestations: Less common than CNS manifestations, PNS and SO related symptoms have been reported in several cases of primary deficiencies. Sensorineural hearing loss (SNHL) is the most frequent PNS phenotype in primary CoQ_{10} deficiency patients, in most of the cases associated with steroid resistant nephrotic syndrome (SRNS) [231–237]. Some patients also presented peripheral neuropathy, optic atrophy (OA) and/or visual dysfunction [235,238–242].

iii. Renal manifestations: Steroid resistant nephrotic syndrome (SRNS) is quite common in primary CoQ_{10} deficiency patients, specifically in those with pathogenic variants of *PDSS2*, *COQ2*, *COQ6* and *COQ8B* [243–245]. It generally starts as proteinuria and derives to end-stage renal disease (ESRD) within childhood, if not treated [245]. Other less frequent renal manifestations are chronic kidney disease (CKD), renal cysts [240,246,247] or tubulopathy (Tp) [248,249].

iv. Cardiac manifestations: Heart is often affected in primary CoQ_{10} deficiency. The most common heart manifestation is hypertrophic cardiomyopathy (HCM). It is particularly frequent in *COQ4* [250–252] and *COQ7* [239,240] patients. Other cardiopathies less frequently found are valvulopathies (Vp), bradycardia, heart failure (HF), cardiomegaly, septal defects or heart hypoplasia (HHyp) [112].

v. Muscle manifestations: Skeletal muscle manifestations are not common in these patients. Isolated myopathy has not been found in individuals with molecularly confirmed primary CoQ_{10} deficiency, and the majority of the patients with a predominantly muscular phenotype have been associated with secondary CoQ_{10} deficiency [253,254]. Myopathy has been described in some patients with a broader multisystem phenotype. Other muscular manifestations include exercise intolerance (EI), muscle weakness (MW) and muscle fatigue (MF) [112,255].

vi. Other manifestations: Other more heterogeneous clinical findings have also been reported in patients affected by mutations in the different *COQ* genes (Figure 1.1 and Table 1.2). Among them, respiratory system alterations are the most frequent. Respiratory distress (RD) and apnea seem to be characteristic of *COQ4* [250–252], *COQ7* [239,240], *COQ9* [246,247,256] and some *COQ2* [257] patients. Oedema is only present in cases with nephrotic syndrome, so it is frequent in probands with pathogenic variants of genes with renal involvement [258]. Less frequent clinical findings include dysmorphic features, metabolic pathologies (diabetes mellitus (DM), obesity and hypercholesterolemia), thyroid disease (goiter, hypothyroidism) and circulatory problems (cyanosis, hypertension (HT), livedo reticularis (LR)), among others [112]. It should be considered that some of these symptoms could be secondary consequences of a more general defect.

Table 1.1. Main clinical manifestations in primary CoQ10 deficiency and abbreviations.

Affected tissue, organ or system				
CNS	**PNS / SENSORY ORGANS**	**KIDNEY**	**MUSCLE**	**HEART**
COGNITIVE-BEHAVIORAL DEFICITS	**PNS**	**RENAL DYSFUNCTION**	**MUSCULAR SIGNS**	**FUNCTIONAL/ MORPHOLO-GICAL DEFECTS**
- Autism - Depression - Developmental delay (DD) - Intellectual deficiency (ID)	- Peripheral Neuropathy (PNSN) - Demyelinating motor neuropathy	- Kidney dysfunction (KD) - Chronic kidney disease (CKD) - End-stage Renal Disease (ESRD) - Steroid resistant nephrotic syndrome (SRNS) - Tubulopathy (Tp)	- Muscle fatigue (MF) - Muscle weakness (MW) - Exercise intolerance (EI)	- Heart Failure (HF) - Diastolic dysfunction - Valvulopathy (Vp) - Pericardial effusion - Septal defects - Heart hypoplasia (HHyp) - Cardio-myopathy - Dilated Cardiomyo-pathy (DCM) - Hypertrophic Cardiomyo-pathy (HCM) - Isolated ventricular non-compactation (IVNC)
EPILEPSY			**MYOPATHY**	
- Epilepsy (Ep) - Seizures (Sz)			- Myopathy	
EYE MOVEMENT DISORDERS	**HEARING**			
- Nystagmus (Ny) - Saccadic eye movements (SEM) - Slow ocular pursuit	- Hearing impairment - Hearing Loss (HL) - Sensorineural hearing loss (SNHL)		**HYSTOLOGY**	
MOVEMENT DISORDERS			- Lipid accumulation in muscle (LAM)	
- Chorea - Dysarthria (Dy) - Dysdiado-chokinesia - Dysmetria - Dystonia - Deteriorated ambulation (DAmb) - Gait instability (GI) - Impaired Handwriting (IH) - Muscle stiffness (MS) - Myoclonus (My) - Opisthotonos - Tremor (Tr) - Spams - Pyramidal syndrome - Spasticity (Sp)	**EYES**	**SIGNS OF RENAL DISEASE**		
	- Astigmatism - Hypermetropia - Myopia - Cataracts - Delayed visual maturation - Optic Nerve Atrophy (OA) - Retinitis Pigmentosa (RP) - Retinopathy (Rp) - Rod-Cone dysfunction - Visual aureas - Visual dysfunction - Exotropia - Strabismus - Non-visual pursuit (nVP) - Ptosis (Pt)	- Hematuria - Proteinuria - Noctural enuresis - Polyuria - Polidypsia		
MOVEMENT DISORDERS				**ARRHYTHMIA**
- Chorea - Dysarthria (Dy) - Dysdiadochokinesia - Dysmetria - Dystonia - Deteriorated ambulation (DAmb) - Gait instability (GI) - Impaired Handwriting (IH) - Muscle stiffness (MS) - Myoclonus (My) - Opisthotonos - Tremor (Tr) - Spams - Pyramidal syndrome - Spasticity (Sp)		**ALTERED MORPHOLOGY**		- Bradycardia - Tachycardia
		- Collapsing focal segmental glomerulo-sclerosis (cFSGS) - Focal segmental glomerulo-sclerosis (FSGS) - Dysplastic kidneys - Enlarged kidneys - Medullary nephron-calcinosis (MNC) - Renal cysts		
STRUCTURAL LESIONS				
- Basal ganglia lessions (BGL) - Cerebellar atrophy (CAt) - Cerebellar hypoplasia (CHyp) - Cerebral atrophy - Cerebral Hypoplasia - Leigh-like Syndrome (LS) - Multifocal global ischemic events (MGIE) - Stroke-like lessions (SLL) - Thalamic hypoplasia (THyp)				
ASPECIFIC SIGNS				
- Headaches - Hypotonia (Ht) - Migraine				
DISEASES/CONDITIONS				
- Autosomal recessive cerebellar ataxia 2 (ARCA2) - Cerebral palsy - Encephalopathy				

Table 1.2. Other clinical manifestations in primary CoQ_{10} deficiency and abbreviations.

Affected tissue, organ or system							
CIRCULATORY DEFECTS	**METABOLIC DISORDERS**	**RESPIRATORY SIGNS**	**THYROID DEFECTS**	**LIVER DEFECTS**	**DEVELOPMENT/ MALFORMATION**	**IMMUNE SYSTEM DYSFUNCTION**	**ASPECIFIC SIGNS**
- Cyanosis - Hypertension (HT) - Hypotension - Livedo Reticularis (LR) - Circulatory collapse - Edema	- Diabetes Mellitus (DM) - Obesity - Hypercholesterolemia	- Respiratory distress (RD) - Neonatal Pneumonia - Respiratory failure (RF) - Apnea - Chronic Lung Disease (CLD) - Recurrent Respiratory infections - Lung Hypoplasia (LHyp) - Dyspnea	- Goiter - Hypothyroidism	- Cholestatic Liver -Hepatomegaly - Hepatosteatosis - Liver failure (LF) - Reduced hematopoiesis in liver	- Dysmorphic features - Hypospadias - Oligohydramnios	- Lupus-like symptoms - Crohn's Disease (CD) - Recurrent Otitis	- Splenomegaly - Coma

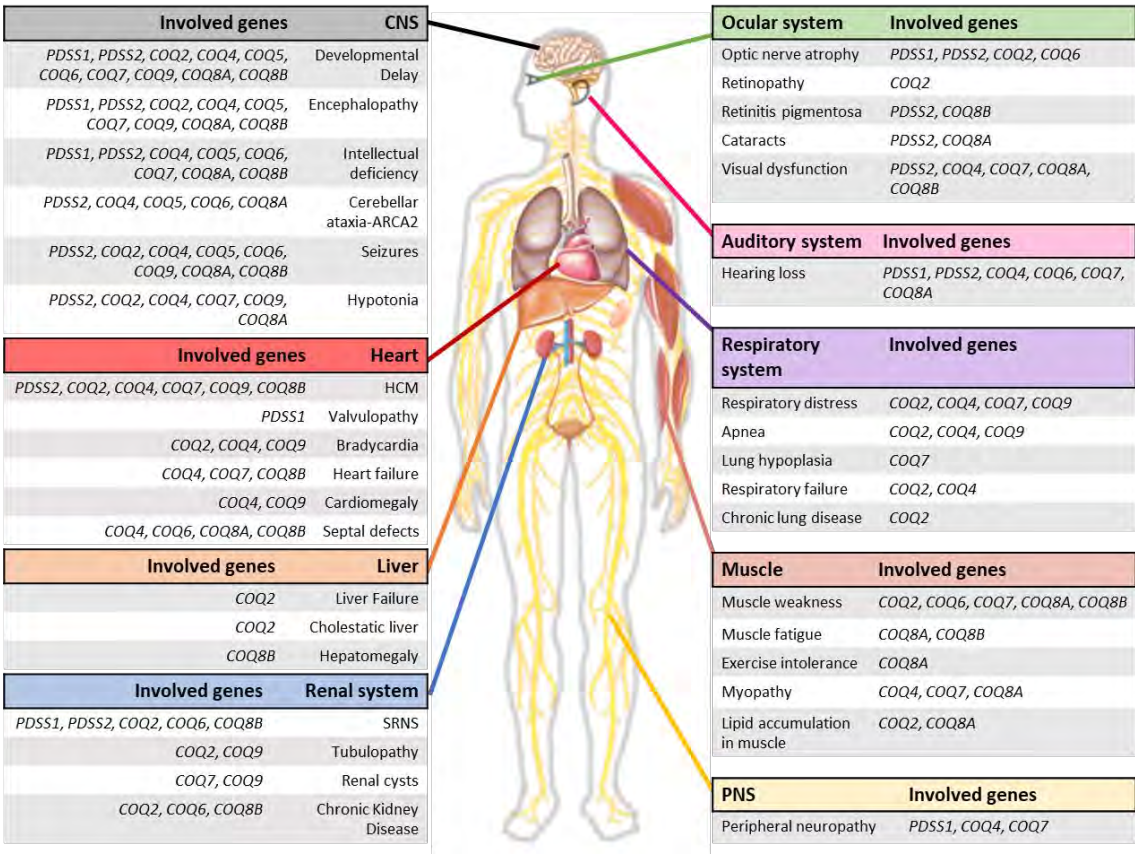

Figure 1.1. Organs and systems involved in primary CoQ_{10} deficiencies.
Organs and systems affected in individuals with primary CoQ_{10} deficiency, associating specific clinical manifestations with the genes involved in each one. For abbreviations refer to Tables 1.1 and 1.2. For frequency of each symptom linked to a specific gene refer to Table 1.3. (Adapted from Alcázar-Fabra et al., 2018 [112]).

Biochemical findings in primary CoQ_{10} deficiency patients

Primary CoQ_{10} deficiency patients can show a high concentration of lactate, pyruvate, growth differentiation factor-15 (GDF-15) and fibroblast growth factor-21 (FGF-21) in plasma or serum[259]. CoQ_{10} levels in skeletal muscle biopsies might be reduced, as well as the enzymatic activities of complex I+III and/or II+III [260]. Biochemically, CoQ_{10} deficiency can also be detected in cultured fibroblast which, together with skeletal muscle, are the preferred diagnosis tissues [261]. However, sometimes fibroblasts do not show reduction while muscle does [261] and vice versa. CoQ_{10} levels can also be measured on white blood cells (WBC), but it has been shown WBC CoQ_{10} levels alone are not reliable to diagnose primary CoQ_{10} deficiency in the setting of nephrotic syndrome [262]. There are concerns about CoQ_{10} plasma measurements for diagnosis since it seems to be influenced by the amount of plasma lipoproteins (carriers of CoQ in circulation) and the dietary intake. Recently, urine CoQ_{10} measurement as a non-invasive approach has been proposed [263] but further research needs to be done to establish this specimen for CoQ_{10} deficiency diagnosis in the clinical setting.

It is important to note that biochemical analysis is unable to distinguish between primary and secondary CoQ_{10} deficiencies [260]. Of note, *de novo* synthesis can also be measured by radioactive precursor incorporation in fibroblasts [177,264], which is especially useful to discriminate between primary and secondary deficiencies.

Pathogenesis in primary CoQ_{10} deficiency

The pathogenesis of primary CoQ_{10} deficiency is far from being simple, and our understanding is still scarce. The reduced OXPHOS activity and an increase of ROS production are certainly crucial factors. However, the wide spectrum of CoQ functions, the unclear roles of some *COQ* gene products and the considerable phenotypic variability, suggest that other mechanisms contribute to the pathogenesis of the disease. Some of the proposed pathogenic mechanism are described below:

i. In cultured cells it has been found that, severe CoQ deficiencies lead to great defects in energy production with no major increase in oxidative stress. In contrast, mild CoQ defects cause a significant increase in ROS production without affecting ATP production, but yielding increased cell death levels [265].

ii. CoQ is required for the biosynthesis of pyrimidine nucleotides since it is an essential co-factor for the dihydroorotate dehydrogenase (DHODH)[123]. *De novo* pyrimidine synthesis is impaired in CoQ_{10} deficiency, further contributing to the development of the disease [266].

iii. CoQ is also an electron acceptor of the sulphide-quinone oxidoreductase (SQOR)[130] during hydrogen sulfide (H_2S) detoxification. Sulphide oxidation pathway has been described to be tissue-specifically defective in primary CoQ_{10} deficiency, leading to an accumulation of H_2S, and thus, an alteration of protein S-sulphydrilation promoting changes in vasorelaxation, inflammation and ROS production [131–133,267–269].

iv. CoQ_{10} deficiency cells also show increased mitophagy, being proposed as a protective mechanism in disease pathogenesis [270], although other authors defined it as detrimental [271].

v. CoQ deficiency has also been linked to development of insulin resistance in human and mouse adipocytes, as a result of increased ROS production via complex II [272].

vi. The disparity on the age of onset and tissues affected, and the specificity of some symptoms associated to certain genes, suggest that *COQ* genes may be involved in other processes and the molecular mechanism of the disease would also be dependent on these yet unknown functions.

Genotype-phenotype correlations in primary CoQ_{10} deficiency

Genotype-phenotype correlations are arduous to establish in this kind of rare diseases, for which the number of diagnosed patients is very low and the complexity of the clinical manifestations hinders the task.

COQ8A and *COQ8B* have the highest number of families with pathogenic variants reported. In the case of *COQ8A* some studies have tried to find clues about genotype-phenotype correlations in this condition with no clear conclusions [273–275]. Some mutations (like c.895C>T, p.Arg299Trp) produced a disease with varied age of onset and severity, while patients harbouring other pathogenic variants (such as c.1042C>T,

p.Arg348Ter) presented similar age of onset and severity of the disease [274]. Multisystemic involvement beyond ataxia was found more prevalent in missense than biallelic loss-of-function variants, for which the phenotype was more frequently found to be an isolated ataxia [275]. This would suggest a possible gain-of-function or dominant-negative mechanism for missense variants in contrast to loss-of-function variants [275]. Preliminary associations between missense variants in specific domains and specific phenotypic outcomes have been proposed. For example, missense variants in the COQ8A protein-specific KxGQ domain seem to be associated with clinical signs reflecting cortical (developmental delay and epilepsy) and pyramidal tract dysfunction [275]. In the case of *COQ8B*, residual activity of mutated versions of *COQ8B* from patients has been studied by expressing these variants in yeast, and no correlations between residual activity of CoQ biosynthesis (CoQ levels) and severity of the symptoms were found [276]. Also, a *COQ8B* polymorphism (c.521A > G, p.His174Arg), present in 50% of the European population, has been found to affect the stability of the protein and could represent a risk factor for secondary CoQ_{10} deficiencies or for other complex traits[276].

For *COQ2* patients (22 families described), with a wide clinical spectrum, it has been proposed that the severity of the disease correlates with the enzymatic residual activity of the COQ2 protein and hence CoQ levels, as shown by expressing mutant proteins in yeast [277]. To date, no clear correlations have been observed for *COQ6* and *COQ4* patients.

Only a few families with mutations in *PDSS1*, *PDSS2*, *COQ5*, *COQ7* or *COQ9* have been described in the literature, being very hard to establish any association. Studies in two different patients' fibroblasts with *COQ7* pathological variants showed that there seems to be a correlation between the residual levels of CoQ_{10} and COQ7 protein, and the severity of the disease. The fibroblasts from the patient with the most severe phenotype showed a drastic CoQ_{10} deficiency [239], while the patient with the milder phenotype had only a 30% decrease in CoQ levels in skin fibroblasts [238]. In the case of *COQ9*, studies in two different knock-in mouse models [278,279] suggested that the degree of stability and residual stability of the CoQ complex is crucial for determining the disease severity, being the diseases less severe when the complex is more stable.

Diagnosis of primary CoQ_{10} deficiency

The diagnosis of primary CoQ_{10} deficiency is established with the identification of biallelic pathogenic variants in any of the genes coding for one of the proteins directly involved in CoQ_{10} biosynthesis [255]. Genome or specific gene sequencing is performed when there is suspicion of mitochondrial disease. Typically, it is suspected by the conjunction of a particular and compatible clinical picture of mitochondrial disease together with the laboratory findings described above (decreased levels of CoQ_{10} or reduced combined activities of complex I+III and II+III in mitochondria of skeletal muscle of patients). Biochemical analysis alone is not a definitive diagnosis. Only a genetic test (using NGS approaches, either genes panels or WES/WGS) will definitively determine the molecular diagnosis of these pathologies [255]. It should bear in mind, that for each new potentially pathogenic variant of the *COQ* genes that is identified by NGS, a functional validation is necessary.

Management of primary CoQ_{10} deficiency patients

Considering the wide clinical spectrum of this condition, any individual with a diagnosis of primary CoQ_{10} deficiency should be assessed, in order to establish the severity of the disease. Importantly, a genetic consultation is recommended for other family members and for recurrence risk of patient's parents. Based on the genetic defect identified in the patient, a specific follow-up should be programmed [112].

Being CNS manifestations very frequent, every patient with a diagnosis of CoQ_{10} deficiency should undergo periodical neurological examinations, even if normal at diagnosis. Evaluation should include an electroencephalogram (EEG) analysis and a brain magnetic resonance imaging (MRI). Also, peripheral nervous system should be assessed for the possible presence of peripheral neuropathy in patients with *PDSS1* and *COQ7* mutations.

Patients with mutations in *PDSS1*, *PDSS2*, *COQ2*, *COQ4*, *COQ6*, *COQ7*, *COQ8A* and *COQ8B* may have eye involvement due to optic atrophy (OA), retinopathy (Rp), retinitis pigmentosa (RP) and even cataracts [112]. They should, therefore, be screened at diagnosis and during the follow-up. Audiometry is necessary in *COQ6* patients who almost invariably manifest SRNS, but should also be performed in patients with mutations in

PDSS1, *PDSS2*, *COQ4*, *COQ7* and *COQ8A* who may sometimes manifest this phenotype [112].

Individuals harbouring mutations in *PDSS1*, *PDSS2*, *COQ2*, *COQ6*, and *COQ8B* may manifest renal involvement with SRNS, whose onset may vary from early childhood to adolescence. Tubulopathy has been reported rarely. These patients thus need to undergo periodical renal function tests with urine analysis for proteinuria and nephrological evaluations for the risk of evolving to ESRD [112].

A cardiologist examination with echocardiogram should be performed in patients with *COQ4, PDSS2, COQ2, COQ7* and *COQ9* mutations (who may present with a severe early-onset cardiomyopathy) and should also be considered in individuals with mutations in *PDSS1, COQ6, COQ8A* and *COQ8B* to exclude the presence of a valvulopathy or septal defects [112].

Treatment of primary CoQ_{10} deficiency

Exogenous CoQ_{10} supplementation is the only therapeutic option currently available for CoQ_{10} deficiency. In general, patients respond quite well to CoQ_{10} supplementation, but this is not always the case. Barriers for tissues CoQ_{10} delivery have been found due to its high molecular weight and poor aqueous solubility, but at high doses, dietary supplementation increases CoQ_{10} levels in all tissues, including heart and brain, especially with certain formulations [280,281]. It also increases in circulating low-density lipoproteins, where it functions as an efficient antioxidant together with α-tocopherol [282,283]. Recently, the EMA approved ubiquinol as an orphan drug for the treatment of primary CoQ_{10} deficiency [79].

CoQ_{10} supplementation at high doses has been demonstrated to be effective for the treatment of both primary and secondary CoQ deficiencies [284]. It is crucial to start the supplementation as soon as possible to get favourable outcomes and to limit irreversible damage in critical tissues such as the kidney or the CNS [255]. Different doses of CoQ_{10} have been employed for the treatment of primary CoQ_{10} deficiencies, ranging from 5 mg/kg/day [285] to 30-50 mg/kg/day for both adults and children [286]. In mouse models of this condition even higher doses (up to 200 mg/kg/day) have been used [287]. With regards to safety, the highest dose for CoQ_{10} supplementation is 1200 mg/day according to well-

designed randomized, controlled human trials, although doses as high as 3000 mg/day have been used in shorter clinical trials [79,288].

Except for *COQ8A* patients, most individuals with primary forms show a good response to CoQ_{10} treatment, which is usually evident after 10-20 days [286]. Different formulations of CoQ are now available, both in the oxidized and the reduced forms, although most of the data available have been obtained in patients treated with ubiquinone. 118 cases of the 276 reported ones (43%) were treated with CoQ_{10} supplementation. The outcome of the treatment will be discussed in the next sections.

Alternatively to CoQ_{10} supplementation, some 4-HB analogues have been proposed as potential bypass molecules with higher bioavailability than CoQ [289]. These molecules provide the defective chemical group and can reactivate endogenous CoQ biosynthesis. They have only been tested in yeast, mammalian cell cultures and mouse models of primary CoQ_{10} deficiency, but have still not been used for patient's treatment, as it will be discussed in Chapter 2 (section 2.1.1).

1.1.2. Secondary CoQ_{10} deficiencies

CoQ_{10} deficiency can also occur in conditions not directly linked to mutations in the *COQ* genes. These secondary deficiencies are more common than the primary ones [290,291], and might exacerbate the phenotype of the conditions to which they are associated. They can be related to oxidative phosphorylation (OXPHOS) defects, other impaired non-OXPHOS mitochondrial processes, or even to a dysfunction in non-mitochondrial functions [291].

How these defects lead to CoQ_{10} deficiency is still unknown, and multiple and very diverse factors are thought to contribute. Some of these factors are the diverse biological functions and metabolic pathways in which CoQ is involved inside and outside the mitochondria, and the different mechanisms that can modulate CoQ levels by regulating CoQ biosynthesis or CoQ turnover [120,291,292]. Due to the high diversity of disorders that can be accompanied by secondary CoQ_{10} deficiency, genotype-phenotype correlations are difficult to establish, and will primarily depend on the nature of the condition and the mutated gene.

Disorders associated to secondary CoQ_{10} deficiency

The clinical spectrum of secondary CoQ_{10} deficiencies is highly dependent on the pathology they derive from. Muscular manifestations in these disorders are myopathies with muscular weakness, hypotonia, exercise intolerance or myoglobinuria. It is clear that isolated mitochondrial myopathies are frequently associated with CoQ_{10} secondary deficiencies and not with primary deficiencies [253,254]. CNS can be also affected in secondary CoQ_{10} deficiencies, presenting ataxia with neurological decline [225,290]. However, there is also a high variability of secondary CoQ_{10} deficiency presence among different patients suffering from the same disorders. This would suggest different susceptibility to the development of CoQ_{10} deficiencies among different individuals. Genetic factors, such as additive hypomorphic mutations or specific polymorphisms, have been proposed to be involved [253,276,290,291].

Amongst OXPHOS pathologies, secondary CoQ_{10} deficiency was found more common in mtDNA depletion syndromes due to nuclear DNA mutations (e.g. *POLG*, *MPV17*, *SUCLA2* or *FBXL4* [291,293]. Moreover, comparative omic studies performed in mouse models of OXPHOS dysfunction caused by nuclear-encoded essential factors for mtDNA maintenance (*Twinkle*, *Tfam*, *Polrmt*, *Lrpprc* and *Mterf4*) showed a general downregulation of CoQ_9 biosynthesis proteins, leading to a secondary CoQ_9 deficiency [294]. Other examples of nuclear genes that when mutated, lead to OXPHOS defects with secondary CoQ_{10} deficiency are: complex III assembly factor *BSC1L* [295]; complex I subunit *NDUFS4* [296,297]; or *EARS2*, which encodes for the mitochondrial aminoacyl-tRNA synthetase specific for glutamate [298,299]. Low CoQ_{10} levels have also been observed in OXPHOS diseases due to point mutations in mtDNA-encoded genes (e.g. *MT-TL1* or *MT-TK*) [253,291,300]. Other very variable non-OXPHOS diseases may display secondary CoQ_{10} deficiency as well, but the mechanisms involved are still elusive [291]:

i. Mutations in *ETFDH*-encoded flavoprotein-ubiquinone oxidoreductase, and in the electron transfer flavoprotein (*ETFA* and *ETFB*), cause multiple acyl-CoA dehydrogenation deficiency (MADD) associated with decreased levels of CoQ_{10} [301,302]. These enzymes are essential for mitochondrial fatty acid β-oxidation, receiving electrons from acyl-CoA and transferring them to CoQ [120]. It should be

noted that not all MADD patients have CoQ_{10} deficiency [303,304], suggesting difference in susceptibility among different patients.

ii. Mutations in *APTX* gene, coding for the single-stranded DNA repair aprataxin, cause ataxia with ocular motor apraxia [305,306], with CoQ deficiency in muscle and fibroblasts [291,307].

iii. Also, it has been shown that patients with Friedrich ataxia can show a decrease of CoQ content in skeletal muscle as a consequence of the mutation in *FXN* gene, which encodes for frataxin, a protein regulating iron transport into mitochondria[291].

iv. Mutations in *ANO10* gene, coding for a member of the anoctamin family of transmembrane proteins with calcium-activated chloride channel activities, cause spinocerebellar ataxia associated to CoQ_{10} deficiency in skeletal muscle, plasma and cerebrospinal fluid [308–310].

v. Another channelopathy with mutations in *SCN2A*-encoded voltage gated sodium channel (Nav1.1) was found to present CoQ_{10} deficiency in muscle, suggesting that CoQ might have a role in CoQ in calcium signalling [291].

vi. A patient with GLUT1 transporter deficiency caused by a heterozygous mutation in the *SLC2A1* gene showed reduced CoQ_{10} levels [311]. However, this is not a common feature in GLUT1 deficiency syndrome [312], indicating that possibly other factors would be involved in the CoQ_{10} defect in this patient.

vii. Patients with mutations in NPC1, with Niemann-Pick C disease presented a reduction of CoQ_{10} biosynthesis probably because of the characteristic accumulation of cholesterol, which may down-regulate HMG-CoA reductase and, consequently, reduce mevalonate and CoQ synthesis [291,301,313]. Something similar was observed in fibroblasts from familial hypercholesterolemia patients, in which the mevalonate pathway was dysregulated, resulting in increased cholesterol levels and CoQ_{10} deficiency [314].

Mechanisms of secondary CoQ_{10} deficiency

The mechanisms underlying CoQ_{10} secondary defects remain largely unknown, but several explanations have been proposed:

i. The rate of CoQ degradation could be increased rate as response to other dysfunctional processes, like a non-functional respiratory chain [290,291].

ii. CoQ biosynthesis pathway could be dysregulated by an interference with its signalling regulatory pathways [290,291]. This could occur because of the malfunctioning of components involved in these signals, or because the signalling pathways activated for a response to certain defect may intrinsically lead to a down-regulation of CoQ synthesis.

iii. Severe mitochondrial deficiencies would cause secondary CoQ deficiency by interfering with the import and formation of mature forms of the COQ proteins in the mitochondria [315].

iv. Certain pathologic environments could lead to a reduction of the stability of the CoQ biosynthetic complex. In this context, a recent study in yeast described the localization of the Coq proteins in specific foci in the IMM, named CoQ domains [1]. The definition of the CoQ domains implies that the spatial localization dimension is essential for CoQ complex formation. These CoQ domains, in yeast, are spatially and functionally related to ERMES (endoplasmic reticulum-mitochondria encounter structure) complex [1,2] and the loss of ERMES structure impairs respiration through reduction of CoQ levels in mitochondria. This could be a mechanism of secondary CoQ deficiency, since many mitochondrial disorders produce a disturbance in IMM structure, which could lead to an impairment in CoQ domain formation and CoQ biosynthesis [316]. Mitochondrial structure disturbances are also observed in aged mitochondria. It has not been demonstrated yet that CoQ domains in mammals are related to ER-mitochondrial contacts.

v. A general deterioration of mitochondrial function could imply CoQ reduction as well [290,291].

Mouse models with secondary CoQ_9 deficiency

The study of some secondary CoQ_9 deficiency mouse models has provided evidence for the understanding of these deficiencies. One example is *Parl*$^{-/-}$ mouse model. *PARL* (coding for Presenilin Associated Rhomboid Like protein) is an IMM intramembrane protease from the rhomboid family [317]. *Parl*$^{-/-}$ mouse model shows a phenotype similar to Leigh syndrome, with a severe complex III defect caused by the disappearance of mature Ttc19, a factor required for complex III stability [318]. Moreover, *Parl*$^{-/-}$ brain mitochondria show a significant decrease of CoQ biosynthesis associated with a reduction of Coq4 and other Coq peptides, and swollen mitochondria with abnormal cristae [319]. Another example is *Mfn2*$^{-/-}$ mouse model. MFN1 and MFN2 are mitochondrial outer membrane proteins that mediate outer membrane fusion and thus, are important for mitochondrial network dynamics. Studies in *Mfn2*$^{-/-}$ mouse model suggested that MNF2 protein is required for maintaining CoQ biosynthesis in mice [320].

1.2. Results and discussion

Primary CoQ_{10} deficiency patients manifest a broad spectrum of clinical phenotypes, affecting different organs, tissues and systems (Figure 1.1).

Currently, over 275 patients from 180 families have been reported to have a primary CoQ deficiency with mutations in one of the *COQ* genes (Table 1.3). Pathogenic variants of *PDSS1, PDSS2, COQ2, COQ4, COQ5, COQ6, COQ7, COQ9, COQ8A* and *COQ8B* have been associated to primary CoQ deficiency in the literature. In this section, we have comprehensively reviewed all primary CoQ_{10} deficiency published cases, in order to provide an overview of the different patterns of the age of onset, clinical presentation and course of the disease, depending on the defective gene. The patterns of clinical presentation and evolution have been evaluated as a whole, for each *COQ* gene involved in primary CoQ_{10} deficiency. This work has been submitted and is now under review[321].

It is important to note that the evaluation of the frequency of some specific manifestations is probably being underestimated because some features are not reported homogeneously among the different published reports. Also, the number of primary CoQ_{10} deficiency patients reported is small, and the number of patients with

pathological variants in the different genes varies widely. This number is especially reduced for *PDSS1*, *PDSS2*, *COQ5*, *COQ7* and *COQ9* genes, so higher frequencies found for some symptoms in these cases can be due to the sampling effect.

1.2.1. General clinical symptoms associated to primary CoQ_{10} deficiency

Primary CoQ_{10} deficiency patients manifest a wide range of clinical phenotypes, affecting several organs, tissues and systems in a highly variable way (Figures 1.1, 1.2, 1.3). The systems mainly affected are the central and peripheral nervous system, kidney, heart and skeletal muscle (Figure 1.2 and Table 1.3). A complete picture of the frequency of all the described symptoms can help to better understand any potential trend in the development of the disease depending on the affected gene.

To make these analyses of frequency openly available to the community, we have created a web-based platform that will be periodically updated with the new literature: https://coenzymeQbiology.github.io/clinic-CoQ-deficiency. Heatmap representation of the frequency of symptoms will give a visual and convenient overview of the disease according to the affected gene. The continuous update of the platform will permit a quasi-real-time overview of the research in the field. With this resource, we aim to contribute not only to a better understanding of the genotype-phenotype correlations of the disease, but also to a more efficient diagnosis of primary CoQ deficiencies.

Table 1.3. Clinical manifestations in primary CoQ_{10} deficiency.

Gene	F	P	Sex	Age		Clinical manifestations						LA	CoQ deficiency	References
				Onset	Last examination (*death)	CNS	PNS/ sensory organs	Kidney	Muscle	Heart	Other			
PDSS1	2	3	F (2), M (1)	Birth (1), 1-2yo (2)	1.5yo* (1), 14-22yo (2)	Encephalopathy (2), ID (2), DD (1)	PNSN (2), OA (2), SNHL (2)	SRNS and ESRD (1)		Vp (2)	LR (2), Obesity (2), HT (1)	(3)	F (2), WBC (1)	241,322
PDSS2	5	7	F (2), M (5)	<1yo (6), 2yo (1)	8mo* (2), 8yo* (1), 8-12yo (2), NK (2)	ARCA2 (3), ID (3), Ht (2), LS (1), Sz (1) Sp (1), Dystonia (1), Ny (1), Pyramidal syndrome (1), Cerebral palsy (1), DD (1), Encephalopathy (1)	SNHL (4), RP (2), Myopia (2), Visual Dysfunction (2), OA (1), Cataract (1)	SRNS (7), ESRD (2)		HCM (2)	Edema (2), Neonatal Pneumonia (1), HT (1)	(2)	M (1), F (1)	245,285,323–325
COQ5	1	3		Early childhood (3)	14-22yo (3)	ID (3), ARCA2 (3), CAt (3), Dy (3), Ny (3), My (2), Sz (2), DD (2), SEM (1), Tr (1), Sp (1)							WBC (3), M (1)	326
COQ7	3	3	F (1), M (2)	Birth (2), 1yo (1)	1yo*(1), 6-9yo (2)	Ht (3), DD (3) BGL (1), Cerebral atrophy (1), Encephalopathy (1), ID (1), Sp (1), Spasms (1)	SNHL (3), PNSN (2), Visual dysfunction (2), nVP (1), Pt (1)	dysplastic kidneys (1), KD (1), renal cysts (1)	MW (3), Myopathy (1)	HCM (2), HF (1)	RD (2), Oligohydramnios (2), HT (1), Dysmorphic features (1), LHyp (1)	(3)	M (1), F (3)	238–240
COQ9	4	7	F (2), M (5)	Birth (6), 9mo (1)	Birth*(2), 12ho*(1), 3do*(1), 18do* (1), 2yo* (1), 3yo (1)	DD (6), Encephalopathy (3), Sz (3), Ht (2), LS (2), CAt (1), CHyp (1), Dystonia (1), MGIE (1), MS (1), BGL (1), Opisthotonus (1)		Renal cysts (2), Tp (1), Enlarged kidneys (1)		Bradycardia (2), Cardio-megaly (1), HCM (1), IVNC (1)	Oligohydramnios (3), RD (3), Apnea (2), Cyanosis (1), Dysmorphic features (1), Reduced hematopoiesis in liver (1), HT (1)	(5)	M (1), F (3)	246–248,256,327

Table 1.3. Clinical manifestations in primary CoQ_{10} deficiency (continued).

Gene	F	P	Sex	Age		Clinical manifestations						LA	CoQ deficiency	References
				Onset	Last examination (*death)	CNS	PNS/ sensory organs	Kidney	Muscle	Heart	Other			
COQ2	22	30	F (15), M (15)	Birth (11), <1yo (10), 1yo-3yo (5), 10yo (1), 16yo-18yo (2), NK (1)	<1mo* (3), 1mo*-1yo* (9), 1yo*-2yo*(2), 1-6yo (8), 12yo (1), 23-37yo (2), NK (5)	Sz (12), Encephalopathy (9), Ht (6), Ny (3) DD (2), Dystonia (2), My (2), SLL (2), BGL (1), CAt (1), MS (1), Tr (1)	Rp (2), OA (1), nVP (1)	SRNS (26), ESRD (10), KD (2), CKD (1), Only proteinuria (1), Tp (1)	LAM (1), MW (1)	HCM (3), Bradycardia (1)	Edema (11), DM (6), RF (5), Oligohydramnios (4), LF (3), Apnea (2), Hypercholesterolemia (2), RD (2), Cholestatic Liver (1), CLD (1), HT (1), Respiratory infections (1)	(12)	M (5), F (3)	232,242,244,245,249,257,262,277,328–334
COQ4	26	35	F (20), M (14), NK (1)	Birth (19), <1yo (11), 4yo (1), 8-9yo (3), NK (1)	<4do* (7), 1mo-3yo* (12), 7yo* (1), 8yo (1), 14-18yo (3), 27-28yo (2), NK (1)	Sz (24), Ht (19), DD (18), Encephalopathy (11), CHyp (10), Sp (8), CAt (8), Cerebral atrophy (6), DAmb (6), Dystonia (6), ID (6), BGL (5), ARCA2 (4), Dy (2), Dysdiadochokinesia (2), Dysmetria (2), LS (2), SLL (2), Spasms (2), Tr (2), My (1), Cerebral hypoplasia (1), Ny (1), SEM (1), THyp (1)	Visual dysfuntion (6), Hearing impairment (2), Delayed visual maturation (1), HL (1), PNSN (1), Demyelinating motor neuropathy (1)		Myopathy (2)	HCM (13), Bradycardia (5), Cardiomegaly (3), HF (2), Tachycardia (2), Diastolic dysfunction (1), HHyp (1), Pericardial effusion (1), Septal defects (1)	RD (14), Apnea (9) RF (5), Cyanosis (2), Hypotension (2), Coma (1), Circulatory collapse (1), Dysmorphic features (1), Oligohydramnios (1), Recurrent Respiratory infections (1)	(24)	M (7), F (10)	250–252,335–341
COQ6	22	30[1]	F (8) M (10) NK (12)	2mo-<1yo (8), 1-2yo (7), 3-4yo (7), 6-10yo (4), NK (4)	5-6yo* (2), 17yo* (1), NK* (2), 0.5-1.5yo (3), 2-10yo (11), 11-17yo (3), 27yo (1), NK (7)	DD (3), Sz (2) ARCA2 (1), ID (1), Ny (1)	SNHL (18), OA (1), Exotropia (1), Pt (1)	SRNS (26), ESRD (16), CKD (1)	MW (2)	Cardiovascular abnormality (1), Septal defects (1)	Edema (2), Dysmorphic features (1), Hypercholesterolemia (1)			231–236,245,258,342,343

1. There are 3 COQ6 patients without any information.

Table 1.3. Clinical manifestations in primary CoQ_{10} deficiency (continued).

Gene	F	P	Sex	Age		Clinical manifestations						LA	CoQ deficiency	References
				Onset	Last examination (*death)	CNS	PNS/ sensory organs	Kidney	Muscle	Heart	Other			
COQ8A	55	77	F (41), M (33), NK (3)	1-4yo (35), 5-11yo (19), 13-15yo (4), 18-20yo (4), 25-27yo (3), NK (12)	22yo*(1), 26yo*(1), 3-11yo (14), 13-25yo (22), 26-54yo (32), 81yo (1), NK (6)	ARCA2 (70), CAt (62), ID (35), Tr (33), Dy (27), Dysmetria (21), Sz (25), GI (16), Dystonia (14), My (14), SEM (14), DD (13), IH (11), Ny (9), Dysdiadochokinesia (8), Sp (8), Ht (7), SLL (6), Migraine (5), Depression (3), Chorea (2), CHyp (2), Encephalopathy (2), Pyramidal syndrome (1), Slow ocular pursuit (1)	Strabismus (4), Pt (3), SNHL (2), Visual dysfunction (1), Cataracts (1), Visual aureas (1), Rod-Cone dysfunction (1)		EI (14), MW (13), MF (3), LAM (3), Myopathy (1)	Cardio-myopathy (1), Septal defects (1)	Dysmorphic features (1), Hepato-steatosis (1), Hypercholes-terolemia (1), Recurrent Respiratory infections (1)	(7)	M (15), F (4), WBC (1)	227,228,273,274,344–361
COQ8B	41	79	F (32), M (31), NK (16)	<1yo-10yo (32) 11yo-21yo (39) 23-32yo (7) NK (1)	13-15yo* (2) 25yo* (1) 29yo* (1) 1-9yo (6) 10-20yo (54) 21-39yo (14) NK (1)	Sz (6), ID (4), Headaches (4), Autism (1), DD (1), Encephalopathy (1)	Hypermetropia, astigmatism (2), Visual dysfunction (1), RP (1)	SRNS (65), ESRD (47), CKD (18), Only proteinuria (8), Hematuria (8), MNC (7), Enlarged kidneys (1), KD (1), Nocturnal enuresis (2), Polidypsia (1), Polyuria (1)	MF (1), MW (1)	HCM (2), Septal defects (2), DCM (1), Cardiomyop athy (1), HF (1), Pericardial effusion (1)	Edema (16), HT (11), Goiter (2), CD (1), Dysplastic ears (1), Dyspnea (1), Hepatomegaly (1), Hypercholesterolemi a (1), Hypospadias (1), Hypothyroidism (1), Lupus-like symptoms (1), Recurrent otitis (1), Splenomegaly (1)		F (5)	229,243,276,362–369

Numbers between brackets indicate the number of patients with the specific manifestation. * These patients died at the indicated age.

Abbreviations: ho: hours old; do: days old; wo: weeks old; mo: months old; yo: years old; NK: not known; F: Number of Families; P: Number of Patients; LA: Lactic Acidosis; CoQ deficiency (WBC: White Blood Cells, F: Fibroblasts, M: Muscle). For Clinical Manifestations abbreviations, refer to Tables 1.1 and 1.2.

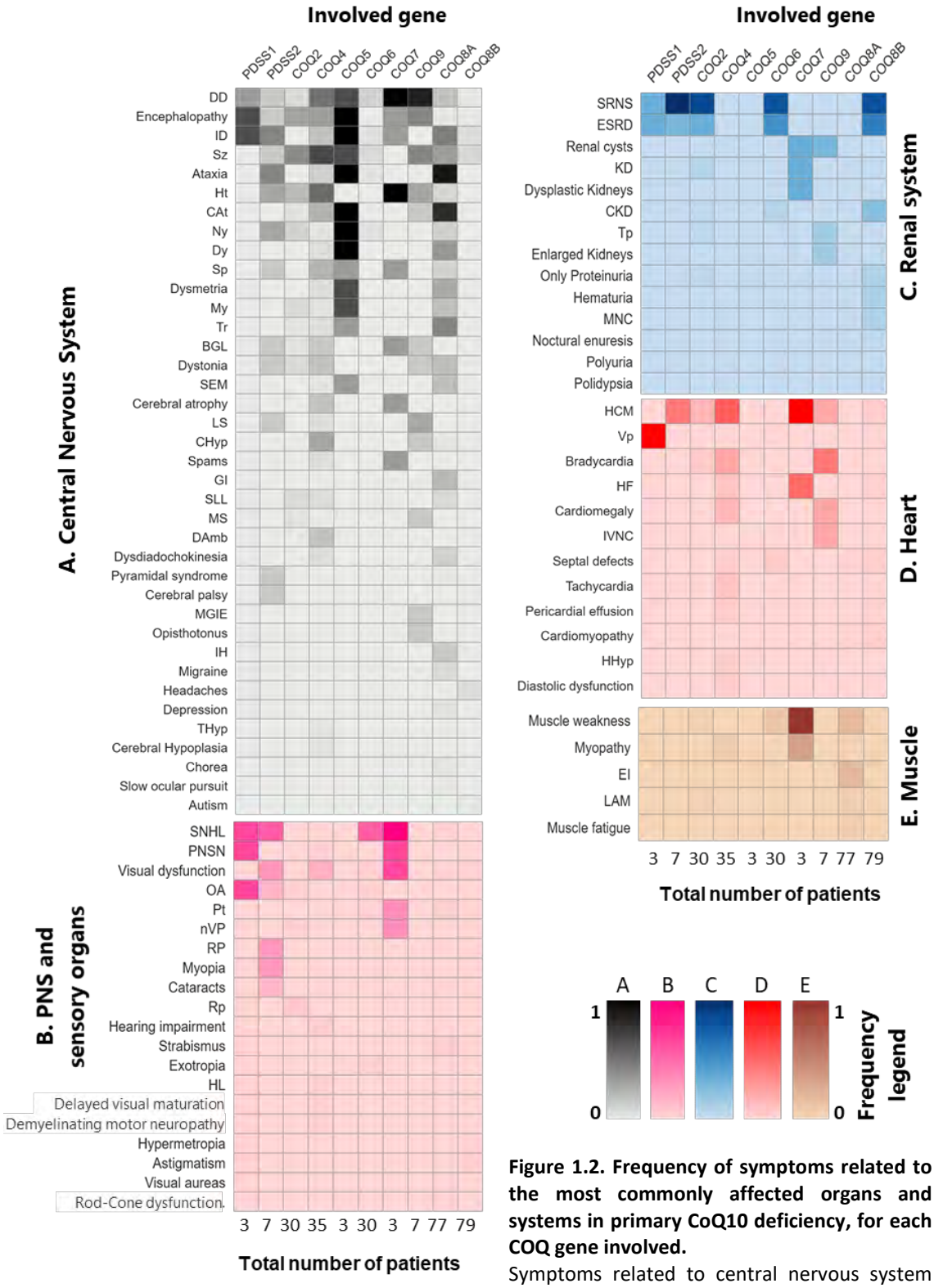

Figure 1.2. Frequency of symptoms related to the most commonly affected organs and systems in primary CoQ10 deficiency, for each COQ gene involved.

Symptoms related to central nervous system (CNS) (A), peripheral nervous system (PNS) and sensory organs (B), renal system (C), heart (D) and muscle (E) are sorted in a decreasing order of frequencies. Total number of patients for each gene is indicated at the bottom of the heatmaps. For Clinical Manifestations abbreviations, refer to Tables 1.1 and 1.2.

CNS manifestations

CNS is often affected in these patients, showing a wide range of clinical manifestations (Figure 1.2.A). These symptoms have been reported in patients with mutations in any of the described *COQ* genes, being less frequent in *COQ6* and *COQ8B* patients. The most common are the following:

i. Disorders or conditions:

The most frequently CNS-related disorders reported are encephalopathy and ARCA2 (autosomal recessive cerebellar ataxia-2, or autosomal recessive ataxia due to CoQ_{10} deficiency), but also, less frequently, cerebral palsy or sporadic multisystem atrophy (MSA).

Encephalopathy is defined as a broad spectrum of brain manifestations, often not described in detail in case reports. It has been found in patients with mutations in each of all the ten genes involved in primary CoQ_{10} deficiency. It has been mainly found in *COQ4* (11/35, 31%) [250–252,336,339–341], *COQ2* (9/30, 30%) [241,242,249,257], *COQ5* (3/3, 100%) [326] and *COQ9* (3/7, 43%) [246–248] patients. It has also been observed in some *PDSS1* (2/3, 67%) [241], *PDSS2* (1/7, 14%) [323], *COQ7* (1/3, 33%) [240], *COQ8A* (2/77, 2.6%) [273,370] and *COQ8B* (1/79, 1.3%) [364] probands.

Progressive cerebellar atrophy and ataxia, also called **ARCA2** is a neurodegenerative disorder defined by an ataxic phenotype with movement disorders, sometimes accompanied by intellectual disability (ID), epileptic seizures (Sz), tremor (Tr), dysarthria (Dy), dysmetria, dysdiadochokinesia, saccadic eye movements (SEM), dystonia or spasticity (Sp) [274,275]. It is the main phenotype in *COQ8A* patients (70/77, 91%). The only family affected by a mutation in *COQ5* up to now also showed a cerebellar ataxic phenotype similar to *COQ8A* patients (3/3, 100%) [326]. A subgroup of *COQ4* patients with childhood-onset also presents this phenotype (5/35 14%) [251,335,338]. Cerebellar ataxia has also been observed in some patients harbouring pathogenic variants of *PDSS2* (3/7, 43%) [285,325] and *COQ6* (1/30, 3%) [233] genes.

ii. Cognitive and behavioral deficits

Developmental delay is defined as a delay in reaching one or more milestones, categorised into motor, cognitive, speech, emotional, social and communication skills[371]. When there is a delay in several of these skills, it is called global DD. It has been found in patients with mutations in each of the ten genes involved in primary CoQ_{10} deficiency, mainly in *COQ4* (18/35, 51%)[250–252,336,372,373], *COQ5* (2/3, 67%) [326], *COQ7* (3/3, 100%) [238–240] and *COQ9* (6/7, 86%) [246–248,327] patients. It has also been observed in some probands with mutations in *PDSS1* (1/3, 33%) [322], *COQ8A* (13/77, 17%) [350,352,354,370], *PDSS2* (1/7, 14%) [323], *COQ6* (3/30, 10%)[231,233,258], *COQ2* (2/30, 7%) [242,334] and *COQ8B* (1/79, 1.3%) [363].

Intellectual disability (ID) is a generalized neurodevelopmental disorder characterized by significantly impaired intellectual and adaptive functioning[374]. It was found in a variable number of cases but in patients of almost all the *COQ* genes: *PDSS1* (2/3, 67%) [241], *PDSS2* (3/7, 43%) [245,285], *COQ4* (6/35, 17%)[251,335,338,341], *COQ5* (3/3, 100%)[326], *COQ6* (1/30, 3%) [231], *COQ7* (1/3, 33%)[239], *COQ8A* (35/77, 45%)[227,273,274,344–346,351,352,354–357,360,370] and *COQ8B* (4/79, 5%) [229,364,366].

Note that some patients present the disease and die in infancy, when DD and ID are difficult to assess.

iii. Epilepsy

Epilepsy and seizures have been reported mainly in *COQ4* (24/35, 69%)[250–252,336–340], *COQ2* (12/30, 40%) [232,241,242,257,332,333], *COQ5* (2/3, 67%) [326] and *COQ9* (3/7, 43%) [247,248,256] patients, generally associated with encephalopathy, but also without such association in some *COQ8A* (25/77, 32%) [227,273,274,345,350,357,360]**,** *PDSS2* (1/7, 14%) [324], *COQ6* (2/30, 7%) [233] and *COQ8B* (6/79, 8%) [364,367] patients.

iv. Hypotonia

Hypotonia (Ht) is a state of low muscle tone. It can be caused by central or peripheral nervous system, as well as by muscle involvement. This feature that has been reported mainly in *COQ4* (19/35, 54%) [251,252,336,340,341], some *COQ2* (6/30, 20%) [242,257,332,333] and in all the three published *COQ7* patients (3/3, 100%) [238–240]. Hypotonia has also been observed in several other *COQ* patients, although the exact frequency might be

especially misleading because of the low number of reported cases (*PDSS2* (2/7, 29%) [323,324], *COQ9* (2/7, 29%) [256]*).* Other groups of *COQ* patients apparently present a lower frequency of hypotonia such as *COQ8A* (7/77, 9%) [354,357,359,370].

v. Others

Other alterations of the CNS reported in the literature with variable frequency include **movement disorders** (dysarthria (Dy), dystonia, dysmetria, dysdiadochokinesia, myoclonus (My), gait instability (GI), tremor, spasticity, etc.) and **eye movement disorders** (nystagmus (Ny), saccadic eye movements (SEM), slow ocular pursuit), among others.

Brain imaging techniques revealed in some cases **structural CNS lesions** (cerebral atrophy, cerebellar atrophy (CAt), cerebellar hypoplasia (CHyp), basal ganglia lesions (BGL), stroke-like lesions (SLL), etc.) Particularly, CAt, which is a hallmark of the ARCA2 phenotype, is a relevant diagnostic feature since it was universally found at brain MRI of a large worldwide cohort of 59 COQ8A patients [275].

Peripheral nervous system and sensory organs manifestations

PNS and sensory organs manifestations have also been reported in several cases of primary deficiencies (Figure 1.2.B). **Sensorineural hearing loss** (SNHL) is the most frequent PNS phenotype in primary CoQ_{10} deficiency patients. SNHL is present in over half of the reported cases of *COQ6* (18/30, 60%) and *PDSS2* (4/7, 57%) patients [285,323,325], being in all those cases associated with SRNS [231–236]. Some probands with *PDSS1* (2/3, 67%) [241], *COQ7* (3/3, 100%) [238–240] and *COQ8A* (2/77, 2.6%) [356] pathogenic variants presented SNHL as well, which in these cases was not linked to SRNS. The PDSS1 patients that presented SNHL were two siblings that suffered peripheral neuropathy, associated with OA and early-onset SNHL [241]. All the three *COQ7* reported patients presented SNHL, and in two cases, they also showed peripheral polyneuropathy and visual dysfunction (2/3, 67%) [238–240]. **Visual dysfunction** was also reported in some *COQ4* (6/35, 17%) [250,340], *PDSS2* (2/7, 29%) [285], *COQ8A* (1/77, 1.3%) [344] and *COQ8B* (1/79, 1.3%) [364] probands. **Optic nerve atrophy** (OA) was reported in very few individuals with *PDSS1* (2/3, 67%) [241], *PDSS2* (1/7, 14%) [285], *COQ2* (1/30, 3%) [242,331,375] and COQ6 (1/30, 3%) [235] pathogenic variants. Other less frequent visual impairments such as **cataracts** [227,285], **retinopathy**

(Rp) [242,332], **retinitis pigmentosa** (RP) [285,323,364] or **delayed visual maturation** [336] have been observed in several cases of *COQ* patients.

Renal manifestations

Renal dysfunction, altered morphology and specific signs and symptoms of renal disease have also been reported in the literature. **Steroid resistant nephrotic syndrome** (SRNS) is very frequent in primary CoQ_{10} deficiency patients (Figure 1.2.C), specifically in those with pathogenic variants of *PDSS2* (7/7, 100%) [245,285,323,324], *COQ2* (26/30, 87%) [232,241,242,245,257,262,329–331,333,334,375,376], *COQ6* (26/30, 87%) [231–233,235,236,342,343,377] and *COQ8B* (65/79, 82%) [229,243,362–365,368]. Importantly, it generally starts as proteinuria and evolves to **end-stage renal disease** (ESRD) within childhood, if not treated (Figure 1.2.C).

The majority of *COQ2* patients manifested early-onset nephrotic syndrome (24/30, 80%) [241,242,245,257,262,329,330,333,334,376], and there was also one family with adolescent-onset and slow progression of the isolated renal disease (2/30, 7%) [232]. The hallmark manifestation of *COQ6* pathogenic variants is childhood-onset SNRS (26/30, 87%) [231–233,235,236,342,343,377], which in around half of the cases was associated with SNHL (17/30, 57%) [231,233,235,236]. *COQ8B* patients mainly manifested SRNS (65/79, 82%) [229,243,362–365,368] due to focal segmental glomerulosclerosis (FSGS), some of them associated with edema (16/79, 20%) [243,362–364]and hypertension (HT) (11/79, 14%) [229,364], which in the most part of the cases progressed to ESRD (47/79, 59%). All of the patients with *PDSS2* (7/7, 100%) [245,285,323,324] mutations and some of those with *PDSS1* (1/3, 33%) [322] variants also manifested SRNS.

Other less frequent renal manifestations are **CKD** (*COQ2* (1/30, 3%) [244], *COQ6* (1/30, 3%) [258], *COQ8B* (18/79, 23%)[229,362,364,366]), **renal cysts** (*COQ7* (1/3, 33%) [240], *COQ9* (2/7, 29%) [246,247]) or **tubulopathy** (*COQ2* (1/30, 3%)[249], *COQ9* (1/7, 14%) [248,327]).

Cardiac manifestations

Heart is often affected in primary CoQ_{10} deficiency (Figure 1.2.D). Arrhythmia and functional and morphological defects have been reported with variable frequency. The most commonly reported heart defect is **hypertrophic cardiomyopathy** (HCM). It is particularly frequent in *COQ4* (13/35, 37%) [250–252] and *COQ7* (2/3, 67%) [239,240] patients

but has also been reported in some *PDSS2* (2/7, 29%) [285,323], *COQ2* (3/30, 10%) [249,328,333], *COQ9* (1/7, 14%) [248,327] and *COQ8B* (2/79, 2.5%) [229,243] patients. Other morphological or functional heart defects less frequently found are **valvulopathies** (*PDSS1* (2/3, 67%) [241]), **cardiomegaly** (*COQ4* (3/35, 9%) [250,252,339], *COQ9* (1/7, 14%) [246]), **septal defects** (*COQ4* (1/35, 3%) [341], *COQ6* (1/30, 3%), *COQ8A* (1/77, 1%) [370] and *COQ8B* (2/79, 3%) [364,365]) or **heart hypoplasia** (HHyp) (*COQ4* (1/35, 3%) [251]). Also, arrhythmia (**bradycardia**) has been observed (*COQ4* (5/35, 14%) [251,252,340], *COQ9* (2/7, 29%) [246,256] and *COQ2* (1/30, 3%) [257]). In some cases, **heart failure** (HF) has been reported as a fatal outcome (*COQ4* (2/35, 5.7%) [251,252], *COQ7* (1/3, 33%) [240] and *COQ8B* (1/79, 1.3%) [364]).

Muscle manifestations

Muscle is less commonly affected in these patients (Figure 1.2.E). **Myopathy** has not been described isolated, but in patients with a broader multisystemic phenotype (*COQ4* (2/35, 6%) [250,341], *COQ7* (1/3, 33%) [240], *COQ8A* (1/77, 1%) [358]). Other muscular manifestations include **exercise intolerance** (EI) (*COQ8A* (14/77, 18%) [344,354,356,357]), **muscle weakness** (MW) (*COQ2* (1/30, 3%) [242], *COQ6* (2/30, 7%) [235], *COQ7* (3/3, 100%) [238–240], *COQ8A* (13/77, 17%) [227,348,354,357], *COQ8B* (1/79, 1%) [243]) and **muscle fatigue** (MF) (*COQ8A* (3/77, 4%) [227,344,347] and *COQ8B* (1/79, 1%) [364]). Also, hypotonia and respiratory alterations may depend on muscular involvement. Some muscle biopsies have shown **lipid accumulation** in this tissue (*COQ8A* (3/77, 4%) [227,357], *COQ2* (1/30, 3%)[328]), but probably this type of study has not been performed for all primary CoQ deficiency patients, so the information is still vastly incomplete. Lipid accumulation in mitochondria from skeletal muscle was also observed in a patient with adult-onset myopathy and CoQ_{10} deficiency. This patient had an haploinsuficiency of *ADCK2* gene, and a mouse model mimicking *Adck2* haploinsufficiency presented a similar phenotype, with defects in fatty acids β-oxidation[378]. This gene seems to participate in lipid homeostasis, regulating mitochondrial CoQ in muscle and organismal fatty acids β-oxidation[378].

Other manifestations

Other more heterogeneous clinical findings have also been reported in patients affected by mutations in the different *COQ* genes (Figure 1.3 and Table 1.2). Among them, respiratory system alterations are the most frequent (Figure 1.3.B). **Respiratory distress**

(RD) and **apnoea** seem to be characteristic of *COQ4* (14/35, 40%; 9/35, 26%) [250–252], *COQ7* (2/3, 67%; None) [239,240], *COQ9* (3/7, 43%; 2/7, 29%) [246,247,256] and some *COQ2* (2/30, 7%; 2/30, 7%) [257]. **Respiratory failure** (RF) occurred in some *COQ2* (5/30, 17%) [242,257,332] and *COQ4* (5/35, 14%) [250,251,336,340] patients. The **liver** is affected in a few patients harbouring mutated versions of *COQ2* (liver failure in 3/30, 10% [241,328]; cholestatic liver in 1/30, 3% [249]), *COQ9* (reduced hematopoiesis in liver in 1/7, 14% [246]), *COQ8A* (hepatosteatosis in 1/77, 1.3% [353]) and *COQ8B* (hepatomegaly in 1/79, 1.3%) (Figure 1.3.A). **Edema** is only present in cases with nephrotic syndrome, so it is frequent in probands with pathogenic variants in genes characterised by renal involvement, such as *COQ8B* (16/79, 20%), *COQ2* (11/30, 37%) [232,242,257,262,330,332–334], *COQ6* (2/30, 7%) [233,258] and *PDSS2* (2/7, 29%) [323,324]. It is highly likely that many of the *COQ6* patients presented edema, but this was underreported in the literature. A more exhaustive comprehension of these disorders might derive from long-term follow-up studies of patients affected by primary CoQ_{10} deficiencies. Less frequent clinical findings include **dysmorphic features** [233,247,341], **metabolic pathologies** (DM, obesity and hypercholesterolemia)[241,249,257,343], **thyroid disease** (goiter, hypothyroidism) [229,363] and **circulatory problems** (cyanosis, hypertension, livedo reticularis)[251,340,364], among others (Figure 1.3.C). It should be considered that some of these symptoms could be secondary consequences of a more general defect.

1.2.2. Biochemical findings

Remarkably, most of the reported cases were not accompanied by a biochemical report. Some of them were reported to show a high concentration of lactate in plasma or serum (56/276, 20%), but the total number of the patients tested is unknown. When enzymatic activities of complex I+III and/or II+III were measured, they generally showed a deficiency.

CoQ_{10} measurement is the most relevant biochemical assay that should be performed when a CoQ_{10} deficiency is suspected. CoQ_{10} levels are measured in skeletal muscle biopsies or in cultured fibroblast, which are the preferred diagnosis tissues. In some cases of the reported cases, CoQ_{10} levels have been measured on white blood cells (WBC), but it has been reported that this measurement is not reliable to diagnose primary CoQ deficiency in the setting of nephrotic syndrome [262].

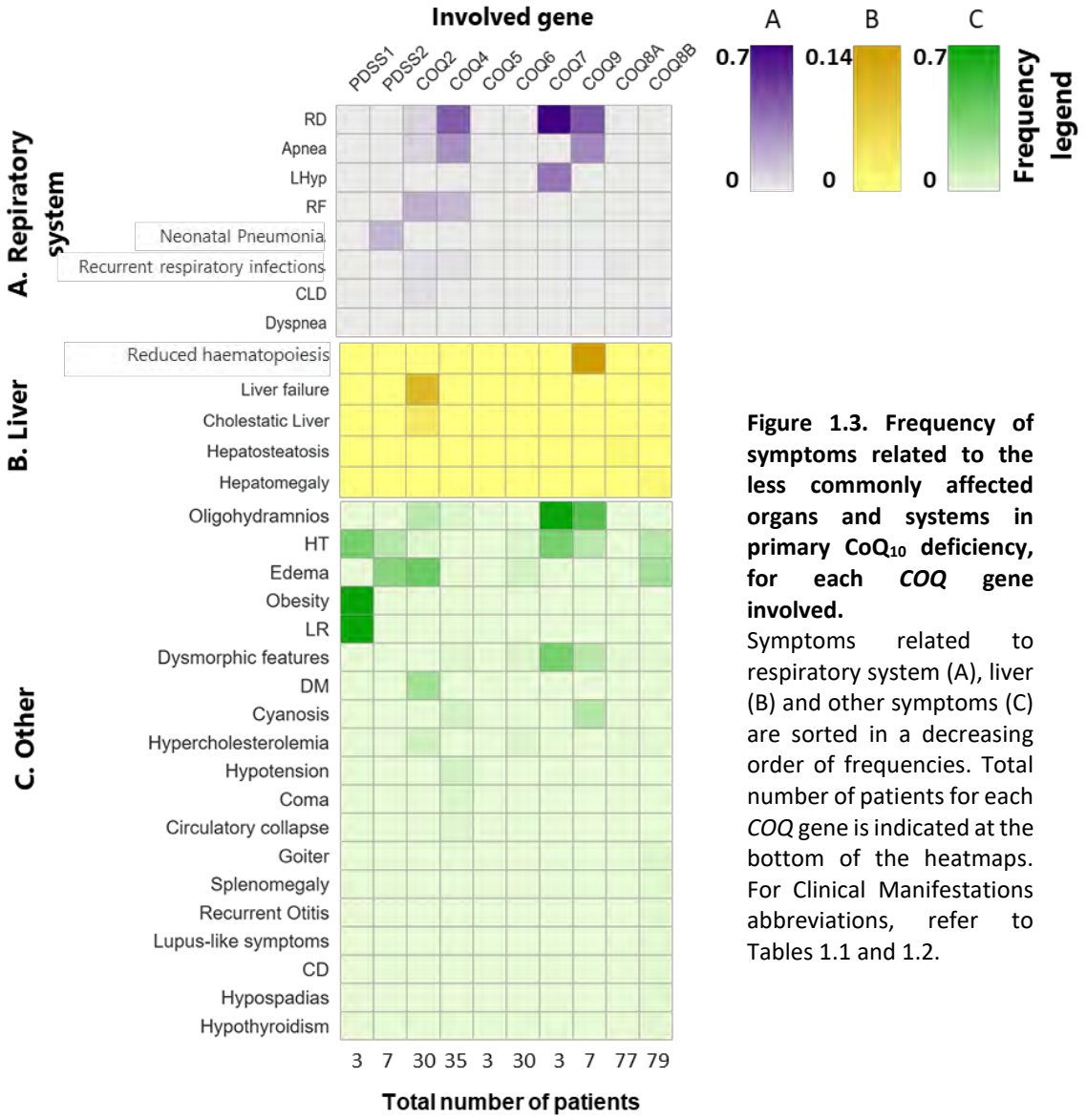

Figure 1.3. Frequency of symptoms related to the less commonly affected organs and systems in primary CoQ_{10} deficiency, for each *COQ* gene involved.
Symptoms related to respiratory system (A), liver (B) and other symptoms (C) are sorted in a decreasing order of frequencies. Total number of patients for each *COQ* gene is indicated at the bottom of the heatmaps. For Clinical Manifestations abbreviations, refer to Tables 1.1 and 1.2.

Of note, only in 61 cases of the 276 reported ones (22%) the diagnosis has been accompanied by a measurement of CoQ_{10} levels in muscle, fibroblasts or white blood cells. This number is extremely low, just considering that the disease being diagnosed is a primary CoQ_{10} deficiency. Additionally, the methods that are being used for this purpose are very heterogeneous, and the control values of CoQ levels also vary from one laboratory to another. Efforts in homogenizing these techniques should be made, in order to improve biochemical diagnosis and reduce variability.

1.2.3. Age of onset, age of death and age of last examination

The age of onset in primary CoQ_{10} is very variable, but each of the affected genes seems to have a distinguishable onset age interval (Figures 1.4.A and 1.5). Moreover, even for the same gene, this range can be extensive (Figure 1.5).

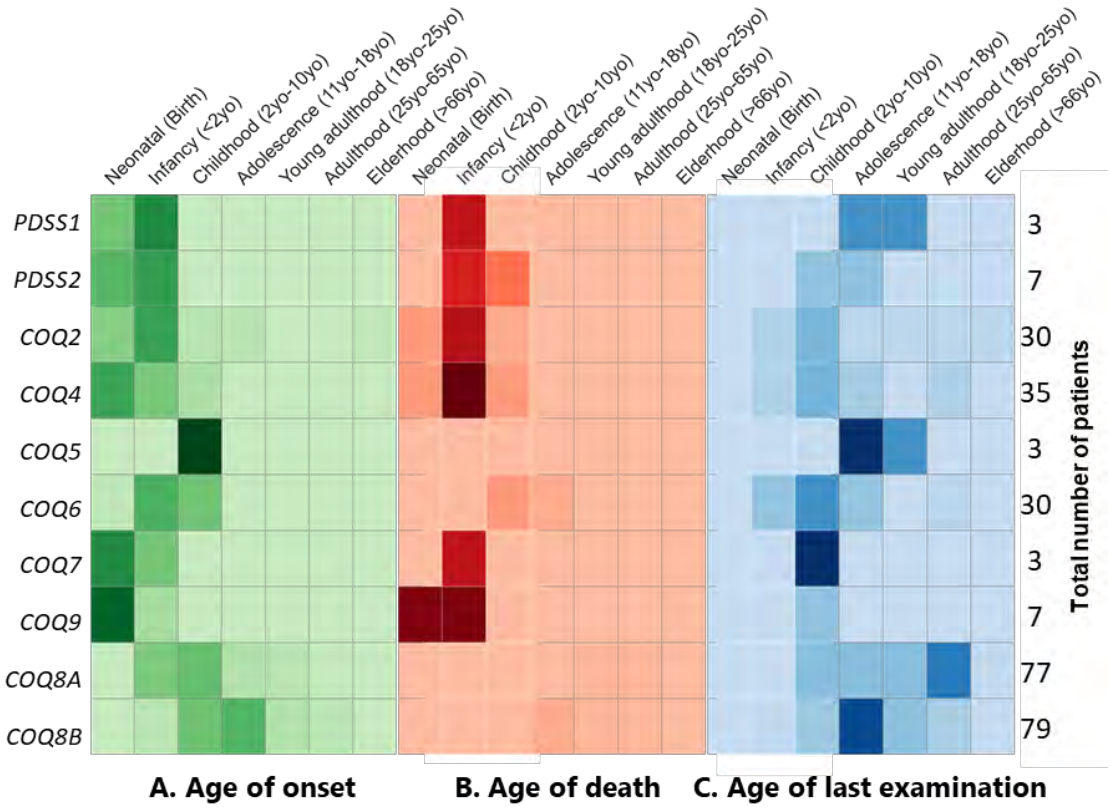

Figure 1.4. Heatmaps representing the age in which patients first manifested (A), died (B) or were examined for the last time (C), for each *COQ* gene involved.
Age has been represented as the percentage of patients belonging to seven different age groups: neonatal (birth), infancy (before 2 years of age), childhood (2-10 years old), adolescence (11-18 years old), young adulthood (18-25 years old), adulthood (25-65 years old) and elderhood (after 66 years old). yo: years old.

The age of onset generally falls between birth and childhood (*PDSS1*, *PDSS2*, *COQ2*, *COQ4*, *COQ5*, *COQ6*, *COQ7*, *COQ9*), or between childhood and adolescence (*COQ8A*, *COQ8B*), but there are also some adult-onset cases (*COQ8A* [227], *COQ8B* [229]) (Figure 1.5). Of note, some COQ2 variants have been reported to increase susceptibility to adult-onset multisystem atrophy (MSA)[379].

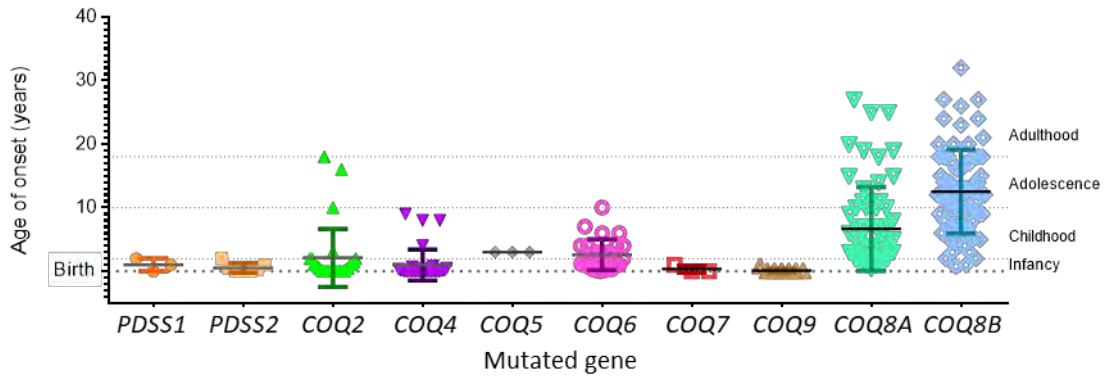

Figure 1.5. Age of onset of patients with primary CoQ_{10} deficiency, for each *COQ* gene involved.
Each point represents one patient, and mean age of onset and standard deviation is calculated for each mutated gene.

Neonatal onset is more frequent in *COQ4* (19/35, 54% of the cases) [240,250,251,336,340,341], *COQ7* (2/3, 67% of the cases) [239,240] and *COQ9* (6/7, 86% of the cases) [246,248,256] patients. Also, many *COQ2* (11/30, 37% of the cases) [241,249,257,328,332,334], and some *PDSS1* (1/3, 33%) [322] and *PDSS2* (3/7, 43%) [245,323,324] patients presented neonatally. It is important to mention the marked lethality of the disease course in the neonatal-onset patients, almost all of them dying in the neonatal or infantile period, and some of them during childhood (Figure 1.4.A and B).

The majority of the *COQ2* patients presented before the age of 2 years (14/30, 47%) [242,245,262,329,376]. This is also true for *PDSS1* (2/3, 67%) [241], *PDSS2* (4/7, 57%) [245,285] and *COQ6* (15/30, 50%) [231–233,235,258,343] patients. Some patients with pathogenic variants of *COQ4* (11/35, 31%) [250,251,340], *COQ7* (1/3, 33%) [238], *COQ9* (1/7, 14%) [247], *COQ8A* (23/77, 30%) [227,273,344,354,356,357,370] and *COQ8B* (4/79, 5%) [363,366] also presented when they were 2 years old or before.

COQ8A patients generally first manifest during childhood (29/77, 38%) [273,274,356,360], as it has been equally reported in previous studies [273–275]. Childhood-onset also occurs in a significant number of *COQ8B* (28/79, 35%) [229,364,365] and *COQ6* (11/30, 37%) [233,235,236] patients, and in the only reported family with *COQ5* defects (3/3, 100%) [326]. Some patients with *COQ2* (2/30, 7%) [262,376] and *COQ4* (4/35, 11%) [335,338] mutations also presented during childhood.

Adolescent-onset is the hallmark of *COQ8B* patients' presentation (35/79,44%)[229,363,364], while also some *COQ8A* (7/77, 9%) [273,274,347] and *COQ2* (2/30, 7%) [232] patients presented

between 11 and 18 years old. Adult-onset is rare, but some patients with *COQ8B* (11/79, 14%) [229,363,364] and *COQ8A* (6/77, 7%) [227,228,273,274] mutations presented when they were adults.

Analysing the age of the last examination, we can infer how patients in the different gene groups or onset-ages were able to live beyond childhood, adolescence or adulthood (Figure 1.4.C). This is just an approximative observation, since it significantly depends on the time when the case was published, which is not homogeneous nor explicative. We can see how some patients that present before 2 years old can progress at least to childhood (*PDSS2*, *COQ2*, *COQ4*, *COQ6*, *COQ7*, *COQ9*, *COQ8A*, *COQ8B*), adolescence (*PDSS1*, *COQ2*, *COQ6*, *COQ8A*) or adult age (*COQ8A*). Equally, some probands that manifested during childhood could achieve the adolescence (*COQ2*, *COQ4*, *COQ5*, *COQ6*, *COQ8A* and *COQ8B*), adult (*COQ4*, *COQ5*, *COQ6*, *COQ8A* and *COQ8B*) or elder age (*COQ8A*). Some of the patients manifesting during adolescence could likewise achieve adult age (*COQ2*, *COQ8A*).

1.2.4. Primary CoQ_{10} deficiency due to mutations in the different *COQ* genes

To shed light on the plethora of symptoms associated with the different cases of primary CoQ_{10} reported, we will discuss the patterns of symptoms at onset (Figure 1.6) and general clinical manifestations for each *COQ* gene. For the genes for which the total number of families with affected patients was sufficiently high (>20), the clinical cases were additionally stratified by age at onset (0/Birth: neonatal-onset; 0-2 years old (yo): infantile-onset; 2–10 yo: childhood-onset; 11–18 yo: adolescence onset; 19-65 yo: adult-onset). We classified patients with mutations in *COQ2* (30 patients from 22 families), *COQ4* (35 patients from 26 families), *COQ6* (30 patients from 22 families), *COQ8A* (77 patients from 55 families) and *COQ8B* (79 patients from 41 families) (Figure 1.7). With this classification, in some cases, patients belonging to the same family were split into different groups. This happened mainly with *COQ8B* patients, in which siblings from the same family first manifested at different ages. There are a very low number of patients with mutations in *PDSS1* (3 patients from 2 families), *PDSS2* (7 patients from 5 families), *COQ5* (3 patients from 1 family), *COQ7* (3 patients from 3 families) and *COQ9* (7 patients from 4 families) to do so. Still, we will equally discuss the global clinical features. We will use abbreviations for clinical manifestations, which are compiled in Tables 1.1 and 1.2.

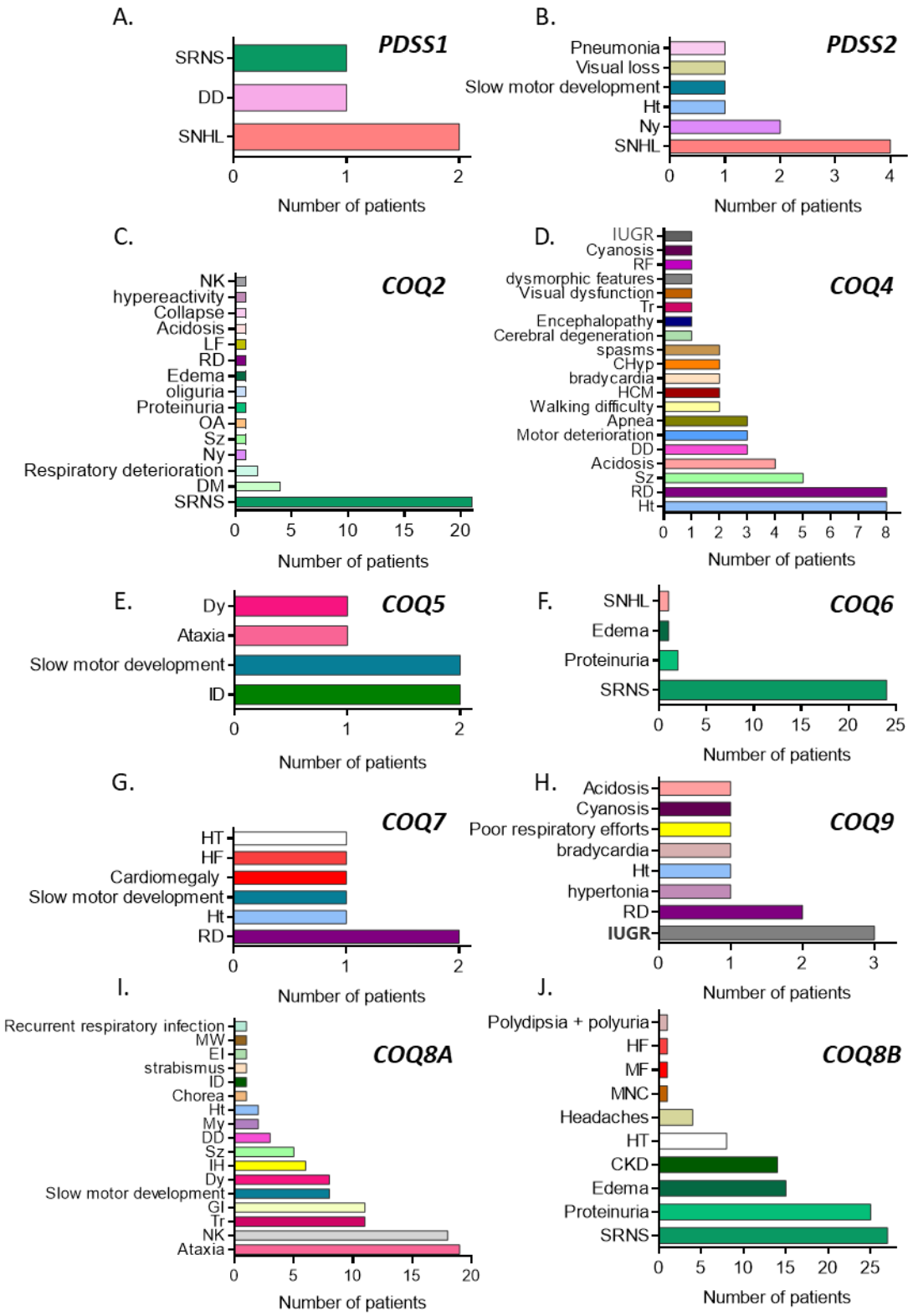

Figure 1.6. Symptoms at onset in patients with mutations in the different *COQ* genes and number of patients associated with each first symptom.

Each graph represents each gene involved in primary CoQ_{10} deficiency. (A) *PDSS1*, 3 patients in total; (B) *PDSS2*, 7 patients in total; (C) *COQ2*, 30 patients in total; (D) *COQ4*, 35 patients in total; (E) *COQ5*, 3 patients in total; (F) *COQ6*, 30 patients in total; (G) *COQ7*, 3 patients in total; (H) *COQ9*, 7 patients in total; (I) *COQ8A*, 77 patients in total and (J) *COQ8B*, 79 patients in total. For abbreviations refer to Tables 1.1 and 1.2.

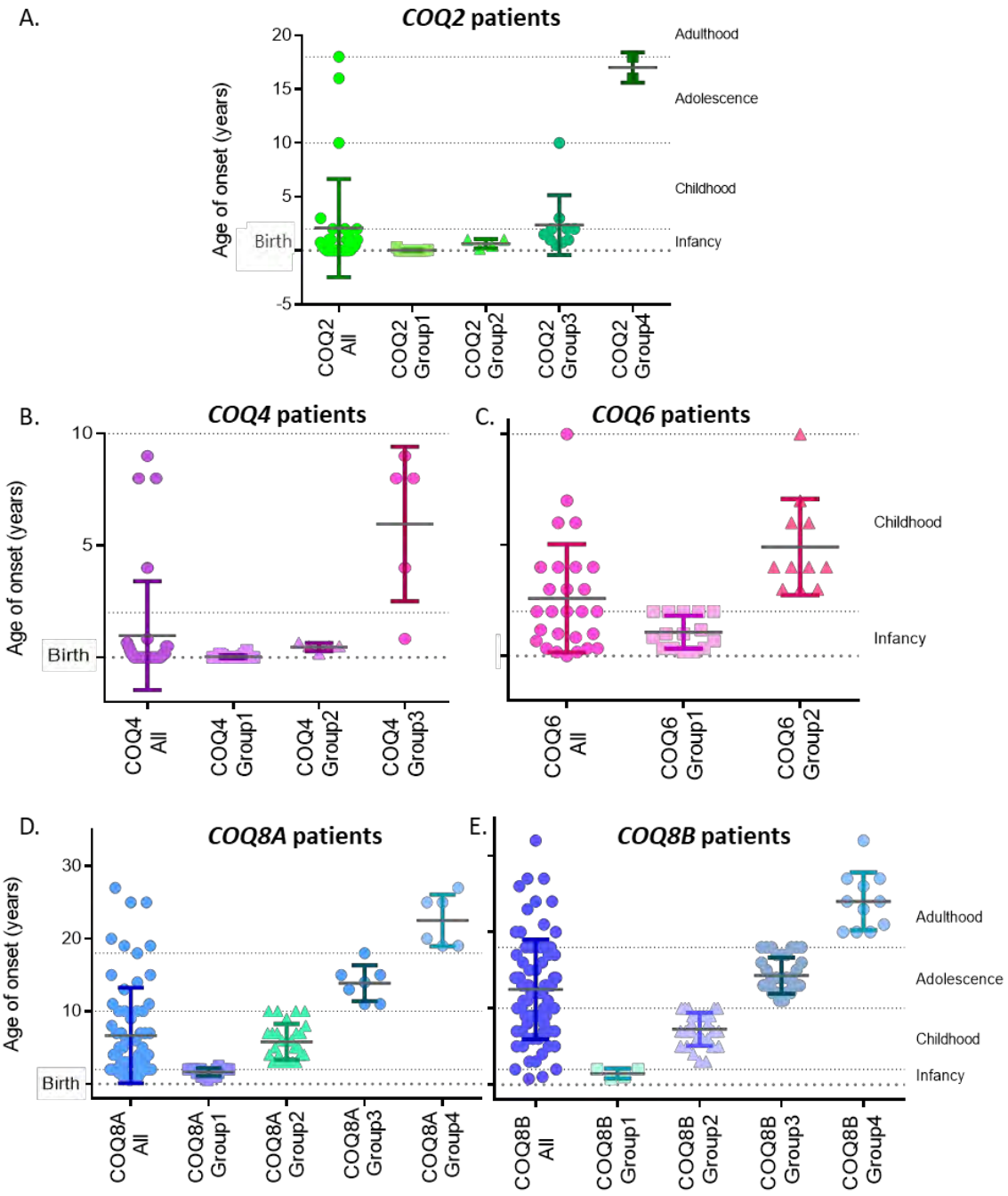

Figure 1.7. Age of onset stratification of patients with primary CoQ_{10} deficiency.

They are classified by the *COQ* gene involved: *COQ2* (30 patients) (A), *COQ4* (35 patients) (B), *COQ6* (30 patients) (C), *COQ8A* (77patients) (D) and *COQ8B* (79 patients) (E). In each graph, the whole group of patients is represented (All), as well as different groups of patients resulting of age-of-onset stratification of the cases (groups 1-4). Each point represents one patient, and mean age of onset and standard deviation is calculated for each mutated gene.

118 cases of the 276 reported ones (43%) were treated with CoQ_{10} supplementation. The outcome of the treatment will be discussed for these cases in this section (Table 1.4).

We also compiled the information about the pathogenicity of the mutations in the literature, reviewing three aspects: (i) the segregation of the mutation in the family; (ii) the biochemical characterisation of the disturbance of CoQ_{10} biosynthesis (measuring CoQ_{10} levels, synthesis rate, levels of COQ proteins or *COQ* transcripts, etc.); (iii) or the functional demonstration of the pathogenicity using a model (yeast, human or mouse cells, induced pluripotent stem cells (iPSCs), etc.). We analysed *in silico* the predicted pathogenicity of the mutations found in these patients. We used SIFT and PolyPhen-2 tools to predict the effect of the missense mutations in the protein function, and SPiCE tool to predict the spliceogenicity of the variant. Furthermore, a pathogenicity score for single nucleotide variants and small insertion/deletions variants was calculated using the Combined Annotation Dependent Depletion (CADD v1.6) tool, which integrates multiple annotations[220]. Most variants analysed display a CADD score higher than 20, the cut-off of deleteriousness that is usually considered.

Additionally, we analysed how the pathogenic variants were distributed concerning the age of onset of the disease (Figure 1.8). All the pathogenic variants of each gene were classified in the onset-age stratified groups, to investigate if some variants can be linked to different phenotypic outcomes. Of note, the majority of variants have been described only in one family, whereas some of them are more represented within the patient cohort. It is not possible to draw definite conclusions for variants that have only been described in a reduced number of families. What is more, for compound heterozygous genotypes, both variants are considered for the classification, but in the absence of functional data, it is not possible to conclude which of them contributes more to the phenotype. Only for those few variants that are represented in several families, we have analysed the possible link to different clinical pictures. In the cases of frameshift or nonsense mutations, when they occur early in the sequence, they could be considered as loss-of-function alleles.

Table 1.4. Response to CoQ_{10} supplementation.

Gene	Total #of patients	CoQ treatment		References
		# of patients treated	Effect	
PDSS1	3	-	-	-
PDSS2	7	2	No benefits (2)	323,324
COQ2	30	14	Neuromuscular functions restored (2), No benefits (2), No benefits on neuromuscular function (3), No benefits on renal function (1), No deterioration (2), Renal function restored (6)	232,242,257,262, 333,334,376
COQ4	35	20	No benefits (7), Improvement of Sz or Ep (3), Improvement in development (2), Improvement of cardiac function (2), Stable condition (2), Subjective response improvement (2), Improvement of ataxia (1), Improvement of lactic acidosis (1), Muscle improvement (1)	250,252,335,338–341
COQ5	3	3	Improvement of ataxia (3)	326
COQ6	30	9	Improved proteinuria (5), Improved renal function (3), Improved groth retardation (2), Improved SNHL (1)	231–234,236,258,343
COQ7	3	3	No deteroration (2), No benefits (1)	238–240
COQ9	7	4	No benefits (3), Plasma lactate reduced (1)	246–248
COQ8A	77	29	No benefits (13), Improvement of ataxia (9), Improvement of tremor and myoclonus (5), Improvement in motor abilities (5), Slight improvement of cerebellar signs (2), Stabilization of the ataxia (2), Improvement in fatigue and speech (1), Improvement of cognitive abilities (1)	227,228,274,345–348,351–354,356,357,359, 360
COQ8B	79	29	No benefits (7), Improvement of proteinuria (18), Improvement of edema (1) , Better physical fitness and reduced fatigue (1), Stabilization of renal function (1), NK (2)	229,243,362–364,366

Abbreviations: NK: Not known. For Clinical Manifestations abbreviations, refer to Tables 1.1 and 1.2.

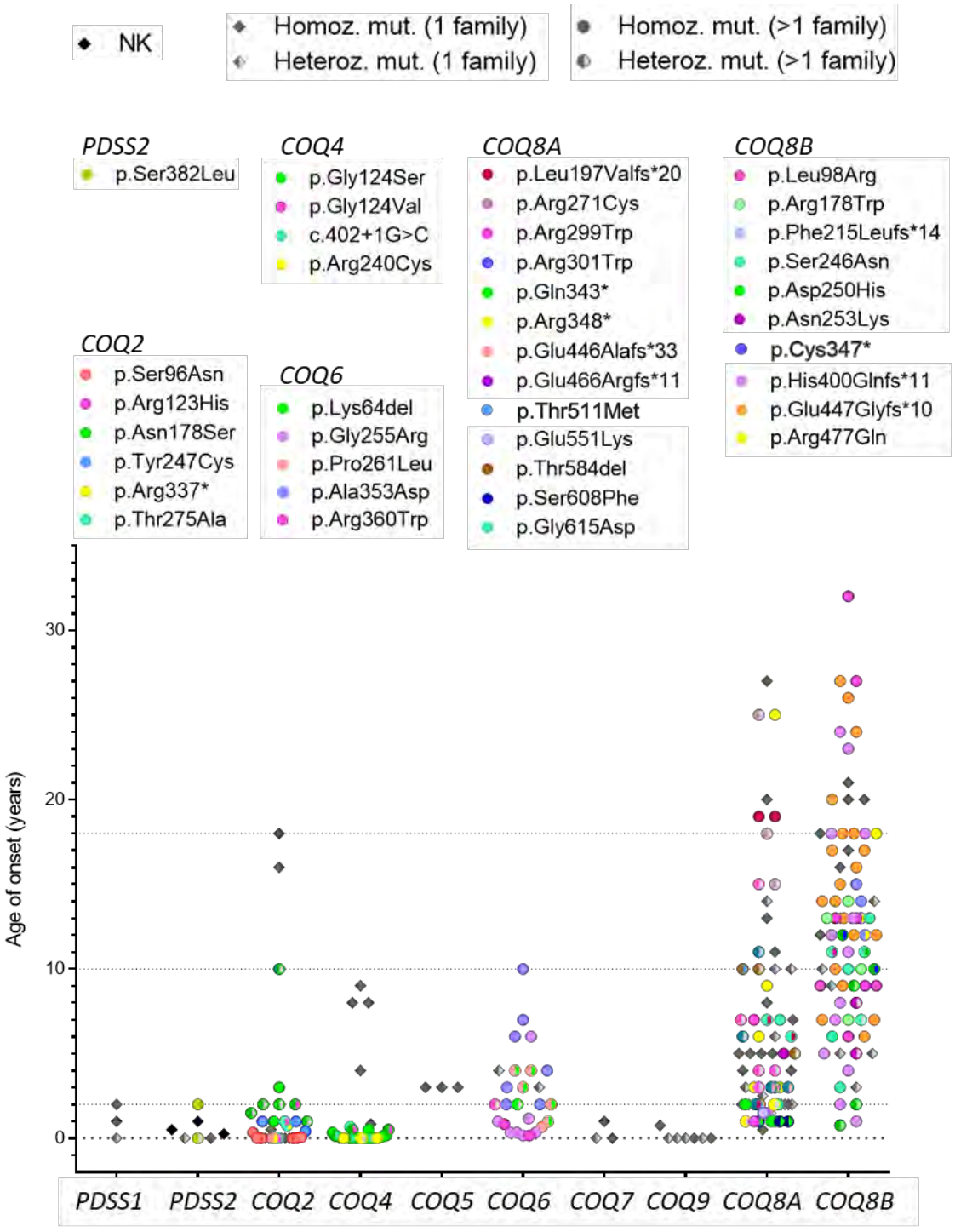

Figure 1.8. Age of onset and genotype of patients with pathogenic variants in one of the ten *COQ* genes involved in primary CoQ_{10} deficiency.

Each point represents one patient. Coloured circles represent mutations that were found in more than one family (each mutation in a different colour, depicted in the legend). Rhombus represent patients with mutations that appeared only in one family (in gray) or unknown mutations (in black). Full-filled symbols represent homozygous mutations, while half-filled ones design heterozygous mutations. Abbreviations: NK: Not known, Homoz: homozygous, Heteroz: heterozygous, mut: mutation.

PDSS1

PDSS1 gene (MIM*607429) is located in the Chr10:26,697,701-26,746,798 (GRCh38.p13), forward strand. The protein-coding transcript (1,584 base pairs (bp)) encodes a 415 amino acid (aa) (12 exons) protein. The gene product, the decaprenyl diphosphate synthase subunit 1, is a monomer of the enzyme that elongates the prenyl side-chain of CoQ_{10}, in order to assemble the complete polyisoprenoid side chain, the first step in CoQ_{10} biosynthesis [380,381]. Defects in this gene is a cause of primary CoQ_{10} deficiency (COQ10D2, MIM#614651).

i. CoQ_{10} *deficiency due to PDSS1 mutations*

Only 3 patients from 2 families with *PDSS1* mutations have been reported so far, so little information is known to draw a disease picture. The mean age of onset was 1 year old (yo) (range birth-2 yo) (Figures 1.5, 1.6.A). These two families manifested very different clinical pictures (Table 1.3).

One family had a birth-onset disease with mainly renal involvement, with a severe SRNS that progressed in an ESRD, with death at 16 months old (mo). The patient from this family also had a marked DD. We could define her clinical picture as a severe multisystem disorder, similar to the primary phenotype of *COQ2* patients. This patient had two compound heterozygous mutations, one frameshift mutation in exon 7 (c.661_662insT), producing an early truncated protein (p.Arg221Leufs*16), and one missense mutation in exon 12, c.1108A>C (p.Ser370Arg)[322] (Table 1.5).

The other family had two siblings with an infancy onset (1-2 yo), who developed a milder disease (Table 1.3). They presented with SNHL, and later in their childhood and adolescence, they developed encephalopathy with a mild ID, and associated peripheral neuropathy with OA. They also presented a valvulopathy, LR and obesity. They did not display any renal involvement, at least at the age of the last examination (14 and 22 yo, respectively). They had a homozygous mutation in exon 10 in both *PDSS1* alleles, c.924T>G (p.Asp308Glu) [241] (Table 1.5).

ii. *CoQ_{10} treatment and effects*

Regarding CoQ treatment and effects, there is no information about CoQ_{10} treatment in these patients (Table 1.4).

iii. Pathogenicity of the mutations

There are 3 mutations in *PDSS1* related with primary CoQ_{10} deficiency in the literature (Figure 1.8 and Table 1.5). Only one of them has been demonstrated pathogenic in a yeast model, c.924T>G (p.Asp308Glu)[241]. The other two mutations are thought to be pathogenic because of the low levels of CoQ_{10} found in patient's cells. The frameshift mutations would probably lead to a loss-of-function allele. The two missense mutations have been predicted pathogenic with SIFT, PolyPhen-2 and CADD tools (Table 1.5).

Table 1.5. Pathogenic variants of *PDSS1* and *PDSS2* genes found in patients.

Gene/ protein	Pathogenic variants				Validation			*In silico* mutagenesis prediction				Ref.
	F (P)	cDNA mutation	aa modification	Exon	Segregation (S), Biochemical (B), Functional (F)			SIFT Patho-genic?	Poly Phen-2 Dama-ging?	SPiCE Probability to alter splicing?	CADD score	
PDSS1 415 aa 12 exons NM_014317.5 NP_055132.2	1 (1)	c.661_662insT	p.Arg221Leufs*	7		B		-	-	-	33	322
	1 (2)	c.924T>G	p.Asp308Glu	10	S	B	F	Pathog.	Probably	-	22.1	241
	1 (1)	c.1108A>C	p.Ser370Arg	12		B		Pathog.	Probably	low	26.4	322
PDSS2 399 aa 8 exons NM_020381.4 NP_065114.3	1 (1)	c.485A>G	p.His162Arg	3	S			Pathog.	Probably	-	25.1	323
	1 (1)	c.964C>T	p.Gln322*	6	S	B		-	-	-	43	324
	1 (1)	c.1042_1148-2816del	p.?	8	S			-	-	low	-	323
	2 (2)	c.1145C>T	p.Ser382Leu	8	S	B		Pathog.	Probably	-	31	245, 324
	1 (1)	c.1151C>A	p.Ala384Asp	8	S			Tole-rated	Probably	-	29.0	245
	1 (3)	NA	NA	NA		B		Pathog.	Probably	-	-	285, 325

Reference sequences correspond to longest transcript. Abbreviations: F: Number of families with each variant, P: Number of patients with each variant, aa: amino acid, Ref: references, NA: not available, Pathog: Pathogenic.

PDSS2

PDSS2 gene (MIM*610564) is located in chr6:107,152,562-107,459,564 (GRCh38.p13), reverse strand. Three different protein coding transcripts are annotated, but only the longest one is thought to produce PDSS subunit 2. This transcript (3,536 bp) encodes a 399 aa (8 exons) protein. The gene product, the decaprenyl diphosphate synthase subunit 2, together with PDSS1, forms the heterotetramer that assemble the complete polyisoprenoid side chain, the first step in CoQ_{10} biosynthesis. Defects in this gene are a cause of CoQ_{10} deficiency (COQ10D3, MIM#614652).

i. CoQ_{10} deficiency due to PDSS2 mutations

7 patients from 5 families with *PDSS2* mutations have been reported so far. The pathology of *PDSS2* deficiency seems to be different from that of *PDSS1* deficiency. *PDSS2* patients presented a **multisystemic disorder with mainly renal involvement**, all of them having SRNS and some of them ending in an ESRD (Table 1.3). However, they had a wide range of neurological manifestations within the different families (Leigh-like syndrome (LS), ataxia, cerebral palsy, encephalopathy). What is clear is that when SNHL was present (in 4 patients of 2 families), it was the first symptom to appear, similarly to one of the two *PDSS1* families [241] (Figure 1.6.B). The two families with SNHL also had an HCM. The disease manifested at a mean age of 6 mo (range birth-2 yo) (Figure 1.5). Three families had a birth onset (3/7 patients, 43%), while two families (4/7 patients, 57%) had an infancy onset (Figures 1.5, 1.6.B).

Two patients with a birth onset died during infancy, but from different causes (epilepsy or ESRD), while the age of the third one is not available. One of these patients presented with hypotonia and developed a LS with basal ganglia lesions (BGL) and seizures, passing away at 8 mo because of a complication of the epileptic status. He had two compound heterozygous mutations, one nonsense variant in exon 6 (c.964C>T), producing an early truncated protein (p.Gln322*), and one missense change in exon 8, c.1145C>T (p.Ser382Leu) [324]. The other patient initially presented with hearing loss (HL), and DD, and later manifested an encephalopathy with hypotonia, RP and HCM. He died because of a renal dysfunction. He had two compound heterozygous mutations, one missense mutation in exon 3, c.485A>G (p.His162Arg), and a 2923bp deletion that affected the 5‘ end of exon 8 [323]. The third patient was described with no other presentation than the SRNS, and had a homozygous missense mutation in exon 8, c.1151C>A (p.Ala384Asp)[245].

There were two families with an infancy onset, and with a less severe phenotype. One of them had three siblings who presented with nystagmus and HL, and then developed visual impairment and an ataxic phenotype, with ID. One of them had HCM. The mutations in these patients were not specified [285,325]. The other family had one patient with cerebral palsy and ID. He had an homozygous missense substitution in exon 8, c.1145C>T (p.Ser382Leu), the same that the LS patient presented [245].

ii. CoQ_{10} treatment and effects

CoQ_{10} treatment was administered to two of the birth-onset cases, but with no apparent benefits (Table 1.4). Two siblings with the ataxic syndrome were treated with ubidecarenone, and after 6 months, they improved their motor performance and general condition [285].

iii. Pathogenicity of the mutations

Five pathogenic variants of *PDSS2* have been related to primary CoQ_{10} deficiency in published patients (Figure 1.8). All the mutations were confirmed to segregate within the different families (Table 1.5). Only the variants identified in the patients with LS (c.964C>T (p.Gln322*) and c.1145C>T (p.Ser382Leu)) were biochemically tested by revealing low levels of CoQ_{10} biosynthesis rate on the patient fibroblasts [324]. The missense mutation was also found in another unrelated patient [245], but with a different disease course (Figure 1.8). The deletion mutation (c.1042_1148-2816del) affects the last part of the last exon and have an uncertain molecular effect [323]. The missense mutation accompanying this deletion, c.485A>G (p.His162Arg), has been predicted to be pathogenic with SIFT, PolyPhen-2 and CADD tools. The last variant, the homozygous missense mutation in exon 8, c.1151C>A (p.Ala384Asp) [245], has been predicted as tolerated by SIFT, but probably damaging by Polyphen-2, whereas it reaches a pathogenicity score (29) with CADD, supporting a deleterious effect of this substitution. Its pathogenicity should be confirmed by an experimental validation (Table 1.5).

COQ2

COQ2 gene (MIM*609825) is located in chr4:83,261,536-83,284,914 (GRCh38.p13), reverse strand. The open reading frame contains four in-frame ATG initiation codons (termed ATG1-4). Traditionally, ATG1 was considered the first translated codon, generating a 421 aa protein with 7 exons. Still, recently, it has been shown that the most abundant *COQ2* transcript in human cells includes only the most downstream initiation codon (ATG4, 1,641 bp), giving rise to a 371 aa protein with 7 exons [277]. The gene product, the para-hydroxybenzoate polyprenyl-transferase, is the enzyme that catalyses the condensation of 4- hydroxybenzoate with polyprenyl-pyrophosphate, generating the first membrane-bound CoQ_{10} intermediate. Defects in this gene are a cause of CoQ_{10} deficiency (COQ10D1, MIM#607426).

i. CoQ_{10} *deficiency due to COQ2 mutations*

30 patients from 22 families with *COQ2* pathogenic variants have been reported up to date. *COQ2* patients manifested a **nephrotic syndrome** with different degrees of severity (Table 1.3). The nephrotic syndrome could be presented either **isolated**, **associated with CNS affections**, or **as a part of a more severe multisystemic disorder**.

a. Age of onset

COQ2 patients manifested at a mean age of 25 mo (range birth-18 yo) (Figure 1.5). We classified the clinical cases by the age of onset in 4 different groups, revealing each of them a different clinical picture (Figures 1.7.A, 1.9.A and B).

Group 1 is the largest one (13/30, 43% of the total number of *COQ2* patients). The mean age of onset in this group was 2 weeks old (wo)(range birth-4 mo). **Group 2** is a small group (6/30, 20% of the total number of *COQ2* patients), which includes 6 patients from 5 different families, in whom the mean age of onset was 9 mo (range 5 mo-1 yo). **Group 3** is composed of patients (9/30, 30% of the total number of *COQ2* patients) that had an infancy (6/9, 78%) or childhood (2/9, 22%) -onset, whose mean age of presentation was almost 3 yo (34 mo) (range 1 yo-10 yo). Only one family (**Group 4**, 2/30, 6.7% of the total number of COQ2 patients) manifested during adolescence, with a mean age of presentation of 17 yo (range 16-18 yo).

b. Symptoms at onset

COQ2 patients mainly displayed a multi-symptom presentation, with a combination of different clinical manifestations. However, the hallmark symptom at onset was SRNS (21/30, 70%). Other symptoms at onset were diabetes mellitus (DM) (4/30, 13%) [257] or respiratory defects (3/30, 10%) [249,332]. Other very variable and less frequent symptoms at onset were seizures, liver failure (LF), collapse, acidosis, hyperreactivity, oliguria, edema, proteinuria, nystagmus or OA (1/30, 3% each of them) (Figure 1.6.C).

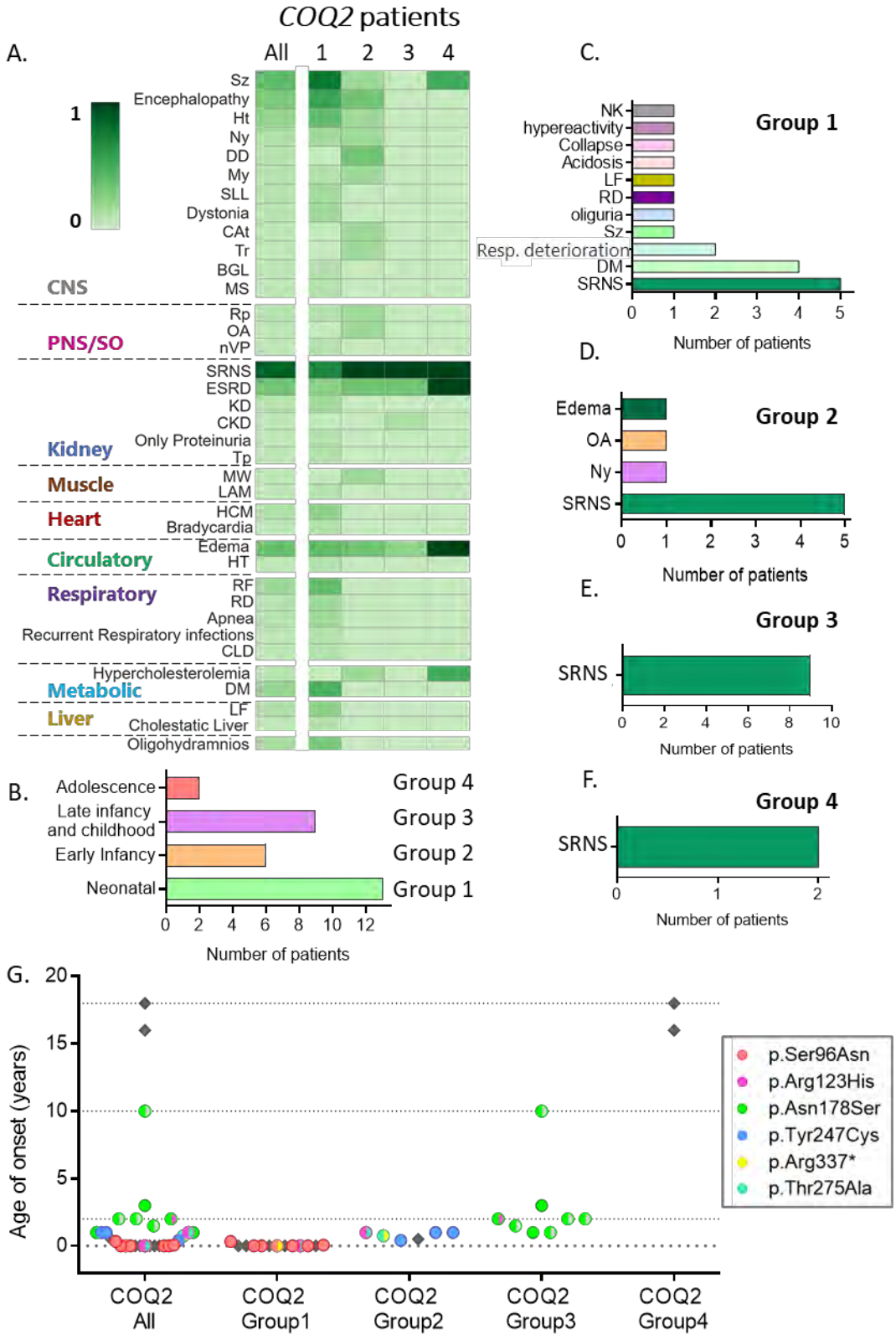

Figure 1.9. Clinical manifestations and genotype of *COQ2* patients.
(A) Symptom frequency found in *COQ2* patients, for each age-of-onset group 1-4. (B) Total number of patients in each age-of-onset group. (C-F) First symptoms at onset, and the number of patients manifesting them, for each age-of-onset group. (G) Age of onset and pathogenic variants of *COQ2* patients. Each point represents one patient. Coloured circles: mutations found in more than one family (see the legend). Rhombus: patients with mutations only present in one family (gray). Full-filled symbols: homozygous mutations, half-filled symbols: heterozygous mutations. Abbreviations: Tables 1.1 and 1.2.

When sorted by age at onset, patients with the earliest onset (group 1) first presented with a wide spectrum of different symptoms (SRNS (5/13, 38%)[241,257], respiratory defects (3/13, 23%) [249,332], DM (4/13, 31%)[257], liver failure (1/13, 8%)[241], seizures (1/13, 8%)[333], acidosis (1/13, 8%)[328], collapse (1/13, 8%) [241] or hyperreactivity (1/13, 8%)[328]) (Figure 1.9.C). For group 2 patients, SRNS was the first symptom in the majority of the cases (5/6, 83%)[242,245,262,330,331,375]. One patient also presented with Ny and OA [331,375], and another one with oedema and proteinuria, which are signs of SRNS (Figure 1.9.D) [334]. The rest of the patients (groups 3 and 4) first presented with SRNS (9 and 2, respectively) (Figure 1.9.E and F) [232,242,244,245,262,329].

c. Clinical manifestations of the disease

COQ2 patients presented a nephrotic syndrome with different degrees of severity, being isolated, with encephalopathy and seizures, or as a part of a multisystemic disorder (Table 1.3). When clinical cases are classified by the age of onset, 4 different groups emerged, revealing each of them a distinct clinical picture (Figure 1.9.A and B).

COQ2 deficiency's main phenotype is an **early-onset severe multisystemic disorder** (group 1), mainly with renal (SRNS (9/13, 69%)) and CNS involvement (encephalopathy (7/13, 54%), epilepsy (2/13, 15%), seizures (10/13, 77%), hypotonia (5/13, 38%), dystonia (2/13, 15%), stroke-like lesions (SLL) (2/13, 15%), nystagmus (2/13, 15%)), but also with other organs and systems' features (HCM (3/13, 23%), LF (3/13, 23%), DM (6/13, 46%), RF (5/13, 38%)) [241,242,249,257,328,333,334]. All patients from group 1 died (13/13, 100%) (Figure 1.4.B) mainly because of multiorgan failure (7/13, 54%)[249,257,333], or a complication of the renal (2/13, 15%) [242,330] or neurological (3/13, 23%) status [257,328]. Infections caused the death of the rest of the patients (2/13, 15%) [332].

Some patients presented an **infancy-onset SRNS that was accompanied by some neurological symptoms** (group 2), such as encephalopathy (2/6, 33%), DD (2/6, 33%), and seizures, nystagmus, hypotonia, myoclonus, CAt, tremor, OA and retinopathy (1/6, 17% each symptom)[242,245,331,334,375].

Group 3 is composed of patients who had infancy (6/9, 67%) or childhood (2/9, 22%) -onset isolated SRNS (9/9, 100%), sometimes associated with oedema (2/9, 22%)[242,244,245,262,329].

Only one family (group 4) manifested during **adolescence an SRNS with a mild CNS involvement** (epilepsy, mild neurological symptoms). They also had edema (2/2, 100%) and hypercholesterolemia (1/2, 50%)[232].

ii. CoQ_{10} *treatment and effects*

CoQ_{10} treatment was administered to 14/30 (47%) of the *COQ2* patients, representing all the four groups described (Table 1.4 and 1.6). In the most severe group (group 1), 4/13 patients were treated. 3/4 normalised glucose and lactate levels, and only one of them decreased proteinuria [257]. None of these 4 patients had any improvement in neurological function. In the group showing SRNS accompanied by encephalopathy (group 2), 4/6 patients were treated, and they restored neuromuscular (2/4) and renal (2/4) functions [242,262,331,334,375]. In the isolated SRNS group (group 3), 4/9 patients were treated, and they ameliorated their renal function (2/4), did not get worse (1/4) or did not benefit from the treatment (1/4)[242,262,376]. From the last group (adolescence onset SRNS), two patients from the same family restored the renal function after the CoQ_{10} supplementation (group 4) [232].

In general, there is a variable response to CoQ_{10} treatment, with no obvious correlation with the mutations of the patient. Renal function often responds well to treatment.

i. Pathogenicity of the mutations

There are 16 reported *COQ2* variants that have been associated with primary CoQ_{10} deficiency in the literature (Figures 1.8, 1.9.G and Table 1.7). Almost all the mutations (13/16, 81%) were confirmed to be segregated on the different families, except the variants c.26dupT (p.Ala10Argfs*33), c.731C>T (p.Thr244Ile) and c.1009C>T (p.Arg337*). Some of the mutations (8/16, 50%) were tested in a yeast model in a study in which a genotype-phenotype correlation for *COQ2* patients is established [277].

Following the age-of-onset stratification of the patients, we analysed the pathogenic variations that were represented within the different groups (Figure 1.9.G and Table 1.6). We observed a correlation in which some variants are associated with more severe phenotypes, while others are associated with less severe ones. This fact fits with the previous study in which *COQ2* variants are associated with the residual CoQ_{10} synthesis ability and the severity of the disease [277].

Table 1.6. *COQ2* patients classified by age of onset. CoQ_{10} treatment and mutations.

Group	# of patients	CoQ_{10} treatment		F (P)	cDNA change	Aa change	Ref.
		# of patients treated	Effect				
Group 1	13	4	Decreased proteinuria (1), Normalised glucose and lactate level (3), No benefits on neurological function (3), No benefits (1)	5 (7)	c.287G>A	p.Ser96Asn	242,249,257,277, 333
				1 (1)	c.368G>A	p.Arg123His	334
				1 (1)	c.395T>G	p.Met132Arg	328
				1 (2)	c.755C>T	p.Ala252Val	277,332
				1 (1)	c.823A>G	p.Thr275Ala	334
				1 (1)	c.1009C>T	p.Arg337*	249,277
				1 (2)	c.1047delT	p.Asn351Ilefs*15	241
Group 2	6	4	Neuromuscular functions restored (2), Renal function restored (2), No benefits on renal function (1), No deterioration (1)	1 (1)	c.368G>A	p.Arg123His	334
				1 (1)	c.682T>C	p.Cys228Arg	330
				2 (3)	c.740A>G	p.Tyr247Cys	242,245,277,331, 375
				2 (2)	c.823A>G	p.Thr275Ala	262, 334
				1 (1)	c.1009C>T	p.Arg337*	262
Group 3	9	4	Renal function restored (2), No deterioration (1), No benefits (1)	1 (1)	c.26dupT	p.Ala10Argfs*33	262
				1 (1)	c.368G>A	p.Arg123His	245
				1 (1)	c.440G>A	p.Arg147His	242,277
				8 (9)	c.533A>G	p.Asn178Ser	242,244,245,262, 277,329
				1 (1)	c.551delT	p.Leu184fs*14	277,329
				1 (1)	c.706C>T	p.Leu236Phe	245
				1 (1)	c.731C>T	p.Thr244Ile	262
Group 4	2	2	Renal function restored (2)	1 (2)	c.1019G>C	p.Gly340Ala	232

Abbreviations: F: Number of families with each variant, P: Number of patients with each variant, aa: amino acid, Ref: references.

We have classified all the variants, but we cannot draw clear conclusions for variants that have been only described in a reduced number of families. Otherwise, we can discuss the phenotypic severity of the variants the most represented in each group (c.287G>A (p.Ser96Asn), c.740A>G (p.Tyr247Cys), c.533A>G (p.Asn178Ser), c.1019G>C (p.Gly340Ala)). For the rest of them, please address to Tables 1.6 and 1.7.

Table 1.7. Pathogenic variants of *COQ2* gene found in patients.

Gene/ protein	Pathogenic variants				Validation			*In silico* mutagenesis prediction				Ref.
	F (P)	cDNA mutation	aa modification	Exon	Segregation (S), Biochemical (B), Functional (F)			SIFT Patho-genic?	Poly Phen-2 Dama-ging?	SPiCE Probability to alter splicing?	CADD score	
***COQ2*[1]** 371 aa 7 exons NM_0013 58921.2 NP_00134 5850.1	1 (1)	c.26dupT	p.Ala10Argfs*33	1				-	-	-	21.8	262
	5 (7)	c.287G>A[2]	p.Ser96Asn	2	S	B	F	Pathog.	Probably	-	25.1	242,249, 257,277, 333
	2 (3)	c.368G>A	p.Arg123His	2	S			Pathog.	Probably	-	25.4	245,334
	1 (1)	c.395T>G	p.Met132Arg	2	S	B	F	Pathog.	Probably	-	27.7	328
	1 (1)	c.440G>A	p.Arg147His	3	S	B	F	Pathog.	Probably	-	31	242,277
	8 (9)	c.533A>G	p.Asn178Ser	3	S	B	F	Tole-rated	Probably	-	26.5	242,244, 245,262, 277,329
	1 (1)	c.551delT	p.Leu184fs*14	4	S	B		-	-	-	32	277,329
	1 (1)	c.682T>C[3]	p.Cys228Arg	5	S			Pathog.	Probably	-	25.3	330
	1 (1)	c.706C>T	p.Leu236Phe	5	S			Pathog.	Probably	-	25.1	245
	1 (1)	c.731C>T	p.Thr244Ile	5				Tole-rated	Probably	-	25.2	262
	2 (3)	c.740A>G	p.Tyr247Cys	5	S	B	F	Pathog.	Possibly	-	25.0	242,245, 277,331, 375
	1 (2)	c.755C>T	p.Ala252Val	5	S	B	F	Pathog.	Probably	-	26.5	277,332
	2 (3)	c.823A>G	p.Thr275Ala	6	S			Tole-rated	Possibly	-	23.7	262,334
	2 (2)	c.1009C>T[2]	p.Arg337*	7				-	-	-	38	249,262, 277
	1 (2)	c.1019G>C	p.Gly340Ala	7	S	B	F	Pathog.	Possibly	-	22.9	232
	1 (2)	c.1047delT	p.Asn351Ilefs*15	7	S	B	F	-	-	-	25.7	241

1. *COQ2* has four in-frame initiation codons. The last proposed nomenclature is used (starting from ATG4), corresponding to a 371-aa-long protein [277].
2. The patient with these two variants also carries a novel mutation in *MT-ND1* (3754C>A) with 22% of heteroplasmy in peripheral blood, which may contribute to the disease [249].
3. The patient with this mutation in homozygosis also carries an additional homozygous mutation in *ARSB* gene (c.1213 + 1G > A), which may contribute to the disease [330].

Reference sequences correspond to longest transcript. Abbreviations: F: Number of families with each variant, P: Number of patients with each variant, aa: amino acid, Pathog: Pathogenic, Ref: references.

p.Ser96Asn mutation is present in 7 patients from 5 different families corresponding to group 1, in homozygous (6/7 patients)[242,257,333] or compound heterozygous state (1/7 patients, with the nonsense mutation p.Arg337*)[249]. Its pathogenicity has been confirmed in a yeast model, where it showed to have very low levels of residual CoQ biosynthesis[277]. We can say that this variant probably leads to a severe infantile multisystemic disorder.

Two families were diagnosed having **p.Tyr247Cys** variant homozygously, and presented a SRNS with neurological symptoms (Group 2)[242,245]. However, the number of cases is small to be able to conclude anything further.

On the other hand, **p.Asn178Ser** variant is present in 9 patients from 8 families grouped in the isolated SRNS clinical group 3, in homozygosis (2/9 patients) [244,262] or compound heterozygosis (7/9 patients, with different missense and frameshift mutations) [242,245,262,329]. Its pathogenicity has been confirmed in a yeast model, where it showed to have 50% of residual CoQ_{10} biosynthesis, compared to the WT allele [277]. This pathogenic variant seems to be less severe.

Only one family manifested during adolescence a SRNS (Group 4) with a mild CNS involvement. These two siblings had **p.Gly340Ala** mutation in homozygosis. The pathogenicity of this variant has been confirmed in a yeast model, where it showed to have a mild effect, retaining almost the 50% of residual CoQ biosynthesis, compared to the WT allele[232].

Finally, some variants were found in heterozygous state in patients belonging to different groups (**p.Arg123His, p.Thr275Ala, p.Arg337***) and predicted pathogenic (Table 1.6 and 1.7)[245,249,262,334]. However, with the available data, it is hard to establish the extent to which each of the heterozygous mutations would contribute to the disease pathogenesis. p.Arg337* is a nonsense change, but since it is in the last exon, the protein only lacks the last 34 amino acids, and its effect on protein function is unknown.

Of note, some studies predict that specific *COQ2* variants increase susceptibility to adult-onset multisystem atrophy (MSA), with Parkinson's-like symptoms, particularly in the East Asian population, but not in the Caucasian one [379,382–384].

COQ4

COQ4 gene (MIM*612898) is located in chr9:128,322,544-128,334,072 (GRCh38.p13), forward strand. Four different protein-coding transcripts are annotated, but only the longest one is thought to produce COQ4 protein. This transcript (1,245 bp) encodes a 265 aa (7 exons) protein. The gene product of COQ4 appears to play a structural role in stabilising a complex that contains most of the CoQ_{10} biosynthesis enzymes. *COQ4* deficiency leads to a form of primary CoQ_{10} deficiency (COQ10D7, MIM#616276).

i. CoQ_{10} *deficiency due to COQ4 mutations*

35 patients from 26 families with *COQ4* mutations have been reported so far. *COQ4* patients mainly showed a **severe neurological affection**, associated with a **cardiomyopathy** (18/35, 51%) and **respiratory distress** (14/35, 40%) in the majority of the cases (Table 1.3).

a. Age of onset

The mean age of presentation was 1 yo (range birth-9 yo) (Figure 1.5), being mostly a neonatal or infancy (19/35, 54% and 11/35, 31%; respectively) presentation (Figure 1.10.B). Likewise *COQ2*, *COQ4* patients present different clinical pictures, and we can classify them in 3 different groups when stratified by the age of onset (Figures 1.7.B, 1.10).

Group 1 is constituted by 25 patients from 18 families (25/35, 71% of the total number of *COQ4* patients), which include all with birth-onset and some presenting the disease within the first months of life. The mean age of onset of patients in this group is 2 wo (range birth-4 mo). **Group 2** is composed of 4 patients from 4 Chinese families (4/35, 11% of the total number of *COQ4* patients), with a mean age of presentation of 6 mo (range 6-8 mo). **Group 3** is the one with less severe phenotype (5/35, 14% of the total number of *COQ4* patients), manifesting at a mean age of 6 yo (range 10 mo-9 yo).

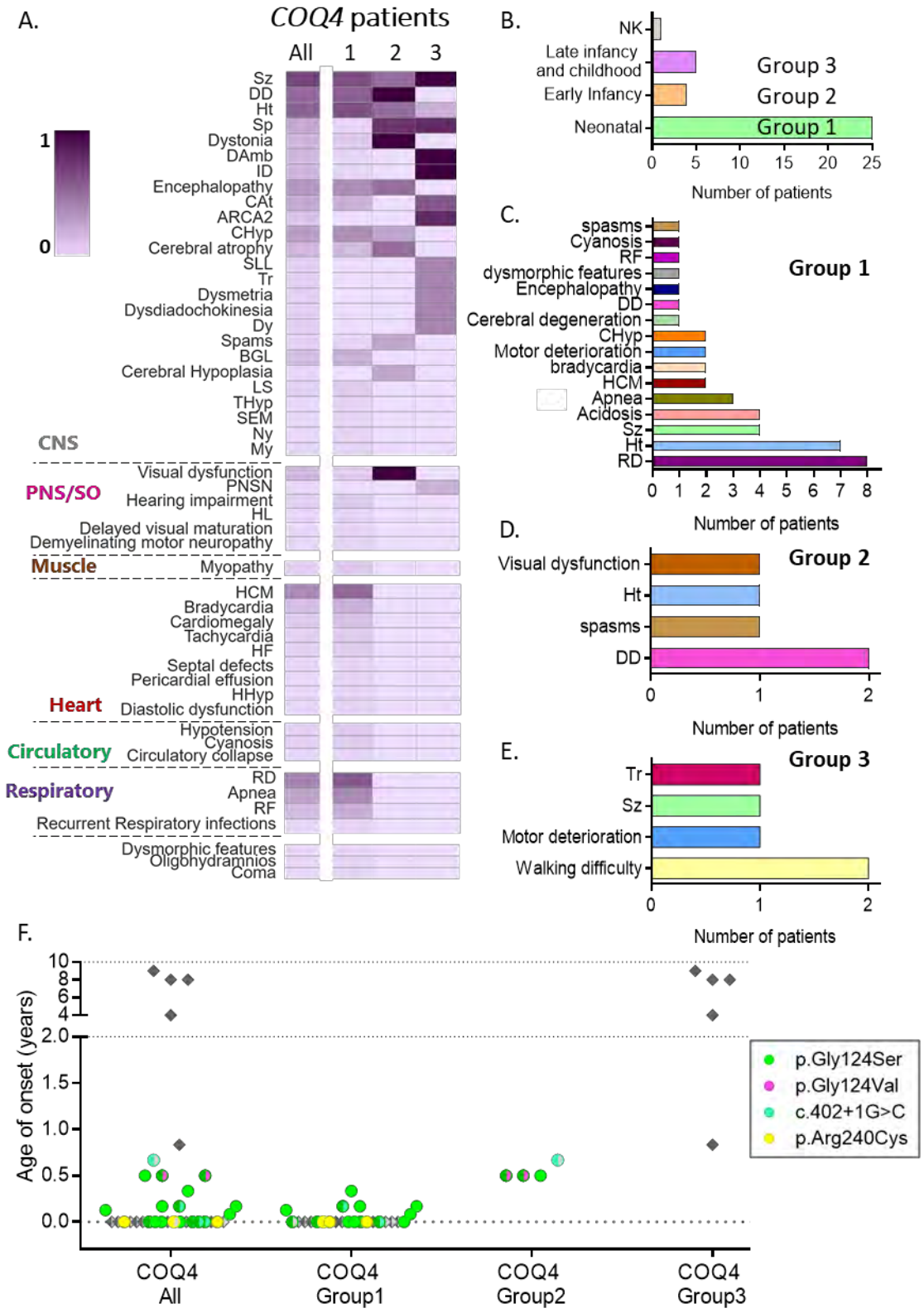

Figure 1.10. Clinical manifestations and genotype of *COQ4* patients.
(A) Symptom frequency found in *COQ4* patients, for each age-of-onset group 1-3. (B) Total number of patients in each age-of-onset group. (C-E) First symptoms and the number of patients manifesting them, for each age-of-onset group. (F) Age of onset and pathogenic variants of *COQ4* patients. Each point represents one patient. Coloured circles: mutations found in more than one family (see the legend). Rhombus: patients with mutations only present in one family (gray). Full-filled symbols: homozygous mutations, half-filled symbols: heterozygous mutations. Abbreviations: refer to Tables 1.1 and 1.2.

b. Symptoms at onset

Patients generally presented with a combination of 1, 2 or 3 clinical manifestations, typical of a severe multisystemic disorder (Figures 1.6.D, 1.10.C-E). The most common symptoms at onset were hypotonia (8/35, 23%), RD (8/35, 23%), seizures (5/35, 14%), acidosis (4/35, 11%), DD (3/35, 9%), motor deterioration (3/35, 9%) and apnea (3/35, 9%). Other less frequent symptoms at onset were walking difficulty, HCM, bradycardia, cerebellar hypoplasia (CHyp) or spasms (2/35, 6% each of them).

We can define different patterns of symptoms at the onset if we analyse them by the age of onset. The majority of *COQ4* patients presented at birth (group 1) with a collection of different symptoms affecting variable systems and organs (RD (8/25, 32%), hypotonia (7/25, 28%), acidosis (4/25, 16%), seizures (4/25, 16%), apnea (3/25, 12%), bradycardia (2/25, 8%), HCM (2/25, 8%)) [250–252,336,340] (Figure 1.10.C). Infantile-onset patients (group 2) presented with DD (2/4, 50%), spasms (1/4, 25%), visual dysfunction (1/4, 25%) and hypotonia (1/4, 25%) (Figure 1.10.D) [250,340]. Some patients presented during childhood (group 3) and their first symptoms were motor deterioration or walking difficulties (3/5, 60%), tremor (1/5, 20%) and seizures (1/5, 20%), being this onset typical of a cerebellar disorder (Figure 1.10.E) [251,335,338].

c. Clinical manifestations of the disease

COQ4 patients mainly showed a severe CNS affection, with encephalopathy (11/35, 31%), seizures (24/35, 69%), hypotonia (19/35, 54%) and CHyp (10/35, 29%), associated to HCM (13/35, 37%) and RD (14/35, 40%) (Figure 1.10.A); and a fatal outcome with death within the first days (2/35, 6%), months (16/35, 46%) or years of life (2/35, 6%) (Table 1.3). Of note, the majority of the identified *COQ4* patients are Chinese (17/35, 49%).

The main phenotype of *COQ4* deficiency is a **neonatal-infantile onset encephalo-cardiomyopathy** (group 1) [250–252,336,339–341]. The most common cardiac manifestations were HCM (13/25, 52%), bradycardia (5/25, 20%), cardiomegaly (3/25, 12%), HF (2/25, 8%), tachycardia (2/25, 8%); while CNS was mainly affected by hypotonia (16/25, 64%), seizures (16/25, 64%), DD (13/25, 52%), encephalopathy (9/25, 36%), CHyp (9/25, 36%), BGL (5/25, 20%), amongst other implications. Additionally to cardiac and CNS

involvement, these patients very often presented RD (14/25, 56%) and apnea (9/25, 36%). Almost all these patients died (19/25, 76%) (Figure 1.4.B) mainly because of a multiorgan failure (7/25, 28%), a complication of the cardiac (4/25, 16%) or respiratory (4/25, 16%) functions, or a severe episode of acidosis (3/25, 12%).

Some patients had a slightly milder outcome (group 2), with an **infantile-onset encephalopathy** mainly with DD (4/4, 100%), dystonia (4/4, 100%), visual dysfunction (4/4, 100%), spasticity (3/4, 75%) and seizures (2/4, 50%). The clinical picture is characterised by the lack of cardiac and respiratory involvement (Figure 1.10.A) [250,340].

The less severe phenotype is that of patients manifesting a **childhood-onset progressive spinocerebellar ataxia** (group 3), similar to *COQ8A* patients' clinical presentation [251,335,338]. After onset, during their childhood and adolescence, they developed ataxia (4/5, 80%), with deteriorated ambulation (DAmb) (5/5, 100%), ID (5/5, 100%), seizures (5/5, 100%), spasticity (4/5, 80%), CAt (3/5, 60%), dysarthria (2/5, 40%), dysdiadochokinesia (2/5, 40%), dysmetria (2/5, 40%), tremor (2/5, 40%), SLL (2/5, 40%), hypotonia (1/5, 20%) and PNSN (1/5, 20%).

ii. CoQ_{10} *treatment and effects*

CoQ_{10} treatment was administered to 20/35 (57%) of the *COQ4* patients, representing all the three groups described (Tables 1.4 and 1.8). In the most severe group (group 1), 12/25 patients were treated. Most of them did not obtain any benefits from the treatment (5/12) [250,252]. Small improvements in cardiac function (1/12) [252], seizures (2/12) [250,339], acidosis (1/12) [252] or subjective response (1/12) [340] were observed in these patients. In group 2, all the 4 patients were treated. Some of them improved the seizures condition (1/4), the general response (1/4) or stabilised the disease progression (1/4), while others did not experience any amelioration (2/4) [250,340]. From the last group, the childhood-onset ataxia, 4/5 patients were treated and one of them reported an improvement of the ataxic condition, while the outcome of the rest of them was not specified (group 3) [335,338].

Table 1.8. *COQ4* patients classified by age of onset. CoQ_{10} treatment and mutations.

Group	# of patients	CoQ_{10} treatment		F (P)	cDNA change	Aa change	Ref.
		# of patients treated	Effect				
Group 1	25	12	No benefits (5), Improvement of lactic acidosis (1), Improvement of cardiac function (2), Muscle improvement (1), Subjective response improvement (1), Improvement of Sz or Ep (2), Stable condition (2), Improvement in development (1)	1 (1)	c.23_33delTCCTCCGTCGG	p.Val8Alafs*19	336
				1 (2)	c.155T>C	p.Leu52Ser	251
				1 (2)	c.197_198delGCinsAA	p.Arg66Gln	252
				1 (2)	c.202G>C	p.Asp68His	252
				1 (2)	c.245T>A	p.Leu82Gln	252
				1 (1)	c.311G>T	p.Asp111Tyr	336
				1 (1)	c.356C>T	p.Pro119Leu	336
				9 (13)	c.370G>A	p.Gly124Ser	250,339,340
				3 (4)	c.402+1G>C	?	250
				1 (1)	c.421C>T	p.Arg141*	251
				1 (1)	c.433C>G	p.Arg145Gly	251
				1 (2)	c.473G>A	p.Arg158Gln	252
				1 (2)	c.521_523delCCA	p.Thr174del	251
				1 (1)	c.533G>A	p.Gly178Glu	340
				3 (3)	c.718C>T	p.Arg240Cys	251,252
				1 (1)	3.9 Mb deletion of chromosome 9q34.13, including COQ4 gene		341
Group 2	4	4	No benefits (2), Subjective response improvement (1), Improvement of Sz or Ep (1)	3 (3)	c.370G>A	p.Gly124Ser	250,340
				2 (2)	c.371G>T	p.Gly124Val	250,340
				1 (1)	c.402+1G>C	?	250
				1 (1)	c.550T>C	p.Trp184Arg	250
Group 3	5	4	Improvement of ataxia (1), NK (3)	1 (2)	c.164G>T	p.Gly55Val	335
				1 (1)	c.190C>T	p.Pro64Ser	251
				1 (2)	c.230C>T	P.Thr77Ile	338

Abbreviations: F: Number of families with each variant, P: Number of patients with each variant, aa: amino acid, Ref: references, NK: not known. For Clinical Manifestations abbreviations, refer to Tables 1.1 and 1.2.

iii. Pathogenicity of the mutations

There are 22 reported *COQ4* mutations associated with primary CoQ_{10} deficiency in the literature (Figures 1.8, 1.10.F, Tables 1.8 and 1.9). Nearly all of them were confirmed to segregate within the different families (18/22, 82%), except for the mutations c.402+1G>C and c.533G>A (p.Gly178Glu), for which no data were available. The pathogenicity of some of the variants (6/22, 38%) was confirmed in a yeast model [251].

Table 1.9. Pathogenic variants of *COQ4* gene found in patients.

Gene/ protein	Pathogenic variants				Validation			*In silico* mutagenesis prediction				Ref.
	F (P)	cDNA mutation	aa modification	Exon	Segregation (S), Biochemical (B), Functional (F)			SIFT Patho-genic?	Poly Phen-2 Dama-ging?	SPiCE Prob. to alter splicing?	CADD score	
COQ4 265 aa 7 exons NM_016035.5 NP_057119.3	1 (1)	c.23_33delTCCTCCGTCGG	p.Val8Alafs*19	1	S			-	-	-	21.1	336
	1 (2)	c.155T>C	p.Leu52Ser	2	S			Pathog.	Probably	-	28.6	251
	1 (2)	c.164G>T	p.Gly55Val	2	S			Pathog.	Probably	-	24.4	335
	1 (1)	c.190C>T	p.Pro64Ser	2	S	B		Pathog.	Probably	-	26.8	251
	1 (2)	c.197_198delGCinsAA	p.Arg66Gln	2	S	B		Pathog.	Probably	-	32	252
	2 (3)	c.202G>C	p.Asp68His	2-3	S	B		Pathog.	Probably	high	35	252,337
	1 (2)	c.230C>T	P.Thr77Ile	3	S	B		Pathog.	Possibly	-	28.7	338
	1 (2)	c.245T>A	p.Leu82Gln	3	S	B		Pathog.	Benign	-	24.6	252
	1 (1)	c.311G>T[1]	p.Asp111Tyr	4		B		Pathog.	Probably	-	27.2	336
	1 (1)	c.356C>T[1]	p.Pro119Leu	4	S		F	Pathog.	Probably	-	26.0	336
	12 (16)	c.370G>A[2]	p.Gly124Ser	4	S	B	F	Pathog.	Probably	-	24.7	250,339, 340
	2 (2)	c.371G>T	p.Gly124Val	4	S			Pathog.	Probably	-	24.4	340
	4 (5)	c.402+1G>C	?	Intron 4	S	B		-	-	high	33	250
	1 (1)	c.421C>T	p.Arg141*	5	S	B	F	-	-	-	41	251
	1 (1)	c.433C>G	p.Arg145Gly	5				Pathog.	Possibly	-	25.1	251
	1 (1)	c.469C>A	p.Gln157Lys	5		B		Tole-rated	Possibly	-	23.5	337
	1 (2)	c.473G>A	p.Arg158Gln	5	S			Pathog.	Probably	-	29.7	252
	1 (2)	c.521_523delCCA	p.Thr174del	5	S			-	-	-	22.1	251
	1 (1)	c.533G>A	p.Gly178Glu	6	S			Pathog.	Probably	medium	33	340
	1 (1)	c.550T>C	p.Trp184Arg	6	S	B		Pathog.	Probably	-	26.2	250
	3 (3)	c.718C>T	p.Arg240Cys	7	S		F	Pathog.	Probably	-	32	251,252
	1 (1)	3.9 Mb deletion of Chr 9q34.13, including *COQ4* gene				B		-	-	-	-	-

1. These two missense variants were identified in a patient in the same allele, paternally inherited. The maternally inherited *COQ4* allele carried the c.22_33delTCCTCCGTCGG deletion (p.Val8Alafs*19) [336].
2. The c.370G>A p.(Gly124Ser) variant in *COQ4* has been described as a founder mutation in southern Chinese population, being identified in 16 patients from 12 Chinese families [250,339,340].

Reference sequences correspond to longest transcript. Abbreviations: F: Number of families with each variant, P: Number of patients with each variant, aa: amino acid, Pathog: pathogenic, Prob: probability, Ref: references, Chr: chromosome.

We classified the mutations into the three age of onset groups (Figure 1.10.F). Here, we will only discuss the most represented variants, which are the c.718C>T (p.Arg240Cys) mutation, found in 3 families; and 3 mutations found in Chinese families, c.370G>A (p.Gly124Ser), c.402+1G>C and c.371G>T (p.Gly124Val).

Three families were diagnosed with **p.Arg240Cys** variant in homozygous (2/3) [252] or heterozygous (1/3) state with the nonsense variant p.Arg141* [251,372], and they all presented a **fatal neonatal onset encephalo-cardiomyopathy**.

p.Gly124Ser mutation has been described as a founder mutation in the southern Chinese population, and it has been described in 16 patients from 12 different families[250,340]. Most of them (13 patients from 9 families) have been associated to the most severe phenotype (group 1), in homozygosis (8/13 patients) or heterozygosis (5/13 patients) with the probably spliceogenous variant **c.402+1G>C** in 4 of the cases [250]. This variant has a high probability of altering splicing, predicted with the SPiCE software (Table 1.9). The rest of the patients with the **p.Gly124Ser** mutation (3 patients from 3 families) are classified in the phenotypic group 2, in homozygosis (1/3 patients) or heterozygosis (2/3 patients) with the c.371G>T **(p.Gly124Val**) variant[250,340]. These three pathogenic variants have all been described in patients with a **neonatal-infantile onset encephalo-cardiomyopathy** or an **infancy-onset encephalopathy**.

A patient with haploinsufficiency of *COQ4* due to a *de novo* heterozygous 3.9-Mb deletion of chromosome 9q34 presented encephalomyopathic manifestations and CoQ_{10} deficiency in fibroblasts [341].

All the 5 patients from 3 families with 3 different mutations in homozygosis (p.Pro64Ser, p.Thr77Ile and p.Gly55Val) [251,335,338] had a **childhood-onset progressive spinocerebellar ataxia** (group 3). These mutations could be considered less severe than the rest of the described *COQ4* mutations, but the number of cases is again too small to reach any sound conclusion.

Finally, there are some other variants found in homozygous or heterozygous state in patients belonging to the different groups. We have predicted their pathogenicity and classified them, but we cannot be certain of how they would contribute to the disease pathogenesis because of their low representation (Tables 1.8 and 1.9).

COQ5

COQ5 gene (MIM*616359) is located in chr12:120,503,279-120,534,434 (GRCh38.p13), reverse strand. Six different protein-coding transcripts are annotated, but only the longest one is thought to produce COQ5 protein. This transcript (1,506 bp) codes for a 327aa (7 exons) protein. The gene product, COQ5, is a methyltransferase required for the methylation of 2-polyprenyl-6-methoxy-1,4-benzoquinol ($DDMQH_2$) to 2-polyprenyl-3-methyl-6-methoxy-1,4-benzoquinol ($DMQH_2$). Defects in this gene have been found to cause primary CoQ_{10} deficiency (COQ10D9, MIM#619028).

i. CoQ_{10} *deficiency due to COQ5 mutations*

Only 3 patients from 1 family with *COQ5* defects have been reported so far. These three female siblings presented varying degrees of an **early childhood cerebellar ataxic phenotype** similar to *COQ8A* patients [326] (Figures 1.5, 1.6.E). The first symptoms they manifested were a slow motor development (2/3) with ID (2/3), ataxia (1/3) or dysarthria (1/3). The age of last examination was between 14 and 22 years old. They mainly presented cerebellar ataxia (3/3), encephalopathy (3/3), generalized tonic-clonic seizures (2/3), and cognitive disability (3/3) (Table 1.3).

ii. CoQ_{10} *treatment and effects*

CoQ_{10} treatment was administered to the three patients and all of them experienced a clinical improvement of their ataxic phenotype.

iii. Pathogenicity of the mutations

This family had a biallelic duplication in the *COQ5* gene (Table 1.10). This duplication of 9,590 bp does not alter the original *COQ5* open reading frame (ORF) and is located about 1 kb after the DNA sequence that encodes the *COQ5* 3' untranslated region (UTR). The duplicated region spans the last four exons of the gene (4-7) and part of the 3' UTR. This duplication creates an abnormal isoform due to an altered splicing event, where the original 3'UTR is partially deleted and fused with duplicated exons (exons 4–7), thus creating a new 3'UTR that appears abnormally long [326].

Table 1.10. Pathogenic variants of *COQ5, COQ6, COQ7* and *COQ9* genes found in patients.

Gene/ Protein	Pathogenic variants				Validation			*In silico* mutagenesis prediction				Ref.
	F (P)	cDNA mutation	aa modification	Exon	Segregation (S), Biochemical (B), Functional (F)			SIFT Patho-genic?	Poly Phen-2 Dama-ging?	SPiCE Prob. to alter splicing?	CADD score	
COQ5 327 aa 7 exons NM_032314.4 NP_115690.3	1 (3)	9590 bp tandem duplication of the last 4 exons of COQ5 after 1Kb of 3'UTR (base pair positions: Chr 12: 120,940,150-120,949,950/hg19)			S	B		-	-	-	-	326
COQ6 468 aa 12 exons NM_182476.3 NP_872282.1	6 (6)	c.189_191delGAA	p.Lys64del	2	S			-	-	-	22.4	235
	1 (1)	c.484C>T[1]	p.Arg162*	5			F	-	-	-	38	233
	1 (1)	c.564G>A[1]	p.Trp188*	5			F	-	-	-	39	233
	1 (1)	c.686A>C	p.Gln229Pro	6	S			Tole-rated	Probably	-	27.5	235
	2 (7)	c.763G>A	p.Gly255Arg	7	S		F	Pathog.	Probably	-	32	233,342
	6 (6)	c.782C>T	p.Pro261Leu	7	S		F	Pathog.	Probably	low	33	232,235
	1 (1)	c.804delC	p.Leu269Trpfs*13	8				-	-	-	32	343
	5 (8)	c.1058C>A	p.Ala353Asp	9	S		F	Pathog.	Probably	-	31	233,234, 236,245, 342
	3 (3)	c.1078C>T	p.Arg360Trp	9	S			Pathog.	Probably	-	32	231,258, 343
	1 (1)	c.1154A>C	p.Asp385Ala	11				Pathog.	Probably	-	29.8	245
	2 (2)	c.1235A>G[1]	p.Tyr412Cys	11			F	Pathog.	Probably	-	25.5	245,342
	1 (1)	c.1341G>A	p.Trp447*	11	S		F	-	-	-	41	233,342
	1 (1)	c.1383delG	p.Gln461fs*478	12	S		F	-	-	-	33	233,342
COQ7 217 aa 6 exons NM_016138.5 NP_057222.2	1 (1)	c.319C>T	p.Arg107Trp	3	S	B		Pathog.	Probably	-	33	240
	1 (1)	c.332T>C (and c.308C>T)[2]	p.Leu111Pro (and p.Thr103Met)	3	S	B	F	Pathog.	Probably	-	28.5 (23.1)	238
	1 (1)	c.422T>A	p.Val141Glu	4	S	B	F	Pathog.	Probably	-	28.8	238,239
	1 (1)	c.599_600delinsTAATGCATC	p.Lys200Ilefs*56	6	S	B		-	-	-	27.1	240
COQ9 318 aa 9 exons NM_020312.4 NP_064708.1	1 (1)	c.384delG	p.Gly129Valfs*17	4	S			-	-	-	23.2	247
	1 (1)	c.521+1delG	p.Ser127_Arg202del	Int.5	S	B	F	-	-	high	24.4	256
	1 (4)	c.521+2T>C	p.Ser127_Arg202del	Int.5	S	B		-	-	high	33	246
	1 (4)	c.711+3G>C	p.Ala203_Asp237del	Int.7	S	B		-	-	high	23.6	246
	1 (1)	c.730C>T	p.Arg244*	7		B	F	-	-	-	46	248,327

1. These pathogenic variants were found in simple heterozygosis in at least one patient [233,342].
2. *COQ7* c.308C>T polymorphism seems to increase COQ7 protein instability and intensify the effect of the mutation. The patient also has a 1555A>G mutation in mtDNA, which may contribute to the disease [238].

Reference sequences correspond to longest transcript. Abbreviations: F: Number of families with each variant, P: Number of patients with each variant, aa: amino acid, Prob: probability, Int: Intron, Ref: references, UTR: untranslated region, Chr: chromosome, Pathog: pathogenic.

COQ6

COQ6 gene (MIM*614647) is located in chr14:73,949,926-73,963,670 (GRCh38.p13), plus strand. At least three alternatively spliced transcript variants encoding different isoforms have been described for this gene. The most represented transcript, the longest one (2,109 bp), encodes a 468 aa (12 exons) protein, COQ6 isoform 1 (or *a*). This protein is an evolutionarily conserved FAD-dependent monooxygenase required for the C5-ring hydroxylation during CoQ biosynthesis. It catalyses the hydroxylation of 3-decaprenyl-4-hydroxybenzoic acid (HHB) to 3-decaprenyl-4,5-dihydroxybenzoic acid (DHHB). The electrons required for the hydroxylation reaction may be obtained indirectly from NADPH via a ferredoxin/ferredoxin reductase system.

There are two additional transcripts (isoforms 2 or *b*; and 3 or *c*), which are present at lower levels in cells and encode different proteins. Transcript variant 2 (1,538 bp), encodes COQ6 isoform 2 (391 aa, 11 exons), which contains an alternative first exon (exon 1b) and lacks exon 3. It is thought that it is not active [342]. The two isoforms differ in the use of alternative exon 1a or 1b and the splicing of exon 3 (absent in isoform 2). Transcript variant 3 (1,608 bp), encodes COQ6 isoform 3 (443 aa, 12 exons). It differs from isoform 1 only for the first exon but it does not rescue CoQ_{10} biosynthesis in human cells lacking *COQ6* [165].

Mutations in this gene are associated with autosomal recessive CoQ_{10} deficiency (COQ10D6, MIM#614650), which manifests as nephrotic syndrome with sensorineural hearing loss.

i. CoQ_{10} *deficiency due to COQ6 mutations*

30 patients from 22 families with *COQ6* mutations have been reported in the literature up to date. *COQ6* patients mainly showed a **nephrotic syndrome** (26/30, 87%), associated in most of the cases **with sensorineural hearing loss** (18/30, 60%) (Table 1.3).

a. Age of onset

The disease was first presented in patients at a mean age of almost 3 yo (32 mo) (range 2 mo-10 yo) (Figure 1.5), having mostly infancy or childhood-onset (15/30, 50% and 11/30, 37%; respectively) (Figure 1.11.B). When classified by the age of onset, the cases

were sorted in 2 different groups, each of them having a slightly different clinical picture (Figures 1.7.C, 1.11).

Group 1 includes 15 patients from 11 families (15/30, 50% of the total number of *COQ6* patients), who first manifested before the age of 2 yo. The mean age of onset of patients in this group is 1 yo (range 2 mo-2 yo). Patients with childhood-onset are grouped together in **group 2**, which includes 12 patients from 10 families (12/30, 40% of the total number of *COQ6* patients). The mean age of presentation was almost 5 yo (range 3 -10 yo).

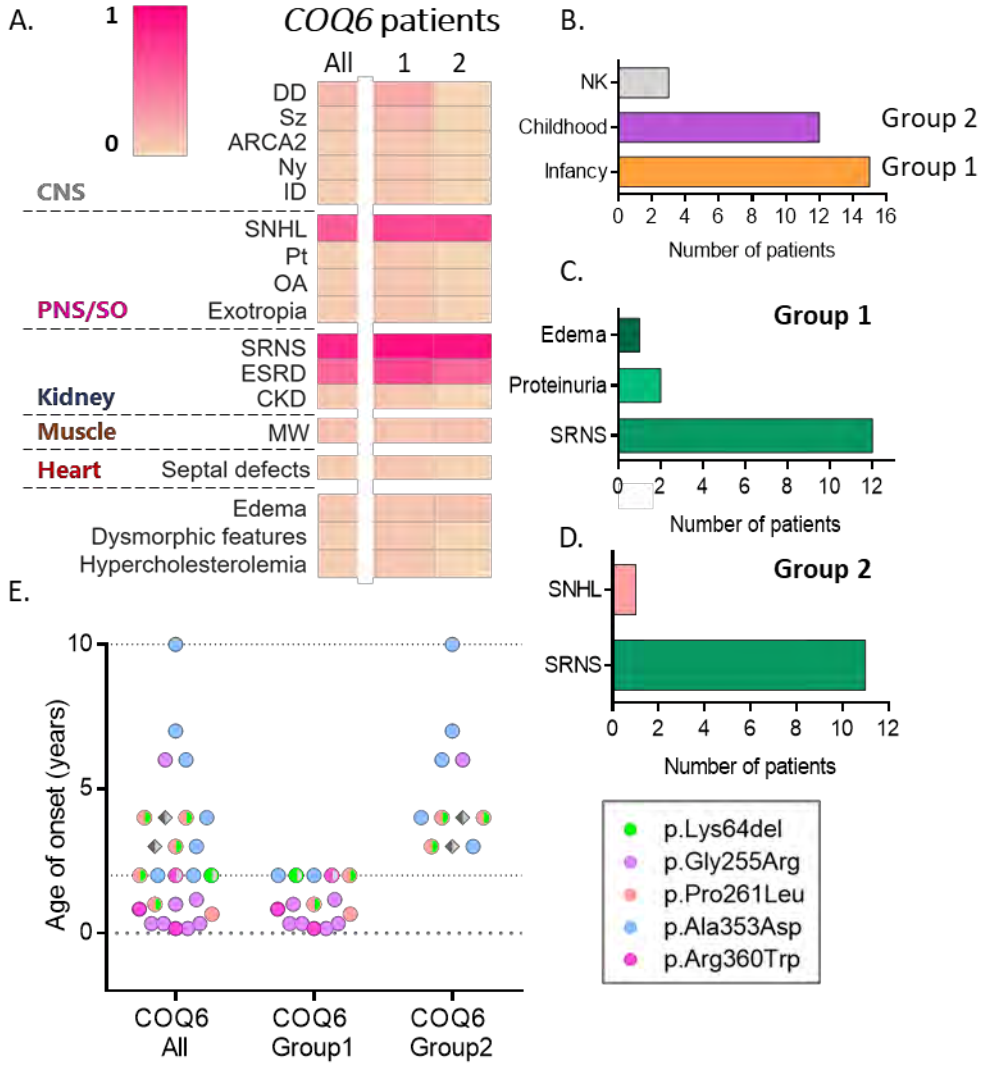

Figure 1.11. Clinical manifestations and genotype of *COQ6* patients.
(A) Symptom frequency found in *COQ6* patients, for each age-of-onset group 1 and 2. (B) Total number of patients in each age-of-onset group. (C-D) First symptoms and the number of patients manifesting them, for each age-of-onset group. (E) Age of onset and pathogenic variants of *COQ6* patients. Each point represents one patient. Coloured circles: mutations found in more than one family (see the legend). Rhombus: patients with mutations only present in one family (gray). Full-filled symbols: homozygous mutations, half-filled symbols: heterozygous mutations. Abbreviations: refer to Tables 1.1 and 1.2.

b. Symptoms at onset

Patients with *COQ6* mutations mainly first presented with SRNS (24/30, 80%) [233,235], but in some cases proteinuria (2/30, 7%), edema (1/30, 3%) or SNHL (1/30, 3%) were found as first manifestations of the disease (Figures 1.6.F, 1.11.C and D).

When stratified by the age of onset, patients with infancy onset (group 1) mainly presented with SRNS (12/15, 80%), but some patients were firstly found having proteinuria (2/15, 13%) [233,343] or edema (1/15, 7%) [258] (Figure 1.11.C). Patients with childhood-onset (group 2) presented with SRNS as the first symptom (11/12, 92%) [233,235,245], and one of them first showed SNHL (1/12, 8%), and he did not develop SRNS afterwards [236] (Figure 1.11.D).

c. Clinical manifestations of the disease

COQ6 patients mainly showed a SRNS (26/30, 87%), associated in most of the cases with SNHL (18/30, 60%) (Table 1.3). Some of them also presented a CNS affection, with seizures (2/30, 7%), ataxia (1/30, 3%), exotropia (1/30, 3%), ID (1/30, 3%), nystagmus (1/30, 3%), or ptosis (1/30, 3%). These neurological manifestations occur mostly in patients manifesting earlier in life (Figure 1.11.A).

Group 1 had an **infantile-onset nephrotic syndrome** (14/15, 93%) that evolved, in most of the cases, to an ESRD (10/15, 67%). These patients also developed **sensorineural hearing loss** (8/15, 53%) [233,235,245]. Group 1's characteristic is that some of the patients (7/15, 47%) also presented a **CNS affection**, with DD (3/15, 20%) [231,233,258], seizures (2/15, 13%) [233], ataxia (1/15, 7%) [233], exotropia (1/15, 7%) [235], ID (1/15, 7%) [231], nystagmus (1/15, 7%) [235] or ptosis (1/15, 7%) [231]. Other less frequent manifestations are OA, MW, cardiovascular abnormalities, septal defects, edema, dysmorphic features or hypercholesterolemia (each of them present in 1/15 patient, 7%).

Patients with **childhood-onset** (group 2) had an **SRNS** (11/12, 92%), **associated with SNHL** (8/12, 67%) [233,235,236,245]. Some of the patients developed an ESRD (6/12, 50%). One of them also had MW (1/12, 8%), and another one, edema (1/12, 8%).

ii. CoQ_{10} *treatment and effects*

CoQ_{10} treatment was administered to 9/30 (30%) of the *COQ6* patients from the two groups described (Tables 1.4 and 1.11). In general, they responded well to the treatment, with some improvements in renal function. 6/15 patients from group 1 were treated, and they improved proteinuria (4/6) [231,233,258], renal function (2/6) [231,343], growth retardation (2/6) [231,258] and SNHL (1) [233]. In group 2, 3/12 patients were treated and only 1 improved proteinuria [233,234,236].

Table 1.11. *COQ6* patients classified by age of onset. CoQ_{10} treatment and mutations.

Group	# of patients	CoQ_{10} treatment		F (P)	cDNA change	Aa change	Ref.
		# of patients treated	Effect				
Group 1	15	6	Improved proteinuria (4), Improved renal function (2), Improved growth retardation (2), Improved SNHL (1)	3 (3)	c.189_191delGAA	p.Lys64del	235
				1 (1)	c.686A>C	p.Gln229Pro	235
				2 (6)	c.763G>A	p.Gly255Arg	233,342
				3 (3)	c.782C>T	p.Pro261Leu	232,235
				1 (1)	c.804delC	p.Leu269Trpfs*13	343
				2 (2)	c.1058C>A	p.Ala353Asp	233,234,342
				3 (3)	c.1078C>T	p.Arg360Trp	231,258,343
Group 2	12	3	Improved proteinuria (1)	3 (3)	c.189_191delGAA	p.Lys64del	235
				1 (1)	c.763G>A	p.Gly255Arg	233,342
				3 (3)	c.782C>T	p.Pro261Leu	235
				4 (6)	c.1058C>A	p.Ala353Asp	233,234,236, 245,342
				1 (1)	c.1154A>C	p.Asp385Ala	245
				1 (1)	c.1235A>G	p.Tyr412Cys	245
				1 (1)	c.1341G>A	p.Trp447*	233,342
				1 (1)	c.1383delG	p.Gln461fs*478	233,342

Abbreviations: F: Number of families with each variant, P: Number of patients with each variant, aa: amino acid, Ref: references, SNHL: sensorineural hearing loss.

iii. Pathogenicity of the mutations

Primary CoQ_{10} deficiency due to *COQ6* mutations has been associated with 13 different variants in *COQ6* (Figures 1.8, 1.11.E, Tables 1.10 and 1.11). Most of them were confirmed to segregate with the disease within the different families (8/13, 62%), while their pathogenicity was predicted and confirmed (8/13, 62%) in a yeast model [342].

We classified the variants into the two age of onset groups. Only the most represented variants will be discussed here, which are 5: c.189_191delGAA (p.Lys64del), c.763G>A (p.Gly255Arg), c.782C>T, (p.Pro261Leu), c.1058C>A (p.Ala353Asp) and c.1078C>T (p.Arg360Trp). Some of these variants appear more frequently in group 1, others in group 2, while some of them are equally represented in the two groups (Figure 1.14 and Table 1.11).

The **p.Gly255Arg** missense change was found in 7 patients from 2 families, 6 of them classified in group 1 and only 1 in group 2 [233]. They presented an infantile-onset nephrotic syndrome with sensorineural hearing loss and a slight CNS involvement. However, the number of cases is small to be able to draw a definite conclusion about genotype-phenotype correlation. The pathogenicity of this mutation has been confirmed in a yeast model [342], in which the mutant allele retained a low residual CoQ biosynthetic function (only 15% of the WT levels).

The **p.Arg360Trp** substitution has been reported in 3 patients of 3 families, in 2 cases in homozygosis[231,258], while in one case in heterozygosis with a frameshift mutation [343]. This variant has been associated with the most severe phenotype (group 1), but the number of patients is still low to be able to define a correlation.

The **p.Ala353Asp** variant was reported in 8 patients from 5 families, always in homozygosis. They were classified mostly in group 2 (6/8 patients)[233,236,245], while two patients belonged to group 1 (being in the upper limit of group1, 2 yo) [233]. These patients mainly presented childhood-onset SRNS, associated with SNHL. The pathogenicity of this mutation has been confirmed in a yeast model [342], in which the mutant allele retained 30% of the WT CoQ biosynthetic function.

p.Lys64del mutation is described in 6 patients from 6 different families, in heterozygosis with the missense mutations **p.Pro261Leu** (5/6) [232,235] or p.Gln229Pro (1/6) [235]. **p.Pro261Leu** was also found in homozygosis in 1 patient [232]. Patients with these mutations are equally found in group 1 or 2, so they might not contribute to the differences in age of onset or clinical presentation. However, the age of presentation of these patients in group 1 is closer to the upper limit, 2 yo, while in group 2 is closer to the lower limit, 3 yo. The pathogenicity of the p.Pro261Leu mutation was confirmed in

a yeast model [232], in which the mutant allele retained a low residual CoQ biosynthetic function (only 10% of the WT levels).

Finally, there are some variants found in homozygosis or heterozygosis in patients belonging to the different groups. We have classified them, but we cannot be certain of how they would contribute to the disease pathogenesis because of their low representation (Table 1.11).

COQ7

COQ7 gene (MIM*601683) is located in chr16:19,067,595-19,080,095 (GRCh38.p13), forward strand. It has two transcript variants, each one with six exons, differing in the first exon. The longest transcript (2,642 bp) encodes a 217 aa long protein, whereas the shorter transcript (819 bp) results in a 179 aa protein. The longest one is thought to be COQ7 protein, which is a mitochondrial di-iron oxidase responsible for hydroxylating 5-demethoxyubiquinol ($DMQH_2$) in the presence of NADH, during CoQ_{10} biosynthesis. Mutations in this gene are a cause of primary CoQ_{10} deficiency (COQ10D8, MIM#616733).

i. CoQ_{10} *deficiency due to COQ7 mutations*

Only 3 patients from 3 families with *COQ7* defects have been reported so far. These patients presented varying degrees of a **neonatal-infancy onset multisystemic disorder**, with CNS, PNS, renal, muscle and heart involvement (Table 1.3). The mean age of onset was 4 mo (range birth -1 yo), and they presented with RD (2/3, 67%) and other symptoms, such as cardiomegaly, HF, hypertension, hypotonia or slow motor development (1/3, 33% for each symptom) (Figures 1.5, 1.6.G). The main manifestations were hypotonia (3/3), DD (3/3), SNHL (3/3), PNSN (2/3), MW (3/3), HCM (2/3) and RD (2/3). However, the three families manifested different clinical pictures.

The most severe case was a Chinese boy, who presented at birth with cardiomegaly, heart failure and respiratory distress. He developed an encephalopathy with DD, hypotonia, BGL and ptosis. He had SNHL and visual impairment, as well as renal cysts and MW, with low muscle bulk. The heart was also affected by an HCM, and he experienced HF. He passed away at 1 year of age due to an episode of sepsis. He had two compound heterozygous mutations in *COQ7*, a missense mutation (c.319C>T,

p.Arg107Trp) and a frameshift variant (c.599_600delinsTAATGCATC, p.Lys200Ilefs*56)[240].

The second case was a Syrian boy who debuted at birth, with hypotonia, RD and hypertension. The patient developed a complex clinical picture with multiorgan involvement, including mild ID, hypotonia, DD. He also had a PNSN, with SNHL and visual impairment. He had MW and HCM. Kidney dysplasia resolved alone within the first year of life. The age of the last examination was 9 years old. He had a missense homozygous mutation (c.422T>A, p.Val141Glu) in *COQ7* gene [239].

The third family presented a less severe phenotype. The patient, a 1-year-old girl, debuted with slow motor development and showed spasticity, hypotonia and DD. She also presented a PNSN, with SNHL and MW. The age of the last examination was 6 years old. She had a missense homozygous mutation (c.332T>C, p.Leu111Pro) in the *COQ7* gene [238].

ii. CoQ_{10} *treatment and effects*

CoQ_{10} treatment was administered to the three patients (Table 1.4). The most severe one didn't benefit from the treatment [240], while the two others experienced a stabilization of the disease progression, with no improvement but no deterioration either [238,239].

iii. Pathogenicity of the mutations

4 pathogenic variants of *COQ7* have been associated to primary CoQ deficiency in the literature so far (Figure 1.8 and Table 1.10). All the mutations segregated within the different families. The pathogenicity of the homozygous mutations from the two less severe cases was confirmed by expressing the variants in mouse cells KO in *Coq7*. The levels of residual CoQ synthesis were consistent with the severity of the disease observed in the patients. The missense mutation from the most severe case, c.319C>T (p.Arg107Trp), has been predicted to be pathogenic with SIFT, PolyPhen-2 and CADD tools (Table 1.10).

COQ9

COQ9 gene (MIM*612837) is located in chr16:57,447,425-57,461,275 (GRCh38.p13), forward strand. The protein-coding transcript (1,630 bp) encodes a 318 aa long protein (9 exons). The gene product, COQ9, is a lipid-binding protein thought to bind CoQ and present it to COQ7 during CoQ biosynthesis. Defects in this gene are a cause of CoQ deficiency (COQ10D5, MIM#614654).

i. CoQ_{10} *deficiency due to COQ9 mutations*

Only 7 patients from 4 families with *COQ9* mutations have been reported so far. These patients presented varying degrees of a severe **neonatal-infancy onset multisystemic disorder**, with CNS, renal and cardiac involvement (Table 1.3) [246–248,256,327]. The mean age of onset was 1 mo (range birth-9 mo) (Figures 1.5, 1.6.H). They presented with intrauterine growth restriction (IUGR) (3/7, 43%), RD (2/7, 29%), poor respiratory efforts accompanied by hypotonia, bradycardia and cyanosis (1/7, 14%) or acute acidosis (1/7, 14%). They had a profound DD (6/7, 86%), with encephalopathy (3/7, 43%), seizures (3/7, 43%), hypotonia (2/7, 29%) and LS (2/7, 29%), among others. There was also renal involvement, with renal cysts (2/7, 29%) and tubulopathy (1/7, 14%). The heart was also affected with bradycardia (2/7, 29%), cardiomegaly (1/7, 14%) and HCM (1/7, 14%). Some patients presented RD (3/7, 43%) and apnea (2/7, 29%).

ii. CoQ_{10} *treatment and effects*

CoQ_{10} treatment was administered to four of the patients (Table 1.4). None of them experienced any clinical improvement, and one of them reduced the plasma lactate levels[248].

iii. Pathogenicity of the mutations

There are 5 pathogenic variants of *COQ9* that have been described in the literature in patients with primary CoQ_{10} deficiency (Figure 1.8 and Table 1.10). There are three intronic mutations, one frameshift and one nonsense mutation. All the mutations were confirmed to segregate with the disease within the different families [246,247,256], except for the nonsense mutation, whose pathogenicity was confirmed biochemically and by heterologous expression of the variant in yeast [248]. There are three intronic mutations with an *in silico* predicted high probability to alter splicing events (Table 1.10). The

pathogenicity of one of these three was confirmed by rescuing the patient's fibroblasts with the expression of WT *COQ9* [256].

COQ8/ADCK proteins

In humans there are five paralogs belonging to the aarF domain-containing protein kinase or UbiB protein kinase-like family (ADCK1-5); among them, COQ8A (ADCK3) and COQ8B (ADCK4) are highly similar, and both are involved in CoQ_{10} biosynthesis. Human COQ8A and COQ8B protein sequences have a 44.23% of identity and a 66.12% of similarity. COQ8A have a longer N-terminal region of 117 aa, while COQ8B has an extended C-terminal region of 18 aa. Both proteins contain the conserved kinase motif in the region responsible for ATP binding and phosphotransfer reaction. Still, they lack the conserved kinase C-term motif, not having canonical protein kinase activity in trans. Instead, they have ATPase activity, whose role in CoQ_{10} biosynthesis still needs to be further studied [385]. They have also been proved to interact with lipid CoQ intermediates and are thought to have a regulatory function, probably redundant being each of them specialised in different tissues. In humans, *COQ8A* expression exceeds *COQ8B* in several tissues with the exception of kidney, in which *COQ8B* is highly expressed [385].

COQ8A

COQ8A gene (MIM*606980) is located in chr1:226,897,536-226,987,545 (GRCh38.p13), forward strand. Two different transcript variants are annotated, and only the longest one is considered to be the canonical sequence or isoform 1. This transcript (2,866 bp) encodes a 647 aa long protein with 15 exons, in which exon 1 is non-coding. Defects in this gene are a cause of CoQ_{10} deficiency (COQ10D4, MIM#612016).

i. CoQ_{10} *deficiency due to COQ8A mutations*

77 patients from 55 families with *COQ8A* mutations have been reported so far. *COQ8A* deficiency results in an **autosomal-recessive cerebellar ataxia type 2** (ARCA2) (70/77, 91%), a slowly progressive ataxic syndrome with cerebellar atrophy (62/77, 81%) (Table 1.3). After the elaboration of this study, a multicentre study of 59 *COQ8A* patients (39 novel) was published, aiming to stablish genotype-phenotype correlations in this

disease[275]. These patients are not included in this study, but the results will be discussed and compared.

a. Age of onset

The mean age of onset was 6.6 years old (range 6 mo-27 yo) (Figure 1.5), being mostly an infancy or childhood presentation (23/77, 30% and 29/77, 38%; respectively) (Figure 1.15.B). When classified by the age of onset, *COQ8A* cases were sorted into 4 different groups (Figures 1.7.D, 1.12).

Group 1 includes 24 patients from 17 families (24/77, 31% of the total number of *COQ8A* patients), which are all of the infancy onset cases. The mean age of onset of patients in this group is 1.6 yo (19 mo) (range 6 mo-2.5 yo). The majority of the *COQ8A* patients were classified in **group 2**, with 32 patients from 24 families (32/77, 42% of the total number of *COQ8A* patients) presenting during childhood. The mean age of presentation in this group is almost 6 yo (range 3-10 yo). **Group 3** includes 9 patients from 8 families (9/77, 12% of the total number of *COQ8A* patients) who first manifested at a mean age of 14 yo (range 11-18 years old). 6 patients from 5 families with *COQ8A* mutations (**group 4**) presented when they were adults (6/77, 8% of the total number of COQ8A patients). This group of patients first manifested at a mean age of 22.5 yo (range 19-27 yo).

b. Symptoms at onset

Patients typically first presented with 1, 2 or 3 clinical manifestations (Figures 1.6.I, 1.12.C-F) including ataxia (19/77, 25%), gait instability (GI) (11/77, 14%), tremor (11/77, 14%), dysarthria (8/77, 10%) or slow motor development (8/77, 10%). Other less frequent symptoms at onset were impaired handwriting (IH) (6/77, 8%), seizures (5/77, 6%) or DD (3/77, 4%). The 59 patients from a very recent study, 39 of them, not included here, mostly presented with ataxia (68%), DD (22%), tremor (13%), epilepsy (8%) and dystonia (7%)[275]. The differences in frequencies probably derives from the small number of patients and the different ways to report the first symptoms in the different reports.

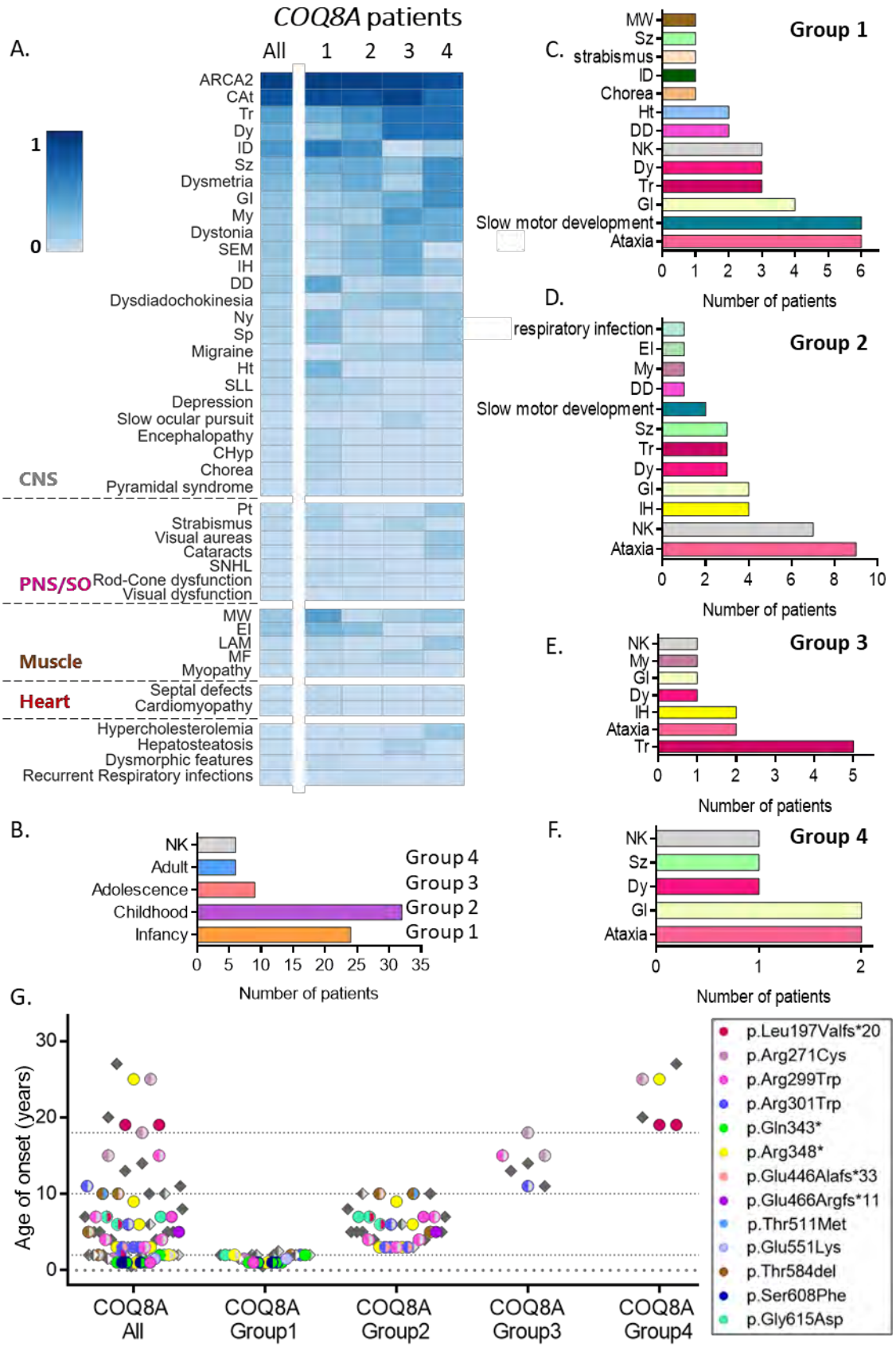
A.
COQ8A patients
All 1 2 3 4
1
0
ARCA2
CAt
Tr
Dy
ID
Sz
Dysmetria
GI
My
Dystonia
SEM
IH
DD
Dysdiadochokinesia
Ny
Sp
Migraine
Ht
SLL
Depression
Slow ocular pursuit
Encephalopathy
CHyp
Chorea
Pyramidal syndrome
CNS
Pt
Strabismus
Visual aureas
Cataracts
SNHL
PNS/SO
Rod-Cone dysfunction
Visual dysfunction
MW
EI
LAM
MF
Muscle
Myopathy
Septal defects
Heart
Cardiomyopathy
Hypercholesterolemia
Hepatosteatosis
Dysmorphic features
Recurrent Respiratory infections
B.
NK
Adult
Adolescence
Childhood
Infancy
Group 4
Group 3
Group 2
Group 1
0 5 10 15 20 25 30 35
Number of patients
C.
Group 1
MW
Sz
strabismus
ID
Chorea
Ht
DD
NK
Dy
Tr
GI
Slow motor development
Ataxia
0 1 2 3 4 5 6
Number of patients
D.
Group 2
respiratory infection
EI
My
DD
Slow motor development
Sz
Tr
Dy
GI
IH
NK
Ataxia
0 2 4 6 8 10
Number of patients
E.
Group 3
NK
My
GI
Dy
IH
Ataxia
Tr
0 1 2 3 4 5
Number of patients
F.
Group 4
NK
Sz
Dy
GI
Ataxia
0 1 2
Number of patients
G.
Age of onset (years)
30
20
10
0
COQ8A All
COQ8A Group1
COQ8A Group2
COQ8A Group3
COQ8A Group4
p.Leu197Valfs*20
p.Arg271Cys
p.Arg299Trp
p.Arg301Trp
p.Gln343*
p.Arg348*
p.Glu446Alafs*33
p.Glu466Argfs*11
p.Thr511Met
p.Glu551Lys
p.Thr584del
p.Ser608Phe
p.Gly615Asp

Figure 1.12. Clinical manifestations and genotype of *COQ8A* patients.
(A) Symptom frequency found in patients, for each age-of-onset group 1-4. (B) Total number of patients in each age-of-onset group. (C-F) First symptoms and the number of patients manifesting them, for each age-of-onset group. (G) Age of onset and pathogenic variants of *COQ8A* patients. Each point represents one patient. Coloured circles: mutations found in more than one family (see the legend). Rhombus: patients with mutations only present in one family (gray). Full-filled symbols: homozygous mutations, half-filled symbols: heterozygous mutations. Abbreviations: refer to Tables 1.1 and 1.2.

When stratified by age of onset, patients with infancy-onset (group 1) mainly first presented with slow motor development (6/24, 25%) and ataxia (6/24, 25%), but also with GI (4/24, 17%), tremor (3/24, 13%), dysarthria (3/24, 13%), DD (2/24, 8%) or hypotonia (2/24, 8%)) (Figure 1.12.C) [227,273,346,351,354,356–360,370]. Probands with childhood-onset (group 2) had ataxia (9/32, 28%), GI (4/32, 13%), IH (4/32, 13%), dysarthria (3/32, 9%), tremor (3/32, 9%), seizures (3/32, 9%) or slow motor development (2/32, 6%) as first symptoms (Figure 1.12.D) [273,274,344–352,355–357,360]. In the case of an adolescence-onset of the disease, the first symptoms were mainly tremor (5/9, 56%), ataxia (2/9, 22%), IH (2/9, 22%), myoclonus (1/9, 11%), GI (1/9, 11%) or dysarthria (1/9, 11%) (Figure 1.12.E) [227,273,274,347,350,352,353,356]. Some patients presented when they were adults with GI (2/6, 33%), gait ataxia (2/6, 33%), dysarthria (1/6, 17%) or seizures (1/6, 17%) (Figure 1.12.F) [227,228,273,274,350].

Ataxia, as the first symptom, is equally frequent in all disease onset groups. We can see that impaired developmental and cognitive manifestations were more common when the disease manifested earlier. In contrast, the opposite trend was observed for other symptoms, such as tremor, gait instability, handwriting or speech difficulties, which become more frequent as first symptoms when the onset of the disease is later in life (Figure 1.12.C-F).

c. Clinical manifestations of the disease

COQ8A deficiency results in an **autosomal-recessive cerebellar ataxia type 2** (ARCA2) (70/77, 91%), a slowly progressive ataxic syndrome with cerebellar atrophy (62/77, 81%), with variable associated clinical features: ID (35/77, 45%), tremor (33/77, 43%), dysarthria (27/77, 35%), seizures (25/77, 32%) and EI (14/77, 18%), amongst others (Table 1.3). The clinical severity of the disease varies with its age of onset, the earlier the disease appears, the more severe it becomes. We can clearly see this when patients are stratified by the age of onset (Figure 1.12.A).

Patients with the earliest onset (group 1) manifested **an infantile-onset cerebellar ataxic syndrome with intellectual disability** (15/24, 63%) and **developmental delay** (9/24, 38%) [227,273,346,351,354,356–360,370]. They also had tremor (8/24, 33%), hypotonia (7/24, 29%), dysmetria (6/24, 25%), seizures (8/24, 33%), spasticity (6/24, 25%), and nystagmus (6/24, 25%). Other less frequent manifestations were dysarthria (5/24, 21%), myoclonus (4/24, 17%), SLL (3/24, 13%), strabismus (3/24, 13%), GI (3/24, 13%) or SEM (3/23, 13%). Some of them had other systems and tissues affected, having MW (10/24, 42%), EI (7/24, 29%), SNHL (1/24, 4%) or cardiac abnormalities (2/24, 8%).

The majority of the *COQ8A* patients (group 2) presented a **childhood-onset cerebellar ataxic syndrome with cognitive impairment** (16/32, 50%), **tremor** (15/32, 47%) and **speech difficulties** (12/32, 38%) [273,274,344–352,355–357,360]. They also manifested dysmetria (11/32, 34%), seizures (11/32, 34%), SEM (8/32, 25%), GI (7/32, 22%) and dystonia (7/32, 22%). Other less frequent manifestations in this group were IH (6/32, 19%), dysdiadochokinesia (5/32, 16%), myoclonus (4/32, 13%) or SLL (3/32, 9%). Other systems were also affected in some patients, manifesting EI (7/32, 22%), MW (1/32, 3%), SNHL (1/32, 3%) or visual dysfunction (1/32, 3%).

Some patients (group 3) manifested an **adolescence-onset cerebellar ataxic syndrome with tremor** (6/9, 67%), **speech difficulties** (6/9, 67%) and **myoclonus** (4/9, 44%) [227,273,274,347,350,352,353,356]. They also manifested GI (3/9, 33%), IH (3/9, 33%), dystonia (3/9, 33%), SEM (3/9, 33%), seizures (2/9, 22%) and dysdiadochokinesia (2/9, 22%). Some of them also suffered from MF (1/9, 11%) or MW (1/9, 11%). Other less frequent manifestations in this group were DD, dysmetria, migraine, strabismus, slow ocular pursuit or hepatosteatosis (1/9, 11% each).

A few patients (group 4) had an **adult-onset cerebellar ataxic syndrome with tremor** (4/6, 67%) and **speech difficulties** (4/6, 67%) [227,228,273,274,350]. These patients also manifested seizures (3/6, 50%), GI (3/6, 50%), dysmetria (3/6, 50%), dystonia (2/6, 33%) and myoclonus (2/6, 33%). Other less frequent manifestations in this group were IH, dysdiadochokinesia, migraine, ID, nystagmus, ptosis, spasticity, cataracts, visual aureas or MW (1/6, 17% each).

Generally, *COQ8A* patients had an ataxic syndrome with cerebellar atrophy, displaying multiple cerebellar and non-cerebellar features whose frequency varies when we

stratify by the age of onset. Developmental delay and cognitive impairment are more frequent with the youngest ages of onset. Muscle or heart involvement is also more frequent in patients that had an earlier presentation. Other symptoms, such as dysarthria, dystonia, GI, myoclonus or tremor become more frequent the later in life the disease manifests (Figure 1.12.A).

ii. CoQ_{10} *treatment and effects*

CoQ_{10} treatment was administered to 29/77 (38%) of the *COQ8A* patients, representing all the four groups described (Tables 1.4 and 1.12). In the youngest onset group (group 1), 11/24 patients were treated [227,273,346,351,354,357,359]. Most of them did not obtain any benefits from the treatment (6/11), while the rest experienced some amelioration of ataxia (4/11), motor performance (3/11) or cognitive abilities (2/11). In group 2, 13/32 patients were treated [345,348,351,352,356,360]. Some of them did not obtain any benefits from the treatment (6/13), and the rest had some improvement of the cerebellar signs: ataxia (5/11), motor skills (2/11) tremor (1/11) and myoclonus (1/11). From the adolescence onset group 3, 5/9 patients were treated and, except from one, 4/5 reported benefits, improving tremor (3/5), ataxia (1/5), motor abilities (1/5), dystonia (1/5), fatigue (1/5) and speech (1/5) [227,274,347,352,353]. 2/6 patients of group 4 were treated, and only one of them reported a slight improvement of the neurological condition [227,228]. There seemed to be no associations between treatment response and age of disease onset or genotype.

i. Pathogenicity of the mutations

There are 49 reported *COQ8A* mutations associated with primary CoQ_{10} deficiency (Figures 1.8, 1.12.G and Tables 1.12 and 1.13). Half of them were confirmed to segregate on the different families (27/49, 55%), while the rest of variants were mostly biochemically checked (by measuring CoQ_{10} levels) (29/49, 57%). The pathogenicity of some of the variants (7/49, 14%) was confirmed in a yeast model [356,357]. The pathogenicity of only a few mutations has not been supported by any other evidence (6/49, 12%) than the *in silico* pathogenicity prediction, being almost all of them predicted as pathogenic (Table 1.13).

Only one variant, the c.993C>T, had a CADD score lower than the cut-off to be considered pathogenic (20). This variant was identified in a patient in *trans* with the c.1645G>A missense change and it was shown to partially affect splicing, leading to an abnormal exon 8 skipping [356]. However, this variant showed an allelic frequency of approximately 1.6% with 38 homozygous individuals in the European non-Finnish population in the gnomAD population database (https://gnomad.broadinstitute.org/) and it is reported in the ClinVar database as likely benign. It is possible that this variant is a functional polymorphism that, when it appears in combination with other variant, may increase the susceptibility to develop a disease, but other studies are required to confirm this hypothesis.

We classified the variants into the 4 age of onset groups (Figure 1.12.G). We will only discuss to the most represented variants: c.589-3C>G (p.Leu197Valfs*20), c.895C>T (p.Arg299Trp), c.901C>T (p.Arg301Trp), c.1027C>T (p.Gln343*), c.1042C>T (p.Arg348*), c.1331_1332insCACAG (p.Glu446Alafs*33), c.1750_1752delACC (p.Thr584del) and c.1844G>A (p.Gly615Asp).

The c.589-3C>G (**p.Leu197Valfs*20**) frameshift variant in intron 3 was in silico predicted as having a high probability of altering splicing (Table 1.13). It was found in 5 patients from 4 families; in heterozygosis with **p.Arg301Trp** in one patient first presenting at 2 years of age (group 1)[351], in heterozygosis with **p.Gly615Asp** mutation, in 2 families presenting during childhood (group 2) [274,351], and in homozygosis in 2 sisters first presenting when they were 19 years old (group 4) [273]. It seems this splicing mutation is less severe when it is found in homozygous state, probably due to the pathogenicity of the mutation that accompanies it. The **p.Gly615Asp** variant was also found in homozygosis in a third family with 2 siblings, presenting at the age of 2 and 7 years old [273]. This mutation mainly produces a childhood-onset disease.

c.895C>T (**p.Arg299Trp**) was found in 7 patients from 5 families, having most of them a childhood-onset (group 2) (5 patients from 3 families)[273,360], but some of them with infancy (group 1) (1 patient) [360] or adolescence (group 3) (1 patient) onset [273].

c.901C>T (**p.Arg301Trp**) was sequenced in 7 patients from 7 families. The majority of them (4) presented during childhood (group 2), in heterozygosis with the frameshift variant c.1331_1332insCACAG (**p.Glu446Alafs*33**) in 3 Italian families [274,351], and with a

unique missense mutation (**p.Arg410Gln**) in one case [350]. Additionally, some of these patients had an infancy (group 1) (1 patient) [351] or adolescence (group 3) (1 patient) onset [352], having this variant in heterozygosis with other mutations.

The nonsense c.1027C>T (**p.Gln343***) mutation was found in 6 patients from 3 families, all of them from Israel, with an infancy onset (group 1) [354]. In one family the mutation was homozygous, while in the other two, it was in compound heterozygosis with the **p.Ser608Phe** variant. A very similar nonsense mutations, c.1042C>T **(p.Arg348***), was found in 8 patients from 5 families, mainly in homozygosis (5/8). Half of them presented during childhood [344,345], while some had infancy (group 1) (2 patients) [344], adult (group 4) (1 patient) [274] or unknown onset [350]. Due to *COQ8A* regulatory role and to the presence of at least another *COQ8* protein with a similar function, the lack of residual functional protein seems to be compatible with life.

c.1750_1752delACC (**p.Thr584del**) deletion variant was found in 5 patients from 4 families, always in heterozygosis. 3 of them presented during childhood (group 2) [346,352,356], 1 of them at 2 years of age (group 1) [346] and the age of first presentation of the other one is unknown [350].

Finally, there are some variants found in homozygous or heterozygous state in patients belonging to the different groups. We have classified them, but we cannot be certain of how they would contribute to the disease pathogenesis, because of their low representation (Table 1.12).

Regarding the recent study of 59 *COQ8A* patients, multisystemic involvement beyond ataxia was more prevalently found in patients with missense variants. Contrarily, patients with biallelic loss-of-function variants more frequently presented an isolated ataxia[275], suggesting a gain-of-function or dominant-negative mechanism for missense variants in contrast to loss-of-function variants[275]. Moreover, they proposed preliminary associations between variants in specific domains and phenotypic outcomes: missense variants in the KxGQ domain seemed to be associated with clinical signs reflecting cortical (developmental delay and epilepsy) and pyramidal tract dysfunction [275].

Table 1.12. *COQ8A* patients classified by age of onset. CoQ_{10} treatment and mutations.

Group	# of patients	CoQ_{10} treatment		F (P)	cDNA change	Aa change	Ref.
		# of patients treated	Effect				
Group 1	24	11	No benefits (6), Improvement of ataxia (4), Improvement in motor abilities (3), Improvement of cognitive abilities (2), Slight improvement of cerebellar signs (1)	1 (1)	c.589-3C>G	p.Leu197Valfs*20	351
				1 (2)	c.637C>T	p.Arg213Trp	273,357
				1 (1)	c.811C>T	p.Arg271Cys	273
				1 (2)	c.815G>T	p.Gly272Val	273,357
				1 (1)	c.827A>G	p.Lys276Arg	358
				1 (2)	c.830T>C	p.Leu277Pro	359
				1 (1)	c.895C>T	p.Arg299Trp	227,360
				1 (1)	c.901C>T	p.Arg301Trp	351
				1 (1)	c.993C>T	p.Lys314_Gln360del	273,356, 361
				3 (6)	c.1027C>T	p.Gln343*	354
				1 (2)	c.1042C>T	p.Arg348*	344
				1 (1)	c.1081_1082dupGTA	p.Gln360_Tyr361ins*	273
				1 (2)	c.1136T>A	p.Leu379*	344
				1 (2)	c.1286A>G	p.Tyr429Cys	227
				1 (2)	c.1506+1G>A	p.Val503Metfs*21	359
				1 (1)	c.1534C>T	p.Arg512Trp	370
				1 (1)	c.1645G>A	p.Gly549Ser	273,356, 361
				1 (1)	c.1651G>A	p.Glu551Lys	357
				1 (1)	c.1702delG	p.Glu568Argfs*	358
				1 (1)	c.1750_1752delACC	p.Thr584del	346
				1 (1)	c.1805C>G	p.Pro602Arg	346
				2 (3)	c.1823C>T	p.Ser608Phe	354
				1 (1)	c.1844G>A	p.Gly615Asp	273
Group 2	32	13	No benefits (6), Improvement of ataxia (5), Improvement in motor abilities (2), Improvement of tremor (1), Improvement of myoclonus (1)	1 (1)	c.500_521del22insTTG	p.Gln167Leufs*36	356
				2 (2)	c.589-3C>G	p.Leu197Valfs*20	274,351
				1 (3)	c.685-690delCTGGCA	p.Leu229_Ala230del	349
				1 (1)	c.815G>A	p.Gly272Asp	273,357
				3 (5)	c.895C>T	p.Arg299Trp	273,360
				4 (4)	c.901C>T	p.Arg301Trp	274,350, 351
				1 (1)	c.913G>T	p.Asp305Tyr	352
				2 (4)	c.1042C>T	p.Arg348*	344,345
				1 (2)	c.1228C>T	p.Arg410*	273
				1 (1)	c.1229G>A	p.Arg410Gln	350
				3 (3)	c.1331_1332insCACAG	p.Glu446Alafs*33	274,351
				1 (1)	c.1396delG	p.Glu466Argfs*11	355
				1 (3)	c.1398+2T>C	p.Asp420Trpfs*40; p.Ile467Alafs*22	356

Table 1.12. *COQ8A* patients classified by age of onset. CoQ_{10} treatment and mutations (Continued).

Group	# of patients	CoQ_{10} treatment		F (P)	cDNA change	Aa change	Ref.
		# of patients treated	Effect				
Group 2	32	13	No benefits (6), Improvement of ataxia (5), Improvement in motor abilities (2), Improvement of tremor (1), Improvement of myoclonus (1)	1 (1)	c.1523T>C	p.Phe508Ser	273
				1 (1)	c.1532C>T	p.Thr511Met	352
				1 (1)	c.1541A>G	p.Tyr514Cys	356
				1 (2)	c.1732T>G	p.Phe578Val	360
				3 (3)	c.1750_1752delACC	p.Thr584del	346,352, 356
				1 (1)	c.1805C>G	p.Pro602Arg	346
				1 (1)	c.1813dupG	p.Glu605Glyfs*125	273,357
				3 (3)	c.1844G>A	p.Gly615Asp	273,274, 351
				1 (1)	c.1844dupG	p.Ser616Leufs*114	347
				1 (1)	29 kb deletion of *COQ8A,* exons 3 to 15 (Chr1:227,150,977-227,195,656, hg19)		273
				1 (1)	2.9Mb duplication of 1q42.11q42.13 (including *COQ8A* gene)		348
Group 3	9	5	No benefits (1), Improvement of ataxia (1), Improvement of tremor (3), Improvement in motor abilities (1), Improvement in fatigue and speech (1), Improvement of dystonia (1)	1 (2)	c.811C>T	p.Arg271Cys	227
				1 (1)	c.895C>T	p.Arg299Trp	273
				1 (1)	c.901C>T	p.Arg301Trp	352
				1 (2)	c.910G>A	p.Ala304Thr	227
				1 (1)	c.1013C>T	p.Ala338Val	353
				1 (1)	c.1334-1335del	p.Thr445Argfs*52	350
				1 (1)	c.1358delT	p.Leu453Argfs*24	273
				1 (1)	c.1398+2T>C	p.Asp420Trpfs*40; p.Ile467Alafs*22	356
				1 (1)	c.1399-3_1408del	?	352
				1 (1)	c.1844dupG	p.Ser616Leufs*114	347
				1 (1)	27.6 kb deletion of 1q42.3 including exons 1-2		274
Group 4	6	2	No benefits (1), Slight improvement of neurological condition (1)	1 (2)	c.589-3C>G	p.Leu197Valfs*20	273
				1 (1)	c.811C>T	p.Arg271Cys	350
				1 (1)	c.911C>T	p.Ala304Val	227
				1 (1)	c.1000C>T	p.Arg334Trp	350
				1 (1)	c.1042C>T	p.Arg348*	274
				1 (1)	c.1511_1512delCT	p.Ala504fs*	228

Abbreviations: F: Number of families with each variant, P: Number of patients with each variant, aa: amino acid, Ref: references.

Table 1.13. Pathogenic variants of *COQ8A* gene found in patients.

Gene/ Protein	Pathogenic variants				Validation			*In silico* mutagenesis prediction				Ref.
	F (P)	cDNA mutation	aa modification	Exon	Segregation (S), Biochemical (B), Functional (F)			SIFT Patho-genic?	Poly Phen-2 Dama-ging?	SPiCE Prob. to alter spli-cing?	CADD score	
COQ8A/ ADCK3 647 aa 15 exons NM_020247.5 NP_064632.2	1 (1)	c.500_521del 22insTTG	p.Gln167Leufs*36	3		B		-	-	-	33	356
	4 (5)	c.589-3C>G[2]	p.Leu197Valfs*20	Int.3	S			-	-	high	23.0	273,274, 351
	1 (2)	c.637C>T	p.Arg213Trp	4		B	F	Pathog.	Probably	-	32	273,357
	1 (3)	c.685-690delCTGGCA	p.Leu229_Ala 230del	5	S			-	-	-	21.1	349
	2 (3)	c.811C>T	p.Arg271Cys	6	S	B		Pathog.	Probably	-	27.1	227,273, 350
	1 (2)	c.815G>T	p.Gly272Val	6		B	F	Pathog.	Probably	-	26.0	273,357
	1 (1)	c.815G>A	p.Gly272Asp	6		B	F	Pathog.	Probably	-	26.5	273,357
	1 (1)	c.827A>G	p.Lys276Arg	6				Pathog.	Probably	-	29.0	358
	1 (2)	c.830T>C	p.Leu277Pro	6	S	B		Pathog.	Probably	-	28.2	359
	5 (7)	c.895C>T	p.Arg299Trp	7	S	B		Pathog.	Probably	-	31	227,273, 360
	3 (3)	c.901C>T	p.Arg301Trp	7	S	B		Pathog.	Probably	-	23.5	350
	1 (2)	c.910G>A	p.Ala304Thr	7	S			Pathog.	Probably	-	24.8	227
	1 (1)	c.911C>T	p.Ala304Val	7	S	B		Pathog.	Probably	-	25.0	227
	1 (1)	c.913G>T	p.Asp305Tyr	7		B		Pathog.	Benign	-	24.8	352
	1 (1)	c.993C>T[3]	p.Lys314_Gln 360del	8 (del of exon 8?)		B		-	-	-	9.753	273,356, 361
	1 (1)	c.1000C>T	p.Arg334Trp	8	S			Pathog.	Probably	-	29.7	350
	1 (1)	c.1013C>T	p.Ala338Val	8				Pathog.	Probably	-	24.8	353
	3 (6)	c.1027C>T	p.Gln343*	8	S			-	-	-	49	354
	5 (8)	c.1042C>T	p.Arg348*	8	S	B		-	-	-	40	274,344, 345,350
	1 (1)	c.1081-1_1082dupGTA	p.Gln360_ Tyr 361ins*	Int.8-Ex.9				-	-	low	18.65	273
	1 (2)	c.1136T>A	p.Leu379*	9	S	B		-	-	-	43	344
	1 (2)	c.1228C>T	p.Arg410*	10	S	B		-	-	-	40	273
	1 (1)	c.1229G>A	p.Arg410Gln	10	S			Pathog.	Possibly	-	26.8	350
	1 (2)	c.1286A>G[1]	p.Tyr429Cys	11	S	B		Tole-rated	Benign	-	22.1	227
	3 (3)	c.1331_1332 insCACAG	p.Glu446Alafs*33	11	S			-	-	-	33	274,351
	1 (1)	c.1334-1335del[1]	p.Thr445Argfs*52	11	S			-	-	-	32	350
	1 (1)	c.1358delT	p.Leu453Argfs*24	11				-	-	-	33	273
	3 (4)	c.1396delG	p.Glu466Argfs*11	11	S			-	-	low	33	355
	1 (4)	c.1398+2T>C[4]	p.Asp420Trpfs*40; p.Ile467Alafs*22	Ex.11 -12	S	B		-	-	high	32	356
	1 (1)	c.1399-3_1408del	?	Int.11 -Ex12	S	B		-	-	high	33	352
	1 (2)	c.1506+1G>A	p.Val503Metfs*21	Int.12	S	B		-	-	high	35	359

Table 1.13. Pathogenic variants of *COQ8A* gene found in patients (Continued).

Gene/ Protein	Pathogenic variants				Validation			*In silico* mutagenesis prediction				Ref.
	F (P)	cDNA mutation	aa modification	Exon	Segregation (S), Biochemical (B), Functional (F)			SIFT Pathogenic?	Poly Phen-2 Damaging?	SPiCE Prob. to alter splicing?	CADD score	
COQ8A/ ADCK3 647 aa 15 exons NM_020247.5 NP_064632.2	1 (1)	c.1511_1512delCT	p.Ala504fs*	13		B		-	-	-	33	386
	1 (1)	c.1523T>C	p.Phe508Ser	13				Pathog.	Probably	-	29.9	273
	2 (2)	c.1532C>T	p.Thr511Met	13	S	B		Pathog.	Probably	-	24.9	350,352
	1 (1)	c.1534C>T[5]	p.Arg512Trp	13	S			Pathog.	Probably	-	23.4	370
	1 (1)	c.1541A>G	p.Tyr514Cys	13		B	F	Pathog.	Probably	-	22.9	356
	1 (1)	c.1645G>A	p.Gly549Ser	14		B	F	Pathog.	Probably	-	26.3	273,356,361
	2 (2)	c.1651G>A	p.Glu551Lys	14		B	F	Pathog.	Probably	-	31	350,357
	1 (1)	c.1702delG	p.Glu568Argfs*	15				-	-	-	34	358
	1 (2)	c.1732T>G	p.Phe578Val	15		B		Pathog.	Probably	-	28.3	360
	4 (5)	c.1750_1752delACC[6]	p.Thr584del	15	S	B	F	-	-	-	22.5	346,350,352, 356
	1 (2)	c.1805C>G	p.Pro602Arg	15				Pathog.	Probably	-	27.3	346
	1 (1)	c.1813dupG	p.Glu605Glyfs*125	15		B		-	-	-	34	273,357
	2 (3)	c.1823C>T	p.Ser608Phe	15	S			Pathog.	Probably	-	31	354
	3 (4)	c.1844G>A[2]	p.Gly615Asp	15	S			Pathog.	Probably	-	29.9	273,274,351
	1 (2)	c.1844dupG	p.Ser616Leufs*114	15	S	B		-	-	-	33	347
	1 (1)	27.6 kb deletion of 1q42.3 including exons 1-2 of *COQ8A*				B		-	-	-	-	274
	1 (1)	29 kb deletion including exons 3 to 15 of *COQ8A*[1] (Chr1: 227,150,977-227,195,656, hg19)						-	-	-	-	273
	1 (1)	2.9Mb duplication at 1q42.11q42.13 (including *COQ8A*)						-	-	-	-	348

1. These pathogenic variants were found in simple heterozygosis in at least one patient [227,273,350].
2. A patient with these two mutations in heterozygosis in *COQ8A* also carries two compound heterozygous mutations in *PAH* gene, which may contribute to the disease[274].
3. The variant c.993C>T in *COQ8A*, which was identified in a patient in *trans* with the c.1645G>A missense change, was shown to partially affect splicing, leading to the production of an abnormal transcript with exon 8 skipping [356]. However, this variant showed an allelic frequency of approximately 1.6% with 38 homozygous individuals in the European non-Finnish population in the gnomAD population database (https://gnomad.broadinstitute.org/) and it is reported in the ClinVar database as likely benign.
4. *COQ8A* c.1398+2T>C6 variant affects a splice donor site, different splice variants are expressed: p.Asp420Trpfs*40 and p.Ile467Alafs*22 [356].
5. The patient with this *COQ8A* mutation in homozygosis also carries an additional homozygous mutation in *MED25* gene (c.518T>C; p.Ile173Thr), which may contribute to the disease [370].
6. This variant is named as c.1749_1751delCAC in Chang et al., 2018 [352].

Reference sequences correspond to longest transcript. Abbreviations: F: Number of families with each variant, P: Number of patients with each variant, aa: amino acid, Int: intron, Ex: exon, Prob: probability, Pathog: pathogenic, Ref: references.

COQ8B

COQ8B gene (MIM*615567) is located in chr19:40,691,529-40,718,207 (GRCh38.p13), reverse strand. Two different protein-coding transcripts are annotated, being the longest one the canonical sequence (isoform 1). This transcript (2,443 bp) encodes a 544 aa protein with 15 exons, being exon 1 non-coding. Defects in this gene are a cause of nephrotic syndrome with primary CoQ_{10} deficiency (NPHS9, MIM#615573).

i. CoQ_{10} *deficiency due to COQ8B mutations*

79 patients from 41 families with *COQ8B* mutations have been reported until now. *COQ8B* deficiency leads to a **steroid-resistant nephrotic syndrome** (SRNS) (65/79, 82%) with **variable neurological involvement** (13/79, 16.5%) (Table 1.3).

a. Age of onset

The mean age of presentation was 12.5 yo (range 9 mo-32 yo) (Figure 1.5), being mostly a childhood or adolescent presentation (28/79, 35% and 35/79, 44%; respectively) (Figure 1.13.B). When classified by the age of onset, *COQ8B* cases were sorted in 4 different groups (Figures 1.7.E, 1.13).

Group 1 is the smallest one, including 4 patients from 4 families (4/79, 5% of the total number of *COQ8B* patients), who had an infancy-onset disease. The mean age of onset in this group is 1.4 yo (17mo) (range 9 mo-2 yo). **Group 2** includes 28 patients from 22 families (28/79, 35% of the total number of *COQ8B* patients) that manifested during childhood, at a mean age of 7.3 yo (range 3-10 yo). The majority of the *COQ8B* patients had an adolescent onset (**group 3**), with 35 patients from 28 families (35/79, 44% of the total number of *COQ8B* patients). The mean age of presentation in this group was 14.3 years old (range 11-18 years old). Adult-onset is less frequent, with 11 patients from 10 families presenting after 20 years of age (**group 4**) (11/79, 14% of the total number of *COQ8B* patients). They manifested at a mean age of 24 yo (range 20-32 years old).

Figure 1.13. Clinical manifestations and genotype of *COQ8B* patients.
(A) Symptom frequency found in patients, for each age-of-onset group 1-4. (B) Total number of patients in each age-of-onset group. (C-F) First symptoms and the number of patients manifesting them, for each age-of-onset group. (G) Age of onset and pathogenic variants of *COQ8B* patients. Each point represents one patient. Coloured circles: mutations found in more than one family (see the legend). Rhombus: patients with mutations only present in one family (gray). Full-filled symbols: homozygous mutations, half-filled symbols: heterozygous mutations. Abbreviations: refer to Tables 1.1 and 1.2.

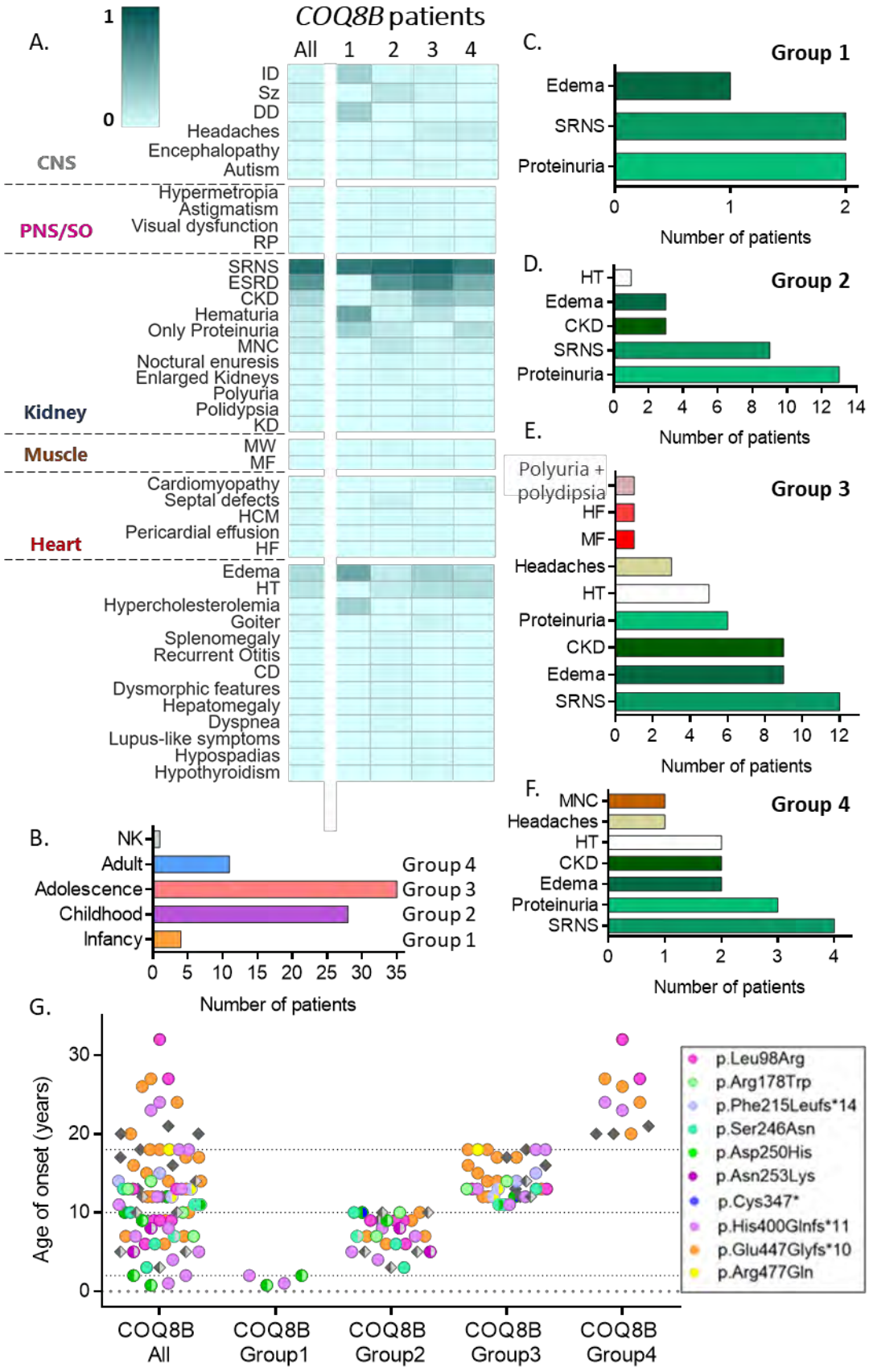
A.
COQ8B patients
All 1 2 3 4
1
0
CNS
ID
Sz
DD
Headaches
Encephalopathy
Autism
PNS/SO
Hypermetropia
Astigmatism
Visual dysfunction
RP
Kidney
SRNS
ESRD
CKD
Hematuria
Only Proteinuria
MNC
Noctural enuresis
Enlarged Kidneys
Polyuria
Polidypsia
KD
Muscle
MW
MF
Heart
Cardiomyopathy
Septal defects
HCM
Pericardial effusion
HF
Edema
HT
Hypercholesterolemia
Goiter
Splenomegaly
Recurrent Otitis
CD
Dysmorphic features
Hepatomegaly
Dyspnea
Lupus-like symptoms
Hypospadias
Hypothyroidism
B.
NK
Adult
Adolescence
Childhood
Infancy
Group 4
Group 3
Group 2
Group 1
0 5 10 15 20 25 30 35
Number of patients
C.
Group 1
Edema
SRNS
Proteinuria
0 1 2
Number of patients
D.
Group 2
HT
Edema
CKD
SRNS
Proteinuria
0 2 4 6 8 10 12 14
Number of patients
E.
Group 3
Polyuria + polydipsia
HF
MF
Headaches
HT
Proteinuria
CKD
Edema
SRNS
0 2 4 6 8 10 12
Number of patients
F.
Group 4
MNC
Headaches
HT
CKD
Edema
Proteinuria
SRNS
0 1 2 3 4
Number of patients
G.
Age of onset (years)
0 10 20 30
COQ8B All
COQ8B Group1
COQ8B Group2
COQ8B Group3
COQ8B Group4
p.Leu98Arg
p.Arg178Trp
p.Phe215Leufs*14
p.Ser246Asn
p.Asp250His
p.Asn253Lys
p.Cys347*
p.His400Glnfs*11
p.Glu447Glyfs*10
p.Arg477Gln

b. Symptoms at onset

COQ8B deficiency patients mainly presented with a renal manifestation (Figures 1.6.J, 1.13.C-F). Patients typically present with SRNS (27/79, 34%), proteinuria (25/79, 32%), edema (15/79, 19%), CKD (14/79, 18%), hypertension (8/79, 10%) or headaches (4/79, 5%). Early detection of proteinuria arose the suspicion of a renal disease[367,377,387]. The majority of the patients firstly referred to the hospitals when they were suffering a nephrotic syndrome.

Patients with infancy-onset (group 1) mainly presented with proteinuria or SRNS (2/4 each, 50%), in one case with edema (Figure 1.13.C) [243,276,363,366]. Childhood-onset (group 2) was mainly characterised by the detection of proteinuria upon scholar medical tests (13/28, 46%) [229,243,362,365,368], but also some other patients presented with SRNS (9/28, 32%)[229,276,363], edema (3/28, 11%)[243,276,364], CKD (3/28, 11%) [229,276] or hypertension (1/28, 4%) [276,364] (Figure 1.13.D). The majority of the *COQ8B* patients had an adolescence onset (group 3), presenting mainly with SRNS (12/35, 34%), CKD (9/35, 26%), edema (9/35, 26%), proteinuria (6/35, 17%), hypertension (5/35, 14%) and headaches (3/35, 9%) [229,276,362–366]. Other less common adolescent-onset first symptoms were muscle fatigue, heart failure and polydipsia plus polyuria (1/35, 3% each) (Figure 1.13.E). Adult-onset cases first manifested with SRNS (4/11, 36%), proteinuria (3/11, 27%), CKD (2/11, 18%), edema (2/11, 18%), hypertension (2/11, 18%), medullary nephrocalcinosis (MNC) (1/11, 9%) and headaches (1/11, 9%) (Figure 1.13.F) [229,276,363,364].

SRNS as the first symptom is equally frequent in all disease onset groups for *COQ8B* cases. Early diagnosis was mainly characterised by the detection of proteinuria before the nephrotic syndrome was established. Edema was found as the first manifestation in some cases, at any age of onset. Extrarenal symptoms as first symptoms were more common with a later onset of the disease. CKD or hypertension become more frequent as first symptoms when the beginning of the disease is later in life (Figure 1.13.C-F).

c. Clinical manifestations of the disease

COQ8B deficiency leads to a **steroid resistant nephrotic syndrome** (SRNS) (65/79, 82%) with variable neurological involvement (13/79, 16.5%) (Table 1.3). Variable associated clinical features include edema (16/79, 20%), hypertension (11/79, 14%), seizures (6/79,

8%), ID (4/79, 5%), headaches (4/79, 5%), HCM (2/79, 3%) or septal defects (2/79, 3%) (Figure 1.13.A).

Patients presenting the earliest (group 1) manifested an **infantile-onset steroid-resistant nephrotic syndrome** (3/4, 75%) **with variable neurological involvement** (2/4, 50%) [243,276,363,366]. They had edema (2/4, 50%), DD (1/4, 25%), ID (1/4, 25%) and hypercholesterolemia (1/4, 25%).

Childhood-onset patients (group 2) manifested a **steroid-resistant nephrotic syndrome** (23/28, 82%) that progressed to an ESRD (17/28, 61%) in most of the cases [229,243,276,362–365,367]. Some of them also suffered from MNC (4/28, 14%), CKD (3/28, 11%), edema (3/28, 11%), hypertension (3/28, 11%), seizures (4/28, 14%), encephalopathy (1/28, 4%), ID (1/28, 4%), HCM (1/28, 4%) or septal defects (2/28, 7%).

The majority of the *COQ8B* patients had an **adolescent-onset** (group 3) **steroid-resistant nephrotic syndrome** (31/35, 89%) that evolved to an ESRD in most of the cases (25/35, 71%) [229,276,362–366]. They had other renal affections, such as CKD (12/35, 34%), hematuria (5/35, 14%), MNC (2/35, 6%) or kidney dysfunction (1/35, 3%). Some of them also had edema (9/35, 26%), hypertension (6/35, 17%) or goiter (2/35, 6%). Some probands reported headaches (3/35, 9%), ID (2/35, 6%), seizures (2/35, 6%) or cardiac abnormalities (4/35, 11%).

Adult-onset is less frequent (group 4) (11/79, 14% of the total number of COQ8B patients). They presented an **adult-onset steroid-resistant nephrotic syndrome** (8/11, 73%) that evolved into an ESRD in some cases (5/11, 45%) [229,276,363,364]. They had other renal affections, such as CKD (3/11, 27%), MNC (1/11, 9%) or isolated proteinuria (2/11, 18%). Some of them also had edema (2/11, 18%), hypertension (2/11, 18%) or a dilated cardiomyopathy (1/11, 9%).

All these patients had a **steroid-resistant nephrotic syndrome**, displaying multiple renal and some extrarenal features with variable frequency. DD and cognitive impairment are more frequent with the youngest ages of onset. Other symptoms, such as chronic kidney disease, hypertension or headaches, are more frequent the later in life the disease manifests (Figure 1.13.A).

ii. CoQ_{10} *treatment and effects*

CoQ_{10} treatment was administered to 29/79 (37%) of the *COQ8B* patients, representing all the four groups described (Tables 1.4 and 1.14). In the youngest onset group (group 1), 4/4 patients were treated, and they improved proteinuria (3/4) and/or edema (1/4) [229,276,363,366], while one did not respond to the treatment [243]. In group 2, 12/28 patients were treated. Half of them improved the proteinuria condition (6/12) [229,276,362], one of them stabilized renal function [243], and another one did not obtain any benefits from the treatment [229,276], while the outcome of three of them was not described [229]. From the adolescence onset group 3, a few probands were treated (7/35). 4/7 improved proteinuria [229,276], while 3/7 did not benefit from the supplementation [229,276,366]. 6/11 patients of group 4 were treated, and while 2 of them did not experience any improvement, 3/6 improved proteinuria and 1/6 ameliorated albuminuria, had better physical fitness and reduced fatigue [229,276,364].

Table 1.14. *COQ8B* patients classified by age of onset. CoQ_{10} treatment and mutations.

Group	# of patients	CoQ_{10} treatment		F (P)	cDNA change	Aa change	Ref.
		# of patient treated	Effect				
Group 1	4	4	Improvement of proteinuria (3), Improvement of edema (1), No benefits (1)	1 (1)	c.532C>T	p.Arg178Trp	366
				2 (2)	c.748G>C	p.Asp250His	243,366
				2 (2)	c.1199dupA	p.His400Glnfs*11	276,363
Group 2	28	12	Improvement of proteinuria (6), Stabilization of renal function (1), Improvement of albuminuria (1), No benefits (1), NK (3)	1 (1)	c.101G>A	p.Trp34*	363
				3 (4)	c.293T>G	p.Leu98Arg	229,364
				1 (2)	c.449G>A	p.Arg150Gln	365
				1 (1)	c.532C>T	p.Arg178Trp	276,364
				1 (1)	c.649G >A	p.Ala217Thr	367
				3 (4)	c.737G>A	p.Ser246Asn	365,368
				1 (1)	c.748G>T	p.Asp250Tyr	367
				2 (2)	c.748G>C	p.Asp250His	243,362
				1 (2)	c.759C>A	p.Asn253Lys	365
				1 (2)	c.857A>G	p.Asp286Gly	276,363
				1 (1)	c.929C>T	p.Pro310Leu	364
				1 (1)	c.954_956dupGAC	p.Thr319dup	363
				1 (1)	c.1041C>A	p.Cys347*	362
				3 (4)	c.1199dupA	p.His400Glnfs*11	229,276
				4 (5)	c.1339dupG	p.Glu447Glyfs*10	229,364
				1 (2)	c.1447G>T	p.Glu483*	276,363
				1 (1)	c.1468C>T	p.Arg490Cys	365
				1 (1)	c.1493_1494CC>AA	p.Ala498Glu	364

Table 1.14. *COQ8B* patients classified by age of onset. CoQ_{10} treatment and mutations (continued).

Group	# of patients	CoQ_{10} treatment		F (P)	cDNA change	Aa change	Ref.
		# of patients treated	Effect				
Group 3	35	7	Improvement of proteinuria (4), No benefits (3)	2 (2)	c.293T>G	p.Leu98Arg	229,364
				2 (2)	c.532C>T	p.Arg178Trp	276,363,364
				3 (4)	c.645delT	p.Phe215Leufs*14	276,363,364
				3 (3)	c.737G>A	p.Ser246Asn	365,366
				1 (2)	c.748G>A	p.Asp250Asn	364
				2 (2)	c.748G>C	p.Asp250His	362,366
				1 (1)	c.759C>A	p.Asn253Lys	365
				1 (1)	c.857A>G	p.Asp286Gly	276,363
				1 (1)	c.958C>T	p.Arg320Trp	276,363
				1 (1)	c.1027C>T	p.Arg343Trp	363
				1 (1)	c.1041C>A	p.Cys347*	362
				4 (5)	c.1199dupA	p.His400Glnfs*11	229,276,364
				7 (11)	c.1339dupG	p.Glu447Glyfs*10	229,276,364
				1 (1)	c.1356_1362delGGGCCCT	p.Gln452Hisfs*	363
				2 (3)	c.1430G>A	p.Arg477Gln	229,276,363
				1 (1)	c.1447G>T	p.Glu483*	276,363
Group 4	11	6	No benefits (2), Improvement of proteinuria (3), Improvement of albuminuria (1), Better physical fitness and reduced fatigue (1)	2 (2)	c.293T>G	p.Leu98Arg	229,364
				1 (1)	c.958C>T	p.Arg320Trp	276,363
				1 (1)	c.1027C>T	p.Arg343Trp	363
				1 (2)	c.1199dupA	p.His400Glnfs*11	229,276
				4 (4)	c.1339dupG	p.Glu447Glyfs*10	229,276,364
				1 (1)	c.1356_1362delGGGCCCT	p.Gln452Hisfs*	363

Abbreviations: F: Number of families with each variant, P: Number of patients with each variant, aa: amino acid, Ref: references.

i. Pathogenicity of the mutations

There are 24 reported *COQ8B* pathogenic variants (Figures 1.8, 1.13.G, Tables 1.14 and 1.15). Most of these mutations were confirmed to be segregated on the different families (15/24, 63%). The pathogenicity of some of the mutations (8/24, 33%) was confirmed in a yeast model [276]. The molecular effect of other variations on the disease have not been supported by any other evidence (8/24, 33%) than the *in silico* pathogenicity prediction, being all of them predicted pathogenic in the case of the missense variants, except for one mutation, the p.Ala498Glu, which was predicted as

pathogenic by SIFT (0.03), but benign by Polyphen-2 (0.08). However, the integrated CADD score was above the threshold for pathogenicity, supporting a deleterious effect of this variant (Table 1.15).

We classified the variants into the 4 age-of-onset groups (Figure 1.13.G). We will only discuss the most represented variants, which are the missense mutations c.293T>G (p.Leu98Arg), c.532C>T (p.Arg178Trp), c.737G>A (p.Ser246Asn) and c.748G>C (p.Asp250His); and the frameshift variants c.645delT (p.Phe215Leufs*14), c.1199dupA (p.His400Glnfs*11), c.1339dupG (p.Glu447Glyfs*10).

c.293T>G (**p.Leu98Arg**) was diagnosed in 8 patients from 4 families, all of them in homozygosis [229,364]. They mainly presented during late childhood (4/8) or early adolescence (2/8), while in 2 cases, they were adults when they debuted (2/8).

The c.532C>T (**p.Arg178Trp**) variant was found in 5 probands from 3 different families. When the mutation was in homozygosis, patients manifested between childhood (2/5) and adolescence (2/5) (7-14yo) [276,363,364], while only in one case, in heterozygosis with the p.Asp250His variant, the patient presented before 1 year of age [366]. This mutation, c.748G>C (**p.Asp250His**), was present in 7 probands from 5 families. One homozygous patient also presented during infancy (2 yo), while his sister presented at 9 yo [243]. Two siblings with this variant in heterozygosis with the non-sense variant c.1041C>A (p.Cys347*) presented when they were 10 and 12 yo [362]. A heterozygous patient, with p.Asp250His and p.Ser246Asn variants presented when she was 11 years old [366]. c.737G>A (**p.Ser246Asn**) mutation was identified in 7 patients from 6 families, the majority of them (4/7) presenting during childhood [365,368], while the rest (3/7) presenting during early adolescence (11-13yo)[365,366].

The frameshift variants c.645delT (p.Phe215Leufs*14), c.1199dupA (p.His400Glnfs*11), and c.1339dupG (p.Glu447Glyfs*10) were respectively found in 4 patients from 3 families, 13 patients from 5 families and 20 patients from 7 families. All the patients with **p.Phe215Leufs*14** mutation presented during adolescence [276,363,364]. c.1199dupA (**p.His400Glnfs*11**) was always found in homozygosis and patients presented in a wide range of ages, since infancy (2/13) to adulthood (2/13), but the majority of them presenting during childhood (4/13) or adolescence (5/13) [229,276,363,364]. c.1339dupG (**p.Glu447Glyfs*10**) variant was always found in homozygosis, and patients mainly

presented during adolescence (11/20)[229,276,364]. Some probands with this mutation also presented during childhood (5/20) or when they were adults (4/20).

Finally, there are some variants found in homozygosis or heterozygosis in patients belonging to the different groups. We have classified them, but we cannot be sure of how they would contribute to the disease pathogenesis because of their low representation (Table 1.14).

Table 1.15. Pathogenic variants of *COQ8B* gene found in patients.

Gene/ Protein	Pathogenic variants				Validation			*In silico* mutagenesis prediction				Ref.
	F (P)	cDNA mutation	aa modification	Exon	Segregation (S), Biochemical (B), Functional (F)			SIFT Patho-genic?	Poly Phen-2 Dama-ging?	SPiCE Prob. to alter splicing	CADD score	
COQ8B/ ADCK4 544 aa 15 exons NM_024876.4 NP_079152.3	1 (1)	c.101G>A	p.Trp34*	2				-	-	low	34	363
	4 (8)	c.293T>G	p.Leu98Arg	5				Pathog.	Probably	-	28.6	229,364
	1 (2)	c.449G>A	p.Arg150Gln	6				Pathog.	Probably	-	29.0	365
	3 (5)	c.532C>T	p.Arg178Trp	7	S	B	F	Pathog.	Probably	-	25.9	276,363,364, 366
	3 (4)	c.645delT	p.Phe215Leufs *14	8	S		F	-	-	-	31	276,363,364
	1 (1)	c.649G >A	p.Ala217Thr	8	S			Pathog.	Probably	-	28.9	367
	6 (7)	c.737G>A	p.Ser246Asn	9	S			Pathog.	Probably	-	27.0	365,366,368
	1 (2)	c.748G>A	p.Asp250Asn	9				Pathog.	Probably	-	26.1	364
	1 (1)	c.748G>T	p.Asp250Tyr	9	S			Pathog.	Probably	-	26.3	367
	5 (7)	c.748G>C[1]	p.Asp250His	9	S			Pathog.	Probably	-	25.6	243,362,366, 369
	2 (3)	c.759C>A	p.Asn253Lys	9				Pathog.	Probably	-	24.4	365
	1 (3)	c.857A>G	p.Asp286Gly	10	S		F	Pathog.	Probably	-	29.7	276,363
	1 (1)	c.929C>T	p.Pro310Leu	10				Pathog.	Probably	-	32	364
	1 (1)	c.954_956dup GAC	p.Thr319dup	11				-	-	-	23.5	363
	1 (2)	c.958C>T	p.Arg320Trp	11	S		F	Pathog.	Probably	-	25.5	276,363
	1 (2)	c.1027C>T	p.Arg343Trp	11	S			Pathog.	Probably	-	29.0	363
	2 (3)	c.1041C>A	p.Cys347*	12	S			-	-	-	38	362,369
	5 (13)	c.1199dupA	p.His400Glnfs *11	13	S	B	F	-	-	-	33	229,276,363, 364
	7 (20)	c.1339dupG	p.Glu447Glyfs *10	15			F	-	-	-	34	229,276,364
	1 (2)	c.1356_1362 delGGGCCCT	p.Gln452Hisfs *	15	S	B		-	-	-	34	363
	2 (3)	c.1430G>A	p.Arg477Gln	15	S		F	Pathog.	Probably	-	29.7	229,276,363
	1 (3)	c.1447G>T	p.Glu483*	15	S		F	-	-	-	40	276,363
	1 (1)	c.1468C>T	p.Arg490Cys	15	S			Pathog.	Probably	-	29.5	365
	1 (1)	c.1493_1494 CC>AA	p.Ala498Glu	15				Pathog.	Benign	-	24.0	364

1. Two siblings with this *COQ8B* variant in homozygosis also had an homozygous mutation in *NPHS1* gene (c.1339G>A; p.Glu447Lys) [243].

Reference sequences correspond to longest transcript. Abbreviations: F: Number of families with each variant, P: Number of patients with each variant, aa: amino acid, Pathog: pathogenic Ref: references.

1.3. Conclusions

Primary CoQ_{10} deficiency patients show a wide and variable range of clinical manifestations. In this work, we have compiled all the reported cases published in the literature and classified them depending on the age of first presentation of the disease. The main conclusions are the following:

i. Each *COQ* gene has a particular phenotypical spectrum of manifestations. However, even patients with mutations in the same gene can manifest different clinical presentation and course of the disease.

ii. In general, the sooner the disease manifests, the more severe it is. Different clinical pictures emerge when patients for each *COQ* gene are classified by age of onset.

iii. CoQ_{10} supplementation is a good therapeutic approach for primary CoQ_{10} deficiency. However, some patients do not benefit from it, especially the most severe phenotypes (*COQ2*, *COQ4*). Renal function responds better to treatment than neurological function.

iv. Genotype-phenotype correlations are difficult to stablish because of the low number of patients. Preliminary associations of mutations with clinical manifestations can be done. Some mutations seem to be more frequent in the different age of onset groups, especially for *COQ2* and *COQ6*. Some less evident associations can also be observed in *COQ4, COQ8A* and *COQ8B.*

Chapter 2

Chapter 2.

Primary CoQ_{10} deficiency study models

2.1. Introduction. Primary CoQ_{10} deficiency models: Characterisation and therapeutic approach

As discussed in Chapter 1, primary CoQ_{10} deficiency disorders are very complex and heterogeneous in terms of molecular causes, pathogenesis and clinical manifestations. This complexity is probably due to the wide range of cellular functions that CoQ exerts, as well as the big number of different components implicated in its biosynthetic pathway, some of which may even perform yet unknown additional roles in mitochondrial homeostasis.

CoQ biosynthesis and functions are extensively conserved across the domains of life, from bacteria to eukaryotic multicellular organisms [381]. We can take advantage of this conservation to deeper understand the human mitochondrial biology and disease, by investigating simpler model organisms.

2.1.1. The use of primary CoQ deficiency models

The use of model organisms has been proven effective to dissect the biosynthetic pathway and the functions of CoQ. What is more, disease modelling with simpler organisms is an extremely useful approach to elucidate the genetic causes and the pathogenesis of the disease, as well as to develop diagnostic tools or preclinical assays for potentially therapeutic molecules (Figure 2.1).

Diagnosis and biochemical studies

In vitro models of primary CoQ_{10} deficiency are useful tools to complement the genetic diagnosis, by biochemically determining the quinone content and the combined enzymatic activity of complexes I+III and/or II+III, which may all be reduced compared to controls. The biochemical diagnosis of CoQ_{10} deficiency is generally based on measurements of CoQ_{10} levels in muscle, which is an invasive technique and not always available. However, most of the patients with primary CoQ_{10} show reduced levels of

CoQ_{10} in cultured skin fibroblasts, so these cells are starting to be used as a diagnostic tool for the biochemical characterisation of the CoQ_{10} biosynthetic defect by measuring the total CoQ_{10} levels by HPLC techniques. Skin fibroblasts offer an additional advantage for the molecular characterisation of the disease, since *in vitro* assessment of CoQ_{10} biosynthetic rate is possible by measuring the incorporation of a labelled CoQ_{10} precursor in this cellular model [177]. Additionally, it is possible to identify the accumulation of abnormal metabolites generated by the defect in a particular *COQ* gene. These molecules could be considered specific molecular markers for the defective *COQ* function. As an example, 6-demethoxy-CoQ_{10} (DMQ_{10}, COQ7 substrate) has been found in high amounts in fibroblasts from *COQ7* and *COQ9* patients [238,239,388]. Western blot of whole cell lysates or purified mitochondria from these different models can show defects in the protein affected by the mutations. Interestingly, other *COQ* protein levels can also be affected.

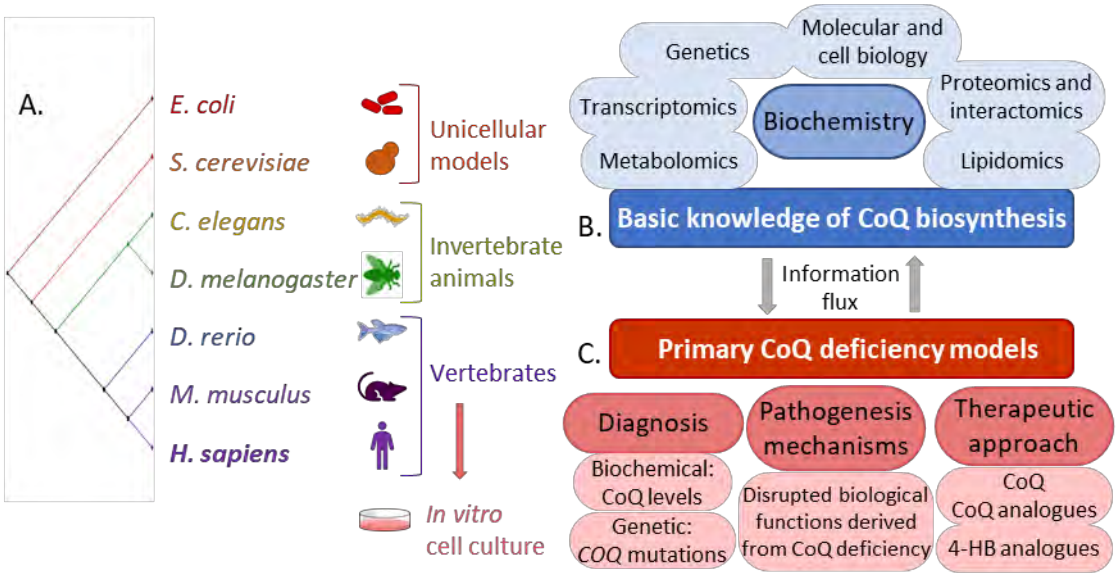

Figure 2.1. The use of model organisms for studying CoQ biosynthesis and primary CoQ deficiency. (A) Phylogenetic tree of the model organisms used for dissecting CoQ biosynthetic pathway, and for studying the physiological significance of a defect in this essential pathway. In vitro cell culture models are usually obtained from clinical patients or from deficient mouse models, or experimentally generated by knock-out/in/down mechanisms. Studying all these models has allowed us to expand the knowledge of CoQ biosynthesis biochemistry (B), but also, understanding the molecular and pathological relevance of primary CoQ deficiency (C).

Pathogenesis

The pathogenesis of primary CoQ_{10} deficiency is very complex (See Chapter 1, section 1.1.1). Different *in vitro and in vivo* models, from yeast to mouse and cell cultures, have contributed to expand our knowledge on CoQ deficiency pathogenesis.

Assessing mitochondrial OXPHOS function has provided insights of the mitochondrial dysfunction caused by CoQ deficiency. This has been performed by measuring the enzymatic activity of the respiratory complexes, and/or analysing the oxygen consumption rate (OCR) by oxygraphy in living cells or in isolated mitochondria. In addition, as CoQ is recognized as an important endogenous antioxidant, oxidative stress produced by this condition has been studied as a mechanism contributing to the pathogenesis [389]. It has been shown that the reduced activity of the OXPHOS system and an increase of ROS are crucial factors involved in the pathogenesis of these disorders.

The use of this models has allowed the molecular characterisation of other pathogenic consequences of reduced levels of CoQ. Some examples are the impairment of different pathways in which CoQ is an important cofactor, such as pyrimidine biosynthesis [266] or H_2S detoxification [267].

Therapeutic approach

As described before, the only therapeutic option currently available for CoQ_{10} deficiency syndrome is CoQ_{10} supplementation. Patients generally respond quite positively to this therapy, but there is a significant group of probands for whom the treatment was not successful. In order to better understand this diversity of responses, different studies have evaluated the effects of CoQ_{10} supplementation as well as other compounds, such as CoQ_{10} analogues with different tail length, vitamin C, vitamin K_2 or probucol in diverse CoQ deficient *in vitro* and *in vivo* models [181,287,390–395].

Moreover, due to the high hydrophobicity and low bioavailability of CoQ_{10}, new approaches are being developed to increase its levels in deficient *in vitro* and *in vivo* models. Some 4-hydrozybenzoate (4-HB) analogues have been proposed as bypass therapies, alternative to CoQ_{10} supplementation [289]. These molecules are CoQ head precursors with additional chemical groups in some of the positions, which are the same

than those found in the final molecule of CoQ (Figure 2.2). These water-soluble compounds with higher bioavailability than CoQ_{10} would bypass certain enzymatic steps disrupted by mutations in *COQ* genes. Their efficacy may differ depending on the stability of the CoQ biosynthetic complex [278] or the residual activity of the mutated enzyme [238], but also by the ability of COQ2 to use them as a substrate to which attach the hydrophobic tail [289]. Some examples of such bypass molecules are vanillic acid (VA) and 3,4-dihydroxybenzoate (3,4-dHB), able to bypass *COQ6* mutations, or 2,4-dHB for *COQ7* defects (Figure 2.2).

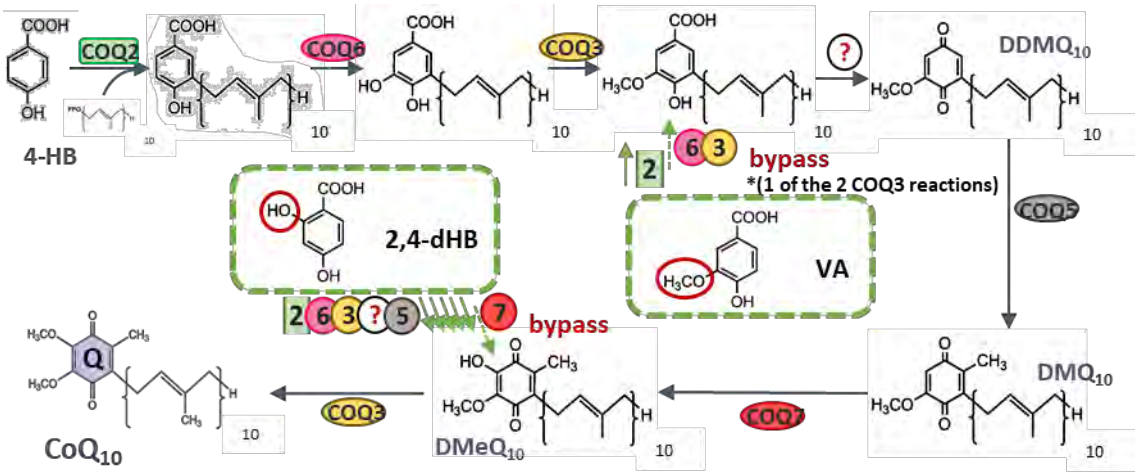

Figure 2.2. Schematic model of human CoQ_{10} biosynthesis pathway.
Gray arrows represent enzymatic reactions and circled numbers represent the different COQ proteins that participate in each step. Circled question mark shows currently unidentified enzymes. Green boxes contain 4-HB analogues, defined as unnatural CoQ precursors, which are able to lead to CoQ production, bypassing defective COQ enzymes such as COQ6 (vanillic acid (VA)) or COQ7 (2,4-dihydroxybenzoate (2,4-dHB). DDMQ: demethoxy-demethyl-coenzyme Q; DMQ: demethoxy-coenzyme Q; DMeQ: demethyl-coenzyme Q (Adapted from Alcázar-Fabra et al., 2018[112]).

The effectivity of VA and 3,4-dHB in restoring CoQ biosynthesis was first demonstrated in *coq6* yeast mutant strains expressing pathogenic versions of human *COQ6* [342], while they were only effective in Δ*coq6* strain after overexpression of Coq8 to stabilize the biosynthetic complex [396]. Treatment with VA has also been tested in mammalian cell lines KO in *COQ6*, rescuing CoQ_{10} biosynthesis and ATP production, in a study that will be described in the results section of this chapter [165]. Notably, VA also stimulates CoQ_{10} synthesis and improves cell viability in *COQ9* patient fibroblasts [388].

2,4-dHB was also first tested in yeast. It was able to restore the CoQ_6 defect in Δ*coq7* strain, only after overexpression of Coq8p to stabilise de complex [397]. 2,4-dHB was also

able to bypass the defective reaction in human fibroblasts with *COQ7* [238,239,388] and *COQ9* mutations [278,388], increasing CoQ_{10} and reducing DMQ_{10} levels. *In vivo*, it increased CoQ_9 levels and lifespan in *Coq7* KO [398] and *Coq9* defective mice ($Coq9^{R239X}$) [278,399]. Particularly, in this model, 2,4-dHB rescued the morphological and histopathological signs of encephalopathy, not by an increase of CoQ_9 but a drastic reduction of DMQ_9. Remarkably, the effectivity of 2,4-dHB depends on the nature of the *COQ7* mutation and the residual activity of the protein [238], being more effective for more severe *COQ7* mutations with less residual activity. A similar effect has been observed for *COQ9* in mouse, in which different mutations in *Coq9* affect differently the stability of the CoQ biosynthetic complex [278], and 2,4-dHB supplementation is more effective when CoQ complex is more stable. 2,4-dHB was also administered to podocyte-specific *Coq6* KO and *Coq8b/Adck4* KO mice models, in which the treatment prevented focal segmental glomerulosclerosis, prolonging their survival [400,401]. In the *Coq6* study, 2,4-dHB treatment was also assayed in a migration assay of cultured podocytes from this mice, and compared with VA supplementation, 2,4-dHB was able to fully recover migration of podocytes, while VA only did it partially [400].

It has also been reported that treatment with high doses of 4-HB, thus increasing COQ2 substrate availability, restores CoQ_{10} synthesis in certain *COQ2* deficient cell lines, which also suggests that these enzyme variants retain some residual activity [402].

2.1.2. Models to study primary CoQ deficiency

In vivo studies with animal models (such as the mouse *Mus musculus* [403] or the fish *Danio rerio* [363]), and *in vitro* studies with mammalian cell cultures (mostly patient's fibroblasts [177,261,301] or cells from defective mice [238]), have been used to study CoQ biology and disease. Additionally, other organisms like invertebrates lacking CoQ have been highlighted important functions of CoQ (the fruit fly *Drosophila melanogaster* or the nematode *Caenorhabditis elegans* [404–410]). Even unicellular eukaryotic (the yeast *Saccharomyces cerevisiae*[380,411380,411]) or prokaryotic (the bacteria *Escherichia coli* [412,413]) organisms have been proven very valuable in this context. Of course, the selection of the model organism is crucial, and the context must be considered in every case (Figure 2.1).

The models that are the most widely used for the study of primary CoQ deficiency disorder are yeast, mouse models and *in vitro* cell cultures (patient's derived cells or other recombinant or KO cell lines).

Saccharomyces cerevisiae

Simple unicellular models, such as *Saccharomyces cerevisiae* and *Escherichia coli,* have been widely used in order to dissect CoQ biosynthetic pathway, to investigate the functions, structure and interactions of each protein involved in the process, and the functions of CoQ itself (Figure 2.1.B). In fact, *coq* genes were first discovered as a complementation group in yeast [414].

Yeast is a powerful model for mitochondrial disease since it can grow in either a fermentative medium or a mandatory respiratory medium, using the mitochondrial respiration. Therefore, mutants in the respiratory function are easily obtained, maintained, and characterised. Examples for such mutants are the strains lacking one of the different *coq* genes, which are unable to synthesise CoQ_6 and grow in a non-fermentable medium. Thanks to the great conservation between yeast *coq* and human *COQ* genes, this eukaryotic unicellular organism has been widely used for evaluating the pathogenicity of the mutations found in primary CoQ_{10} deficiency patients. Yeast deleted-strains in almost all *coq* genes (*coq1* [241]*, coq2* [232,241,277,328]*, coq4* [251,341]*, coq6* [232,233,342]*, coq8* [276,356,357]*, coq9* [248]) have been used to better understand the pathogenicity of the mutation. The null mutants are transformed with the WT or mutant version of the respective gene (human or yeast gene), which is followed by a functional complementation assay, analysing the transformants ability to grow in a respiratory medium or to produce CoQ_6.

Yeast have also been proven a useful model for therapeutic assays. For example, the bypass therapy with 4-HB analogues with the defective chemical group was first assayed in yeast, as described above [342,395–397,415]. Very recently, yeast deficient in some *coq* genes (Δ*coq6* and Δ*coq4* strains with Coq8p overexpression) have been described to be a useful platform to perform a high throughput screening of natural extracts to identify molecules bypassing primary CoQ_6 deficiency in *Saccharomyces cerevisiae* [416].

Mus musculus

Although studies in simple model organisms have been extremely useful, the generation of multicellular animal models deficient in CoQ is paramount to reveal the complex pathogenic consequences of CoQ deficiency in the physiological context of a whole animal. Mouse models recapitulating primary CoQ deficiency disease pathogenesis are extremely valuable, since their complexity, anatomy, physiology, and metabolism are relatively close to humans. In fact, they allow to study the tissue-specific damage that mutations in some *COQ* genes produce, providing deeper knowledge about CoQ biosynthesis and regulation in a whole organism. Furthermore, the use of mouse models is contributing to the development of new therapeutic approaches. Different mouse models with primary CoQ_9 and CoQ_{10} deficiency have been developed and studied in CoQ biosynthesis research [403].

i. Knock-out (KO) and Knock-in (KI) models

The International Mouse Phenotyping Consortium (IMPC, www.mousephenotype.org) and the European Conditional Mouse Mutagenesis Program (EUCOMM), together with different gene specific studies have generated constitutive KO mouse models for the different *Coq* genes [403]. In the case of *Pdss1* (IMPC), *Pdss2* [417,418], *Coq2* (EUCOMM), *Coq3* [419], *Coq4* (EUCOMM), *Coq6* [400], *Coq7* [419–421] and *Coq8b/Acdk4* [401], constitutive homozygous KO resulted in embryonic lethality. This suggests CoQ biosynthesis has a crucial role during development. Interestingly, the heterozygous *Coq7*$^{+/-}$ mice were viable and displayed an increased lifespan, lower levels of DNA damage in liver, decreased ROS levels, respiratory dysfunction and an altered distribution of CoQ_9 and CoQ_{10} in submitochondrial membranes [419,422]. Immunoblots showed the heterozygous mice had 50% of Coq7 signal in brain extracts, in comparison to the controls [420]. The increase in lifespan was previously reported in *clk-1* (ortholog of *COQ7* gene) *C. elegans* null mutant [423]. In contrast, *Coq3*$^{+/-}$ mice had a normal lifespan and had no defects in mitochondrial function or ubiquinone distribution [419].

Contrarily, constitutive Coq8a/Adck3 [424] and Coq9 [278] knocking-out resulted in viable mice. Homozygous mice were born and recapitulated the clinical disorder. In the case of *Coq8a/Adck3*$^{-/-}$ mice, they displayed a cerebellar ataxia (ARCA2), mimicking

COQ8A/ADCK3 patients' main clinical phenotype [424]. On the other hand, the effects of defects on *Coq9* were studied in two different KI mouse models [278,279]. The complete lack of Coq9 protein due to a very early nonsense mutation (*Coq9*^{Q95X}) resulted in a moderate CoQ deficiency and a late-onset mild mitochondrial myopathy, with decreased levels of Coq7 and Coq5 proteins and, in agreement with what was observed in the *Coq7*$^{+/-}$ mice, an increase in lifespan. This mouse did not respond to 2,4-dHB supplementation. Contrarily, defects on Coq9 due to a late-truncation of the protein (*Coq9*^{R239X}) produced a severe widespread CoQ deficiency associated with fatal encephalomyopathy, responding to 2,4-dHB supplementation. These mice had a generic decrease of Coq proteins, suggesting that the presence of a truncated Coq9 induces instability of the CoQ multiprotein complex and contributes in this way to the genetic and tissue-specific pathomechanisms of the disease [278,279].

ADCK2 is a gene of a yet unknown function that is part of the *ADCK* family to which *ADCK3* (*COQ8A*) and *ADCK4* (*COQ8B*) also belong. Recently, it has been shown that *ADCK2* haploinsufficiency reduces mitochondrial lipid oxidation and causes liver dysfunction and myopathy associated with CoQ deficiency in the skeletal muscle of an *Adck2*$^{+/-}$ mouse model [378]. Fibroblasts from a patient with mutations in this gene also showed CoQ_{10} deficiency[378]. *ADCK2* is proposed to be involved in organismal fatty acid metabolism and in CoQ biosynthesis in skeletal muscle[378].

ii. Conditional KO models

To overcome the issue of embryonic lethality, some tissue-specific or adult-onset KO mice in some of the *Coq* genes were developed and studied. Conditional *Pdss2* KO in kidney [393,418] and cerebellum [417] were generated, and they recapitulated the organs damage found in the patients. Conditional *Clk-1/Coq7* KO in liver [425] revealed a defect in CoQ_9, an accumulation of DMQ_9 and a mild respiratory impairment in liver that was responsive to CoQ_{10} supplementation. An induced adult-onset global *Coq7* KO mouse was also generated [398], developing a severe depletion of CoQ_9 in almost all organs, with DMQ_9 accumulation, gradual loss of mitochondrial function, gradual development of disease phenotypes and shortened lifespan. CoQ deficiency was not rescued by CoQ_{10} treatment in this case, but it was partially recovered with 2,4-dHB. Podocyte-specific *Coq6* KO and *Coq8b/Adck4* KO mice models were also produced, recapitulating the focal

segmental glomerulosclerosis observed in the nephrotic syndrome caused by *COQ6* and *COQ8B/ADCK4* mutations in patients. In these two mouse models 2,4-dHB treatment ameliorated the kidney disease and prolonged their survival [400,401].

iii. Spontaneous mutant models

A mouse with a spontaneous missense mutation (p.Val117Met) in Pdss2 developed a kidney disease responsive to CoQ_{10} supplementation [287,394,418,426–428].

In vitro cellular models

Cell cultures of isolated mammalian cells are a fast and powerful tool to extract information from a eukaryotic system. However, the mechanisms studied *in vitro* occur in a simplified, highly controlled intracellular and extracellular environment, so conclusions must be drawn carefully.

i. Patient's fibroblasts

Primary skin fibroblasts derived from patients carrying mutations in one of the *COQ* genes are a model widely used to study primary CoQ_{10} deficiency, especially for its biochemical diagnosis. They are very valuable, since they are easily obtained by less invasive techniques than muscle biopsies -which is preferred by families-, and they come directly from the studied patient. However, they have some limitations, after all the experiments are performed in optimum conditions outside their normal biological context and adaptations may occur. In addition, as they are primary cells, they can only divide a certain number of times, after which experiments should not be performed. Of note, due to the low number of described patients, the number of available cell lines is limited, and not a huge number of studies have been performed. They have also been used to study certain pathogenic mechanisms of the disease, as well as for *in vitro* assessments of efficacy of CoQ or 4-HB analogues supplementation (see section 2.1.1).

ii. Human induced pluripotent stem cells model (iPSCs)

One of the greatest breakthroughs that redefined the fields of stem cell biology, regenerative medicine and disease modelling was the discovery of the induced pluripotent stem cells (iPSCs) technology in 2006 by Shinya Yamanaka *et al* [429]. Fully differentiated adult somatic cells were reprogrammed into a pluripotent state, by using

four defined transcription factors: Oct3/4, Sox2, c-Myc and Klf4. The resulting cells, the iPSCs, exhibited the morphology and growth properties of stem cells and had the capacity to differentiate into any cells of the three germ layers. The selection of the appropriate type of somatic cells, reprogramming factors and the method for delivering these factors to the cells are the most important parameters influencing the reprogramming process.

This technology allows to create patient-specific and healthy donor iPSCs, suitable for disease modelling[430]. Moreover, it allows to obtain and work with hard-to-reach cell types, such as neurons, cardiomyocytes or myotubes, as well as to study their differentiation process and how the disease may alter it. The development of this iPSC model, in combination with genome-editing strategies for correcting or introducing disease-causing mutations, has led to numerous advances in modelling neuro-degenerative disorders, neuropathies, myopathies and mitochondrial diseases [430–434].

However, the use of iPSCs has some disadvantages. They are expensive and complex to be generated. Besides, induction of pluripotency is accompanied by epigenetic reprogramming and metabolic shift from OXPHOS to glycolytic, and sometimes the nuclear and mitochondrial genomes have been reported to be genetically instable [434].

In the context of primary CoQ_{10} deficiency, an iPSC model was generated from human dermal fibroblasts from a patient harbouring a heterozygous mutation in *COQ4* gene (c.483G>C, p.Glu161Asp)[435]. The patient was a 4-year-old girl diagnosed with lethal rhabdomyolysis associated with CoQ_{10} deficiency. These iPSCs had impaired mitochondrial function and CoQ_{10} deficiency, which was rescued when the mutation was corrected by CRISPR/Cas9. Differentiation to neurons was not impaired in these iPSCs, while differentiation to skeletal muscle was compromised and the resulting muscle also displayed respiration defects. Remarkably, this was reproducing the disease phenotype observed in the patient, and the CRISPR/Cas9 corrected iPSCs did not show the defects[436].

iii. Continuous cell lines defective/overexpressing one COQ gene

Continuous cell lines are a useful model often employed in research to study different biological problems. They offer some advantages over the primary cultures, such as the

big amount of material they can provide in a short time, their ease to use, and their high transfection efficiency. Thanks to this last point, knock-down (KD), KO, KI or tagged expression of COQ proteins have been achieved in cell lines in order to study CoQ biosynthesis (see also Chapter 3, CRISPR/Cas9). KO and KD have been used to study the functional defects of the lack of a certain COQ protein [165,315,394,437]. Also, ectopic overexpression of the different tagged COQ proteins has been used for localisation of the labelled protein by microscopy [277] or mitochondrial fractionation [276,378] and for searching interactors of the tagged protein with other proteins [401,438]. Some examples of cell lines commonly used are HeLa [277,394], HEK293 (and other lines derived from it) [378,385,400,401,438], HepG2 [438] or 143B [315,437] cells.

HEK293 is a cell line derived from human embryonic kidney cells grown in tissue culture[439]. It is a hypotriploid cell line with a modal chromosome number of 64. These cells are popular for their ease of growth and high transfection efficiency, as well as their ability to produce exogenous proteins in large amounts. They are widely used in biomedical research in general, and have helped for great advances in mitochondrial research. For example, they have been used for mitochondrial localisation characterisation of the mammalian mitochondrial proteome by tagged protein expression and microscopy [69], or for the characterisation of functional and interaction partners of some unknown mitochondrial proteins -the COQs proteins among them- by tagged expression of these proteins in HEK293 cells, affinity purification of the tagged protein and mass spectrometry of the affinity enriched fraction (AE-MS)[438].

The Flp-In™ T-REx™-293 cell line is derived from HEK293. It allows the rapid generation of stable cell lines that ensure homogenous expression of a protein of interest from a Flp-In™ expression vector. These cells contain a single stably integrated FRT site at a transcriptionally active genomic locus. Co-transfection of the Flp-In™ Cell Lines with a Flp-In™ expression vector and the Flp recombinase vector, pOG44, results in targeted integration of the expression vector to the same locus in every cell (the FRT site), ensuring homogeneous levels of gene expression. These cells have been used for mitochondrial protein expression, for example, in the recent generation of a high resolution human mitochondrial protein proximity map using BioID [440], characterising

proteins belonging to the different mitochondrial compartments and sub-compartments.

2.2. Results and discussion

In this chapter, we worked with different *in vitro* cellular models of primary CoQ_{10} deficiency with three main objectives:

i. Biochemical and molecular diagnosis of the primary CoQ_{10} deficiency, and report of new cases.

ii. Determination of the pathogenesis and physiopathology of the mitochondrial defects associated to a primary CoQ_{10} deficiency.

iii. Treatment evaluation with 4-HB analogues.

For the completion of these objectives, several human cellular models with defects in one of the genes involved in CoQ_{10} biosynthesis were obtained.

On one hand, in collaboration with different hospitals (see Table M.1), we received skin biopsies or fibroblasts of patients with clinical suspicion of suffering CoQ_{10} deficiency. After genetic tests to confirm the primary CoQ_{10} deficiency, due to mutations in one of the genes involved in CoQ_{10} biosynthesis, five patients were found to have compound heterozygous or homozygous mutations in *COQ4* or *COQ7* genes. These patients and the genetic defects producing their disease are being firstly reported in this PhD project. The studies on the fibroblasts have been performed with the three previously mentioned objectives in mind: diagnosis, study of the pathogenesis and therapeutic approach with 4-HB analogues.

On the other hand, HEK293T cells were genetically modified to knock out *COQ6* or *COQ4* genes, and used as models of deficiency of these genes. The studies with HEK cell lines have been mainly performed with the objective of characterising the pathogenicity of the mutations, studying the physiopathology of the total defect of CoQ_{10} due to a total lack of one of the proteins involved in its synthesis (COQ6 or COQ4), as well as for therapy evaluation with 4-HB analogues.

Biochemical and physiological studies have been performed in order to determine how the mitochondrial function is altered. Additionally, some molecular studies have also been done in order to confirm the pathogenicity of the mutations.

The first step consisted in confirming the CoQ_{10} deficiency by measuring steady state levels of CoQ_{10} in cells by HPLC. Sometimes, CoQ_{10} levels have already been measured in skeletal muscle from patients, before the arrival of the fibroblasts to our laboratory. Anyway, CoQ_{10} assessment in fibroblasts is very useful to corroborate the condition of CoQ_{10} deficiency. It would be also possible to detect the accumulation of intermediates of the synthesis, as it has been described for *COQ7* and *COQ9* patient fibroblasts[388]. To deeper investigate how this function is altered, we also measured CoQ_{10} biosynthetic rate, by analysing the incorporation of radiolabelled 4-HB, which is the precursor for the CoQ_{10} quinone head. This technique allows us to confirm the biosynthetic defect.

Then, we measured the mitochondrial respiratory performance, by measuring the enzymatic activity of the respiratory complexes, and/or analysing the OCR by oxygraphy using a SeaHorse XF24 Extracellular Flux Analyzer in living cells. OCR measurement by the Seahorse XF Cell Mito-Stress Test uses modulators of cellular respiration that specifically target components of the electron transport chain (ETC) to reveal key parameters of the metabolic function: basal respiration, ATP-linked or coupled respiration, proton leak, maximal respiration, spare respiratory capacity, and non-mitochondrial respiration (See Material and Methods, Section M2.5 for more details).

For treatment evaluation, CoQ_{10} levels and mitochondrial performance have been assayed in cells after the administration of different analogues of 4-HB that could bypass the defective enzymatic step, in order to test their therapeutic potential effect.

Primary deficiencies due to defects in *COQ7*, *COQ6* and *COQ4* genes have been studied in this chapter.

2.2.1. Primary CoQ_{10} deficiency due to defects in *COQ7* gene

COQ7 is a di-iron oxidase responsible for the C6-hydroxylation of DMQ_{10}. Mutations in *COQ7* are very rare and only three cases have been reported in the literature so far (see Chapter 1, section 1.2.4). Here, we report two new patients with mutations in *COQ7*.

One of them, P102, is similar to the patients reported in the literature, while the other one, P112, is strikingly different, with the disease onset during adolescence.

Mutations in COQ7 gene produce different clinical manifestations

P102 patient is a Spanish child who showed a pronounced neonatal generalized hypotonia. He developed hypoxic-ischemic encephalopathy during the neonatal period. He mainly had a neurological affection, with sensorineural hearing loss, and there were no signs of renal involvement. At the age of 8 months, he developed epileptic crisis with tonic movement in upper limbs. Because of the acute hypotonia, he could not hold his head at the age of two. At this age, he had lack of language and a severe intellectual disability, with cerebral atrophy. Metabolic studies showed persistently elevated lactate.

In contrast, P112 presented a different and milder clinical picture. This patient is a Spanish 55-year-old woman who had walking difficulty since the age of 15 years. She had a pyramidal syndrome, with hearing loss and neuropathic gait. Up to now, all *COQ7* reported patients were paediatric patients presenting very early in life, being P112 the first patient with adolescence-onset and a mild progressive disorder.

P102 and P112 have biallelic mutations in COQ7 gene

Exome sequencing and bioinformatic analysis revealed these patients had potential pathological variations in the *COQ7* gene.

In the case of P102, a panel exome sequencing was performed, and after data analysis, two compound heterozygous mutations in *COQ7* gene were found as candidates to produce the disease (Figure 2.3). One of the variants is a deletion of one nucleotide, resulting in a frameshift (c.161_161delG, p.Val55Trpfs*94, NM_016138.5) in exon 2, with a premature stop codon 94 amino acid downstream the frameshift mutation. The variant is predicted pathogenic by CADD (score=29.4) tool. The other variant corresponds to a missense mutation (c.319C>T, p.Arg107Trp, NM_016138.5) in exon 3. This mutation has also been reported in another *COQ7* patient [240] and it is predicted to affect the protein stability, changing a very conserved arginine (positive) for an hydrophobic amino acid (tryptophan). The change is predicted to be pathogenic by SIFT

(score=0.01), PolyPhen-2 (score=1) and CADD (score=33) tools (Table 1.10). Sanger sequencing confirmed the segregation of the variants in parental DNA. Both parents were heterozygous carriers of each of the mutated alleles. The frameshift variant was maternally inherited while the missense variant was carried by the father.

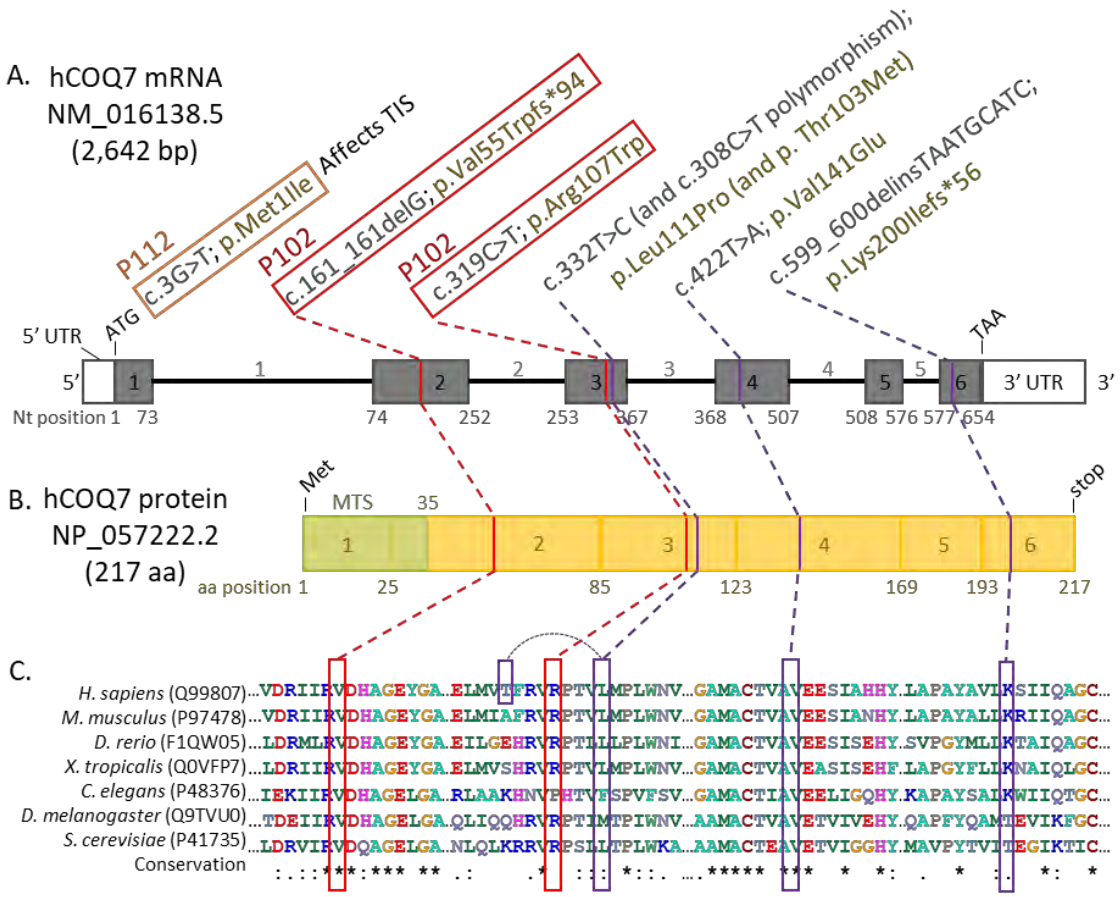

Figure 2.3. Schematic representation of COQ7 mRNA (A) and protein (B).
The localization of the two mutations from P102 patient are shown with red lines and boxes, showing the residue conservation in the alignment of COQ7 protein from different species (C). The localization of the mutation of P112 is shown with an orange box, being located in the translation initiation site (TIS). The rest of mutations shown (purple boxes) correspond to the 3 COQ7 patients reported previously [238–240]. The multiple alignment was performed with the protein sequences obtained in Uniprot, using Clustal X2 and BioEdit to visualize the results. UTR (untranslated region); MTS (mitochondrial targeting sequence; aa (amino acid); * (asterisk: single and fully conserved residue); : (colon: conservation between groups of strongly similar properties); . (period: conservation between groups of weakly similar properties).

The nature of P112's mutations is different. In this case, exome sequencing revealed a homozygous mutation in the translation initiation codon (c.3G>T, p.Met1Ile, NM_016138.5) (Figure 2.4). The change is predicted to be pathogenic by SIFT (score=0.00), PolyPhen-2 (score=1) and CADD (score=24.9) tools. This extremely rare case of primary CoQ_{10} is the first one reported to have a mutation altering the translation initiation codon of a COQ protein.

Significance of the c.3G>T, p.Met1Ile mutation in P112

Translation initiation in eukaryotic mRNAs mainly occurs via a scanning mechanism which identifies a start AUG codon in a Kozak context[441]. Mutations affecting this initiation codon will probably have important biological consequences, and there are several examples of different diseases caused by mutations in the initiation AUG codons [442–449]. The characterisation of the pathogenicity of mutations disturbing translation initiation codon is very useful to study not only the impaired biological process (in this case, CoQ_{10} biosynthesis), but also the pathological relevance of translation initiation defects.

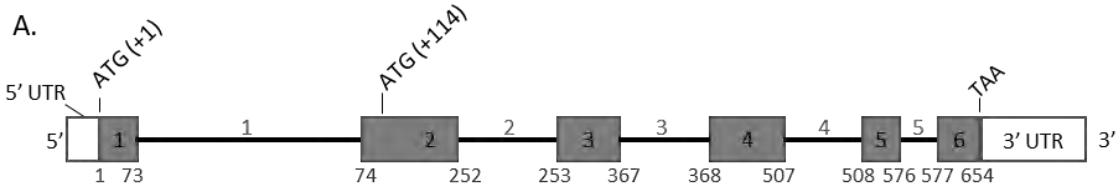

B.

ATG (nt)	Met (aa)	NetStart score WT/MUT	ATGpr score WT/MUT	ORF length (aa)	Uniprot isoform
+1	1	0.248/-	0.55/-	217	1
+114	39	0.591/0.591	0.16/0.38	179	2

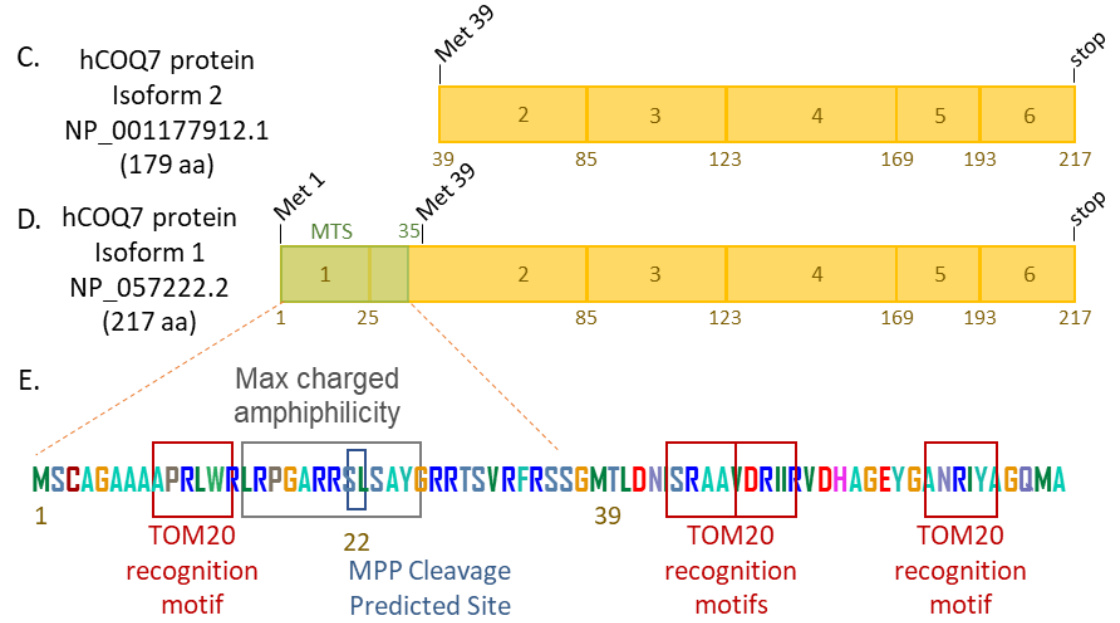

Figure 2.4. Alternative translation initiation of COQ7.
P112 c.3>G mutation in AUG (+1) could lead to alternative translation initiation in a downstream AUG (+114) (A). (B) The table indicates the probability of translation initiation in these two AUGs calculated by NetStart and ATGpr tools. Translation from AUG (+114) would give rise to a 179 amino acid long protein (COQ7 isoform 2), starting from Met39, and lacking the mitochondrial localization signal (MTS) (C). The presence of a MTS in COQ7 isoform 1 (D) has been predicted using MitoFates (E).

The pathogenicity of the c.3G>T, p.Met1Ile mutation would mainly rely on the impaired translation of the protein, and not exclusively on the amino acid change from methionine to isoleucine. For this kind of mutation, it is possible that downstream AUG codons could be used as alternative translation initiation (ATI) sites, leading to shorter versions of the protein lacking the N-terminal region. ATI diversifies the proteome and may alter a protein's function or cellular location [450]. COQ7 isoform 1 has an MTS in the N-terminal of the protein, leading to a protein with mitochondrial localisation (Figure 2.4.D and E). Of note, COQ7 protein has also been attributed a role in the nucleus, with the nuclear localisation signal (NTS) adjacent to the mitochondrial transit peptide (mitochondrial targeting sequence, MTS) [451]. However, this fact is still controversial [373].

In this context, we subjected WT and mutated *COQ7* mRNA sequence (NM_016138.5) to a translation initiation site (TIS) prediction using NetStart1.0 [204] and ATGpr [205]. *COQ7* translation initiation sites prediction did not give very high scores for any of the methionines, and the scores given by the two tools were not comparable to each other (Figure 2.4.A and B). However, ATG(+114) has one of the highest scores when ATG(+1) is mutated, so we could hypothesise that COQ7 translation can initiate from ATG(+114), besides from ATG(+1) (and specially in the context of the c.3G>T mutation). Translation from this site would lead to a 179aa protein that is annotated as COQ7 isoform2 and lacks the MTS (and the NTS) (Figure 2.4.C). This phenomenon would produce a protein with no mitochondrial (nor nuclear) localisation.

It is also possible that the new non-AUG codon (in this case, AUU) could be also used for initiation of translation, but in a lesser efficient way, compared to the AUG codon [449,452,453]. In this case, COQ7 protein would be produced and probably translocated to the mitochondria, having no differences with a WT COQ7 protein after removal of the MTS. A reduction in the levels of WT COQ7 may not be deleterious, and even in some organisms it induces an increase in lifespan [422,454]. We could speculate that this non-AUG translation could become less efficient with age [455], leading to a later onset of the disease.

The effect of the p.Met1Ile mutation on COQ7 translation and localisation has not been experimentally studied yet, but it will provide important information about its pathogenicity.

COQ7 patients' fibroblasts have drastically reduced CoQ_{10} levels, impaired CoQ_{10} biosynthesis and accumulation of DMQ_{10}.

In order to investigate the degree of affectation of CoQ_{10} biosynthesis due to these *COQ7* mutations, total levels of CoQ_{10} were analysed in patients' fibroblasts (Figure 2.5).

P102 patient's fibroblasts showed an 80% CoQ_{10} deficiency (Figure 2.5.A) and a high accumulation of DMQ_{10} (Figure 2.5.B), the natural substrate for COQ7 enzyme, which was undetected in cells from a neonatal control (HDF Neo). The identity of the DMQ_{10} peak was confirmed by HPLC-coupled mass spectrometry, showing a prominent ion with a mass-to-charge ratio (*m/z)* of 850.70, which is compatible with the mass of DMQ_{10} ($M+NH4^+$). P112's fibroblasts equally showed an 80% of CoQ_{10} deficiency (Figure 2.5.E) and a high accumulation of DMQ_{10}, undetected in cells from an adult control (B003) (Figure 2.5.F). Accumulation of this molecule seems to be a hallmark for *COQ7* deficiencies, so it could be considered a molecular marker for this defect [388]. *COQ9* deficiency has also been reported to show accumulation of DMQ_{10}, which reflects its role in supporting COQ7 function [388].

CoQ_{10} biosynthesis rate was also measured, by analysing the incorporation of ^{14}C-4-HB to the quinone extract. While the control cells showed a radioactive CoQ_{10} peak, the fibroblasts from both patients only presented radioactivity corresponding to the DMQ_{10} peak (Figure 2.5.D and H). This probably indicates that CoQ_{10} pathway is slow and the lack of a functional COQ7 enzyme is the bottleneck, provoking the accumulation of the radiolabelled substrate of COQ7, DMQ_{10}.

P102 and P112 show the same defects in terms of CoQ_{10} levels, biosynthesis rate and accumulation of DMQ_{10}. However, it should be considered that fibroblasts were obtained from the patients with a great age difference. It is possible that CoQ_{10} levels and biosynthesis rate from the adult patient were not so highly impaired when the patient was younger. It is also possible that any systemic adaptation that could compensate the late-onset deficiency could be abolished in the context of an *in vitro* cellular model of the disease.

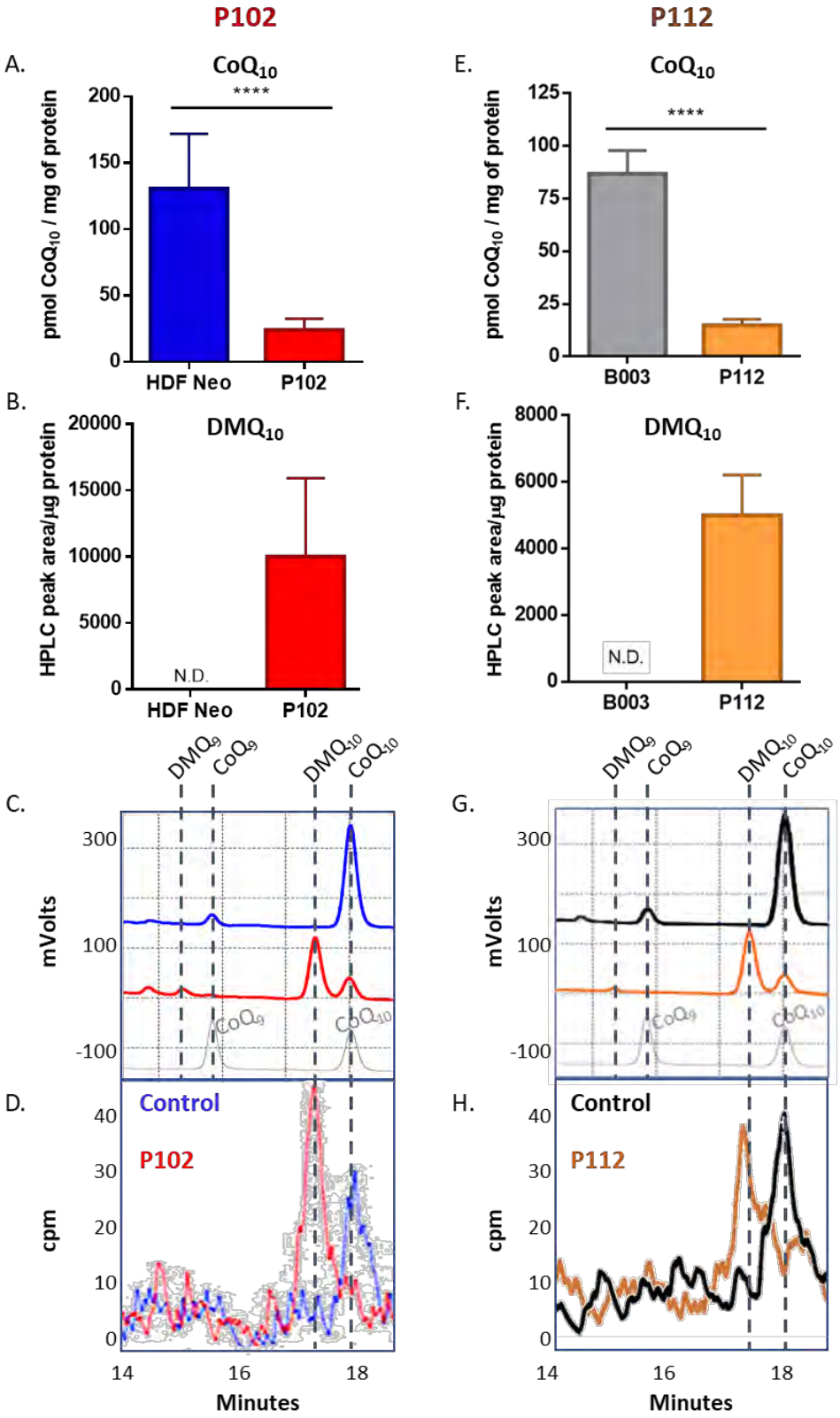

Figure 2.5. Quinone content in *COQ7* Mutant Fibroblasts, P102 (A-D) and P112 (E-H).
Both patient fibroblasts (P102: A; P112:E) show an 80% CoQ_{10} deficiency (Unpaired two-tailed t-test; p value<0.0001) and (B, F) a big accumulation of 6-demethoxyubiquinone (DMQ_{10}) , the natural substrate for COQ7 enzyme, undetected (N.D.) in control cells. (C, G) The HPLC-ECD chromatogram showed the presence of the two peaks (DMQ_{10} peak, retention time (rt): 17.5min; CoQ_{10} peak, rt:18min) in lipids extracts from patients' fibroblasts. It is also possible to see lower amounts of CoQ_9 in controls and DMQ_9 in patients. The HPLC-radioactivity chromatogram (D, H) showed the incorporation of ^{14}C-4-HB to the quinone extract; in controls, in a radioactive CoQ_{10} peak; in patients, in a radioactive DMQ_{10} peak.

Patients' fibroblasts respiration is impaired in different degrees

Respiration studies in *COQ7* mutant fibroblasts and controls were performed to evaluate the effect of the dysfunctional CoQ_{10} synthesis on the mitochondrial respiratory function (Figure 2.6).

Patient P102 fibroblasts showed a marked decrease in CII+CIII activity, while isolated CIII was also reduced (Figure 2.6.A). However, these differences were not statistically significant. OCR profile showed a marked respiratory defect in patient's fibroblasts. This phenomenon was mainly observed with the decrease of the maximal respiration rate, as well as the spare capacity (Figure 2.6.B and C) (see Matherials and Methods for more details). These results suggest that patient's cells are less able to respond to energetic demands than control cells. These effects can be a combined action of CoQ_{10} deficiency and DMQ_{10} accumulation, as it has been proposed that DMQ_{10} could compete with CoQ_{10} to bind to CoQ_{10}-binding sites in the MRC and inhibit electron transport [238,409,456].

P112 fibroblasts also showed defects in CII+CIII and isolated CIII but a less severe respiratory impairment, measured by oxygraphy (Figure 2.6.E and F). Remarkably, these fibroblasts also showed an increased CIV activity. These fibroblasts have a mild respiratory defect, which fits with the fact that the patient had a milder disease. However, it is surprising because of the profound CoQ_{10} deficiency measured in fibroblasts, and the high levels of DMQ_{10} accumulated. In fact, both CoQ_{10} and DMQ_{10} levels are comparable to those of P102 fibroblasts. However, respiratory efficiency is higher in P112 than in P102. This observation could rely on other compensatory or adaptation mechanisms still to be defined. Increased CIV activity in P112 fibroblasts could partially explain the higher respiratory efficiency in P112 compared to P102.

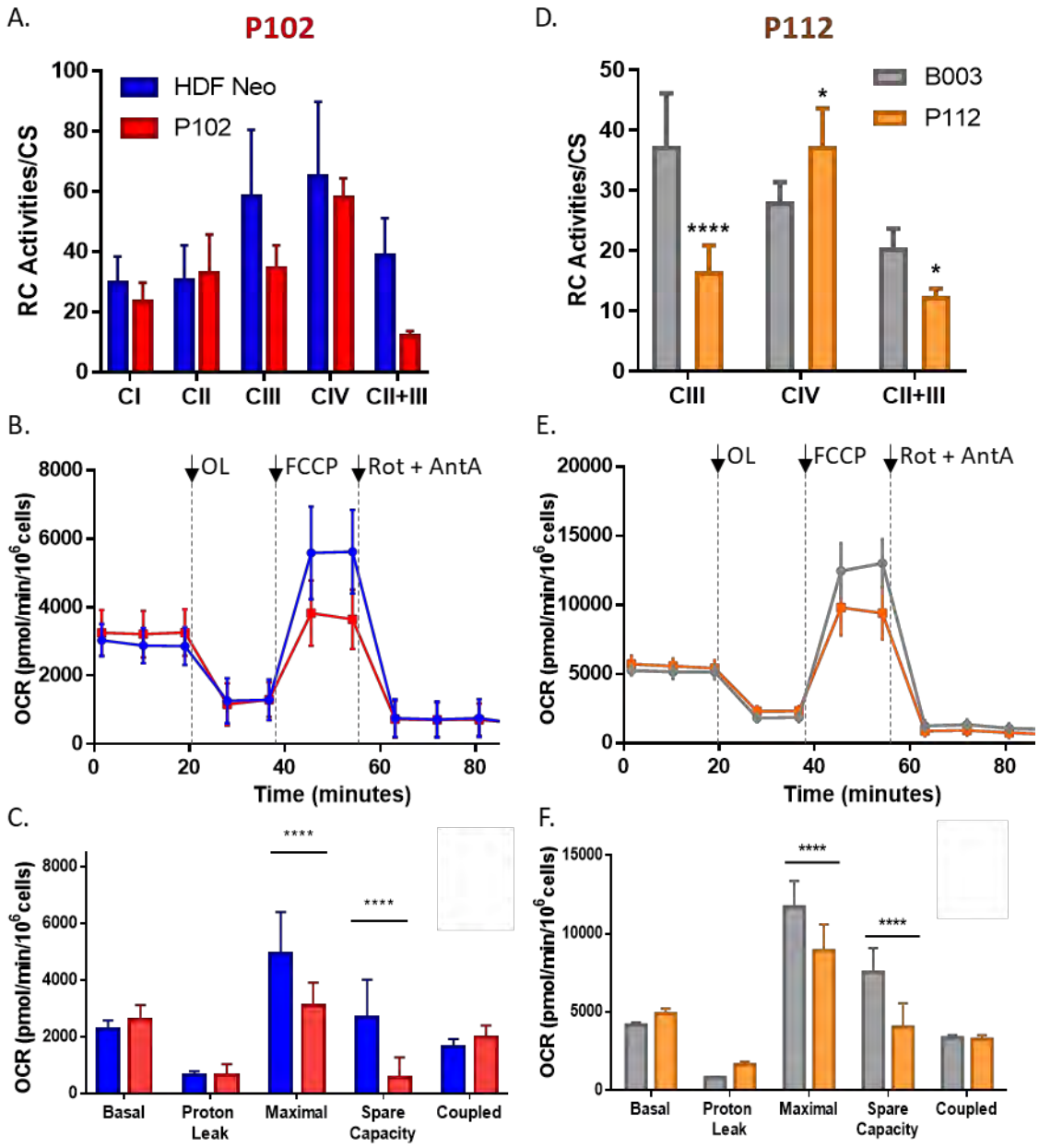

Figure 2.6. Respiration Studies in *COQ7* Mutant Fibroblasts, P102 (A-C) and P112 (D-F).
(A, D) Mitochondrial Respiratory Chain (RC) activities were measured in patient's fibroblasts and controls (Two-way ANOVA with Sidak's multiple comparison test (p value<0.05 (*), <0.0001(****)). (B, E) Oxygen consumption rate (OCR) profile shows a respiratory defect in both patient's fibroblasts. Arrows indicate the addition of the individual inhibitors. Quantitative data are graphed on C and F as mean ± SD (Two-way ANOVA with Sidak's multiple comparison test (p value<0.0001(****)). OL (oligomycin 4 µM); FCCP (Carbonyl cyanide 4-(trifluoromethoxy)phenylhydrazone 1 µM); Rot (rotenone 1 µM); AntA (antimycin A 2.5 µM).

COQ7 protein levels are drastically reduced in both patients, and P102 point mutation is predicted to alter the protein structure stability.

COQ7 protein levels were analysed in whole cell lysates from controls' and patients' fibroblasts, revealing extremely low levels of the polypeptide in both the cases (Figure 2.7.A and C).

The low levels of the protein resulting from the c.161_161delG mutation in patient P102 were expected and are explained by the frameshift mutation that produces an early STOP codon and, thus, does not produce any full length COQ7 protein. However, the missense mutation in this patient is predicted to give rise to a full-length COQ7 protein that should be detected by western blot. The inability to detect the protein could be explained by a dramatically decrease in protein stability induced by the mutation. Human COQ7 protein homology model was generated using a ferritin as template (PDB:5HJH, [224]) (Figure 2.7.D). The mutated amino acid (p.Arg107Trp), labelled in red (Figure 2.7.D), was also found in another *COQ7* patient [240] and it is predicted to affect the protein stability, changing a positive (arginine) for an hydrophobic (tryptophan) amino acid. It is also very close to the region that is proposed to interact with COQ9 protein [224]. We cannot know if these extremely low protein levels (probably because low protein stability) are the cause of the enzymatic defect, or if the mutation itself also alters COQ7 enzymatic function. What is clear is that the combination of these effects leads to a highly impaired COQ7 function. Other previously reported mutations in COQ7 had been identified with the same extremely low expression feature. The mutations were p.Leu111Pro (very close to the here studied mutation) and p.Val141Glu (in the predicted di-iron center active site). After a treatment with a protease inhibitor, in order to prevent protein degradation, CoQ levels were not increased in those cases [238].

P112 fibroblasts also show very low levels of COQ7 protein (Figure 2.7.A and C). This could be explained by the translation initiation defect induced by the homozygous mutation in the first codon. Localization studies have not been performed, but they would be interesting to decipher the mechanism by which COQ7 is translated (ATI or non-AUG translation) and translocated to mitochondria.

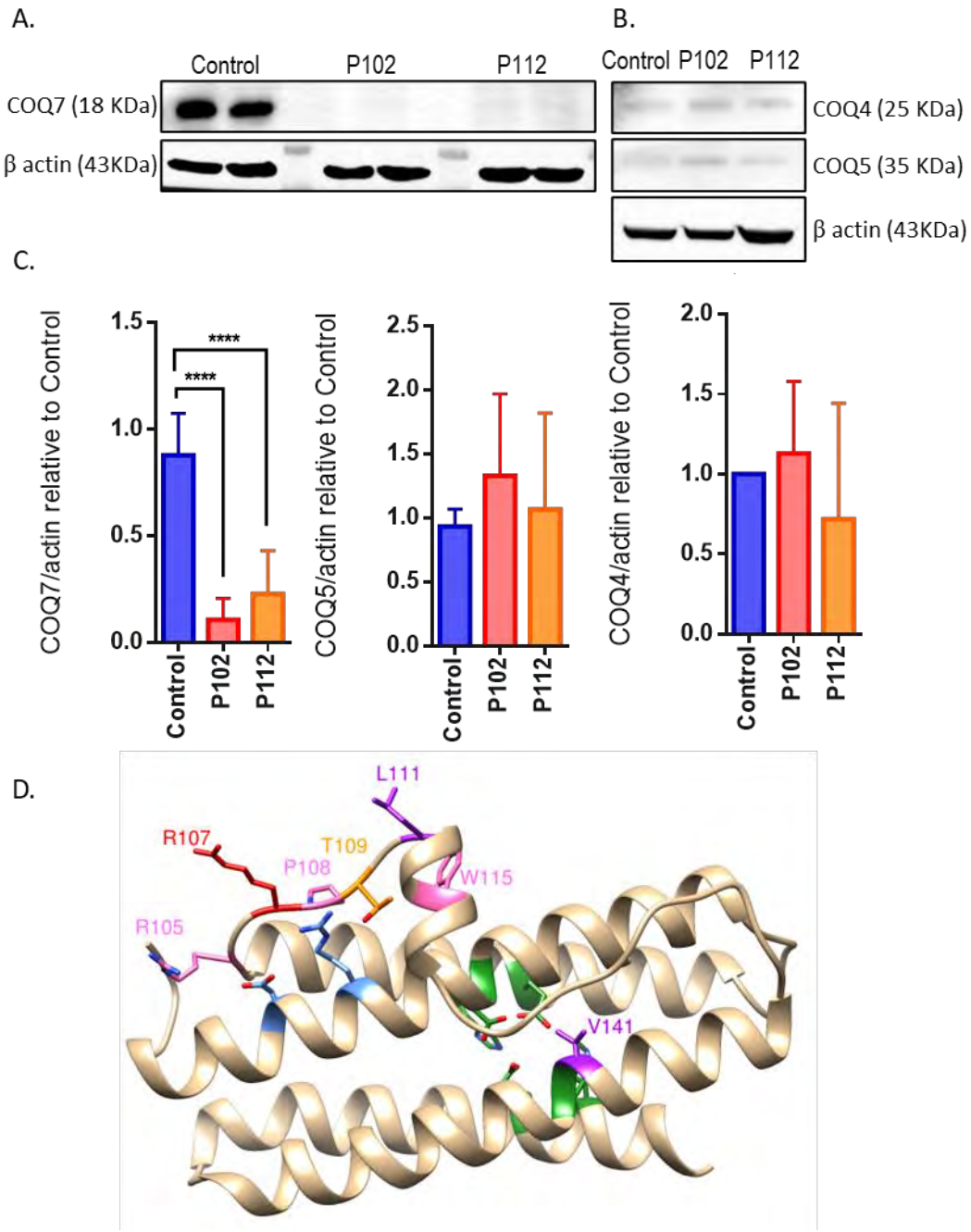

Figure 2.7. COQ7 and other COQ proteins levels in *COQ7* Mutant Fibroblasts.
Western blot analysis of COQ7 (A) and other COQ proteins (B) levels in whole fibroblasts lysates and their quantification (One-way ANOVA, Dunnett's multiple comparison test, p-values<0.0001 (****))(C). An antibody against beta-actin (43KDa) was used as a loading control. (D) Predicted structure of COQ7 (PDB:5HJH, (Lohman et al., 2019)[224]) with different residues labeled: R107, the mutated amino acid found in P102 patient (red); the region proposed to interact with COQ9 protein (pink)[224]; L111 and V141, amino acids found mutated in other patients (purple)[238,239]; the predicted di-iron center active site (E60, E90, H93, E142, E178 and H181) (green)[457]; other two amino acids reported important for protein activity (D50, R54) (blue) [458].

We also checked the levels of other COQ proteins and they seem to be dysregulated, but this measurement was not significant. COQ4 and COQ5 seem to be upregulated, especially in P102 cells (Figure 2.7.B and C). This fact is probably caused by the low levels

of *COQ7,* and would contribute to the instability and/or malfunctioning of the CoQ_{10} biosynthetic machinery. We also tried to measure COQ6 and COQ2 levels, but the antibodies used did not show a clear signal.

CoQ_{10} is increased with 2,4-dihydroxybenzoic acid treatment in a dose dependent manner, and DMQ_{10} is markedly reduced in both patient fibroblasts.

We performed a supplementation with 2,4-dihydroxybenzoic acid (2,4-dHB), a structural analogue of 4-HB, that could be able to bypass the COQ7 deficiency. 2,4-dHB is a water-soluble molecule that has the same structure than the quinone head precursor, 4-HB, and it also contains a hydroxyl group at C6, which is the position that COQ7 hydroxylates (Figure 2.8.A). With this molecule entering CoQ_{10} biosynthetic pathway, COQ7 activity would not be needed so it would be bypassed. It has already been demonstrated that 2,4-dHB is able to increase lifespan and improve the phenotype in Coq7 [398] and Coq9 defective mice [278,399]. It also has been proven to bypass the reaction in human fibroblasts with *COQ7* [238,239,388] and *COQ9* mutations [278,388]. Remarkably, the effectivity of 2,4-dHB to bypass COQ7 reaction depends on the nature of the COQ7 mutation itself and the residual activity of the protein [238]. This has been already shown in fibroblasts from two different patients, in which 0.1mM 2,4-dHB supplementation during one week induced an increase in CoQ_{10} levels in the cells with the most severe CoQ_{10} deficiency (with a p.Val141Glu homozygous mutation in the predicted active site), while it did not have any effect in cells with a mild deficiency (with the p.Leu111Pro mutation). The treatment highly decreased DMQ_{10} accumulation in both cell lines [238].

Particularly in our cases, we have observed that a 10 days treatment with 2,4-dHB is able to dose-dependent- and significantly increase cellular CoQ_{10} levels, while it has an inhibitory effect in controls (Figure 2.8.B and D). The effect on DMQ_{10} levels is even more drastic. DMQ_{10} levels are highly reduced at all concentrations of 2,4-dHB in both patients' fibroblasts (Figure 2.8.C and E), while in controls it starts to be detectable only in the case of the neonatal control (HDF Neo) (Figure 2.8.F) but not in the adult control (B003).

Figure 2.8. Quinone content after 2,4-dHB treatment in *COQ7* Mutant Fibroblasts.
(A) Structure of 2,4-dHB compared to 4-HB. P102 (B) and P112 (D) fibroblasts increase CoQ10 levels after 10 days of 2,4-dHB treatment, while in controls it has an inhibitory effect. DMQ10 levels are drastically reduced at all concentrations of 2,4-dHB in P102 (C) and P112 (E). (One-way ANOVA with Dunnett's multiple comparison test; each non-treated cell vs treated; p values: <0.05(*); <0.01(**); 0.001(***); <0.0001(****)).(F) Representative chromatograms from P102 and HDF Neo samples.

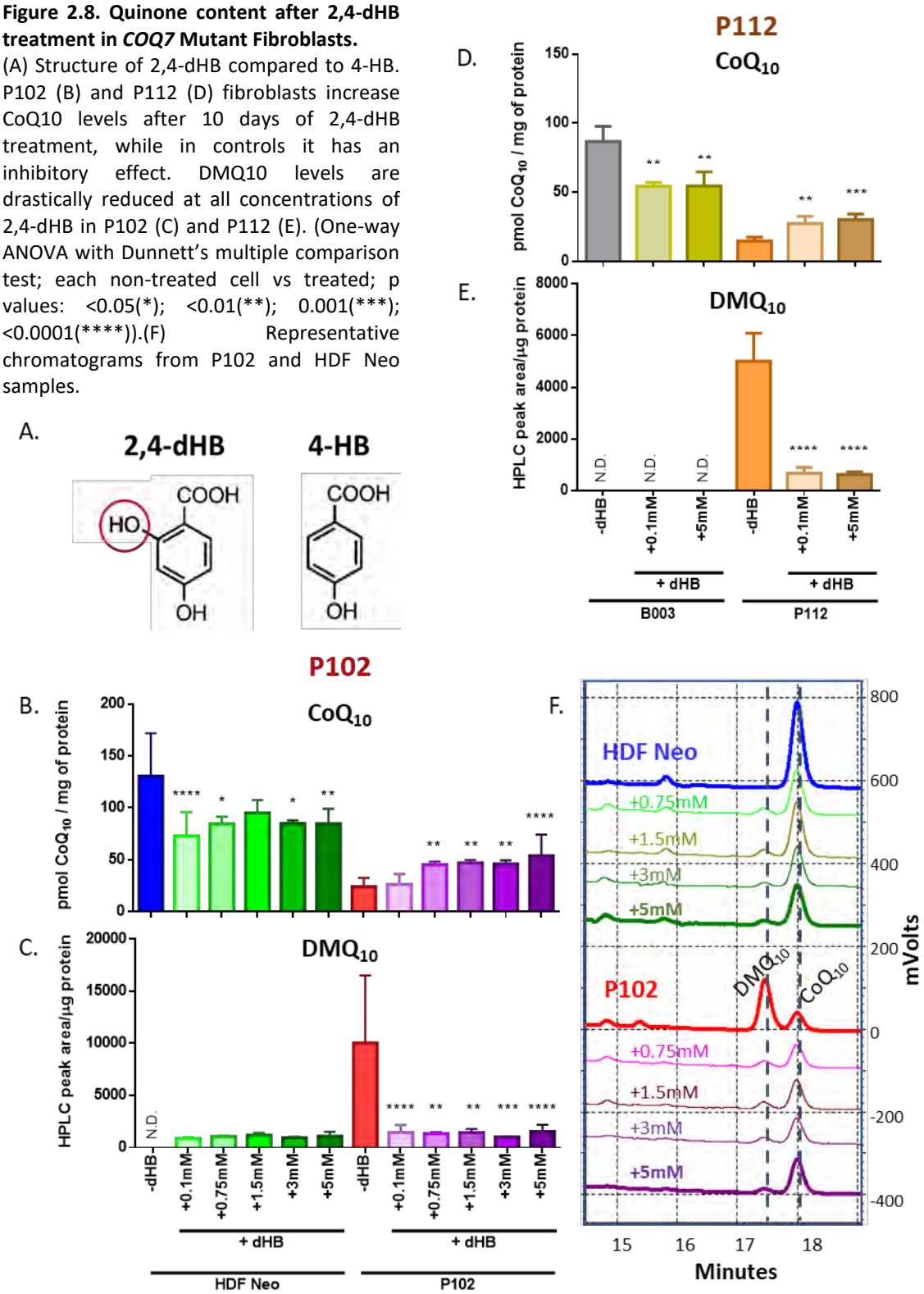

In comparison with the previously published treatments, in which only the cells from the V141E patient were increasing dose-dependently CoQ_{10} levels, higher concentrations of 2,4-dHB were needed in order to see any effect on CoQ_{10} levels in P102. That could mean

that the pathogenicity of the R107W mutation is probably in between the two mutations studied in the literature (V141E and L111P). For P112, which has a mutation probably affecting translation efficiency, treatment with 2,4-dHB (0.1mM and 5mM) significantly increases CoQ_{10} levels.

The hallmark of 2,4-dHB treatment, more than increasing CoQ_{10}, is significantly reducing the accumulation of DMQ_{10}, which is probably in the core of the pathogenesis of the disease. This effect has been observed here and in all the other cases reported in the literature, with COQ7 and COQ9 patients' fibroblasts or mice defective in the two same genes. In the case of the controls, an inhibitory effect of 2,4-dHB is always observed, leading to reduced levels of CoQ_{10}. This could be probably due to a substrate competition between the 2,4-dHB and 2,4-dHB-derived molecules and the 4-HB endogenous substrate and intermediates, for the access to the enzymes upstream of the COQ7-hydroxilation step.

Respiratory deficit is restored with 2,4-dihydroxybenzoic acid treatment.

P102 showed a marked respiratory defect, while it was milder in P112 cells, as described before (Figure 2.6). After the 10 days of 2,4-dHB treatment, we observed a recovery in the respiratory capacity, being the response different in each patient fibroblasts (Figure 2.9).

P102 OCR showed a clear dose-dependent recovery after the treatment (Figure 2.9.A and C). The effects can be seen with the 0.1mM treatment, and they become more obvious with the high dose 5mM treatment. Especially, we can see a great recovery of the maximal respiration and the spare capacity. We can also observe an increase in the basal and coupled respiration rate. Controls show the opposite behaviour, being the treatment dose-dependently detrimental.

In the case of P112, only 0.1mM of 2,4-dHB leaded to an improvement in mitochondrial performance (Figure 2.9.B and D). The treatment with the highest concentration, 5mM, did not influence in the OCR of these cells. This suggests that the dose of the treatment is important and specific for each cell line. The treatment is less detrimental for this control than for the neonatal control.

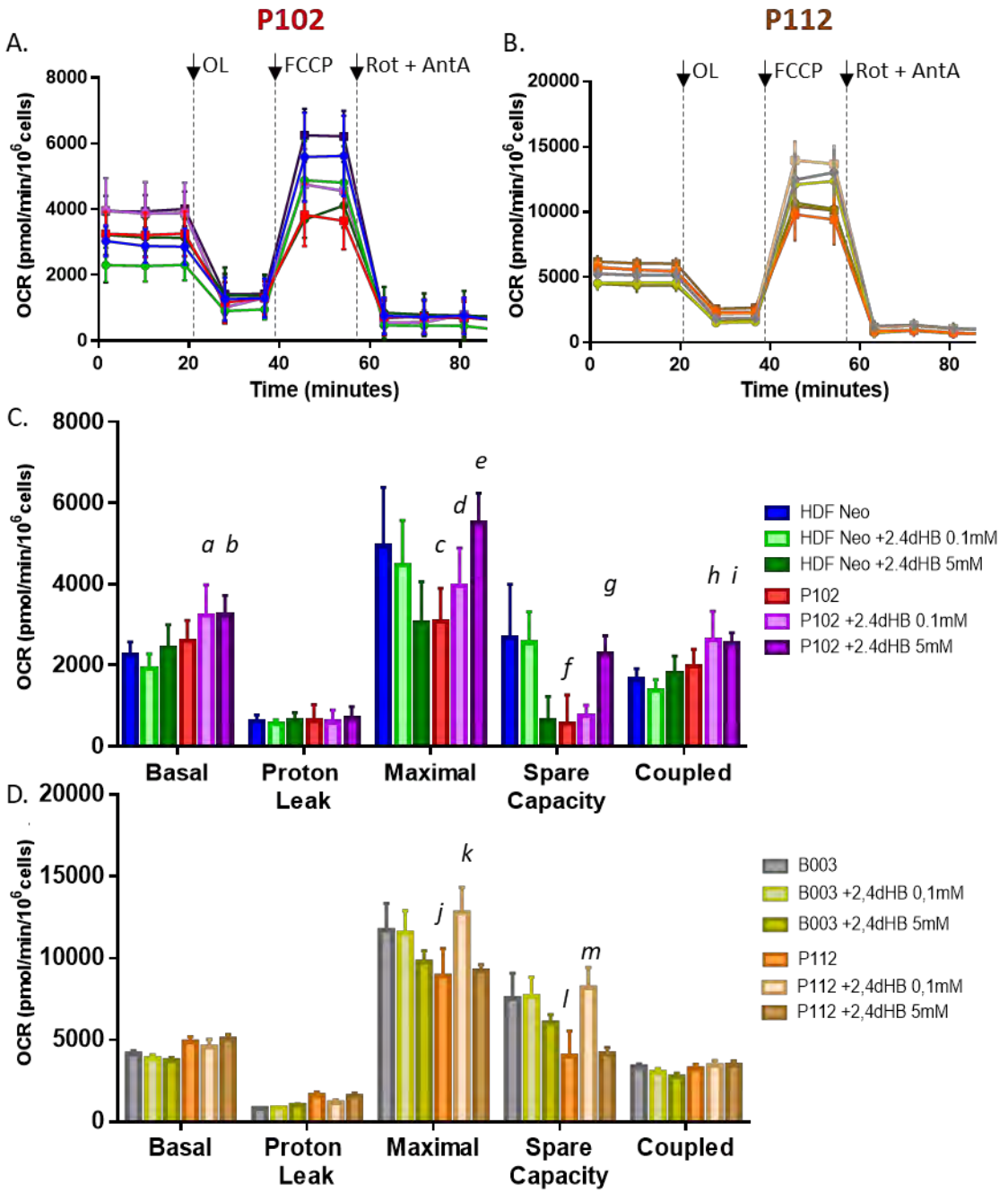

Figure 2.9. Oxygen consumption rate (OCR) after 2,4-dHB treatment in *COQ7* Mutant Fibroblasts.
OCR profile shows a respiratory defect in P102 (A and C) and P112 (B and D) patients' fibroblasts, and a recovery when they are treated with 2,4-dHB. Controls show the opposite behavior. Arrows indicate the addition of the individual inhibitors. (C, D) Seahorse quantitative data are graphed as mean ± SD ((n = 6–17/group). OL (oligomycin 4µM); FCCP (Carbonyl cyanide 4-(trifluoromethoxy)phenylhydrazone 1µM); Rot (rotenone 1µM); AntA (antimycin A 2.5µM).
Two-way ANOVA with Sidak's multiple comparison test:
P102 vs HDF Neo (c, f:, p value<0.0001(****)).
P112 vs B003 (j, l:, p value<0.0001(****)).
Two-way ANOVA with Dunnett's multiple comparison test:
P102 vs 0.1mM treated P102 (a: p value<0.01(**), d: p value<0.0001(****), h: p value<0.001(***))
P102 vs 5mM treated P102 (b: p value<0.05(*), e: p value<0.0001(****), g: p value<0.0001(****), i: p value<0.05(*))
P112 vs 0.1mM treated P112 (k,m: p value<0.0001(****))
P112 vs 5mM treated P112 (non-significant)

The benefits of 2,4-dHB treatment on mitochondrial respiratory rate can be explained by a combination of the induced CoQ_{10} increase and DMQ_{10} decrease. DMQ_{10} decrease is very drastic even with the lowest 2,4-dHB concentration (0.1mM), indicating that the treatment is inhibiting the natural CoQ_{10} biosynthetic pathway, from 4-HB to DMQ_{10}, decreasing the DMQ_{10} accumulation. It seems CoQ_{10} production from 2,4-dHB (bypassing COQ7) would be slower than from 4-HB, and at this lowest concentration, CoQ_{10} synthesis from 2,4-dHB is not remarkable. When the concentration of the treatment is increased (5mM), the inhibition of the production of DMQ_{10} through the natural pathway stays the same, but more CoQ_{10} is being produced from 2,4-dHB. This can explain why the respiration rate is even better with this treatment (5mM) than with the 0.1mM in the case of P102. P112, however, behaves differently. The molecular mechanism explaining these differences needs further studies. Maybe other pathways or biological functions are responsible for this different behaviour.

In the case of the controls, the picture is different. All the treatments lead to the same result on DMQ_{10} and CoQ_{10} levels. DMQ_{10} levels increase from not being detected, to be at the same levels than the treated patient cells, at least for the neonatal control. CoQ_{10} levels decrease almost to the same levels than the 5mM treated patient cells. So, in this picture, control and patient cells treated with 5mM of 2,4-dHB have the same levels of DMQ_{10} and CoQ_{10}, but the effect on the respiration capacity is totally different. Respiratory capacity of control cells is negatively affected with this treatment, while patient cells benefit from it. This could be explained as WT cells in normal conditions have higher CoQ_{10} levels and no detectable DMQ_{10}, so they are adapted to this situation and the decrease in CoQ_{10} and increase in DMQ_{10} dysregulates the mitochondrial performance. In the patient's cell lines, mitochondrial respiration would be adapted to be efficient enough in its basal conditions with a drastic CoQ_{10} deficiency and high DMQ_{10} accumulation, so they can significantly benefit when CoQ_{10} is slightly increased and DMQ_{10} is highly decreased.

2,4-dihydroxybenzoic acid induces an increase in COQ7 protein levels

Only P102 samples have been analysed in this section. Drastically reduced levels of mutant COQ7 protein are slightly increased with 2,4-dHB treatment (Figure 2.10). This effect is not only seen in the mutant protein, but also in the controls. This could mean that 2,4-dHB can be somehow stimulating COQ7 protein production or stabilising it. An effect on *COQ7* expression has been observed previously in the literature [388], in controls and in *COQ4* deficient fibroblasts. Also, COQ4 levels were increased with the treatment in controls and *COQ9* and *COQ7* deficient fibroblasts. COQ9 levels are increased as well in controls and *COQ4* deficient fibroblasts with the treatment [388]. The same effect was observed in *COQ9* defective mice after 2,4-dHB treatment, in which this molecule increased COQs protein levels (COQ4, COQ5, COQ6, COQ8A) in some tissues [399]. Other 4-HB analogues have been proven to increase COQs proteins levels, such as VA. VA treatment increased COQ9, COQ7 and COQ4 levels in controls, COQ4 levels in *COQ9* deficient cells, COQ4, COQ7 and COQ9 in *COQ7* deficient cells, and COQ7 and COQ9 in *COQ4* deficient cells [388]. Thus, regulation of other COQ proteins seems not to be a specific *COQ7* phenomenon, but rather a generalised one.

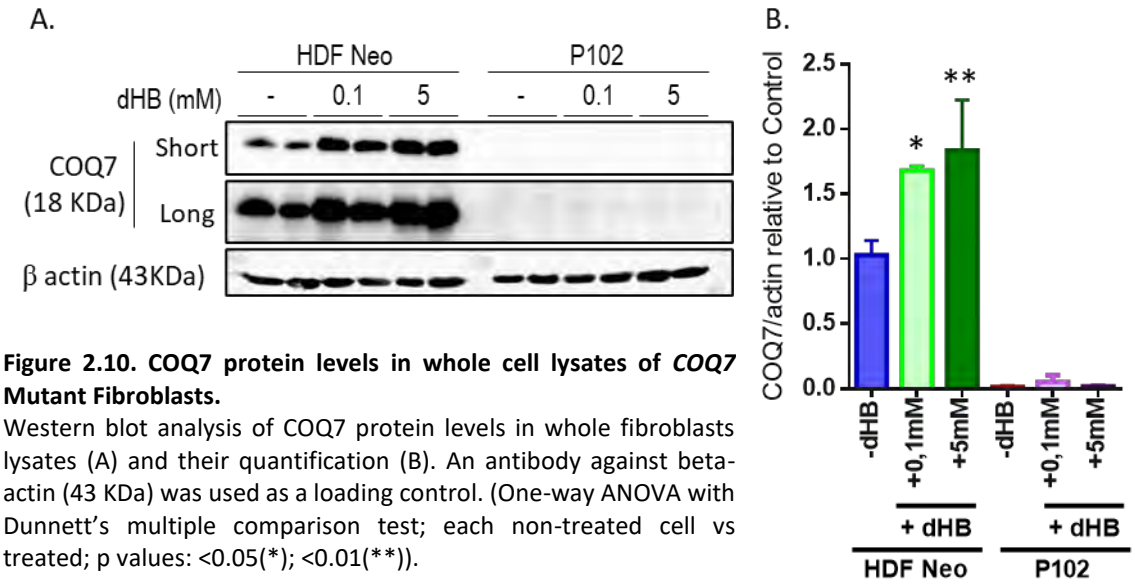

Figure 2.10. COQ7 protein levels in whole cell lysates of *COQ7* Mutant Fibroblasts.
Western blot analysis of COQ7 protein levels in whole fibroblasts lysates (A) and their quantification (B). An antibody against beta-actin (43 KDa) was used as a loading control. (One-way ANOVA with Dunnett's multiple comparison test; each non-treated cell vs treated; p values: <0.05(*); <0.01(**)).

2.2.2. Primary CoQ_{10} deficiency due to defects in *COQ6* gene

COQ6 encodes a mono-oxygenase responsible for the addition of the hydroxyl group in position C5 of quinone ring [396]. Patients with mutations in *COQ6* present with a steroid-resistant nephrotic syndrome (SRNS) associated with sensorineural deafness, and variable degree of encephalopathy (see Chapter 1, section 1.2.4) [233,459]. In collaboration with Prof Leonardo Salviati's group, we have studied CoQ_{10} deficiency in a continuous cell line lacking COQ6 protein. This cell line was generated in their laboratory, derived from HEK 293 cells by using the CRISPR/Cas9 technique. The results of this study have been recently published [165]. In this section I present a brief summary of the research I have been directly involved in.

COQ6 KO cells have extremely low CoQ_{10} levels and their CoQ_{10} biosynthesis is impaired, accumulating 4-HP_{10}

CoQ_{10} levels were markedly reduced in *COQ6* KO cells compared to wild-type cells (Figure 2.11.A). Incorporation of ^{14}C-labelled 4-HB to CoQ_{10} was virtually undetectable, indicating that the residual CoQ_{10} detected in these cells is not produced endogenously but it is derived from the medium (Figure 2.11.B). The chromatogram showed an additional radioactive peak only present in *COQ6* KO cells, which eluted faster than CoQ_{10} (rt: 13 min). This peak was also observed with the ECD, meaning that this molecule has electrochemical activity. When the sample was oxidised before the injection in the HPLC, this 13 min rt peak shifted to a time very close but slightly before of the CoQ_{10} peak (Figure 2.11.B). HPLC-coupled mass spectrometry of lipid extracts from WT and *COQ6* KO cells allowed the characterisation of this compound as 3-decaprenyl-1,4-benzoquinone (4-HP_{10}), in agreement with the accumulation of 4-HP previously reported in yeast (*Δcoq6* cells with *coq8* OE [396] or expressing *coq6* with point mutations[342]) and bacterial [460] models with a deficient C5 hydroxylation function.

This result suggests that decarboxylation and hydroxylation of C1 can occur before or independently on C5 hydroxylation, and that this step is not dependent on COQ6 function (Figure 2.12).

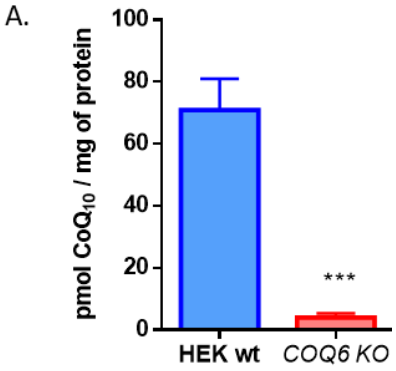

Figure 2.11. Quinone content in *COQ6* KO cells.
(A) Total CoQ_{10} levels of HEK 293T *COQ6* KO and wild type cells (Unpaired two-tailed t-test; p value<0.001). (B) Both cell lines were cultured with radiolabelled ^{14}C-4-HB. Labelled quinones were detected by HPLC with a radio-flow detector (Rad), while total quinone content was detected by a electrochemical detector (ECD). COQ6 KO samples showed a preCoQ_{10} peak (rt 13 minutes), detected by Rad and ECD. This peak shifts to rt 18min when it is oxidised (right panels, with the oxidizing guard cell after the injector). This peak was identified as 4-HP_{10} (by MS).

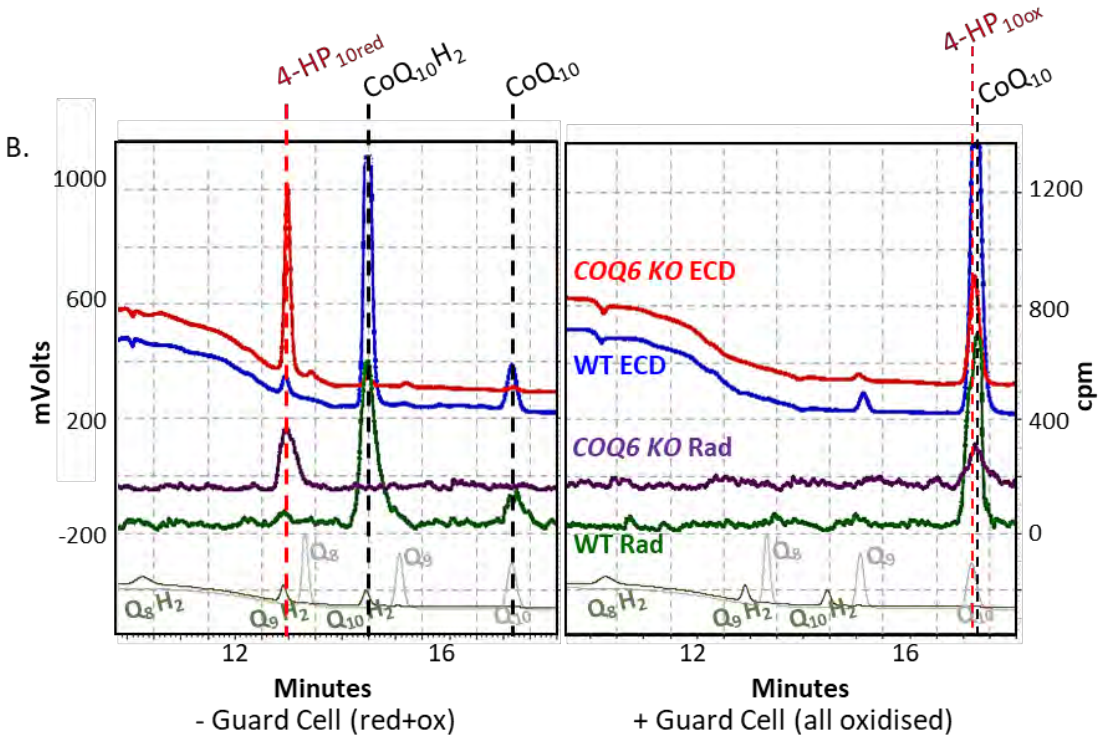

Vanillic Acid Restores CoQ_{10} Biosynthesis and Cellular Respiration in COQ6 KO cells

As presented in the introduction to this section, a possible therapeutic alternative to CoQ_{10} for *COQ6* defects can be a bypass therapy based on vanillic acid (VA) supplementation (Figure 2.13.A). The capacity of VA to restore CoQ synthesis has been already proven in yeast expressing pathogenic versions of Coq6p. In this work, VA has been shown to restore CoQ_{10} production and mitochondrial respiration in a human cell line completely lacking COQ6 protein function.

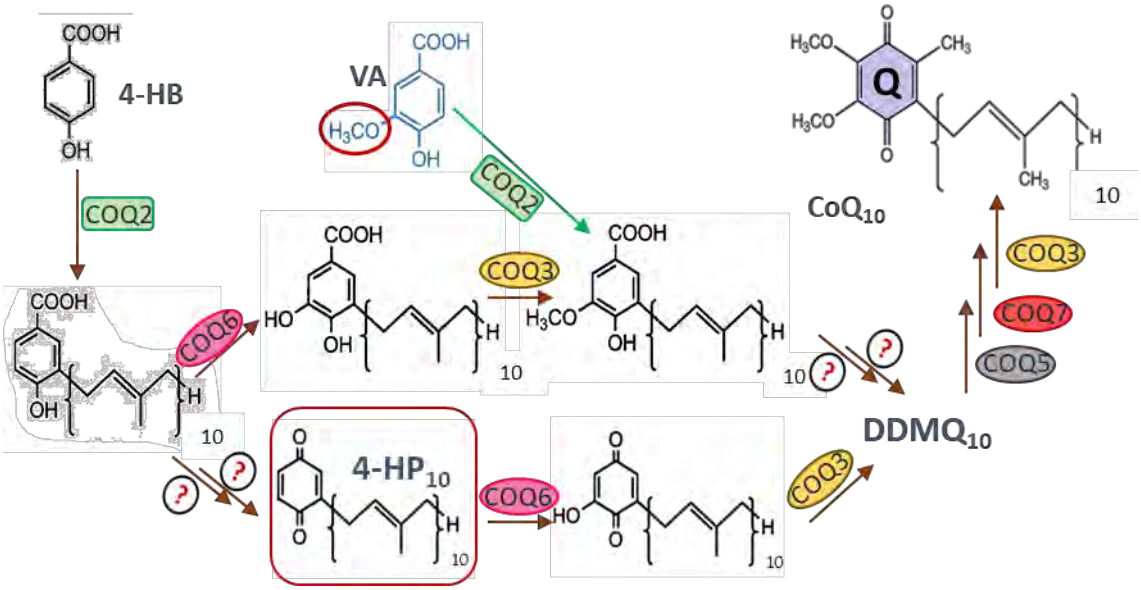

Figure 2.12. Proposed model of CoQ_{10} biosynthetic pathway in mammals.
The fact that *COQ6* KO cells accumulate 4-HP_{10} (red box) suggests that decarboxylation and hydroxylation of C1 can occur before or independently on COQ6 function (C5 hydroxylation).

VA treatment is able to restore CoQ_{10} synthesis to WT levels (Figure 2.13.B) and, importantly, it also prevents the accumulation of the 4-HP_{10} intermediate. *COQ6* KO cells are unable to respire, and after VA treatment, their OCR profile becomes very similar to the controls' one (Figure 2.13.C and D). Treatment with VA is more efficient than CoQ_{10} administration (Figure 2.13.C and D). This can be explained by the fact that VA supplementation allows CoQ production in the optimal concentrations and located in the natural environment, in the CoQ complex, next to the mitochondrial inner membrane, where it is needed for electron transport. In the case of CoQ_{10} supplementation, is must arrive to this location to participate in this function. Although incorporation of CoQ_{10} in cell membranes after supplementation is demonstrated, its distribution and proper localisation could be suboptimal (See Chapter 4, section 4.2.3 and Figure 4.22.B).

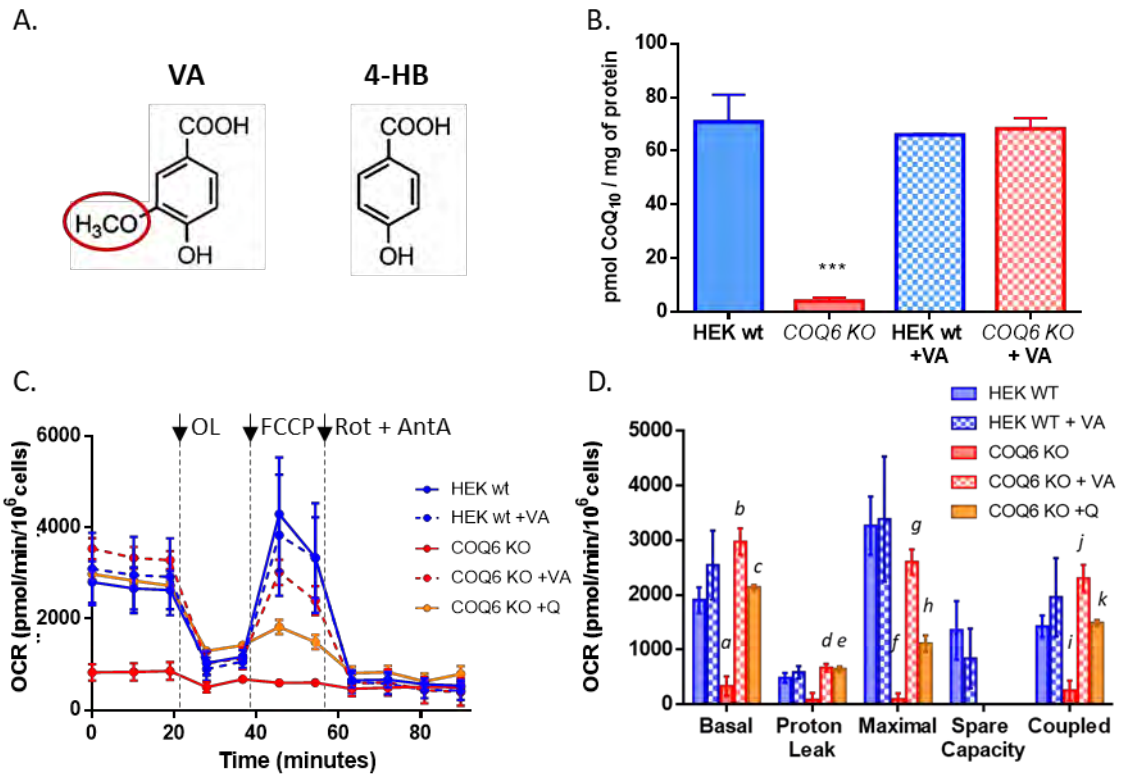

Figure 2.13. Quinone content and OCR after vanillic acid (VA) treatment in *COQ6* KO cells.
(A) Structure of VA compared to 4-HB. (B) *COQ6* KO cells treated with VA have wild type levels of CoQ_{10}, and the treatment does not show an inhibitory effect in controls (One-way ANOVA, Tukey's multiple comparison test, p-value: <0.001 (***)) (C) Oxygen consumption rate (OCR) profile shows a total respiratory defect in *COQ6* KO cells, and a partial recovery when they are treated with VA or CoQ_{10}. VA treatment is more effective than CoQ_{10}. Arrows indicate the addition of the individual inhibitors. OL (oligomycin 1µM); FCCP (Carbonyl cyanide 4-(trifluoromethoxy)phenylhydrazone 0.2µM); Rot (rotenone 1µM); AntA (antimycin A 2.5µM).
(D) Seahorse quantitative data are graphed as mean ± SD.
Two-way ANOVA with Sidak's multiple comparison test:
COQ6 KO vs HEK WT (a, f, i:, p value<0.0001(****)).
Two-way ANOVA with Dunnett's multiple comparison test:
COQ6 KO vs VA treated COQ6 KO (b, d, g, j:, p value<0.0001(****));
COQ6 KO vs CoQ treated COQ6 KO (c, e, h, k:, p value<0.0001(****)).

2.2.3. Primary CoQ_{10} deficiency due to defects in *COQ4* gene

COQ4 is an essential protein for CoQ biosynthesis in eukaryotes. Its precise function is not known, but it has been shown that it interacts with other components of the CoQ biosynthetic complex. As for the other *COQ* genes, defects in *COQ4* gene are a cause of CoQ_{10} deficiency. 35 patients from 26 families with *COQ4* mutations (Figure 2.14) have been reported so far, presenting mostly as a fatal neonatal-infantile onset encephalo-cardiomyopathy, and in a lesser percentage, as a childhood onset progressive spinocerebellar ataxia (see Chapter 1, section 1.2.4).

Here, we report two new families with mutations in the *COQ4* gene. One of them with one patient, P105, is similar to the majority of the patients reported in the literature. The second family is composed by two twin sisters (P108 and P109), with a milder progressive disease. To further investigate basic and disease-associated aspects of *COQ4*, we have also worked with a continuous cell line lacking this gene and the results will be detailed in Chapter 4.

Mutations in COQ4 gene produce a severe disease with different clinical presentations

P105 case was a girl from Denmark, who presented a birth-onset disease compatible with a *COQ4* deficiency, but strikingly, instead of hypotonia, she showed hypertonia. She was suspected of a mitochondrial disease, so she started a CoQ_{10} treatment to try to avoid the worsening of the symptoms. Unfortunately, the development of the disease was very fast, and she died at the age of 16 months.

P108 and P109 are two 14-years-old twin females who presented early-onset severe hypotonia, developmental delay and regression, seizures and hypertrophic cardiomyopathy. Plasma and cerebrospinal fluid lactate were normal and did not raise the suspicion of a mitochondrial disorder. P109 fatally progressed and recently died at 17 years-old.

Figure 2.14. Schematic representation of COQ4 mRNA (A) and protein (B).
Mutations from P105 (orange), P108 and P109 (blue) patients are highlighted with boxes, showing the residue conservation in the alignment of COQ4 protein from different species (C). The rest of mutations shown (red boxes) correspond to the rest of *COQ4* patients reported in the literature. The multiple alignment was performed with the protein sequences obtained in Uniprot, using Clustal X2 and BioEdit to visualize the results. UTR (untranslated region); MTS (mitochondrial targeting sequence; aa (amino acid); * (asterisk: single and fully conserved residue); : (colon: conservation between groups of strongly similar properties); . (period: conservation between groups of weakly similar properties).

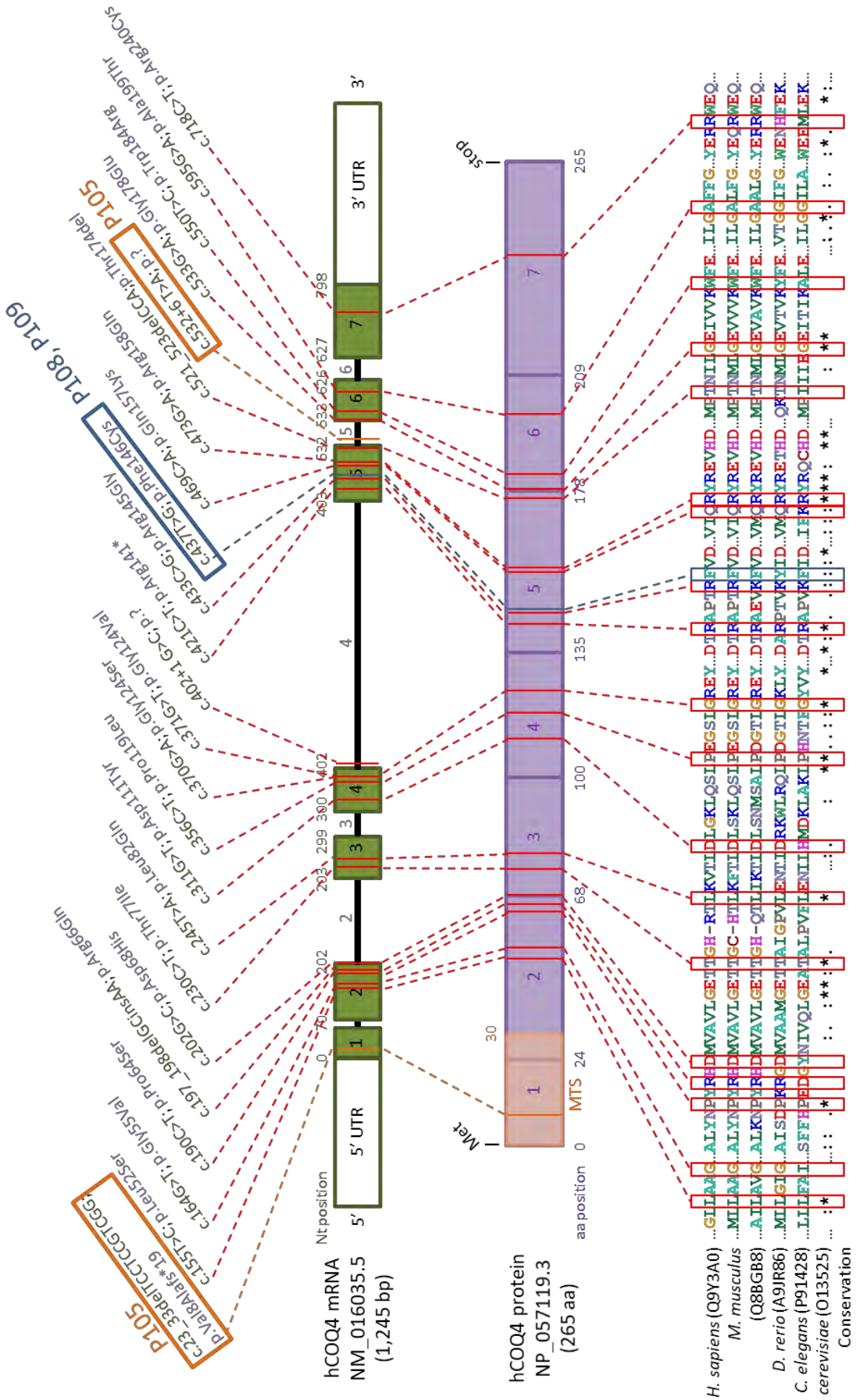
hCOQ4 mRNA
NM_016035.5
(1,245 bp)
hCOQ4 protein
NP_057119.3
(265 aa)
5' UTR
3' UTR
Met
stop
MTS
Nt position
aa position
P105
P108, P109
H. sapiens (Q9Y3A0)
M. musculus (Q8BGB8)
D. rerio (A9JR86)
C. elegans (P91428)
S. cerevisiae (O13525)
Conservation

P105, P108 and P109 have biallelic mutations in COQ4 gene

i. P105 case

Exome sequencing of P105 revealed two heterozygous compound mutations in *COQ4* gene, and both parents were carriers of the mutations (Figure 2.14).

One of the mutations (c.23_33delTCCTCCGTCGG, p.Val8Alafs*19, NM_016035.5) is a deletion of 10 nucleotides in exon 1, so a frame shift and an early truncated protein are predicted to be generated. This mutated allele is predicted to produce loss of function, since the defect occurs very early in the sequence, and the CADD *in silico* pathogenicity prediction tool also classify it as pathogenic (score=21.1) tool. To check its pathogenicity, *COQ4* KO HEK cell line was transfected with this allele, and it was not able to restore CoQ_{10} biosynthetic function, confirming the lack of function of this aberrant allele (see Chapter 4, section 4.2.1). This mutation has been described previously in another *COQ4* patient with a birth onset encephalopathy with seizures, hypotonia and developmental delay. He also presented hearing loss and delayed visual maturation. He had hypertrophic cardiomyopathy and bradycardia, and he succumbed after a respiratory failure at 4 months of age. The other allele of *COQ4* in this published case was also affected by the combination of two other mutations, c.311G>T and c.356C>T (p.Asp111Tyr and p.Pro119Leu)[336].

The other *COQ4* mutation present in P105 is a point substitution in intron 5 (c.532+6 T>A, p.?, NM_016035.5). This mutation is in the 5' donor splice site of intron 5, so it may produce an aberrant *COQ4* RNA splicing. This mutation is not described in the literature and nor present in the ClinVar database. Further details on this potential pathogenic variant will be provided in this section.

ii. P108 and P109 cases

Genetic tests revealed a novel homozygous mutation in *COQ4* gene (c.437T>G, p.Phe146Cys, NM_016138.5) being both parents carriers of the mutation (Figure 2.14). This missense variant is located in exon 5, and it would probably affect protein stability, since it changes a very conserved phenylalanine (with an aromatic and hydrophobic side chain) to a cysteine (with a tiny sulfur-containing hydrophobic side chain). This mutation is not described in the literature, but it has an entry in the ClinVar database, with

conflicting interpretations of pathogenicity. It is predicted to be pathogenic by SIFT (score=0), PolyPhen-2 (score=0.999) and CADD (score=29.2) tools. Sanger sequencing confirmed the segregation of the variants in parental DNA, being both parents heterozygous carriers. To check its pathogenicity, *COQ4* KO HEK cell line was transfected with this allele. Overexpressing COQ4 with p.Phe146Cys mutation was able to restore COQ4 function and CoQ_{10} production to WT levels, indicating that this mutation is probably hypomorphic and it only partially affects COQ4 function (see Chapter 4, section 4.2.1), which will also explain the milder phenotype of the siblings.

Significance of the intronic c.532+6 T>A mutation in P105: Splicing alterations

c.532+6 T>A is a point substitution mutation in intron 5, precisely, inside the 5' donor splice site. Its pathogenicity may rely in the alteration of COQ4 pre-mRNA splicing.

Pre-mRNA splicing is an essential process for the production of a functional protein. Mutations can alter this mechanism, affecting the RNA processing in different ways (skipped exons, alternative 5' donor splice sites, alternative 3' acceptor splice sites, retained introns and mutually exclusive exon usage) and these diverse molecular phenotypes can result in disease. Mutations that affect splicing of pre-mRNA account for at least 15% of disease-causing mutations with up to 50% of all mutations described in some genes [461].

Understanding the molecular mechanisms through which a mutation is pathogenic is crucial for understanding the clinical phenotype, in order to advance for the development of novel therapeutic approaches. NGS has allowed identifying an enormous number of new genomic variants with unknown significance. The development of *in silico* prediction methods based on bioinformatical algorithms is very useful for a preliminary approach to classify the variants for later *in vitro* studies.

In order to bioinformatically predict the spliceogenicity of the variant of interest, we have used a prediction tool called SPiCE [219]. It works with two probability thresholds to set optimal sensitivity (ThSe=0.115) and specificity (ThSp=0.749). The tool provides a P probability for a given variant, that must be above the 2 optimal thresholds, to be classified as variant with high probability to alter splicing.

SPiCE P for c.532+6 T>A variant is 73.382%, just below ThSp (74.9%) (Figure 2.15). It is in the region predicted to have medium probability to alter splicing, but very close to be considered to have high probability.

A.

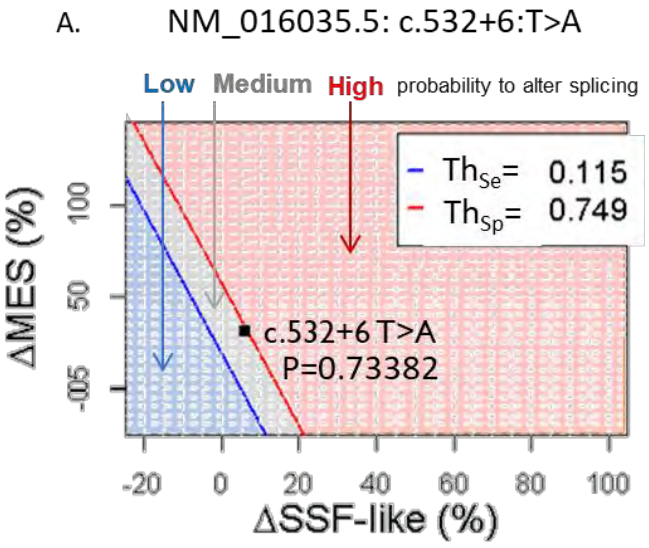

B.

Wt sequence	TGGgtgagt
Mutant sequence	TGGgtgaga
Distance to nearest splice site	6
Splice site type	Donor
Variant Type	substitution
SSF-like_wt score	84.23
SSF-like_mut score	78.86
ΔSSF-like (%)	-6.4
MES_wt	8.73
MES_mut	6.04
ΔMES (%)	-30.9
SPiCE probability (%)	73.382
Medium probability to alter splicing	

Figure 2.15. NM_016035.5: c.532+6T>A variant spliceogenicity prediction by SPiCE program.
(A) Graph shows that probability of c.532+6T>A variant to alter splicing is in the area considered of medium probability to alter splicing (grey), but close to the high probability (red). (B) Table shows detailed information about the prediction.

We have also used the RNAfold server[206] to predict the secondary structure of the pre-mRNA that would contribute a state of minimum free energy (Figure 2.16). As input, we have used a sequence containing the nucleotide that is found mutated in P105 patient and 100 (Figure 2.16.A) or 200 nucleotides (Figure 2.16.B) flanking it upstream and downstream. By comparing the WT and the mutant predicted RNA secondary structure, we find differences in the resulting structures. In both tested cases (100 or 200 nucleotides flanking the mutation), the mutant sequence folding is different than the WT, changing the position and the pairing of some loops. Moreover, the mutant sequence also reduces the base pairing probabilities for several base-pairs that are not only close, but also far away from the mutation (Figure 2.16). Maybe, all these possible changes in the structure are affecting the process of splicing of the pre-mRNA.

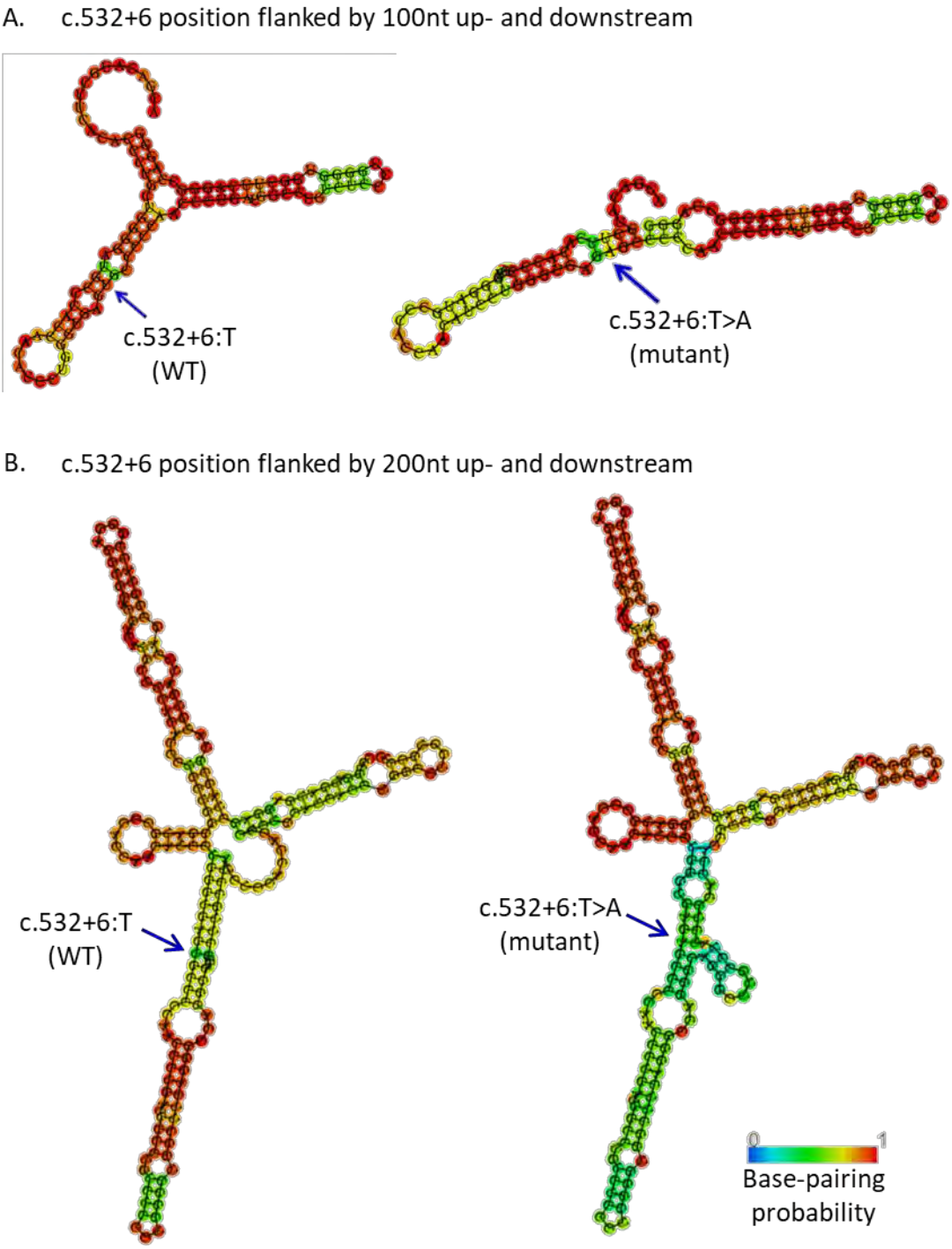

Figure 2.16. Minimum free energy structure of WT and c.532+6T>A mutant pre-mRNA.
The minimum free energy RNA structure of a sequence containing the NM_016035.5: c.532+6 position and the upstream and downstream 100 (A) or 200 (B) flanking positions was calculated by using RNAfold server. WT (right) and c.532+6T>A mutant (left) structures are represented. The colour of each base pair indicates their probability to be paired (see colour legend). Blue arrows point the c.532+6 position.

Further *in vitro* studies are needed to confirm the spliceogenicity of this variant, in order to confirm if its pathogenicity rely in the alteration of pre-mRNA splicing and to specifically identify which is the effect on *COQ4* mRNA. The most commonly used *in vitro* methods for validating mutant mRNA are minigene constructs expression and RT-PCR analysis of the patient mRNA. The development of high throughput transcriptomics, such as RNA-Seq, has brought the possibility of studying alternative splicing events in a genome wide context, with computational tools that use the RNA-Seq data. All these approaches show some advantages and some limitations. The minigene approach is able to analyse the transcript produced by a single allele, while this is not possible when analysing of the patients' transcriptome by RT-PCR or RNA-Seq. In contrast, RT-PCR can analyse the effect of a certain mutation in the splicing of the whole transcript, while the minigene analyses each variant separately from the natural whole mRNA context. Moreover, RNA-Seq has the advantages of being high throughput and non-targeted [462,463].

i. Minigene constructs

In collaboration with Dr Eva Trevisson's laboratory in Padova, minigene constructs were used to analyse the spliceogenicity of this variant (Figure 2.17). The patient's genomic DNA fragment carrying the c.532+6 T>A variant to analyse was amplified and subsequently cloned inside the ß-globin minigene contained in a pcDNA™3.1/Hygro(+) vector (Figure 2.17.A), as well as the equivalent WT sequence. The fragment amplified consisted in the exon closest to the intronic variant to analyse, in this case, *COQ4* exon 5, and a portion of 100 bp of flanking intronic regions upstream and downstream. WT, mutant and empty ß-globin vector were transfected in HEK293 cells that do not express ß-globin. 24 hours after transfection, total RNA was extracted, retrotranscribed and the resulting cDNA was amplified with a semiquantitative-PCR, using specific primers for the ß-globin gene, designed on exon 2 (forward) and exon 3 (reverse).

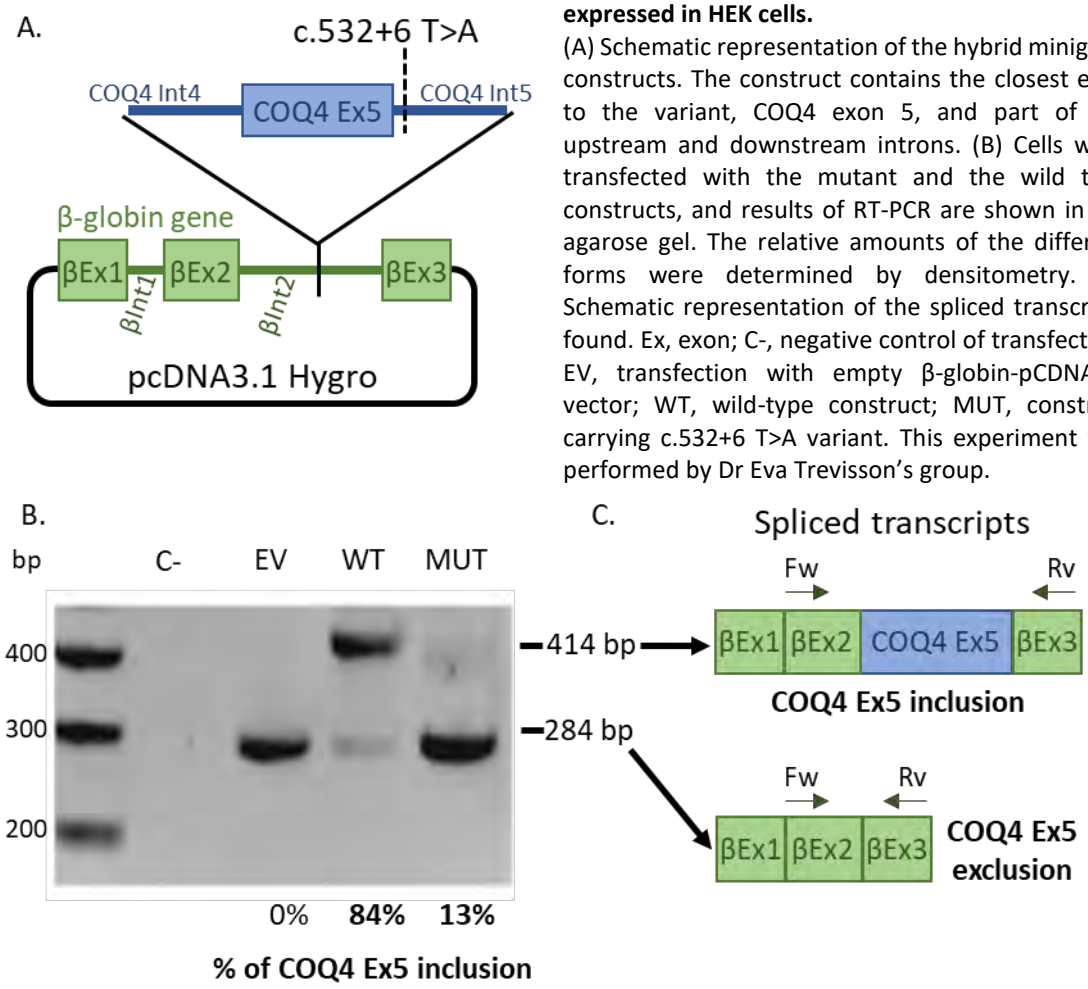

Figure 2.17. RT-PCR analysis of the *COQ4* (c.532+6T>A variant) minigene constructs expressed in HEK cells.
(A) Schematic representation of the hybrid minigene constructs. The construct contains the closest exon to the variant, COQ4 exon 5, and part of the upstream and downstream introns. (B) Cells were transfected with the mutant and the wild type constructs, and results of RT-PCR are shown in the agarose gel. The relative amounts of the different forms were determined by densitometry. (C) Schematic representation of the spliced transcripts found. Ex, exon; C-, negative control of transfection; EV, transfection with empty β-globin-pCDNA3.1 vector; WT, wild-type construct; MUT, construct carrying c.532+6 T>A variant. This experiment was performed by Dr Eva Trevisson's group.

Both the WT and the c.532+6 T>A variant in intron 5 yielded two products, but in different proportions (Figure 2.17.B and C). The mutated construct predominantly produced a fragment lacking exon 5 (87% of the total amplification), but also produced the WT fragment (13% of the total amplification). This splicing mutation seems to be an hypomorphic allele mutation, predominantly leading to exon 5 skipping, at least when it is studied in exon 5 context. Curiously, WT construct also led to the fragment lacking exon 5, but in a smaller proportion (16%), indicating this alternative splicing event can also occur with the WT sequence.

ii. RT-PCR

In order to have a wider picture, we amplified *COQ4* whole transcript from patient and control fibroblasts RNA (converted to cDNA). The semiquantitative PCR product was run into agarose gels, showing different results for controls and patient (Figure 2.18.A-C). Control samples showed a predominant band with *COQ4* whole transcript length (Band 1). In patient samples, this band was less intense, and several bands with lower molecular weight were more predominant. These 4 extra bands (Bands 2-5) were also present in control samples, but fainter. We interpreted these bands could be different molecular products of *COQ4* pre-mRNA splicing, that are present naturally in the control, but enhanced in the mutant. It needs to take into account that we are looking at a picture of the effect of both mutations in the two *COQ4* alleles. Our results suggest that the presence of the splicing mutation leads to unbalancing the normal splicing of *COQ4*, favouriting the presence of this alternative splicing. It is also possible that the frameshift mutation leads to NMD, which could affect the whole *COQ4* transcript with that mutation, while the alternative spliced isoforms coming from the other allele would proportionally increase their presence. Of course, the final effect can be an addition of the effects of these two factors, or even others.

Each of these bands was purified, subcloned and sequenced. Sequencing told us that, both in controls and patient, alternative *COQ4* splicing occurs, producing different *COQ4* isoforms (Figure 2.18.D and Table 2.1). The first band (Band 2), included 2 different isoforms, one of them lacking exon 3 (p.Asp68Glyfs*34) and the other one lacking exon 5 (p.Arg135Glyfs*5). Both of these isoforms would lead to a frameshift and truncated form of *COQ4*. The second band (Band 3) resulted to be *COQ4* lacking both exon 3 and 5, which would have the same frame shift than the one lacking only exon 3 (p.Asp68Glyfs*34). The third band (Band 4) was identified as a *COQ4* isoform lacking exons 3 to 5. This isoform was interpreted as a deletion of all the amino acids present in exons 3 to 5 (p.del68-177). The last band (Band 5) was sequenced as an unspecific amplification, since it contained a sequence different to *COQ4*.

A.

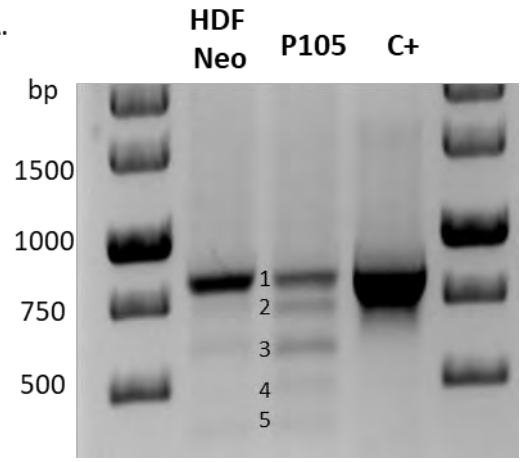

Figure 2.18. RT-PCR analysis of *COQ4* transcripts in P105 and control fibroblasts. (A) Five (1-5) bands appeared in both P105 and control cDNA samples. C+ is a positive control from a plasmid with full-length *COQ4* cDNA. (B) The relative amounts of the different forms were determined by densitometry and expressed as a percentage (B and C). (Two-way ANOVA, Sidak's multiple comparison test, p-values: <0.001 (***)). (D) Schematic representation of the spliced transcripts found in each band. Iso, isoform.

B.

Band	Average Band %	
	HDF Neo	P105
1	90.5%	59.2%
2	4.7%	17.5%
3	4.2%	19.8%
4	0.6%	3.6%
5	unspecific amplification	

C.

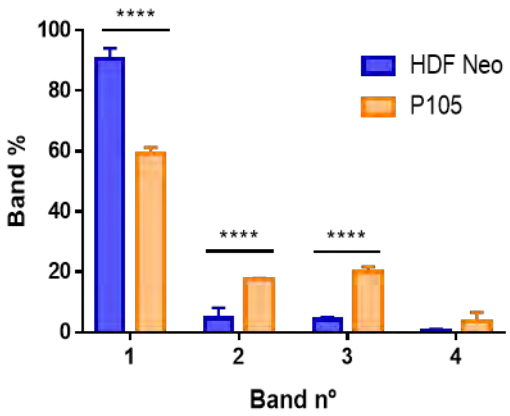

D.

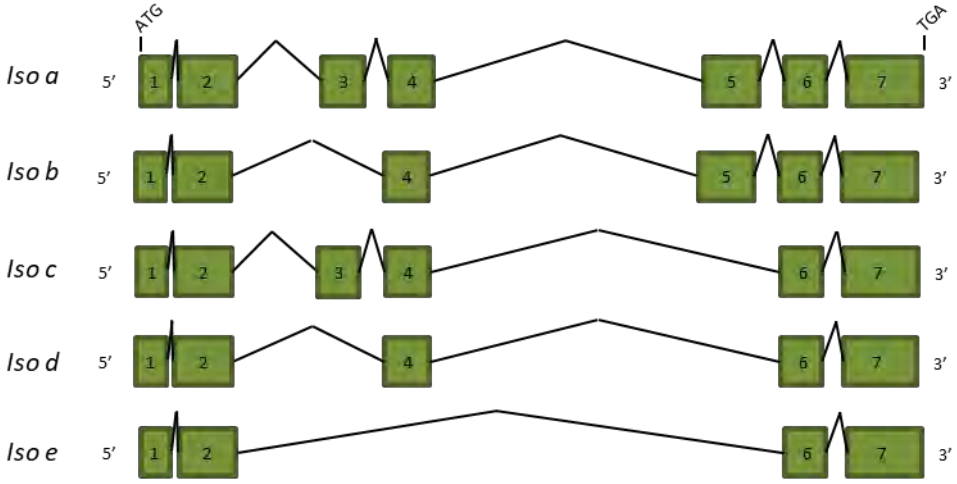

Curiously, the two most frequently excised exons (3 and 5) are preceded by the longest introns (1,995 bp and 6,271 bp, respectively). Maybe the presence of the mutation in the 5' donor splice site of exon 5 is altering the pre-mRNA secondary structure and therefore, affecting the coordination of the splicing process across the whole COQ4 transcript. This could result in the alteration of the order of intron splicing, or even to the inhibition of certain splice events, leading to the various effects that we have observed.

Table 2.1. Identity of COQ4 mRNA isoforms found in P105 and controls' cDNA.

COQ4 Isoform	Found in band	Characteristics	Length (pb)	Changes in protein sequence	Estimated protein MW (KDa)
Iso a	1	Full length *COQ4* mRNA	798	-	29.6
Iso b	2	Missing Exon 3	701	Asp68Glyfs*34	10.7
Iso c	2	Missing Exon 5	668	Arg135Glyfs*5	15.3
Iso d	3	Missing Exons 3 and 5	571	Asp68Glyfs*34	10.7
Iso e	4	Missing Exons 3 to 5	468	del68-177	17

In order to characterise if these isoforms had COQ4 function, bands were cloned in pcDNA5, and transfected into HEK *COQ4* KO cells. Only the whole *COQ4* transcript expression was able to restore COQ4 function and CoQ_{10} production in these cells, meaning these isoforms can't replace COQ4 function in CoQ biosynthesis when it is absent (See Chapter 4, section 4.2.1).

iii. RNA sequencing

Total RNA from patient and control fibroblasts was also subjected to RNA-Seq analysis, in order to validate the increased alternative splicing events that were observed with the minigene and the RT-PCR analysis. From the read histogram, we can see how P105 sample shows lower number of reads of exon 3, mainly, and also exon 5 (Figure 2.19.A and B). Different splicing events were detected, and splice junctions reads were quantified (Figure 2.19.A, B and C). All splicing events were quantified as a percent spliced, which represents the percentage of a gene's mRNAs transcripts that include a specific splice junction (Figure 2.19.D). These results are very similar to what was observed by RT-PCR and minigenes. Exons 3 and 5 are more frequently excised in cells from patient P105, which carry the c.532+6 T>A variant in intron 5.

The splicing event found in the variant named *Iso e* (Table 2.1), from exon 2 to exon 6, was not found by the RNA-Seq. It is possible that the reads depth of this experiment was not enough to capture it. However, it is also possible that it is only produced anecdotally, and was only amplified by chance by the RT-PCR. Also, an alternative splicing event was also observed in the middle of intron 2, leading to a very short transcript.

We are only seeing the final effect of the mutation (in combination with the c.23_33delTCCTCCGTCGG deletion mutation in the other allele). To exclude a general splicing defect, we checked splicing events in COQ2 and TFAM mRNAs and there were no differences between the control and P105 samples. To check both alleles were being produced in the same amount, and discard an effect of NMD, the number of reads of

the nucleotides that are deleted in one of the alleles of the patient, c.23_33delTCCTCCGTCGG, were measured and compared with the number of reads of the 10 nt downstream this deletion (control region, c.33-42). In the case of the WT, both regions had the same number of reads, while in the patient's RNA, the control region had the double of reads than the deletion. This indicated that *COQ4* mRNA is being produced from both alleles in a 1:1 proportion (Table 2.2).

Table 2.2. Number of reads of the *COQ4* c.23-32 and c.33-42 regions, to distinguish transcripts produced from each allele of P105.

Region	Chr. Position (GRCh38)	Nt	P105 (reads)	WT (reads)	P105 (average reads)	WT (average reads)	R105 (%reads/ control region)	R02 (%reads/ control region)
deletion in one allele of P105	chr9:128,322,881	T	47	274	49 ± 1	281 ± 6	45% ± 1%	95% ± 2%
	chr9:128,322,882	C	48	275				
	chr9:128,322,883	C	48	275				
	chr9:128,322,884	T	49	278				
	chr9:128,322,885	C	49	279				
	chr9:128,322,886	C	49	279				
	chr9:128,322,887	G	49	287				
	chr9:128,322,888	T	49	283				
	chr9:128,322,889	C	51	287				
	chr9:128,322,890	G	52	289				
Control region	chr9:128,322,891	G	104	290	108 ± 3	297 ± 6	100% ± 3%	100% ± 2%
	chr9:128,322,892	C	104	291				
	chr9:128,322,893	T	105	290				
	chr9:128,322,894	C	107	294				
	chr9:128,322,895	T	108	294				
	chr9:128,322,896	G	109	299				
	chr9:128,322,897	C	109	302				
	chr9:128,322,898	G	112	304				
	chr9:128,322,899	G	110	302				
	chr9:128,322,900	G	112	303				

How the c.532+6 T>A variant (in combination with the c.23_33delTCCTCCGTCGG deletion mutation in the other allele) leads to an aberrant splicing alteration is unknown yet. Elucidating the mechanisms by which *COQ4* pre-mRNA is spliced and the effects of this mutation could be a target for therapy design.

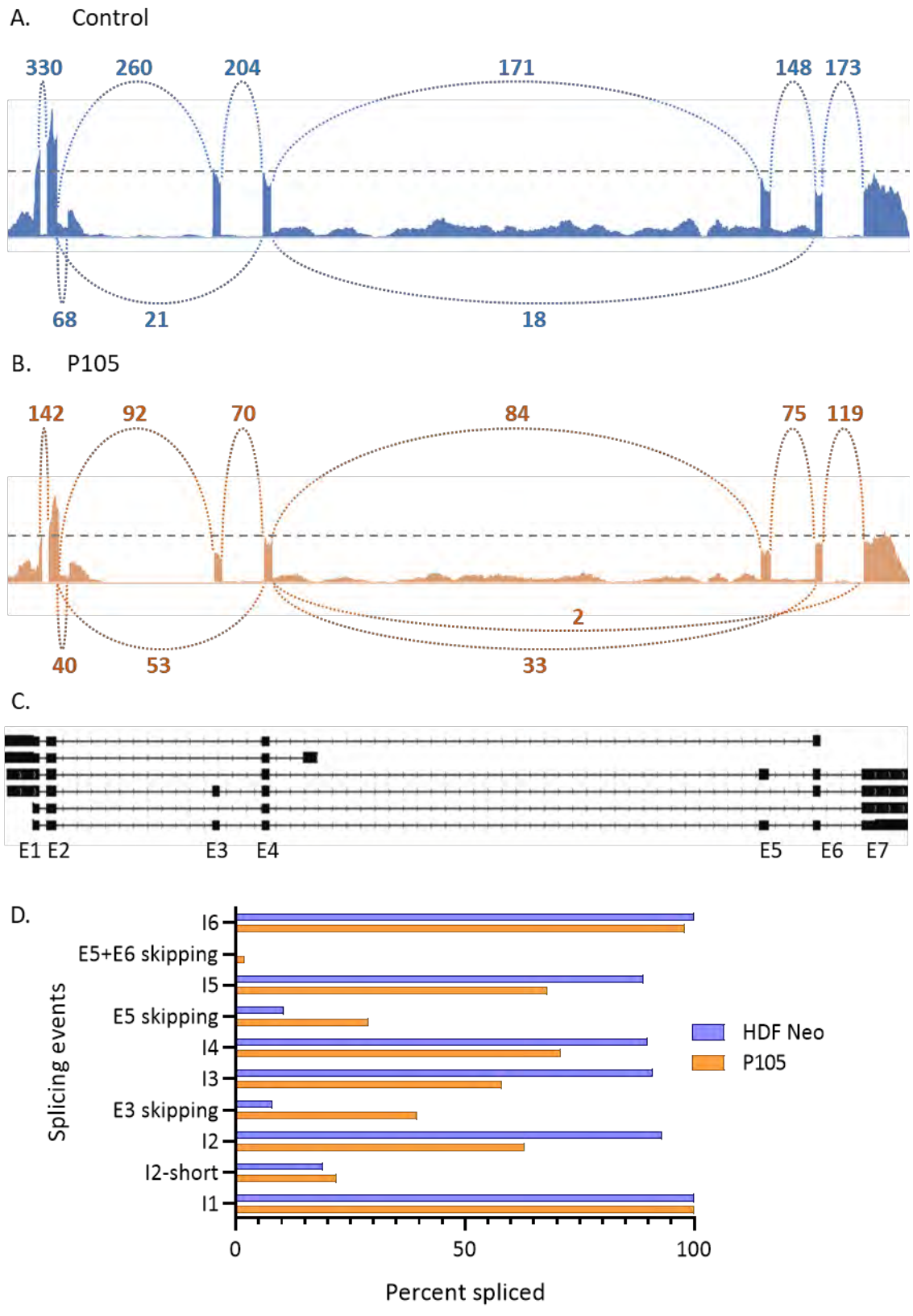

Figure 2.19. RNA-Seq analysis of *COQ4* transcripts in P105 and control fibroblasts.
RNA-Seq histogram plots of control (A) and P105 (B) RNA samples. Height of the bars represents read coverage. Splice junctions are displayed as arcs, each one with its own number of reads. Canonical splicing events are indicated above the histograms, while alternative splicing events are displayed below the histograms. (C) Transcript models representing the different splice variants, according to the splicing events. (D) Percent spliced value for each splicing event.

COQ4 patients' fibroblasts have drastically reduced CoQ_{10} levels, impaired CoQ_{10} biosynthesis and accumulation of a specific intermediate.

In order to investigate the degree of affectation of CoQ_{10} biosynthesis due to these *COQ4* mutations, total levels of CoQ_{10} were analysed for all the three patients.

CoQ_{10} concentration in skin fibroblasts was measured by HPLC, and, in the case of P105, we were able to analyse CoQ_{10} levels in skeletal muscle as well. In this patient, CoQ_{10} levels in skeletal muscle (154.37 pmol CoQ_{10}/mg of protein, control range 300-700) (Table 2.3) and skin fibroblasts (more than 50% of deficiency) were found to be severely reduced (Figure 2.20.A). Citrate synthase activity was also found to be slightly reduced in skeletal muscle (82.8 CS units/L, control range 88-240), indicating that this primary CoQ_{10} defect could lead to a defect in mitochondria in muscle (Table 2.3). In the case of P108 and P109, two different control fibroblasts were used, HDF Neo (neonatal control fibroblasts) and B003 (fibroblasts from a 20-year-old healthy person), because we did not have the information about the age of the patients when the skin biopsy was performed. P108 and P109 fibroblasts showed a 65% of CoQ_{10} deficiency comparing to HDF Neo control and a 53-55% of deficiency comparing to B003 control (Figure 2.20.C).

Table 2.3. P105 CoQ_{10} levels in skeletal muscle.

Skeletal muscle	CoQ_{10} levels (pmol CoQ_{10}/mg protein)	CS activity (Units/L)
P105	154.37	82.8
Controls	300-700	88 - 240

Incorporation of radiolabelled 4-HB, the quinone head precursor, revealed a drastic defect on CoQ_{10} biosynthetic rate in all the three patients' fibroblasts, and the appearance of a radioactive peak different to CoQ_{10} (rt:13.5min), and different to the intermediates accumulated in the cases of *COQ7* (DMQ_{10}) and *COQ6* (4-HP_{10}) deficiency (Figure 2.20.B and D). This could indicate that CoQ_{10} synthesis is impaired at some specific step in which COQ4 would participate, assist, or be needed to.

This is the first time that mammalian *COQ4* deficiency is described to produce the accumulation of a yet unknown intermediate of the pathway, which provides key insights about COQ4 function in CoQ_{10} biosynthesis. Efforts on identifying this molecule will be described in next sections (see Chapter 4, section 4.2.1).

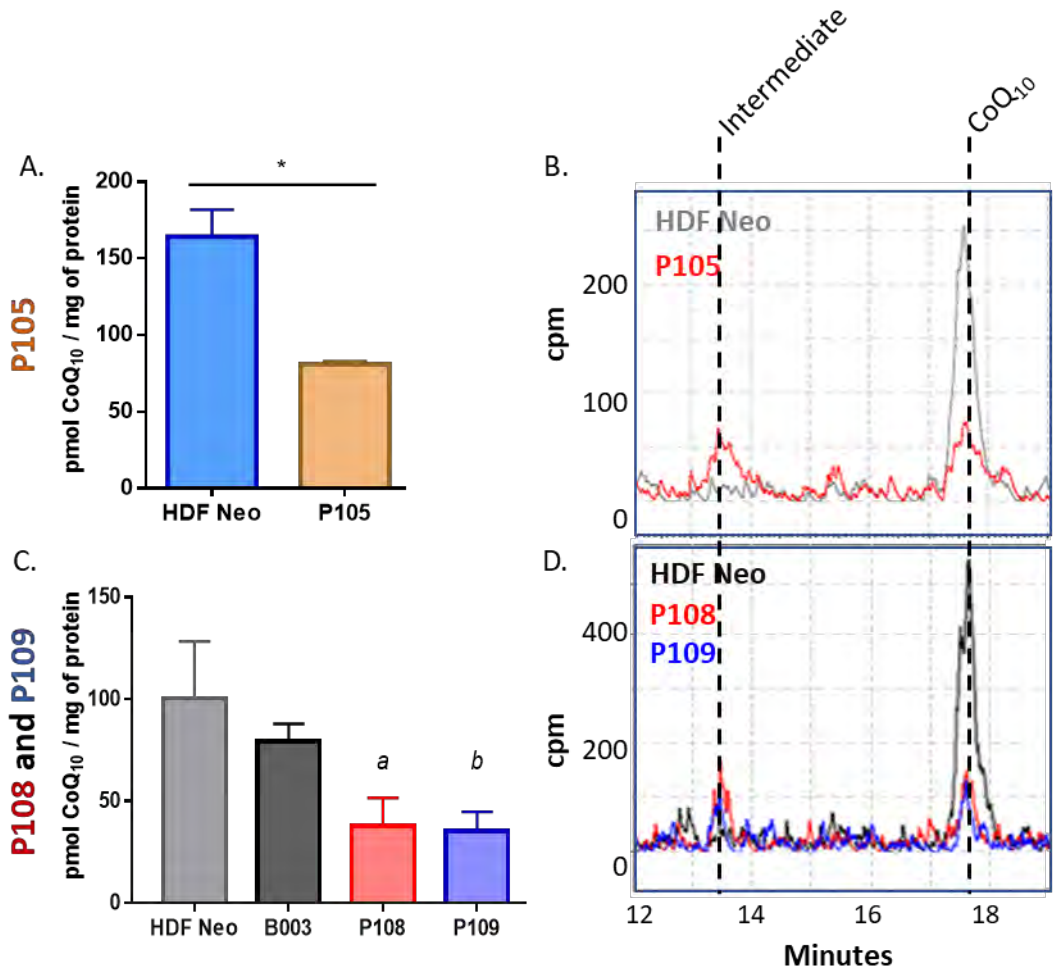

Figure 2.20. Quinone content in *COQ4* Mutant Fibroblasts, P105 (A, B) and P108 and P109 (C, D).
(A) P105 shows CoQ_{10} deficiency in fibroblasts (Unpaired two-tailed t-test; p value<0.05 (*)). (C) P108 and P109 fibroblasts also show low levels of CoQ_{10} (Two-way ANOVA, Tukey's multiple comparison test, p-values: a= P108 vs. HDF Neo, p<0.0001 (****), P108 vs. B003, p<0.0001 (****); b= P109 vs. HDF Neo, p<0.0001 (****), P109 vs. B003, p<0.001 (***)). The HPLC-radioactivity chromatogram (B, D) showed the incorporation of ^{14}C-4-HB to the quinone extract. While control cells show a radioactive CoQ_{10} peak, all patients' fibroblasts present 2 peaks, one corresponding to CoQ_{10}, and another probably corresponding to an intermediate molecule of CoQ_{10} synthesis (retention time: 13-13.5min).

Patients' fibroblasts respiration is impaired in different degrees

Respiration studies in *COQ4* mutant fibroblasts and controls were performed, and P105 and P108/P109 displayed a different behaviour.

P105 fibroblasts showed a significant decrease in OCR, especially observed through a lower maximal respiration rate and spare capacity (Figure 2.21.A and B). This means that P105 cells are less able to respond to energetic demands than control cells, which may be due to CoQ_{10} deficiency, but also because of the accumulation of the unknown intermediate, as it occurs with DMQ_{10} in *COQ7* and *COQ9* deficiency.

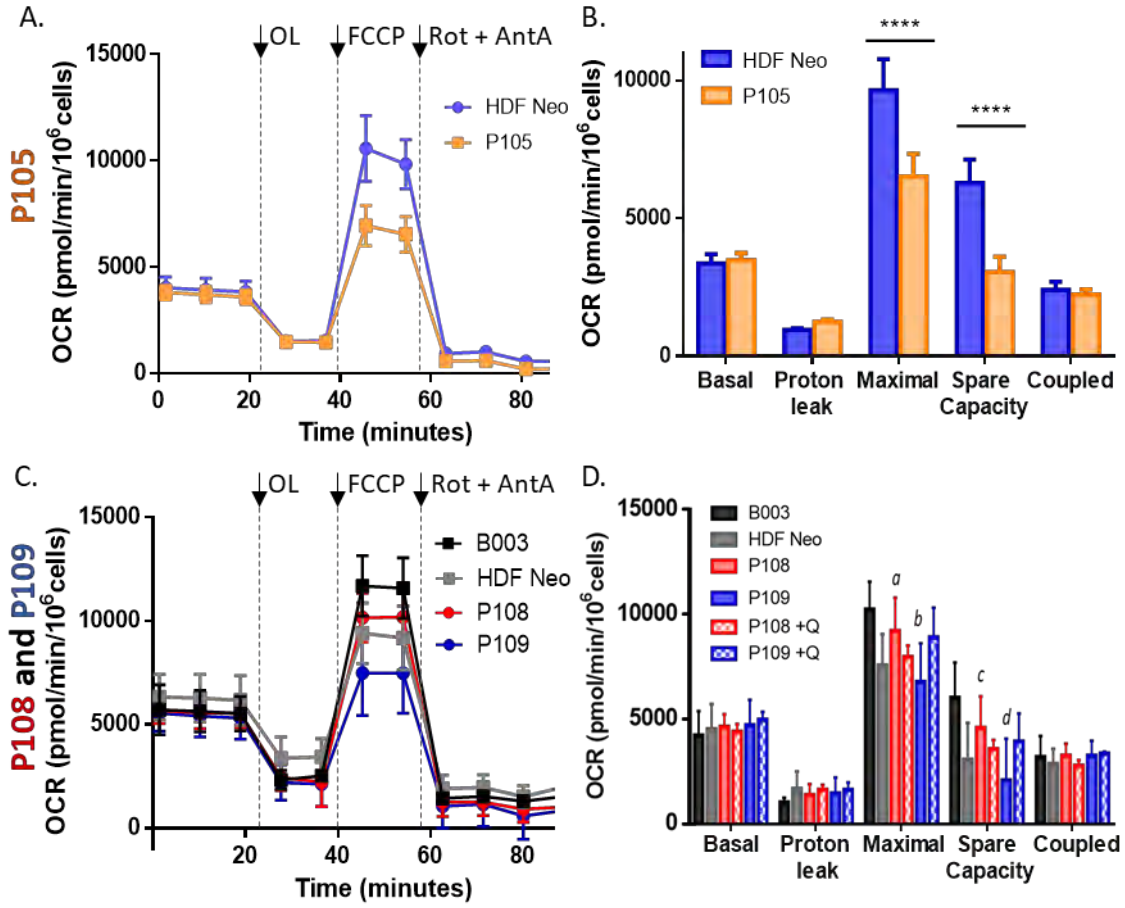

Figure 2.21. Oxygen consumption rate (OCR) in *COQ4* Mutant Fibroblasts.
OCR profile shows a respiratory defect in P105 (A) and P109 fibroblasts, but not in P108 (C). Arrows indicate the addition of the individual inhibitors. OL (oligomycin 4µM); FCCP (Carbonyl cyanide 4-(trifluoromethoxy)phenylhydrazone 1µM); Rot (rotenone 1µM); AntA (antimycin A 2.5µM).
(B, D) SeaHorse quantitative data are graphed as mean ± SD.
(B) P105 vs. HDF Neo. Two-way ANOVA with Sidak's multiple comparison test.
p values<0.0001 (****).
(D) Two-way ANOVA with Tukey's multiple comparison test. p values:
a: P108 vs. B003, p<0.05; P108 vs. HDFNeo, p<0.0001; P108 vs. P109, p<0.0001.
b: P109 vs. B003, p<0.0001; P108 vs. P109, p<0.0001.
c: P108 vs. B003, p<0.001; P108 vs. HDFNeo, p<0.0001; P108 vs. P109, p<0.0001.
d: P109 vs. B003, p<0.0001; P109 vs. HDFNeo, p<0.05; P108 vs. P109, p<0.0001.

In the case of P108 and P109, both cells behaved differently (Figure 2.21.C and D). P109 presented lower maximal respiration rate and spare capacity compared to both controls used, while P108 had these two parameters in between the two controls. This characteristic fits with the fact that P109 fibroblasts grow slower and show a more senescent phenotype in culture, compared to P108 fibroblasts. Comparing both patients' cells to B003 control, they have a decreased capacity to respond to energetic demands, which is indicative of reduced cell fitness or adaptability. When treated with 5 µM of CoQ_{10} for 10 days, P109 experienced a slight improvement in maximal respiration and spare capacity, becoming more similar to P108 and controls (Figure 2.21.D).

COQ4 protein levels are drastically reduced in patients, and other COQ proteins are dysregulated.

COQ4 protein levels were analysed in whole cell lysates from controls' and patients' fibroblasts, showing extremely low levels of mutant COQ4 protein in the fibroblasts of all patients compared to controls (Figure 2.22.A and B). In the case of P105, the very low levels of COQ4 protein agrees with the fact that the frameshift mutation is not predicted to produce any full length COQ4 protein, and it seems that it would happen the same with the splicing mutation. In the case of P108 and P109, the homozygous mutation could destabilize the protein, leading to its degradation, or could destabilize the mRNA, leading to NMD.

We also checked the levels of other COQ proteins, since the alteration in one of the proteins of the CoQ_{10} biosynthetic complex could have effects on the stability of the rest of the proteins participating in the complex. Our results show that some of these proteins seem to be dysregulated (Figure 2.22.A and C-E). COQ7 is downregulated in comparison to controls, while COQ5 seems to be upregulated in P108 and P109 cells. COQ6 showed unclear results.

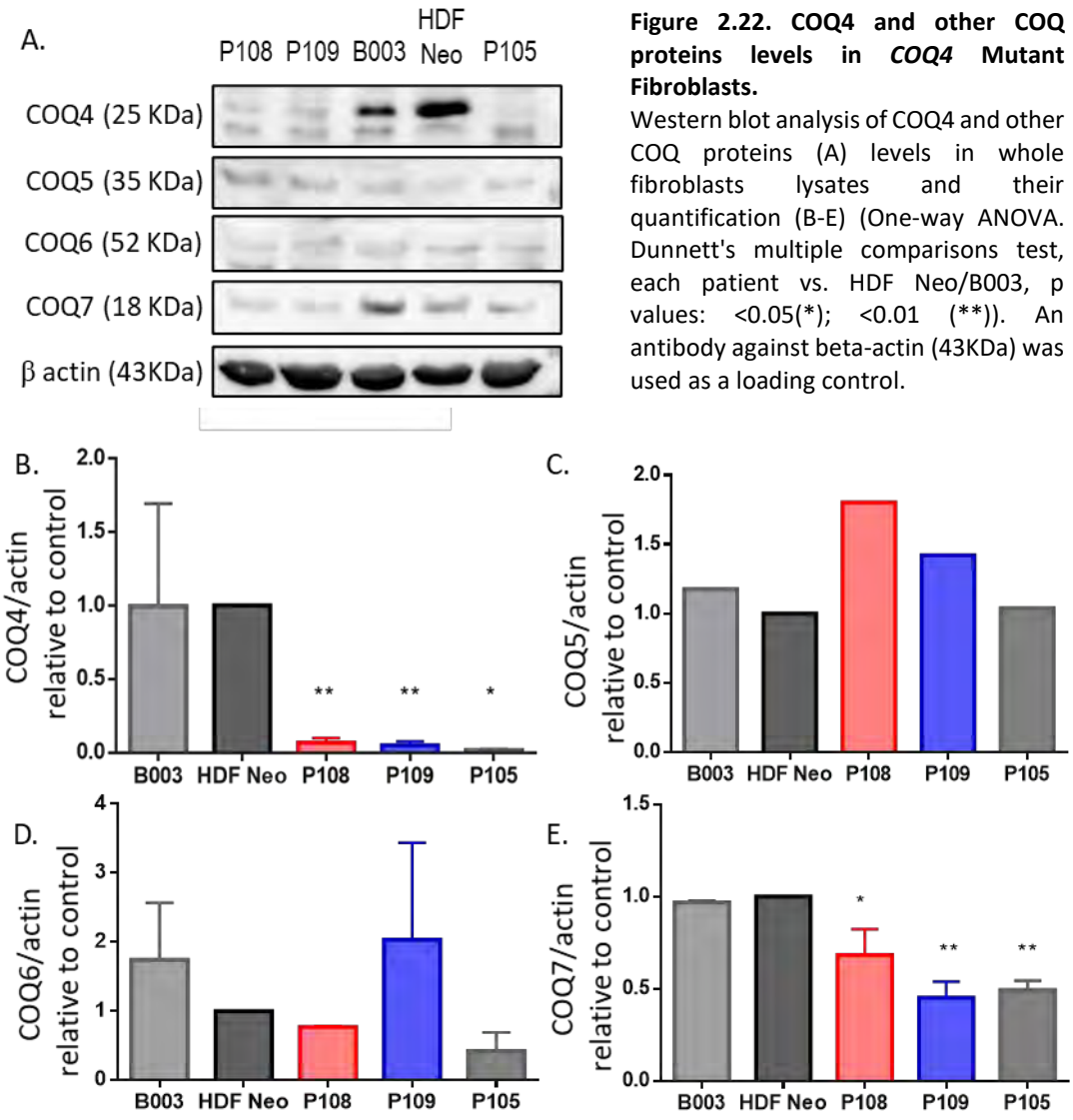

Figure 2.22. COQ4 and other COQ proteins levels in *COQ4* Mutant Fibroblasts.
Western blot analysis of COQ4 and other COQ proteins (A) levels in whole fibroblasts lysates and their quantification (B-E) (One-way ANOVA. Dunnett's multiple comparisons test, each patient vs. HDF Neo/B003, p values: <0.05(*); <0.01 (**)). An antibody against beta-actin (43KDa) was used as a loading control.

2.3. Conclusions

In this chapter, we worked with different *in vitro* cellular models of primary CoQ_{10} deficiency: *COQ4* and *COQ7* patients' fibroblasts and immortal HEK cell lines knocked-out in *COQ4* and *COQ6.* The main conclusions derived from this work are the following:

i. New cases of primary CoQ_{10} deficiency due to mutations in *COQ4* and *COQ7* genes have been described, widening the clinical phenotype attributed to these disorders. Unreported variants in *COQ4* and *COQ7* expand the genotype of these disorders.

ii. Cell models with mutations in *COQ4*, *COQ6* or *COQ7* have low levels of CoQ_{10} and impaired biosynthesis, reduced CII+III activity and impaired respiratory performance.

iii. Primary CoQ_{10} deficiency cell models accumulate diagnostic intermediates, specific for each *COQ* defect. *COQ6* deficient cells accumulate 4-HP_{10}, *COQ7* deficient cells accumulate DMQ_{10} and *COQ4* deficient cells accumulate a yet unknown intermediate of CoQ_{10} synthesis.

iv. Treatment with 4-HB analogues is effective in some of the primary CoQ_{10} deficiency cell models. 2,4-dHB decreases DMQ_{10} accumulation, increases CoQ_{10} levels and ameliorate respiratory function in COQ7 mutant fibroblasts. Vanillic acid restores CoQ_{10} biosynthesis and respiration in *COQ6* KO cells.

Chapter 3

Chapter 3.

COQ4 gene and protein characterisation

3.1. Introduction

3.1.1. *COQ4* yeast gene and protein

COQ4 gene was first described as one of the genes needed for CoQ_6 production in the yeast *S. cerevisiae* [464]. *coq4* yeast gene, also known as *YDR204W*, is located in chromosome IV 858,137-859,144, and it spans 1,008 bp. The transcript (NM_001180512.1) produces a 335 aa-long protein (O13525) with a calculated molecular mass of 38.6 kDa.

Work in yeast have provided comprehensive knowledge on CoQ biosynthesis in general, and *coq4*, in particular. *coq4* null yeast has proven that *coq4* is essential for CoQ production in yeast, but its exact function remains unclear. Coq4 yeast protein (Coq4p) has been shown to be peripherally associated to the matrix side of the mitochondrial inner membrane [464] and it has been suggested to play a structural role in stabilizing the CoQ biosynthetic complex, which contains most of the CoQ biosynthetic enzymes [465,466]. The lack of *coq4* in *S. cerevisiae* causes the instability of several Coq proteins, such as Coq7p and Coq3p and, importantly, the accumulation of hexaprenyl-hydroxybenzoate (HHB), an early precursor of the pathway (the molecule resulting when Coq2p binds the quinone head to the lipid tail) [467,468] (See Chapter 4, Section 4.1.5.).

3.1.2. *COQ4* human gene and protein

Human *COQ4* gene was first identified by Casarin and colaborators [469]. It is located in the long arm of chromosome 9, specifically in the cytogenetic region 9q34.11 (Figure 3.1.A). *COQ4* genomic sequence spans chr9:128,322,544-128,334,072 (GRCh38.p13), in the forward strand (11,528 bp). Four different protein coding transcripts are annotated, but only the longest one is thought to produce a functional COQ4 protein (isoform 1) (Figure 3.1.B). This transcript (1,245 bp, NM_016035.5) encodes a 265 aa (7 exons) protein with a predicted molecular mass of 29.7 KDa (NP_057119.3) (Figure 3.1.C). Human COQ4 has 39% of identity and 55% of similarity with yeast Coq4p, and it is able

to complement *coq4* function in a *coq4* null yeast mutant [469]. Human COQ4 has a mitochondrial localization signal, leading to a mitochondrial targeted protein. Another transcription initiation site located within intron 1 was described to produce a shorter transcript and a shorter protein COQ4 (isoform 2). Isoform 2 starts at methionine 25 in exon 2, and it's not targeted to mitochondria, as it lacks the amino acids that specify the predicted mitochondrial targeting sequence, so it would probably lead to a cytoplasmatic protein [469]. This phenomenon is known as alternative translation initiation, and it can generate proteins targeted to different cell compartments, where they may exert different functions [450].

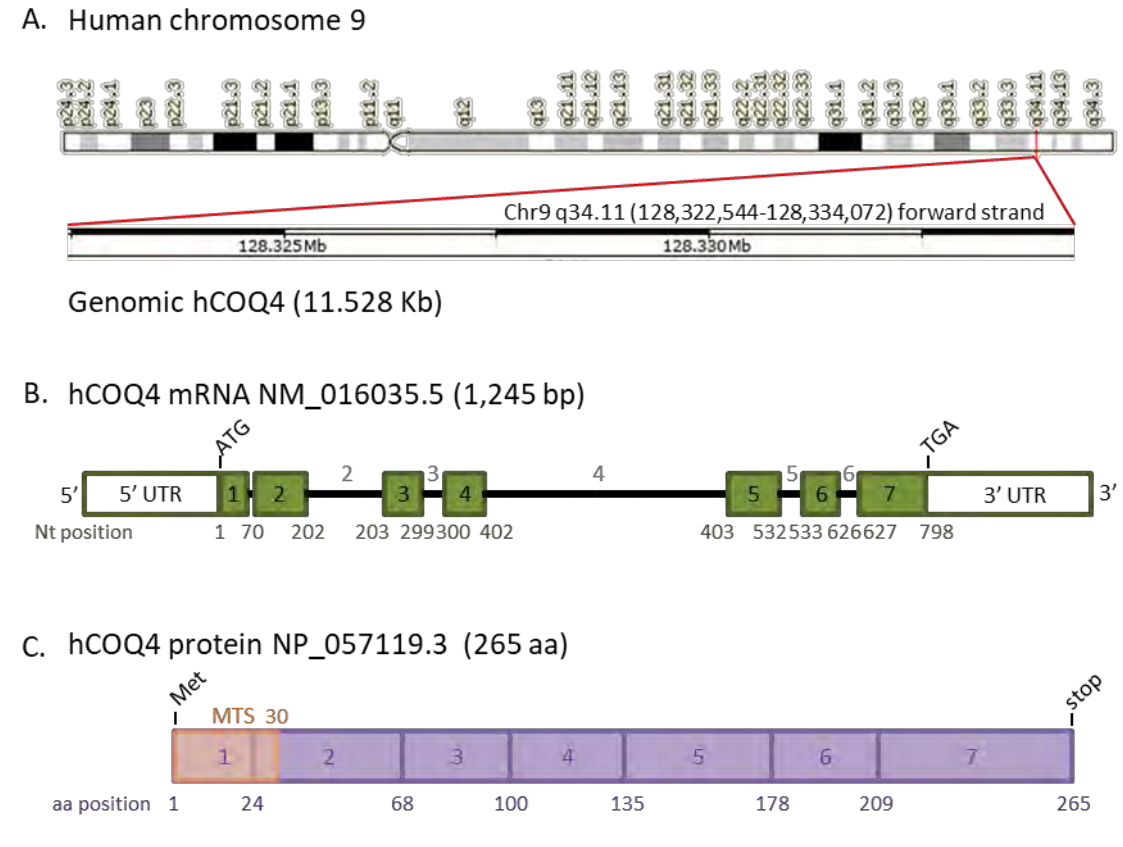

Figure 3.1. Schematic representation of *COQ4* genomic localization (A), mRNA (B) and protein (C) sequences.
Legend shows the scale of the sequences represented. UTR (untranslated region); MTS (mitochondrial targeting sequence; aa (amino acid); nt (nucleotide).

COQ4 function in mammals is still unknown, but it has been identified as a part of a putative biosynthetic complex, with interactions with some COQ proteins (See Chapter 4, sections 4.1.5 and 4.2.2.). For example, tagged COQ5 and COQ4 proteins co-immunoprecipitated when co-expressed in HEK293 cells [470]. Additionally, numerous interactions between different COQ proteins were also confirmed by cell-free protein expression and purification studies [438]. Recently, a COQ4-containing protein complex in the range from 66 kDa to below 480 kDa was detected by 2D-BN-PAGE [315]. Defects in COQ4 gene are a cause of CoQ_{10} deficiency, as we have seen in Chapter 1 (section 1.2.4) and 2 (section 2.2.3).

Further insights in human COQ4 function are needed, in order to understand how this protein contributes to CoQ biosynthetic pathway, and how this process is altered in primary CoQ deficiency due to *COQ4* mutations. This is crucial, so we could improve early diagnosis, therapeutic approaches and genetic advising. With this in mind, we can consider human cellular models a useful tool to better understand the disease mechanisms. Some examples of this models are skin fibroblasts from patients or immortal cell lines genetically modified to knock out the *COQ* gene we are interested in studying (see Chapter 2). Studies with immortal KO models can be greatly valuable, since these cells grow easily, and they can provide a homogeneous genetic background to study different defects. The recent advances in effective genome editing tools, such as CRISPR-Cas9, allows us to easily generate these models of extraordinary applicability in rare diseases research.

3.1.3. Generation of *KO* models using the CRISPR/Cas9 system

CRISPR (Clustered Regularly Interspaced Short Palindromic Repeats) sequences and Cas (CRISPR-associated) proteins are the two elements of an ancient microbial adaptive immune system [471–473], converted into the most powerful genome editing tool [474] (Figure 3.2). The repeats (CRISPRs) are short, directly repeating nucleotide sequences flanked by short unique DNA fragments (protospacers), which have been acquired by bacteria from infections with invading phages. The CRISPR sequences are transcribed to make the pre-CRISPR RNA (pre-crRNA), which is then processed into individual crRNAs by a trans-activating crRNA (tracrRNA) with homology to the short palindromic repeat.

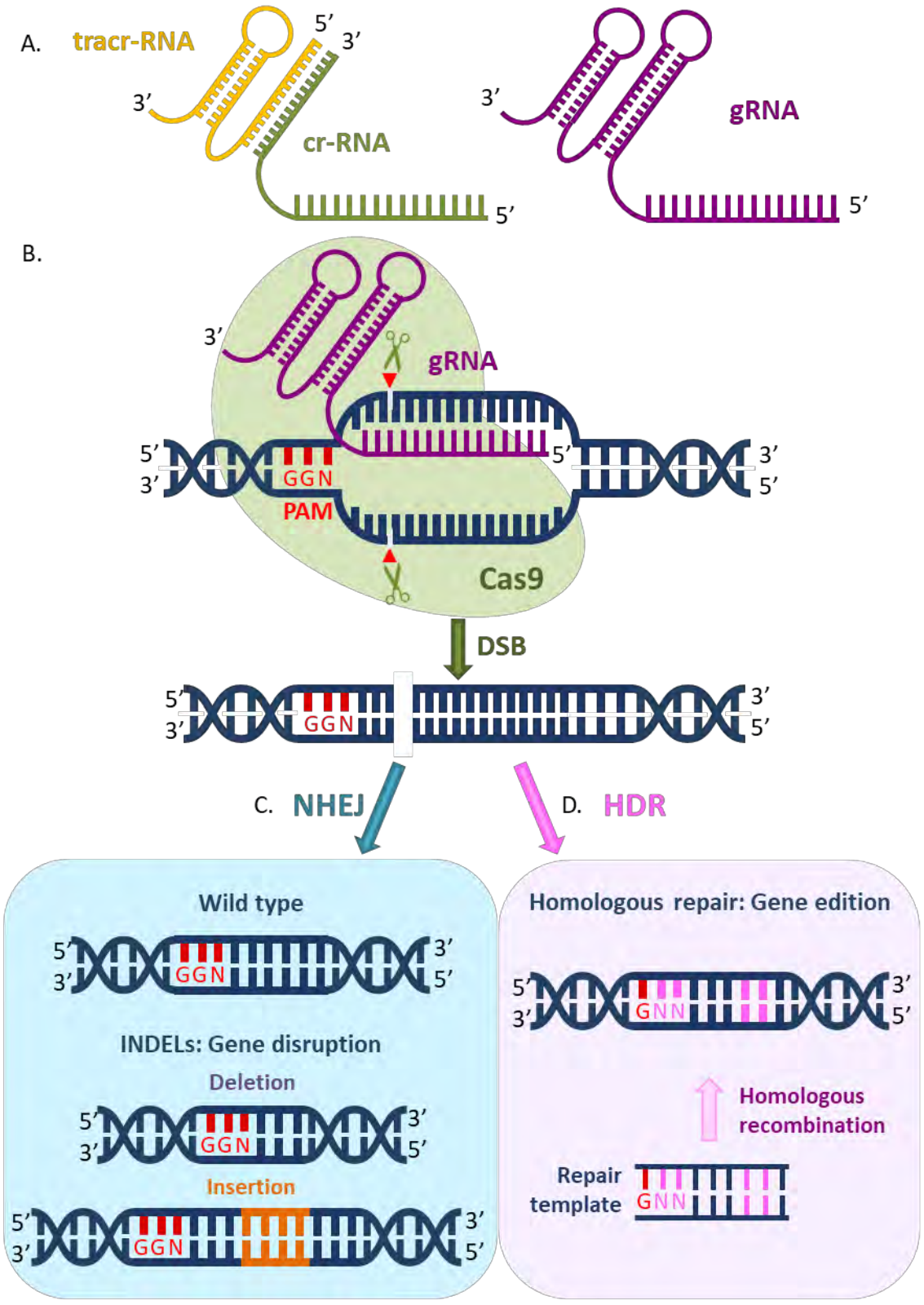

Figure 3.2. Overview of CRISPR-Cas9 technique for gene editing, and the endogenous mechanisms of DNA repair of the cell (NHEJ/HDR).

(A) The crRNA:tracrRNA from bacteria have been fused in a synthetic guide RNA (gRNA) to simplify its use for genome editing. (B) Cas9/gRNA complex produces a double strand break (DSB) at the target genomic locus, which have to be adjacent to a PAM (Protospacer Adjacent Motif; NGG in Cas9 from *S. pyogenes*). Repair will proceed through non-homologous end-joining (NHEJ) (C) or homologous directed repair (HDR) (D) depending on the experimental conditions.

The tracrRNA helps recruit RNAse III and Cas9 enzymes, which together separate the individual crRNAs, forming the crRNA:tracrRNA:Cas9 complexes, each one having a specific crRNA sequence (protospacer). Each complex can bind infectious DNA molecules complementary to the crRNA's protospacer, and the nuclease Cas9 produces a double strand break (DSB), cleaving and destroying the invader. After the DSB, the crRNA:tracrRNA:Cas9 complex unbinds. In Type II CRISPR systems, a potential target sequence is only valid if it contains a special Protospacer Adjacent Motif (PAM) directly after where the crRNA would bind. The most commonly-used Cas9 from *Streptococcus pyogenes* recognizes the PAM sequence 5'-NGG-3' (where N can be any nucleotide base) (Figure 3.2).

To translate a complex prokaryotic system into a simple genome editing tool, the crRNA and the tracrRNA were fused in a synthetic small guide RNA (gRNA), composed by a hairpin RNA structure linked to a 20 bp sequence homologous to the target DNA (Figure 3.2.A). Then, the Cas9 nuclease can complex to the gRNA, and be guided to the genome region complementary to the gRNA, where it cleaves both strands of the DNA (Figure 3.2.B). At this point, the cell will try to repair the break and that is when the potential for genome editing arises. The cells repair these DSBs by standard cellular repair mechanisms, either by non-homologous end joining (NHEJ), introducing small insertions or deletions into the sequence (Figure 3.2.C), or homologous directed repair (HDR), copying the genetic information from homologous DNA molecules (Figure 3.2.D). Depending on the mechanism used, the sequence at the repair site can be modified by indels, or new genetic information can be inserted [166,475]. HDR needs the use of a repair template with the desired modifications (such as point mutations that affect the targeted sequence, and even the PAM, to prevent repeated cleavage of already repaired sequences (Figure 3.2.D).

Knock-out generation benefits from the indels generated with NHEJ repair (Figure 3.2.C), that alter the original sequence, and by probability, can produce a shift in the ORF and a generation of a new stop codon, early in the protein. If the defects occur in all the alleles, the cell will not be able to produce the WT protein, meaning it will be knocked out for this gene [476].

Cas9 generates DBSs in the region of the genome where the gRNA has guided to. However, off-target activity can also occur, sometimes very frequently, inducing mutations at sites other than the intended on-target site. One strategy to reduce this off-target activity is the use of two paired nickases, guided by two different gRNAs. Cas9 nickase is a catalytically mutant Cas9 that is able to introduce a single-strand break (SSB) with the same specificity as a regular Cas9 nuclease. These SSBs can be repaired without inducing indels. In order to create DSBs, two paired nickases guided by two gRNAs targeting adjacent regions must be used. Because both nickases must effectively nick their target DNA, paired nickases have significantly lower off-target effects compared to the regular CRISPR/Cas9 system [477].

3.2. Results and discussion

We have previously seen that COQ4 is an essential protein for CoQ biosynthesis. In this Chapter we will extract as much information as we can from its gene and protein sequences, and we will generate a model to study *COQ4* function.

3.2.1. COQ4 *in silico* characterisation

Gene sequence localization and genomic context

COQ4 human gene is located in chr9:128,322,544-128,334,072 (GRCh38.p13), in the forward strand (Figure 3.1). Different transcripts are annotated. Five of them are protein coding, but only the longest one is thought to produce COQ4 protein (isoform 1). This transcript (1245bp, NM_016035.5) encodes a 265aa (7 exons) protein with a predicted molecular mass of 29.7 KDa (NP_057119.3).

COQ4 (plus strand) shares 5' regulatory region with *TRUB2* gene (minus strand) (Figure 3.3), which encodes a mitochondrial mRNA pseudouridine synthase essential for the mitochondrial 16S rRNA, thus, for mitochondrial protein translation [478,479]. However, the functional significance of pseudouridinilation in mRNA is not characterised yet. This disposition is conserved throughout vertebrates, with some exceptions. The significance of this conservation is unknown, but it could suggest a shared or opposite regulation of the expression of these two genes and therefore a potential functional interaction between them.

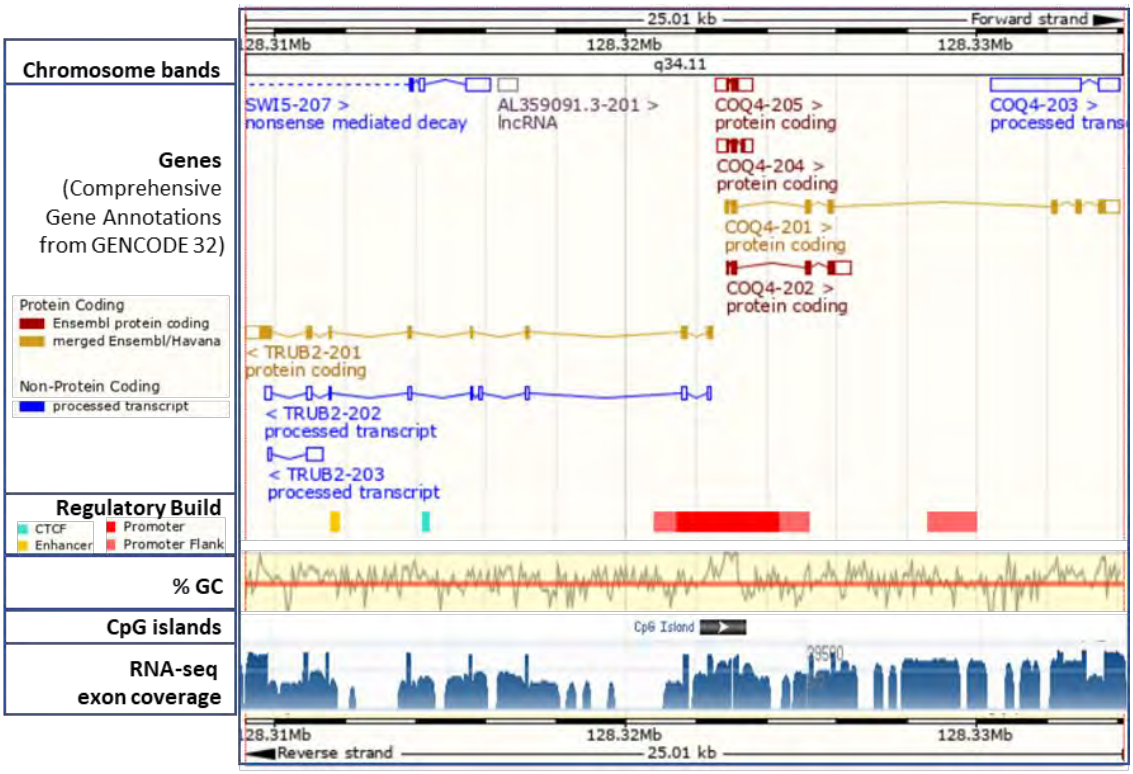

Figure 3.3. Visualization of human *COQ4* gene in its genomic context.
Data obtained and visualised with UCSC genome browser, Genome Data Viewer (NCBI's genome browser) and Ensembl Genome Browser.

This head-to-head arrangement of gene pairs on opposite strands is not rare in the human genome. More than 10% of protein-coding genes are arranged this way, with transcription start sites (TSS) that are separated by less than 1,000 base pairs, being this percentage significantly larger than expected by chance [480]. These gene pairs are termed 'bidirectional', and the regions between the TSS of these gene pairs (their regulatory region) are known as bidirectional promoters. These sequences can regulate the genes in both directions. Bidirectional promoters are associated with gene pairs whose levels of transcription need to be expressed in a co-ordinately mechanism, such as genes co-expressed in the same biological pathway. The bidirectional arrangement of promoters is also highly conserved among different species, which indicates functional importance[481].

Some data support the definition of this *COQ4-TRUB2* region as a bidirectional regulatory region for both *COQ4* and *TRUB2*. It has been described that TATA box occurrence in bidirectional promoters is significantly lower compared to the genome average, being the motif of TATA sequence mostly found in non-bidirectional promoters

[482]. An *in silico COQ4* promoter region study, revealed the absence of a classical TATA box, in line with the mentioned observation [469].

Moreover, bidirectional promoters are GC rich, and CpG-islands are present in 90% of bidirectional promoters compared to 45% of non-bidirectional promoters [482]. In the case of *COQ4-TRUB2*, the region annotated as promoter (regulatory build annotation by ENSEMBL) has a GC % of 53.73% (chr9:128,321,400-128,324,401), and a CpG island (with 60.06% of GC) is annotated in this region (chr9:128,322,080-128,323,376 bp) (Figure 3.3).

A study performed in HeLa cells used RNA polymerase II (RPol II) ChIP-seq data to identify and classify the bidirectional promoters. The gene pair *COQ4-TRUB2* has a very short TSS distance (93 bp). This gene pair was identified as one of the 932 pairs whose promoter was covering the two genes, inducing the expression of both of them. This was elucidated by the presence of a single central RPol II peak from ChIP-seq data [481]. However, more studies would be needed to prove the co-expression of these two genes.

COQ4 protein sequence conservation

COQ4 protein sequence is highly conserved through the evolution (Figure 3.4). By analysing its sequence, it has no homology with any other known protein or domain that would indicate it has any specific enzymatic activity. It only has an inherent characteristic domain, so-called the COQ4 domain, which is very conserved, found in 1770 sequences from 1345 species (data from Pfam database [483]). *COQ4* gene has homologous sequences in all eukaryotic genomes, and some of them are also found in some bacteria, and cyanobacteria, even though some of these species do not even have any form of CoQ. This COQ4 domain has a very conserved putative catalytic zinc binding motif, HDxxH-$(x)_{10}$-GE [466] (Figure 3.4).

We predicted secondary structures (alpha helixes) from the sequence, and the position of these helixes seem to be conserved through COQ4 sequences from different species (Figure 3.4).

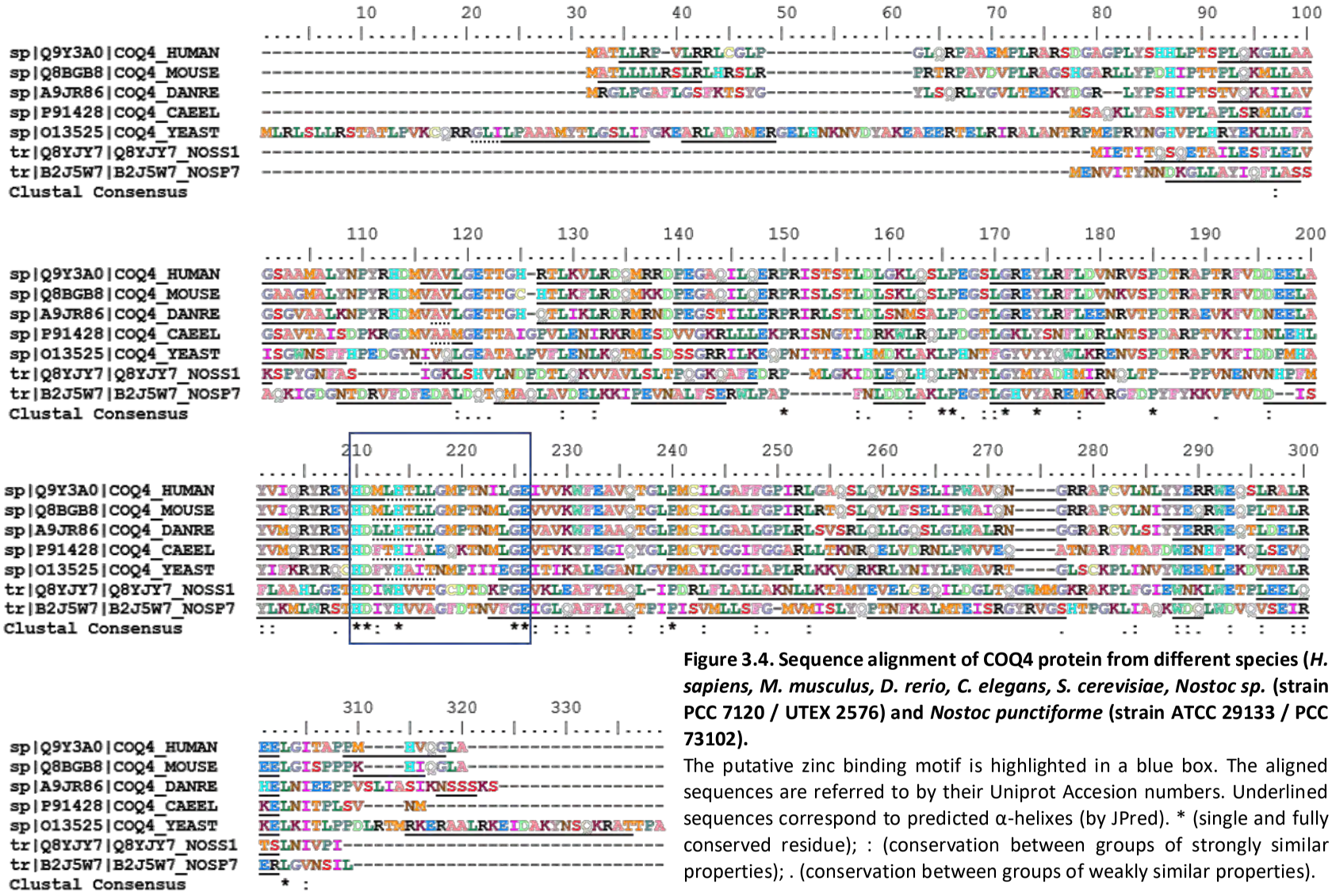

Figure 3.4. Sequence alignment of COQ4 protein from different species (*H. sapiens, M. musculus, D. rerio, C. elegans, S. cerevisiae, Nostoc sp.* (strain PCC 7120 / UTEX 2576) and *Nostoc punctiforme* (strain ATCC 29133 / PCC 73102).

The putative zinc binding motif is highlighted in a blue box. The aligned sequences are referred to by their Uniprot Accesion numbers. Underlined sequences correspond to predicted α-helixes (by JPred). * (single and fully conserved residue); : (conservation between groups of strongly similar properties); . (conservation between groups of weakly similar properties).

COQ4 protein 3D Structure

COQ4 3D structure has not been dilucidated yet. Only two ortholog proteins from cyanobacterial genus *Nostoc* have been crystallised so far, which are Alr8543 (17.82% of identity and 44.36% of similarity with human COQ4, calculated by pairwise alignment) and Npun_R0350 (18.15% of identity and 48.75% of similarity with human COQ4, calculated by pairwise alignment).

Structural properties of COQ4 orthologous proteins from Nostoc

Alr8543 protein from the cyanobacteria *Nostoc sp. (strain PCC 7120)* was crystallised by X-Ray diffraction in a 2.4 Å resolution structure deposited in PDB as 6E12 (Figure 3.5.A). This protein crystallised as a homodimer, co-crystallising with a molecule of oleic acid in a deep binding pocket. Oleic acid is a mono-unsaturated fatty acid found to represent 10% of the total fatty acid content in several species of cyanobacteria from genus *Nostoc*[484]. Additionally, a magnesium ion (Mg^{2+}) was chelated by the putative zinc (Zn^{2+})-ligand motif, HDxxH-$(x)_{10}$-GE [466]. The 6E12 PDB entry superseded the entry 3KB4, which crystallised similarly as a homodimer. This previous structure had co-crystallised with a molecule of geranylgeranyl monophosphate in the binding pocket, as well as the magnesium ion (Mg^{2+}) [485] (Figure 3.5.B). On the other hand, Npun_R0350 from *Nostoc punctiforme (strain PCC 73102)* was crystallised by X-Ray diffraction in a 2.85 Å resolution structure found in the PDB entry 3MSQ (Figure 3.5.C). This protein crystallised as a homotetramer, without any ligands. It contains a helix predicted to be a transmembrane domain.

We can see that the three protein structures have a similar globular structure (Figure 3.5), and that the dimeric and tetrameric forms are compatible. The helixes and the structured regions are arranged in a not very different way in all the three crystal structures. To be able to study the structural features of COQ4 proteins, we selected Alr8543 protein model. One of the reasons of this choice is the structural arrangement of the residues coordinating the divalent cation. Since this motif seems to be important, based on its high conservation, we selected the structure in which these residues are positioned towards the pocket. Also, the fact that a lipidic molecule co-crystallised in a

putative binding pocket allows us to hypothesise that COQ4 may be able to bind lipids, such as the polyisoprenoid tail of CoQ.

We thus analysed and visualised the conservation of the residues in the 6E12 structure (Figure 3.6). It can be observed that the most conserved features (in red) are the residues involved in the divalent cation coordination. The lipid binding pocket surface show a relatively high conservation while the rest of the protein surface shows regions with different degrees of conservation.

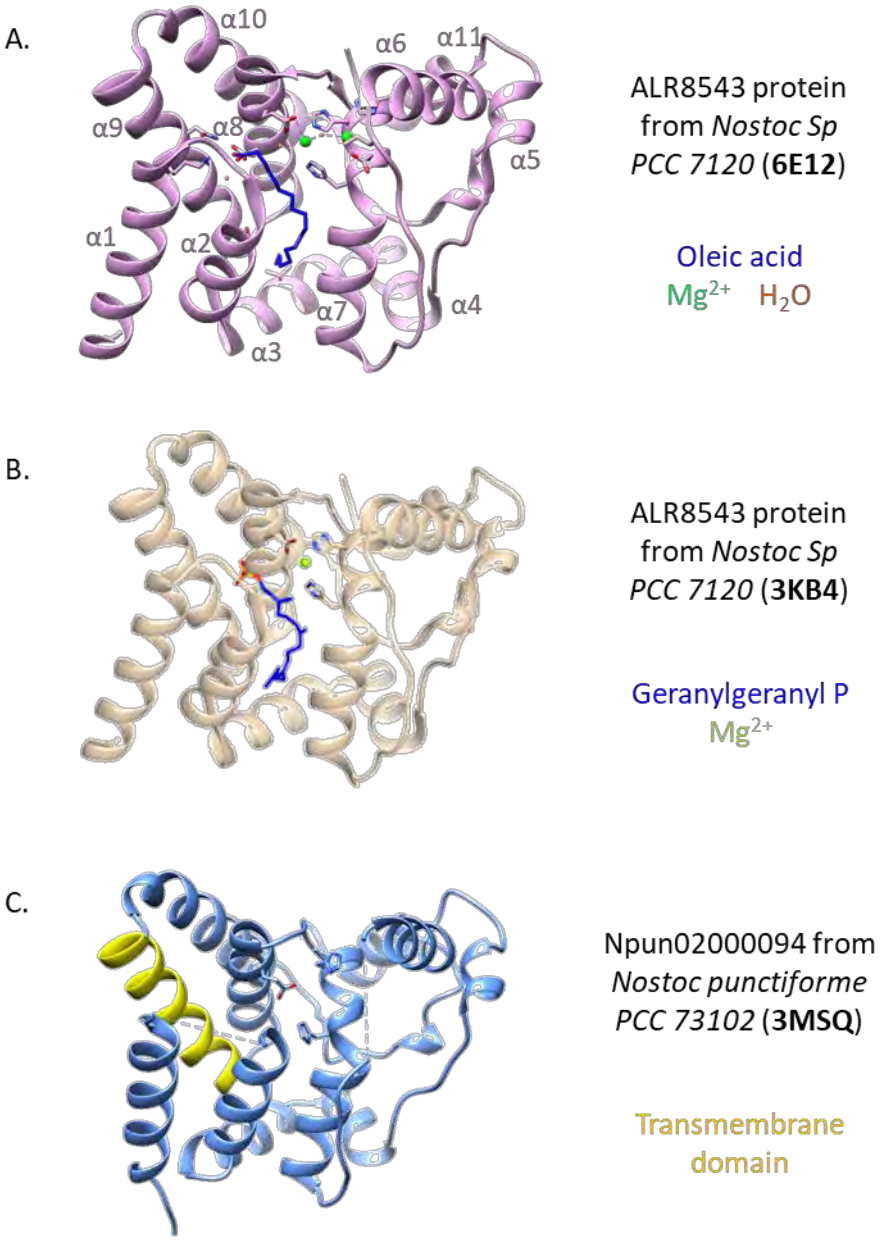

Figure 3.5. Ribbons visualization of 3D structures from COQ4 homologous proteins from cyanobacteria from genus *Nostoc*.
Ligands crystallised with the proteins are shown in different colours. Side chains of the residues that chelate the divalent cation are also displayed. (A) PDB: 6E12, (B) PDB: 3KB4, (C) PDB: 3MSQ. Alpha helixes are labelled in (A).

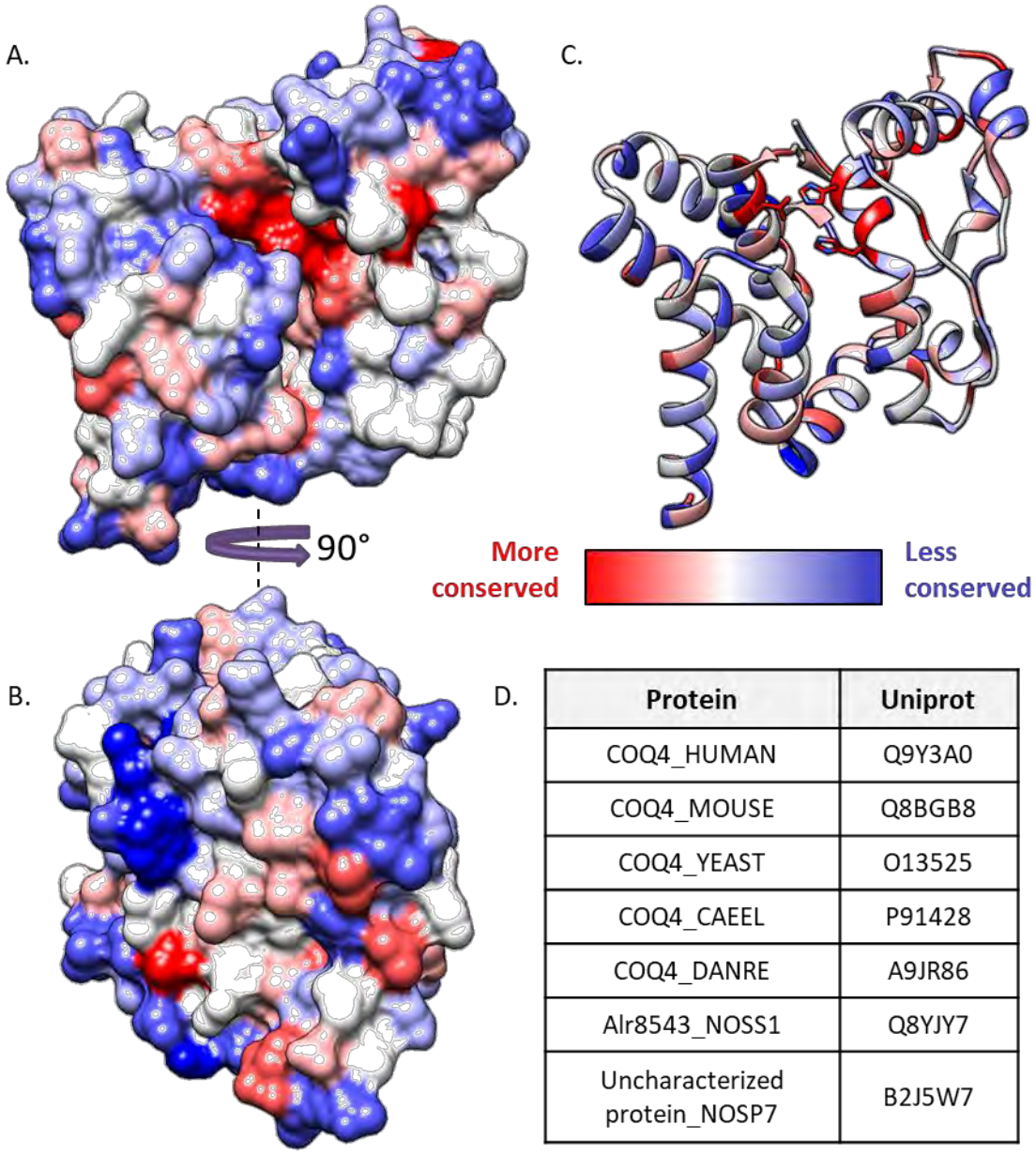

Protein	Uniprot
COQ4_HUMAN	Q9Y3A0
COQ4_MOUSE	Q8BGB8
COQ4_YEAST	O13525
COQ4_CAEEL	P91428
COQ4_DANRE	A9JR86
Alr8543_NOSS1	Q8YJY7
Uncharacterized protein_NOSP7	B2J5W7

Figure 3.6. COQ4 evolutionary residue conservation mapped onto COQ4 protein 3D structure.
The residue conservation was calculated with AL2CO method and mapped onto 6E12 structure using Chimera software. (A, B) Protein surface view, from different angles. (C) Ribbons view. (D) Table with the COQ4 protein sequences used for the multialignment (*H. sapiens, M. musculus, D. rerio, C. elegans, S. cerevisiae, Nostoc sp.* (strain PCC 7120 / UTEX 2576) and *Nostoc punctiforme* (strain ATCC 29133 / PCC 73102).

Figure 3.7. 6E12 homodimer structure and interface.
6E12 homodimer structure (A: surface, C: ribbons), and visualization of the opened interface, like a book (B: surface, D: ribbons). Contact residues are highlighted in different colours (pink and yellow) and listed in (E), with the corresponding residue in human COQ4 protein. The conservation of the residues with the human sequence is indicated in different tones of red: *(single and fully conserved residue); : (strong similar properties); . (weak similar properties).

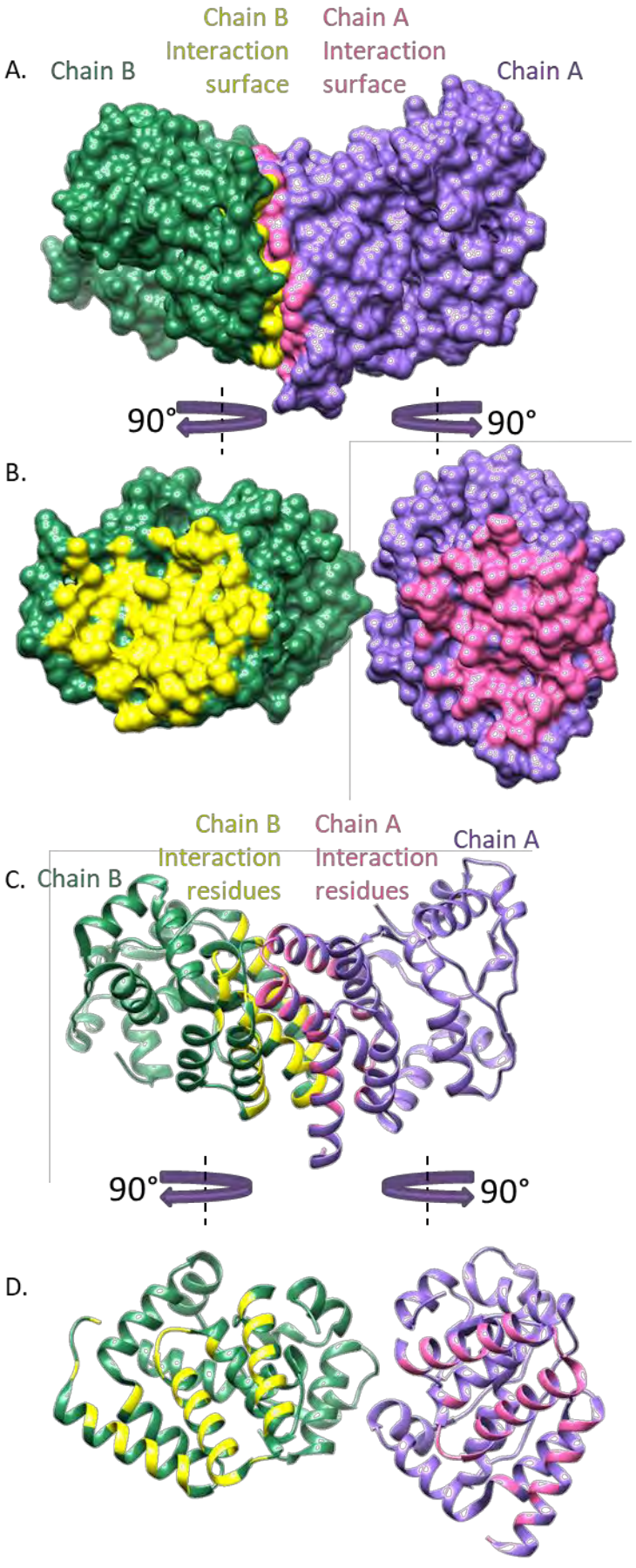

E.

6E12	Human COQ4
M1	Y38
I5	L42
E10	Q48
I13	L51
L14	L52
F17	A57
L18	A58
V21	L61
K22	Y62
L38	T76
T144	A187
I148	L192
P149	P193
D150	M194
R151	C195
L154	G198
A155	A199
L157	F201
A158	G202
L161	R205
L162	L206
T164	A208
A165	Q209
M166	S210
Y167	L211
E168	Q212
V169	V213
E170	L214
C172	S216
E173	E217
L176	I219
D177	-
L179	-
T180	-
W183	W221
M184	A222
K187	R227

Conservation

	.	:	*

Regarding the possible oligomerization, this protein crystallised as a homodimer (Figure 3.7). We cannot know if this is the physiological arrangement of the protein, but it should be taken into account that this structure should be only used within the context of a dimer. In this context, the monomers would reflect the phenomenon of *induced fitting*, by which they help each other to fold in a complementary manner, which would be different to the monomeric state. We were able to visualise the region involved in the dimerization and contact between the two chains of 6E12 structure (Figure 3.7.A-D), and we listed the amino acids that would be involved in this process (Figure 3.7.E). We could see how the hydrophobic residues are sequestrated at the binding interphase. If COQ4 functions as a dimer, these residues would be important for its stability. It can be observed that most of these residues are conserved in the human sequence, or at least have the same chemical properties than the cyanobacterial ones (Figure 3.7.E). The α-helixes that are mainly involved in these interactions are α1, α9 and α10, and some residues from α2 and α8 (see helixes labelling in figure 3.5.A).

Interaction with ligands is also an important feature for protein function. We analysed the residues that interacted with the different ligands in the 3KB4 and 6E12 structures (Figure 3.8). The majority of the residues interacting with the two lipidic ligands were common for both structures, and some of them shared biochemical properties with the corresponding residues in the human COQ4 sequence (Figure 3.8.E). These residues are mainly belonging to α2 and α9, and some to α3 and α8. The residues chelating the divalent cation, located in α7 and α8, were the same in both structures (H120, H124 and E136) and fully conserved in the human sequence (H163, H167, E179).

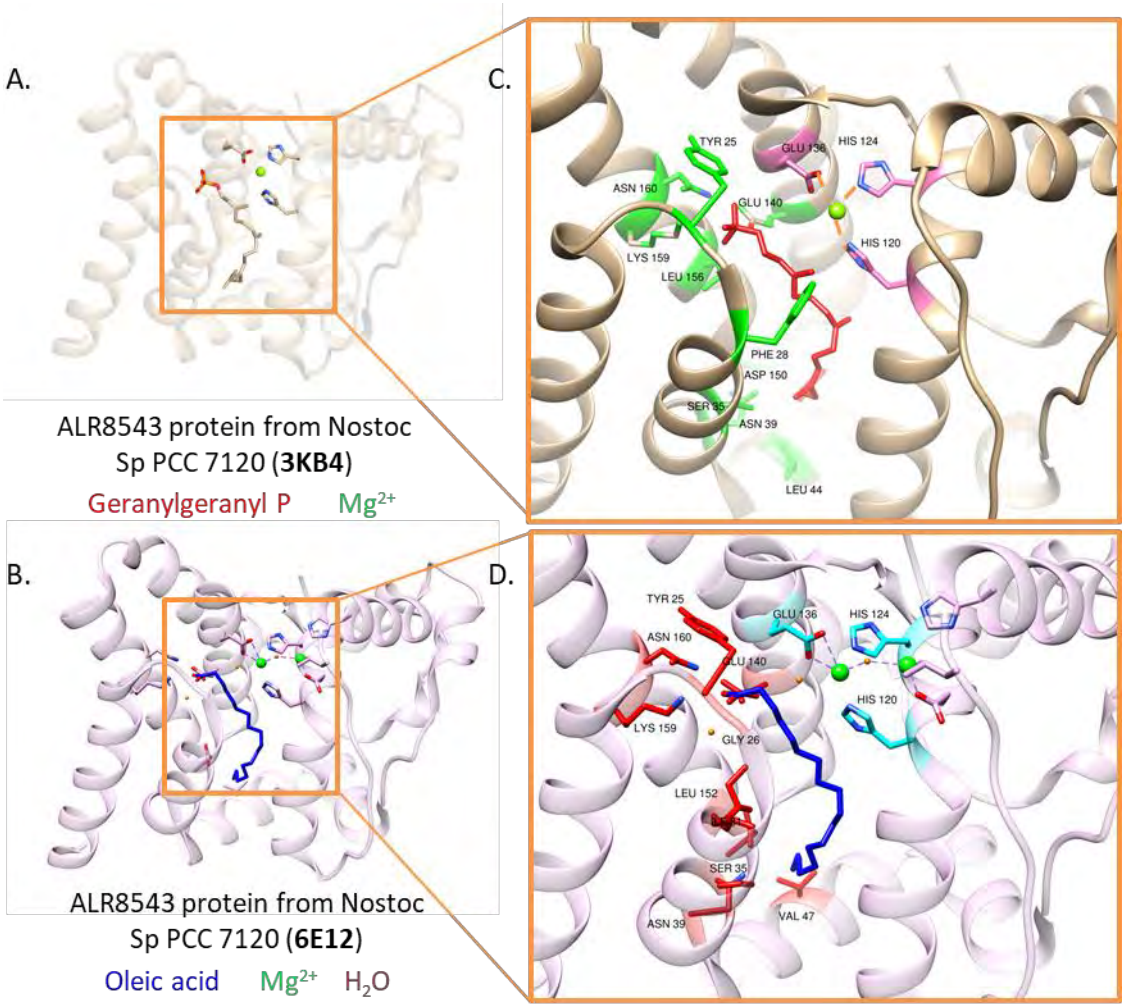

E.

Conservation

	.	:	*

3KB4	6E12	Human COQ4
Interactions with Mg2+		
H120	H120	H163
H124	H124	H167
E136	E136	E179

3KB4	6E12	Human COQ4
Interactions with lipids		
GR	OLA	-
Y25	Y25	Y65
-	G26	R66
F28	-	V70
-	I31	L73
S35	S35	-
N39	N39	T77
L44	-	L82
-	V47	L85
E140	E140	K183
D150	D150	M194
-	L152	I196
L156	-	G198
K159	K159	P203
N160	N160	I204

Figure 3.8. 3KB4 (A) and 6E12 (B) structure and ligands.
Ligands are in an orange box, which is zoomed in (C) and (D). In the zoomed regions, residues involved in ligand binding are labelled. In 3KB4 (C), residues binding geranylgeranyl phosphate molecule (in red) are marked in green, showing their side chains; and residues binding the Mg2+ ion (in green) are marked in pink. In 6E12 (D), residues binding oleic acid molecule (in dark blue) are marked in red, showing their side chains; and residues binding the Mg2+ ion (in green) are marked in cyan. Contact residues are highlighted in list (E), with the corresponding residues in human COQ4 protein. The conservation between them is indicated in different tones of red: *(single and fully conserved residue); : (strong similar properties); . (weak similar properties).

Human COQ4 structure model

We generated human COQ4 models by using the three previously mentioned structures as templates (Figure 3.9). There are some structural differences between the different models, but they are mostly compatible (Figure 3.9.D). We focused on the model that used 6E12 as template, and localised the features we know from the primary sequence, such as the exons, in an attempt to understand how each exon contributes to the protein structure (Figure 3.10).

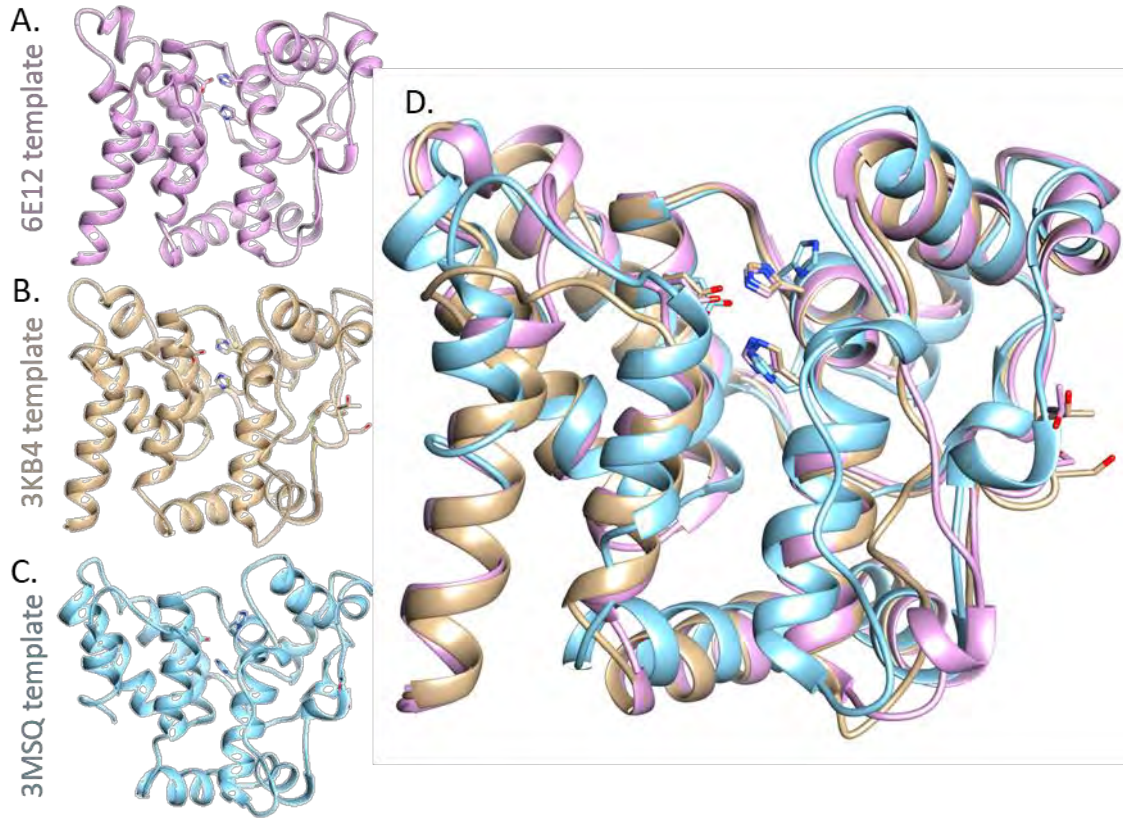

Figure 3.9. Human COQ4 protein models.
Human COQ4 protein models using (A) PDB: 6E12, (B) PDB: 3KB4, (C) PDB: 3MSQ structures as templates. (D) Visualization of the three models matched together. They have been matched using the match command in Chimera software on the three residues that were found to bind a cation in the original Nostoc structures (H163, H167, E179), since they seem to be important for the function of COQ4. Sidechains of these residues are shown.

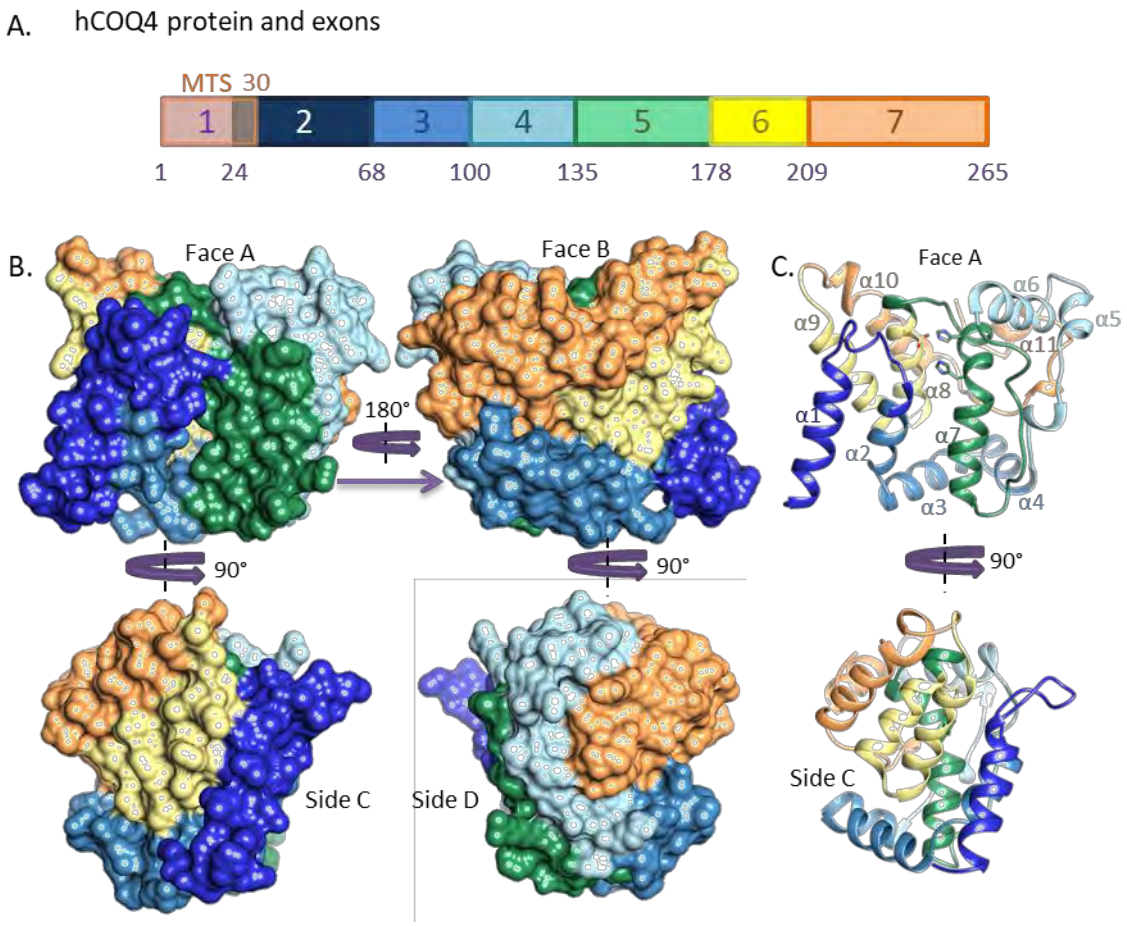

Figure 3.10. Distribution of exons in the structure of human COQ4 protein model.
(A) Human COQ4 protein sequence representation, each coloured box representing a different exon. (B) Four views of the model from 6E12 and mapped exons. (C) Distribution of the different helixes through the structure. Side C would correspond to the putative dimer interface.

Information extracted previously from the Alr8543 protein structure has been annotated to this model in the Figure 3.11. If COQ4 had the same properties as Alr8543, we hypothesise that α1, α9 and α10 would be important for protein dimerization; helixes α2, α9, α3 and α8 would form a pocket with lipid binding capacity; and α7 and α8 would be involved in zinc or other cation binding.

Additionally, we compared the human COQ4 model to the original structure, studying different properties of the protein surface. The representation of the spatial distribution of hydrophobicity, hydrophilicity and electrostatic potential on the molecular surface of proteins is critical for the understanding of the interaction with small molecules and other proteins.

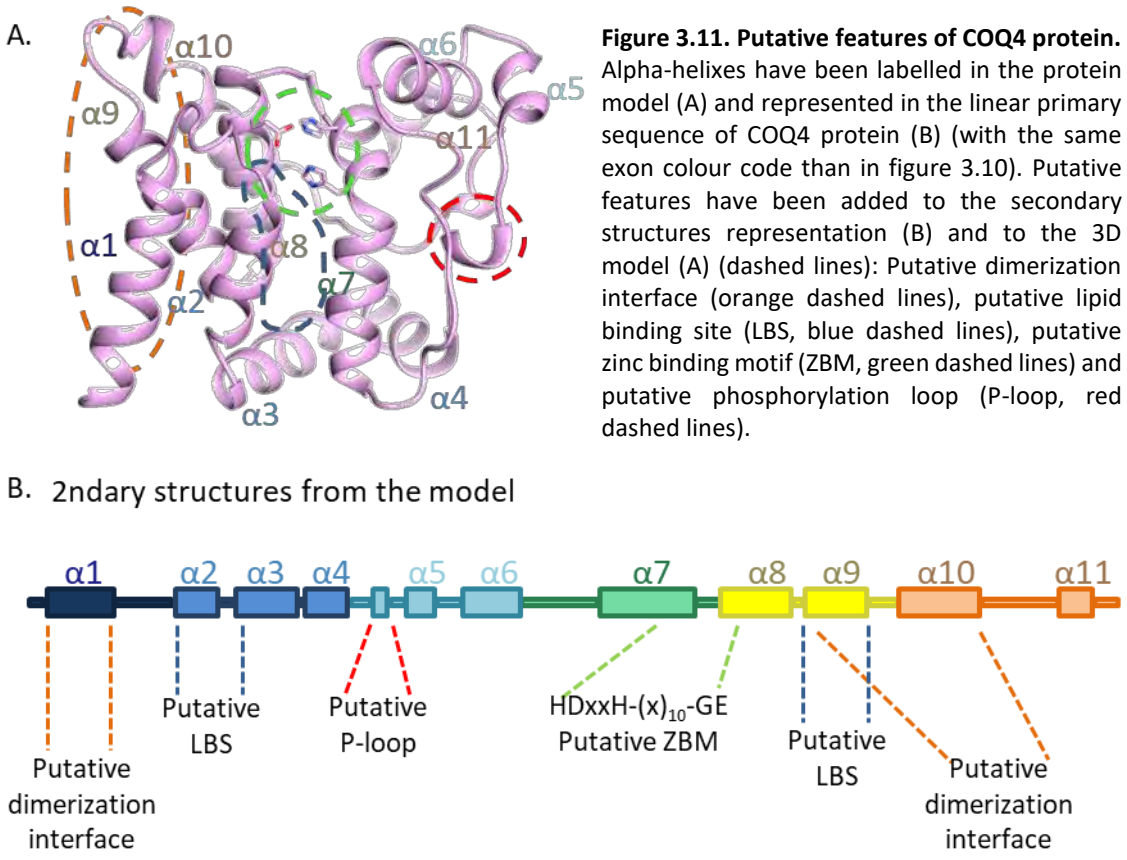

Figure 3.11. Putative features of COQ4 protein. Alpha-helixes have been labelled in the protein model (A) and represented in the linear primary sequence of COQ4 protein (B) (with the same exon colour code than in figure 3.10). Putative features have been added to the secondary structures representation (B) and to the 3D model (A) (dashed lines): Putative dimerization interface (orange dashed lines), putative lipid binding site (LBS, blue dashed lines), putative zinc binding motif (ZBM, green dashed lines) and putative phosphorylation loop (P-loop, red dashed lines).

The hydrophobicity properties of Alr8543 structure surface were displayed and compared with the human COQ4 model (Figure 3.12). Alr8543 crystal structure has a hydrophobic pocket in which the lipidic ligand was crystallised (Figure 3.12.A. Face A). Hydrophobicity in this pocket seems to be conserved in the human structure model, indicating that this pocket could conserve lipid binding properties (Figure 3.12.B. Face A). Another characteristic hydrophobic patch in Alr8543 surface is the dimer interface between two crystallised units of Alr8543 protein (Figure 3.12.A. Side C). The hydrophobicity of the surface of the putative dimer interface seems to be reproduced in the human COQ4 model (Figure 3.12.B. Side C). There are other hydrophobic patches on the surface of these structures, which are concentrated in Face A, Face B and Side C and almost absent in Side D (in both structures). These patches could be involved in interactions with other proteins or with membranes.

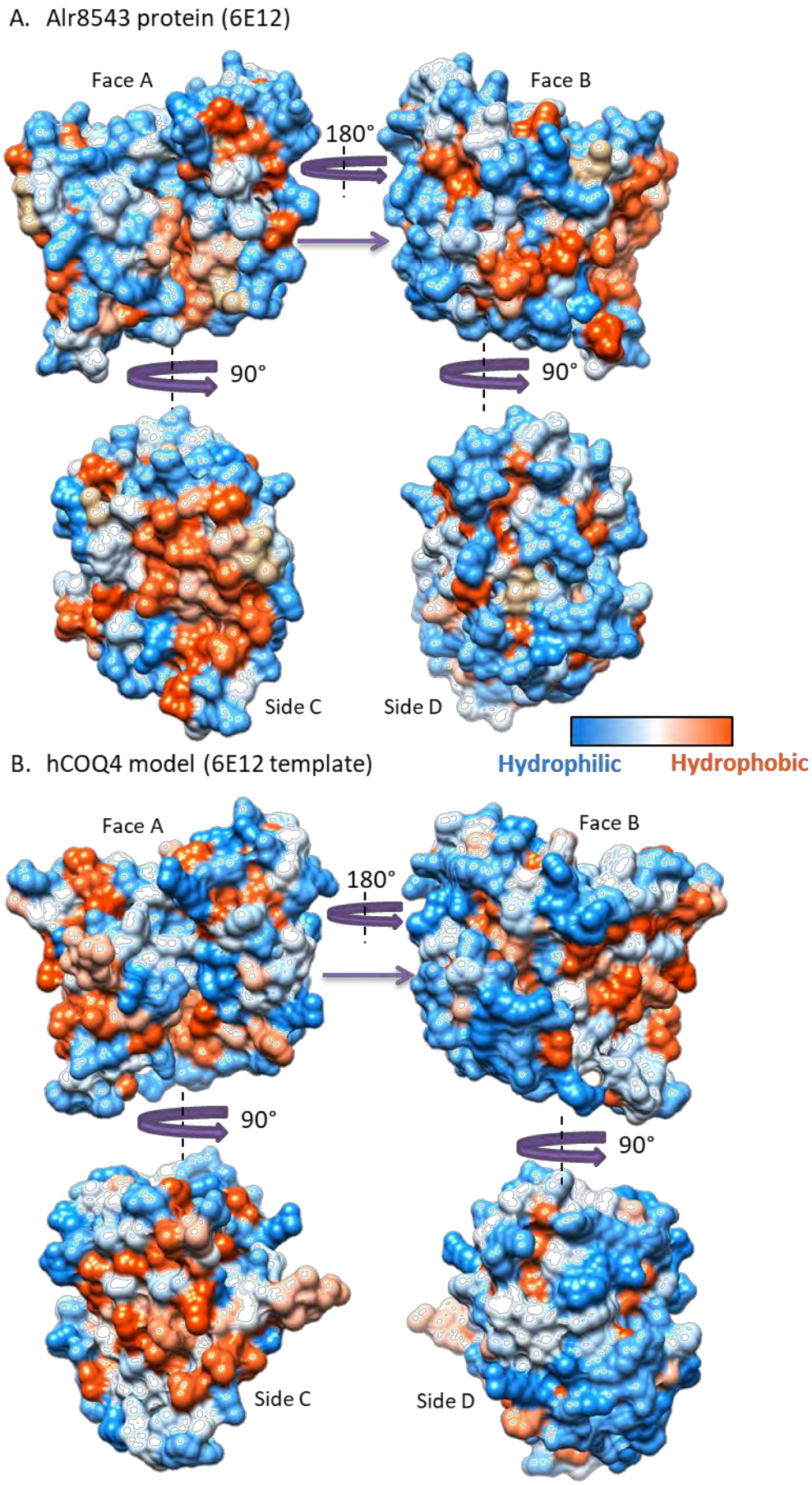

Figure 3.12. Surface hydrophobicity of Alr8543 (A) and human COQ4 (B) protein structures.

Electrostatic potential distribution on the molecular surfaces of Alr8543 and COQ4 model are substantially different (Figure 3.13). However, conservation of the charges in the very conserved divalent cation chelating pocket as well as in the putative lipid binding pocket is high. Absence of positive or negative charges is observed in the putative dimer interface of both protein structures (Side C).

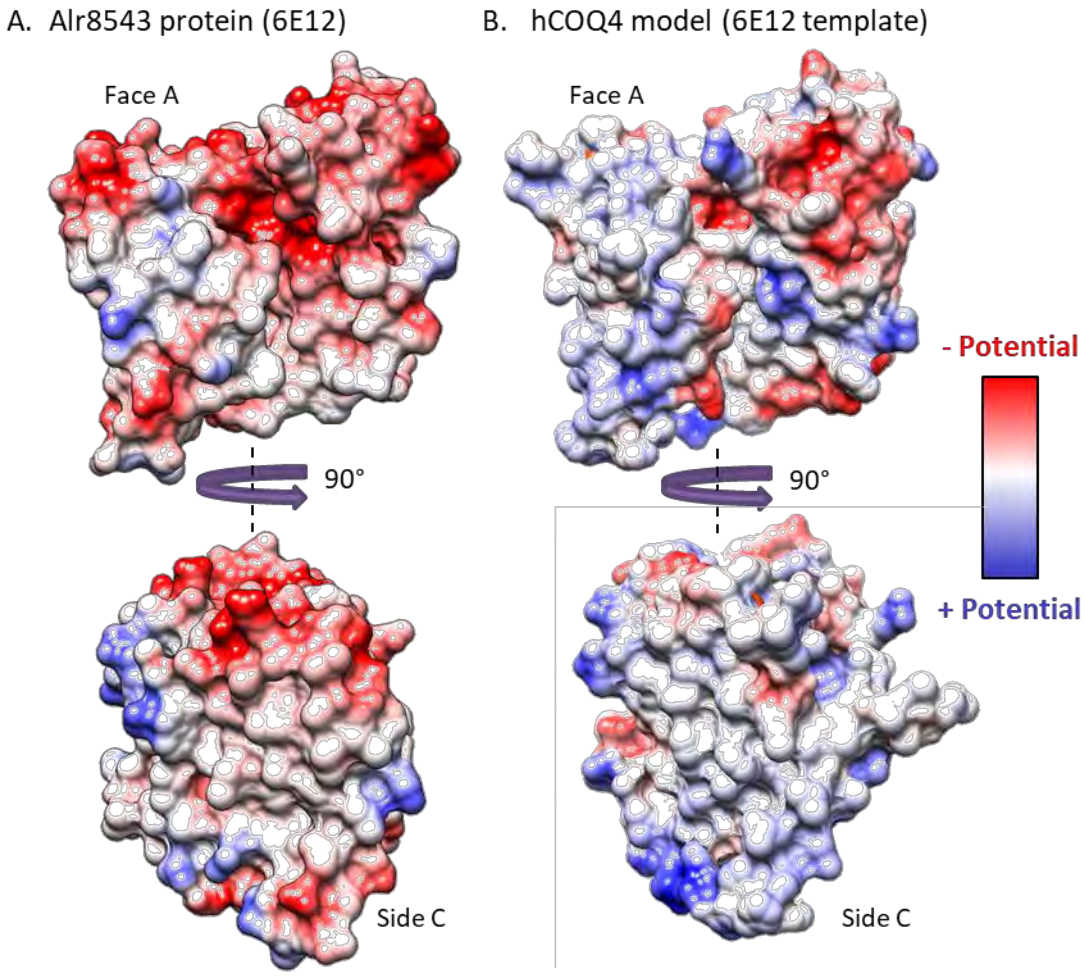

Figure 3.13. Surface Coulombic electrostatic potential of Alr8543 (A) and human COQ4 (B) protein structures.

These are only preliminary observations, since optimisation and energy minimisation of the model should be performed in order to be able to draw more conclusions about the protein structure and surface. Molecular dynamics modelling of the protein would reveal important information about its features.

Other features of COQ4 protein

i. Mitochondrial localisation prediction

Human COQ4 protein is a 265 amino acids polypeptide with a mitochondrial localization[469]. COQ4 is included in the MitoCarta2.0 inventory as one of the 1158 human genes encoding proteins with strong support of mitochondrial localization[69].

Different *in silico* approaches classify COQ4 as a mitochondrial protein, with a mitochondrial localisation peptide in the N-terminal end of the protein. Uniprot database indicates a mitochondrial subcellular localisation by manual annotation with a mitochondrial localization signal corresponding to the first 30 amino acids of the protein (Figure 3.14). MitoMiner [208] and MitoFates [209] bioinformatics tools predict a N-terminal cleavable targeting signal (presequence) with a high composition of arginine and no negatively charged residues (Figure 3.14).

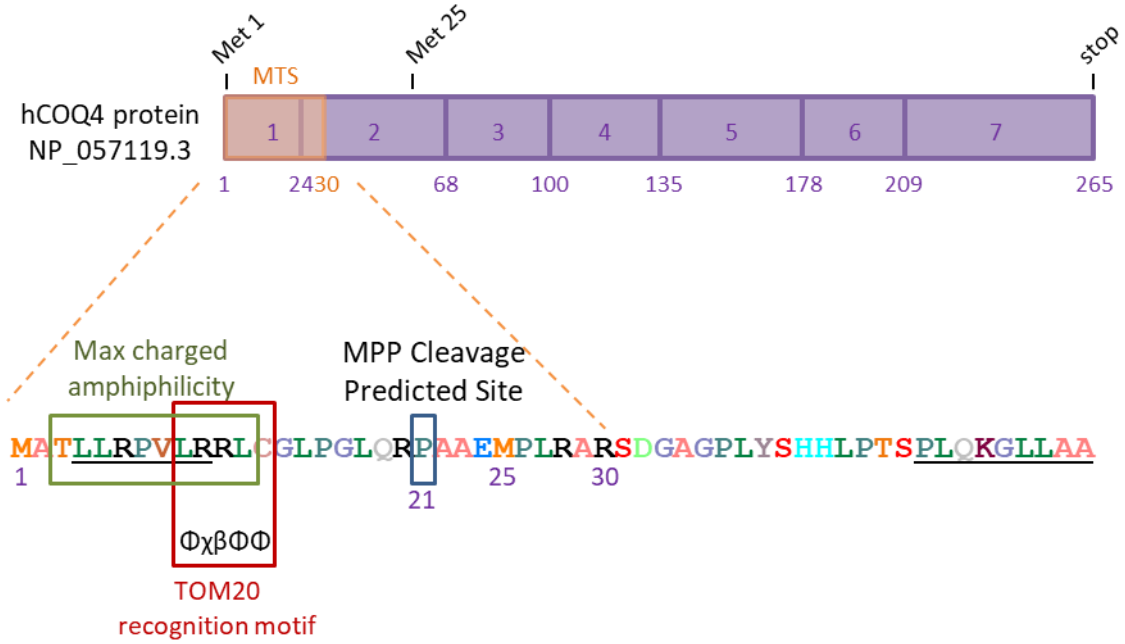

Figure 3.14. Human COQ4 contains mitochondrial localization signals.
Prediction of a mitochondrial targeting signal and cleavage sites in COQ4 was performed using MitoMiner and MitoFates. Proteolytic cleavage site for mitochondria processing peptidase (MPP) was predicted at proline in position 21 (Φ(hydrophobic), β(basic)).

This presequence is called mitochondrial targeting sequence (MTS) and is predicted to form an amphiphilic α-helix with positively charged residues on one side and hydrophobic residues on the opposite face. This helical structure is meant to be recognised by TOM20 in order to initiate the import of the protein to the mitochondria,

through the TOM and TIM complexes. Upon import into mitochondria, this presequence is predicted to be cut by the heterodimer mitochondrial processing peptidase (MPP) in the mitochondrial matrix. The cleavage consensus site is predicted to be at proline 21 (Figure 3.14).

ii. Phosphorylation predictions

Phosphorylation is an essential signalling process that is involved in the regulation of many cellular functions, such as bioenergetic metabolism, growth, differentiation or apoptosis. Mitochondrial phosphorylation is central to the regulation of the organelle functions, and proteins such as those belonging the respiratory chain [486,487] or pyruvate dehydrogenase subunits [488,489] are regulated by this post-translational mechanism. Phosphorylation plays a crucial role in CoQ biosynthesis. For example, phosphorylation of Coq3p, Coq5p, and Coq7p is altered in *coq8* yeast [490,491]. On the other hand, phosphorylation of Coq7p induces reduction of CoQ synthesis[492]. The phosphatase responsible for its dephosphorylation and activation is Ptc7p in yeast [493] and its homologous phosphatase in mammals is PPTC7[494,495]. Since phosphorylation seems to be an important process in the regulation of CoQ biosynthesis, and COQ4 has been defined as a regulatory protein, we were interested in determining if COQ4 was a phosphoprotein.

In order to do so, human COQ4 sequence and some COQ4 ortholog sequences from model organisms with different phylogeny (mouse, zebra fish, yeast and worm) were aligned and subjected to different *in silico* analysis for phosphorylation prediction. Conservation in the position of the phosphorylation site could suggest that the function of the phosphorylation event is important for the organism. We selected potentially phosphorylatable residues, such as serine, threonine and tyrosine, which were conserved in at least 2 of these species (human's, among these two).

In total, 22 selected residues were analysed by seven different *in silico* phosphorylation prediction tools or phosphorylation databases. For each selected residue, a tools score was calculated, representing the number of tools for which the residue was positive for phosphorylation (tools score: 0-7) (Table 3.1).

Table 3.1. COQ4 protein phosphorylation prediction.

Selected conserved residues					Tools score		3D structure score		Solvent accessibility score	
Human	Mouse	Fish	Worm	Yeast	Human	Mouse	Human	Mouse	Human	Mouse
S106	**S107**	**-**	**S76**	**T153**	**6**	**6**	**2**	**2**	**3.75**	**4**
S108	**S109**	**S107**	**-**	**-**	**5**	**6**	**2**	**2**	**4**	**3.5**
T107	**-**	**-**	**-**	**T154**	**5**	**-**	**2**	**-**	**4**	**-**
S31	S32	-	-	T77	5	5	1	1	3	3
S122	S123	T121	T92	T169	4	5	1.5	1.5	2.5	2.75
T77	T78	T76	T46	T123	4	4	1.5	1.5	2.75	2.25
T140	T141	T139	-	T187	4	4	2	2	3.75	3.75
S45	T46	S44	-	-	4	4	1	1	4	4
S117	S118	-	-	-	4	4	2	1.5	4	4
T144	T145	-	-	-	4	4	2	2	3	4
S137	S138	T136	S107	S184	4	1	2	2	4	4
T255	S256	-	T225	T302	3	4	2	2	3.75	4
T168	T169	T167	-	-	3	3	0	0	0.25	0.25
T190	T191	T189	-	-	3	3	1.5	0.5	2	2
T109	**T110**	**T108**	**T79**	**-**	**3**	**2**	**2**	**2**	**3**	**4**
S56	-	S55	S25	S102	2	-	1	-	3	-
S210	S211	-	-	-	2	4	0.5	1.5	3.5	3.75
S216	S217	-	-	-	2	3	0	0	1	4
T44	T45	T43	-	-	2	2	1	1	2	3
T81	T82	T80	-	-	2	2	0	0	2.75	1.75
T3	T3	-	-	-	2	1	-	-	-	-
T174	T175	T173	T144	-	1	1	2	2	2.75	2.75
-	T247	-	S216	T293	-	2	-	0	-	4

The tools score is coloured in a gradient from green (the highest values) to red (the lowest values).

Phosphorylation at a site depends on many factors, including the structure and solvent accessibility of the phosphorylation site. Phosphorylation, as well as other post translational modifications, predominantly occurs in regions of intrinsic disorder [212]. Disordered regions provide a flexibility that facilitates different conformational requirements for binding the modifying enzymes. Intrinsically disordered regions are often found as flexible linkers or loops connecting domains [496].

In order to introduce 3D structure information in our study, protein structures for human and mouse were modelled using the only homolog structure available at that time, PBD 3KB4. We considered the position of the residue in the 3D model, and depending on its structural position, it manually received a score. When the residue was on the surface of the protein, in a disordered region or loop, the score was the highest, and when it was totally buried in an ordered region of the protein structure, the score was the lowest (3D structure score: 0-2). We also considered the solvent accessibility predicted by JPred, giving the maximum score when the residue was exposed in a disordered region and the minimum score when it was buried and inside an ordered region (solvent accessibility score: 0-4).

We compiled the three scores for the 22 different residues and selected the ones with the highest scores. The tools score is considered to be the most relevant one, since it results from an assemblage of diverse *in silico* tools, each of them employing different algorithms to calculate the probability prediction, each of one with its advantages and limitations.

The three amino acids with the highest scores were contiguous, in the positions 106 to 108, serine, threonine and serine. Threonine 109 was also considered but reached significant lower scores. If we travel to the predicted 3D structure, we can localise these four residues in a loop, probably flexible, that would allow the conformational requirements of a post-translational modification such as phosphorylation (Figure 3.15.B). Moreover, and interestingly, they are localised in the opposite side (Side D) to the putative dimerization interface (Side C) (Figure 3.11). This loop appeared after Nostoc in the evolution since it is absent from its sequence. In addition, the residues flanking this putative phosphorylation loop are very conserved (Figure 3.15.A), which could mean that a conserved kinase able to recognize this region is responsible for the phosphorylation.

A.

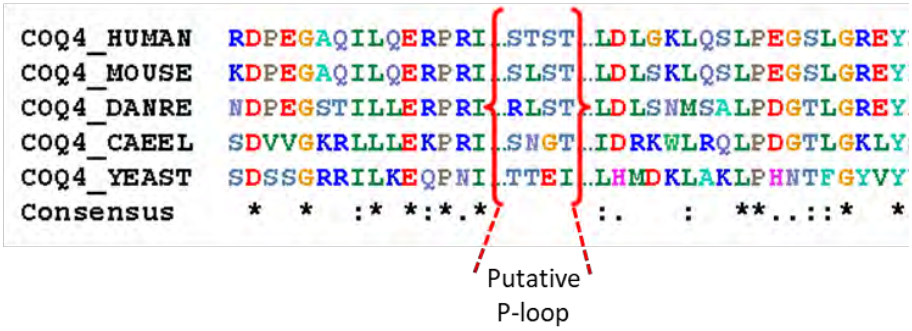

B.

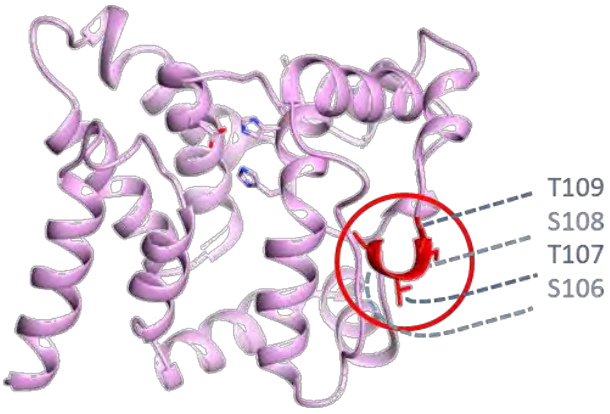

Figure 3.15. Putative phosphorylation loop in COQ4 protein.
Phosphorylation prediction revealed a putative phosphorylation loop (P-loop), which is conserved in terms of presence of at least 2 serine or threonine residues (A). Flanking residues of this putative phosphorylation loop have a high degree of conservation (A). If we localise these 4 residues in the 3D model, they are located in a probably flexible loop, towards the surface of the protein (B).

Of note, there is evidence of phosphorylation in COQ4 but only from global phosphoproteomics MS assays, reported in PhosphoSitePlus. Four high-throughput studies found the same residue (from human, mouse and rat) in a phosphorylated state. S108 human residue was found phosphorylated in HeLa and K562 cells [497]. It is conserved in mouse (S109), in which it was found phosphorylated in three different studies, in murine pancreatic cells [498], hearts [499] and kidneys [500]. The same residue from rats (S108) was found phosphorylated in different rat tissues [501]. For all these reasons, we selected these four residues for ulterior experimental studies (see Chapter 4, section 4.2.1).

Mutations affecting COQ4: mutations found in patients

35 patients from 26 families with *COQ4* mutations have been reported to have a CoQ_{10} deficiency. There are 22 published *COQ4* variants associated to this disease in the literature. Here, we add 2 more to the list: the intronic mutation of P105 and the homozygous mutation of P108 and P109 (See Chapter 2, Section 2.2.3.). The reported mutations are distributed throughout the entire coding sequence (CDS), being less frequent in the first and last exons, and especially abundant in exon 5. All the residues involved in point mutations causing disease occur in conserved positions (Figure 2.14).

Figure 3.16 shows the localization of the residues affected by missense (and one nonsense) mutations from all the published *COQ4* patients in the 3D protein structure. We have classified the mutations in 2 groups, depending on the severity of the disease: early-onset severe multisystemic disorder (which corresponds to Group 1 and 2 of the age-of-onset classification done in Chapter 1) and milder disease with adolescence progression (which corresponds to Group 3) (see Chapter 1, section 1.2.4). We have added the homozygous mutation found in P108 and P109, F146C, to the less severe group, because the age of last examination of these patients was 17 years old.

The mutations seem to accumulate in a face of the protein surface which contains the putative lipid binding pocket, face A (Figure 3.16). Additionally, the mutations classified in the milder disease group, except for the F146C mutation, appear to be buried in the protein structure, while the majority of the mutations classified in the severe group seem to be exposed on the surface of the protein. This may have a significance, reinforcing the idea that COQ4 surface interactions are important for its function.

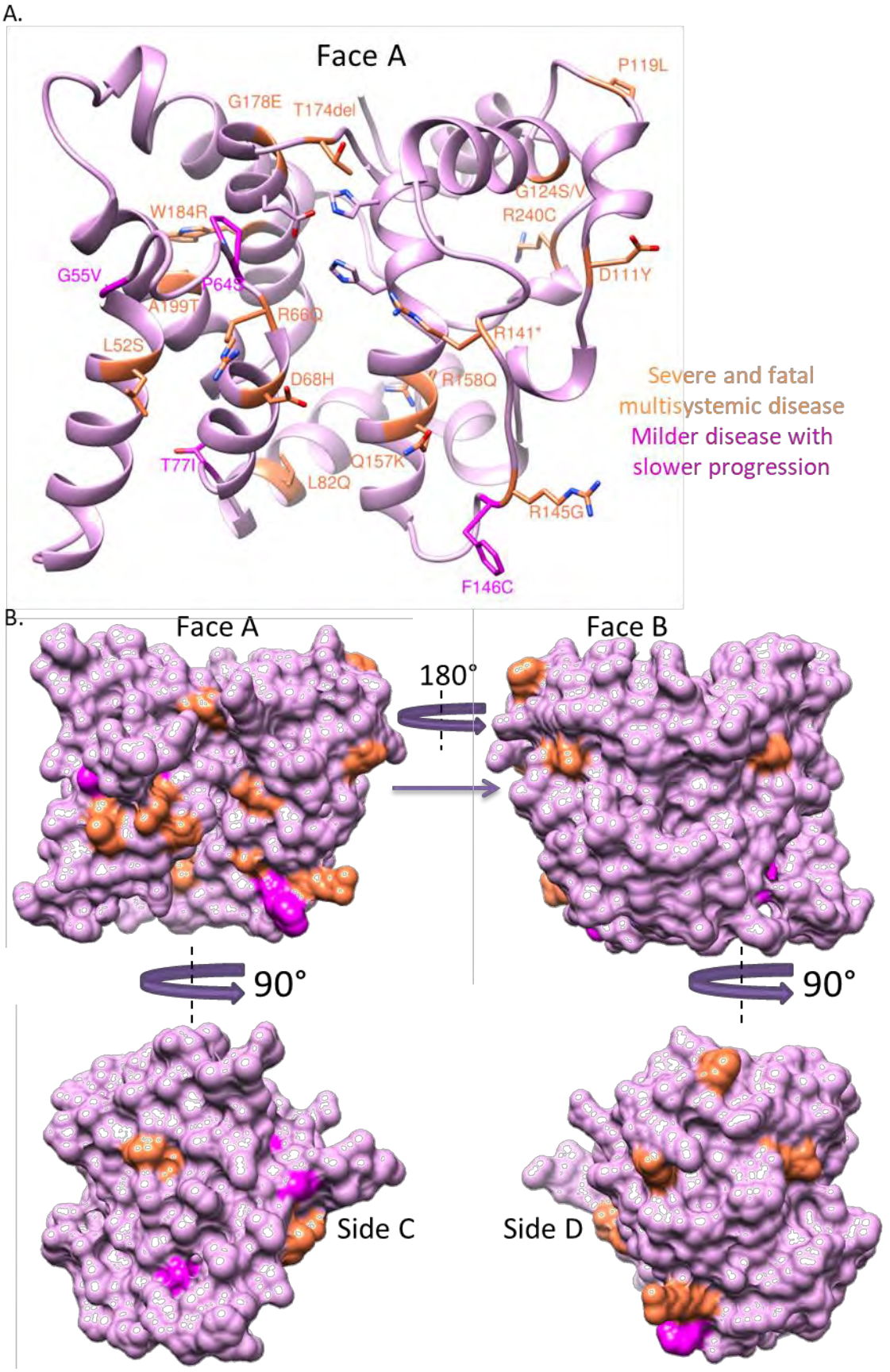

Figure 3.16. Patients' mutations mapped on human COQ4 protein structure model (PDB template: 6E12).

(A). Surface models showing the mutated residues' distribution on the surface of the protein (B). Mutated residues are labelled in orange or pink, depending of the severity of the disease manifested in the patients.

3.2.2. *COQ4* cellular models' generation

COQ4 KO cell line was generated in a HEK 293T-Rex/Flp-In

i. Selection of the cell line HEK 293T-Rex/Flp-In

HEK 293T-Rex/Flp-In WT cell line was chosen to generate our *COQ4* KO mutant cell line. Human embryonic kidney (HEK) 293T cells grow fast so big amounts of cells can be obtained in a short period of time and they can be efficiently transfected. Moreover, these cells are very convenient for biochemical approaches since they can be detached from the plate surface easily, considerably shortening the processing time for cell collection. The specific Flp-In genomic background was selected because it contains a single stably integrated FRT site at a transcriptionally active genomic locus. This feature would allow us to easily insert different versions of *COQ4* gene in the *COQ4 KOs* genome by flippase (Flp)-FRT site directed recombination in this FRT-site and then, control their expression by inducing with doxycycline (See Materials and Methods, section M2.1 and Figure M.1 for more details).

ii. Selection of the Paired nickases CRISPR/Cas9 3 plasmid strategy

Paired nickases CRISPR/Cas9 3 plasmid strategy was used to generate the *COQ4 KO* in a HEK 293T-Rex/Flp-In WT background. Paired nickases strategy was selected over the WT Cas9 in order to decrease the number of off-targets. Cas9-D10A or Cas9 nickase is a catalytically mutant Cas9 that is able to introduce a SSB with the same specificity as a regular Cas9 nuclease. Two paired nickases guided by two gRNAs targeting adjacent regions were used in order to reduce off-target activity.

iii. gRNA design and off target analysis

Guide RNAs (gRNAs) were designed to target exon 2, to make sure the expression of COQ4 protein would be effectively disrupted. Exon 1 was not targeted in order to avoid a possible alternative translation initiation, which would more likely occur at the beginning of the transcript [450].

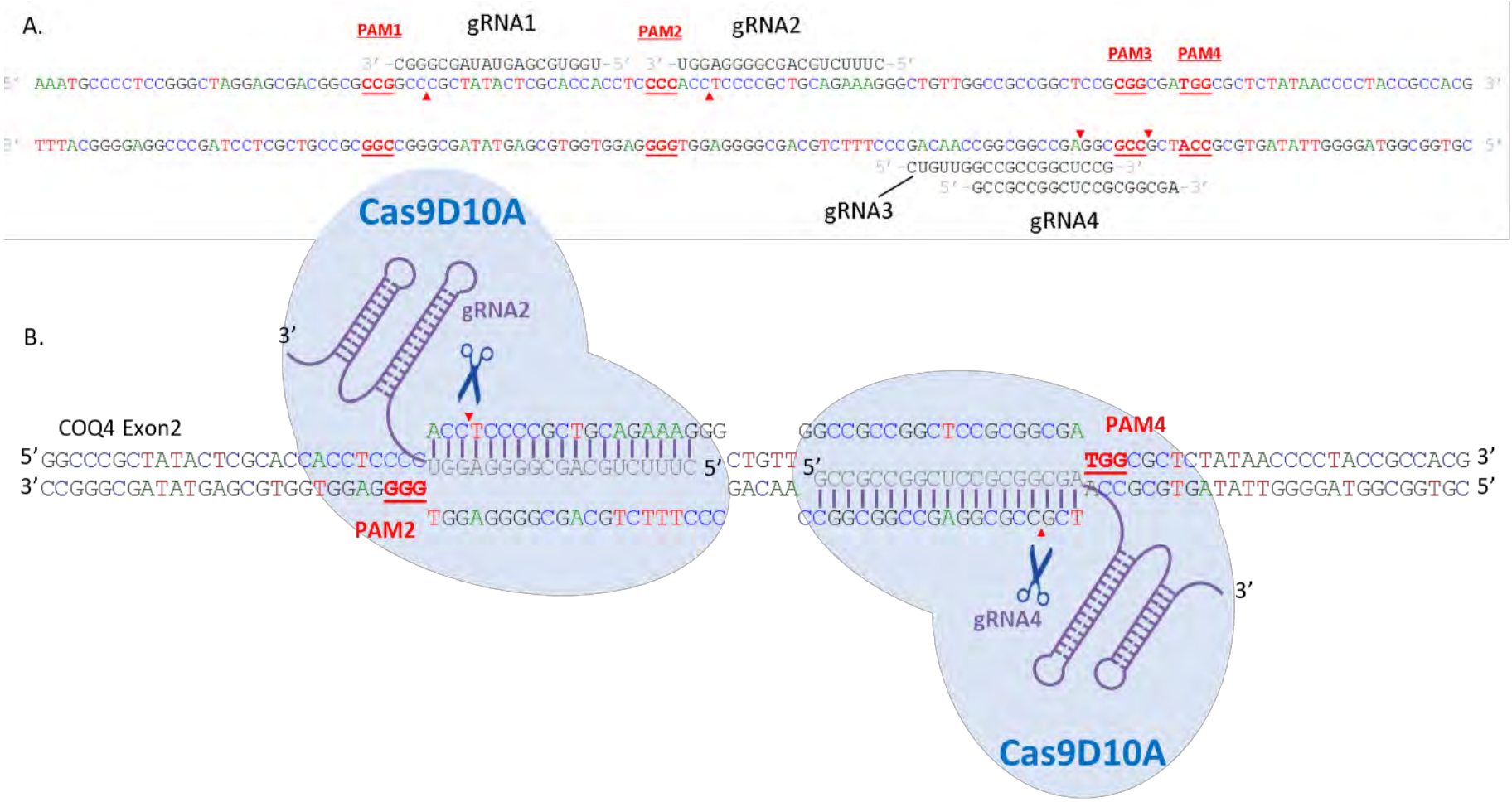

Figure 3.17. Designed gRNAs for CRISPR paired nickase strategy.
(A) Four different target sequences in *COQ4* exon 2 (2 forward and 2 reverse), adjacent to PAMs, were used for gRNA design. 4 different combinations of Forward and Reverse gRNA were assayed (gRNA1-3, gRNA1-4, gRNA2-3, gRNA2-4). (B) Schematic representation of the paired nickases-gRNAs complexes formed in *COQ4* exon 2 genomic sequence, highlighting the cleavage point where the nickases produce the single-strand breaks (SSBs) (one in each strand). Sequences of gRNAs 2 and 4 have been used as an example.

Four different sequences adjacent to PAMs were selected to design the gRNAs (Figure 3.17). These gRNAs were designed to target *COQ4* exon 2 (2 forward and 2 reverse), and 4 different combinations of Forward and Reverse gRNA were used. Potential off-target sites were analysed computationally, and while each gRNA separately has predicted off-target sites, the 4 pairs of gRNAs were considered to have high quality, with 0 predicted off-target sites. (Table 3.2).

Table 3.2. Off-target analysis of selected gRNAs.

Off-target analysis of single gRNAs			
gRNA	**Quality score**	**On-target locus**	**# of off-target sites**
gRNA1	97 (high)	chr9:-131,085,324	29 (4 are in genes)
gRNA2	49 (medium)	chr9:-131,085,348	384 (56 are in genes)
gRNA3	66 (high)	chr9:+131,085,373	171 (67 are in genes)
gRNA4	70 (high)	chr9:+131,085,379	167 (85 are in genes)

Off-target analysis of gRNAs pairs for paired nickases				
CRISPR pair	**gRNAs**	**Nt between cleavage sites**	**Quality score**	**# of off-target sites**
CRISPR1	gRNA1+gRNA3	60	65 (high)	0
CRISPR2	gRNA1+gRNA4	66	62 (high)	0
CRISPR3	gRNA2+gRNA3	34	17 (medium)	0
CRISPR4	gRNA2+gRNA4	40	35 (high)	0

iv. Several clones with deletions at exon 2 of COQ4 were isolated and they did not express COQ4 protein

WT HEK293T-Rex/Flp-In cells were transfected with 3 plasmids (pCMV-Cas9-nickase GFP, pU6gRNA1/2, pU6gRNA3/4) (Figure 3.18.A). 48h after transfection, they were FACS-sorted by GFP fluorescence (Figure 3.18.B), and the cells with high levels of GFP fluorescence were selected (Figure 3.19). The GFP-transfection efficiency was between 20 and 25% (Figure 3.19.D). For each reaction, one pool and several individual clones were grown and genotyped by PCR amplification of the genomic targeted region (Figure 3.18.C and D). This amplification would lead to a 499 pb fragment, according to the designed genotyping primers.

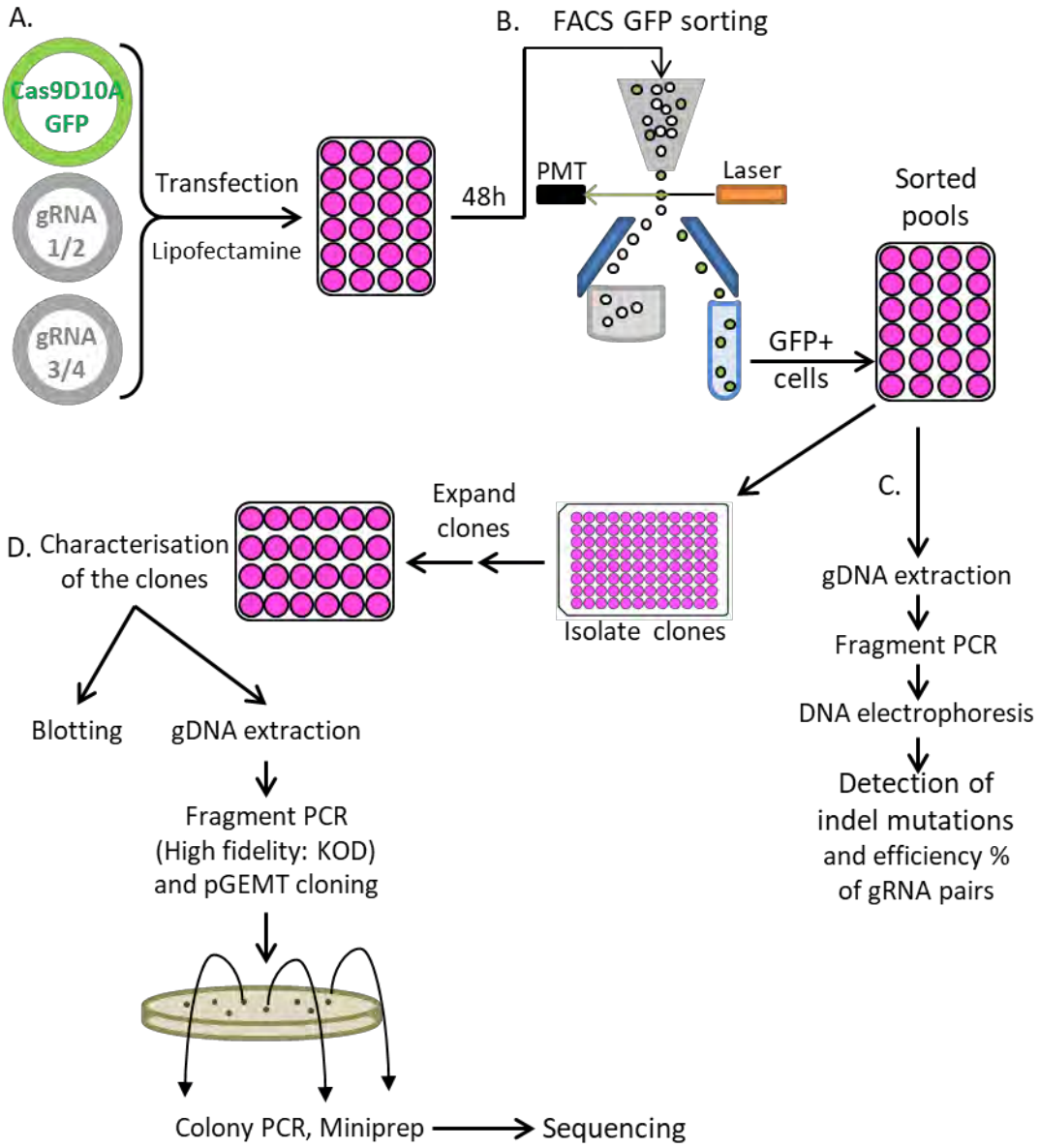

Figure 3.18. Generation of *COQ4* KO cells overview.
(A) Wild type HEK293T-Rex/Flp-In cells were transfected with 3 plasmids (pCMV-Cas9-nickase GFP, pU6gRNA1/2, pU6gRNA3/4), and 48h after transfection, (B) they were FACS sorted for GFP fluorescence. Sorted pools were grown and genotyped by PCR amplification of the genomic targeted region (C). Clones from each pool were isolated, expanded and characterised (D). They were genotyped by PCR, pGEMT cloning and sequencing. COQ4 western blot analysis of total protein extracts of these cells was also performed to check the lack of COQ4 expression.

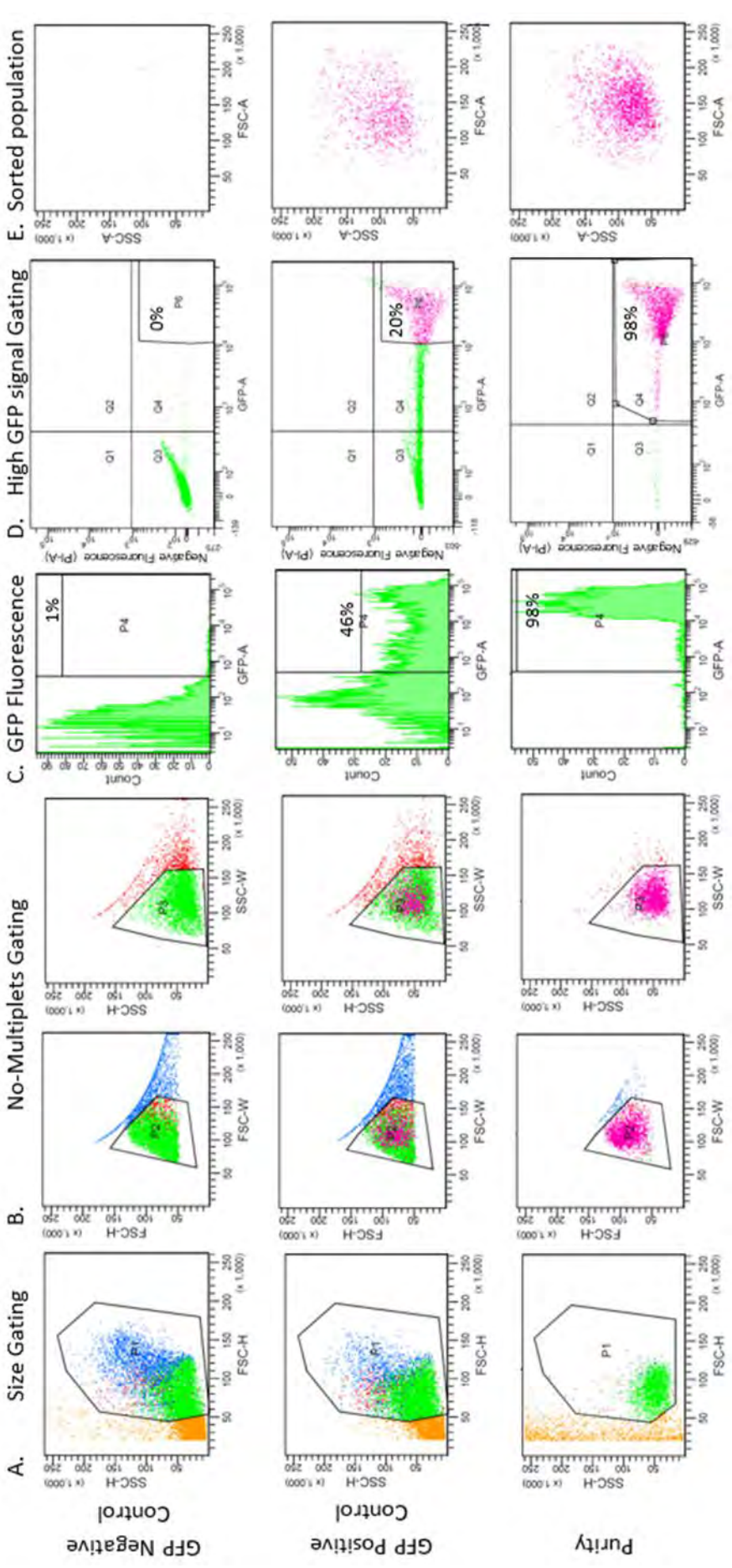

Figure 3.19. Fluorescence-activated cell sorting (FACS) Gating Strategy for GFP sorting.
Each row of graphs corresponds to a different sample. Sorted GFP positive control (second row) was re-sorted to evaluate the purity of the sorted sample (third row). Each column of graph corresponds to each step of gating. All events are labelled in yellow, while the different gated populations (P1-P6) are labelled in different colors. (A) First level gating (P1: blue), forward versus side scatter (FSC vs SSC) dot plots for identifying our cell population and excluding debris (at the bottom left corner), based on size and granularity. (B) Doublet and multiplet exclusion gating, FSC-Height (H) vs FSC-Width (W) (P2: red) and SSC-H vs. SSC-W (P3: green) dot plots, for increasing the purity and gating out doublets and clumps of cells. (C) GFP fluorescence histograms, for identifying cells with GFP expression (P4). (D) GFP vs a negative fluorescence dot plots (P6: pink), to gate

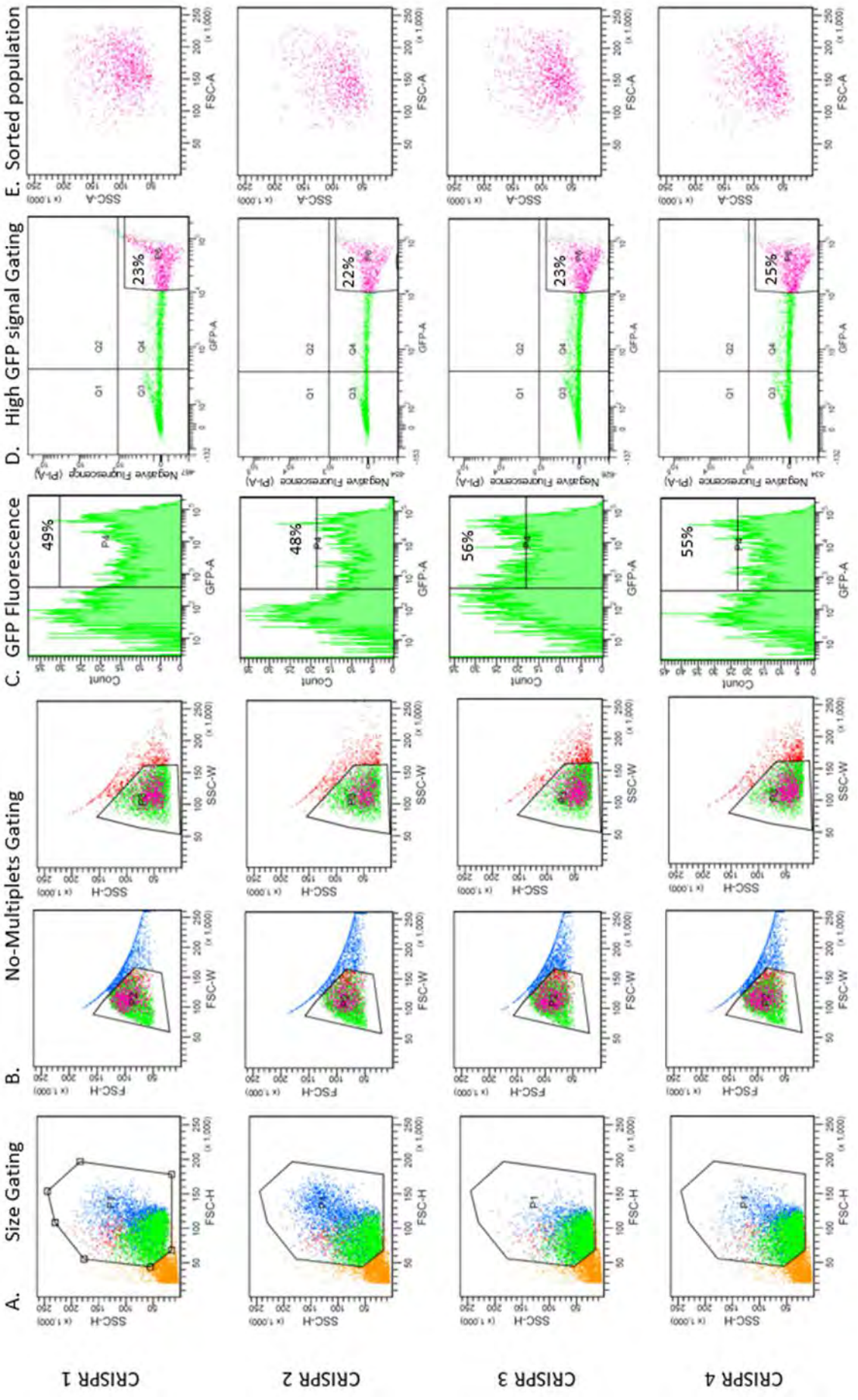
A. Size Gating
B. No-Multiplets Gating
C. GFP Fluorescence
D. High GFP signal Gating
E. Sorted population
CRISPR 1
CRISPR 2
CRISPR 3
CRISPR 4
49%
48%
56%
55%
23%
22%
23%
25%

PCR revealed that COQ4 and positive control CRISPR reactions had some amplicons that were smaller to the expected size, indicating that deletions may have occurred (Figure 3.20.A and B). Further genotyping techniques, as detecting mismatches or surveyor nuclease test, were not needed because all the CRISPR reactions tested appeared to produce a big deletion, easily detectable by PCR amplification.

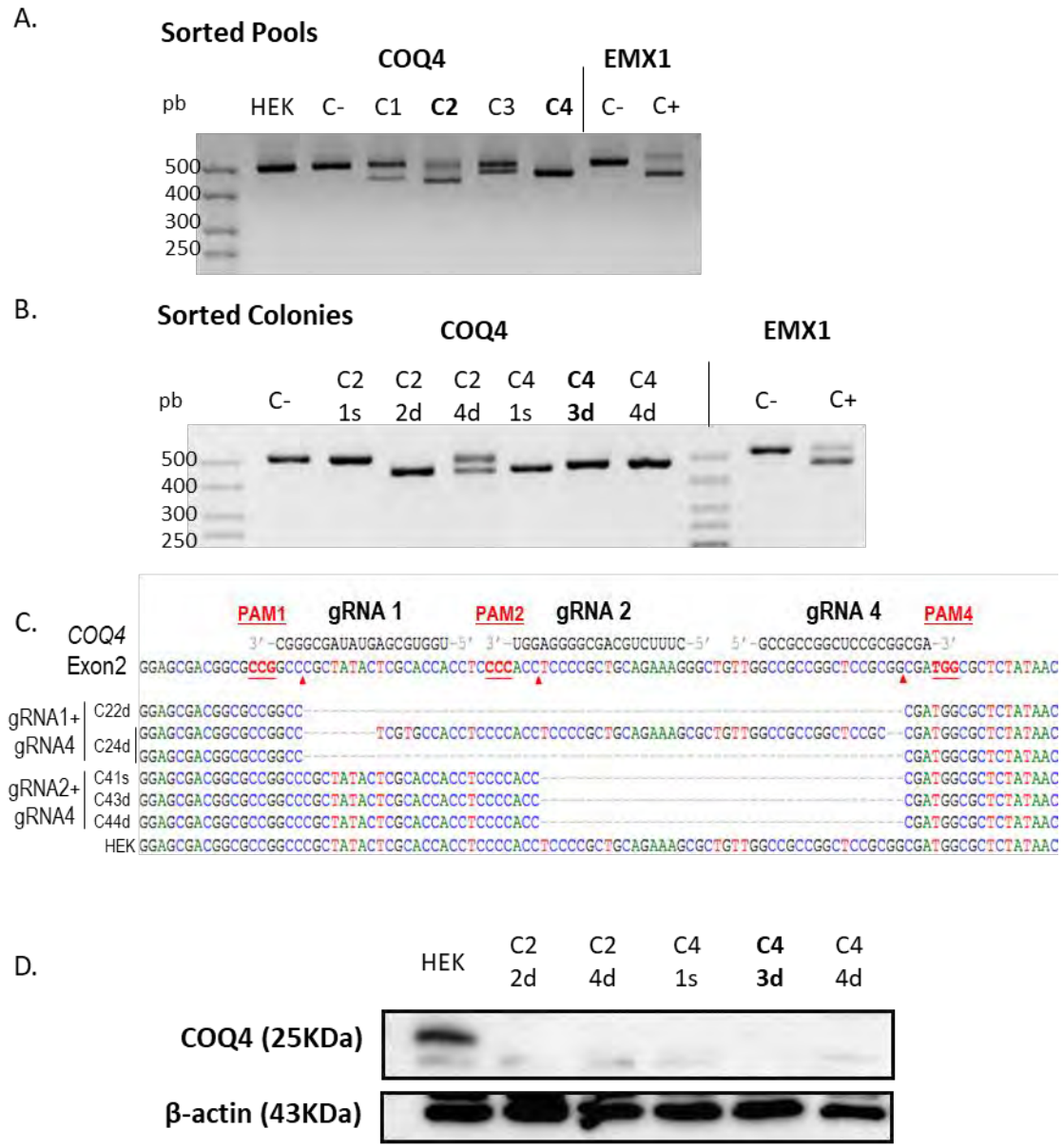

Figure 3.20. Identification of *COQ4* KO cell lines.
(A) PCR amplification of a genomic fragment containing the gRNAs binding site in COQ4 exon 2 revealed the presence of deletions in some pools of CRISPR transfected cells. C2 and C4 seemed to be the most efficient ones. Non-transfected cells (HEK) and cells transfected with the CRISPR negative control (C-) were used as negative controls. Genomic EMX1 fragment was also amplified in the cells that were transfected with the CRISPR positive control (gRNAs guided to a EMX1 genomic region) and with the C-. (B) The same PCR amplification was performed with genomic DNA from some cloned derived from C2 and C4 pools, and 5 of them showed a deletion in the amplified fragment. (C) This was confirmed by pGEMT cloning, colony PCR and sequencing. (D) None of the clones express COQ4 protein, analysed by immunoblots.

At first, PCR amplification of pools revealed different efficiency of producing a deletion for the different gRNAs pairs, being CRISPR2 (C2) and CRISPR4 (C4) more efficient (Figure 3.20.A). Then, 6 individual clones from these CRISPR reactions were genotyped by PCR (Figure 3.20.B). 5 of them showed a clear deletion in the targeted region, and this was confirmed by pGEMT cloning, colony PCR and sequencing (Figure 3.20.C and Table 3.3).

One clone of CRISPR2, C22d showed a deletion of 66 nt between the 2 Cas9 cutting sites, and the other one, C24d, showed 2 different sequences, the same 66 nt deletion and also the original sequence with short deletions (8 and 2 nt) close to the cutting sites (Figure 3.20.C and Table 3.3). All analysed clones coming from CRISPR4 reaction harboured a deletion of 40 nucleotides (Figure 3.20.C and Table 3.3).

All these deletions would produce a drastic change in COQ4 protein, that would lead to its lack of function (Table 3.3). In the clones from CRISPR2 reaction, the deletion causes a deletion of 22 amino acids in exon 2, probably leading to a non-functional COQ4 protein. In the clones from CRISPR4 reaction, the deletion would produce a frameshift of the ORF and a premature stop codon, producing the lack of COQ4 in these cells.

Western blot analysis of total protein extracts of the cells showed an absence of COQ4 protein in all mutant clones (Figure 3.20.D). From now on, all experiments have been performed with one of the obtained clones, 43d, which we are going to call *COQ4* KO cell line. We chose this clone because it would have a frameshift and an early truncated protein, which is the most similar situation to a real knock-out.

Table 3.3. *COQ4* cDNA and predicted protein changes in CRISPR clones.

Clones	Deletion length	cDNA mutation	Predicted protein change
22d 24d	66nt	c.107_172del	p.Leu37_Ala58del
24d	8nt + 2nt	c.107_114del_171_172del	p.Pro35Leufs*35
41s 43d 44d	40nt	c.133_172del	p.Ser45Argfs*15

COQ4 KO expressing different versions of COQ4

In order to evaluate COQ4 function, we transfected *COQ4* KO with different versions of *COQ4*. The transfections were performed by using a lipid-based reagent and pcDNA5 and pOG44 plasmids (See Materials and Methods, section M2.3). All COQ4 transfected

variants were contained in the pcDNA5 plasmid (the transfected plasmids are detailed in Materials and Methods, Table M.12). After transfections, the expression of the transgene was induced with different amounts of doxycycline and measured by western blot. We were able to obtain different cell lines KO in *COQ4*, which stably expressed different versions of the gene. Details of levels and effects of expression of these ectopic *COQ4* variants will be explained in the next sections (See Chapter 4, section 4.2.1).

3.2.3. *COQ4* molecular localisation characterisation

As we just discussed, different *in silico* approaches classify COQ4 as a mitochondrial protein. Additionally, some experimental assays found it located inside the mitochondria [469]. In order to experimentally test human COQ4 mitochondrial location in our cellular model, we have performed several experiments: immunofluorescence and colocalisation with mitochondrial proteins by confocal microscopy and cell subfraccionation and biochemical coexistence by western blot.

For these experiments, we used a cell line previously generated, the HEK 293T-Rex/Flp-In *COQ4* KO cell line transfected with untagged COQ4 wt gene, as well as COQ4 gene tagged in C-terminal with a FLAG-Strep tag (COQ4-FS). These cells overexpress the transfected gene, expression that it dose-dependently induced with the addition of doxycycline (DOX) to the medium, since the transgene expression is regulated by a DOX inducible promoter.

Tagged COQ4 colocalizes with TOM20 staining

To start COQ4 localisation characterisation, we used a FLAG-tagged COQ4 WT protein in the HEK 293T-Rex/Flp-In human cell line. Cells were transfected and selected with hygromycin. 48h before the immune staining, cells were seeded onto poly-D-Lysine treated coverslips. 24h before the staining, the expression of the exogenous COQ4-FS was induced by adding 0.5ng/ml of doxycycline. The day after, cells were fixed and stained. COQ4 protein was visualised in green, by using a primary mouse antibody against FLAG tag, and the anti-Mouse Alexa^{488} antibody (Figure 3.21). As a mitochondrial marker, we used the outer membrane mitochondrial protein TOM20, stained in colour red (by using a primary TOM20 antibody with conjugated fluorescence). The nucleus of the cells was stained with DAPI (See Materials and Methods, section M3.4).

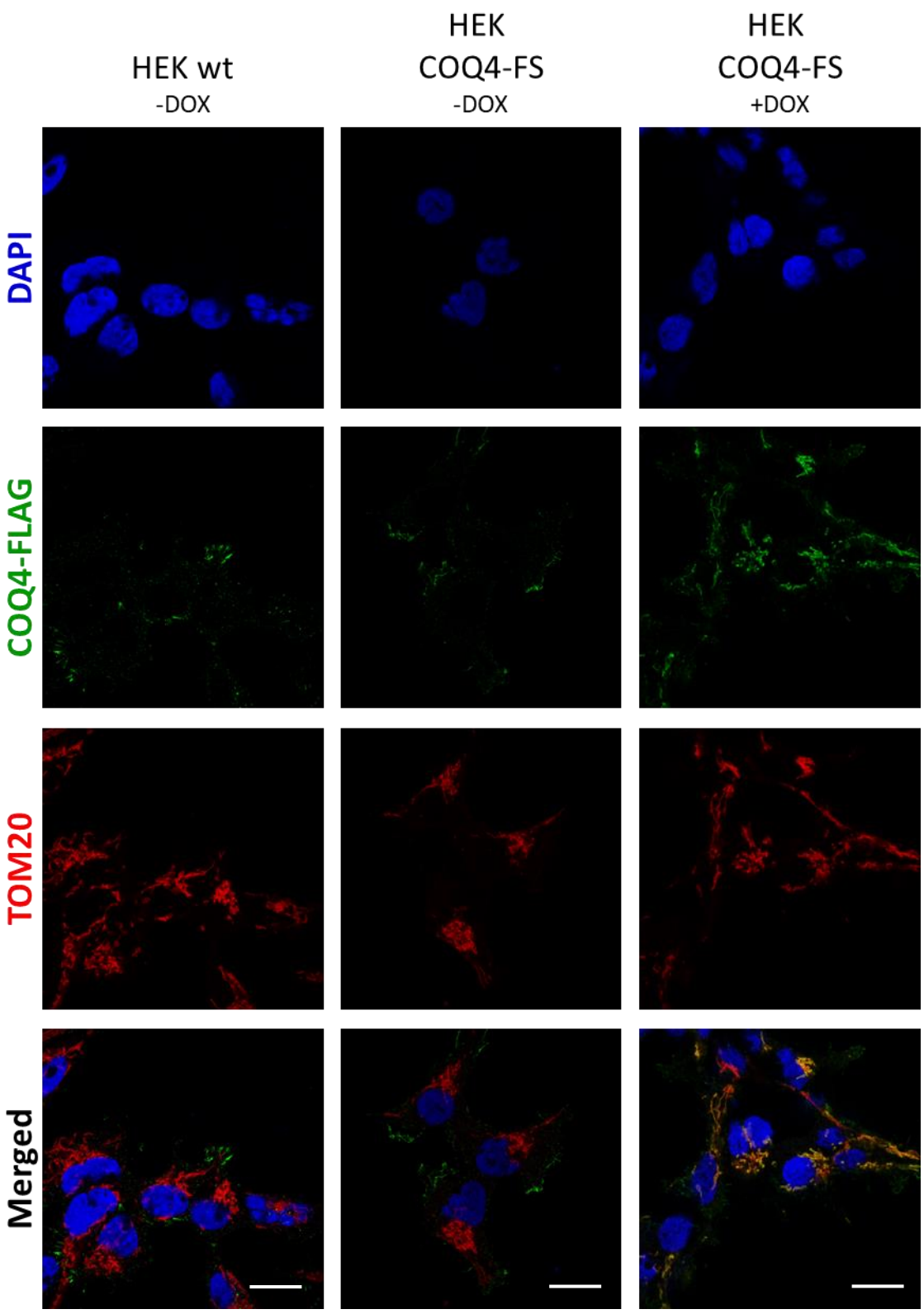

Figure 3.21. COQ4-FS colocalizes with TOM20 staining.
Immunofluorescence staining of HEK 293T-Rex/Flp-In cells (HEK wt), and the same cells transfected with a flag-strep tagged form of COQ4 (HEK COQ4-FS). Overexpression of the transgene is observed after a doxycycline treatment (+DOX: 0.5ng/ml doxycycline during 24h). Images show that in induced cells (+DOX), COQ4-FS (green) localize to the mitochondria (TOMM20 red stain), while the non-induced cells show the same pattern than the non-transfected controls. Scale bar = 15 µm.

Images of induced COQ4-FS transfected cells show that COQ4-FS green stain colocalizes to the TOM20 red stain, meaning that the overexpressed COQ4 protein seems to localize mainly to the mitochondria (Figure 3.21). As a negative control, non-transfected HEK cells as well as non-induced COQ4-FS transfected cells were also stained. Anti-FLAG antibody seems to non-specifically recognize some areas in the cellular periphery, also in both the controls. Even if we know non-induced COQ4-FS transfected cells are also expressing COQ4-FS protein to some extent due to a leaky effect (see Chapter 4, section 4.2.1 and Figure 4.8), they do not show the green and red colocalization pattern, but they are more similar to negative controls. This is probably is due to its leaky expression, that it is not enough to be visualized with the antiFLAG antibody.

Endogenous and tagged COQ4 follow the same localization pattern than mitochondrial proteins after mitochondrial fractionation

COQ4-FS transfected HEK cell line was expanded and fractionated in different subcellular compartments by differential centrifugation. Samples of total homogenate (nucleus free), cytosol, crude mitochondria, mitochondrial associated membranes (MAMs) and pure mitochondria were run in acrylamide gels and subjected to western blot (Figure 3.22). Mitochondrial external membrane protein TOM20 is predominantly in the mitochondrial fractions, and not in the cytosol. It also appears partially in the MAMs fraction, which has been described before [502]. ATAD3A protein is mainly a mitochondrial IMM protein, where the N-terminal domain interacts with the OMM, being essential for mitochondria-ER contacts (See Chapter 5, section 5.1.6), and the C-terminal domain localizes in a specific matrix compartment, where it is associated with nucleoids [175]. It can be observed that it follows a mitochondrial localisation pattern, the same as TOM20, being also present in MAMs, which has been also reported before [4]. Remarkably, both endogenous and tagged-COQ4 protein follow the same fractionation pattern than mitochondrial proteins TOM20 and ATAD3A, being predominantly present in pure mitochondria, but also a small fraction in the MAMs and in the cytosolic fractions (Figure 3.22). Lack of lactate dehydrogenase A (LDH-A) signal in pure mitochondria [503] confirms the purity of the fractions.

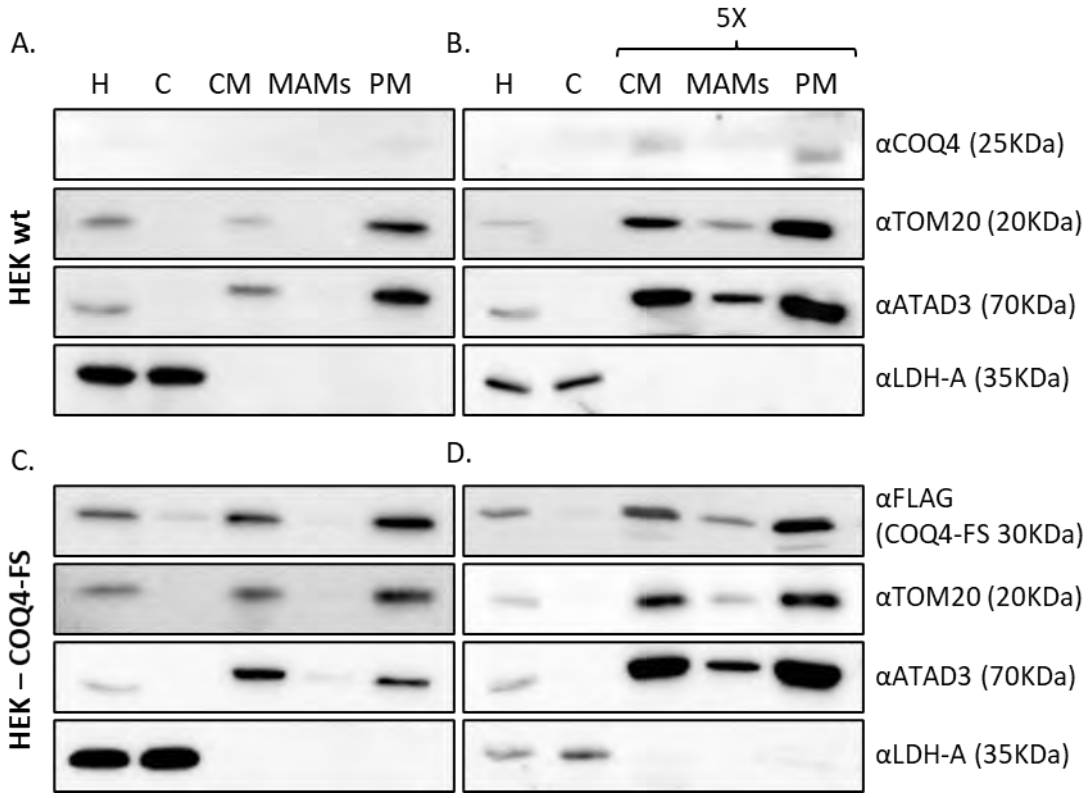

Figure 3.22. Endogenous and tagged COQ4 are enriched in mitochondrial fractions.
Cellular and mitochondrial subfractionation of HEK 293T-Rex/Flp-In cells (HEK wt) (A and B), and the same cells transfected with a flag-strep COQ4 (HEK COQ4-FS) (C and D). TOM20 is a mitochondrial outer membrane protein, ATAD3 is a mitochondrial inner membrane protein and LDH-A is a cytosolic soluble protein. Endogenous COQ4 expression is very low (A), so the same blots with a higher concentration of the mitochondrial fractions (5x) are shown in B and D. H: Homogenate, C: Cytosol, CM: Crude Mitochondria, MAMs: Mitochondrial associated membranes, PM: Pure Mitochondria.

Endogenous COQ4 and COQ4-FS are resistant to mild trypsin treatment.

Whether the protein is in the mitochondrial matrix can be assayed biochemically by incubating mitochondria with trypsin (5mg/ml trypsin at 30ºC) in a hypotonic buffer. In this hypoosmotic conditions, mitochondrial outer membrane is firstly broken, and then, trypsin sequentially degrades the intermembrane space proteins, the external face of the IMM, the IMM and finally if incubated for enough time, the matrix (Figure 3.23.C).

Immunoblots show that endogenous COQ4 is protected from trypsin digestion in the same manner than HSP60, which resides in the mitochondrial matrix (Figure 3.23.A). This also occurs with the COQ4-FS tagged protein, meaning that it behaves similarly to the endogenous protein, at least, in terms of localisation (Figure 3.23.B). At the same

time, we can see how proteins belonging to the mitochondrial outer (TOM20) or inner (TIM23, ATAD3A) membranes are being sequentially degraded with the same treatment.

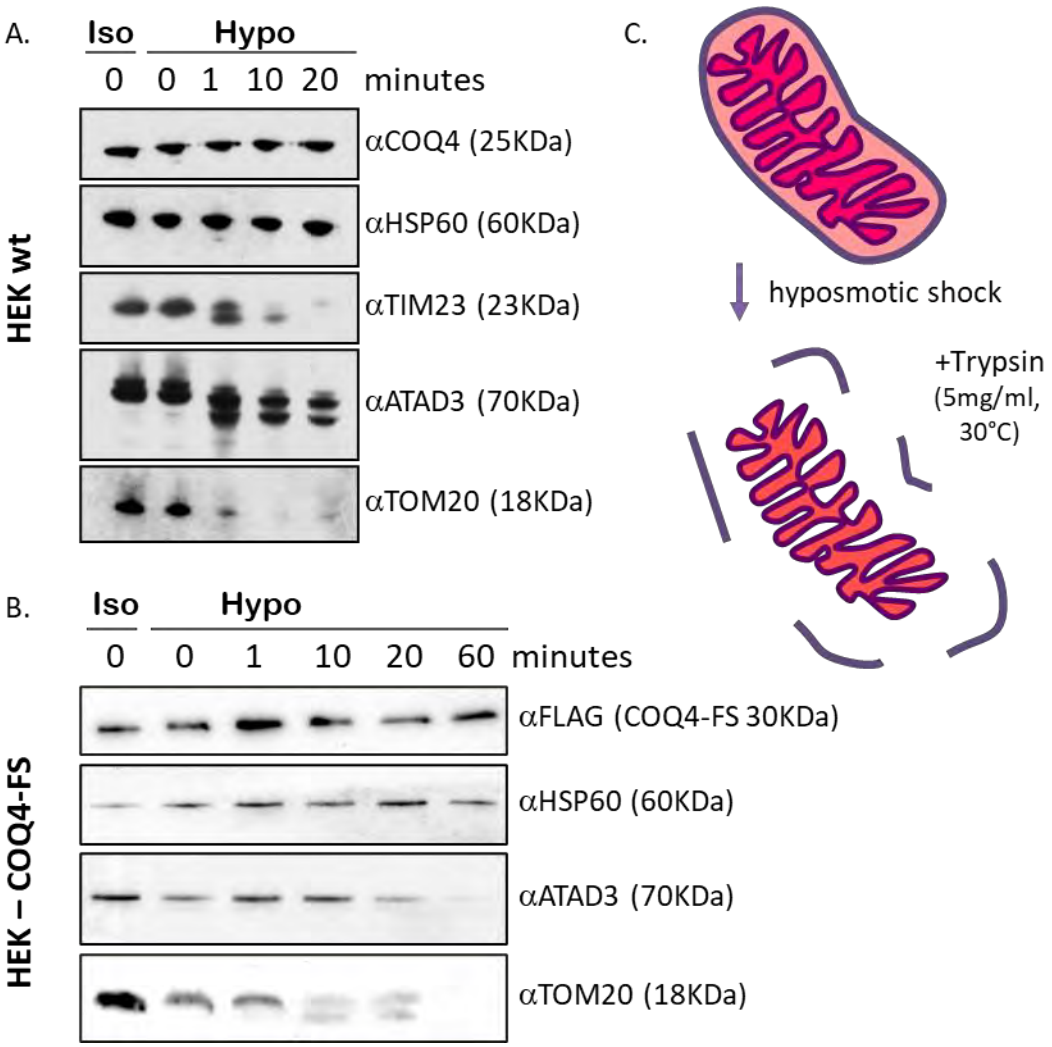

Figure 3.23. Endogenous and tagged COQ4 are protected from a mild trypsin treatment.
Mild trypsin treatment of pure mitochondria sequentially degrades the different mitochondrial compartments: outer membrane (TOM20), intermembrane space, the inner membrane (ATAD3) and finally, the matrix (HSP60). Immunoblots show that endogenous COQ4 (A) and FS-tagged COQ4 (B) are both protected from trypsin digestion in the same way that HSP60, which is a matrix protein. (C) Schematic representation of the experiment, in which the combination of a hypoosmotic buffer and trypsin treatment (5mg/ml trypsin at 30°C), firstly breaks the outer membrane, and then the rest of components that are more protected.

3.3. Conclusions

In this chapter, we studied *COQ4* gene and protein characteristics and we generated a *COQ4* KO cell model. The main conclusions derived from this work are the following:

i. Based on studies with COQ4 orthologues, it could be possible that human COQ4 protein forms a homodimer, binds a lipid in a lipid binding pocket and chelates a divalent cation in the very conserved putative zinc-ligand motif, HDxxH-$(x)_{10}$-GE.

ii. It could be possible that human COQ4 phosphorylation in the residues S106, T107, S108 and T109 is important for COQ4 function.

iii. Mutations from patients are distributed along the whole protein (in a human COQ4 protein model), mainly exposed on the surface of the protein in one face of the protein, indicating that COQ4 surface interactions in this face of the protein could be important for its function.

iv. COQ4 has a N-terminal MTS, and the mature protein seems to reside inside the mitochondrial matrix.

v. CRISPR-Cas9 paired nickases 3-plasmid assay is a useful method for generating a *COQ4* KO cell model in a HEK 293T-Rex/Flp-In background.

Chapter 4

Chapter 4.

COQ4 participation in CoQ_{10} Biosynthesis and mitochondrial respiratory chain

4.1. Introduction. CoQ biosynthesis pathway from bacteria to eukaryotes

CoQ is an isoprenoid quinone endogenously synthesized by organisms belonging to all domains of life [381]. The length of the polyisoprenoid tail differs among species (6 isoprene units in the yeast *Saccharomyces cerevisiae*, 8 units in the bacteria *Escherichia* coli, 9 or 10 units in mouse and 10 units in humans). The tail gives CoQ extremely hydrophobic properties, which therefore localizes in cellular membranes.

In eukaryotes, CoQ is synthesized by a set of nuclear-encoded proteins that reside in the matrix side of the mitochondrial inner membrane, through a pathway that is not still completely understood. It has been proposed that, although most eukaryotic CoQ is produced in the mitochondria, some amount of CoQ may be generated in different cellular compartments, such as Golgi apparatus or ER [504,505], although it is controversial because the CoQ biosynthesis proteins are located inside mitochondria[381].

Most of the work on CoQ biosynthesis has been done in *Saccharomyces cerevisiae*, in which at least 13 yeast genes (*coq1 – coq11*, *Yah1*, *Arh1*) have been identified as players of the process. Some of the products of these genes assemble in a multienzymatic complex (CoQ complex) located in the matrix side of the IMM [292,464–466,506].

Orthologues of most of the yeast *coq* genes have been identified in humans [380], but the assembly and regulation of the CoQ complex have not yet been wholly demonstrated in this case. A similar complex has been described in *E.coli,* with the peculiarity that it is described as a soluble cytosolic complex [413].

The synthesis of CoQ occurs via the formation of highly hydrophobic intermediates. For this reason, lipid-binding proteins have a crucial role in chaperoning these intermediates, attaching the hydrophobic tails in their binding pockets [507].

CoQ synthesis requires several processes to occur in order to get the final product. The biosynthesis pathway starts with the synthesis of the precursors of the quinone head (Figure 4.1) and the polyisoprenoid tail. Then, these two precursors are condensed to form the first lipophilic quinone intermediate of this pathway. Finally, a set of head group chemical modifications give rise to the final molecule of CoQ.

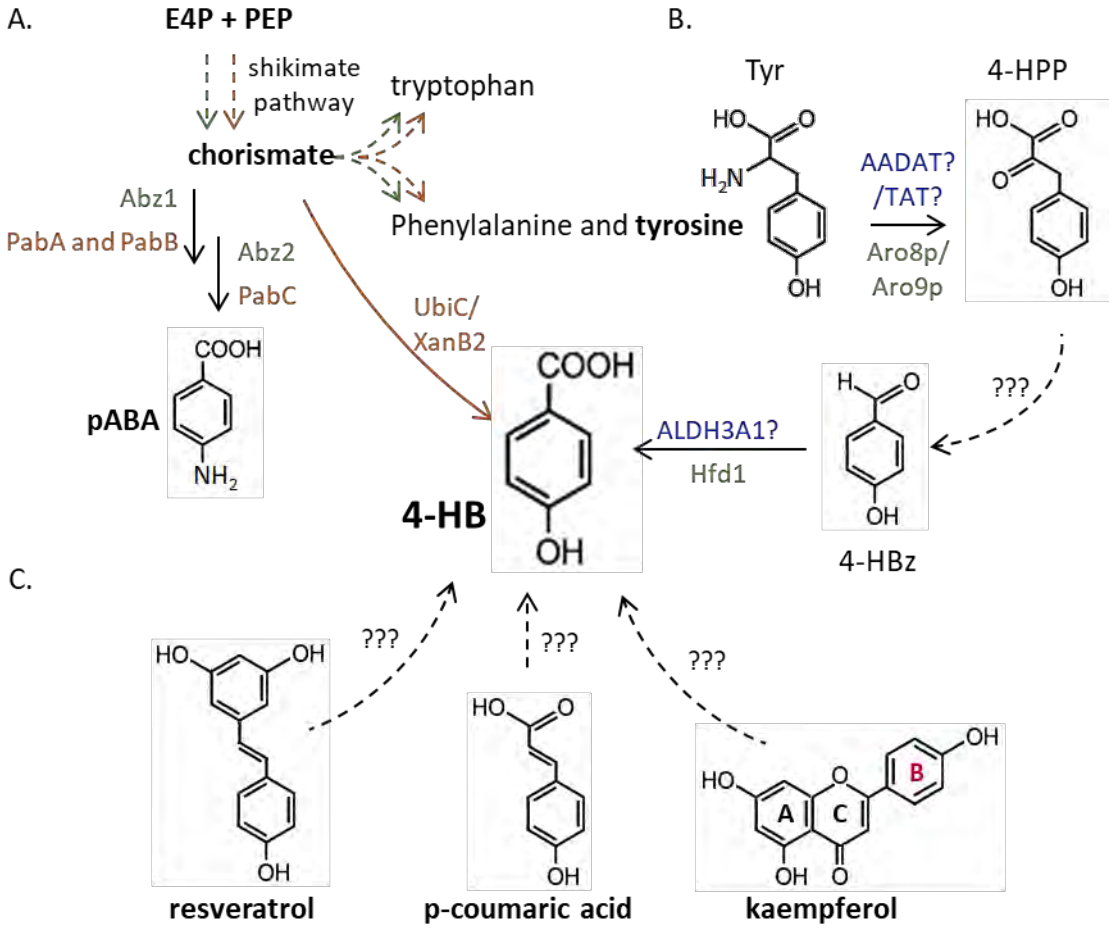

Figure 4.1. 4-HB and pABA CoQ head precursors synthesis.
(A) Chorismate is synthesized via the shikimate pathway in yeast and bacteria, and it is the precursor for phenylalanine, tyrosine, tryptophan and pABA. In bacteria, it can be directly transformed to 4-HB by UbiC or XanB2. (B) In yeast and mammals, 4-HB is synthesised from tyrosine (or phenylalanine) through some known and unknown steps. (C) Resveratrol, p-coumarate and kaemferol can also be used as 4-HB ring precursors. Black arrows indicate general pathways, while coloured arrows are pathways or reactions exclusive to bacteria (orange) or yeast (green). Dashed arrows indicate several reactions, while continuous arrows represent only one reaction. Coloured names of enzymes are unique for humans (blue), yeast (green) or bacteria (orange). Abbreviations: E4P, erythrose-4-phosphate; PEP, phosphoenolpyruvate; 4-HBz, 4-hydroxybenzaldehyde; 4-HPP, 4-hydroxyphenylpyruvate; pABA, p-aminobenzoate; 4-HB, 4-hydroxybenzoate.

4.1.1. Synthesis of the precursors of CoQ

Quinone head precursors synthesis

4-Hydroxybenzoate (4-HB) is the main precursor of the benzoquinone ring. Yeast and bacteria can synthetize it *de novo* through the shikimate pathway via chorismate [508] (Figure 4.1.A). This pathway is highly conserved in fungi, bacteria, and some plant species, but it is not present in mammals [509]. Chorismate, synthesized from erythrose-4-phosphate (E4P) and phosphoenolpyruvate (PEP) also serves as precursor for aromatic amino acids (tryptophan, phenylalanine and tyrosine) and para-amino benzoic acid (pABA) biosynthesis [510]. *E. coli* is able to directly transform chorismate to 4-HB, step catalysed by UbiC protein, the chorismate lyase [511]. Interestingly, other bacteria lack any UbiC gene or homologue and, instead, they have XanB2 protein, which converts chorismate to 3-HB and 4-HB with catalytic domains not related to UbiC [512]. Mammals and yeast use tyrosine to produce 4-HB. The pathway converting Tyr to 4-HB is poorly characterized, and only the first and the last yeast enzymes have been identified in yeast, so far (Figure 4.1.B) [381]. In this organism, tyrosine is first deaminated by the aromatic amino acid transaminases Aro8p or Aro9p, and after several unknown modifications to 4-hydroxybenzaldehyde (4-HBz), it is finally oxidized to 4-HB by the aldehyde dehydrogenase Hfd1 [513,514]. Human orthologs of Aro8p/Aro9p function in this pathway are not identified, but Aro8p/Aro9p homolog AADAT (mitochondrial alpha-aminoadipate amino- transferase) and the tyrosine aminotransferase TAT are candidates [381]. In the case of Hfd1, human ALDH3A1 (aldehyde dehydrogenase 3A1) is able to restore CoQ synthesis in yeast lacking Hfd1 [513], but ALDH3A1 participation in 4-HB production has not been demonstrated in mammals yet [381]. Mammals can also use phenylalanine to produce CoQ, which is converted to tyrosine, and then to 4-HB [515].

Resveratrol and para-coumarate can also be used as alternative ring precursors by bacteria, yeast and mammals, probably through 4-HB transformation (Figure 4.1.C) [515]. The polyphenol kaempferol has also been described to be an alternative biosynthetic ring precursor. While in yeast its use was very limited, in mammals it has been shown to be a precursor of the ring, even inducing the increase of CoQ levels in mouse and human kidney cells [380,516]. It has been recently shown that the B-ring of kaempferol is the part

of the molecule entering CoQ biosynthesis (Figure 4.1.C) [517]. It is cleaved by still unknown peroxidases, producing 4-HB which directly enters the CoQ biosynthesis pathway [517,518]. This mechanism seems to be conserved in mammals and plants, but not in yeast [516–518].

pABA is an alternative ring precursor for CoQ biosynthesis. Interestingly, only yeast but not mammals or bacteria (*E. coli)* are able to use this molecule to synthesise CoQ [289,515,519,520]. pABA is a well-known precursor of folate that has an amino group in C4, instead of the C4-hydroxyl group of 4-HB. In yeast, pABA is synthesized from chorismate, which is transformed to pABA by Abz1 and Abz2 enzymes in two steps via the intermediate 4-amino-4-deoxychorismate (Figure 4.1.A) [519]. pABA is then imported to mitochondria, being the FOL1 gene product required for this import [519] for its use in CoQ biosynthesis. In the case of *E. coli*, pABA is synthesized from chorismate via the shikimate pathway. PabA and PabB convert glutamine and chorismate to glutamate and 4-amino-4-deoxychorismate, which is subsequently transformed to pABA by PabC [521]. It can be prenylated by UbiA, but it cannot progress down the whole CoQ biosynthesis pathway. Vertebrates cannot synthesize pABA, but it can be partially modified by COQ proteins. However, as it occurs in bacteria, this molecule cannot fully progress to CoQ, and it can inhibit CoQ production from 4-HB.

Polyisoprenoid precursors synthesis and tail assembly

The isoprene units of the tail come from the mevalonate pathway. It is a common pathway for the biosynthesis of a variety of isoprenoid molecules, like CoQ, cholesterol, dolichol, vitamin D and isoprenylated proteins (Figure 4.2). Pyruvate is decarboxylated to acetyl-CoA, and then, three molecules of acetyl-CoA are bound together to form 3-hydroxy-3-methylglutaryl-CoA [522]. This molecule is converted to mevalonate by the enzyme 3-hydroxy-3-methylglutaryl-CoA (HMG-CoA) reductase, which is a key step for the regulation of the whole pathway [522,523]. Mevalonate can be phosphorylated by the mevalonate kinase and transformed to isopentenyl diphosphate (IPP). IPP is a building block for the production of farnesyl diphosphate (FPP) and geranyl diphosphate (GPP), and short-chain poly-prenyl diphosphate synthases (poly-PDS), such as FPP synthase and GPP synthase perform these reactions [522,524]. IPP, FPP and GPP are an essential supply

of precursors for CoQ side chain, dolichol and squalene (cholesterol precursor) biosynthesis, as well as for protein farnesylation and geranylgeranylprenylation [522].

The mevalonate pathway takes place in the extra-mitochondrial membranes. In eukaryotes, the following steps of CoQ biosynthesis occur in mitochondria, associated to mitochondrial membranes, so a specific transporter for these molecules to mitochondria may exist in the IMM, but it is not known yet [381]. It has been proposed that the ER-mitochondria contact sites are required for this transport, in order to proceed with CoQ biosynthesis[1,2,320]. The prokaryotic pathway is performed in the cytosolic compartment, with some steps associated to the cell membrane [413].

Next, these isoprenoid units are assembled together by a trans long-chain poly-PDS: Coq1p in yeast [525], PDSS1 and PDSS2 in human [526], IspA and IspB in *E. coli* [527]. This long-chain PDS adds IPP molecules to FPP, GPP or dimethylallyl diphosphate (DMAPP) in multiple steps. DMAPP is probably obtained through IPP isomerization by a yet unknown isomerase. If the isomerization occurs outside or inside the mitochondria is still unknown, but only two IPP isomerases (IDI1 and IDI2) have been described in mammals so far, which are products of a gene duplication and localize into peroxisomes [528,529].

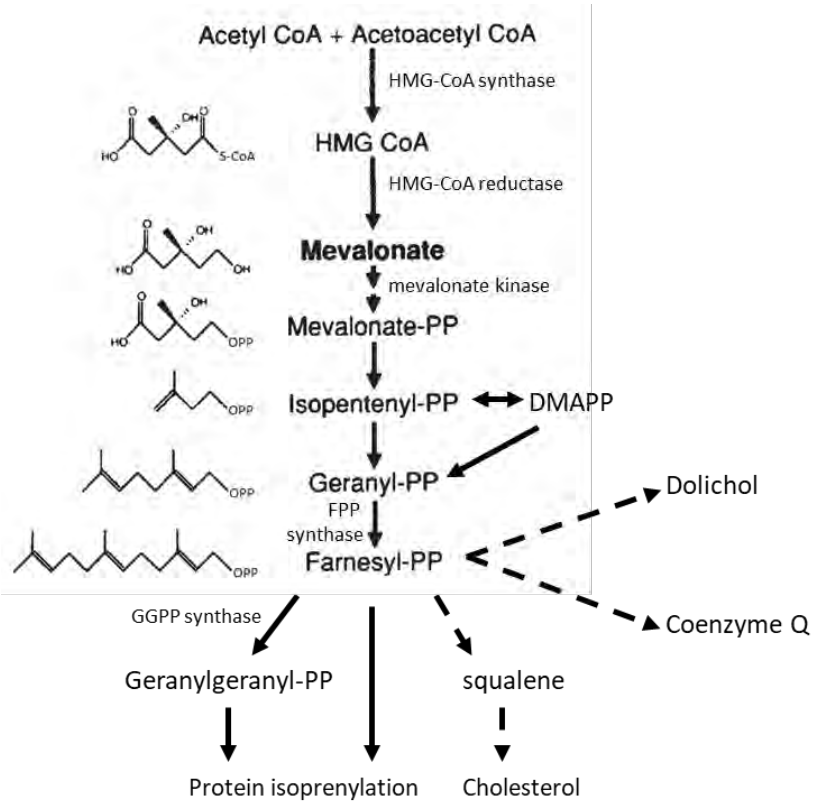

Figure 4.2. Mevalonate pathway.
The end product of glycolysis, acetyl-CoA, is metabolized through the mevalonate pathway, also known as the isoprenoid pathway or HMG-CoA reductase pathway. These produce two five-carbon building blocks called isopentenyl pyrophosphate (IPP) and dimethylallyl pyrophosphate (DMAPP), which are used to make isoprenoids, essential biomolecules for the biosynthesis of cholesterol, dolichols and coenzyme Q, and for protein isoprenylation. (Adapted from Goldstein et al., 1990[523])

Long-chain poly-PDS can be classified into homodimeric (octa-PDS IspB in E. coli, hexa-PDS in *S. cerevisiae*), heterodimeric (hepta-PDS in *B. subtilis*) and heterotetrameric (deca-PDS PDSS1 and PDSS2 in humans, deca-PDS Dps1 and Dlp1 in *S. pombe* or nona-PDS Pdss1 and Pdss2 in mouse) and this multimerization is essential for the CoQ side chain length determination [524,526,530]. Thus, length of CoQ isoprenoid tail is determined by the specific long-chain poly-DPS and its multimerization, differing among species (8 isoprene units in bacteria, 6 in yeast, mostly 10 (and some amount of 9) in humans, mostly 9 (and some of 10) in mice, etc.).

4.1.2. Head precursor prenylation

Head and tail are next conducted to the mitochondrial inner membrane by unknown mechanisms, probably involving ER-mitochondria contacts[1], and Coq2p (in yeast)/COQ2 (in humans), an integral protein of the IMM, condensates the two precursors [531,532]. In the case of bacteria, UbiA is the polyprenyltransferase that binds head and tail, and it is embedded in the cell membrane [533]. These polyprenyl-transferase proteins produce the first highly hydrophobic prenylated ring CoQ intermediate. In yeast, this intermediate (HHB) accumulates in most of the *coq* null mutants, as we will discuss later (section 4.1.5).

4.1.3. Modifications of the quinone ring: genes and proteins involved

The resulting molecule undergoes subsequent modifications of the ring moiety performed by the Coq proteins in yeast and the COQ proteins in humans, which form a complex associated to the IMM. In prokaryotes, the following steps occur instead in the cytosol and are performed by the Ubi proteins forming a soluble multiprotein complex.

Genes and proteins involved in this part of the pathway are presented in this section, referring to the human/*S. cerevisiae* /*E. coli* enzymes, in this order. COQ3/Coq3p/UbiG is an O-methylase which modifies C5 and C6 [534–538]; COQ5/Coq5p/UbiE C-methylates C2 [470,539,540] and COQ6/Coq6p/UbiI [396,460,541] and COQ7/Coq7p/UbiF [542–548] are hydroxylases modifying C5 and C6 respectively (Table 4.1). CoQ synthesis requires a C1-decarboxylation and hydroxylation catalysed by enzymes that have not yet been identified in eukaryotes. In *E. coli*, UbiD and UbiX perform the C1-decarboxylation [549,550] and UbiH, the C1-hydroxylation [551–553] (Table 4.1).

Table 4.1. Enzymes involved in CoQ biosynthesis.

Reaction	Enzymes catalysing the reaction				References
	Human	*M. musculus*	*S. cerevisiae*	*E. coli*	
Isoprenoid chain polymerization	PDSS1 and PDSS2	Pdss1 and Pdss2	Coq1p	IspA and IspB	525–527
C1-decarboxylation	NK	NK	NK	UbiD and UbiX	549,550
C1-hydroxylation	NK	NK	NK	UbiH	551–553
C2-methylation	COQ5	Coq5	Coq5p	UbiE	470,539,540
C3- Prenylation	COQ2	Coq2	Coq2p	UbiA	531–533
C5-hydroxylation	COQ6	Coq6	Coq6p	UbiI	396,460,541
C6-hydroxylation	COQ7	Coq7	Coq7p	UbiF	542–548
C5 and C6 O-methylations	COQ3	Coq3	Coq3p	UbiG	534–538

COQ3/Coq3p/UbiG

COQ3 in eukaryotes (UbiG in prokaryotes) is an O-methyltransferase required for 2 steps in the biosynthetic pathway of CoQ, O-methylation of C5 and C6, after the hydroxylation of these carbons by COQ6 and COQ7, respectively [534,535,537,538]. This enzyme methylates an early CoQ intermediate, the 3-polyprenyl-4,5-dihydroxybenzoic acid, as well as the final intermediate in the pathway, converting 2-polyprenyl-5-hydroxy-3-methyl-6-methoxy-1,4-benzoquinone (6-demethyl-CoQ, DMeQ) to CoQ (Table 4.1). COQ3 proteins are Class I S-adenosylmethionine (SAM)-dependent methyltransferases (SAM-MTases) that use the methyl donor SAM as a cofactor and catalyse the transfer of the methyl group from SAM to oxygen, requiring a divalent cation for the reaction [381,411,554]. UbiG crystal structure has been determined, and it displayed the typical class I SAM-MTase Rossman-like fold, with some additional features characteristic of COQ3 proteins [554]. COQ3 proteins typically show three conserved regions. The first one is the classical glycine-rich motif (DXGXGXG) of class I SAM-MTases to interact with the methyl donor SAM. The other two are particular to COQ3 proteins: a short helix (α6) between β4 and α7 with unknown function, and an insertion of two hydrophobic helixes (α8, α9) between β5 and α10 that has been proposed to be essential for membrane binding.

COQ5/Coq5p/UbiE

COQ5 in eukaryotes (UbiE in prokaryotes) is a C-methyltransferase that methylates C2 of the quinone ring, requiring SAM as methyl donor (Class I SAM-MTase) [470,539,540]. COQ5

catalyses the only C-methylation of CoQ biosynthetic pathway, the conversion of 2-polyprenyl-6-methoxy-1,4-benzoquinone (2-demethyl-6-demethoxy-CoQ, DDMQ) to 2-polyprenyl-3-methyl-6-methoxy-1,4-benzoquinone (6-demethoxy-CoQ, DMQ) (Table 4.1). NADH has been reported to enhance the reaction through a yet unknown mechanism [539]. Coq5p yeast protein has been crystallised as a dimer, and its structure shows a typical class I SAM-MTase Rossman-like fold, with some peculiarities [555]. COQ5 proteins have the typical glycine-rich SAM-binding site, in this case with a minor variation in the sequence: DVAGGSG. They also have a conserved insertion of two helixes (α6, α7) between β5 and α8, which participate in the hydrophobic interface of the dimer. Another feature that is conserved is a hydrophobic pocket predicted to be a putative DDMQ binding site [555]. Interestingly, UbiE bacterial protein is only able to restore Coq5p methylation in yeast expressing an enzymatically inactive Coq5p enzyme, but not when they totally lack Coq5p protein [556]. This fact indicates that besides the enzymatic function, Coq5p probably has an important function in stabilizing the other Coq proteins.

COQ6/Coq6p/UbiI

COQ6 in eukaryotes (UbiI in prokaryotes) is an evolutionarily conserved FAD-dependent monooxygenase required for the C5 hydroxylation (Table 4.1) [396,460,541]. COQ6 proteins have three conserved motifs that are present in the larger family of flavin-dependent monooxygenases (FMOs): an ADP-binding motif, a NAD(P)H recognition and FAD-pyrophosphate moiety binding site and a FAD-ribityl moiety binding motif [411,541]. Crystal structure of UbiI protein from *E. coli* has been partially resolved, revealing that it has a typical FAD-binding domain, similar to that of several FMOs [460]. COQ6 enzymes catalyse the hydroxylation of 3-polyprenyl-4-hydroxybenzoic acid to 3-polyprenyl-4,5-dihydroxybenzoic acid. The electrons required for the hydroxylation reaction are indirectly obtained from NAD(P)H via a ferredoxin/ferredoxin reductase system. In yeast, these are Yah1 and Arh1, encoding mitochondrial ferredoxin and ferredoxin reductase [520]. FDXR and FDX1L are the human orthologues, but their possible implication in CoQ biosynthesis is unknown [381]. Additionally, it has been shown that Coq6p acts as a C4-deaminase in yeast as well, whenever pABA is used as a precursor [557].

COQ7/Coq7p/UbiF

COQ7 (Clk-1 or Cat5) in eukaryotes is a monooxygenase, member of the carboxylate-bridged diiron hydroxylases family [542,543,547,558]. It is responsible for the C6 hydroxylation of the quinone moiety in CoQ biosynthesis, catalysing the conversion of DMQ to DMeQ (Table 4.1), the penultimate step of the pathway [546]. The protein seems to be associated to the IMM [547,559]. The hydroxylation reaction catalysed by COQ7 has been proposed to occur through a DMQ substrate-gated reduction of the diiron centre by NADH (and not NADPH), and then, a subsequent dioxygen activation and DMQ hydroxylation [542,543]. COQ7 protein structure has not been dilucidated yet, but structural models of COQ7 protein from different organisms (human [224,543], *S. cerevisiae* [458], rat [558], *P. aeruginosa* [547] have been obtained by using other diiron proteins as templates. They show to have a four-helix bundle, with a highly conserved diiron active site with the $EX_{n1}EXXH\text{-}X_{n2}\text{-}EX_{n3}EXXH$ binding motif [458,543,558]. Each pair of helixes (α1 and α2; α3 and α4) contains a single iron binding site, that consists in one iron-coordinating E residue in the first helix (α1 and α3) and a EXXH motif in the second helix (α2 and α4), which chelate the iron atom. Then, there is a hydrophobic cavity leading to the diiron site, that could serve as DMQ binding pocket [547,558]. UbiF is the monooxygenase that performs the C6-hydroxylation in *E. coli* and other bacteria [548,551]. It is an FMO, more similar to COQ6/Coq6p/UbiI, and unrelated to COQ7. Despite using different cofactors, UbiF performs the same function than COQ7/Coq7p and it is able to complement *S. cerevisiae coq7* null mutants when it is targeted to the mitochondria [544]. Also, Coq7 homologues from *Pseudomonas aeruginosa*, *Thiobacillus ferroxidans*, and *C. elegans* were demonstrated to complement an *E. coli* mutant with defects in UbiF [545,547].

UbiD-UbiX system and UbiH

In *E. coli*, the UbiD-UbiX system performs the C1-decarboxylation. UbiX is a flavin prenyltransferase that produces prenyl-FMN, a cofactor for UbiD decarboxylation reaction [549,550]. UbiH is a FMO that hydroxylates C1 [551–553]. Eukaryotic homologues of these three proteins have not been yet found, suggesting that the reactions mechanisms in eukaryotes might be different from the bacterial ones.

Order of the reactions in CoQ biosynthesis

The accepted order of reactions involved in the modifications of the aromatic ring of CoQ is slightly different between eukaryotes and prokaryotes, and some steps are still unclear (Figure 4.3). It is possible that for some reactions the active site of the enzyme requires the presence of a chemical group previously added by a different Coq protein. This is obvious for Coq3 O-methylation, which requires a previous hydroxylation to perform the O-methylation. But this fact could be also true for other modifications, considering the chemical logic of the reactions and the possible regioselectivity of active sites [381]. It is also possible that other enzymes could catalyse their reaction independently of other modifications, so they could occur before or after these other reactions.

The accepted eukaryotic model after 4-HB prenylation by COQ2 starts with a C5 hydroxylation of the head group performed by COQ6 [411], followed by the O-methylation of these C5 group by COQ3. Next, unidentified decarboxylase and hydroxylase enzymes perform the C1-decarboxylation and hydroxylation. Then, COQ5 would C-methylate C2 and COQ7 would hydroxylate C6. The last step of the pathway would be the O-methylation of C6 by COQ3 (Figure 4.3 and Table 4.2). However, yeast and human *COQ6* knockout cells accumulate 4-HP, a compound that is decarboxylated and hydroxylated in position C1 of the ring. Therefore, these reactions (which are catalysed by still unidentified enzymes) must occur before or independently on C5 hydroxylation by COQ6 (Figure 4.3, Table 4.2 and Chapter 2, section 2.2.2) [165,396].

In prokaryotes like *E. coli*, the sequence of reactions is described to be different. 4-HB is firstly synthetized by UbiC, directly from chorismate (Figure 4.1.A). Following 4-HB prenylation by UbiA, UbiX-UbiD system performs the C1-decarboxylation [549,550]. Then, the monooxygenase UbiI performs C5-hydroxylation, and UbiG O-methylates this same position. Next, UbiH FMO hydroxylates C1, followed by C2-methylation by UbiE. Then, UbiF hydroxylates C6 and subsequently, UbiG O-methylates this position to form CoQ_8 (Figure 4.3 and Table 4.2) [512]. Similar to what occurs in eukaryotes, *E. coli* defective in UbiI accumulates $4\text{-}HP_8$, indicating that UbiH is able to perform C1-hydroxylation in the absence of the methoxyl group in C5 (Figure 4.3 and Table 4.2) [460,512].

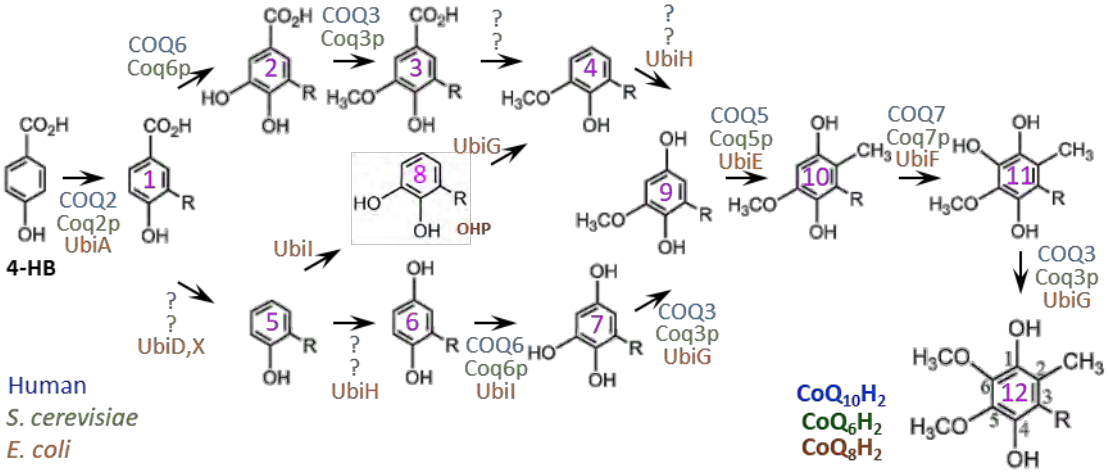

Figure 4.3. CoQ biosynthesis pathway from 4-HB in human, yeast and bacteria.
Human COQ proteins are indicated in blue, yeast Coqp proteins in green and bacterial Ubi enzymes in orange. Each intermediate compound is labelled with a number and described in Table 4.2. Human and yeast canonical pathway is the 1-2-3-4-9-10-11-12 pathway, while bacterial canonical pathway is the 1-5-8-4-9-10-11-12. Pathways involving 5, 6 and 7 would be also possible, since human, yeast and bacterial models defective in COQ6/Coq6p/UbiI accumulate compound 6 (4-HP).

Table 4.2. Intermediate molecules of CoQ biosynthesis from 4-HB.

#	Compound	Abbreviations		
		Human (poly=deca)	*S. cerevisiae* (poly=hexa)	*E. coli* (poly=octa)
1	3-polyprenyl-4-hydroxybenzoate	DHB	HHB	OHB
2	3-polyprenyl-4,5-dihydroxybenzoate	DDHB	DHHB	DOHB
3	3-polyprenyl-4-hydroxy-5-methoxybenzoate	DHMB	HHMB	OHMB
4	2-polyprenyl-6-methoxyphenol	DMP	HMP	OMP
5	2-polyprenyl-phenol	DPP	HPP	OPP
6	3-polyprenyl-1,4-benzoquinone/quinol	4-HP$_{10}$	4-HP$_6$	4-HP$_8$
7	3-polyprenyl-5-hydroxy-1,4-benzoquinone/quinol	DHDP	DHHP	DHOP
8	2-hydroxy-3-polyprenylphenol			OHP
9	2-polyprenyl-6-methoxy-1,4-benzoquinone/quinol (2-demethyl-6-demethoxy-coenzyme Q)	DDMQ$_{10}$	DDMQ$_6$	DDMQ$_8$
10	2-polyprenyl-6-methoxy-3-methyl-1,4-benzoquinone/quinol (6-demethoxy-coenzyme Q)	DMQ$_{10}$	DMQ$_6$	DMQ$_8$
11	2-polyprenyl-5-hydroxy-6-methoxy-3-methyl-1,4-benzoquinone/quinol (6-demethyl-coenzyme Q)	DMeQ$_{10}$	DMeQ$_6$	DMeQ$_8$
12	Coenzyme Q	CoQ$_{10}$	CoQ$_6$	CoQ$_8$

Regarding the three hydroxylation reactions of the pathway, it has been shown that while in eukaryotes, two known (COQ6 and COQ7) and one unknown specialist hydroxylases participate in these three reactions, the picture in bacteria is more complex. There are some bacteria that have three specialist enzymes (like UbiF, UbiH and UbiI in *E. coli* or UbiH, UbiI and Coq7 in *P. aeruginosa*), while some other bacteria have one or two generalist enzymes of broader regioselectivity, able to perform hydroxylation reactions in different positions of the quinone ring in CoQ biosynthesis (like UbiM and UbiL FMOs) [551]. Interestingly, a O_2-independent CoQ biosynthesis pathway has been described in bacteria, in which the O_2-dependent FMO hydroxylases are replaced by the Fe-S hydroxylases UbiU and UbiV [560,561].

The use of pABA in CoQ biosynthesis

Yeast can synthesise and use pABA for CoQ_6 biosynthesis (Figures 4.1.A and 4.4.A), for which it is prenylated by Coq2p protein, competing with 4-HB for Coq2p active site [519,520]. C4 amino group must be then replaced by a hydroxyl group. The monooxygenase Coq6p is reported to perform C4 deamination and hydroxylation, in addition to C5 hydroxylation, but at an undefined step [557]. Specifically, C-terminal region of Coq6p is reported to be essential for C4 deamination, and Coq9p may have an indirect roll in this reaction, since some mutations in the C-terminal region of Coq6p or the lack of Coq9p promote severe defects in C4 deamination, while partially preserve C5 hydroxylation function [557]. When the C4 deamination step is defective, 4-imino-6-demethoxyCoQ_6 ($IDMQ_6$) is mainly accumulated, meaning that all Coq biosynthetic enzymes up to Coq7p (Coq2p, Coq6p, Coq3p (at least for the first reaction catalysed by Coq3), unknown C1-decarboxylase and hydroxylase and Coq5p) can accommodate and transform substrates with a C4-amino group (Figure 4.4.A) [289,557].

In *E. coli,* pABA is endogenously synthesised (Figure 4.1.A). It can be prenylated by UbiA, and then decarboxylated (by UbiD/X) and hydroxylated (by UbiI) to yield 2-amino-3-octaprenylphenol (OAP), a “dead-end” aminated product that cannot progress further in the pathway (Figure 4.4.B) [515]. This means prenylated pABA cannot be C4-deaminated by UbiI in *E. coli* and the OAP product cannot be modified by UbiG.

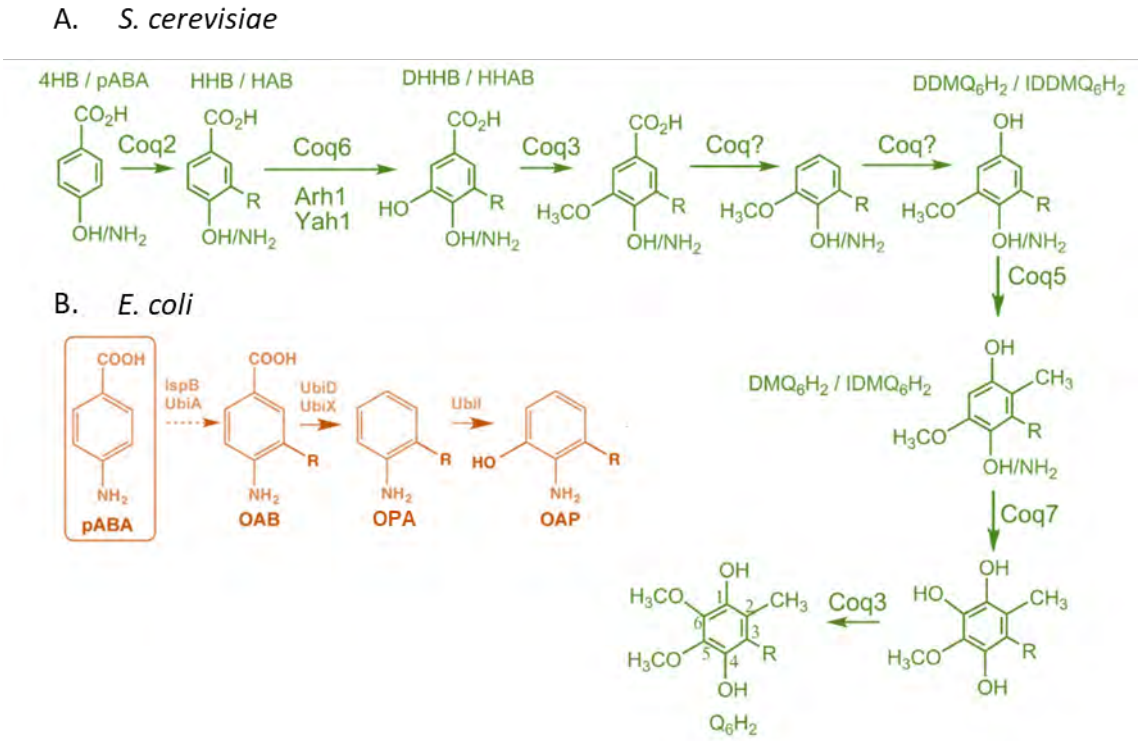

Figure 4.4. The use of p-aminobenzoic acid (pABA) in CoQ biosynthesis.
(A) *S. cerevisiae* (green) can use either 4-HB (4- hydroxybenzoate) or pABA for CoQ_6 biosynthetic pathway. 4-HB and pABA differ by the presence of a hydroxyl or an amino group at position C4. The C4-deamination reaction is performed by Coq6p and it occurs at an undefined step, being 4-imino-6-demethoxycoenzyme Q ($IDMQ_6$) the most downstream amino-containing intermediate identified to date. (B) *E. coli* (orange) can transform pABA into 4-amino-3-octaprenyl-benzoate (OAB). UbiD and/or UbiX catalyze the decarboxylation of the aromatic ring forming 2-octaprenyl-aniline (OPA). UbiI adds the first hydroxyl to the ring to form 2-amino-3-octaprenylphenol (OAP). The pABA branch of the pathway stops at this step. R represents the polyprenyl tail, with 6 units of isoprene in yeast and 8 in bacteria. (Adapted from Ozeir et al., 2015 [557] and Xie et al., 2015 [515])

Vertebrates cannot synthesize pABA. In mammalian cell cultures, pABA supplementation decreases CoQ total levels and leads to the accumulation of 4-imino-6-demethoxycoenzyme Q (IDMQ) [289], similarly to what happened in yeast defective in the C4-deamination reaction [397]. This fact suggested that IDMQ cannot be further modified by COQ7, and that deamination does not occur in cell cultures, interfering with endogenous CoQ biosynthesis. However, pABA supplementation in mice did not alter CoQ levels or accumulate IDMQ in the different tissues analysed, suggesting that pABA does not perturb CoQ biosynthesis in the context of a whole organisms, at least in mouse[289].

4.1.4. Other important non-enzymatic or uncharacterised proteins in CoQ biosynthesis

There are other COQ/Coq/Ubi proteins that are essential for CoQ biosynthesis, but their precise molecular function is still unknown (Table 4.3). In eukaryotes, these are COQ4/Coq4p, COQ8A (or ADCK3/CABC1) and COQ8B (or ADCK4) /Coq8p, COQ9/Coq9p, COQ10A and COQ10B/Coq10p and Coq11p. In bacteria, there are three Ubi proteins of unknown function which are required for CoQ synthesis: UbiB, UbiJ and UbiK [512].

Table 4.3. Other important functions involved in CoQ biosynthesis.

Other important functions in CoQ biosynthesis	Protein				References
	Human	***M. musculus***	***S. cerevisiae***	***E. coli***	
ATPase activity	COQ8A and COQ8B	Coq8a and Coq8b	Coq8p	UbiB	385,397,460
Complex stabilization? Lipid binding?	COQ4	Coq4	Coq4p	UbiK?	465,466,469,412
Membrane and lipid binding, substrate presentation to COQ7	COQ9	Coq9	Coq9p	UbiJ?	224,278,468,562–564,512
CoQ binding and transport?	COQ10A and COQ10B	Coq10a and Coq10b	Coq10p	UbiJ?	565–568
Decarboxylase or reductase?	NK	NK	Coq11p	NK	506

COQ4/Coq4p

COQ4 is essential for CoQ biosynthesis in eukaryotes. It has been proposed that COQ4's function is related to the CoQ biosynthetic complex stabilization (Table 4.3) [465,466,469]. COQ4 protein family has homologues in eukaryotes and also in some prokaryotes (See Chapter 3). These proteins have a conserved motif predicted to bind a divalent cation. For all the details about this protein and its features, please refer to Chapter 3. In the present chapter we will try to elucidate COQ4 molecular function in CoQ biosynthesis and mitochondrial respiration (section 4.2).

COQ8A and COQ8B/Coq8p/UbiB

The ancient UbiB protein kinase-like (PKL) family is very conserved in archaea, bacteria, and eukaryotes. These proteins are needed for efficient CoQ production, but their molecular function still remains unclear (Table 4.3). *E. coli* UbiB was thought to be a monooxygenase performing the first hydroxylation of CoQ [569], but later studies revealed that UbiI performs this step [460]. UbiB has three yeast (Coq8p, YLR253W and YPL109C) and five human orthologues (AarF Domain Containing Kinases, ADCK1-5) [385]. Amongst these orthologues, only Coq8p in yeast and COQ8A (or ADCK3/CABC1) and COQ8B (or ADCK4) in humans have been reported to participate in CoQ biosynthesis. Human *COQ8A* and *COQ8B* protein sequences have a 44.23% of identity and a 66.12% of similarity, and patients with mutations in both genes have been found to present primary CoQ_{10} deficiency [112].

The three other genes of the ADCK family (ADCK1, ADCK2 and ADCK5) have been suggested to be involved in the CoQ biosynthetic process and diverse functions have been shown for some of them. ADCK1 has been proposed to participate in the structural maintenance of mitochondrial membranes in muscle [570]. ADCK2 has been described to participate in CoQ biosynthesis and in the fatty acid metabolism in skeletal muscle[378], as well as in the distribution of CoQ from mitochondria to other membranes [571].

Initially, Coq8p was thought to be a kinase participating in phosphorylation of Coq3p, Coq5p and Coq7p in yeast [397,490,491], since phosphorylation of these proteins is altered in a *coq8* null mutant yeast. However, the crystallisation of COQ8A revealed a kinase-like fold protein with unique UbiB-specific features demonstrated to inhibit protein kinase activity. These features are an N-terminal domain that occupies the typical substrate binding pocket and a A-rich loop that replaces the canonical G-rich nucleotide binding loop and provides an unusual selectivity for ADP over ATP [385]. Moreover, COQ8A/ADCK3 has recently been shown to lack canonical protein kinase activity in *trans* [424] and have an ATPase activity that is enhanced by binding cardiolipin containing membranes or small phenolic molecules resembling to CoQ pathway intermediates [572]. It has been hypothesised that it could couple the hydrolysis of ATP to the extraction of the quinone heads of CoQ intermediates out of the membrane and allow their chemical modification [316,413,572]. Still, its mechanistic role is unclear and needs to be further studied.

COQ9/Coq9p

COQ9 are lipid-binding proteins present in a wide range of eukaryotes, but not in bacteria [468,562]. COQ9 functionally and physically interacts with COQ7, to favour C6-hydroxylation reaction, stabilizing CoQ biosynthetic complex [224,278,563,564]. COQ9 deficiency leads to a drastic reduction of COQ7 levels and activity, accumulating DMQ, in all models studied [278,388,397]. It has also been reported that yeast Coq9p supports Coq6p in the deamination of the intermediates derived from pABA precursor [573]. The X-ray structure of human COQ9 protein was obtained, showing the presence of a conserved lipid-binding pocket, able to specifically bind aromatic isoprenes [224,564]. The structure revealed structural homology to an ancient TetR family of transcriptional regulator (TFRs) with an amphipathic C-terminal helix. COQ9 protein structural and molecular dynamics studies suggested that this C-terminal hydrophobic helix controls membrane binding, and the association is favourited in cardiolipin-rich membranes. When COQ9 binds this part of the IMM, a local deformation occurs and lipids are orthogonally displaced, entering their hydrophobic tail inside the cavity of COQ9. Afterwards, COQ9 is able to lift the bound lipid off the membrane, and present it to COQ7, to promote C6-hydroxyltion [224].

COQ10A and COQ10B/Coq10p/pasT

COQ10 are mitochondrial proteins belonging to the START (steroidogenic acute regulatory protein-related lipid transfer) domain protein family, which have a hydrophobic tunnel specialised in binding lipids. Coq10p is not essential for CoQ biosynthesis since yeast null mutants present normal levels of CoQ [566]. However, *de novo* CoQ biosynthesis and mitochondrial respiration of these mutants is less efficient than in WT yeast, and they are highly sensitive to H_2O_2. These defects can be restored by exogenous CoQ supplementation or Coq10p WT expression [565–567]. Human COQ10A and COQ8B expression, CC1736 bacterial START domain protein from *Caulobacter crescentus* expression or yeast Coq8p overexpression were also able to rescue the respiratory defect and the sensitivity to oxidative stress in this mutant [565,566,574], and only partially the defect in *de novo* CoQ synthesis. Interestingly, levels of Coq10p protein are important since Coq10p overexpression has an inhibitory effect on mitochondrial

respiration, which is partially restored by Coq8p overexpression [567,575]. *S. pombe* Coq10p protein has been demonstrated to specifically accommodate the quinone head ring of CoQ in a binding site included in the START domain [576]. Very recently, an *E. coli* protein displaying the same functions of COQ10 proteins has been identified [560,577]. *E. coli* mutants lacking *pasT* displayed the same pleiotropic phenotypes as yeast *coq10* mutants, including decreased membrane potential, increased sensitivity to oxidative stress, and modestly decreased ubiquinone biosynthesis. Moreover, these phenotypes were rescued by ectopic expression of human *COQ10A* [560,577].

It is suggested that Coq10 proteins bind CoQ and late-stage CoQ-intermediates, probably chaperoning them to the sites where they are needed within the mitochondrial membranes, facilitating *de novo* CoQ biosynthesis and respiratory electron transport [560,565–567,574,577].

Coq11p

Coq11p yeast protein was first found as a component of the CoQ biosynthesis complex by immunoprecipitation studies [506]. It is present in fungal genomes and in photosynthetic genomes or genomes with a photosynthetic ancestor. Yeast *coq11* null mutants have an impaired but not completely abolished CoQ biosynthesis, and they retain some respiratory growth. Coq11p is thought to be necessary for efficient *de novo* CoQ synthesis in yeast, with a predicted role as a FMN-dependent decarboxylase or reductase, but it has no clear human orthologue [506].

Interestingly, *coq11* gene was found to be fused to *coq10* gene in some fungal genomes from *Ustilaginaceae*, suggesting some functional link between these two proteins [506,574,578]. Indeed, *coq11* gene deletion in yeast has been recently reported to rescue the respiratory deficiency, sensitivity to oxidative stress and decreased *de novo* CoQ biosynthesis in *coq10* null mutant. *coq10* and *coq11* double mutant showed increased CoQ levels in mitochondria, which were suggested to rescue the phenotype of *coq10* mutant [579]. Coq11p is suggested to be a negative modulator of CoQ biosynthesis in yeast, but the mechanisms underlying this phenomenon are still elusive [579]. It does not have a clear homologue in human, but it has been shown by a protein similarity network analysis that the taxonomy of Coq11p-like proteins include the short-chain

dehydrogenases/reductases subfamily protein NDUFA9, an accessory CI subunit required for CI stability in humans [380,506].

UbiJ and UbiK

UbiJ [568] and UbiK [412] are bacterial proteins essential for CoQ biosynthesis. They have been found to physically bind to each other in a heterocomplex UbiK-UbiJ (2:1) that is able to bind lipids. UbiJ is a lipid binding protein capable of binding CoQ and CoQ intermediates. UbiK-UbiJ complex has been found part of a bigger 1-MDa multiprotein complex, in which 5 other Ubi proteins were also found (Ubi E, F, G, H, I), localised in the cytosolic fraction. UbiJ has a key role in binding the isoprenoid intermediates, through its SCP2 (sterol carrier protein 2) domain, inside the complex and is essential for complex formation. The current hypothesis is that UbiJ and UbiK assist several steps of CoQ biosynthesis by presenting intermediates to the Ubi enzymes inside the biosynthetic complex [560]

4.1.5. Structural organization of CoQ biosynthetic proteins: CoQ biosynthesis complex

The enzymes modifying CoQ quinone head are described to form a multiprotein complex, the CoQ synthome or CoQ complex. There is evidence that yeast Coq3p-Coq9p proteins are organized in a complex located on the matrix side of the IMM [490,580], and this architecture seems to be conserved in mammals (Figure 4.5.B and C). As detailed in the previous section, in prokaryotes, an Ubi-metabolon has also been described, but in this case, in the cytosolic soluble fraction (Figure 4.5.D). Importantly, CoQ intermediates of the pathway are also needed for complex formation and stability. The organization of the CoQ biosynthetic proteins and CoQ intermediates in a complex would be essential for shielding the hydrophobic intermediates from the hydrophilic environment. Moreover, in addition to enhancing the catalytic efficiency of the pathway, by correctly orientating the substrates and active sites of the enzymes, or allowing the functional regulation of the different components, the complex would sequester the reactive hydrophobic intermediates, having them in a controlled environment [507].

Yeast CoQ complex

The existence of a CoQ biosynthetic complex containing Coq3p-Coq9p proteins was first described in yeast. A common feature for *coq3-coq9* null mutants was the lack of the final product CoQ and the accumulation of the same early precursor, hexaprenyl-hydroxybenzoate (HHB), Coq2p's product [467,468], instead of the substrate of the lacking enzyme (Table 4.4). This observation indicated that Coq proteins were needed not only for their enzymatic function but also for the activity and stability of the other Coq enzymes. This possibility was supported by the fact that some point *coq* mutants (*coq5, coq6* and *coq7*) had a lesser drastic phenotype, accumulating their corresponding diagnostic intermediate. For example, some point mutations of Coq7p led to the accumulation of Coq7p substrate, DMQ_6 (Table 4.4) [456,544,546]. Moreover, this mutant but not the *coq7* null mutant, was rescued by low copy expression of *ubiF* [544]. Similarly, some respiratory deficient mutants with point mutations in *coq5*, affecting the catalytic activity, but not *coq5* null mutant, were rescued by the expression of *ubiE* [556].

Table 4.4. Intermediates accumulated in yeast defective in CoQ biosynthesis.

Yeast	Intermediate accumulated			References
Mutant gene	Null mutant	Point mutant	Null mutant + Coq8 OE	
coq1	No prenylated quinones	-	No prenylated quinones	397
coq2	No prenylated quinones	-	No prenylated quinones	397
coq6	HHB	4-HP	4-HP/4-AP	342,396,467
coq3	HHB	HHB	HHB (DMQ when VA added)	397
coq5	HHB	DDMQ	DDMQ	397,467,470
coq7	HHB	DMQ	DMQ	397,415,467,546
coq9	HHB	-	DMQ and 4-HP	397,468
coq4	HHB	HHB	HHB/HHAB	397,467
coq8	HHB	-	-	467
coq10	HHB/HAB	-	-	565
coq11	HHB and DMQ	-	-	506

Moreover, in several of these mutants, the lack of one Coq protein (Coq3p, Coq4p, Coq6p, Coq7p or Coq9p) produced the depletion of other Coq polypeptides, while point mutations didn't have such effect [464,468,544,556,563,580,581]. All these data indicated that Coq proteins were also playing a structural role, besides their enzymatic one, forming a multiprotein complex, whose stability is essential for the function of the individual components.

Importantly, it has also been demonstrated that some intermediates of the synthesis and CoQ itself are important integral components of the complex [395,415,424,465,506]. Furthermore, it is known that CoQ intermediates are needed for complex formation and stabilization [1]. In agreement with this, there are some Coq proteins that have been shown to directly bind lipids inside a lipid-binding domain of the protein. It is the case of Coq9p [224] and Coq8p [424], which both co-immunopurified with several intermediates of CoQ biosynthesis.

Overexpression (OE) of Coq8p in some of the *coq* mutants stabilized the levels of other Coq polypeptides [397,575] and their organization as a complex [395], resulting in the accumulation of the respective substrates of the lacking enzyme, instead of HHB (Table 4.4). Coq8p OE in *coq* null mutants has been then a useful tool for confirming the specific enzymatic activities of different components of the complex, such as *coq7*, which accumulates DMQ_6 [397,415], *coq5*, which accumulates $DDMQ_6$ [397,470] or *coq6*, which accumulates 4-HP_6 [396]. Because of the complex-stabilising effect, OE of Coq8p has also been useful to explore the use of 4-HB analogues as bypass molecules for some specific Coq protein defects, such as vanillic acid in *coq6* for Coq6p bypass [396] or 2,4-dHB in *coq7* for Coq7p bypass [397] (see Chapter 2), or even as a screening platform to look for new bypass molecules for some *coq* defects [416]. As explained before, it has been hypothesised that Coq8p's role in CoQ biosynthesis could be the extraction of the CoQ intermediates out of the membrane, coupled to ATP hydrolysis [316,413,572]. In this context, Coq8p would act as a lipid chaperon, providing the lipid intermediates needed for complex nucleation and maintenance, but not being an integral component of the complex [1]. In the condition of suboptimal complex stability, due to the lack of one of the components, Coq8p overexpression would rescue this instability, probably by providing more intermediates to nucleate and maintain the complex [1].

Biochemical and proteomic analyses provided physical evidence of protein-protein interactions (PPI) between the complex Q components. Different co-immunoprecipitation studies found that Coq3p-Coq9p co-precipitated together in different combinations [465,506,563], and one of them identified Coq11p as part of the complex [506]. By size-exclusion chromatography, Coq3p, Coq4p, Coq6p and Coq7p were found together in a 700KDa-1300KDa complex which had O-methylase activity [465,466,544].

2D BN-PAGE assays also demonstrated that several Coq proteins (Coq3p, Coq4p, Coq5p, Coq7p and Coq9p) co-migrate as part of complexes with a molecular weight higher than 1MDa [2,395,465,466,490,544,563,574]. BN-PAGE separation profiles of Coq2p, Coq8p and Coq10p suggested that these proteins would probably not be integral and structural part of the >1MDa complex, but some weak or transient interactions between these proteins and the complex may be occurring [316,490].

In vivo fluorescence microscopy in yeast has also provided evidence of CoQ complex formation, being Coq3, 4, 5, 6, 7, 9, and 11p the core components (Figure 4.5.C) [1]. Tagged Coq proteins were visualised, and only some of them (Coq3p, Coq4p, Coq5p, Coq6p, Coq7p, Coq9p and Coq11p) were found to have a focal localisation into discrete *foci* in the IMM named CoQ domains [1]. On the contrary, Coq1p, Coq2p, Coq8p and Coq10p had a uniform distribution within mitochondria. The lack of Coq1p-Coq9p totally prevented CoQ domain formation, while *coq10* mutants were only partially affected, and *coq11* mutants just slightly affected in CoQ domain formation.

Coq8p overexpression was also shown to rescue CoQ domain formation in *coq5*, *coq6*, *coq7* and *coq9* null mutants, but not in *coq1*, *coq2*, *coq3* and *coq4*, in agreement with the previous biochemical data [1,395,397]. In the case of *coq1* and *coq2*, it is understandable, because the lack of these enzymes prevents the presence of prenylated intermediates, which are essential for CoQ domain formation [1,316]. In the case of *coq3* and *coq4*, the proteins coded by these genes are thought to be critical structural components of the complex [1,465,466], so that is the hypothetical reason why Coq8p overexpression do not rescue the CoQ domain formation. All these data fully agree with the previous biochemical data for CoQ complex formation, additionally suggesting that Coq8p is not an integral part of the CoQ complex, but it interacts with it dynamically, being essential for complex formation.

Importantly, these CoQ domains are spatially and functionally related to ERMES (endoplasmic reticulum-mitochondria encounter structure) complex, also known as ER-mitochondria contacts [1,2] and the loss of this structure impairs respiration through reduction of CoQ levels and accumulation of CoQ intermediates (See Chapter 5, section 5.1.6). This could be a mechanism of secondary CoQ deficiency [316].

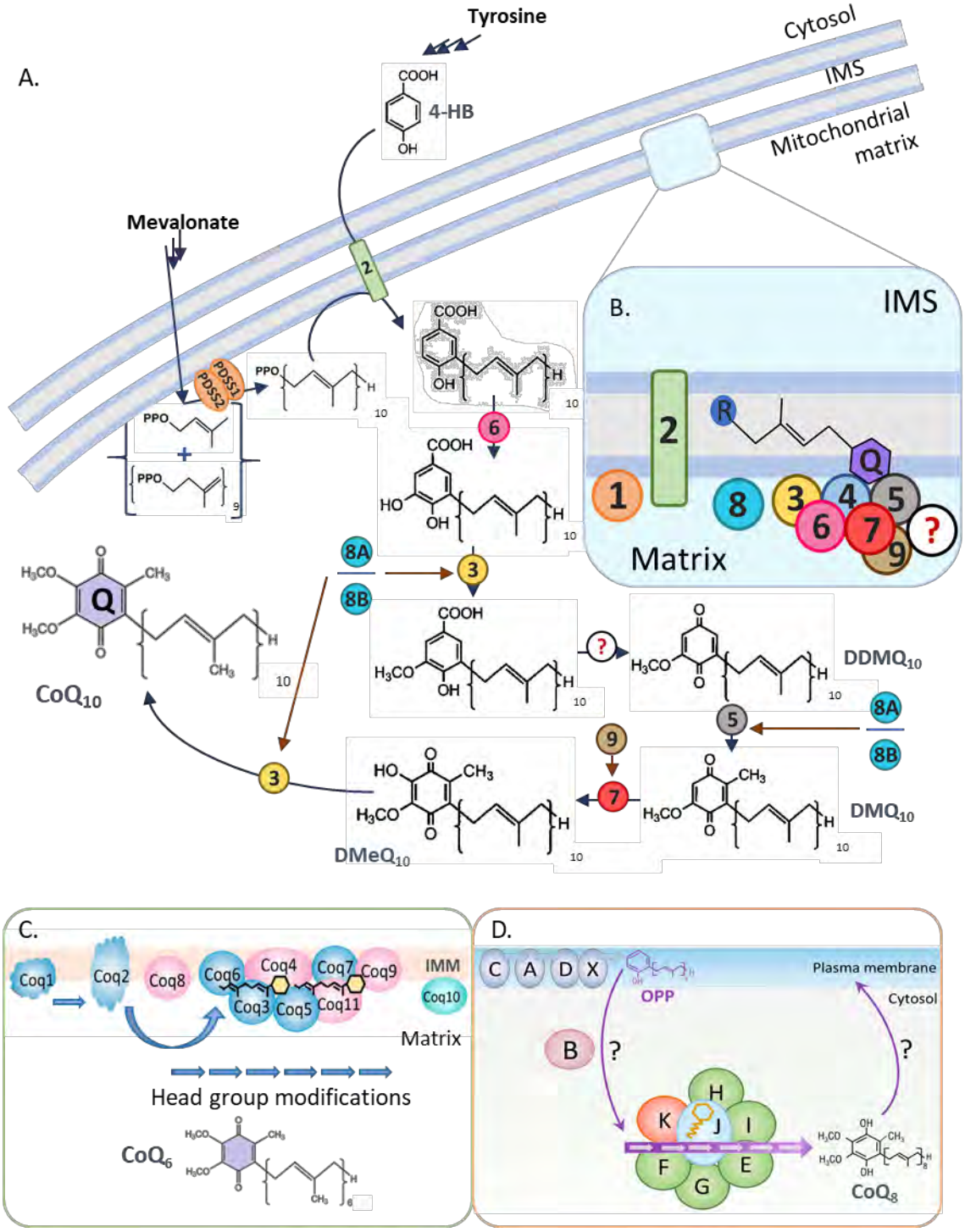

Figure 4.5. Models of CoQ biosynthesis complex.

(A) Human CoQ_{10} biosynthesis pathway and model of the biosynthetic complex. Blue arrows represent enzymatic reactions and circled numbers represent the different COQ proteins that participate in each step. Brown arrows indicate regulatory mechanisms. Circled question mark shows currently unidentified enzymes. (B) Model of human CoQ_{10} biosynthetic complex, containing at least COQ3–COQ9 and lipids, such as CoQ_{10} itself. Other CoQ biosynthesis complex models are also represented: yeast (C) and bacteria (D). CoQ_{10}, coenzyme Q_{10}; 4-HB, 4- hydroxybenzoate; $DDMQ_{10}$, demethoxy-demethyl-CoQ_{10}; DMQ_{10}, demethoxy-CoQ_{10}; $DMeQ_{10}$, demethyl-CoQ_{10}; IMS, inter-membrane space. (Adapted from Alcázar-Fabra et al., 2018[112] and Wang et al. 2019[316])

Mammalian CoQ complex

CoQ complex seems to be conserved in mammals. Unlike in yeast, only some mammal CoQ intermediates accumulation experiments have been performed, and only a few of them are in models with a total lack of a specific COQ protein (Table 4.5). Likewise *coq6* null yeast (overexpressing Coq8p or expressing mutated Coq6p), *COQ6 KO* human cells (HEK293) accumulated 4-HP_{10}, but in this case with no need of COQ8 overexpression or inactive COQ6 expression [165]. Something similar occurred in $Coq7^{-/-}$ embryos at E9.5 (the lack of Coq7 in these mice was embryonic lethal), which accumulated DMQ_9 [421]. Two different KI mouse models with non-sense mutations in Coq9 ($Coq9^{Q95X}$ and $Coq9^{R239X}$) also accumulated DMQ_9 [278,279]. Patient fibroblasts with mutations in *COQ7* or *COQ9* accumulated DMQ_{10} [238,239,248,388]. *COQ4* patient fibroblasts also showed a small accumulation of DMQ_{10} [388]. Patient fibroblasts with mutations in *COQ2* accumulated decaprenyl-pyrophosphate [241]. *COQ7* KD in 143B cells also accumulated DMQ_{10} [315]. Human fibroblasts KD of *COQ3*, *COQ4*, *COQ5*, *COQ6*, *COQ7* and *COQ9* genes (but not *COQ2*) also showed an accumulation of DMQ, being observed the highest accumulation in the *COQ7* KD [388].

Table 4.5. Intermediates accumulated in mammalian models defective in CoQ biosynthesis.

Mammals	Intermediate accumulated			References
Mutated gene	KO	KD	Point mutations (Patient cell line)	
COQ2	-	-	Decaprenol	241
COQ6	4-HP	-	-	165
COQ3	-	DMQ	-	388
COQ5	-	DMQ	-	388
COQ7	DMQ	DMQ	DMQ	238,315,388,420,421,425
COQ9	DMQ	DMQ	DMQ	248,278,279,388
COQ4	-	DMQ	-	388

Depletion of specific COQ proteins has been observed in some mouse models with primary CoQ deficiency. Coq3-9 proteins were depleted across different tissues in $Coq8a^{-/-}$ mice at different degrees [424], and the same was observed in *Coq9* mutant mice [278,564]. This phenomenon has also been studied in some human cell lines. COQ4, COQ7 and COQ9 levels were measured in patient fibroblasts with mutations in *COQ4*, *COQ7* and *COQ9* [388]. In these specific cell lines, defects in *COQ9* led to a depletion in COQ4 and COQ7; mutations in *COQ7* also depleted COQ4 levels but not COQ9; and *COQ4* deficiency

did not affect COQ7 or COQ9 levels [388]. In human 143B cells, the KD of some of the *PDSS* and *COQ* genes resulted in the alteration of other COQ protein levels [315]. In these cells, the KD of some genes, such as *PDSS1*, *PDSS2* and *COQ3*, produced a general depletion of COQ3-COQ9 proteins. In contrast, knocking-down the rest of the *COQ* genes had a more discreet effect, reducing or increasing the levels of other specific COQ polypeptides. For example, *COQ4* KD displayed an overproduction of COQ5 and COQ6, while *COQ7* KD only showed an overproduction of COQ4. In contrast, *COQ5* KD produced a reduction in COQ7; *COQ6* KD, a reduction in COQ3 levels and *COQ9* KD, a decrease in COQ5 levels. In these studies, KD of *COQ2* and *COQ8A* did not show an effect in other COQ proteins levels [315].

COQ PPI have also been described in mammalian cells. COQ8B co-immunoprecipitated with COQ6 and COQ7 in cultured human podocytes [363] and with COQ5 in HEK293 overexpressing COQ8B-FLAG [401]. Tagged COQ5 and COQ4 proteins coimmunoprecipitated when coexpressed in HEK293 cells [470], and COQ8A-FLAG co-purified with COQ5-HA when co-expressed in COS cells [424]. Wider affinity enrichment mass spectrometry (AE-MS) studies of HEK293 and HepG2 cells expressing the different tagged-COQ proteins revealed a highly interconnected CoQ biosynthetic complex, with a big number of PPI between the different components [438,514]. Interestingly, the abundance of PPI involving COQ8A and COQ8B were reciprocally regulated depending on the cellular metabolic status, being COQ8A interactions more abundant when cells were grown in galactose medium, while COQ8B's were predominant in cells grown in dextrose medium [438].

Cell-free protein translation and co-immunoprecipitation showed that nearly all COQ proteins were unstable alone but stabilised when co-expressed in pairs [438]. With this same approach, a complex containing COQ3, 4, 5, 6, 7 and 9 was purified in vitro, indicating that the presence of these six core components is enough to produce the complex (Figure 4.5.C) [438]. These 6 core components are the same that, in yeast, were reported to localize in the *foci* so-called the CoQ domain (in yeast, Coq11p is also part of these CoQ domains) [1,438]. COQ8A and COQ8B seem to interact with the different COQ proteins of the complex in a more dynamic way, and are required for its stability and probably its regulation (Figure 4.5) [438].

Also, 2D BN-PAGE experiments showed the presence of different COQ proteins (PDSS2, COQ3, COQ4, COQ5, COQ6, COQ7 and COQ9) in high-molecular weight complexes in human osteosarcoma 143B cells [315,437], but smaller than the ones found in yeast. These proteins were mainly found in a dissociated state, but some high-molecular weight signals were observed. PDSS2 was observed in two major complexes of approximately 146KDa and 242KDa, and very faint signals up to 1MDa. One of the two small complexes were hypothesized to be the heterotetramer configuration of PDSS2 in association with PDSS1, maybe with contacts with other proteins too [315]. COQ3 was found in small complexes from 66 to 146KDa, and COQ7 also around the 146KDa marker with some faint signals up to 242KDa [315]. COQ4 and COQ6 were found in a range from 66 to 480KDa [315], and COQ5 in the range of 242KDa to 400KDa [437]. COQ9 was found in complexes of 66KDa-146KDa [437]. The presence of the different proteins in fractions of diverse molecular weight would support the idea of a dynamic CoQ biosynthetic complex in mammals. CoQ complex configuration should be studied under specific metabolic conditions in order to better understand its assembly and regulation.

As in yeast, some COQ proteins have been shown to bind lipids or small molecules, like CoQ precursors, which are thought to be integral and important componets of the complex as well [224,424,564]. For example, mouse Coq8a was found to bind lipid membranes [424] and its human homologue was able to bind small molecules like CoQ-intermediates and phenol derivatives [572]. Human COQ9 protein co-crystallised with phosphorylated lipids [564] and co-immunopurified with aromatic isoprenes [224].

The CoQ domains observed in yeast were also observed in human osteosarcoma U2OS cells by immunohistochemistry and fluorescence microscopy. Endogenous human COQ9 localized to discrete *foci* that colocalised to Mitotracker Red staining [1].

Bacterial CoQ complex

The structural organization of the CoQ biosynthetic proteins is evolutionary very conserved, and the pathway in *E. coli* has been equally studied, to characterize the Ubi proteins and how they function as a metabolon. Mutations varying from point mutations to total ablation of some *ubi* genes resulted in the accumulation of various CoQ intermediates of the pathway (Table 4.6) [512], such as OHB for *UbiD* and *UbiX*

mutations[550], OPP for *UbiB* [569], *UbiJ* [568], *UbiK* [412], *UbiG* [538] and *UbiH* [552] mutations, 4-HP_8 for *UbiI* mutations[460], $DDMQ_8$ for *UbiE* mutations [540] or DMQ_8 for *UbiF* mutations [548].

Table 4.6. Intermediates accumulated in bacterial models defective in CoQ biosynthesis.

Bacteria	Intermediate accumulated		References
Mutated gene	**Null mutant**	**Point mutant**	
UbiC	-	None + Low CoQ	[511]
UbiA	-	No prenylated quinones	[533]
UbiD	OHB + Low CoQ	-	[550]
UbiX	OHB + Low CoQ	-	[550]
UbiI	4-HP + Low CoQ	-	[460]
UbiG	-	OPP and DMeQ	[538]
UbiH	-	OPP, OHP, OMP	[552]
UbiE	DDMQ	DDMQ	[540]
UbiF	DMQ	DMQ	[548]
UbiB	OPP	OPP	[569]
UbiJ	OPP	-	[568]
UbiK	OPP	-	[412]

Recent studies reported that Ubi proteins are organised into a multiprotein complex of 1MDa [413,507]. Surprisingly, this complex seems to be in the cytosolic fraction, forming a stable and soluble metabolome able to transform a highly hydrophobic molecule in a hydrophilic environment [413] (Figure 4.5.D). The seven core components of this complex are five Ubi enzymes (UbiI, G, H, E, and F) and two accessory factors (UbiJ and UbiK) [413]. This complex would catalyse OPP transformation to CoQ in the cytosol. UbiJ is a lipid-binding protein capable of binding CoQ and CoQ intermediates, through its SCP2 domain, inside the complex, and is essential for complex formation [412,568].

4.1.6. Regulation of CoQ biosynthesis

Little is known about the regulation of CoQ biosynthesis. Still, such a complex pathway must have an elaborated regulatory mechanism operating at very different levels: nuclear transcriptional factors, posttranscriptional and post-translational modifications, or even assembly of the complex in time and space might be important for the regulation of this process.

Transcriptionally, several nuclear transcription factors have emerged along the last years as candidates for regulating the expression of the *COQ* genes, such as PPARα [582], RXRα [583] or NFκB [584]. However, an in-depth study of promoters and regulatory sequences of the *COQ* genes still lacks. PPARα has been shown to respond to its ligands, the

peroxisome proliferators, by dimerizing with another receptor, the retinoid X receptor (RXRα, β or γ). This heterodimeric complex, when it is active, induces a wide range of lipid anabolic and catabolic processes, and increases CoQ content in all tissues except for the brain. In a *PPARα* null mouse, CoQ, cholesterol or dolichol levels are the same than in a WT mouse, so the constitutive synthesis of these lipids is not affected. However, while a WT mouse experiences an increase in CoQ levels upon administration of a peroxisome activator, the *PPARα* null mouse is unable to induce CoQ synthesis, indicating this receptor participates in CoQ induction via peroxisome proliferators, but it is not essential for constitutive CoQ synthesis [582,583]. RXR is able to form dimers with a number of other receptors, such as retinoic acid receptor, vitamin D receptor, thyroid hormone receptor, PPAR, RXR itself and other orphan receptors. The RXRα was found to be essential for CoQ biosynthesis regulation by studying a hepatocyte-specific *RXRα* deficient mouse. These mice had 50% of CoQ WT levels in liver, while cholesterol and dolichol were unchanged. *In vivo* CoQ biosynthesis rate was reduced when compared to controls, but the CoQ induction after peroxisome proliferators was not affected. All these observations indicated that RXRα is important for constitutive CoQ biosynthesis and not for induction by peroxisome proliferators [582,583]. NFκB was found to upregulate the expression of *COQ7* gene, and therefore CoQ synthesis, by binding to *COQ7* gene's 5' flanking region. This activation was found to occur under stress conditions, such as treatment with cancer drugs like camptothecin [584,585]. In contrast, the tricyclic antidepressant amitriptyline has been proposed as an antitumoral drug that down-regulates CoQ biosynthesis in cancer cells, by reducing *COQ4* mRNA levels, and COQ4 and COQ6 protein levels by unknown mechanisms [586]. However, this treatment also upregulated *COQ7* mRNA and protein levels, similarly to camptothecin treatment, and it has been suggested that this is probably caused by the increase in ROS through activation of NFκB [584,586].

At the post-transcriptional level, several studies have identified some RNA binding proteins (RBPs) which modulate the stability of *COQ* transcripts, regulating therefore their ability to be translated. The yeast RBP Puf3p has been reported to bind *coq5* mRNA, and control its translation, to avoid the detrimental overproduction of this protein [587]. Moreover, it also binds to other mRNAs of proteins related to mitochondrial biogenesis

for their repression during fermentation, which means that Puf3p is involved in a regulatory network that coordinates CoQ production and mitochondrial biogenesis [587]. Some human RBPs have also been found to be involved in CoQ biosynthesis regulation. It is the case of HuR and hnRNP C1/C2, which have been reported to bind to *COQ7* mRNA 3' UTR with opposite regulatory outcomes [588]. HuR enhances *COQ7* mRNA stability and helps maintain physiological *COQ7* mRNA, COQ7 protein levels, and CoQ_{10} biosynthesis; while hnRNP C1/C2 binds to *COQ7* mRNA by interacting with HuR and triggers its degradation [588]. These findings suggest that RBPs have crucial roles in regulating CoQ biosynthesis.

There is also evidence showing that CoQ biosynthesis can be regulated at a post-translational level. For example, yeast Coq5p requires to be processed at the N-terminus directly by the mitochondrial protease Oct1p (human orthologue MIPEP) to improve its stability in yeast [589]. The unprocessed Coq5p protein has a reduced half-life and leads to a decrease in CoQ levels [589]. Yeast Coq7p is also post-translationally regulated by a phosphorylation cycle, being active when it is dephosphorylated by the mitochondrial phosphatase Ptc7 in yeast (human orthologue PPtc7) [493]. However, the kinase responsible for its phosphorylation is not known yet. Additionally, human COQ7 activity also depends on the interaction with COQ9 protein, which seems to present the lipid cargo DMQ to COQ7 to allow its modification [224,564]. Additionally to Coq7p, Coq3p and Coq5p also seem to be regulated by phosphorylation modifications by an unknown kinase [397,490,491]. Coq8p seems to indirectly participate in these phosphorylations, since phosphorylation states of these proteins are altered in a *coq8* null mutant yeast [397,490,491]. However, *COQ8* lacks canonical protein kinase activity in *trans* [424] and have an ATPase activity instead [572].

4.2. Results and discussion

In this chapter, we will focus on the molecular characterisation of human *COQ4*, and how it is involved in the CoQ biosynthesis process and in the mitochondria respiratory chain. In order to do so, we will study in-depth our *COQ4* KO cellular model, and how CoQ biosynthesis and mitochondrial respiration are affected in this model. Also, we will analyse COQ4 protein interaction partners to provide a wider picture of COQ4 function.

4.2.1. COQ4 is essential for CoQ_{10} synthesis in human cells

COQ4 KO cells show drastically reduced CoQ_{10} levels, impaired CoQ_{10} biosynthesis and accumulation of a specific intermediate

CoQ_{10} levels were measured in the five *COQ4* KO clones previously described (See Chapter 3, section 3.2.2), lacking COQ4 protein expression (Figure 3.20.D). CoQ_{10} levels were extremely reduced, near to be undetectable, in *COQ4* KO cells compared to WT cells (Figure 4.6). This means that CoQ_{10} biosynthetic pathway is highly impaired in these cells.

In order to analyse how this pathway was affected, we measured the incorporation of ^{14}C-labelled 4-HB to CoQ_{10}, which was virtually undetectable (Figure 4.6.B). This suggests that the residual CoQ_{10} detected in these cells is not produced endogenously but it is derived from the medium, in agreement with what we observed in *COQ6* KO cells. Moreover, the chromatogram showed an additional radioactive peak in *COQ4* KO sample (rt: 13.5 min), which eluted faster than CoQ_{10} (rt:17.5-18 min), which is probably an intermediate of CoQ_{10} synthesis (Figure 4.6.B). This peak was also observed in samples from patients' fibroblasts with mutations in *COQ4* (see Chapter 2, section 2.2.3, Figure 2.18).

The pre-CoQ_{10} peak was electrochemically active, since it was also observed with the ECD, like the intermediates found in the cases of *COQ6* (4-HP_{10}) and *COQ7* (DMQ_{10}) deficiency (see Chapter 2, sections 2.2.2 and 2.2.1, respectively). However, in contrast with the *COQ6* and *COQ7* deficiency intermediates, *COQ4* deficiency pre-CoQ_{10} peak did not shift when the sample passed through the oxidizing guard cell before entering the chromatographic column (Figure 4.6.B). This probably indicates that this molecule would need a greater potential to be oxidised or that it is already in the oxidized form.

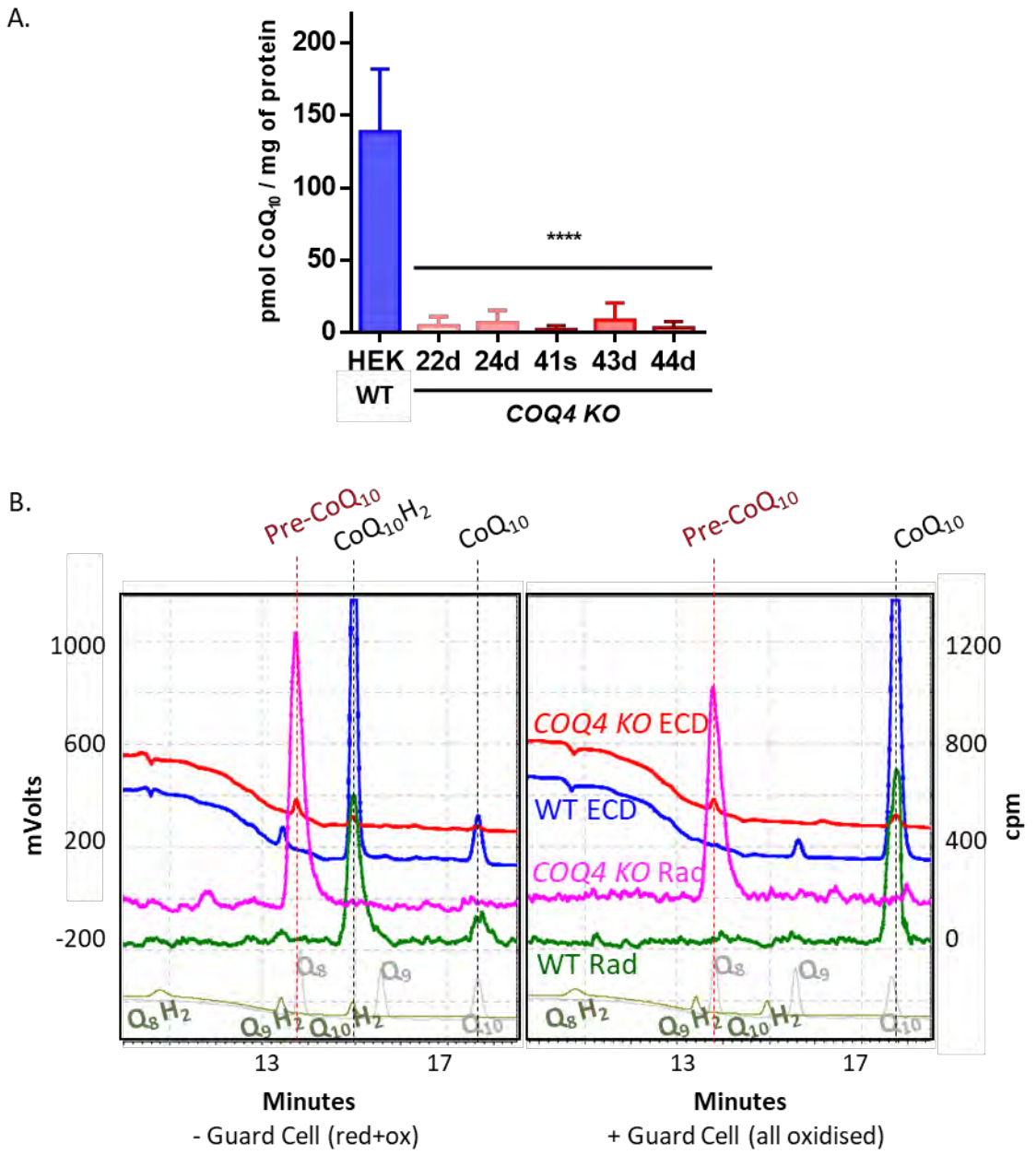

Figure 4.6. Quinone content in *COQ4* KO cell lines.
(A) All *COQ4* KO clones had almost null levels of CoQ_{10} in total lipid extracts (One-way ANOVA, Dunnett's multiple comparison test (each KO vs. WT); p value<0.0001). (B) Both cell lines were cultured with radiolabelled ^{14}C-4-HB. Labelled quinones were detected by HPLC with a radio-flow detector (Rad), while total quinone content was detected by a electrochemical detector (ECD). *COQ4* KO samples showed a pre-CoQ_{10} peak (retention time: 13.5 minutes), detected by Rad and ECD and not detected in WT. This peak do not shift when it is subjected to oxidation by the guard cell (right panels, with the oxidizing guard cell after the injector).

HPLC-coupled MS and mass scanning of lipid extracts from WT and *COQ4* KO cells was performed to characterise this compound. A list with all the possible intermediates of the pathway, according to the current knowledge for CoQ biosynthesis in mammals, was generated, with molecular formulas and calculated molecular mass of the different

compounds (Table 4.7, for abbreviations of the compounds' names, please refer to Table 4.2). This list was used as the input for the mass spectrometry experiment, meaning that if the mass found in the samples was not previously in the list, we would not be able to identify the compound.

Table 4.7. List of possible intermediates of CoQ_{10} biosynthesis, input for MS identification.

Abbreviation	Formula	M (u)	$[M+NH_4]^+$	Redox state
DHB	$C_{57}H_{86}O_3$	818,657695	836,692069	
DDHB	$C_{57}H_{86}O_4$	834,65261	852,686983	
DHMB	$C_{58}H_{88}O_4$	848,66826	866,702634	
DMP	$C_{57}H_{88}O_2$	804,678429	822,712804	
DPP	$C_{56}H_{86}O$	774,667865	792,702239	
4-HP_{ox}	$C_{56}H_{84}O_2$	788,64713	806,681504	ox
4-HP_{red}	$C_{56}H_{86}O_2$	790,66278	808,697154	red
$DHDP_{ox}$	$C_{56}H_{84}O_3$	804,642045	822,676419	ox
$DHDP_{red}$	$C_{56}H_{86}O_3$	806,657695	824,692069	red
$DDMQ_{10}$	$C_{57}H_{86}O_3$	818,657695	836,692069	ox
$DDMQ_{10}H_2$	$C_{57}H_{88}O_3$	820,673344	838,707719	red
DMQ_{10}	$C_{58}H_{88}O_3$	832,673344	850,707719	ox
$DMQH_2$	$C_{58}H_{90}O_3$	834,688995	852,723369	red
$DMeQ_{10}$	$C_{58}H_{88}O_4$	848,66826	866,702634	ox
$DMeQ_{10}H_2$	$C_{58}H_{90}O_4$	850,68391	868,718284	red
CoQ_{10}	$C_{59}H_{90}O_4$	862,68391	880,718284	ox
$CoQ_{10}H_2$	$C_{59}H_{92}O_4$	864,69956	882,733934	red

Six different samples from WT and *COQ4* KO cells were analysed and some intermediate candidates were obtained (Figure 4.7 and Table 4.8). While in WT samples we found CoQ_{10} in its oxidized (*m/z* 880.7 [M+NH4$^+$]) or reduced (*m/z* 882.7 [M+NH4$^+$]) form, in *COQ4* KO we found molecules with different *m/z* ratio. In 4 out of 6 samples, we found an ion with *m/z* 866.7 [M+NH4$^+$], corresponding to the formula $C_{58}H_{88}O_4$. There are two intermediates from the list with that formula. One of them is 3-decaprenyl-4-hydroxy-5-methoxybenzoate (DHMB), product of COQ3. The enzyme that decarboxylates it in C1 is still unknown, so it could be a good candidate. However, with the same $C_{58}H_{88}O_4$ formula there is 2-decaprenyl-5-hydroxy-6-methoxy-3-methyl-1,4-benzoquinone ($DMeQ_{10}$), product of COQ7 and substrate of COQ3. We have also found in 3 out of 6 samples a *m/z* of 868.7 [M+NH4$^+$], compatible with the reduced form of this last molecule, 2-decaprenyl-5-hydroxy-6-methoxy-3-methyl-1,4-hydroquinone ($DMeQ_{10}H_2$). Another *m/z* found in 1 out of 6 sample was 836.7, which can correspond to the formula $C_{57}H_{86}O_3$ [M+NH4$^+$]. There are two molecules of the list with this formula, 4-hydroxy-3-

decaprenylbenzoic acid (DHB) and 2-decaprenyl-6-methoxy-1,4-benzoquinone (DDMQ). DHB is an early intermediate, product of COQ2, which can be modified by COQ6 or the unknown carboxylase previously mentioned; and DDMQ appears later, product of COQ3 or an unknown hydroxylase, which is afterwards methylated by COQ5. Ubiquinol was also found in 2 out of 6 samples (*m/z* 882.7 [M+NH4$^+$]).

Table 4.8. MS candidates for pre-CoQ_{10}.

Sample	#	Compound	Mol. Formula	Selected ion	Err (ppm)	mSigma	m/z calculated	m/z measured
HEK WT	1	$CoQ_{10}H_2$	$C_{59}H_{92}O_4$	$[M+NH_4^+]$	9.3	113.6	882.7334	882.7251
	2	CoQ_{10}	$C_{59}H_{90}O_4$	$[M+NH_4^+]$	2	101.6	880.7177	880.7195
	3	CoQ_{10}	$C_{59}H_{90}O_4$	$[M+NH_4^+]$	1.4	102.1	880.7177	880.7165
	4	$CoQ_{10}H_2$	$C_{59}H_{92}O_4$	$[M+NH_4^+]$	6	127.4	882.7334	882.7281
		CoQ_{10}	$C_{59}H_{90}O_4$	$[M+NH_4^+]$	2.3	16.9	880.7177	880.7197
	5	$CoQ_{10}H_2$	$C_{59}H_{92}O_4$	$[M+NH_4^+]$	6	127.4	882.7334	882.7281
		CoQ_{10}	$C_{59}H_{90}O_4$	$[M+NH_4^+]$	2.3	15.8	880.7177	880.7197
	6	$CoQ_{10}H_2$	$C_{59}H_{92}O_4$	$[M+NH_4^+]$	6.3	105.7	882.7334	882.7278
COQ4 KO	1	DHB or $DDMQ_{10}$	$C_{57}H_{86}O_3$	$[M+NH_4^+]$	6.8	101	836.6915	836.6858
	2	DHMB or $DMeQ_{10}$	$C_{58}H_{88}O_4$	$[M+NH_4^+]$	-3	63.2	866.7021	866.7047
		$DMeQ_{10}H_2$	$C_{58}H_{90}O_4$	$[M+NH_4^+]$	-4.7	28.8	868.7177	868.7218
	3	DHMB or $DMeQ_{10}$	$C_{58}H_{88}O_4$	$[M+NH_4^+]$	-4.9	98.1	866.7021	866.7063
		$DMeQ_{10}H_2$	$C_{58}H_{90}O_4$	$[M+NH_4^+]$	-6.5	66.5	868.7177	868.7234
	4	DHMB or $DMeQ_{10}$	$C_{58}H_{88}O_4$	$[M+NH_4^+]$	3.3	98.2	866.7021	866.6993
	5	$CoQ_{10}H_2$	$C_{59}H_{92}O_4$	$[M+NH_4^+]$	2.8	124.6	882.7334	882.7358
	6	DHMB or $DMeQ_{10}$	$C_{58}H_{88}O_4$	$[M+NH_4^+]$	8.7	76	866.7021	866.7096
		$DMeQ_{10}H_2$	$C_{58}H_{90}O_4$	$[M+NH_4^+]$	3.9	80.4	868.7177	868.7212
		$CoQ_{10}H_2$	$C_{59}H_{92}O_4$	$[M+NH_4^+]$	0.8	111.2	882.7334	882.7341

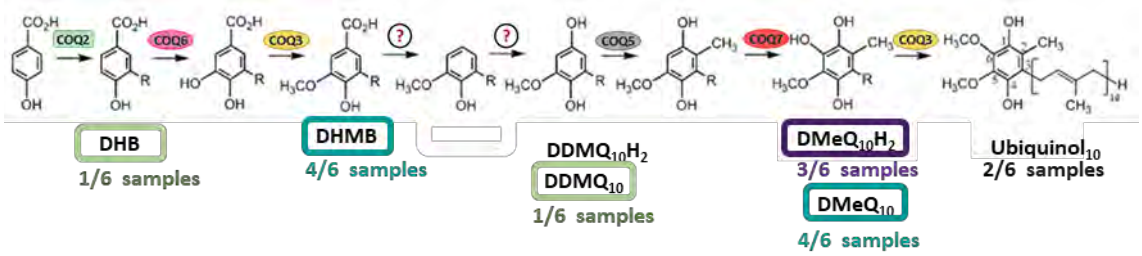

Figure 4.7. Candidates for pre-CoQ_{10} identity.
Mass spectrometry identified some possible intermediates (in boxes) of CoQ_{10} biosynthesis.

We obtained some candidates to be possibly accumulated in *COQ4* KO cells. However, the confidence of the results was not very high (mSigma<50 indicates high probability of correct formula, and in most of the results it was >50) (Table 4.8). Additionally, we were unable to distinguish between molecules with the same molecular formula. It should be bear in mind that only the results that were compatible with the initial list of known intermediates were obtained, meaning we were very limited in terms of possible outputs. It is possible that the molecules we were looking for are not in the list, since the pathway is not entirely deciphered yet. For this reason, nuclear magnetic resonance (NMR) experiment in our pre-CoQ_{10} compound was decided to be performed, to elucidate the exact structure of the intermediate. Significant amounts of the pure compound are needed to this end, so currently the pre-CoQ_{10} peak is being purified by HPLC in order to get enough material to be subjected to NMR analysis.

Treatment with 4-HB analogues and other quinone molecules did not have any effect on CoQ_{10} biosynthesis in COQ4 KO cells

In an effort to explore potential bypass therapies for *COQ4* defects, and at the same time, to gain more insight on the role of this protein, we used *COQ4* KO cell model to test whether some molecules could rescue CoQ synthesis in the absence of the protein. *COQ4* KO and control cells were treated with diverse 4-HB analogues that would potentially bypass some CoQ biosynthesis defects (VA for C5-hydroxylation (COQ6) and O-methylation (COQ3); 2,4-dHB for C6-hydroxylation (COQ7)) and other molecules that could serve as bypass molecules for the still unknown C1-decarboxylation step (hydroquinone (HQ) or 2-methoxy-hydroquinone (2-moHQ). The effect on CoQ_{10} biosynthesis was measured for all the treatments (Table M.2). None of the compounds had a great impact on CoQ_{10} biosynthesis in *COQ4* KO cells or controls (not shown). These results confirm that COQ4 has a different enzymatic role from COQ6 or COQ7 and does not act by supporting their function. Although HQ and 2-moHQ are structurally equivalent to the C1 decarboxylation and hydroxylation putative resulting intermediates, none of them were able to rescue the synthesis of CoQ in *COQ4* KO cells. In order to enter the CoQ pathway, both molecules should be prenylated. It is possible that COQ2 is enzymatically unable or do not recognize the structure of HQ or 2-moHQ, since they are not 4-HB analogues [289].

WT versions of tagged or untagged COQ4 restore CoQ levels and biosynthesis in COQ4 KO, regardless of expression levels

The whole *COQ4* cDNA sequence was amplified by PCR and cloned into a pcDNA5 plasmid, using HindIII and XhoI restriction enzymes (restriction sequences were included in the PCR primers, Table M.11, primers #1 and #2). An intermediate T-A cloning of the PCR bands in pGEMT plasmid was performed. pGEMT plasmids with the different inserts were sequenced and, when the sequences were correct, they were double digested with HindIII and XhoI, as well as pcDNA5 plasmid was. *COQ4* sequences were finally subcloned in pcDNA5, and confirmed by restriction enzyme digestion and sequencing. Tags were introduced by different approaches. Flag-strep (FS) tag was already included in the backbone sequence of the pcDNA5 plasmid, so for FS tagging, *COQ4* was cloned without stop codon. For HA tagging, HA sequence was included, together with a stop codon, in the reverse PCR primer (Table M.11, primer #3), and then, the resulting fragment of DNA was digested and cloned into pcDNA5 in the same way than *COQ4*.

WT COQ4 protein expression in *COQ4* KO cells was achieved after co-transfection of pcDNA5 carrying *COQ4* sequence (untagged or FS/HA tagged) together with pOG44 in these cells (see Materials and Methods, section M2.3 and Figure M.1). Cells expressing these 3 different forms of WT COQ4 were obtained after transfection. Since the sequences introduced are under the expression of a tetracycline/doxycycline inducible promoter, induction tests were performed, by incubating the cells with different concentrations of doxycycline for 24h, before harvesting them. Expression was checked by western blot of total cell lysates. Of note, for all these 3 cell lines, COQ4 protein expression was observed even for not induced samples, and the levels of non-induced expression were some fold higher than endogenous COQ4 expression in HEK WT cells (Figure 4.8.A). This means our models are overexpressing COQ4, even without induction by doxycycline. Induction leads to an even higher overexpression of the transgene.

CoQ_{10} levels in *COQ4* KO cells transfected with *COQ4* WT cDNA were comparable to WT levels, which are very low in both non-induced and induced samples (Figure 4.8.B). Achieving COQ4 protein expression to levels comparable to endogenous expression, thus, is enough to restore CoQ_{10} biosynthesis. Notably a significant overexpression of COQ4 protein does not affect positively nor negatively CoQ_{10} total levels. FS or HA-

tagged COQ4 behave similarly to untagged COQ4, meaning the tags do not impede COQ4 function in CoQ_{10} biosynthesis.

Importantly, accompanying the rescue of CoQ_{10} levels, pre-CoQ_{10} intermediate accumulation is suppressed when COQ4 expression is restored (Figure 4.8.C). This result supports the idea that pre-CoQ_{10} is an intermediate of the pathway.

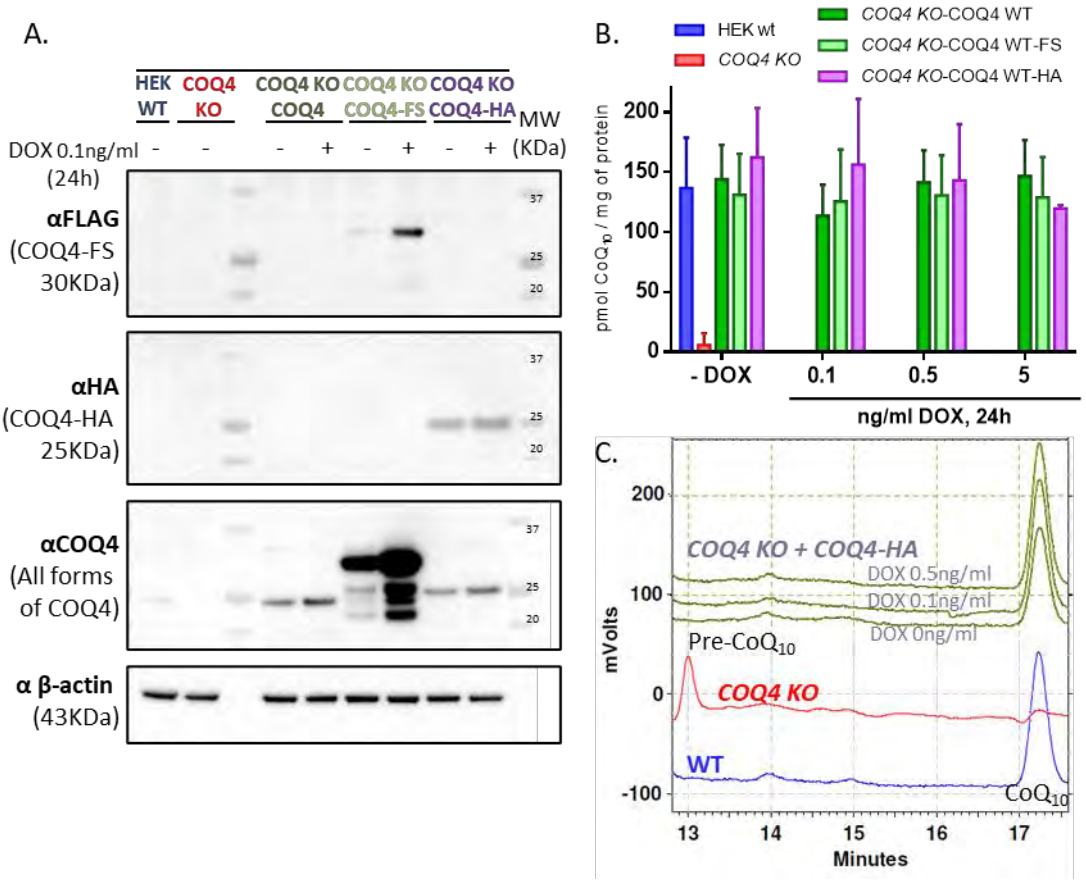

Figure 4.8. *COQ4* KO transfected with WT versions of the gene recovers COQ4 protein expression and CoQ_{10} levels.
(A) Levels of COQ4 proteins in WT, *COQ4* KO and *COQ4* KO transfected with untagged or FS/HA tagged WT COQ4. Membranes developed with antibody against each tag or anti COQ4. Cells were incubated with 0.1ng/mL of doxycycline (DOX) for 24h. (B) CoQ_{10} levels in the same cells with or without doxycycline induction. (C) Representative HPLC-ECD chromatograms from WT, *COQ4* KO and *COQ4* KO + COQ4-HA samples, showing the CoQ_{10} and the pre-CoQ_{10} peaks.

Mutations in the phospho-loop do not affect COQ4 function in CoQ synthesis in COQ4 KO cells overexpressing the mutant versions

We selected the amino acids Ser106, Thr107, Ser108 and Thr109 as a putative phosphorylation loop, based on *in silico* phosphorylation prediction studies previously detailed (see Chapter 3, section 3.2.1 and Figure 3.15). S108 has also been found phosphorylated in global phosphoproteomics mass spectrometry assays [497–501].

Modifying this loop with different mutations would allow us to determine if these amino acids and their phosphorylation state contribute to COQ4 function in CoQ_{10} biosynthesis (Figure 4.9).

Site-directed mutagenesis to study protein phosphorylation is widely used (Figure 4.9.A). Ser/Thr to Ala mutation is considered to prevent phosphorylation of the mutated residue. On the contrary, Ser/Thr mutations to Asp/Glu residues are used to mimic constitutive phosphorylation in Ser/Thr. It has even been proposed that Asp/Glu residues are in some cases ancestral precursors of phosphorylation sites [590].

Thus, to study the putative phosphorylation loop, we performed site-directed mutagenesis in pcDNA5 plasmid containing WT COQ4-FS cDNA sequence to obtain different mutant versions of the gene (M1, M2 and M3) (Figure 4.9.C) with primers described in Table M.11 (primers #22 to #29). M1 has the four amino acids of the loop (Ser106, Thr107, Ser108 and Thr109) converted to Ala, so they would no longer be phosphorylatable. M2 has a point substitution of the residue that has been found phosphorylated before (Ser108) to a constitutively negatively charged Glu, to mimic this phosphorylation. In M3, all amino acids are mutated to Ala, except for this Ser108, that is mutated to Glu. These different versions of the *COQ4* gene were transfected in *COQ4* KO cells, and after selection with hygromycin, they were analysed. If phosphorylation in these residues was important for CoQ biosynthesis, we would expect different outcomes for each of the mutants.

CoQ_{10} levels in *COQ4* KO cells transfected with *COQ4* phospho-mutants were similar in M1, M2 and M3 and comparable to WT levels (in all the samples, non-induced and induced) (Figure 4.9.D). Inducible expression of the transgene was checked by immunoblotting (Figure 4.9.E). Results suggested that these mutations in COQ4 do not affect CoQ synthesis, at least in this model and in the conditions we tested. These mutations are not loss-of-function; however, we cannot discard they are hypomorphic and the high levels of expression do not allow to determine their residual activity. Further studies would be needed to ultimately unveil the significance of these residues in CoQ biosynthesis regulation under different conditions.

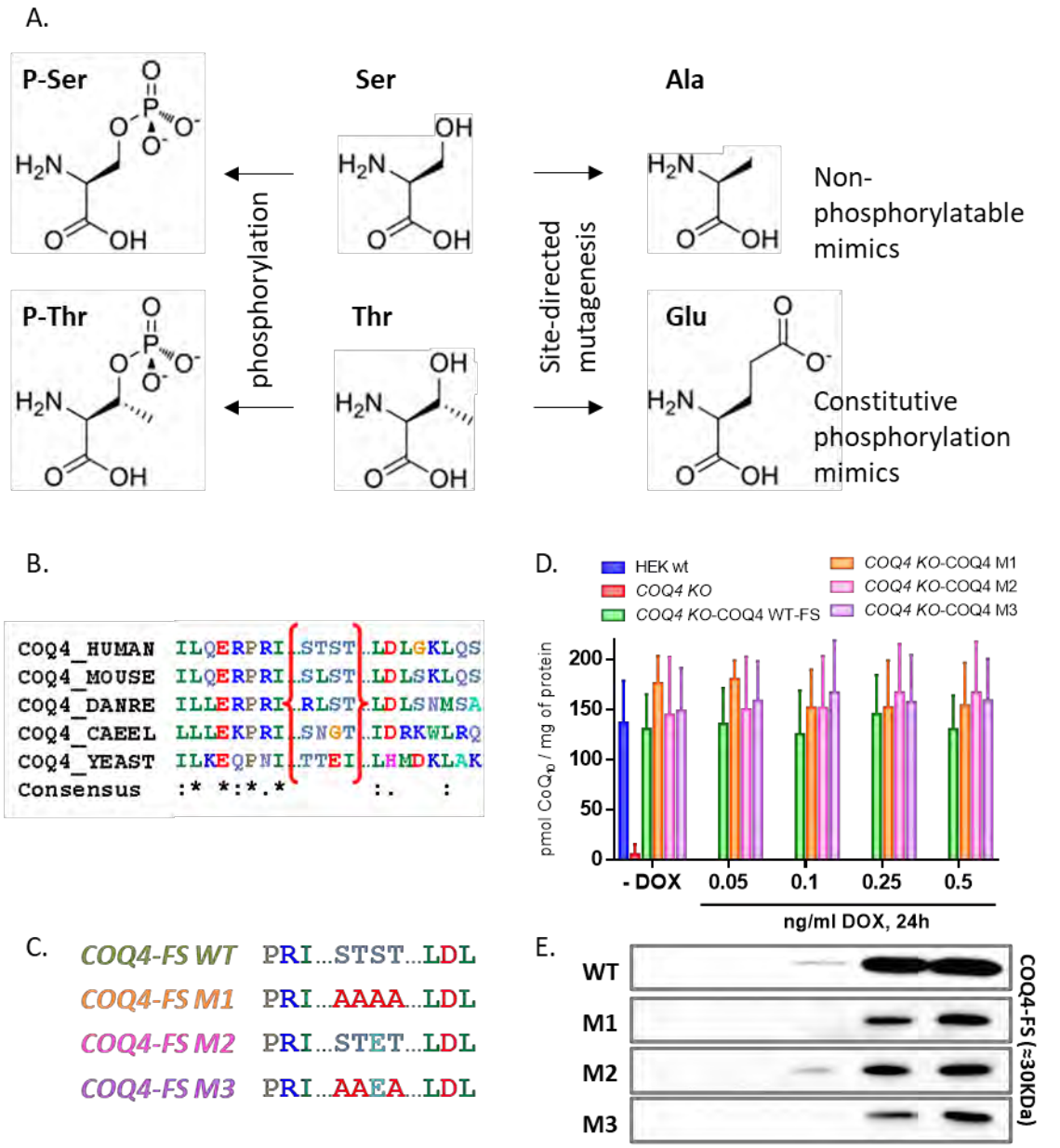

Figure 4.9. *COQ4* KO transfected with phospho-mutant versions of the gene recovers COQ4 protein expression and CoQ_{10} levels.

(A) Changes of serine (Ser) and threonine (Thr) after phosphorylation (left) and mutations for phosphorylation (Glu, glutamic acid) and non-phosphorylation (Ala, alanine) mimics (right). (B) Conservation of the region of the putative phosphorylation loop, between brackets (positions 106, 107, 108 and 109 in human sequence). (C) Changes in this region introduced by site-directed mutagenesis. (D) CoQ_{10} levels in WT, *COQ4* KO and *COQ4* KO cells transfected with WT and mutant M1, M2 and M3 versions of COQ4. (E) Levels of COQ4 proteins in the same cells, developed with antibody against FLAG tag. Before these experiments, cells were incubated with doxycycline (DOX) for 24h.

COQ4 KO cells overexpressing COQ4 protein with mutations found in patients have different outcomes in terms of CoQ biosynthesis

i. Some patient variants restore CoQ biosynthesis in *COQ4* KO cells, while others do not.

Several mutations in *COQ4* have been reported in patients with CoQ deficiency (Figure 2.13), being distributed throughout the whole structure of the protein (Figure 3.17). We wanted to analyse the effect of these mutations on *COQ4* function using a homogeneous background, in this case, the *COQ4* KO cell line. We selected all the variants affecting the coding region (excluding intronic mutations) and introduced them into pcDNA5 plasmid containing HA-tagged WT *COQ4* cDNA sequence by site-directed mutagenesis (Val8Alafs*19, Leu52Ser, Gly55Val, Pro64Ser, Arg66Gln, Asp68His, Thr77Ile, Leu82Gln, Asp111Tyr, Pro119Leu, Asp111Tyr + Pro119Leu, Gly124Ser, Arg141*, Arg145Gly, Phe146Cys, Gln157Lys, Arg158Gln, Thr174del, Arg240Cys) with primers described in Table M.11 (primers #30 to #65). Some of the variants in Figure 2.13 have not been included in this study because they were reported after the design of the experiment (Gly178Glu, Trp184Arg, Ala199Thr). The different versions of the *COQ4* gene were transfected in *COQ4* KO cells, and after selection with hygromycin, they were analysed. As all these mutations have been detected by NGS in patients in a primary CoQ_{10} deficiency disease context, we expected they would probably affect *COQ4* function in CoQ_{10} biosynthesis.

We checked the inducible expression of the different mutated COQ4 versions by immunoblot (Figure 4.10.A). Most of them had a leaky expression of the genes and achieved a high level of COQ4 protein after induction with doxycycline. Some of them showed very low (Val8Alafs*19, Asp111Tyr + Pro119Leu, Arg240Cys-1) or even null (Arg141*) levels of *COQ4* expression.

Figure 4.10. *COQ4* KO transfected with COQ4 mutant versions from patients recovers COQ4 protein expression and CoQ_{10} levels in different degrees.
(A) Levels of COQ4 proteins in HEK WT (WT), *COQ4* KO (KO) and *COQ4* KO transfected with WT COQ4 (WT) or with COQ4 mutated variants from patients. Membranes developed with antibody against COQ4. Before these experiments, cells were incubated with doxycycline (DOX) for 24h. CoQ_{10} (C) and pre-CoQ_{10} (B) levels in HEK WT, *COQ4* KO and *COQ4* KO cells transfected with WT and patients' mutant versions of COQ4 (Two-way ANOVA, Dunnett's multiple comparison test (each transfected cell line (induced+non-induced) vs. WT); p values: ****, $p<0.0001$; ***, $p<0.001$; **, $p<0.01$). Grey area represents CoQ_{10} levels range found in controls.

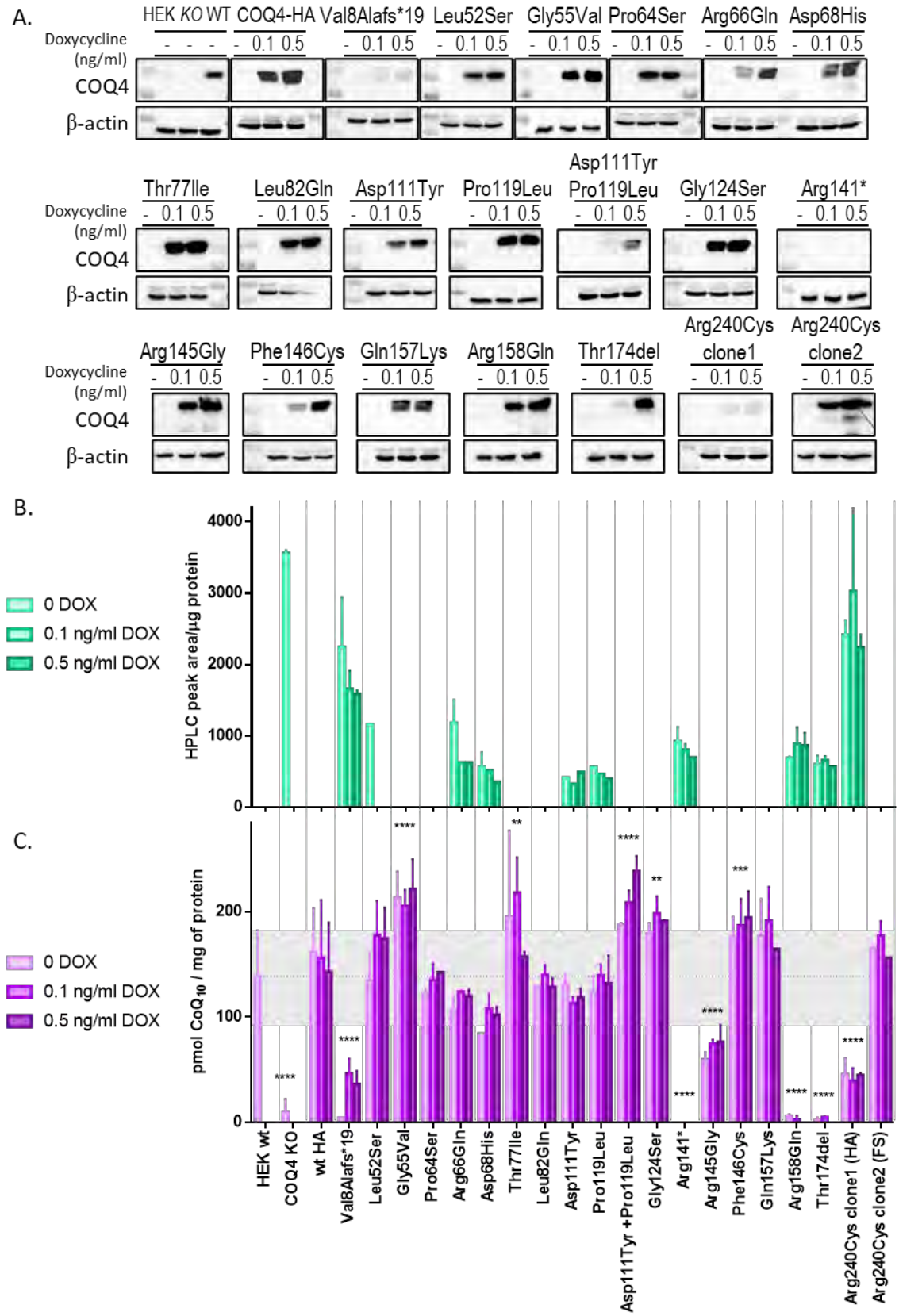
A.
HEK KO WT
COQ4-HA
Val8Alafs*19
Leu52Ser
Gly55Val
Pro64Ser
Arg66Gln
Asp68His
Doxycycline (ng/ml)
- - - - 0.1 0.5
COQ4
β-actin
Thr77Ile
Leu82Gln
Asp111Tyr
Pro119Leu
Asp111Tyr Pro119Leu
Gly124Ser
Arg141*
Arg145Gly
Phe146Cys
Gln157Lys
Arg158Gln
Thr174del
Arg240Cys clone1
Arg240Cys clone2
B.
0 DOX
0.1 ng/ml DOX
0.5 ng/ml DOX
HPLC peak area/µg protein
4000
3000
2000
1000
0
C.
pmol CoQ10 / mg of protein
200
100
0
HEK wt
COQ4 KO
wt HA
Val8Alafs*19
Leu52Ser
Gly55Val
Pro64Ser
Arg66Gln
Asp68His
Thr77Ile
Leu82Gln
Asp111Tyr
Pro119Leu
Asp111Tyr +Pro119Leu
Gly124Ser
Arg141*
Arg145Gly
Phe146Cys
Gln157Lys
Arg158Gln
Thr174del
Arg240Cys clone1 (HA)
Arg240Cys clone2 (FS)

We analysed CoQ levels in all these *COQ4* KO transfected cells (Figure 4.10.C), and also quantified the levels of the pre-CoQ intermediate, which seems to be a marker of *COQ4* deficiency (Figure 4.10.B). Surprisingly, most of the mutations were able to restore WT levels of CoQ, to the same extent than the WT gene did (Leu52Ser, Pro64Ser, Arg66Gln, Asp68His, Leu82Gln, Asp111Tyr, Pro119Leu, Gln157Lys). At the same time, these mutations abolished pre-CoQ accumulation, in line with what we observed when we transfected with the WT protein. The rest of the mutations had other different effects.

There were 6 mutations that produced a significant decrease in CoQ levels and, parallelly, an increase in pre-CoQ accumulation (Val8Alafs*19, Arg141*, Arg145Gly, Arg158Gln, Thr174del, Arg240Cys-1). Two of them are mutations not expected to produce any functional COQ4 protein: the frameshift (Val8Alafs*19, one of the mutations of P105, see Chapter 2, section 2.2.3), and the non-sense (Arg141*) mutations, which create premature STOP codons. Null or almost null levels of COQ4 protein were observed by immunoblot of cells carrying these two mutations. The deletion mutation (Thr174del) produces a protein, observed by western blot, but extremely low levels of CoQ. The negative effect of this mutation can be explained by its localisation in the protein structure, inside the loop between helixes α7 and α8, in which the putative Zinc-binding motif is located (Figure 3.16). The lack of this threonine probably affects the correct orientation and function of the Zinc-binding motif. The rest of the mutations producing a decrease in CoQ are 3 missense mutations (Arg145Gly, Arg158Gln, Arg240Cys). Among them, Arg145Gly mutant is the one with the highest levels of CoQ and the only one with no pre-CoQ accumulation. Regarding COQ4 protein expression, Arg145Gly and Arg158Gln produced COQ4 protein levels comparable to the rest of the mutations, but Arg240Cys levels were very low. In order to check if the decrease of CoQ in this mutant (Arg240Cys-1) was an effect of the low expression, we re-cloned the mutated gene in pcDNA5 with FS tag and transfected *COQ4* KO cells again (Arg240Cys-2). In this second mutant clone, COQ4 protein levels were higher and CoQ levels were now in a WT range.

There is another set of 5 mutations that produced a surprising phenotype in *COQ4* KO cells: an increase in CoQ levels (Gly55Val, Thr77Ile, Asp111Tyr + Pro119Leu, Gly124Ser, Phe146Cys). Curiously, 3 of them (Gly55Val, Thr77Ile, Phe146Cys) were included in the

"Milder disease" group described in Chapter 3, section 3.2.1 (Figure 3.17). It is challenging to explain how could mutations that produce primary CoQ deficiency in patients produce an increase in CoQ levels in the *COQ4* KO cellular model. However, we should bear in mind that variants are overexpressed in the KO mutants, and, although mutated, the high load of protein could compensate for a putative reduced enzymatic activity. There is also the possibility that these mutations would affect somehow COQ4 regulation, that could be differentially exerted in a patient or an immortal cell line's context. Our observation raises concerns about the general use of this kind of models to study the pathogenicity of different mutations. Our results would suggest that this approach is only useful to determine the pathogenicity of very drastic mutations with no residual COQ4 activity. For the rest of the cases, it would be difficult to distinguish between the non-pathogenic and the hypomorphic variants. The latter would have a decrease in protein activity but could act as WT COQ4 when they are overexpressed.

For example, P108 and P109 patient fibroblasts, which harbour the Phe146Cys homozygous mutation, show extremely low levels of COQ4 protein, accumulation of the intermediary and reduced levels of CoQ (Chapter 2, section 2.2.3 and Figure 2.19.A and B). However, *COQ4* KO models expressing this variant accumulate high amounts of protein and recover CoQ biosynthesis. The mutation may lead to an unstable mRNA or protein, and the degradation at one of those levels in fibroblasts. Artificially high amounts of protein would compensate for the COQ4 enzymatic defect. Alternatively, it could be possible that this mutation did not affect the activity, but only the stability of the protein and a high and continuous expression would compensate for the rhythm of degradation.

Endogenous expression under the natural promoter of the patient's variants in a homogeneous background would help to clarify these cases, but it would need techniques such as CRISPR-Cas-driven modification of the genome.

ii. Para-amino benzoic acid (pABA) treatment can help us determine *COQ4* patients' mutations pathogenicity and *COQ4* function

Para-amino benzoic acid (pABA) has an amino group in C4, instead of the C4-hydroxyl group of the CoQ head precursor. Yeast, but not mammals, bacteria (*E. coli)* or the plant *A. thaliana* are able to use this molecule to synthesise CoQ (see the introduction of this

chapter, section 4.1.1). In vertebrates, it is not synthetized endogenously, and in mammalian cell cultures, pABA supplementation decreases CoQ total levels and leads to the accumulation of 4-imino-6-demethoxycoenzyme Q (IDMQ), which seems to be a dead end product [289].

We performed a very preliminary assay of pABA supplementation in WT, *COQ4* KO cells and *COQ4* KO cells expressing some of the *COQ4* patient variants (Leu52Ser and Phe146Cys). pABA supplementation would reduce the rate of endogenous CoQ_{10} synthesis from 4-HB, by competing for COQ2 active site to be prenylated [289]. We wanted to check how these different variants would perform in a context of low CoQ_{10} synthesis, and thus, if there were any differences between variants' residual activity to produce CoQ_{10}.

However, by analysing CoQ_{10} levels, we did not observe any difference between the WT and the cells expressing the patients' variants. In terms of CoQ_{10} final product content, CoQ_{10} was equally inhibited in the three cell lines, and with the different times of inhibition (Figure 4.11.A). We could also see a peak probably corresponding to DMQ_{10}, that usually appears upon CoQ_{10} inhibition by pABA [289]. This peak has a retention time slightly shorter than CoQ_{10}. On the other hand, DMQ_{10} content was higher in WT than in the cells expressing mutant COQ4, and it increased with the time of the treatment (Figure 4.11.C). Even if CoQ_{10} levels are the same in the three cell lines, the increased amount of DMQ_{10} in the controls would suggest that COQ4 WT protein is working more efficiently than the mutated COQ4 proteins to produce DMQ_{10} (together with the rest of COQ proteins). The lack of DMQ_{10} accumulation in *COQ4* KO cell line is suggesting that COQ4 functions upstream DMQ_{10} formation.

Figure 4.11. Para-amino benzoic acid (pABA) treatment has different effects on quinone content of *COQ4* KO transfected with COQ4 mutant versions from patients.
Quantification of different quinones after pABA treatment: CoQ_{10} (A), pre-CoQ_{10} (B), DMQ_{10} (C) and $IDMQ_{10}$ (D) peaks (Two-way ANOVA, Dunnett's multiple comparison test (each pABA treated cell line vs. WT with the same treatment for CoQ_{10} (A), DMQ_{10} (C) and $IDMQ_{10}$ (D); each pABA treated cell line vs. the same untreated cell line for pre-CoQ_{10} (B)); p values: ****, p<0.0001; ***, p<0.001; **, p<0.01; *, p<0.05)). (E) HPLC-ECD chromatograms from the same samples, showing the peaks.

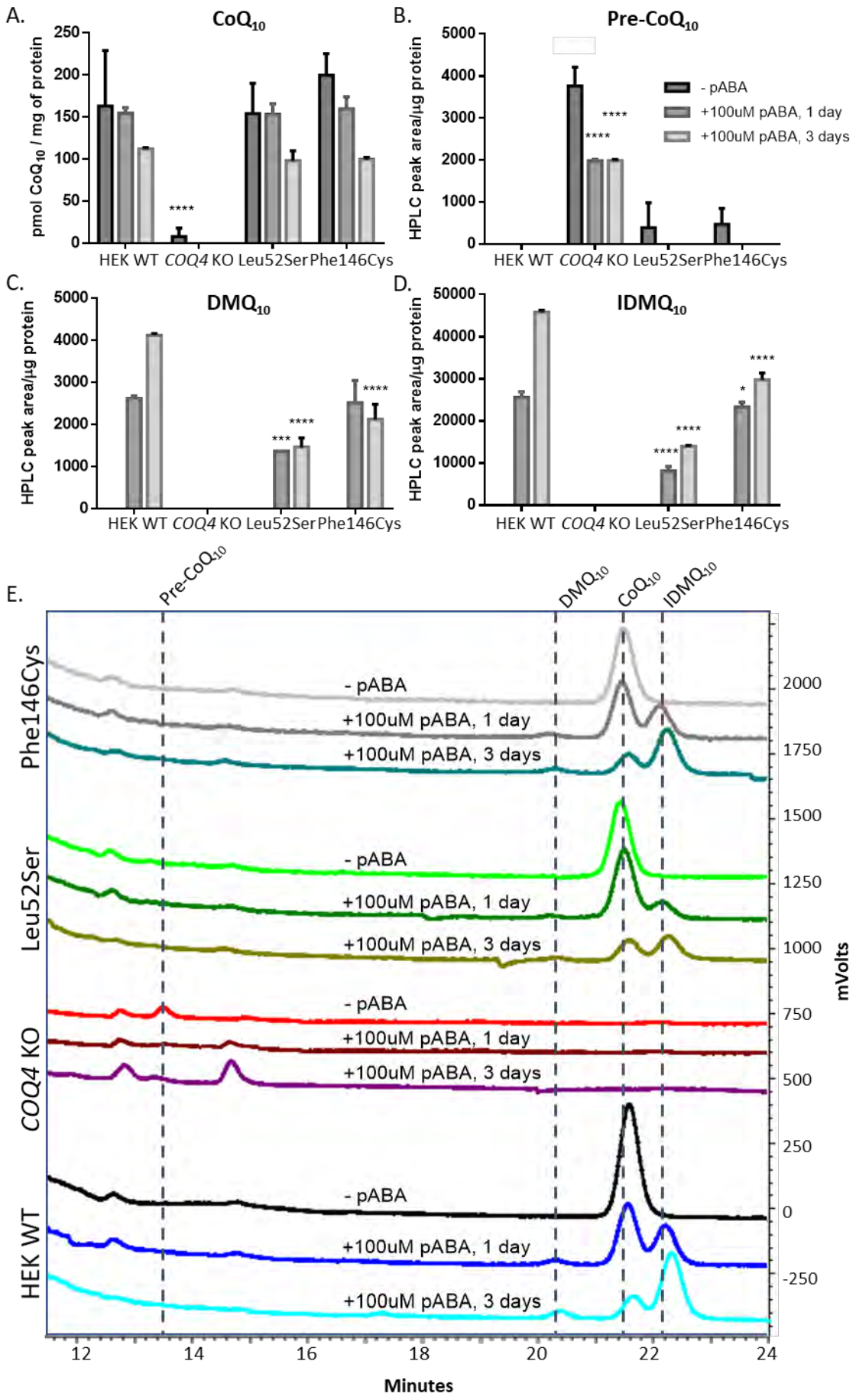
A.
CoQ10
pmol CoQ10 / mg of protein
HEK WT
COQ4 KO
Leu52Ser
Phe146Cys
B.
Pre-CoQ10
HPLC peak area/µg protein
- pABA
+100uM pABA, 1 day
+100uM pABA, 3 days
C.
DMQ10
D.
IDMQ10
E.
Pre-CoQ10
DMQ10
CoQ10
IDMQ10
Phe146Cys
Leu52Ser
COQ4 KO
HEK WT
mVolts
Minutes

Additionally, we could see how pABA is also modified to a dead-end product that is accumulated (putatively $IDMQ_{10}$, based on the bibliography [289]). It appears as a peak after CoQ_{10} in the chromatograms (Figure 4.11.D). It is possible that the accumulation of $IDMQ_{10}$ and the probable inability of COQ7 to transform it are the reasons why DMQ_{10} is also being accumulated. The presence of this putative $IDMQ_{10}$ peak in all cells except from the *COQ4* KO cells indicates that COQ4 protein (WT or mutated) is able to modify the amino containing prenylated quinone. This post- CoQ_{10} peak is higher in WT than in cells expressing mutated *COQ4*, similarly to what was observed with DMQ_{10} accumulation. This fact is in agreement with the suggestion that WT COQ4 is functioning more efficiently to modify the amino-containing prenylated quinone than the mutated COQ4 proteins.

In the case of *COQ4* KO supplemented with pABA, the COQ4-specific intermediate we observed before (pre-CoQ_{10} peak) was reduced, and another peak slightly after appeared instead (Figure 4.11.B and E). This fact probably indicated that when using pABA as a substrate, the intermediate accumulated due to the lack of COQ4 is different than the endogenous one, and probably this difference is the presence of the amino group instead of the hydroxyl. This fact supports the idea that COQ4 acts directly or indirectly upstream DMQ_{10} production.

We did not obtain clear results of pathogenicity of patients' mutations in *COQ4* when expressing the variants in a *COQ4* KO HEK cell line, presenting most of the variants WT levels of CoQ_{10}. With this preliminary study of pABA supplementation we have been able to determine that Leu52Ser and Phe146Cys mutations in *COQ4* affect COQ4 function, since *COQ4* KO cells overexpressing these variants are less efficient in producing late intermediates of the pathway, such as DMQ_{10} or the dead-end product when using pABA, $IDMQ_{10}$. A more comprehensive study including further variants is planned to be performed, to be able to check the pathogenicity and functionality of the mutations found in patients.

COQ4 Isoforms lacking exon 3, 4 and 5, in different combinations, fail to restore CoQ biosynthesis in a COQ4 KO cell line

Different *COQ4* isoforms not previously described were found expressed in fibroblasts (see Chapter 2.2.3, Table 2.1 and Figure 2.17). *COQ4* mRNAs lacking several exons in different combinations were found in fibroblasts from controls and from P105 patient (who carried the splicing mutation c.532+6 T>A). In fibroblasts from this patient, mRNAs lacking exon 3, exon 5, both exons 3 and 5 or exons from 3 to 5, were found to be relatively more abundant than the canonical *COQ4* mRNA, compared to controls. We wanted to check if these putative isoforms were functional and whether they could play a similar role than *COQ4* in CoQ_{10} biosynthesis. For this purpose, we subcloned the cDNA obtained from fibroblasts in pcDNA5 and transfected them into HEK *COQ4* KO cells.

Only the WT *COQ4* cDNA expression was able to restore *COQ4* function and CoQ_{10} production in these cells (Figure 4.12.A). Also, the WT *COQ4* expression suppressed the intermediate accumulation, while expression of the different isoforms did not (Figure 4.12.B). These results would suggest that these isoforms are unable to replace *COQ4* function in CoQ_{10} biosynthesis when it is absent.

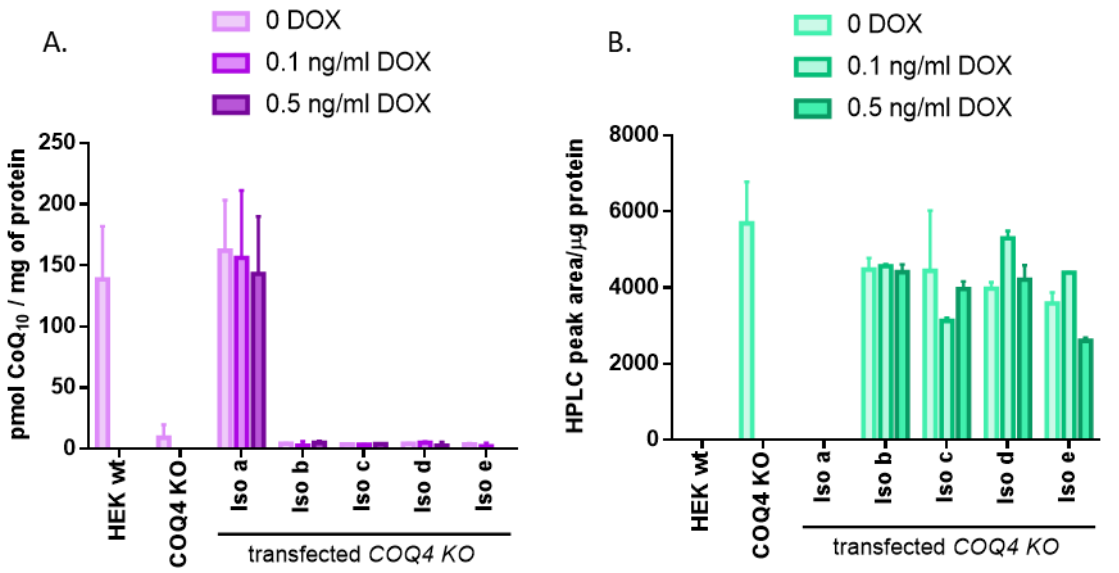

Figure 4.12. Quinone content of *COQ4* KO cells transfected with COQ4 isoforms found in P105 patient's and control's fibroblasts.
Quantification of CoQ_{10} (A) and pre-CoQ_{10} (B) show that only the full length isoform *(iso a)* is able to restore CoQ_{10} WT levels (A) and abolish pre-CoQ_{10} accumulation (B) in induced and non-induced samples.

However, we were not able to detect any *COQ4* isoform protein levels by western blot, even after doxycycline induction. These isoforms are indeed predicted to lead to significant changes in COQ4 protein sequence (Table 2.1), and it is probable that all these aberrant forms of COQ4 are readily degraded in the cells. Future experiments will include inhibition of proteasome to check a putative accumulation of the small proteins. In any case, further phenotyping of these cells to check plasmid integration into the cells' DNA or the RNA isoforms expression levels will help to elucidate whether the isoforms are definitively unable to substitute COQ4 function in CoQ_{10} biosynthesis.

4.2.2. Effects of *COQ4* deficiency in mitochondrial respiration

CoQ-dependent enzymatic activities of combined respiratory complexes are markedly reduced in COQ4 KO cell, while isolated activities are normal.

Respiration studies in *COQ4* KO cells and controls were performed to test the effect of the lack of COQ4 or the consequent dysfunctional CoQ_{10} synthesis on the mitochondrial respiratory function. Activities of individual respiratory chain enzymes were normal, *COQ4* KO only showed a slight tendency to have decreased CI activity and increased CII activity (Figure 4.13.A). However, combined activity of CI+III and CII+III were markedly reduced in these cells, consistent with a severe defect in CoQ_{10} levels (Figure 4.13.B). This deficiency was restored with the expression of *COQ4* WT gene. Reduced CoQ-dependent respiratory activities is the typical phenotype of a CoQ_{10} deficiency, indicating these defects are mostly due to the severely reduced levels of CoQ_{10} in *COQ4* KO cells.

COQ4 KO cells show a defective cellular respiration, that is completely restored with COQ4 gene expression or exogenous CoQ_{10} supplementation

Cellular respiration in living cells was measured by using the Seahorse XF24 Extracellular Flux Analyzer. *COQ4* KO cells showed a completely deficient OCR profile, with all respiratory parameters' levels near to zero (Figure 4.14). This result suggested these cells were unable to use mitochondria for respiration because of the enormous CoQ_{10} deficiency.

WT *COQ4* gene transfection restored all the respiratory parameters to WT levels. The same rescuing effect was observed in *COQ4* KO cells treated with 5µM of CoQ_{10} for 96h hours before the assay, confirming that the respiratory defect is caused by the CoQ_{10} deficiency.

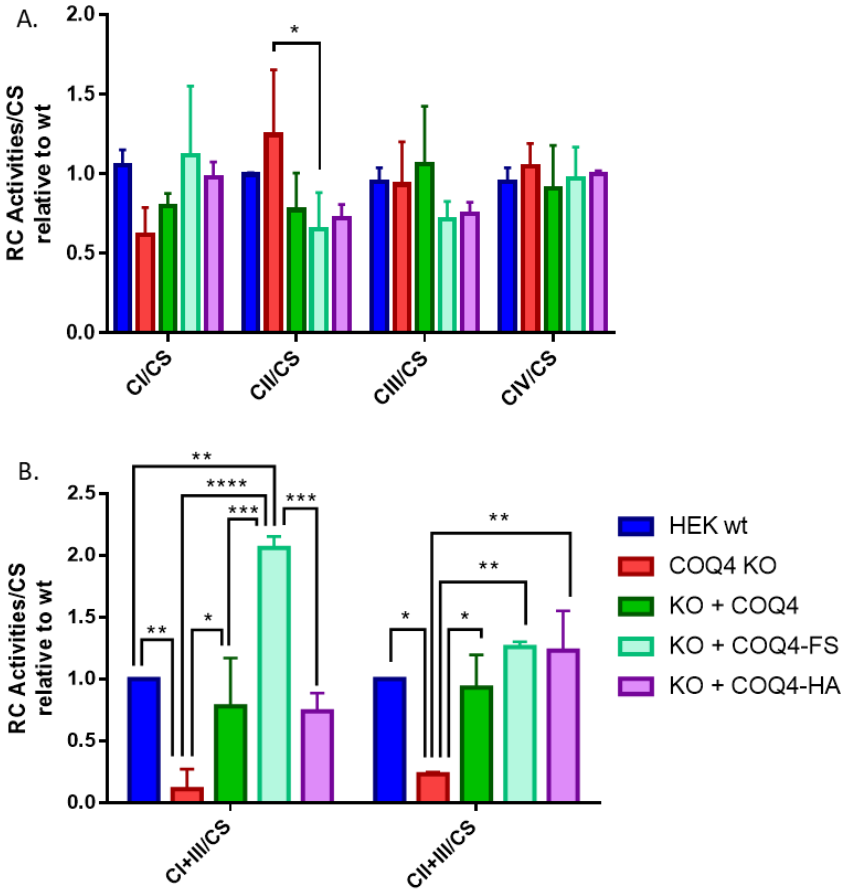

Figure 4.13. Mitochondrial Respiratory Chain (RC) activities in *COQ4* KO cells and the same cells transfected with WT versions of the gene.
(A) Isolated RC activities of *COQ4* KO were normal compared to controls, while (B) CoQ_{10} dependent activities (CI+III and CII+III) were significantly reduced. Specific activities are represented as a normalized value (by the specific activity of citrate synthase (CS)) and relative to WT (Two-way ANOVA with Tukey's multiple comparison test (p values: ****, p<0.0001; ***, p<0.001; **, p<0.01; *, p<0.05)).

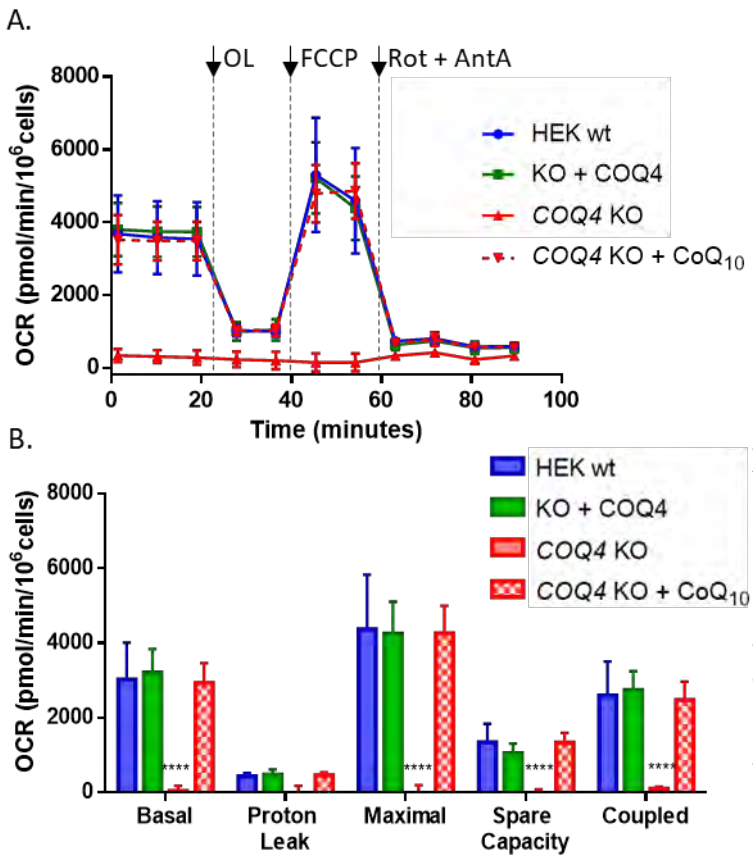

Figure 4.14. *COQ4* KO cells have a respiratory deficiency that is rescued with COQ4-WT expression or CoQ_{10} supplementation.
(A) Oxygen consumption rate (OCR) profile shows a profound respiratory defect in *COQ4* KO cells, restored with WT COQ4 expression or CoQ_{10} supplementation (5μM for 96h). Arrows indicate the addition of the individual inhibitors: OL (oligomycin 1μM); FCCP (Carbonyl cyanide 4-(trifluoromethoxy) phenyl-hydrazone 0.2μM); Rot (rotenone 1μM); AntA (antimycin A 2.5μM). Quantitative data are graphed on B as mean ± SD (Two-way ANOVA with Tukey's multiple comparison test (p value<0.0001(****)).

4.2.3. COQ4 interacts with the rest of the COQ proteins in a dynamic complex

It is clear that CoQ biosynthesis is performed by a complex of proteins in yeast, and in recent years, there is increasing evidence of the formation of such a complex in mammals as well. As a part of our research in COQ4 protein function, we wanted to investigate if COQ4 protein is present in protein complexes, and which are its partners. In order to do so, we performed BN-PAGE and immunocapture of COQ4, with or without SILAC labelling. We were especially interested in determining the composition of the CoQ_{10} biosynthesis complex in human cell lines.

Identification of protein complexes containing COQ4 protein by BN-PAGE

Cell pellets of HEK WT, *COQ4* KO and *COQ4* KO expressing different tagged versions of COQ4 WT protein were enriched in mitochondria with a digitonin treatment. Then, they were prepared for Blue Native-PAGE, solubilizing with two non-denaturing detergents, n-dodecyl-β-D-maltoside (DDM) and digitonin. 2D-BNGE membranes were probed for COQ4 presence and also with a cocktail of antibodies against subunits of MRC

Complexes I, II, III, IV and V (Mitoprofile), as a control of the size of the complexes. The results of the digitonin solubilized mitochondrial enriched pellets are shown in Figure 4.15. The same results were obtained with the harsher solubilization detergent DDM (not shown).

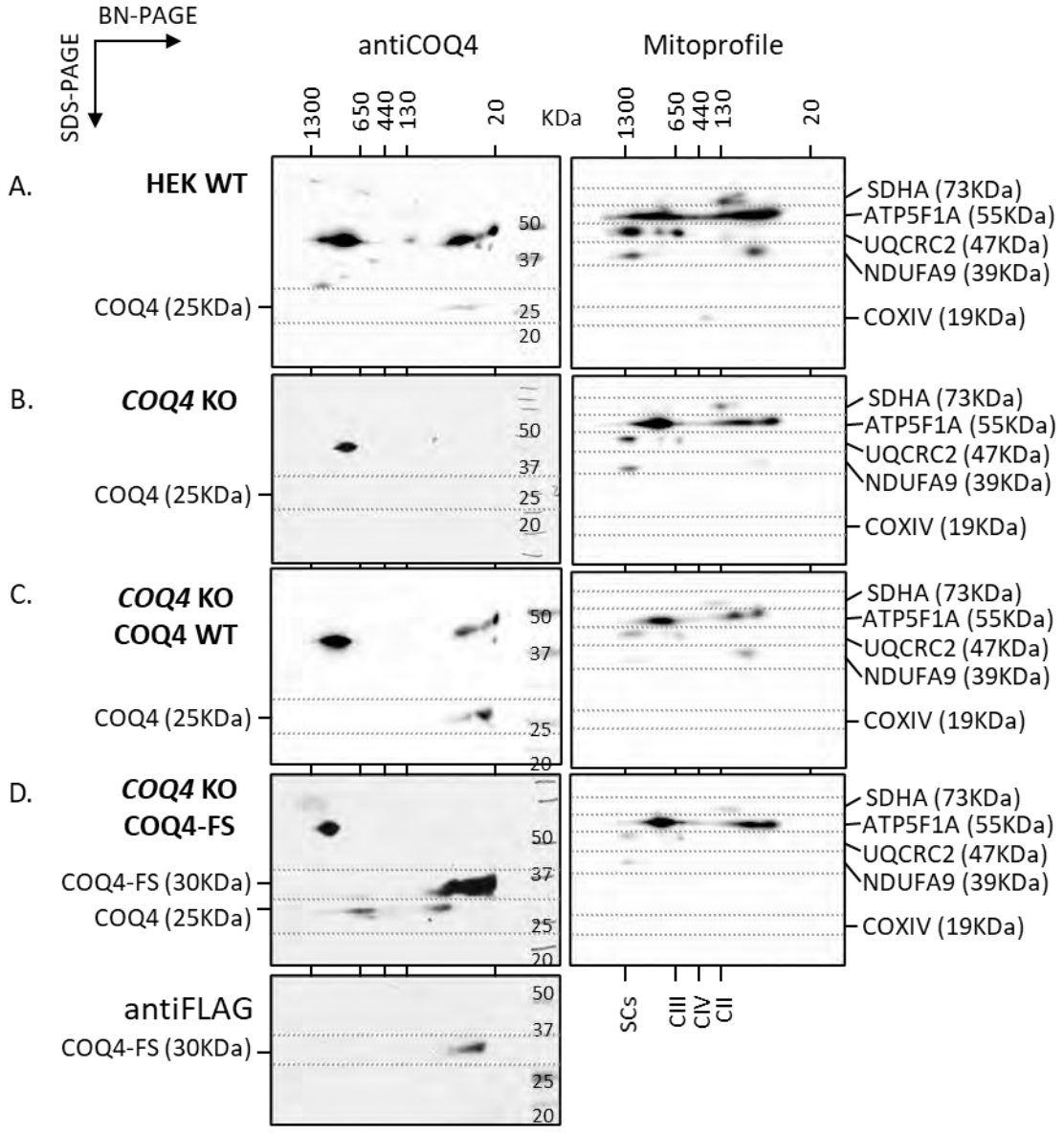

Figure 4.15. 2D BN-PAGE of digitonin-solubilised samples.
Digitonin-solubilised pellets from WT (A), *COQ4* KO, and *COQ4* KO transfected with WT COQ4 (C) or COQ4-FS (D) were run in 1D-BN-PAGE and lanes were subjected to a 2D-SDS-PAGE. Western blot and immunodetection was performed with antiCOQ4 antibody (left) and a cocktail of antibodies against subunits of the mitochondrial respiratory complexes I, II, III, IV and V (Mitoprofile, right).

COQ4 protein (developed with an anti-COQ4 antibody, 25KDa) migrated to the bottom of the gel (low molecular weights) in both WT and *COQ4* KO expressing WT *COQ4* samples (Figure 4.15.A and C). These results suggested that COQ4 is not stably interacting in high molecular weight complexes in our experimental conditions. If COQ4 was part of a complex, its interactions would be transient (or stimulated in some specific metabolic states) or they would be unable to be maintained in the solubilization or the electrophoresis conditions. To test if this low molecular weight conformation was due to the metabolic state of the cells, the same experiments were performed by treating the cells with a low glucose medium for 24h to boost respiration and, thus, the need of CoQ biosynthesis. No differences were observed by comparing the high glucose to the low glucose conditions (not shown).

Comparing these two blots with *COQ4* KO blot, there are two main differences (Figure 4.15.A-C). On one hand, as expected, *COQ4* KO blots lack the 25KDa band corresponding to COQ4 protein, which corroborates that our model is a total knock out of COQ4 protein. On the other hand, a 50 KDa band is differentially detected also at the low molecular weights' region. We could not confirm the nature of this band, but we could speculate that it could be a very stable dimeric form of COQ4 (resistant to SDS treatment), that it is not forming higher molecular weight complexes. These 50KDa band, not present in *COQ4* KO cells, could not be distinguished by SDS-PAGE probably because of the presence of another overlapping 50KDa band result of an unspecific binding of the anti-COQ4 antibody (which can be observed by BN-PAGE, at the 50KDa size, but running in high molecular weight complexes).

COQ4 KO expressing FLAG-strep (FS)-tagged COQ4 behave slightly different in 2D BN-PAGE experiments (Figure 4.15.D). COQ4-FS was detected by an anti-FLAG antibody, with the expected size (around 30KDa). It was detected in the low molecular weight region of the gel, similar to the localization of WT COQ4 in HEK WT samples. However, when we developed the blot with an anti-COQ4 antibody, we saw some differences compared to the untagged COQ4 protein. Overexpression of COQ4-FS led to a big accumulation of tagged COQ4 at around 30KDa. Surprisingly, a band corresponding to the size of untagged COQ4 also appeared, forming complexes of higher molecular weight (from around 50 to 650 KDa). This band was undetected by the antiFLAG

antibody, suggesting that FS-tagged COQ4 was probably being processed to remove the tag. These COQ4-containing high molecular weight complexes observed could be an artifact related to the processing of the tag, which would not occur naturally or could be real complexes only visible now because of the high expression of the protein. Despite this model being useful for recovering COQ4 function in CoQ biosynthesis, this anomalous behaviour in terms of protein complexes should be considered. The unspecific 50KDa detection at high molecular weights is still there, but the one at low molecular weights is not detectable. Maybe the processing of the tag is needed for the putative dimerization and functionality.

Quantitative proteomics with SILAC labelling after immunocapture of COQ4 revealed measurable interactions with mitochondrial chaperones and actin related proteins

To characterise the interaction partners of COQ4 protein, we carried out a comparison of COQ4 immunopurified from digitonised cells of *COQ4* KO overexpressing COQ4 (tagged or untagged) and *COQ4* KO cells as a negative control for COQ4 expression. They were analysed by quantitative mass spectrometry (MS) using stable isotope-labelled amino acids in cell culture (SILAC). Three different experiments were performed, with immunocapture of COQ4-FS with antiFLAG beads, untagged COQ4 with antiCOQ4 antibody crosslinked to agarose beads, and COQ4-HA with antiHA beads. Each of these three experiments were performed in duplicates with reciprocal isotopic labelling between the *COQ4* expressing cell line and the *COQ4* KO.

Firstly, we performed the immunocapture of FLAG-tagged COQ4 from a 1:1 mix of mitoplasts from *COQ4* KO and *COQ4* KO overexpressing COQ4-FS, differently labelled. COQ4-FS enrichment was checked by immunoblot (Figure 4.16.A). The mass spectrometric analysis of affinity-purified COQ4 and associated partners identified 148 different proteins, but only 73 of them were quantifiable (Figure 4.16.B). From these 73, only three of them showed a significant enrichment in the COQ4-FS overexpressing sample over the negative control. The first one was COQ4 itself, which demonstrated that the immunocapture worked, as we had already seen by western blot. Then, only HSPA9 (HSP70) and HSPD1 (HSP60) were significantly enriched in COQ4-FS eluates (Figure 4.16.B). They are both mitochondrial heat-shock chaperones with important

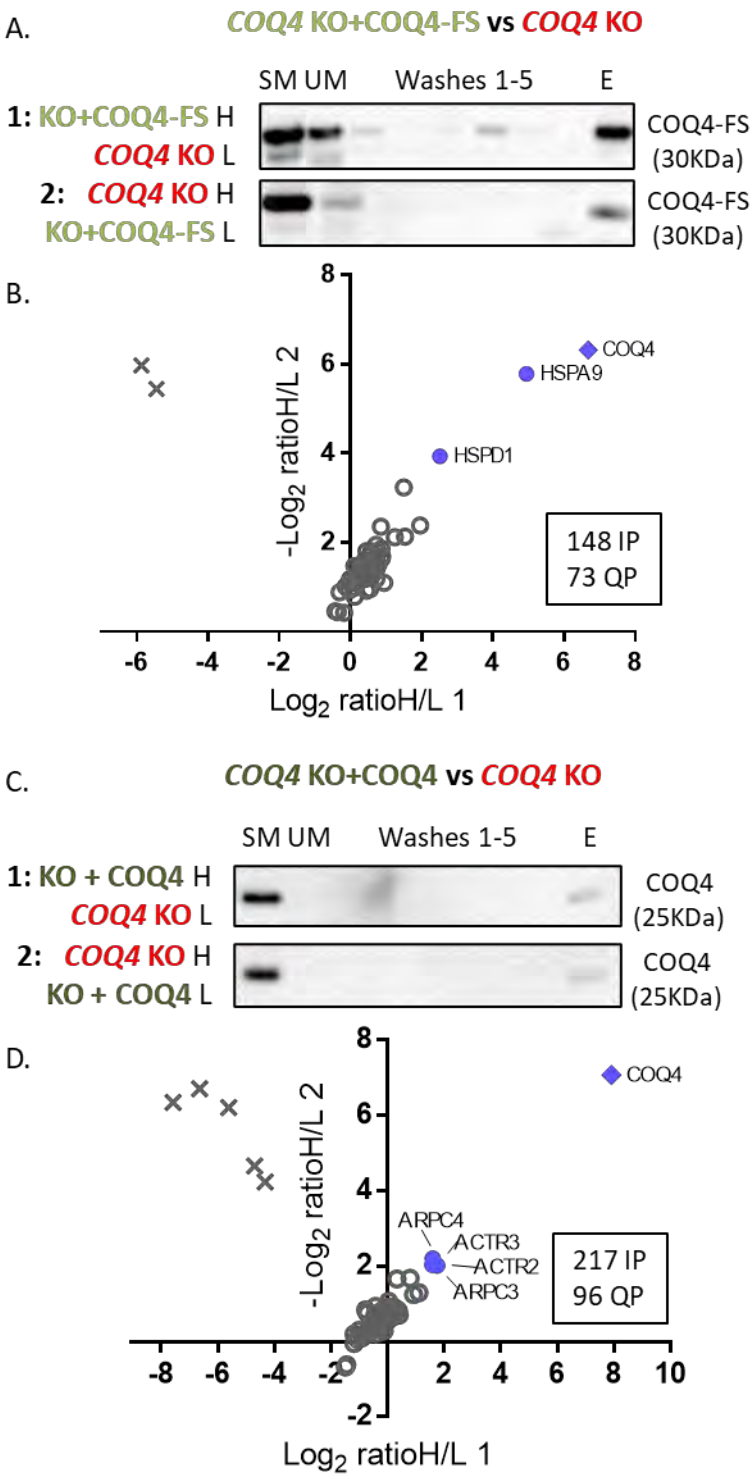

Figure 4.16. COQ4 co-purified with mitochondrial chaperones and actin related proteins, measured by quantitative proteomics with SILAC labelling.

Immunocapture of COQ4 (FS-tagged (A, B) or untagged (C, D)) was checked by immunoblot (A, C). Before the experiments, expression of COQ4 was induced with 24h of doxycycline 0.1 ng/mL. Scatterplots show the $\log_2$ and $-\log_2$ H/L ratios obtained after mass spectrometry analysis of anti-FLAG (B) or anti-COQ4 (D) co-immunoprecipitation fractions of bidirectional SILAC labelled *COQ4* KO and *COQ4* KO expressing COQ4-FS (B) or COQ4 WT (D). Each point represents a specific protein. COQ4 protein is plotted with a rhombus and co-immunopurified proteins with circles. Statistically significant interactions are plotted in blue (based on significance B, Perseus analysis platform). Crosses represent exogenous contaminants. SM, soluble material; UM, unbound material; E, elution fraction; IP, identified proteins; QP, quantified proteins.

functions in stress response, maintenance of the mitochondria and correct folding of imported proteins[591,592]. This would suggest that the overexpression of COQ4-FS is producing stress, and these proteins are interacting with the excess of tagged COQ4 to fold it correctly. Going back to the BN-PAGE results, maybe the complexes we were observing were related with this kind of interactions (Figure 4.15.D). However, it could be possible that these significantly quantified interactions are meaningful, and there is some relationship between COQ4 or CoQ biosynthesis with mitochondrial heat shock proteins. More in-depth studies would be needed to confirm this.

After observing that COQ4-FS overexpression could be producing artifacts, we purified untagged COQ4 from *COQ4* KO overexpressing untagged COQ4 and *COQ4* KO as negative control (Figure 4.16.C). MS identified 217 different proteins and only 96 of them were measurable (Figure 4.16.D). Five of them showed a significant enrichment in the COQ4 overexpressing sample. Again, the most enriched one was COQ4 itself, proving that the immunocapture worked. The other four significantly enriched proteins were ACTR2, ACTR3, ARPC3 and ARPC4, four of the seven subunits of the ARP2/3 complex (Figure 4.16.D). This actin-related complex mediates actin polymerization in the cytoplasm (essential for the cytoskeleton function, cell shape and motility) and the nucleus (provides the motility needed for gene transcription and DNA repair). The hypothetical relationship between COQ4 and these complex from non-mitochondrial cell compartment would require further studies.

The third assay tried to increase the number of interactions found, by treating purified mitochondria with a disuccinimidyl suberate (DSS) before immunocapture. DSS is a non-cleavable and membrane-permeable crosslinker that contains an amine-reactive (NHS) ester at each end of an 8-carbon spacer arm. NHS esters react with primary amines at pH 7-9 to form stable amide bonds, along with the release of the N-hydroxysuccinimide leaving group (Figure 4.17.A). Proteins generally have several primary amines in the side chain of lysine (K) residues and the N-terminus of each polypeptide that are available as targets for NHS-ester crosslinking reagents. With DSS crosslinking, we expected to capture also transient or very dynamic interactions with COQ4. We did a test with different times and concentrations of DSS, crosslinking isolated mitochondria of *COQ4* KO expressing COQ4-HA. We could see the formation of new bands with increasing the

concentration and time, while at the same time, the single protein was disappearing (Figure 4.17.B). We hypothesized that the new bands were COQ4-HA crosslinked to other proteins which it interacts with. We decided to continue with the SILAC-MS experiment, to identify these captured associations. We treated isolated mitochondria from SILAC labelled cells with DSS (1mM, 30min), performed the immunocapture (Figure 4.17.C) and analysed the eluates by MS. MS only identified 81 different proteins, only 5 of them being measurable. Only COQ4, HSPA9 (Hsp70) and HSPD1 (Hsp60) were significantly enriched in COQ4-HA eluates, the same results obtained in the first experiment (Figure 4.17.D).

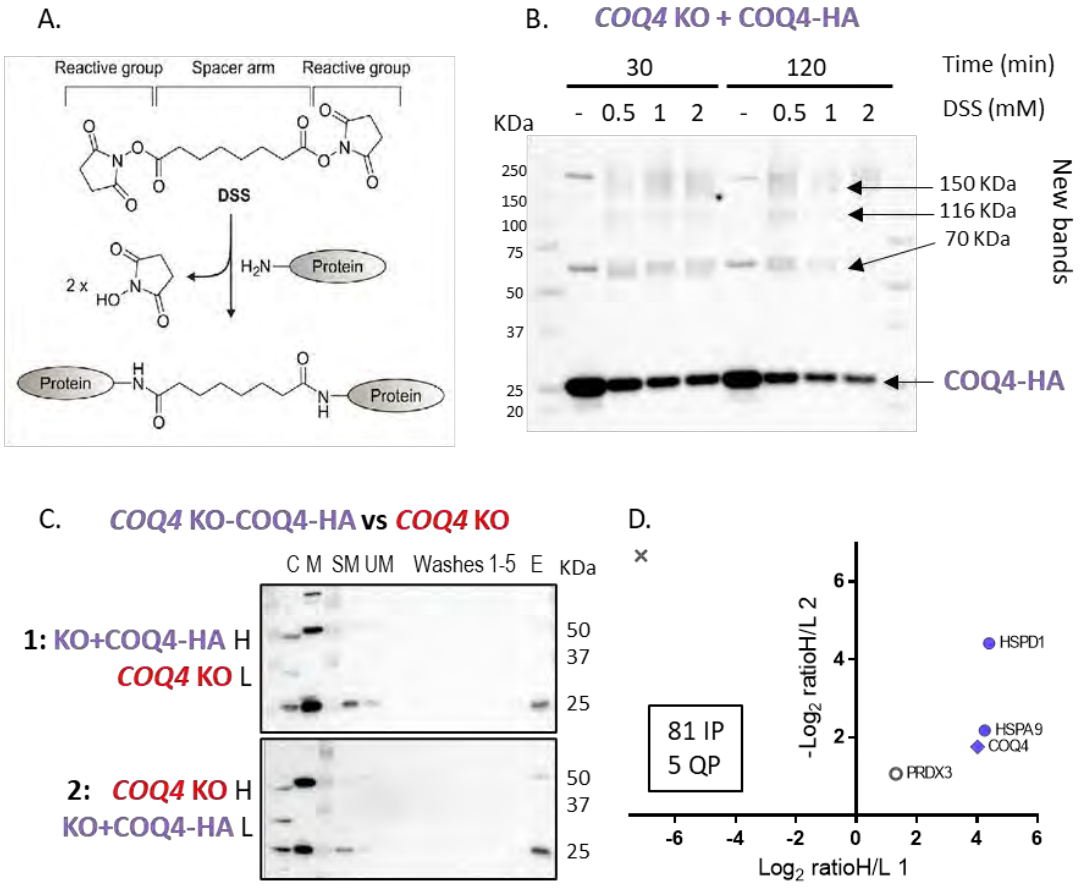

Figure 4.17. COQ4 co-purified with mitochondrial chaperones, measured by quantitative proteomics with SILAC labelling after crosslinking of crude mitochondria.

(A) Disuccinimidyl suberate (DSS) crosslinker. (B) Crude mitochondria were SDS treated with different DSS concentrations an times, and after SDS-PAGE and antiHA immunodetection, new bands of high molecular weight were detected. (C) Immunocapture of DSS treated (1mM, 30min) mitochondria from SILAC labelled cells was performed and checked by immunoblot. Before the experiments, expression of *COQ4* was induced with 24h of doxycycline 0.1 ng/mL. (D) Scatterplot show the $\log_2$ and $-\log_2$ H/L ratios obtained after mass spectrometry analysis of the co-immunoprecipitation fractions of bidirectional SILAC labelled *COQ4* KO and *COQ4* KO expressing COQ4-HA and crosslinked (D). Each point represents a specific protein. COQ4 protein is plotted with a rhombus and co-immunopurified proteins with circles. Statistically significant interactions are plotted in blue (based on significance B, Perseus analysis platform). Crosses represent exogenous contaminants. C, cytosol; M, mitochondria; SM, soluble material; UM, unbound material; E, elution fraction; IP, identified proteins; QP, quantified proteins.

None of the three experiments detected any of the COQ proteins, putatively forming the CoQ biosynthesis complex. The inability to detect any interaction partners for COQ4 could be due to the fact that COQ proteins are expressed in very low levels in the cell, or that these interactions are not stable in the conditions we used for the affinity purification, even if crosslinked.

COQ4-FS copurified with COQ3-COQ9 proteins, and with other mitochondrial and non-mitochondrial proteins.

We performed a less restrictive qualitative proteomic analysis without SILAC (Figure 4.18). Mitoplasts from *COQ4* KO and *COQ4* KO overexpressing COQ4-FS (induced with doxycycline) were subjected to affinity purification with anti-FLAG beads in native conditions. Subsequent analysis of the eluates was performed by MS. The experiment was performed twice, and we only considered the identified proteins as positive results when they were found in both experiments in the pulled down COQ4-FS sample (and not in the negative controls).

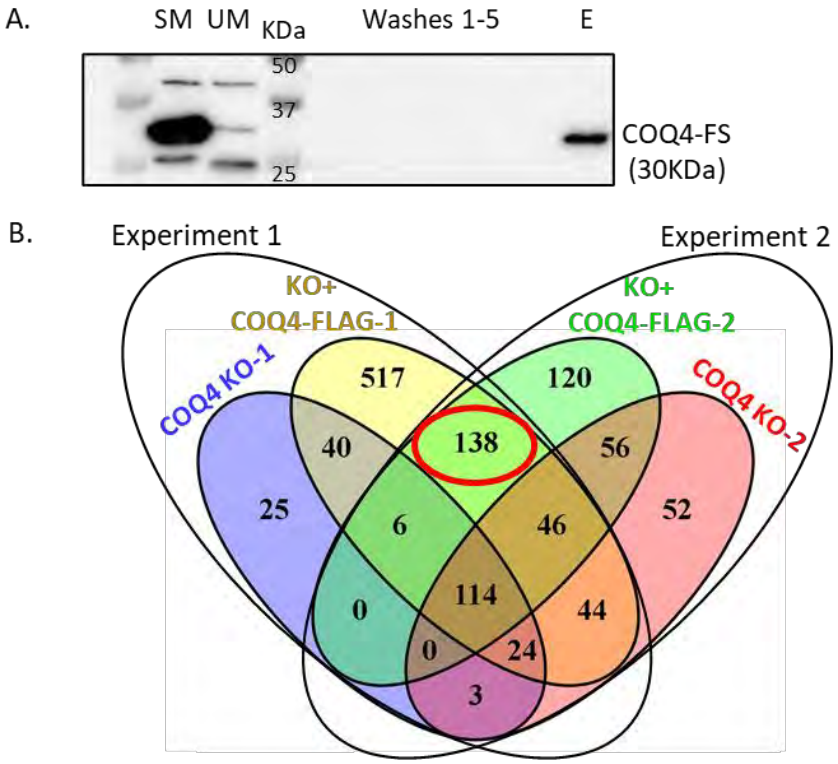

Figure 4.18. COQ4 co-purified with COQ proteins and other mitochondrial proteins.
(A) Immunocapture of COQ4-FS was checked by immunoblot. Before the experiments, expression of COQ4 was induced with 24h of doxycycline 0.1 ng/mL. (B) The elution fraction was subjected to mass spectrometry analysis, and identified proteins (by gene names) were plotted in Venn diagrams. 138 proteins were considered positive in both experiments. SM, soluble material; UM, unbound material; E, elution fraction.

In the first experiment, 929 proteins were identified in the COQ4-FS sample and 212 in the negative control (*COQ4* KO), from which 184 were common to both samples. The second experiment identified 480 proteins in the COQ4-FS sample and 339 in the negative control, being 216 common to both samples. Combining the results of both experiments, we observed that 138 proteins in total were identified as potential interactors of COQ4, since they were found in the two COQ4-FS samples, and not found in any of the negative controls (Figure 4.18.B). By manually analysing these proteins, we eliminated 7 of them that were duplicated in the list. We subjected the protein list (by gene names) to a Gene Ontology (GO) PANTHER overrepresentation analysis, by cellular component, biological process and molecular function.

Among the 131 positive results, 37 were mitochondrial proteins (Table 4.9). We could see this mitochondrial enrichment by the cell component GO analysis. Interestingly, mitochondrial subcompartments like mitochondrial nucleoids and respiratory complexes were overrepresented. ER, Golgi and lysosomes also seemed to be significant locations for COQ4 identified putative partners. In general, cell component GO terms that were overrepresented were mainly related to membranes (plasma, mitochondrial, vesicle membranes) and to complexes that are mainly localised in membranes, such as ATPase or GTPase complexes (Figure 4.19.A). We have to take into account that the immunoprecipitation of COQ4 was performed with digitonised cells (mitochondria enriched fractions) as starting material, so the enrichment in mitochondrial and membrane proteins probably derives from this approach. Molecular function GO analysis showed that the detected proteins mainly exert the following functions: aminoacyl tRNA editing, transferase activity, ion transport across the membrane, oxidoreductase activity, purine nucleotide (ATP, ADP, GTP, GDP) binding, GTPase and ATPase activity, constituent of the cytoskeleton, etc (Figure 4.19.B).

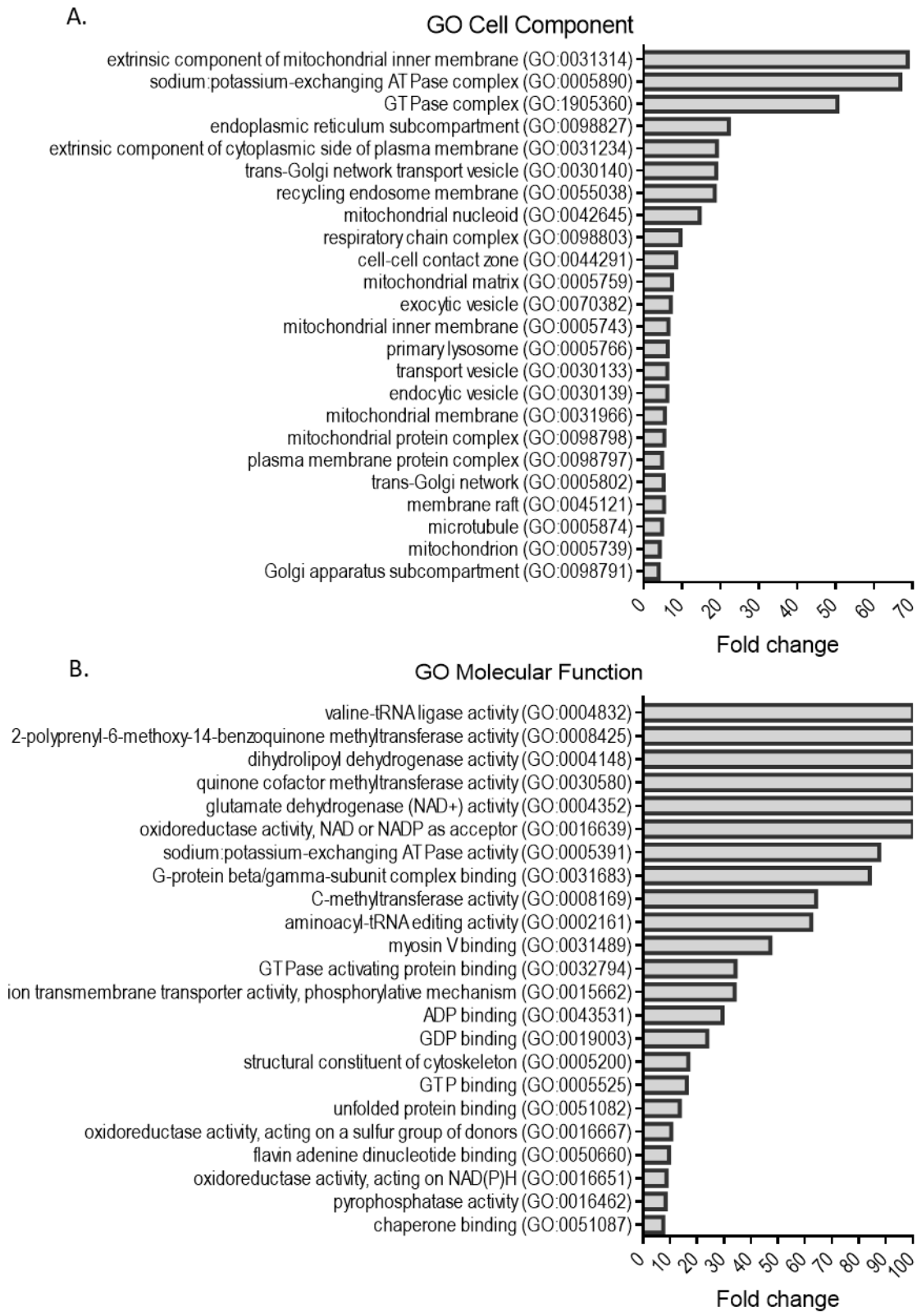

Figure 4.19. Gene Ontology (GO) terms enrichment in COQ4 co-purifing list of proteins.
Representative GO cell component (A) and molecular function (B) terms enriched in putative COQ4 interaction partners.

Table 4.9. Mitochondrial proteins identified in COQ4-immunopurified eluates.

CoQ biosynthesis	OXPHOS	Response to ROS	mtDNA metabolism/ maintenance	RNA metabolism
COQ3	ATP5F1A	PRDX3	POLDIP2	FASTKD4
COQ4	COX4I1	PYCR2	LONP1	FASTKD5
COQ5	NDUFA2			NIPSNAP1
COQ6	NDUFS1			AARS
COQ7	NDUFS7			DARS2
COQ8B	UQCRC1			VARS2
COQ9				
Pyruvate, TCA and other mitochondrial metabolism	**Fatty acids β-oxidation**	**Aa metabolism**	**Chaperones/ protein folding**	**Protein import to mitochondria**
D2HGDH	HADHB	MCCC2	FKBP8	TIMM44
DLD	IVD	PYCR2	TRAP1	TIMM50
GLUD1		GLUD1		GRPEL1
IDH3B		GLUD2		HAX1
GLUD2				

Importantly, amongst the mitochondrial-positive results, all the COQ proteins putatively forming the CoQ biosynthetic complex (COQ3, COQ5, COQ6, COQ7, COQ8B and COQ9) were identified as COQ4 interactors (Table 4.9). The fact that they all co-purified with COQ4-FS provides strong evidence for the mammalian CoQ biosynthesis complex and its composition. Biological process GO analysis also showed an enrichment in ubiquinone biosynthetic process terms (Figure 4.20.A). We found COQ8B and not COQ8A in our experiments. It has been suggested that they are reciprocally regulated depending on different metabolic conditions [438], and it is possible that in our model, the kidney HEK293 cell line, the COQ8 protein that is mostly working is COQ8B. Notably, this observation fits with the fact that the most predominant clinical phenotype of COQ8B patients is a nephrotic syndrome, meaning that COQ8B function is more important in kidney than in other organs.

In addition to the COQ proteins, other mitochondrial proteins involved in different processes were identified as candidates for COQ4 interaction partners (Table 4.9 and Figure 4.20.B). Six of them are components of the mitochondrial respiratory chain, from CI (NDUFA2, NDUFS1, NDUFS7), CIII (UQCRC1), CIV (COX4I1) and CV (ATP5F1A). Some proteins involved in pyruvate metabolism, TCA cycle, fatty acids beta-oxidation and amino acids biosynthesis and catabolism were also identified (D2HGDH, DLD, GLUD1, GLUD2, IDH3B, HADHB, IVD, MCCC2, PYCR2). Proteins involved in protein import to mitochondria maybe were captured when they were transporting COQ4 into the

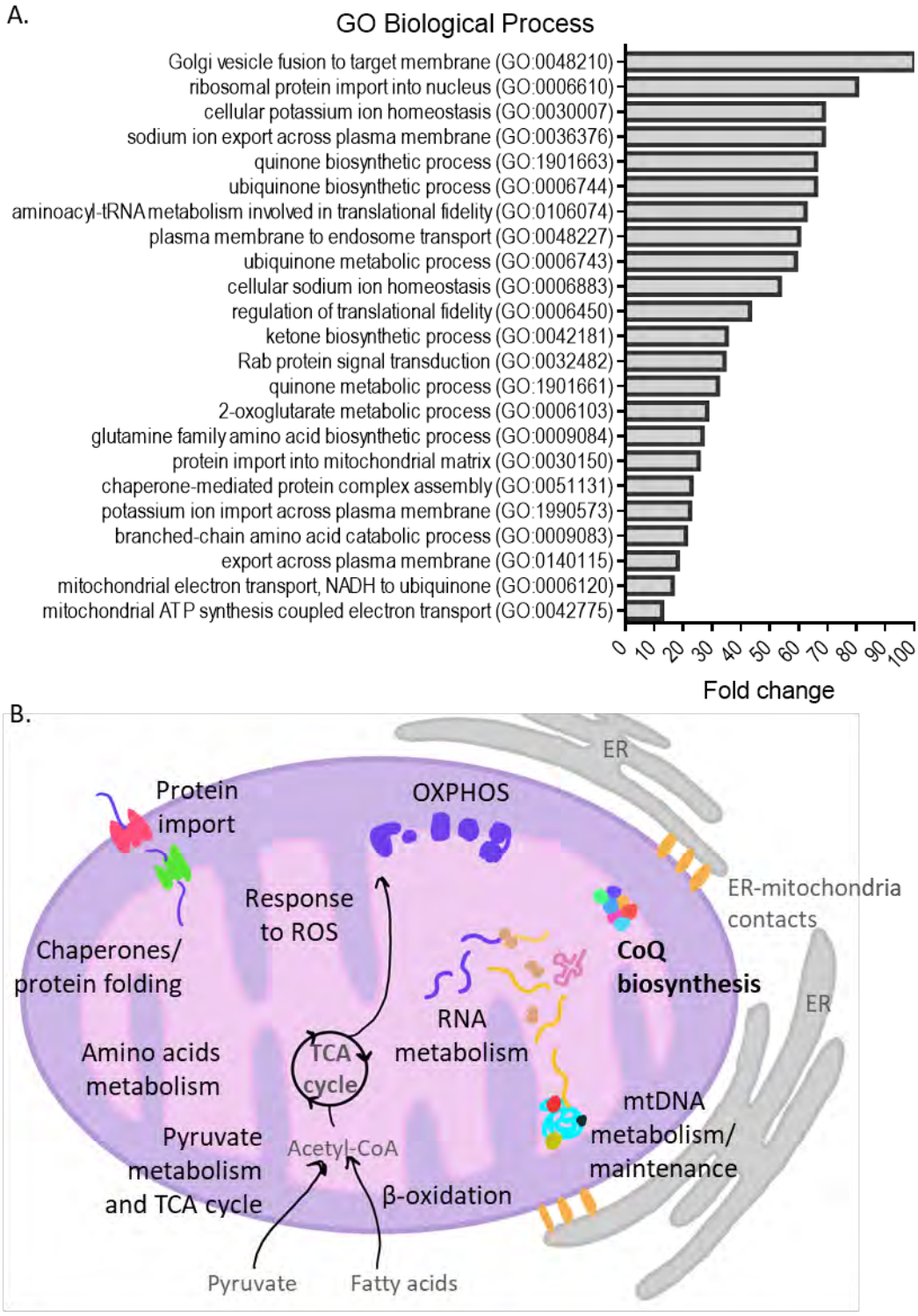

Figure 4.20. Biological processes and mitochondrial functions enriched in COQ4 co-purifing list of proteins.

(A) Representative GO biological process terms enriched in putative COQ4 interaction partners. (B) Representative functions of the 37 identified mitochondrial proteins.

mitochondria (TIM44, TIM50, HAX1, GRPEL1). Proteins related to mtDNA metabolism and maintenance (POLDIP2, LONP1), mitochondrial RNA processing (FASTKD4, FASTKD5, NIPSNAP1) and mitochondrial translation (AARS, DARS2, VARS2) were also found. We also detected chaperones or proteins involved in protein folding (TRAP, FKBP8). The biological process GO analysis showed an overrepresentation of these different mitochondrial functions in the list of COQ4 potential partners: aminoacyl-tRNA metabolism, mitochondrial respiration, 2-oxoglutarate metabolism, ketone and glutamine biosynthesis, etc (Figure 4.20.A).

Besides mitochondrial proteins, other proteins localised to the cytosol or other parts of the cell (plasma membrane, ER, Golgi, lysosome, vesicles, nucleus, cytoskeleton) were also found. Moreover, cell component GO analysis showed an overrepresentation of these cellular locations. ATPases from non-mitochondrial membranes (ATP12A, ATP1A1, ATP1A2, ATP1A3, ATP1A4, ATP1B3, ATP2A2, ATP5F1A, ATP6V1A), proteins related to cytoskeleton (tubulins), Ras-related proteins, guanine nucleotide-binding proteins, cytoplasmic ribosomal proteins and heat shock proteins were also identified as potential COQ4 partners. However, the functional significance for many of these interactions would need deeper analysis.

COQs proteins levels are altered in COQ4 and COQ6 KO cells

Almost all COQ proteins (only with the exception of COQ8A) co-purified with COQ4, providing more evidence to the existence of a COQ multienzymatic complex. It has been suggested that its stability is essential for CoQ biosynthesis. The presence of all components of the complex seems to be essential for maintaining this stability, meaning that these proteins are important building blocks of the complex, besides their catalytic activity.

Our *COQ4* KO and *COQ6* KO cell lines (see Chapter 2, section 2.2.2, for more details of *COQ6* KO cell line) are unique models of human cell lines completely lacking one of the components of this complex. We wanted to determine if the stability of the rest of the COQ proteins was affected by the lack of one of these two proteins. We subjected total protein lysates of the two KO cell lines, as well as a control cell line, to western blotting,

using antibodies against COQ4, COQ5, COQ6 and COQ7 proteins, and the constitutive β-actin as a loading control (Figure 4.21).

In these blots, we can see how COQ4 and COQ6 are indeed knocked out in *COQ4* and *COQ6* KO cells, respectively (Figure 4.21). But they are not the only COQ proteins with altered levels. *COQ4* KO cells show significantly high levels of COQ5 and COQ7 proteins, while COQ6 levels also seem to be slightly incremented. Similarly, *COQ6* KO cells show a significant overexpression of COQ4 protein, COQ5 is only slightly increased, and COQ7 remains the same than in controls. The lack of COQ4 or COQ6 proteins seems to induce an increase of other COQ proteins (Figure 4.21), maybe as an attempt to compensate for the lack of these two components for the stabilisation of the complex.

Similar effects have been observed before in the literature, using human 143B cells [315]. In these cells, *COQ4* KD showed an overproduction of COQ5 and COQ6, and *COQ6* KD, only showed a reduction in COQ3 levels [315].

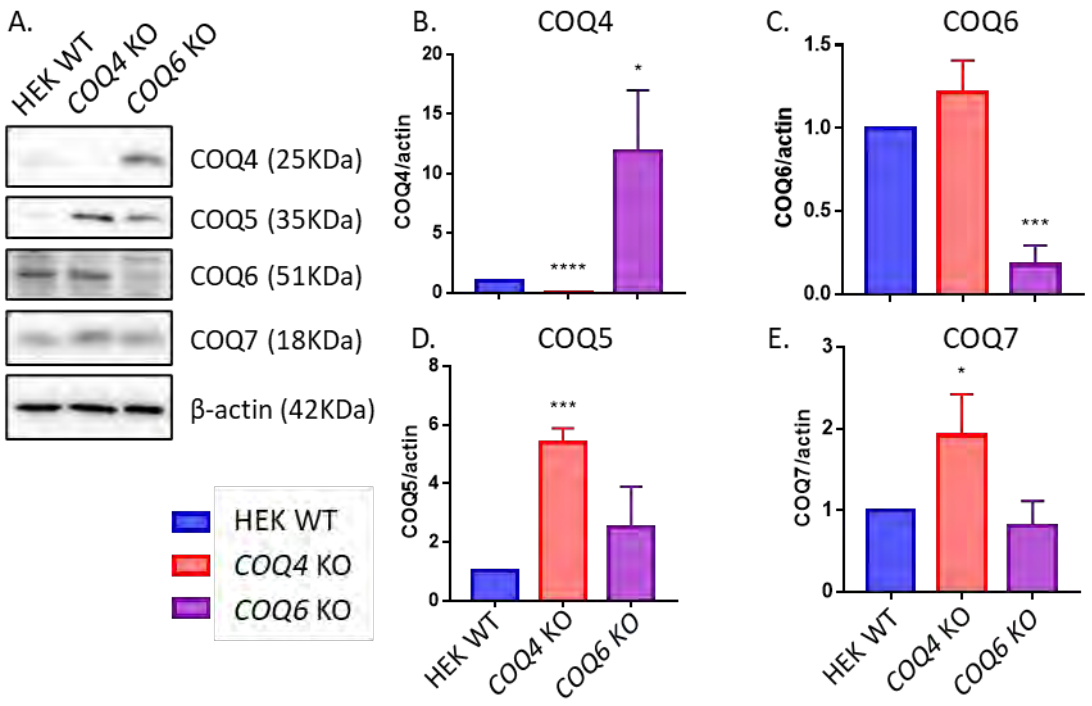

Figure 4.21. Western blot analysis of COQ4 and other COQ proteins in whole cell lysates.
Western blot analysis of COQ4 and other COQ proteins (A) levels in whole cell lysates and their quantification (B-E) (Two-tailed unpaired t-test, each KO vs. HEK WT; p values: <0.05(*), <0.001 (***), <0.0001 (****)). An antibody against β-actin (43KDa) was used as a loading control.

Exogenous CoQ_{10} enters mitochondria upon treatment and produces some changes in COQs proteins levels in COQ4 and COQ6 KO cells

We wanted to check if supplementation of exogenous CoQ_{10} had an effect on COQ proteins levels, in order to understand if the specific COQ proteins overproduction we were observing was due to the lack of the final product or to the absence of one of the components of the CoQ complex and its instability. We treated controls, *COQ4* KO and *COQ6* KO with 5µM of CoQ_{10} for 96 hours. We first checked if exogenous CoQ_{10} was able to enter the mitochondria, for which cell subfractionation was performed and CoQ_{10} levels were measured in the mitochondrial fraction. CoQ_{10} levels were similar in the three treated cell lines, and around 7 times higher than WT levels (Figure 4.22.B). This result was indicating that a big amount of exogenous CoQ_{10} was reaching the mitochondria. Then, we subjected mitochondrial protein to western blotting, to measure COQ4, COQ5, COQ6 and COQ7 proteins' levels, and TOM20 as a mitochondrial control.

CoQ_{10} treatment seems to have a greater effect in terms of COQ proteins levels in the *COQ6* KO (Figure 4.22). In these cells, the high amounts of COQ4, COQ5 and COQ7 are reduced when treated with exogenous CoQ_{10}. CoQ_{10} supplementation does not show a significant effect in the regulation of other COQ protein levels in *COQ4* KO cells, except for a slight decrease in COQ5 levels. Our results could indicate that CoQ_{10} treatment is more likely to stabilize a complex lacking COQ6 than a complex lacking COQ4, maybe because COQ4 is a more important structural unit of this complex.

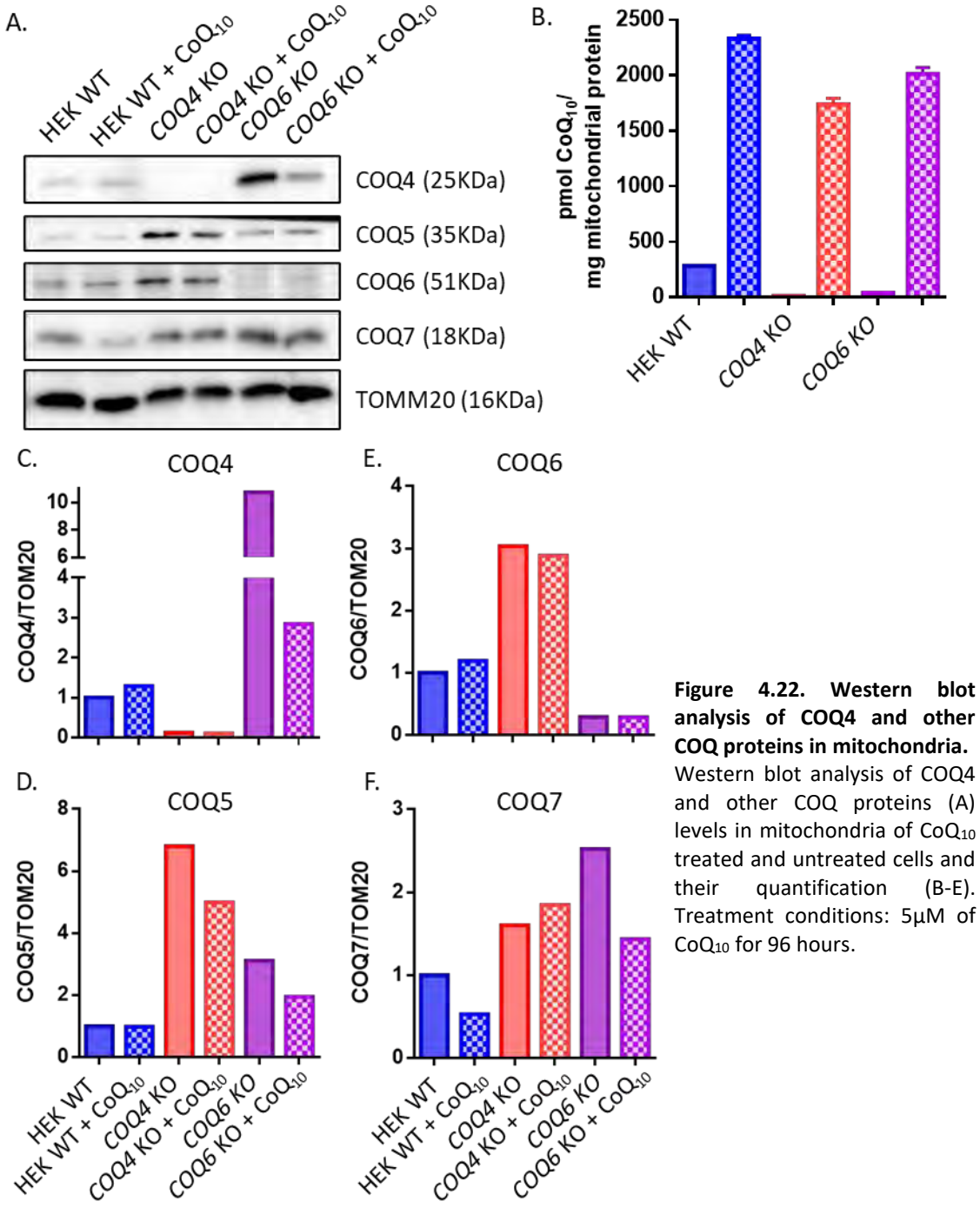

Figure 4.22. Western blot analysis of COQ4 and other COQ proteins in mitochondria. Western blot analysis of COQ4 and other COQ proteins (A) levels in mitochondria of CoQ_{10} treated and untreated cells and their quantification (B-E). Treatment conditions: 5µM of CoQ_{10} for 96 hours.

4.3. Conclusions

A *COQ4* KO cellular model has been useful to dissect human COQ4 function in CoQ biosynthesis. The main conclusions derived from this work are the following:

i. COQ4 protein is essential for CoQ_{10} biosynthesis in human cells. The lack of COQ4 leads to drastically reduced CoQ_{10} levels, which causes a great respiratory defect that is rescued with CoQ_{10} treatment or WT *COQ4* expression.

ii. Impaired CoQ_{10} biosynthesis due to the absence of COQ4 protein produces the accumulation of a specific intermediate, which could be considered as a marker for CoQ_{10} deficiency in human cells.

iii. COQ4 may act directly or indirectly upstream DMQ_{10} production.

iv. Mutations in the phospho-loop do not affect *COQ4* function in CoQ_{10} synthesis, at least in the tested conditions.

v. Most of the mutations described in patients are hypomorphic, and when overexpressed in *COQ4* KO cells they cannot be distinguished from the wild type version of the protein.

vi. *COQ4* Isoforms lacking exon 3, 4 and 5, in different combinations, do not have the same function than full-length *COQ4* in CoQ_{10} biosynthesis.

vii. COQ4 protein interacts with COQ3-COQ9 proteins in a dynamic complex, and the lack of COQ4 or COQ6 proteins alters the levels of other COQs proteins, probably modifying the stability of the biosynthetic complex.

viii. Other mitochondrial proteins involved in different processes were identified as candidates for COQ4 interaction partners. They were involved in different functions, such as OXPHOS, pyruvate metabolism, TCA cycle, fatty acids beta-oxidation, amino acids biosynthesis and catabolism, protein import to mitochondria, mtDNA metabolism and maintenance, mitochondrial RNA processing, mitochondrial translation or protein folding.

Chapter 5

Chapter 5.

COQ4 involvement in mtDNA metabolism

5.1. Introduction. Human mtDNA and its metabolism

The human mitochondrial genome is a 16,569 bp-long circular and double-stranded DNA molecule. It exists in multiple copies in the mitochondrial matrix, in both somatic tissues and germ cells [9]. According to the endosymbiotic theory, mitochondria originated from α-proteobacteria that were endocytosed by a primitive archaebacterium during the eukaryotic evolution [593]. The observed similarities between mtDNA and the bacterial chromosome probably derive from the endosymbiotic origin of mitochondria.

The mtDNA molecule is very compact since most of the mitochondrial genes were lost or transferred to the nucleus throughout evolution. Mitochondrial genes retained by different organisms are variable. The reason why some of the genes were maintained in an organelle-specific genome like the mtDNA is unclear, but it is possible that the local regulation of gene expression is key for the control of the energy production metabolism and the redox state of mitochondria [594]. Also, it has been hypothesized that highly hydrophobic proteins, such as CYTB or COXI, are difficult to import across the outer membrane and correctly insert them in the IMM [594,595].

5.1.1. Organization of the mitochondrial genome: mitochondrial genes

The mitochondrial genome has a remarkable economy of sequence, with a compact gene organization in which there are no introns and almost no intergenic regions or non-coding regions [596]. In humans, only 37 genes are encoded by the mtDNA; 13 of them correspond to structural subunits of the MRC (transcribed in 11 mRNAs and translated to 13 proteins) and the rest code for RNA components of the mitochondrial translation machinery: 22 mitochondrial transfer RNAs (mt-tRNAs) and 2 mitochondrial ribosomal RNAs (mt-rRNAs, 12S and 16S) (Figure 5.1.A) [9,596].

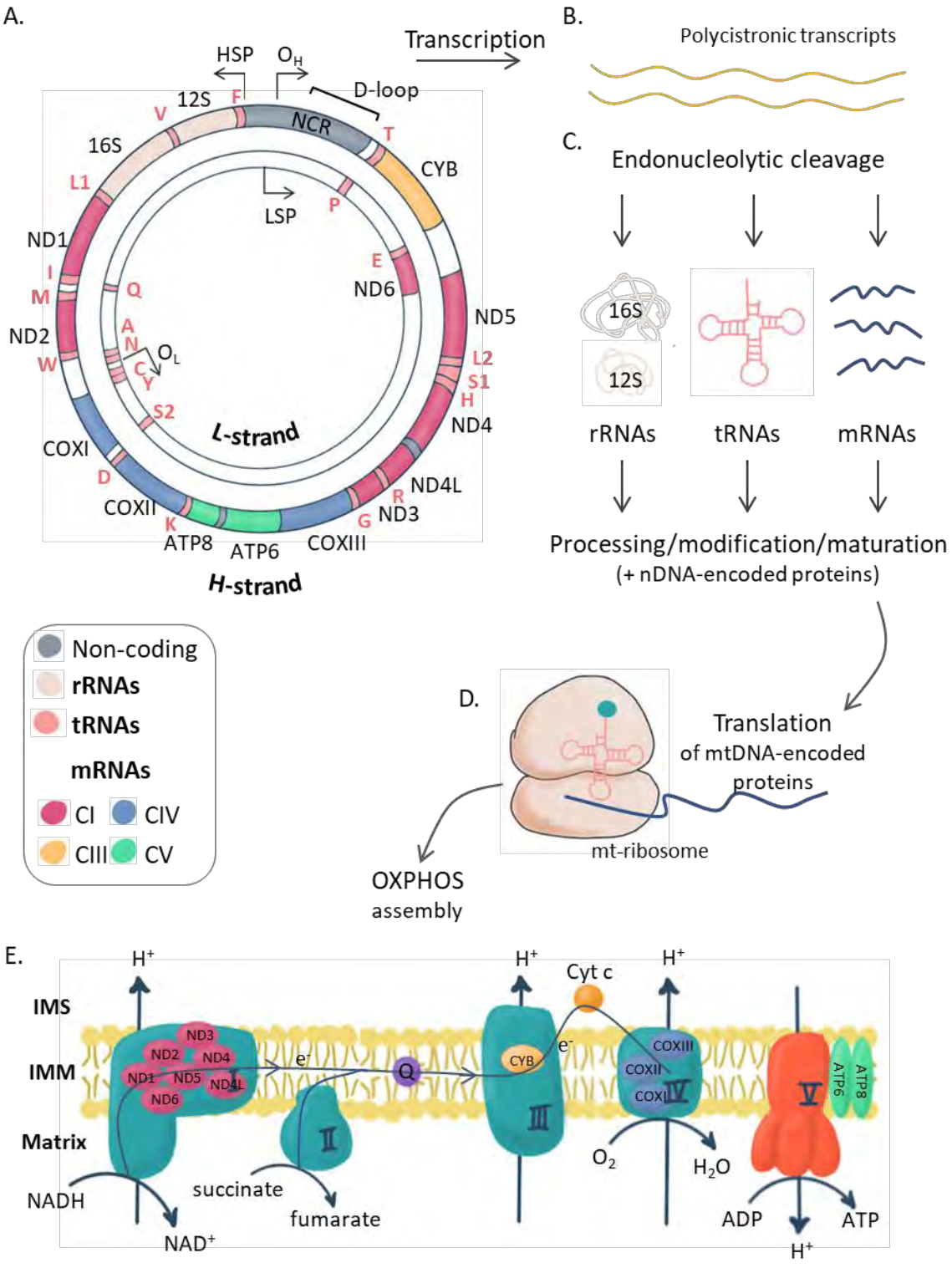

Figure 5.1. The human mitochondrial genome and its metabolism.
(A) mtDNA sequence structure, with the different genes coloured (see legend). (B) Transcription from LSP and HSP promoters produces long polycistronic transcripts. (C) These long transcripts must be cleaved and processed to produce mature rRNAs, tRNAs and mRNAs. (D) Mitoribosomes are assembled with rRNAs and proteins, and the translation machinery produces the mtDNA-encoded proteins, that are assembled with the nDNA-encoded proteins to form the OXPHOS complexes (E).

The 13 mtDNA-encoded subunits of the MRC represent a small fraction of the OXPHOS subunits, but they are nevertheless essential for the correct functioning of the OXPHOS system. These genes include 7 subunit of complex I (ND1–6, ND4L), 1 subunit of complex III (cytochrome b), 3 subunits of complex IV (COXI, COXII and COXIII) and 2 subunits of the ATP synthase or complex V (ATP6 and ATP8) [9,67]. The rest of the structural subunits of the respiratory complexes (around 77), as well as all the factors needed for the correct assembly of the respiratory complexes (around 57 known so far), are encoded by the nDNA (Table 5.1 and Figure 5.1) [9,36].

Table 5.1. Number of nDNA- and mtDNA-encoded subunits and assembly factors for each mitochondrial respiratory complex.

Polypeptides	CI	CII	CIII	CIV	CV
mtDNA-encoded subunits	7	0	1	3	2
nDNA-encoded subunits	~38	4	10	10	~14
nDNA-encoded assembly factors	~11	~4	~9	~30	~3

Colours are the same than in Figure 5.1. CII do not have subunits encoded by the mtDNA.

5.1.2. mtDNA inheritance and segregation

The mtDNA is almost exclusively maternally inherited. While oocytes contain around 10^5 copies of mtDNA, mtDNA copy number is actively downregulated in spermatogenesis, so the sperm cell contains around 100 copies of mtDNA [597]. Moreover, sperm mitochondria that may enter the oocyte are specifically marked for degradation after fertilization [9,598,599]. When the mechanisms of selective elimination of paternal mitochondria are defective, paternal mtDNA transmission can occur, but this is a rare phenomenon [600–603].

MtDNA molecules from the oocyte segregate into the daughter cells after fertilization, and mtDNA replication in the embryos starts after implantation [9,604]. There are mechanisms that prevent the transmission of mtDNA mutations in the germline. The mtDNA bottleneck phenomenon occurs in the early development of the oocyte, and it highly reduces the number of different molecules of the pool of maternal mtDNAs which will be transmitted to the next generation [605]. Moreover, mtDNA mutations affecting codons of the protein-coding genes or the tRNAs are negatively selected in the female germline or during embriogenesis, respectively, phenomenon known as purifying selection [606,607]. The molecular mechanisms underlying these two levels of purifying

selection are still elusive. Moreover, females with mtDNA mutations in the germline are reported to have a reduced fertility [607].

Conversely to what happens in the germline, in somatic tissues, mtDNA molecules segregate randomly to the daughter cells during mitosis, by a process of relaxed replication [9]. This means there is non-stringent control of mtDNA replication during the cell cycle, which could lead to different mtDNA molecules replicating at different rates, within the same cell [607].

Heteroplasmy and mutation rate

Given that mitochondria enclose multiple copies of mtDNA and each cell can contain a variable number of these organelles, there can be several hundreds or thousands copies of mtDNA per cell [66]. Therefore, if there is a mutation in the mtDNA, it can be present in just a fraction of the mtDNA molecules. The homoplasmic state is when all the cells or the tissues contain the same identical copy of mtDNA, while various levels of heteroplasmy can occur when there is a mix of different molecules of mtDNA. Generally, we refer to heteroplasmy when there is a mix of wild type mtDNA molecules and mutated mtDNA molecules with a disease-causing mutation [66,608,609]. In this case, the mitochondrial dysfunction and the clinical phenotype associated to this condition will depend on the proportion of wild type and mutated mtDNA genomes (heteroplasmy load), and it will appear only when the proportion of WT mtDNA drops below a threshold level. This phenomenon is known as mitochondrial threshold effect, and it can be specific for the mutation, the tissue or even the patient [66,610].

Besides, mtDNA has a high mutation rate, 10-17-fold higher than nDNA mutation rate. It can be explained by different factors: mtDNA is less protected by a chromatin-like packaging than nDNA, it resides in an environment with high exposure to oxidative stress and there are less mechanisms of mtDNA repair in mitochondria. This mutagenesis can lead to the phenomenon of heteroplasmy [66]. Also, paternal mtDNA leakage can be a rare cause of heteroplasmy [601].

5.1.3. mtDNA expression and maintenance

The two strands of the human mtDNA have different nucleotide composition so they are designated heavy (H) and light (L), since they can be separated by CsCl density centrifugation gradients [611]. The H-strand is rich in guanines, and it contains most of the coding material (12 of the 13 protein-coding genes, the two rRNAs, and 14 of the 22 tRNAs) (Figure 5.1.A). In contrast, the L-strand encodes one protein (ND6) and eight tRNAs. There is only one major non-coding region (NCR), 1.1 Kb long, which contains *cis*-elements for replication and transcription [612]. Promoters of both H and L strands are located in the NCR, as well as the origin of mtDNA replication of the strand H (O_H). Moreover, it has been observed that, in vertebrates, many molecules of mtDNA contain a short and stable triple-stranded region, or displacement loop (D-loop), located in the NCR [9,612–615]. The proportion of molecules containing a D-loop is very variable, ranging from 10% to 90% in different cell lines and times [613]. The third strand of the D-loop, the 7S DNA, is around 650 bp long in humans, and its synthesis is thought to be primed using the 7S RNA molecules (of about 200 nt) derived from transcription from the light strand promoter [614]. The precise function of the D-loop is not clear, but it could be related to mtDNA replication from O_H origin, mtDNA recombination, membrane association or topology, or even mitochondrial dNTP pools metabolism [613].

The regulation of mtDNA expression and maintenance is a complex process since it involves many different levels, such as mtDNA replication, mtDNA transcription, the processing of primary transcripts, RNA modification and stability and the translation by mitochondrial ribosomes (Figures 5.1 and 5.2). The structural organization of these machineries within the mitochondria is essential for a tight regulation of the different processes. In this chapter, we provide an overview of these processes and how they are structurally and functionally regulated in the different compartments within the mitochondria.

mtDNA replication

mtDNA replication is a key process that occurs independently of the cell cycle [66]. Human mtDNA molecules have two origins of replication, one for each strand: O_H (origin of H-strand synthesis), at the NCR, and O_L (origin of L-strand synthesis), within a tRNA cluster

around 11,000 bp downstream of O_H [612] (Figure 5.1.A). L-strand transcription generates the RNA primers needed for replication initiation. The mtDNA replication machinery involves several proteins: the mtDNA polymerase (POLG) [9,612], the DNA helicase TWINKLE [616], the mitochondrial single-stranded DNA-binding protein (mtSSB) [9], and probably other factors [612,614,617].

Several modes of mtDNA replication have been proposed to operate in mammalian mitochondria:

i. Strand displacement replication (SDR) or strand asynchronous replication: The initiation of the replication occurs at the O_H [9,612,618]. Then, the replisome proceeds unidirectionally to produce the nascent H-strand. The displaced, parental H-strand is stabilized by mtSSB. When the second origin (O_L) is displaced as a single-stranded template, DNA replication of the other strand begins in the opposite direction, with no generation of small replication intermediates (RIs). For this purpose, mitochondrial RNA polymerase (POLRMT) produces small primers at the loop originated at O_L, which are used to initiate L-strand DNA synthesis [619]. The mtDNA replication is carried out by POLG. TWINKLE is required for DNA unwinding when replication initiates at the H-strand [9].

ii. Bootlace/RITOLS strand-asynchronous replication: The finding of RNA hybridized to the parental H-strand, led to propose that Ribonucleotides are Incorporated ThroughOut the Lagging Strand (RITOLS) [615,620,621]. Replication of this mode initiates with the synthesis of an H-strand, similarly to SDR. H-strand DNA synthesis (leading-strand synthesis) proceeds unidirectionally, but RNA is incorporated to the lagging strand, instead of being coated by mtSSB. Delayed L-strand DNA synthesis is initiated at O_L and proceeds unidirectionally, removing RNA lagging strands in the process.

iii. Strand coupled replication (SCR): Conventional coupled leading and lagging strand DNA synthesis, similar to nuclear DNA replication [612,615]. Characterisation of RIs from this process suggests that the synthesis of the leading and the lagging strands are synchronous and both strands are essentially composed of DNA. However, the mechanism of lagging-strand synthesis remains to be elucidated.

mtDNA transcription

Transcription from the light-strand promoter (LSP) and the heavy-strand promoter (HSP) produces polycistronic RNA precursors that are almost the same size of the mtDNA [9,622] (Figure 5.1.B). This transcription is carried out by the mitochondrial RNA polymerase POLRMT, which specifically binds the sequence of the LSP and HSP. The process requires the presence of mitochondrial transcription factor A (TFAM) and the mitochondrial transcription factor B2 (TFB2M) to start transcription. TFAM binds sequence-specifically to mitochondrial promoters and creates a 180° bend in DNA. Then POLRMT is recruited by TFAM and the DNA sequence. When the polymerase binds to the DNA-TFAM complex, it undergoes a conformational change that allows its interaction with TFB2M, forming the initiation of transcription complex. After the initiation of transcription, elongation goes on with the help of the mitochondrial transcription elongation factor (TEFM), which interacts with the catalytic C-terminal domain of POLRMT and is thought to be an accessory subunit of the polymerase [623]. A second heavy-strand promoter was proposed to be at the boundary between the $tRNA^{Phe}$ and the 12S rRNA genes and mainly dedicated to producing the two rRNAs for mitochondrial ribosomes [624]. However, recent research suggested that H strand transcription occurs only from HSP, and rRNA abundance may be due to different turnover rate [622]. In any case, when transcription is terminated, the RNA precursors must be processed via endonucleolytic cleavage to release the individual mRNAs, tRNAs and rRNAs (Figure 5.2.C).

mtRNAs processing

Mt-RNA processing and maturation occurs in specialized compartments in the mitochondria, known as mitochondrial RNA granules (MRG), in close proximity to the mtDNA nucleoids [440,625,626].

Most of the tRNA genes are flanking rRNA and protein-coding genes, and it is described that polycistronic RNA processing is performed by the recognition and cleavage of these tRNA, known as the tRNA punctuation model [627], which leads to the release of the rRNAs and mRNAs. The cleavage is performed by two enzymes that recognise tRNAs ends and catalyse 5’ and 3’ cleavage, respectively: a mitochondria-specific protein-only RNase P complex and the RNase Z endonuclease ELAC2 [626,628,629]. For the genes that are not

localized in these tRNAs junctions, other proteins have been identified to be responsible for their processing, such as FASTK, FASTKD4, FASTKD5 and GRSF1. After endonucleolytic cleavage, the individual mRNAs, tRNAs and rRNAs are post transcriptionally modified. Curiously, two mRNAs are bicistronic (mRNAs for ND4/ND4L and ATP6/ATP8) [623].

The mRNAs are added a 3' poly-A tail by the mitochondrial poly(A) polymerase (mtPAP) and stabilized by binding to factors like the PPR-containing proteins (such as LRPPRC) [622,630,631]. tRNAs undergo nucleotide modifications, such as the 5-formyl modification of the cytosine residue in the wobble position of the anticodon in human mt-tRNAMet by NSUN3 and ABH1 [626]. Some mRNAs, tRNAs and rRNAs are also pseudouridylated in specific positions by different pseudouridine synthases (PUS1, RPUSD3, RPUSD4, and TRUB2), but the exact function of these modifications is still not clear [478,479,626,632]. rRNAs are also modified with methylations by methyltransferases (TFB1M, NSUN4, MRM1, MRM2, MRM3, TRMT61B), being these modifications important for mitoribosome assembly, which occurs also in the MRGs [595,626,630,633].

mtRNA translation

Translation of the mt-mRNAs takes place in the mitochondrial matrix by the mitoribosomes and different proteins associated (Figure 5.1.D). All these protein factors are transcribed in the nucleus, translated in the cytosol and imported to the mitochondria via the translocases of the outer and inner membrane (TOM and TIM, respectively) complexes.

Proteins involved in the mtRNA translation are the 80 or more mitoribosomal proteins (MRP), aminoacyl synthetases (ARSs), the already mentioned tRNA modifying enzymes, translation initiation (IF2mt and IF3mt), elongation (EFG1, EFG2, EF-Tsmt, and EF-TUmt/TUFM), termination (mtRF1a, mtRF1, C12ORF65 and ICT1) factors, and two mitoribosome recycling factors (mtRRF1 and mtRRF2) [630].

Firstly, MRPs bind to rRNAs 12S and 16S to form the mature mitorribosomes subunits, 28S and 39S, respectively. Then, mitochondrial protein synthesis occurs in four major steps: initiation, elongation, termination and ribosome recycling.

Initiation is the rate limiting step, in which IF3mt binds the 28S subunit and the mRNA. When a proper start codon is found, formyl-Met-tRNA bind to the first codon and IF2mt associates to form the initiation complex. This allows the binding to the 39S subunit to form a 55S monosome and releases the initiation factors.

The machinery proceeds then to elongation, in which a charged aminoacyl-tRNA enters the A site of the monosome (in a ternary complex with EF-TUmt-GTP). If the codon:anticodon pairing is correct, EF-TUmt hydrolyses GTP and EF-TUmt-GDP is released. Then, the nascent amino acid chain is transferred from the tRNA in the P site to the new aminoacyl-tRNA in the A site by peptidyl-transferase activity of the 39S subunit. Then, the monosome moves along the mRNA towards the 3' direction by the action of EFG1 in a GTP-dependent manner, allowing a new codon to enter the A site. At this point, EF-TUmt-GTP is regenerated by EF-TSmt and binds a new aminoacyl-tRNA.

Elongation cycle continues until a termination codon is recognized in the A site. When this occurs, the termination factor mtRF1a-GTP binds to the complex, which leads to hydrolysis of the peptide bond between the nascent chain and the tRNA in the P site thereby releasing the mature polypeptide from the ribosome. Other factors homologous to mtRF1a (ICT1, C12ORF65, and mtRF1), may also be involved in translation termination.

When translation is terminated, mtRRF1 and mtRRF2/EFG2 bind to the A site and dissociate the 55S monosome, releasing the mRNA and tRNA and allowing mitoribosome recycling [624,634].

5.1.4. Coordination of nDNA and mtDNA gene expression

As we have seen, mitochondria need much more than the 37 genes on the mitochondrial genome to work. Actually, it has been estimated that these organelles contain around 1,500 proteins, which are needed for all the different processes that occur inside them [69,440,635]. All these proteins are encoded by the nuclear genome, and must be translated on the cytosol and imported to mitochondria. For the correct functioning of all mitochondrial processes, an accurately regulated coordination of mtDNA and nDNA expression must exist. The coordination of mitochondrial-nuclear DNA expression can operate in different levels.

There is a set of transcription factors, called coactivators, that regulate both nuclear and mitochondrial gene expression in response to environmental changes or external stimuli (i.e. caloric intake or exercise). In this context, there is a change in the gene activation program that affects both mitochondrial and nuclear gene expression. For example, the peroxisome-proliferator-activated receptor coactivator-1 (PGC-1) is considered a universal regulatory system for mitochondrial biogenesis in vertebrates [636].

However, since mitochondrial genomes encode a small subset of proteins, precise mRNA-specific mechanisms have evolved. mRNA-specific nuclear encoded translation activators can regulate the synthesis of a specific mitochondrial protein by regulating their abundance in mitochondria. In yeast, many transcript-specific activators have been described [637]. However, only one mitochondrial translation activator has been identified in mammalian mitochondria, the *TACO1* gene encoding a translational activator of COXI. This suggests the mechanisms of mammalian mitochondrial gene regulation are significantly different from the yeast ones [626].

Also, translational activators can directly regulate mitochondrial gene expression by evaluating the efficiency of OXPHOS complex assembly. A failed assembly would lead to a decrease in the synthesis of the key subunit. These feedback mechanisms have been extensively studied in yeast, but less is known about the mammalian system. A study in human mitochondria described that mitochondrial translation displays plasticity and adapts to the availability of nDNA-encoded complex subunits [638]. According to their findings, the translation of COXI is paused in the absence of COXIV, and, interestingly, ribosomes carrying nascent COXI peptides prime complex IV assembly. Whether this kind of feedback mechanism, with translation coupled to complex assembly, exists for the rest of the mitochondrial encoded MRC proteins remains to be elucidated [626].

5.1.5. Packaging mtDNA into mitochondrial nucleoids

MtDNA molecules need to be compacted to fit inside the mitochondrial network. MtDNA is organized into compact nucleoprotein complexes named nucleoids, which are considered to be the mitochondrial genetic segregating unit (Figure 5.2) [639]. They can be visualized as punctate foci evenly distributed inside the mitochondria (Figure 5.2.A). Thanks to the development of super-resolution techniques, the size, number and

organization of the nucleoids have been elucidated [640–643]. Mitochondrial nucleoids are slightly elongated with a size around 0.1 µm of diameter. Depending on the cell type, there is a wide range of nucleoids per cell. It has been shown that each mammalian mitochondrial nucleoid contains only one copy of mtDNA, which is compacted with different proteins [641,643].

TFAM is the major constituent of the mammalian nucleoid and sufficient for nucleoid compaction, while other proteins can associate to it temporarily for replication or transcription purposes (Figure 5.2.B and C) [641,644]. When it binds to mtDNA, it produces a U-turn bend, facilitating the folding of the mtDNA molecule [645]. TFAM is very abundant in mammalian cells, present in about 1,000 molecules per mtDNA molecule [641].

Different degrees of nucleoid compaction have been observed at different physiological TFAM/mtDNA ratios (Figure 5.2.C) [639,643,646]. When TFAM/mtDNA ratio is high, the nucleoids are fully compacted, and their transcription and replication is blocked [646]. This means that nucleoid compaction by TFAM protein levels is an important mechanism for control of mtDNA expression, selecting which nucleoids undergo transcription or replication [9,643–646].

Besides TFAM, a large number of other mitochondrial proteins have been found to be part of the nucleoids, exerting different functions. Mitochondrial transcription (POLRMT, TFB2M, TEFM) and replication (POLG, Twinkle, mtSSB) machineries are prominently represented (Figure 5.2.B). The MRGs are located in close proximity of the nucleoids, so various RNA-metabolism proteins have been found in nucleoid-rich preparations [647].

Nucleoids distribution depends on the mitochondrial fusion and fission dynamics, probably by nucleoid attachment to the IMM, and coordinated with mtDNA replication [3,648,649]. For this purpose, ER-mitochondria contact sites are essential. In fact, the subset of nucleoids that is replicatively active has been shown to be associated with the IMM through cholesterol-rich areas within these ER-mitochondria contact sites (Figure 5.2.B) [4]. These membrane-attached nucleoids are also rich in ATAD3 protein, which is a AAA (ATPases Associated with diverse cellular Activities) only present in multicellular eukaryotes [650–652].

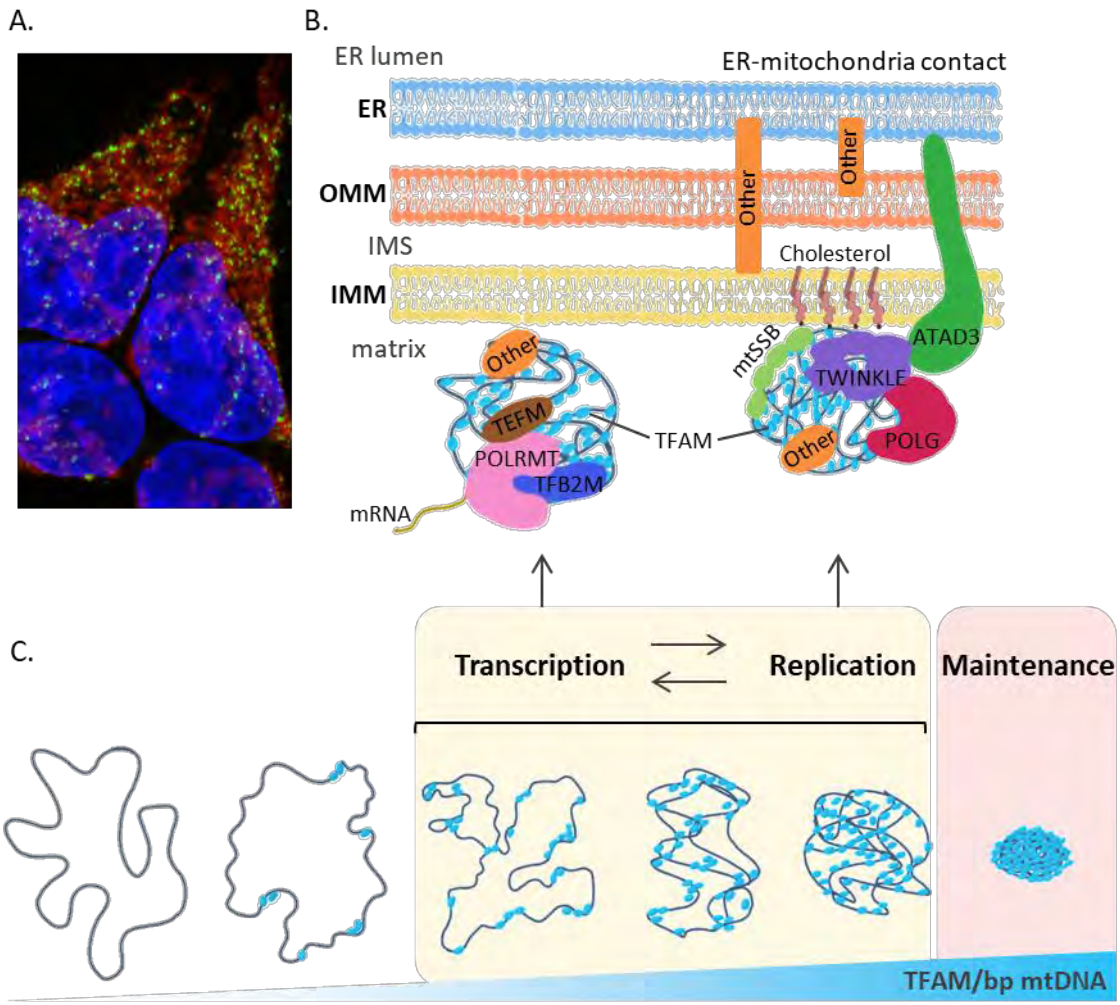

Figure 5.2. Mitochondrial DNA organisation in nucleoids.
(A) Mitochondrial nucleoids visualised by fluorescence microscopy as punctate foci (antiDNA stained in green). AntiTOM20 stained in red shows the mitochondrial network and DAPI blue staining shows the nucleus of HEK cells. (B) Schematic representation of transcriptionally (left) or replicatively (right) active nucleoids, in close contact with IMM and ER-mitochondria contacts, with different proteins associated (not in scale) (image elaborated with data from different references, see main text). (C) Different degrees of compaction of mtDNA by TFAM association. At intermediate stages, mtDNA can still be used for replication and/or gene expression. At the tightly packaged stage, TFAM blocks DNA unwinding and makes mtDNA inaccessible to the replication and transcription machineries (Adapted from Gustafsson et al., 2016[9]).

5.1.6. ER-mitochondria contact sites and relationship with mtDNA

Membranes from two different organelles can be tightly connected through specialized structures named membrane contact sites, which are maintained via dynamic protein-protein and protein-lipid interactions. These contact sites have essential functions in intracellular signalling, mediating a wide range of cellular processes, which include calcium homeostasis, lipid metabolism, membrane biogenesis and organelle remodelling [653]. ER-mitochondria contact sites are unique microenvironments for the localization and activity of components with inter-organellar functions. They have been

associated to different processes, such as cellular and mitochondrial calcium homeostasis, mitochondrial division and motility, apoptosis, autophagy and lipid metabolism and trafficking (Figure 5.3) [15,654,655].

Mitochondrial division and distribution of nucleoids

ER-mitochondria contact sites are also important for mitochondrial dynamics. It has been demonstrated that mtDNA replication marks the site for ER-recruitment, coordinating mitochondrial genome replication and segregation to mitochondrial division [3]. ER binding to this site drives pre-constriction of the membrane, and oligomeric forms of dynamin-like protein 1 (Drp1) accumulate in a ring-like structure. GTP-hydrolysis leads to Drp1 conformational change, enhancing membrane constriction. The composition in phospholipids of the OMM also regulates Drp1 assembly and activity. Then, Dnm2 is recruited to the constriction site and terminates membrane scission [23]. The molecular mechanism explaining how mitochondria-ER contacts occur at the replicative mtDNA spots remains to be completely elucidated.

Moreover, it has been proposed that ER-mitochondria contacts promote mtDNA nucleoids active transportation via KIF5B-driven mitochondrial dynamic tubulation. The MICOS (mitochondrial contact site and cristae organizing system) complex links nucleoids to Miro1, a KIF5B receptor on mitochondria, at the ER-mitochondria contact sites. This active transportation of nucleoids is distinct from mitochondrial fusion or fission and is an essential mechanism for the proper distribution of nucleoids in the peripheral zone of the cell [656].

Lipids metabolism and trafficking and its importance for mtDNA maintenance

The proper distribution and abundance of different lipids in the mitochondrial membranes allow the correct assembly of membrane protein complexes, cristae biogenesis, fusion/fission of mitochondrial membranes and even mtDNA maintenance. Some lipids are synthesised in the mitochondria, but the majority of them come from the ER. ER-mitochondria junctions are sites for non-vesicular lipid transport to allow mitochondrial membrane biogenesis [657–661].

i. Mitochondrial cholesterol

Cholesterol is an important lipid of all membranes, and its distribution influences membrane fluidity, curvature, permeability and membrane protein function. *De novo* sterol synthesis takes places in the ER, through the mevalonate pathway, and afterwards, it is rapidly distributed to other organelles and membranes [662]. It is imported to the IMM mainly through the ER-mitochondrial contacts by a complex formed by the translocator protein (TSPO) and VDAC in the OMM, and the ATPase family AAA domain-containing protein 3 (ATAD3) bridging to the IMM (Figure 5.3.A) [661–663].

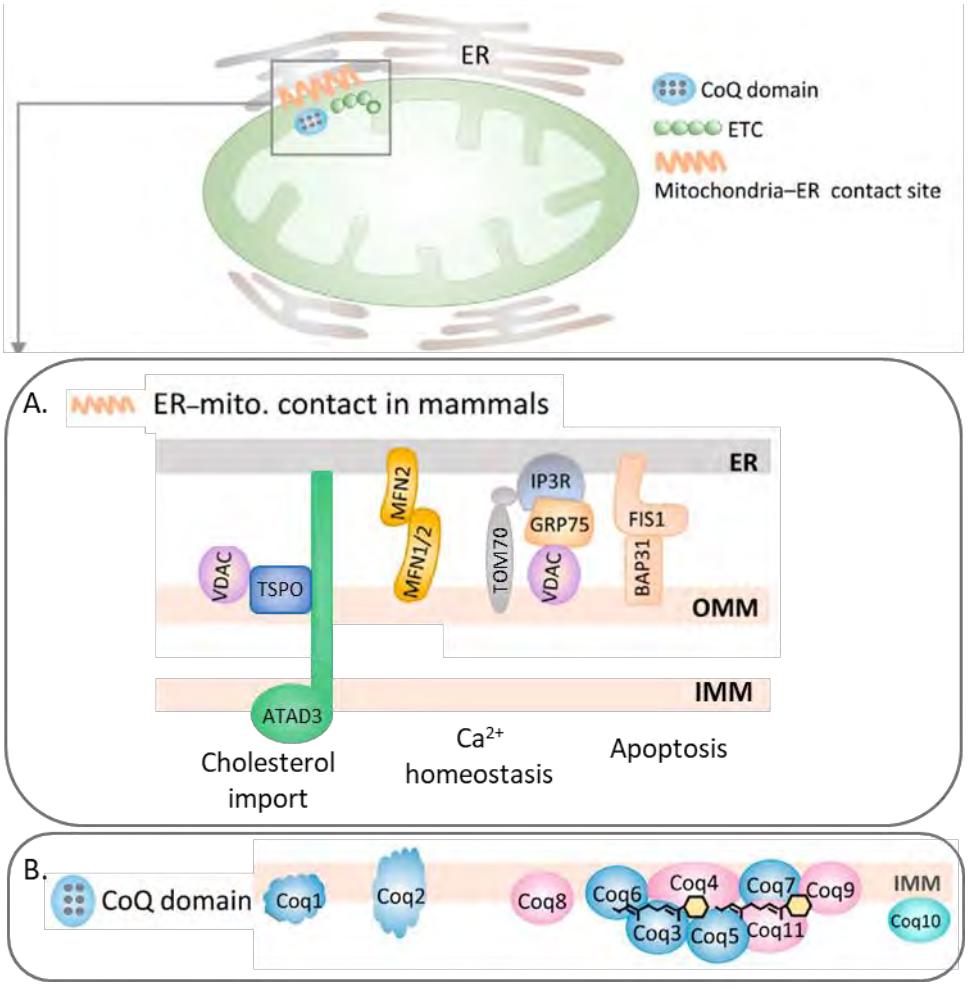

Figure 5.3. ER-mitochondria contact sites and CoQ biosynthesis.
(A) Schematic representation of ER–mitochondria contact sites. The ER– mitochondria contact sites in mammalian cells are not yet completely defined. Shown are several of the relatively better understood components and their functions associated. (B) Diagram of current model of CoQ biosynthetic pathway in eukaryotes. In the inner mitochondrial membrane (IMM), a cohort of Coq proteins (Coq3–9 and Coq11) are assembled into a supramolecular complex, the CoQ complex. This complex is localized into discrete foci, called mitochondrial CoQ domains, which are positioned close to the ER– mitochondria contact sites. In addition to the protein constituents, generation of polyisoprenylated UQ intermediates is also required for the formation and stabilization of the CoQ synthome and the CoQ domains. Coq proteins with known enzymatic functions are shown in blue (Adapted from Wang et al., 2019[316] and Elustondo et al., 2017[661])

Cholesterol levels in mitochondrial membranes are extremely low, being concentrated in the ER-mitochondria contact sites, in association with ATAD3 and membrane attached nucleoids (Figure 5.2.B) [4]. Yeast do not have cholesterol, but the structurally similar lipid ergosterol. It has been reported that ergosterol reduction impairs mtDNA maintenance in these microorganisms [664]. Abnormal levels of cholesterol in mitochondria have been observed in a wide range of pathological conditions with a mitochondrial dysfunction and an impaired mtDNA maintenance. One example is ATAD3 dysfunction.

ATAD3 membrane proteins are specific to multicellular eukaryotes. They are encoded by the *ATAD3* gene cluster, composed of three paralogs formed by tandem duplication (*ATAD3A*, *ATAD3B* and *ATAD3C*). *ATAD3A* and *ATAD3B* differ in a stop-loss mutation in *ATAD3B* that makes the protein 62 aa longer. *ATAD3C* is not known to be expressed [665]. ATAD3A is a transmembrane ATPase that anchors in the IMM and spans to the OMM [175,644,666]. It is predicted to form hexamers. The N terminus of ATAD3 contains 50 aa that have been proposed to be inserted into the OMM and associated to organelles such as the ER [175]. Interestingly, ATAD3 has been found associated to membrane-attached nucleoids [4,650] and proposed to be important for mtDNA maintenance and cholesterol levels in mitochondrial membranes [665,667].

Several patients have been reported with a wide variety of disease-causing mutations in the *ATAD3* gene cluster, including biallelic hypomorphic variants, biallelic deletions, monoallelic dominant-negative missense variants and monoallelic de novo dominant-negative duplications. This genetic variety also produces a broad phenotypic spectrum: pontocerebellar hypoplasia [667], hereditary spastic paraplegia [668], syndromic neurological disorder (peripheral neuropathy, hypotonia, cardiomyopathy, optic atrophy, cerebellar atrophy, and seizures) [669–671] or an ataxic syndrome (with CAt and DD)[672].

At the cellular level, defects in ATAD3 impair mitochondrial structure and function in different ways, leading to loss of cristae [673], dysfunctional mitochondrial morphology and dynamics [663,668], mtDNA abnormalities, perturbed cholesterol distribution, reduced steroid hormone formation and OXPHOS dysfunction [4,663,667–669,673]. It is not clear if the origin of these defects is the lack of a functional ATAD3 protein or the changes in membrane structure caused by altered cholesterol levels, or even a combination of both phenomena.

ii. Coenzyme Q

Remarkably, CoQ biosynthesis has also been related to ER-mitochondria contact sites. CoQ head-modifying enzymes have been found to resolve in discrete loci, so-called CoQ domains, adjacent to ER-mitochondria contact sites (Figure 5.3.B) [1,2,316]. Yeast defective in ER-mitochondria contact site components display defects in CoQ domain copy number and CoQ biosynthesis. They have increased cellular CoQ levels and accumulation of early and late CoQ biosynthetic intermediates in whole cells, while in mitochondria, CoQ and some late intermediates were significantly reduced [2]. These findings suggest that ER-mitochondria contacts could function to control the spatial organization of CoQ biosynthesis and distribution within mitochondrial and extramitochondrial membranes, being essential for CoQ homeostasis and cellular respiration [1,2,316].

CoQ levels and mtDNA maintenance have been linked in the context of disease, being mtDNA depletion syndromes the most common cause of secondary CoQ deficiency (See Chapter 1, section 1.1.2). A reciprocal effect has been observed in the literature, in a yeast model, in which several *coq* null mutants (*coq2*, *coq4* and *coq10*) had an increased mtDNA instability [674].

Moreover, CoQ and cholesterol share part of their biosynthetic pathways and levels of both molecules could be coregulated in the cells. Recently, cellular models of pharmacological inhibition of COQ2 protein displayed high levels of cholesterol [675]. The same happened in a KD of UBIAD1, a nonmitochondrial prenyltransferase involved in CoQ synthesis in the Golgi [676]. In a disease context, Niemann-Pick disease type C is a cholesterol trafficking disorder that causes high levels of cholesterol in endosomes and mitochondria [661,677]; and, in line with the previous section, mtDNA abnormalities, such as aggregation [667]. Some patients with this disorder presented also a secondary CoQ_{10} deficiency, probably due to a downregulation of the mevalonate pathway caused by high cholesterol [291,301,313]. Similarly, low CoQ_{10} levels were detected in fibroblasts from familial hypercholesterolemia patients [314].

Other functions of ER-mitochondria contacts

ER-mitochondria contact sites are where Ca^{2+} is released from the ER to the mitochondria (Figure 5.3.A). The Ca^{2+}, released from inositol-triphosphate receptors (IP_3Rs) at the ER, passes the OMM through VDAC and the IMM via the mitochondrial calcium uniporter (MCU) [15,655]. HSPA9/HSP70/GRP75 protein links IP_3R and VDAC [678], and the OMM protein TOM70 also binds to IP_3R [502]. Dimerization of mitofusin 2 (MFN2) also controls the tethering of ER to OMM [679,680]. Mitochondrial Ca^{2+} uptake has been linked to energized mitochondria, by enhancing the activity of TCA cycle dehydrogenases required for OXPHOS. Mitochondrial Ca^{2+} and ER-mitochondria contacts are also involved in the control of apoptosis and ROS signalling [15,681–683].

5.2. Results and discussion

All biological processes occurring inside the mitochondria are tightly interconnected and regulated, functionally and spatially. This regulation involves a complex interaction between mtDNA replication and transcription machinery, functional components of the ETC, the structural conformation of IMM, selective clearance of mitochondria, nuclear gene expression, and probably other cellular processes.

CoQ biosynthesis is a crucial process in mitochondria that has been recently linked to ER-mitochondria contact sites [1,2], a mitochondrial location in which other important mitochondrial functions take place, as presented in the introduction above. Very interestingly, it has been described in yeast that several *coq* null mutants (*coq2*, *coq4* and *coq10*) have an increased mtDNA instability, compared to controls, with a high rate of rho^- cell formation [674]. The authors proposed that this mtDNA instability was due to elevated ROS production in cells defective in CoQ function.

COQ4 deficiency leads to a respiratory defect due to an impaired CoQ biosynthetic process. We wanted to further investigate if CoQ deficiency due to *COQ4* defects, specifically, or CoQ biosynthesis defects, in general, may lead to an impairment in other important mitochondrial functions related to mtDNA metabolism, such as replication, maintenance or expression.

Moreover, in the InterPro database of protein families, the Coq4 domain (IPR007715) (which includes the whole Coq4 protein sequence), appears in architecture with other

types of domains in some proteins. The most frequent functions of these other domains are RNA metabolism and metal binding, which may be related with COQ4 function.

5.2.1. mtDNA copy number is decreased in cells lacking *COQ4*

We subjected our *COQ4* KO model to mtDNA copy number measurements. We used different probes for real-time PCR to quantify mtDNA and nDNA, obtaining the same results for all of them. MtDNA copy number seems to be reduced in cells lacking COQ4 protein, with varying percentage of deficiency (between 25 and 60%), depending on the mitochondrial and nuclear probes used (Figure 5.4.A). This deficiency shows a trend to be rescued with the overexpression of different forms of COQ4, such as WT COQ4 with or without a FLAG tag, or COQ4 with mutations in the putative phosphorylation loop (Figure 5.4.B), which were shown no to have any effect in CoQ biosynthesis as well.

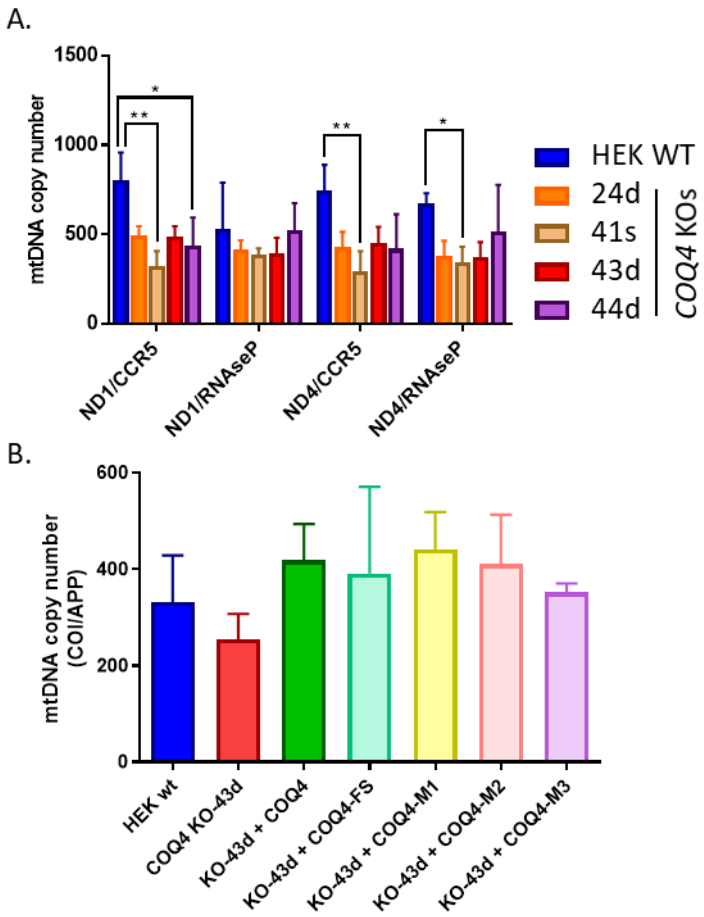

Figure 5.4. mtDNA copy number in *COQ4* KO cells and *COQ4* KO cells transfected with different COQ4 variants.
(A) mtDNA copy number of the different *COQ4* KO cell lines and HEK WT control. (Two-way ANOVA, Tukey's multiple comparison, p-values < 0.05 (*), < 0.01 (**)). (B) mtDNA copy number of *COQ4* KO (43d) cell lines, the same KO transfected with different versions of *COQ4* gene and HEK WT cells. (One-way ANOVA, Tukey's multiple comparison, p-values > 0.05 (non significant)).

5.2.2. mtDNA transcription is not altered at the level of transcripts in *COQ4* KO cells

Another critical and tightly regulated phenomenon related to mtDNA metabolism and the correct functioning of mitochondria is mtDNA transcription. Transcripts of several mtDNA-encoded subunits of the respiratory chain complexes were measured by qPCR, using the actin transcript as a constitutive control for normalization. The expression of the nDNA-encoded SDHB subunit of CII was equally measured. No significant changes in mtDNA transcription were found between the cells lacking COQ4 and the controls, or between the expression of nDNA-encoded SDHB and the mtDNA-encoded transcripts (Figure 5.5). These results indicated the transcription of mtDNA is not affected in *COQ4* KO mutant cells.

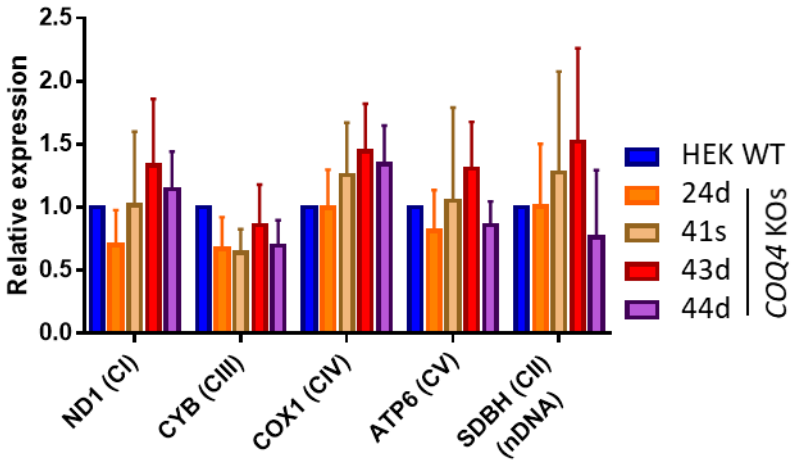

Figure 5.5. Mitochondrial transcripts expression in *COQ4* KO cells, relative to HEK WT control. Quantitative PCR of several transcripts of mtDNA-encoded (ND1 for Complex I, CYB for Complex III, COXI for complex CIV and ATP6 for Complex V) and nDNA-encoded (SDBH for Complex II) subunits of the respiratory chain complexes, using the actin transcript as a constitutive control for normalization. (Two-way ANOVA, Tukey's multiple comparison, p-values > 0.05 (non significant)).

5.2.3. *COQ4* KO cells have a slight increased translation of mtDNA-encoded COXI protein

We wanted to analyse the participation of COQ4 protein in the translation of mitochondrial proteins. The small number of proteins encoded by mtDNA (13 polypeptides) makes it easy to label, detect, and quantify these mitochondrial translation products. With this purpose, cells were incubated with [^{35}S]-methionine, which is incorporated into newly synthesized proteins. To avoid the labelling of new cytosolic proteins, cells were treated with emetine, a cytoplasmic translation inhibitor, before the addition of radioactive methionine. After a 60 min pulse with the labelled amino acid, cells are harvested, washed, lysed, and finally subjected to SDS-PAGE, to later detect the radioactively labelled polypeptides. The *in vivo* mitochondrial protein labelling assay was carried out 3 times, testing mitochondrial translation in HEK WT cell line, *COQ4* KO (with a low number of passages and with a high number of passages since the ablation of *COQ4* gene), and *COQ4* KO complemented with COQ4-FS.

We observed that the *COQ4* KO cells showed a significant specific increase in the translation of COXI, which was rescued by WT COQ4 gene expression (Figure 5.6.A-C). Steady-state levels of COXI were also analysed by Western Blot, being the same in all cell lines (Figure 5.6.D). Maybe the increase in translation could be due to a slower turnover rate of this protein in the *COQ4* KO cells, compared to the controls, but the significance of these results and the eventual molecular mechanism of this phenomena remains to be elucidated.

A slight but not significant decrease in the translation of ATP6 and ATP8 was also observed, but cells expressing COQ4-FS did not revert this effect (Figure 5.6.A-C). Interestingly, the same phenotype was described for a *TRUB2* gene KD (Antonicka et al., 2015), a gene that shares a 5'UTR region with *COQ4*. In order to check that the ablation of *COQ4* gene did not have an effect on *TRUB2* expression, causing an indirect impact on mitochondrial translation, we performed a western blot of TRUB2 protein. TRUB2 levels were the same in all cells (Figure 5.6.D), so this effect could be related to the lack of COQ4, or any of the consequences derived from this deletion.

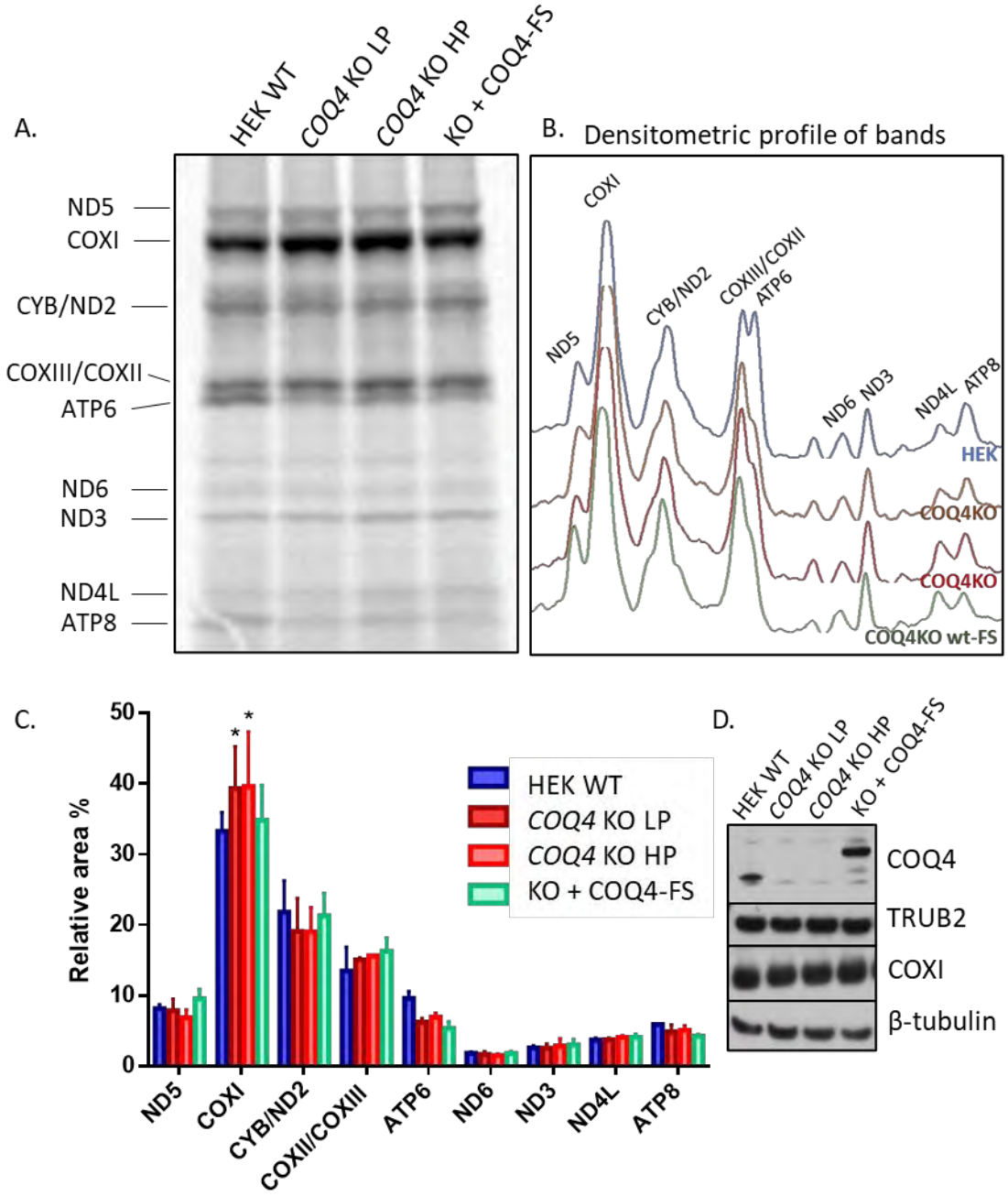

Figure 5.6. Increased COXI and slightly decreased ATP6 and ATP8 translation in *COQ4* KO cells, compared to controls.

(A) L-[^{35}S]-Methionine labelling (pulse of 1 hour) of mtDNA-encoded proteins in control HEK WT, in *COQ4* KO (43d) with high (HP) and low (LP) number of passages after *COQ4* ablation, and in *COQ4* KO cells transfected with *COQ4-FS*. (B) Densitometric profile of each lane of the gel and (C) densitometric quantification of the signal intensities of the labelled peptides (Two-way ANOVA Dunnett's multiple comparisons test, all samples vs. HEK WT; p-values<0.05 (*)). (D) Immunoblot of total lysates of the same cells, showing COQ4, TRUB2, COXI and β-tubulin levels.

5.2.4. Recovery after EtBr depletion

Next, we were interested in understanding if the correct functioning of CoQ biosynthetic function was also important for the balance of mtDNA maintenance and replication, and for the cellular response to mtDNA stress. With this purpose in mind, we treated *COQ4* KO and control cells with ethidium bromide (EtBr) at concentrations that induced a loss of mtDNA, to study the effects of mtDNA depletion in both genomic backgrounds.

EtBr is a DNA intercalator that preferentially binds to the mtDNA, disrupting its tertiary structure and leading to inhibition of its replication and transcription, but not stopping cell proliferation. Thus, cells continue to divide and, consequently, mtDNA is diluted into the daughter cells. This is a reversible process since upon withdrawal of the intercalator, cells are able to restore mtDNA replication if they still have some molecules of it [684]. So that, after a certain time, cells will have recovered their initial levels of mtDNA, with a recovery rate that may be different for different cell types.

It has been shown in the literature that, upon EtBr intercalation, not only the DNA topology changes, but it also neutralizes the charge of mtDNA and alters the binding ability for TFAM [685]. The release of TFAM into the mitochondrial matrix would lead to its specific degradation by Lon protease. After the loss of TFAM, mtDNA nucleoids tend to cluster, as a protecting mechanism for newly replicated mtDNA against intercalators mediating genotoxic stress [685]. This clusters mostly contained nucleoids in a replicative state, while the nucleoids which were not in replication tended to remain outside the clusters [685]. Nucleoid clustering has been also observed under other circumstances of mtDNA stress, such as POLG [614], TWINKLE and TFAM overexpression [686] or TFAM or CLPX protease downregulation [687,688].

We wanted to test the effect of *COQ4* deficiency in the response to mtDNA stress caused by EtBr treatment, in order to understand if *COQ4* in particular, or CoQ biosynthesis in general are important for mtDNA metabolism.

COQ4 KO recovers faster the mtDNA copy number after depletion induced by ethidium bromide (EtBr) treatment

MtDNA depletion was induced with with EtBr up to a 10% of the initial amount of mtDNA. After removing the intercalator, cells were let to recover mtDNA over time, and the recovery rate was quantified. Wild type cells, *COQ4* KO, and *COQ4* KO transfected with different versions of *COQ4* gene (COQ4-FS, COQ4, COQ4 M1-FS, COQ4 M2-FS and COQ4 M3-FS) were used in this assay. Firstly, the optimal duration of the EtBr treatment was determined to be 4 days for the cells to reach the 10% of the initial mtDNA. For the following experiments, cells were treated for 4 days and thenwashed and re-seeded. Every 24h, up to 7 days, two samples were collected, for DNA and protein extraction. The experiment was performed in triplicate, and with two conditions, with doxycycline and without doxycycline (which induces the expression of the transfected gene) (Figure 5.7).

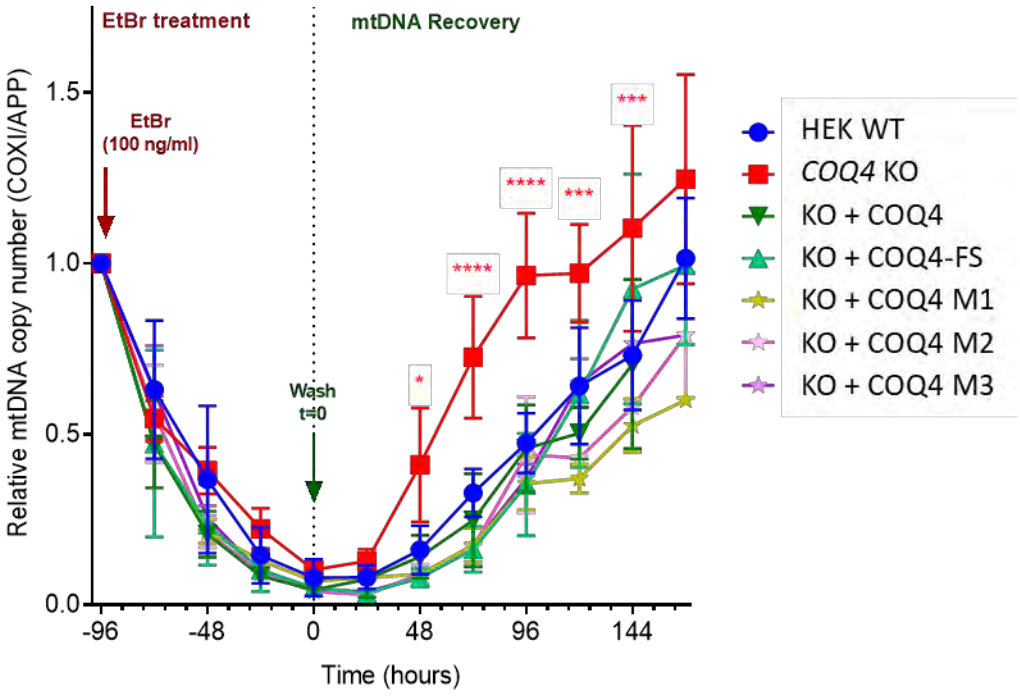

Figure 5.7. Increased mtDNA recovery rate in *COQ4* KO ethidium bromide mtDNA-depleted cells, compared to controls.
Cells were treated for four days (96h) with 100 ng/mL) of ethidium bromide (EtBr), for mtDNA depletion, until they had a 10% of the initial copy number. After withdrawal of the treatment (wash, t=0), mtDNA was recovered at different rates by the different cell lines. mtDNA copy number was measured at each time-point by quantitative PCR, using the nuclear gene (APP) for normalisation (Two-way ANOVA Dunnett's multiple comparisons test, all samples vs. HEK WT; p-values<0.05(*), <0.001 (***), <0.0001 (****)).

Strikingly, after quantifying the recovery rate of mtDNA (measured by qPCR MT-COXI/APP), we observed that the lack of COQ4 accelerated the recovery of mtDNA, reaching 50% of the initial copy number approximately 48 hours earlier than wild type cells or *COQ4* KO cells transfected with any of the versions of the gene. The latter recovered more slowly than wild type cells (Figure 5.7). The results were the same in the presence or absence of doxycycline (Figure 5.7). This surprising phenomenon has not been observed before in the literature. It could be directly related to the lack of COQ4, indicating that this protein could have some regulatory function in this process; or indirectly, related to the lack of CoQ_{10}, the lack of a functional CoQ_{10} biosynthetic complex or the accumulation of specific lipidic intermediates. Alternatively, it could also be caused by differences between *COQ4* KO cells and controls in the protective mechanism of nucleoid clustering that is caused by TFAM loss after EtBr intercalation, as described in the literature [685]; or even a differential efficiency in mitochondrial biogenesis in the two cell lines.

Several proteins, COQ4 amongst them, are lost and then recovered at different times during the mtDNA depletion and recovery process induced by EtBr treatment and withdrawal.

In order to gain further insight into the changes in mtDNA and mitochondrial mass following EtBr exposure, levels of proteins involved in different mitochondrial processes were analysed in the different conditions. In particular, levels of mitochondrial transcription factor (TFAM), proteins involved in mitochondrial RNA processing and translation (TRUB2, LRPPRC, TUFM, MRPS18B), subunits of the respiratory complexes encoded by the mtDNA (COXI, COXII) or the nDNA (NDUFS3, NDUFA9) and controls for mitochondrial mass (HSP60, VDAC1) were assayed. Steady-state levels of these proteins were analysed before the treatment (Figure 5.8), and during depletion (Figure 5.9) and recovery of mtDNA (after EtBr treatment and withdrawal) (Figure 5.10), at different time points.

The levels of all these proteins before the EtBr treatment were the same in *COQ4* KO and controls (HEK WT and *COQ4* KO transfected with *COQ4* (FS-tagged or untagged) (Figure 5.8).

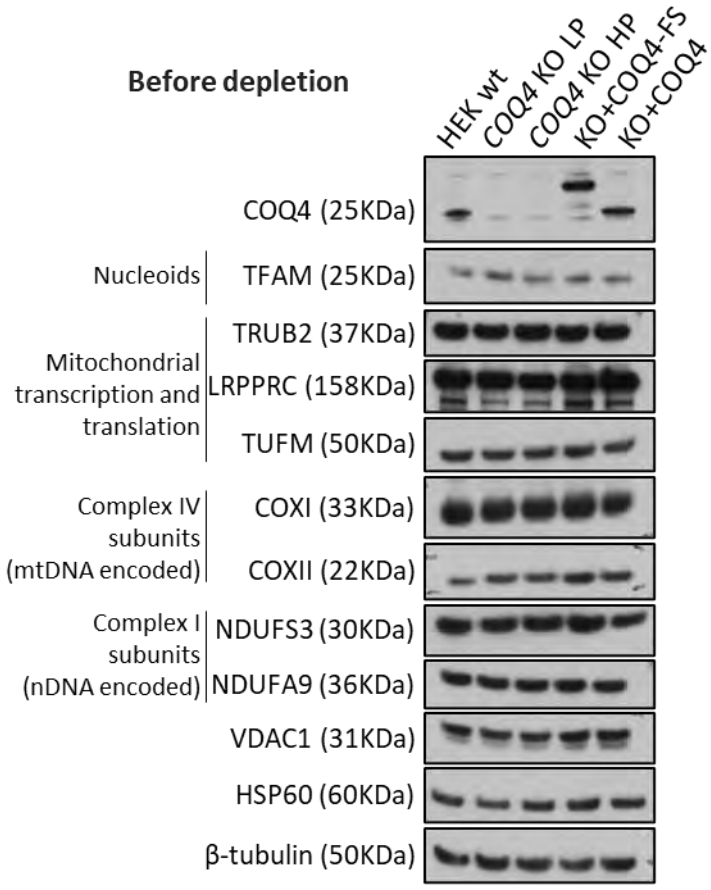

Figure 5.8. Steady-state levels of proteins involved in different mitochondrial processes were the same in *COQ4* KO and controls.
Western blot and immunodetection analysis of SDS-PAGE of total lysates from HEK WT, *COQ4* KO and *COQ4* KO transfected with COQ4 (FS-tagged or untagged), before ethidium bromide treatment.

Consistent with the reduction in mtDNA content during EtBr treatment, the steady state levels of TFAM decreased in *COQ4* KO and in controls, being slightly faster degraded in *COQ4* KO cells (Figure 5.9). TRUB2, the mitochondrial mRNA pseudouridine synthase whose coding gene shares 5' UTR with *COQ4* gene, was very rapidly depleted in all the three cell lines. LRPPRC, a protein involved in RNA metabolism, was partially degraded with the 4 days treatment, similarly to what happened to the mitochondrial ribosomal protein S18B (MRPS18B). The mitochondrial translation elongation factor TUFM was only very slightly degraded at 4 days of treatment, being in *COQ4* KO slightly more abundant than in the controls. MRC subunits were also affected by mtDNA depletion, especially the mtDNA encoded COXII. COXII was very rapidly degraded, and this degradation seemed to be somehow slower in *COQ4* KO. nDNA encoded complex I subunit NDUFA9 was slowly degraded in the three cell lines. HSP60 levels did not experienced major changes during depletion, suggesting the mitochondrial mass was not being affected, at least at 4 days of treatment with EtBr (Figure 5.9).

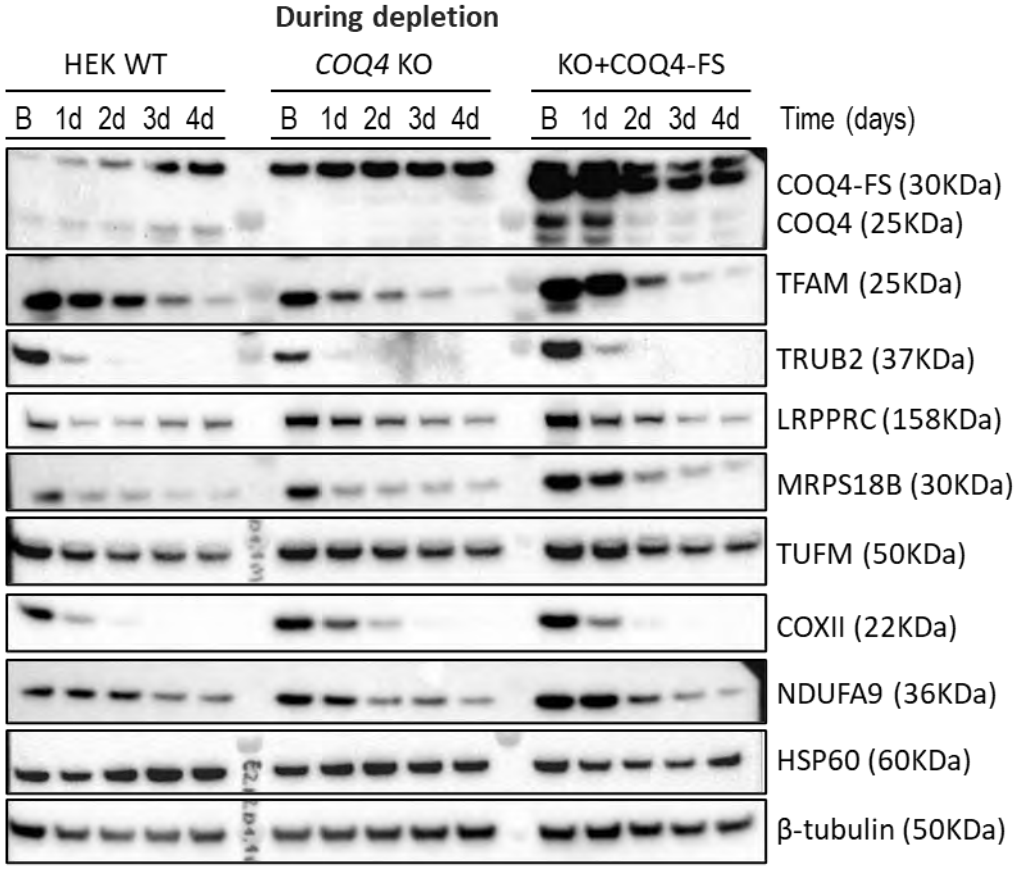

Figure 5.9. Protein levels during mtDNA depletion caused by ethidium bromide treatment.
(A) Western blot and immunodetection analysis of SDS-PAGE of total lysates from HEK WT, *COQ4* KO and *COQ4* KO transfected with COQ4-FS, at different time-points of mtDNA depletion. B: before depletion, d: days with ethidium bromide treatment.

After the removal of EtBr and during the mtDNA recovery phase, the proteins measured behaved in accordance with the mtDNA content and the faster recovery of mtDNA in *COQ4* KO (Figure 5.10.A). Proteins that were lost (or partially degraded) during the depletion phase, were gradually recovered (TFAM, TRUB2, LRPPRC, MRPS18B, MT-COII), being the recovery faster in *COQ4* KO cells. Other proteins that were only partially degraded behaved differently. This is the case of nDNA encoded complex I subunits NDUFA9 and NDUFS3, which continued to be degraded after EtBr withdrawal, and then, they experienced a delayed recovery that was similar in the three cell lines. Interestingly, COQ4 protein was also modulated in a similar way than NDUFA9 and NDUFS3 (nDNA-encoded complex I proteins). This effect is independent of the endogenous genomic locus and promoter, because it also occurred in COQ4 KO cells overexpressing COQ4 (tagged and untagged) from a different locus of the genome (Figure 5.10.B). This depletion of COQ4 probably occurs by direct degradation of the protein or by

degradation of the transcript. The delayed depletion and repletion of nuclear-encoded proteins directly involved in energy production (MRC components, or CoQ biosynthesis) is probably a mechanism to adapt to the retarded mtDNA-encoded protein synthesis.

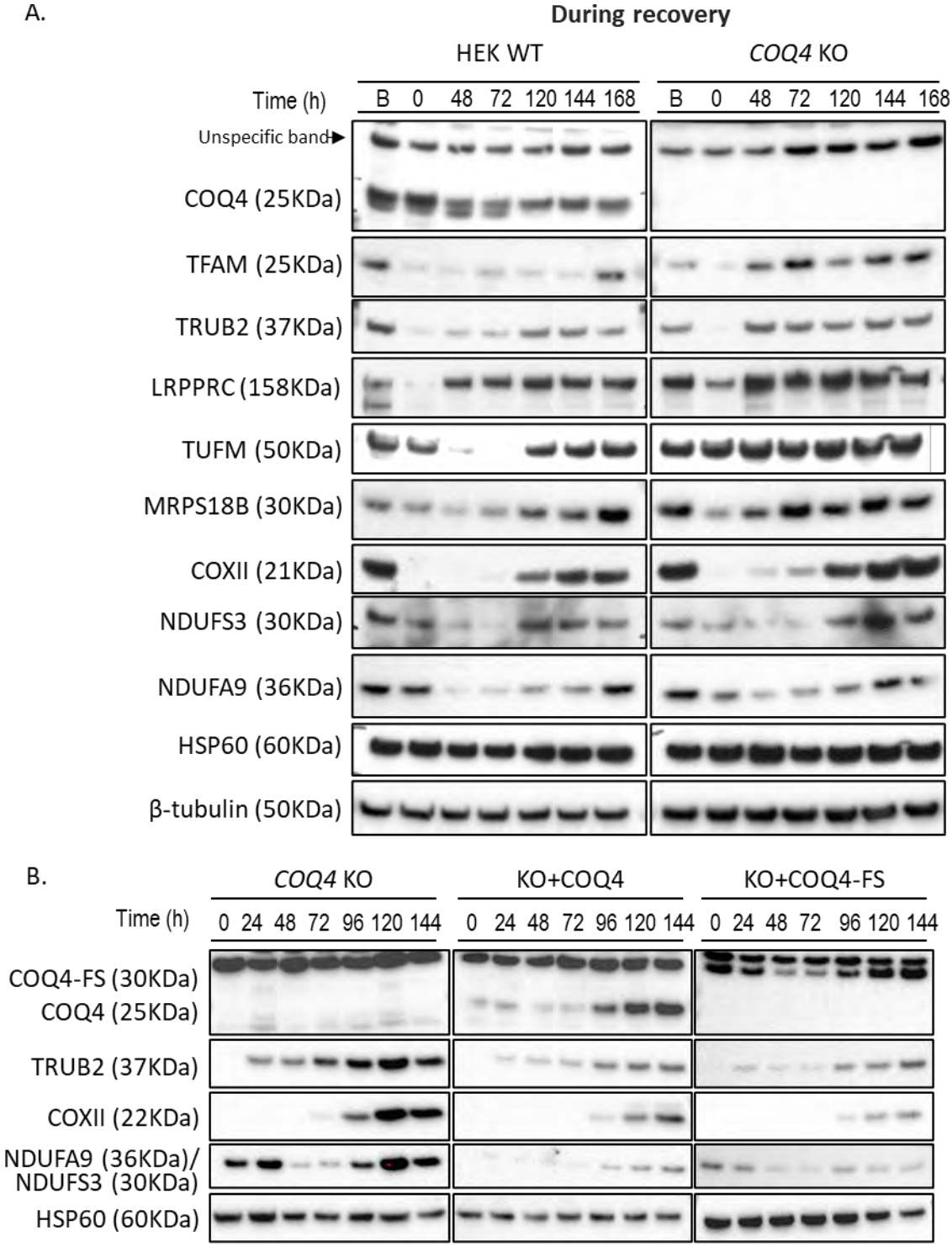

Figure 5.10. Protein levels during mtDNA recovery after ethidium bromide treatment.
Western blot and immunodetection analysis of SDS-PAGE of total lysates from HEK WT, *COQ4* KO (A) and *COQ4* KO transfected with COQ4-FS or untagged COQ4 (B), at different time-points of mtDNA recovery. B: before depletion, t=0: withdrawal of ethidium bromide treatment.

Faster mtDNA recovery in COQ4 KO is not due to the lack of CoQ_{10}, and also occurs in a COQ6 mutant (+/- CoQ_{10})

We wanted to unravel if the faster recovery was directly due to the absence of COQ4, or it was produced by other causes, such as the consequently significant CoQ_{10} deficiency, the lack of a functional CoQ biosynthetic process derived from the lack of COQ4, or the perturbance in lipids metabolism. To distinguish whether the increased rate of recovery was derived from the lack of CoQ, mtDNA depletion and recovery experiments were assayed in control and *COQ4* KO cells, with or without CoQ_{10} supplementation. To better understand if the effect was due specifically to the lack of COQ4 or the accumulation of specific intermediates, a *COQ6* KO cell line was also tested for mtDNA recovery rate.

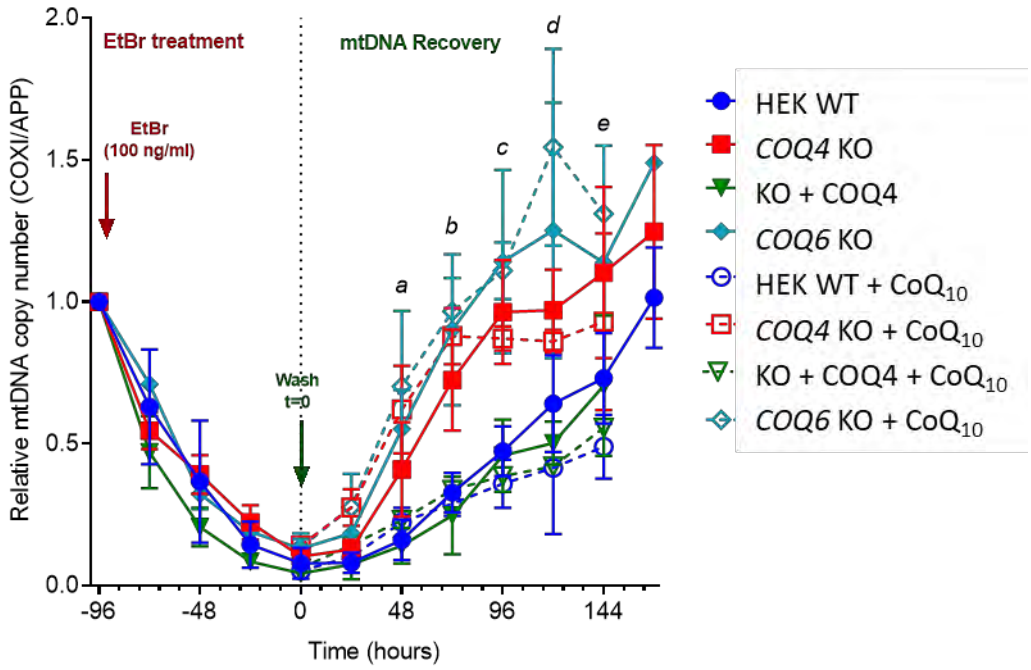

Figure 5.11. Increased mtDNA recovery rate in *COQ4* KO and *COQ6* KO ethidium bromide mtDNA-depleted cells, compared to controls (with no effect of CoQ_{10} treatment).
Cells were treated for four days (96h) with 100 mg/mL) of ethidium bromide (EtBr), for mtDNA depletion, until they had a 10% of the initial copy number. After withdrawal of the treatment (wash, t=0), mtDNA was recovered at different rates by the different cell lines. CoQ_{10} treatment was performed at 5µM during the recovery phase. mtDNA copy number was measured at each time-point by quantitative PCR, using the nuclear gene (APP) for normalisation, and represented as a percentage relative to mtDNA copy number before EtBr treatment. (Two-way ANOVA Dunnett's multiple comparisons test, all samples vs. HEK WT. p-values<0.05(*), <0.01 (**), <0.001 (***), <0.0001 (****):
a: *COQ4* KO (*), *COQ6* KO (**), *COQ4* KO + CoQ_{10} (**), *COQ6* KO + CoQ_{10} (****);
b: *COQ4* KO (****), *COQ6* KO (****), *COQ4* KO + CoQ_{10} (****), *COQ6* KO + CoQ_{10} (****);
c: *COQ4* KO (****), *COQ6* KO (****), *COQ4* KO + CoQ_{10} (**), *COQ6* KO + CoQ_{10} (****);
d: *COQ4* KO (***), *COQ6* KO (****), *COQ4* KO + CoQ_{10} (non-significant), *COQ6* KO + CoQ_{10} (****);
e: *COQ4* KO (***), *COQ6* KO (**), *COQ4* KO + CoQ_{10} (non-significant), *COQ6* KO + CoQ_{10} (**).

Our results show that the mere lack of CoQ_{10} does not influence the rate of mtDNA recovery in *COQ4* KO, since the same phenotype was observed when cells were supplemented with 5µM of CoQ_{10} during the recovery phase (Figure 5.11). Very interestingly, a faster recovery of mtDNA in *COQ6 KO* cells (+/- CoQ_{10}) was also observed, indicating that both *COQ4* and *COQ6* KO cell lines have something in common that induces a rapid repletion of mtDNA copy number after EtBr-induced depletion (Figure 5.11). Determining the cause of this phenomenon would shed light into the possible link between CoQ biosynthesis and mtDNA metabolism, a currently unexplored field. One possibility is that the disassembly of the CoQ biosynthetic complex itself could influence mtDNA metabolism.

5.2.5. Study of mitochondrial cholesterol and nucleoid proteins distribution

Considering the shared pathway between CoQ and cholesterol biosynthesis, and the link between mitochondrial cholesterol and replicative nucleoids, we wanted to explore if these relationships could be a clue for explaining the phenotype of fast mtDNA recovery after EtBr induced depletion.

Mitochondrial cholesterol concentration is the same in COQ4 KO cells and controls

Given that CoQ and cholesterol biosynthesis have in common the mevalonate pathway, a blockage in CoQ synthesis could lead to an accumulation of isoprenoid precursors in mitochondrial or extramitochondrial membranes that may increase cholesterol synthesis. In fact, higher levels of cholesterol have been observed in cellular models upon pharmacological inhibition of COQ2 protein by the addition of 4-nitrobenzoic acid (4-NB) [675], and in a KD of *UBIAD1*, a nonmitochondrial prenyltransferase involved in CoQ synthesis in the Golgi [676].

As we have seen in the introduction, mitochondrial cholesterol has been shown to be concentrated in the membrane fractions where replicative nucleoids attach [4]. We hypothesised a possible cholesterol raise could increase the number of cholesterol platforms in mitochondria membranes, which would anchor more replicatively-active nucleoids. In order to test this, we measured total cholesterol levels in mitochondria, comparing the *COQ4* KO cell line to controls.

In terms of total mitochondrial cholesterol concentration, the two cell lines have the same concentration in pure mitochondria (Figure 5.12.A). This finding made us conclude that cholesterol levels in mitochondria may not be the reason of the fast mtDNA copy number recovery in *COQ4* KO cells, compared to controls. However, we cannot rule out the possibility that small changes in concentration or distribution in specific domains in the IMM would be responsible for the modulation of cholesterol platforms and mtDNA stability.

COQ4 KO cells seem to have a slightly altered nucleoid structure in mitochondria

It has been suggested that cholesterol distribution in specific structures in the ER-mitochondria contact sites is important for the association of replicative mtDNA nucleoids [4]. Additionally, the CoQ biosynthesis machinery also localises in focal regions within ER-mitochondria contacts and, in yeast, the lack of Coq4p or Coq6p abolishes this focal localisation [1,2].

We wanted to examine if the lack of COQ4 protein had an effect on the distribution of nucleoid components and cholesterol within IMM. Thus, pure mitochondria from *COQ4* KO and controls (HEK WT and *COQ4* KO transfected with WT COQ4) were subjected to a DDM solubilization and a top-down fractionation on an iodixanol density gradient (Figure 5.12.B).

TFAM, ATAD3 and COQ4 were localized in the different fractions of the gradient (Figure 5.12.C). TFAM was considered a marker of mtDNA (and nucleoids), as it has been suggested to possibly be the only factor that is permanently associated with mtDNA [641]. ATAD3 was measured as an indicator of membrane-bound nucleoids, that are considered to be in a replicatively-active state [644,650]. ATAD3 is also thought to determine mitochondrial localization of cholesterol in this same area [4].

TFAM staining showed two distinct protein populations in mitochondria (Figure 5.12.C). The majority of the TFAM signal was part of high-density structures (being detected mainly in fractions 8 and 9). Likewise, a small proportion of TFAM staining was found in less dense fractions (12, 13 and 14). This distribution was in accordance with the literature, where dense structures are considered nucleoids containing mtDNA, TFAM, and also replication factors (TWINKLE), which would be tightly bound to the IMM [650].

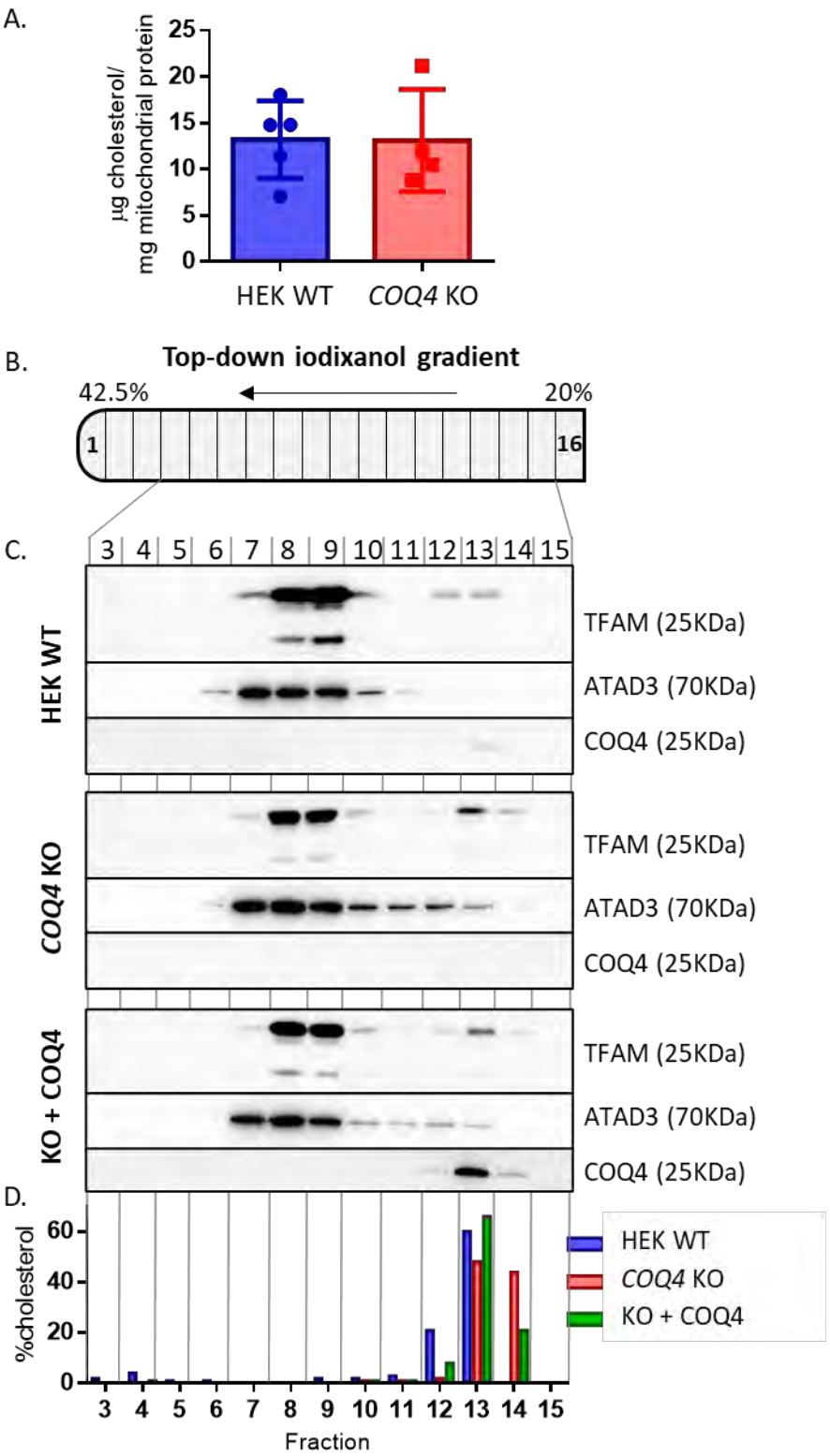

Figure 5.12. Cholesterol levels in mitochondria, and distributions of proteins and cholesterol on top-down iodixanol gradients of total mitochondrial DDM lysates.
(A) Cholesterol levels in pure mitochondria of HEK WT and *COQ4* KO cells (non-significant differences by unpaired two-tailed t-test). (B) Total pure mitochondrial DDM lysates from HEK WT, *COQ4* KO and *COQ4* KO transfected with COQ4 cells were separated on top-down iodixanol gradients. (C) Western blot and immunodetection analysis of SDS-PAGE of each fraction of the iodixanol gradients. (D) Cholesterol quantification in each fraction of the gradients, represented as a percentage of the total cholesterol measured.

The less-dense structures found in iodixanol gradients could be nucleoids associated with a lower amount and diversity of proteins or even free TFAM (we did not measure mtDNA presence). In our system, TFAM signal found in less dense structures (fractions 12, 13 and 14) is higher in COQ4 KO cells than in controls. This would suggest that in a steady-state situation, *COQ4* KO cells have more nucleoids in a non-replicative state and not attached to membranes, or that they have more free-TFAM.

ATAD3 protein was mainly found in dense fractions, being mostly in fractions 7 to 9, co-fractioning with TFAM-dense structures. Also, a small part appeared in less dense fractions (10 to 13) (Figure 5.12.C). This results agreed with previous observations described in the literature, in which they propose that TWINKLE-containing mammalian nucleoids attach to the IMM by ATAD3, in association with ER-mitochondrial junctions[4]. ATAD3 found in dense structures (fractions 7 to 9) is relatively less abundant in *COQ4* KO cells. This could mean that in a steady-state situation, *COQ4* KO cells have less ATAD3 coordinating nucleoids organisation, and more free-ATAD3.

COQ4 signal was also measured and found in the same low-density fractions than TFAM (13 and 14) in controls (Figure 5.12.C). This distribution of COQ4 protein probably indicates that it is not part of high-density complexes with nucleoids or other proteins, and is probably not tightly attached to the membrane. On the contrary, it is located in low-density fractions, cosedimenting with a fraction of TFAM that may correspond to nucleoids in a non-replicative state and/or not attached to membranes. This colocalisation could have some importance in the context of a regulation between mtDNA expression and CoQ_{10} biosynthesis.

Cholesterol levels were also measured in each of the fractions. In the literature, cholesterol was found in the low-density fractions of a flotation gradient (bottom-up) from mitochondrial membranes preparations, Triton X-100 solubilized [4]. In this type of gradients, IMM-associated nucleoids also migrated from the bottom of the tube to the low-density fractions. In our experiments, we used DDM lysates from total mitochondria separated by top-down iodixanol density gradients. Cholesterol was found next to the top of the gradient, in low-density fractions (12 to 14), and not in the fractions associated to ATAD3, in all the 3 cell lines (Figure 5.12.D). It is possible that the technical differences between protocols could have influenced results. It should be taken into

account that we made gradients from total pure mitochondria instead of membrane-enriched samples, performed DDM instead Triton X-100 solubilisation and used top-down gradient instead of bottom-up flotation gradient.

We repeated the experiments with a digitonin pre-treatment before running the gradient, to produce a mitochondrial membrane pellet sample and a supernatant sample containing soluble components. The membrane-rich pellet sample was solubilised with DDM, and both the pellet and the supernatant were fractionated on top-down iodixanol density gradients.

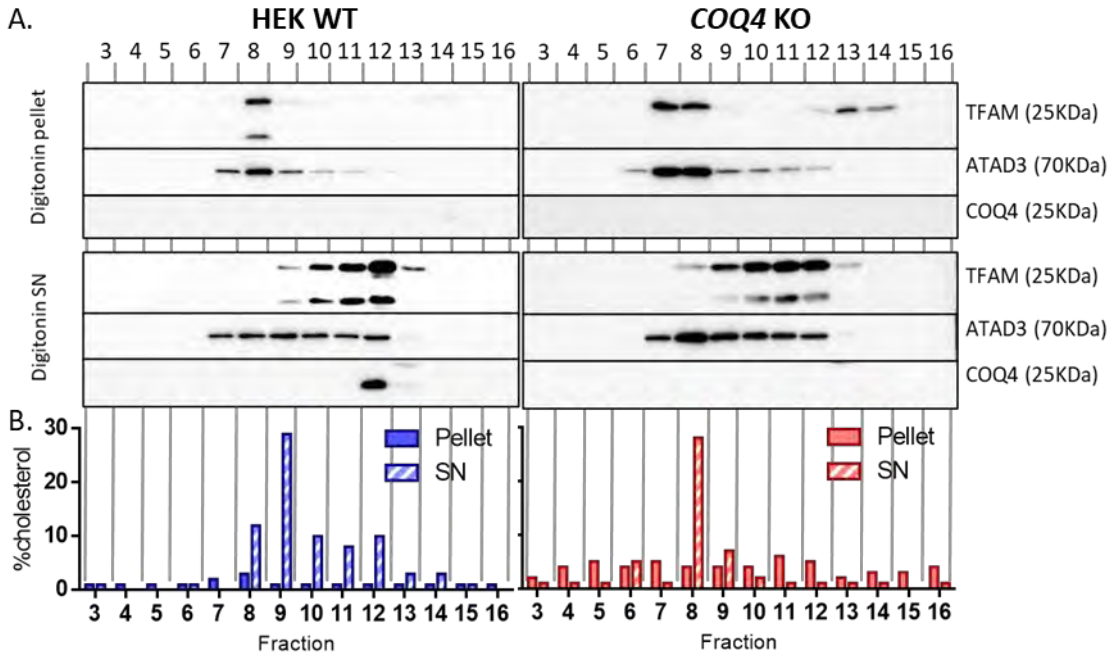

Figure 5.13. Distribution of proteins and cholesterol on top-down iodixanol gradients of membrane and soluble fractions of pure mitochondria.
Pellet and supernatant preparations from digitonin treated purified mitochondria from HEK WT and *COQ4* KO cells were separated on top-down iodixanol gradients and their protein (A) and cholesterol (B) contents were analysed.

The pellet fraction, rich in mitochondrial membranes, showed the same distribution of TFAM and ATAD3 observed with total mitochondria (Figure 5.13.A). We could see that TFAM and ATAD3 were more abundant in less dense fractions in the *COQ4* KO cell line compared to the control. COQ4 was not detected in the control pellet, probably indicating COQ4 is not tightly associated with the membranes. Cholesterol was almost undetected and equally distributed along the fractions in the pellet samples, contrarily to what was observed in the literature (Figure 5.13.B). It seems the digitonin treatment

removed the cholesterol from the membrane fraction, or that the combination of digitonin and DDM treatment totally solubilise cholesterol from the membranes. Technical improvements should be performed in order to confidently measure cholesterol in this kind of samples.

In the supernatant samples, TFAM and ATAD3 became more soluble, part of less dense fractions in both *COQ4* KO cells and controls. Soluble TFAM was no longer at high density 8 and 9 fractions, but it moved to fractions 9 to 13. ATAD3 spread to low-density fractions, but it was still more abundant in fractions 8 and 9. Curiously, cholesterol was detected in supernatant fractions (which were not treated with DDM), being concentrated in fractions 8 and 9, following ATAD3 distribution, with no significant differences between *COQ4* KO and control. This result fits with the literature [4].

With these very preliminary experiments, we have observed that mitochondrial cholesterol does not seem to change its levels or localisation in the absence of COQ4, although cholesterol distribution in compromised cells by mtDNA depletion should be further investigated. However, there seem to be slight differences between *COQ4* KO and control cells in terms of nucleoid proteins (TFAM and ATAD3) distribution in density gradients. Maybe these subtle changes are behind the *COQ4* KO fast mtDNA recovery after induced depletion. However, there is still a lot of work to be done to better understand the relationship between CoQ biosynthesis and mtDNA metabolism.

5.3. Conclusions

CoQ biosynthesis is an essential process taking place inside the mitochondria and influencing its physiology. When CoQ is altered, it could affect other essential mitochondrial functions such as mtDNA metabolism. The main conclusions derived from this work are the following:

i. The lack of COQ4 leads to a slight decrease of mtDNA copy number, with no effect on mtDNA transcription and a very subtle effect on mtDNA-encoded proteins synthesis.

ii. The lack of COQ proteins, such as COQ4 or COQ6, induces a faster mtDNA recovery rate after depletion induced by ethidium bromide (EtBr) treatment. This phenomenon does not seem to be due to the lack of CoQ_{10}.

iii. Faster mtDNA recovery rate is not due to mitochondrial cholesterol total levels, which overall are not altered in cells lacking COQ4.

iv. Density gradients of pure mitochondria show that the lack of COQ4 slightly alters nucleoid structure in mitochondria. ATAD3 and TFAM show a wider distribution towards the low-density fractions when COQ4 protein is missing.

v. COQ4 protein is found in low-density fractions of a density gradient, cosedimenting with a fraction of TFAM that may correspond to nucleoids in a non-replicative state and/or not attached to membranes. This colocalisation could have some importance in the context of a regulation between mtDNA expression and CoQ_{10} biosynthesis.

Discussion

Discussion

D1. Primary CoQ_{10} deficiency

D1.1. Phenotypic variability and attempt for genotype-phenotype associations

Primary CoQ_{10} deficiency is a rare mitochondrial disorder caused by mutations in one of the nuclear genes participating in the CoQ_{10} biosynthesis pathway, such as *PDSS1*, *PDSS2*, *COQ2*, *COQ4*, *COQ5*, *COQ6*, *COQ7*, *COQ8A/ADCK3*, *COQ8B*/ADCK4 or *COQ9* [112,225]. Patients show a broad spectrum of clinical manifestations, with different organs and tissues affected in a variable way, mainly depending on the affected gene and probably on many other factors still to be completely defined. The most affected organs and systems are the central and peripheral nervous system, kidney, heart and skeletal muscle, but other more heterogeneous findings have also been reported.

In this work, we have compiled and analysed the patients described in the literature so far for each mutated gene, according to the age of onset of the disease. We have studied the manifestations of the disease, the pathogenic mutations present in each family and other aspects, such as the response to CoQ_{10} treatment (Chapter 1). In this context, we have been able to describe the main phenotypic patterns of primary CoQ_{10} deficiency for each mutated gene, depending on the age when the patient first manifested the condition. These patterns are summarised in Table D.1. We have also checked for putative associations between some specific variants and these clinical phenotypic patterns.

Mutations in some *COQ* genes produce a multisystemic affection. This is the case of *PDSS1*, *PDSS2*, *COQ2, COQ4, COQ7* and *COQ9* pathogenic variants, which are also the ones that produce a disease that manifests the earliest in life. The most predominant phenotype in *PDSS2* and *COQ2* patients is the renal affection mainly with some neurological manifestations [242,245,277,323,324]. *COQ4* patients mainly displayed encephalopathy with cardiomyopathy in many cases [250–252,336]. The number of patients with mutations in *PDSS1, COQ7* and *COQ9* is too low to achieve a general conclusion, but they generally presented a multisystemic disease [238–241,246,248,256,322].

Pathogenic variants of other *COQ* genes show a more specific phenotype. Patients with mutations in *COQ6* manifest a nephrotic syndrome, with sensorineural hearing loss in many cases [233,235]. *COQ8B/ADCK4* patients had a steroid-resistant nephrotic syndrome, with multiple renal and some extrarenal features with variable frequency [229,363,364]. The hallmark phenotype of patients with pathogenic variants of *COQ8A/ADCK3* is cerebellar ataxia, often associated with cerebellar atrophy and other neurological abnormalities like epilepsy or movement disorders [274,275,357]. Only one family with a mutation in *COQ5* has been described so far, having an ataxic phenotype similar to *COQ8A'* s one [326]. Only one patient with *ADCK2* haploinsufficiency has been described, presenting at adult age a mitochondrial myopathy[378].

Age of onset of the disease is very variable among the different families, ranging from birth to early childhood (*PDSS1*, *PDSS2*, *COQ2*, *COQ4*, *COQ5*, *COQ6*, *COQ7*, *COQ9*), from childhood to adolescence (*COQ8A*, *COQ8B*), or even during adulthood (*COQ8A*, *COQ8B*). Generally, the disease seems to be more severe when the first symptoms appear earlier in life. We classified the clinical cases described in the literature according to their age of onset, as an attempt to draw more specific clinical patterns between patients with mutations in the same gene. We have done this for the genes for which the total number of families with affected individuals was higher than 20 (*COQ2*, *COQ4*, *COQ6*, *COQ8A* and *COQ8B)*. After the classification, we observed how different phenotypic clinical patterns appeared in some of the age of onset groups, which are detailed in Table D.1 and Chapter 1 (Section 1.2.4).

Many mutations associated with primary CoQ_{10} deficiency are rare or private. We have analysed, for each gene, the most common ones, and how they are distributed within the different age-of-onset groups of patients (Table D.1). For some genes, like *COQ2* and *COQ6*, some specific variants are clustered in the different age-of-onset groups (Table D.1). Based on some functional studies found in the literature, it seems that the residual activity of the mutated protein is essential for determining the severity of the disease [232,277]. A profound functional study on how all these mutations affect protein functionality could shed light to this hypothesis. No clear associations have been observed for *COQ4, COQ8A/ADCK3* or *COQ8B/ADCK4* mutations.

This distinction of different phenotypic patterns depending on the mutated gene, the age of onset of the disease and the pathogenic variants has been previously observed in several specific studies, focused in one particular gene or clinical case. We believe its application to the whole group of primary CoQ_{10} patients can be clinically useful for the early diagnosis and management of patients with primary CoQ_{10} deficiency suspicion. To contribute to this purpose, we have also built a web-based database that will grow with all the published primary CoQ_{10} deficiency clinical cases and their features: https://coq-biology.github.io/clinic-CoQ-defects. Heatmap representation of the frequency of symptoms will give a visual and convenient overview of the disease according to the affected gene, which we think will be useful in a clinical context.

Table D.1. Main clinical phenotypes of primary CoQ_{10} deficiency patients, classified by the mutated gene and subclassified by age-of-onset.

Gene (P)	Group (P)	Mean age of onset	Main phenotype	Most represented mutations (F)
PDSS1 (**3**)	All (**3**)	1 yo	Only two families with different presentation: nephropathy or peripheral neuropathy	-
PDSS2 (**7**)	All (**7**)	6 mo	multisystem disorder with mainly renal involvement and a wide range of neurological manifestations	c.1145C>T (p.Ser382Leu) (**2**)
COQ2 (**30**)	1 (**13**)	2 wo	early-onset severe multisystemic disorder, mainly with renal and CNS involvement	c.287G>A (p.Ser96Asn) (**5**)
	2 (**6**)	9 mo	infancy-onset SRNS that was accompanied by some neurological symptoms	c.740A>G (p.Tyr247Cys) (**2**), c.823A>G (p.Thr275Ala) (**2**)
	3 (**9**)	34 mo	infancy or childhood -onset isolated SRNS	c.533A>G (p.Asn178Ser) (**8**)
	4 (**2**)	17 yo	Adolescence-onset SRNS with a mild CNS involvement	c.1019G>C (p.Gly340Ala) (**1**)
COQ4 (**35**)	1 (**25**)	2 wo	Neonatal or infantile-onset encephalo-cardiomyopathy	c.370G>A (p.Gly124Ser) (**9**), c.402+1G>C (**3**), c.718C>T (p.Arg240Cys) (**3**)
	2 (**4**)	6 mo	infantile-onset encephalopathy	c.370G>A (p.Gly124Ser) (**3**), 371G>T (p.Gly124Val) (**2**)
	3 (**5**)	6 yo	childhood-onset progressive spinocerebellar ataxia	c.190C>T (p.Pro64Ser) (**1**), c.230C>T (p.Thr77Ile) (**1**), c.164G>T (p.Gly55Val) (**1**)
COQ5 (**3**)	All (**3**)	Early chilhood	early childhood cerebellar ataxic phenotype	-

Abbreviations: P: number of patients; F: number of families; SRNS: steroid resistant nephrotic syndrome; CNS: central nervous system; SNHL: sensorineural hearing loss.

Table D.1. Main clinical phenotypes of primary CoQ_{10} deficiency patients, classified by the mutated gene and subclassified by age-of-onset (Continued).

Gene (P)	Group (P)	Mean age of onset (years old)	Main phenotype	Most represented mutations (F)
COQ6 (**30**)	1 (**15**)	1 yo	infantile-onset SRNS, sometimes with SNHL and CNS affection	c.763G>A (p.Gly255Arg) (**2**), c.1078C>T (p.Arg360Trp) (**3**), c.189_191delGAA (p.Lys64del) (**3**), c.782C>T (p.Pro261Leu) (**3**)
	2 (**12**)	5 yo	childhood-onset SRNS, sometimes with SNHL	c.1058C>A (p.Ala353Asp) (**4**), c.189_191delGAA (p.Lys64del) (**3**), c.782C>T (p.Pro261Leu) (**3**)
COQ7 (**3**)	All (**3**)	4 mo	neonatal-infancy onset multisystemic disorder with CNS, PNS, renal, muscle and heart involvement	-
COQ9 (**7**)	All (**7**)	1 mo	neonatal-infancy onset multisystemic disorder, with CNS, renal and cardiac involvement	-
COQ8A (**77**)	1 (**24**)	19 mo	infantile-onset cerebellar ataxic syndrome with intellectual disability and developmental delay	c.1027C>T (p.Gln343*) (**3**), c.1823C>T (p.Ser608Phe) (**2**)
	2 (**32**)	6 yo	childhood-onset cerebellar ataxic syndrome with cognitive impairment, tremor and speech difficulties	c.901C>T (p.Arg301Trp) (**4**), c.895C>T (p.Arg299Trp) (**3**), c.1331_1332insCACAG (p.Glu446Alafs*33) (**3**), c.1844G>A (p.Gly615Asp) (**3**), c.1750_1752delACC (p.Thr584del) (**3**)
	3 (**9**)	14 yo	adolescence-onset cerebellar ataxic syndrome with tremor, speech difficulties and myoclonus	-
	4 (**6**)	22.5 yo	adult-onset cerebellar ataxic syndrome with tremor and speech difficulties	-
COQ8B (**79**)	1 (**4**)	17 mo	infantile-onset SRNS with variable involvement of other organs	c.748G>C (p.Asp250His) (**2**), c.1199dupA (p.His400Glnfs*11) (**2**)
	2 (**28**)	7.3 yo	infantile-onset SRNS with variable involvement of other organs	c.1339dupG (p.Glu447Glyfs*10) (**4**), c.293T>G (p.Leu98Arg) (**3**), c.737G>A (p.Ser246Asn) (**3**), c.1199dupA (p.His400Glnfs*11) (**3**), c.748G>C (p.Asp250His) (**2**)
	3 (**35**)	14.3 yo	adolescence-onset SRNS with variable involvement of other organs	c.1339dupG (p.Glu447Glyfs*10) (**7**), c.1199dupA (p.His400Glnfs*11) (**4**), c.737G>A (p.Ser246Asn) (**3**), c.645delT (p.Phe215Leufs*14) (**3**)
	4 (**11**)	24 yo	adult-onset SRNS with variable involvement of other organs	c.1339dupG (p.Glu447Glyfs*10) (**4**)

Abbreviations: P: number of patients; F: number of families; SRNS: steroid resistant nephrotic syndrome; CNS: central nervous system; SNHL: sensorineural hearing loss.

D1.2. Expanding phenotypes and genotypes

We also worked with primary fibroblasts from previously unreported cases of primary CoQ_{10} deficiency. In this context, we contributed to the biochemical diagnosis of the CoQ_{10} deficiency in fibroblasts from 5 patients with CoQ_{10} deficiency, with biallelic mutations in *COQ7* and *COQ4* genes (Chapter 2, sections 2.2.1 and 2.2.3). They had low levels of CoQ_{10} and impaired biosynthesis, reduced CII+III activity and impaired respiratory performance.

P102 and P112 are two patients with new pathogenic variants in *COQ7*. P102 presented clinical manifestations similar to the three *COQ7* patients reported in the literature. They all showed early-onset multisystemic disease, mainly with neurological involvement. In contrast, P112 presented an adolescence-onset and a mild progressive disorder with a pyramidal syndrome, hearing loss and neuropathic gait, expanding the phenotype of the disease with a strikingly different one. Interestingly, the genotype of this patient is also very different from all primary CoQ_{10} deficiency patients reported to date. P112 has a homozygous mutation in the translation initiation codon (c.3G>T, p.Met1Ile, NM_016138.5). This extremely rare case of primary CoQ_{10} deficiency is the first one reported to have a mutation altering the translation initiation codon of a COQ protein. The pathogenicity of the mutation may primarily rely on the efficiency of COQ7 translation or even in the mislocalization of the protein, rather than on a dysfunctional COQ protein. This fact should be taken into account for the possibility to design personalised therapeutic options.

P105, P108 and P109 are three patients with new pathogenic variants in *COQ4*. P105 presented a birth-onset disease compatible with a *COQ4* deficiency, but manifesting hypertonia instead of hypotonia. She died prematurely at the age of 16 months old. P108 and P109 presented early-onset severe hypotonia, developmental delay and regression, seizures and hypertrophic cardiomyopathy. P109 died at the age of 17 years old. All these patients presented new pathogenic variants in *COQ4* gene. One of the mutations found in P105 is a point substitution in intron 5 (c.532+6 T>A, p.?, NM_016035.5), specifically in the 5' donor splice site. We have observed that this mutation produces an aberrant *COQ4* mRNA splicing pattern, inducing the skipping of exons 3 and 5, mainly. In this case, we observe how the pathogenicity of the mutation

would rely on the process of splicing of the *COQ4* pre-mRNA, that would reduce the levels of properly spliced variants and, consequently, would impact the rate and efficiency CoQ_{10} biosynthesis process. As explained before, it is important to consider this fact for possible and personalised therapeutic options in this kind of mutations.

D1.3. Intermediates of the pathway as diagnostic markers

CoQ is synthesised by a multienzymatic complex composed by different proteins involved in the process. Defects in one of these components sometimes lead to the accumulation of specific intermediates in certain yeast, bacteria and mammalian models (Chapter 4, section 4.1.5 and Tables 4.4, 4.5 and 4.6)). However, not a great number of studies of the accumulated intermediates have been performed in human models of primary CoQ_{10} deficiency disease. DMQ_{10}, the substrate of COQ7 enzyme, has been found accumulated in several models of CoQ_{10} deficiency. Specifically, it has been described as a diagnostic intermediate for *COQ7* and *COQ9* deficiency, in primary fibroblasts from patients with mutations in these two genes [239,388]. Interestingly, it was also found in lower amounts in patient fibroblasts with mutations in *COQ4* [388].

In this work, we equally found high amounts of DMQ_{10} accumulated in patients with mutations in *COQ7*. Moreover, we were able to find other diagnostic intermediates accumulated in models with defects in COQ6 and COQ4 proteins. Human *COQ6* KO cells accumulate 4-HP_{10} intermediate [165], in agreement with the accumulation of 4-HP reported in yeast [342,396] and bacterial [460] models deficient in C5 hydroxylation function. Human *COQ4* KO cells also accumulate a not previously reported specific intermediate that we have been able to observe in the HPLC chromatograms. Consistently, patient fibroblasts with mutations in *COQ4* equally show this peak. Currently, we are trying to identify this molecule which could be a very valuable marker for the diagnosis of CoQ_{10} deficiency due to *COQ4* mutations.

D1.4. Primary CoQ_{10} deficiency: a treatable disorder

Supplementation with CoQ_{10} or derivatives is the only therapeutic option currently available for CoQ_{10} deficiency. Patients generally respond quite well to CoQ_{10} supplementation, but in some cases, the treatment does not have any effect. The treatment with CoQ_{10} seems to be more effective in less severe disease stages, in which

the irreversible damage in critical tissues has not been completely established yet [255]. However, no other clear predictors of treatment response have been identified. There are difficulties that hinder our understanding of this variable response to treatment.

CoQ_{10} treatment and the patient's response to it has been described in almost half of the reported primary CoQ_{10} deficiency cases in the literature. However, among these reports, response to treatment has been measured in different and not standardised ways, generally as an amelioration of the specific reported symptoms. Due to the small number of patients and the diversity of the reports, it is difficult to establish quantitative data regarding the response to CoQ_{10} treatment.

Moreover, CoQ_{10} delivery in muscle and brain tissue is generally limited, due to its high molecular weight and lipophilicity. However, at high doses, dietary supplementation has been proved to increase CoQ_{10} levels in all tissues, especially in the case of certain lipid-soluble formulations [280,281,689]. For these reasons, patients are worldwide treated with very different doses and formulations of CoQ_{10}. Doses range from 5 mg/kg/day [285] to 30-50 mg/kg/day for both adults and children [286]. Different formulations of CoQ_{10} are now available and being used in a clinical context. There are CoQ_{10} drugs both in the oxidized and the reduced forms, with different properties. All this variability may also contribute to the differences in treatment response.

Alternatively to CoQ_{10} supplementation, some soluble 4-HB head precursor analogues have been proposed as potential therapeutic molecules with higher bioavailability than CoQ_{10} [289]. These molecules provide the defective chemical group and can reactivate endogenous CoQ biosynthesis. Currently, they have not been yet utilised for patients' treatment, but they have been proven useful in yeast, mammalian cell cultures and mouse models of primary CoQ_{10} deficiency [238,239,342,399–401]. In this work, we have observed that vanillic acid treatment is more effective than CoQ_{10} treatment in a *COQ6* KO human cell line [165]. We have also observed how 2,4-dHB treatment is generally beneficial in fibroblasts from patients with mutations in *COQ7*. Taking these facts together, 4-HB analogues could be considered as promising potential therapeutic agents for specific defects in CoQ_{10} biosynthesis. However, the conditions of the treatment should be personalised for each patient, since these molecules seem to be more effective when the CoQ_{10} biosynthetic defect is more severe.

D2. Investigating COQ4 function

D2.1. COQ4 function in CoQ_{10} biosynthesis and mitochondrial respiration

COQ4 protein has an essential role in CoQ_{10} biosynthesis. It was first described and studied in yeast, in which it was suggested to play a structural role in stabilizing the CoQ biosynthetic complex [465,466]. In our work, we have demonstrated that human COQ4 protein is essential for CoQ_{10} biosynthesis in human cells (Chapter 4, section 4.2.1). The lack of COQ4 leads to drastically reduced CoQ_{10} levels (Figures 4.6, 4.8 and 4.14), which causes a great respiratory defect that is rescued with CoQ_{10} treatment or WT *COQ4* expression. Moreover, knocking-out COQ4 protein produces the accumulation of a specific intermediate, as described in section D1.3. It is possible that the lack of COQ4 and its structural function in the CoQ_{10} biosynthesis complex derives in a destabilisation of contacts between the different COQ proteins, ending up in the accumulation of an intermediate molecule of the pathway. Other possibility is that, in addition to the important structural function of COQ4, it could have other roles directly or indirectly on a specific enzymatic reaction in the pathway and its defect would lead to the accumulation of the intermediate.

We have used our CRISPR/Cas9 produced *COQ4* KO to try to study other aspects related to COQ4 function. We predicted the presence of a potential phosphorylatable loop, composed of the residues S106, T107, S108 and T109 andused site-directed mutagenesis to study this possible protein phosphorylation, changing Ser/Thr to Ala to prevent phosphorylation, and Ser/Thr to Glu to mimic constitutive phosphorylation. Expression of these mutants on a *COQ4* KO background recovered COQ4 function, restoring CoQ_{10} levels, at least in the conditions tested (Figure 4.9). It could be also possible that these variants affect somehow COQ4 function, but our system is not fine enough to distinguish differences in residual activity due to a high expression of the transgene. Further studies would be needed to ultimately unveil the significance of these residues in CoQ_{10} biosynthesis regulation under different conditions.

We also expressed *COQ4* carrying the pathogenic variants found in patients in the *COQ4* KO background, in order to analyse the pathogenicity of the mutations. Surprisingly, most of the mutations described in patients were found to be hypomorphic, fully

recovering CoQ_{10} biosynthesis in the *COQ4* KO cells when overexpressed (Figure 4.10). The expression system we used seem to be unable to discern different levels of activity of the mutated COQ4 proteins. However, it seems to be useful for examining the pathogenicity of loss-of-function variants. For the rest of mutations, we propose a combination of the mutant *COQ4* variant overexpression and a pABA treatment that partially inhibits CoQ_{10} biosynthesis from 4-HB (Figure 4.11). This combined system could help us to elucidate the pathogenicity of the mutations found in patients, by understanding the levels of residual activity that the mutant proteins may have.

Treatment with pABA also helped us in the task of investigating COQ4 function. When comparing pABA-treated *COQ4* KO cells with WT cells or cells expressing a WT or mutant version of COQ4, we could observe how all of them, except *COQ4* KO, presented an accumulation of DMQ_{10}, due to a partial inhibition of the endogenous CoQ_{10} synthesis from 4-HB (Figure 4.11). This fact supports the idea that COQ4 may act directly or indirectly upstream DMQ_{10} production, or that its specific function precedes DMQ_{10} formation, since it is not found when COQ4 is totally abstent.

D2.2. COQ4 forms a dynamic complex with COQ3-9 proteins, essential for CoQ_{10} synthesis

CoQ_6 biosynthesis complex has been extensively studied in yeast, in which it is described to be composed by Coq3p-Coq9p proteins. Some recent studies identify Coq8p dynamically interacting with the complex, but not as an integral component [1,316,438]. There is increasing evidence of the formation of such a complex in mammals as well. With this work, we aimed to provides further insights about the CoQ_{10} biosynthesis complex and its composition in humans. Specifically, we were interested in studying COQ4 interaction partners. In order to do so, we performed BN-PAGE and immunocapture of COQ4, with or without SILAC labelling (Chapter 4, section 4.2.3).

BN-PAGE and blots of COQ4 protein showed that this protein migrated to the bottom of the gel, in low molecular weights (Figure 4.15.A and C). These results suggested that COQ4 is not stably interacting in high molecular weight complexes, at least in our experimental conditions of cell growth, or even solubilization or electrophoresis. Additionally, 2D BN-PAGE showed a 50 KDa band at the low molecular weights' region,

in the controls but not in the *COQ4* KO. We could speculate that it could be a very stable dimeric form of COQ4 (resistant to SDS treatment), that it is not forming higher molecular weight complexes.

We were able to identify proteins that copurified with COQ4 after immunocapture. Interestingly, all the COQ proteins (except for COQ8A) were found significantly overrepresented in the eluates of COQ4 purification (Table 4.9). The fact that they all co-purified with COQ4-FS provides evidence for the mammalian CoQ biosynthesis complex and its composition. Moreover, we observed by Western blot that the lack of COQ4 or COQ6 proteins alters the levels of other COQs proteins, probably modifying the stability of the biosynthetic complex.

Interestingly, recent studies in yeast localised the CoQ-head modifying enzymes in discrete loci named CoQ domains, spatially and functionally related to ERMES[1,2,316]. A similar distribution of COQ9 protein was also observed in human cells[1]. Further research is needed to analyse if this relationship between ER-mitochondria contacts and CoQ_{10} biosynthesis is also conserved in mammals and to understand its implications.

D2.3. Studying the relationship between CoQ_{10} biosynthesis and mtDNA metabolism.

Different studies have reported an important link between ER-mitochondria contacts and proper nucleoids distribution in mitochondria [3,656]. Remarkably, the cholesterol content in these areas seems to be key for mtDNA replication of membrane-attached nucleoids [4]. Moreover, CoQ biosynthesis has also been related to ER-mitochondria contact sites, since CoQ head-modifying enzymes resolved in discrete loci, the so-called CoQ domains, adjacent to ER-mitochondria contact sites [1,2,316]. Besides this newly described spatial localisation in mitochondria, CoQ and cholesterol also share part of their mevalonate-derived lipid chain biosynthesis in the ER [522,523]. Therefore, all these processed must be tightly regulated, and it is possible that if one of them is altered, the others can be affected.

That is why we wanted to further investigate if CoQ deficiency due to COQ4 defects, may lead to an impairment in other important mitochondrial functions related to mtDNA metabolism, such as replication, maintenance or expression (Chapter 5). In this

context, we found that the lack of COQ4 led to a slight decrease of mtDNA copy number, with no effect on mtDNA transcription and a very subtle effect on mtDNA-encoded proteins synthesis (Chapter 5, sections 5.2.1, 5.2.2 and 5.2.3).

However, regarding mtDNA replication, we observed a surprising phenotype in the *COQ4* and *COQ6* KO cells (Chapter 5, section 5.2.4). The lack of these two COQ proteins induced a faster mtDNA recovery rate (compared to controls) after depletion induced by ethidium bromide treatment indicative of a more efficient mtDNA replication. This phenomenon does not seem to be due to the lack of CoQ_{10} because it was equally observed after CoQ_{10} supplementation. We suspected it could be rather related to an altered mitochondrial cholesterol content or distribution that may affect mtDNA replication. Reduced CoQ biosynthesis may lead to an accumulation of upstream intermediaries that would be available for more cholesterol biosynthesis and/or more stable cholesterol platforms in the IMM. However, we found that total cholesterol levels were not altered in mitochondria, although this does not rule out the possibility of changes in the micro-domains of cholesterol platforms. To study cholesterol distribution, as well as the distribution of related proteins within mitochondria, we performed very preliminary studies using density gradients. Interestingly, we found subtle differences between *COQ4* KO and control cells in terms of nucleoid proteins (TFAM and ATAD3) distribution in these gradients, which maybe are behind the *COQ4* KO fast mtDNA recovery after induced depletion. However, there is still a lot of work to be done to better understand the relationship between CoQ biosynthesis and mtDNA metabolism. Super-resolution microscopy of nucleoids may help us describe these possible differences in nucleoids structure and distribution, which we think is essential for the next steps of this project. Many mtDNA depletions are associated with CoQ secondary reduced levels. The understanding of the possible mtDNA metabolism and CoQ biosynthesis interplay in mitochondria would represent a milestone for unveiling the complexity of mitochondrial and specifically CoQ deficiencies conditions.

Bibliography

Bibliography

1. Subramanian, K. *et al.* Coenzyme Q biosynthetic proteins assemble in a substrate-dependent manner into domains at ER–mitochondria contacts. *J. Cell Biol.* **218**, 1353–1369 (2019).
2. Eisenberg-Bord, M. *et al.* The Endoplasmic Reticulum-Mitochondria Encounter Structure Complex Coordinates Coenzyme Q Biosynthesis. *Contact* **2**, 251525641882540 (2019).
3. Lewis, S. C., Uchiyama, L. F. & Nunnari, J. ER-mitochondria contacts couple mtDNA synthesis with mitochondrial division in human cells. *Science (80-.).* **353**, aaf5549 (2016).
4. Gerhold, J. M. *et al.* Human Mitochondrial DNA-Protein Complexes Attach to a Cholesterol-Rich Membrane Structure. *Sci. Rep.* **5**, 15292 (2015).
5. Benda, C. Ueber die Spermatogenese der Vertebraten und höherer Evertebraten, II. Theil: Die Histiogenese der Spermien. *Arch. für Anat. und Physiol.* **73**, 393–398 (1898).
6. Lynn Margulis. *Origin of Eukaryotic Cells. Evidence and Research Implications for a Theory of the Origin and Evolution of Microbial, Plant, and Animal Cells on the Precambrian Earth*. *Yale University Press* (1970).
7. Mitchell, P. Protonmotive redox mechanism of the cytochrome b-c1 complex in the respiratory chain: Protonmotive ubiquinone cycle. *FEBS Lett.* **56**, 1–6 (1975).
8. Alberts, B. *et al.* Molecular biology of the cell. *Garl. Sci.* **6th editio**, (2015).
9. Gustafsson, C. M., Falkenberg, M. & Larsson, N.-G. Maintenance and Expression of Mammalian Mitochondrial DNA. *Annu. Rev. Biochem.* **85**, 133–160 (2016).
10. Schmidt, O., Pfanner, N. & Meisinger, C. Mitochondrial protein import: from proteomics to functional mechanisms. *Nat. Rev. Mol. Cell Biol.* **11**, 655–667 (2010).
11. Grevel, A., Grevel, A., Becker, T. & Becker, T. Porins as helpers in mitochondrial protein translocation. *Biological Chemistry* vol. 401 699–708 (2020).
12. Lill, R. & Neupert, W. Mechanisms of protein import across the mitochondrial outer membrane. *Trends in Cell Biology* vol. 6 56–61 (1996).
13. Voos, W., Martin, H., Krimmer, T. & Pfanner, N. Mechanisms of protein translocation into mitochondria. *Biochimica et Biophysica Acta - Reviews on Biomembranes* vol. 1422 235–254 (1999).
14. Schlame, M. & Greenberg, M. L. Biosynthesis, remodeling and turnover of mitochondrial cardiolipin. *Biochim. Biophys. Acta - Mol. Cell Biol. Lipids* **1862**, 3–7 (2017).
15. Paupe, V. & Prudent, J. New insights into the role of mitochondrial calcium homeostasis in cell migration. *Biochem. Biophys. Res. Commun.* **500**, 75–86 (2018).
16. Kozjak-Pavlovic, V. The MICOS complex of human mitochondria. *Cell and Tissue Research* vol. 367 83–93 (2017).
17. van der Laan, M., Horvath, S. E. & Pfanner, N. Mitochondrial contact site and cristae organizing system. *Current Opinion in Cell Biology* vol. 41 33–42 (2016).
18. Saita, S. *et al.* PARL partitions the lipid transfer protein STARD7 between the cytosol and mitochondria. *EMBO J.* **37**, (2018).
19. Herrmann, J. M. & Riemer, J. The intermembrane space of mitochondria. *Antioxidants and Redox Signaling* vol. 13 1341–1358 (2010).
20. Edwards, R., Gerlich, S., Gerlich, S. & Tokatlidis, K. The biogenesis of mitochondrial intermembrane space proteins. *Biological Chemistry* vol. 401 737–747 (2020).

21. Mordas, A. & Tokatlidis, K. The MIA Pathway: A Key Regulator of Mitochondrial Oxidative Protein Folding and Biogenesis. *Acc. Chem. Res.* **48**, 2191–2199 (2015).
22. Signes Marrahi, A. Identification and characterisation of new factors and mechanisms regulating human cytochrome c oxidase biogenesis. *University of Cambridge* (University of Cambridge, 2019). doi:https://doi.org/10.17863/CAM.39069.
23. Tilokani, L., Nagashima, S., Paupe, V. & Prudent, J. Mitochondrial dynamics: Overview of molecular mechanisms. *Essays in Biochemistry* vol. 62 341–360 (2018).
24. Villanueva Paz, M. Autophagy and mitophagy flux disruption in cellular models of MERRF syndrome. *Universidad Pablo de Olavide* (Universidad Pablo de Olavide, 2019).
25. Campello, S. & Scorrano, L. Mitochondrial shape changes: Orchestrating cell pathophysiology. *EMBO Reports* vol. 11 678–684 (2010).
26. Suárez-Rivero, J. *et al.* Mitochondrial Dynamics in Mitochondrial Diseases. *Diseases* **5**, 1 (2016).
27. Kunji, E. R. S. & Robinson, A. J. Coupling of proton and substrate translocation in the transport cycle of mitochondrial carriers. *Current Opinion in Structural Biology* vol. 20 440–447 (2010).
28. Alcázar-Fabra, M., Navas, P. & Brea-Calvo, G. Coenzyme Q biosynthesis and its role in the respiratory chain structure. *Biochim. Biophys. Acta - Bioenerg.* **1857**, 1073–1078 (2016).
29. Hirst, J. & Roessler, M. M. Energy conversion, redox catalysis and generation of reactive oxygen species by respiratory complex I. *Biochim. Biophys. Acta - Bioenerg.* **1857**, 872–883 (2016).
30. Sun, F. *et al.* Crystal Structure of Mitochondrial Respiratory Membrane Protein Complex II. *Cell* **121**, 1043–1057 (2005).
31. Van Vranken, J. G., Na, U., Winge, D. R. & Rutter, J. Protein-mediated assembly of succinate dehydrogenase and its cofactors. *Critical Reviews in Biochemistry and Molecular Biology* vol. 50 168–180 (2015).
32. Crofts, A. R. *et al.* The Q-cycle reviewed: How well does a monomeric mechanism of the bc1 complex account for the function of a dimeric complex? *Biochim. Biophys. Acta - Bioenerg.* **1777**, 1001–1019 (2008).
33. Cramer, W. A., Hasan, S. S. & Yamashita, E. The Q cycle of cytochrome bc complexes: A structure perspective. *Biochim. Biophys. Acta - Bioenerg.* **1807**, 788–802 (2011).
34. Crofts, A. R. The cytochrome bc1 complex: Function in the context of structure. *Annu. Rev. Physiol.* **66**, 689–733 (2004).
35. Wikström, M., Sharma, V., Kaila, V. R. I., Hosler, J. P. & Hummer, G. New perspectives on proton pumping in cellular respiration. *Chemical Reviews* vol. 115 2196–2221 (2015).
36. Signes, A. & Fernandez-Vizarra, E. Assembly of mammalian oxidative phosphorylation complexes I-V and supercomplexes. *Essays Biochem.* **62**, 255–270 (2018).
37. Walker, J. E. The ATP synthase: The understood, the uncertain and the unknown. *Biochem. Soc. Trans.* **41**, 1–16 (2013).
38. Zhou, A. *et al.* Structure and conformational states of the bovine mitochondrial ATP synthase by cryo-EM. *Elife* **4**, (2015).
39. Mukherjee, S. & Warshel, A. The FOF1 ATP synthase: from atomistic three-dimensional structure to the rotary-chemical function. *Photosynthesis Research* vol. 134 (2017).
40. Schägger, H. & Pfeiffer, K. Supercomplexes in the respiratory chains of yeast and mammalian mitochondria. *EMBO J.* **19**, 1777–83 (2000).

41. Acín-Pérez, R., Fernández-Silva, P., Peleato, M. L., Pérez-Martos, A. & Enriquez, J. A. Respiratory active mitochondrial supercomplexes. *Mol. Cell* **32**, 529–39 (2008).

42. Gu, J. *et al.* The architecture of the mammalian respirasome. *Nature* **537**, 639–643 (2016).

43. Guo, R., Gu, J., Wu, M. & Yang, M. Amazing structure of respirasome: unveiling the secrets of cell respiration. *Protein Cell* **7**, 854–865 (2016).

44. Guo, R., Zong, S., Wu, M., Gu, J. & Yang, M. Architecture of Human Mitochondrial Respiratory Megacomplex I2III2IV2. *Cell* **170**, 1247-1257.e12 (2017).

45. Wu, M., Gu, J., Guo, R., Huang, Y. & Yang, M. Structure of Mammalian Respiratory Supercomplex I1III2IV1. *Cell* **167**, 1598-1609.e10 (2016).

46. Letts, J. A., Fiedorczuk, K. & Sazanov, L. A. The architecture of respiratory supercomplexes. *Nature* **537**, 644–648 (2016).

47. Lobo-Jarne, T. & Ugalde, C. Respiratory chain supercomplexes: Structures, function and biogenesis. *Semin. Cell Dev. Biol.* **76**, 179–190 (2018).

48. Enriquez, J. A. & Lenaz, G. Coenzyme Q and the respiratory Chain: Coenzyme Q pool and mitochondrial supercomplexes. *Mol. Syndromol.* **5**, 119–140 (2014).

49. Lapuente-Brun, E. *et al.* Supercomplex Assembly Determines Electron Flux in the Mitochondrial Electron Transport Chain. *Science (80-.).* **340**, 1567–1570 (2013).

50. Fedor, J. G. & Hirst, J. Mitochondrial Supercomplexes Do Not Enhance Catalysis by Quinone Channeling. *Cell Metab.* **28**, 525-531.e4 (2018).

51. Hirst, J. Open questions: respiratory chain supercomplexes-why are they there and what do they do? *BMC Biol.* **16**, 111 (2018).

52. Guda, P., Guda, C. & Subramaniam, S. Reconstruction of Pathways Associated with Amino Acid Metabolism in Human Mitochondria. *Genomics, Proteomics Bioinforma.* **5**, 166–176 (2007).

53. Wang, L. Mitochondrial purine and pyrimidine metabolism and beyond. *Nucleosides, Nucleotides and Nucleic Acids* vol. 35 578–594 (2016).

54. Kastaniotis, A. J. *et al.* Mitochondrial fatty acid synthesis, fatty acids and mitochondrial physiology. *Biochim. Biophys. Acta - Mol. Cell Biol. Lipids* **1862**, 39–48 (2017).

55. Issop, L. *et al.* Mitochondria-Associated membrane formation in hormone-stimulated leydig cell steroidogenesis: Role of ATAD3. *Endocrinology* **156**, 334–345 (2015).

56. Paul, B. T., Manz, D. H., Torti, F. M. & Torti, S. V. Mitochondria and Iron: current questions. *Expert Review of Hematology* vol. 10 65–79 (2017).

57. Swenson, S. A. *et al.* From Synthesis to Utilization: The Ins and Outs of Mitochondrial Heme. *Cells* **9**, 579 (2020).

58. Maio, N. & Rouault, T. A. Iron-sulfur cluster biogenesis in mammalian cells: New insights into the molecular mechanisms of cluster delivery. *Biochimica et Biophysica Acta - Molecular Cell Research* vol. 1853 1493–1512 (2015).

59. Stehling, O. & Lill, R. The role of mitochondria in cellular iron-sulfur protein biogenesis: Mechanisms, connected processes, and diseases. *Cold Spring Harb. Perspect. Biol.* **5**, (2013).

60. Solano-Gálvez, S. *et al.* Apoptosis: Activation and Inhibition in Health and Disease. *Med. Sci.* **6**, 54 (2018).

61. Baines, C. P. The molecular composition of the mitochondrial permeability transition pore. *Journal of Molecular and Cellular Cardiology* vol. 46 850–857 (2009).

62. Chinopoulos, C. Mitochondrial permeability transition pore: Back to the drawing board. *Neurochemistry International* vol. 117 49–54 (2018).

63. Baines, C. P. & Gutiérrez-Aguilar, M. The still uncertain identity of the channel-forming unit(s) of the mitochondrial permeability transition pore. *Cell Calcium* vol. 73 121–130 (2018).

64. Russell, O. M., Gorman, G. S., Lightowlers, R. N. & Turnbull, D. M. Mitochondrial Diseases: Hope for the Future. *Cell* **181**, 168–188 (2020).

65. Gorman, G. S. *et al.* Mitochondrial diseases. *Nat. Rev. Dis. Prim.* **2**, 16080 (2016).

66. Chinnery, P. F. & Hudson, G. Mitochondrial genetics. *British Medical Bulletin* vol. 106 135–159 (2013).

67. Schon, E. A., DiMauro, S. & Hirano, M. Human mitochondrial DNA: roles of inherited and somatic mutations. *Nat Rev Genet* **13**, 878–890 (2012).

68. Frazier, A. E., Thorburn, D. R. & Compton, A. G. Mitochondrial energy generation disorders: Genes, mechanisms, and clues to pathology. *J. Biol. Chem.* **294**, 5386–5395 (2019).

69. Calvo, S. E., Clauser, K. R. & Mootha, V. K. MitoCarta2.0: An updated inventory of mammalian mitochondrial proteins. *Nucleic Acids Res.* **44**, D1251–D1257 (2016).

70. Thompson, K. *et al.* Recent advances in understanding the molecular genetic basis of mitochondrial disease. *Journal of Inherited Metabolic Disease* vol. 43 36–50 (2020).

71. Suomalainen, A. & Battersby, B. J. Mitochondrial diseases: the contribution of organelle stress responses to pathology. *Nat. Rev. Mol. Cell Biol.* **19**, 77–92 (2018).

72. Lightowlers, R. N., Taylor, R. W. & Turnbull, D. M. Mutations causing mitochondrial disease: What is new and what challenges remain? *Science* vol. 349 1494–1499 (2015).

73. Viscomi, C. & Zeviani, M. MtDNA-maintenance defects: syndromes and genes. *J. Inherit. Metab. Dis.* 1–13 (2017) doi:10.1007/s10545-017-0027-5.

74. Craven, L., Alston, C. L., Taylor, R. W. & Turnbull, D. M. Recent Advances in Mitochondrial Disease. *Annu. Rev. Genomics Hum. Genet.* **18**, 257–275 (2017).

75. Garone, C. & Viscomi, C. Towards a therapy for mitochondrial disease: An update. *Biochemical Society Transactions* vol. 46 1247–1261 (2018).

76. Zhang, L. *et al.* Advances in drug therapy for mitochondrial diseases. *Ann. Transl. Med.* **8**, 17–17 (2020).

77. El-Hattab, A. W., Zarante, A. M., Almannai, M. & Scaglia, F. Therapies for mitochondrial diseases and current clinical trials. *Molecular Genetics and Metabolism* vol. 122 1–9 (2017).

78. Viscomi, C. Toward a therapy for Mitochondrial disease. *Biochem. Soc. Trans.* **44**, 1483–1490 (2016).

79. Hernández-Camacho, J. D., Bernier, M., López-Lluch, G. & Navas, P. Coenzyme Q10 Supplementation in Aging and Disease. *Front. Physiol.* **9**, 44 (2018).

80. Hirano, M., Garone, C. & Quinzii, C. M. CoQ 10 deficiencies and MNGIE: Two treatable mitochondrial disorders. *Biochimica et Biophysica Acta - General Subjects* vol. 1820 625–631 (2012).

81. Viscomi, C. & Zeviani, M. Strategies for fighting mitochondrial diseases. *J. Intern. Med.* **287**, 665–684 (2020).

82. Beyrath, J. *et al.* KH176 Safeguards Mitochondrial Diseased Cells from Redox Stress-Induced Cell Death by Interacting with the Thioredoxin System/Peroxiredoxin Enzyme

Machinery. *Sci. Rep.* **8**, 6577 (2018).

83. Cámara, Y. *et al.* Administration of deoxyribonucleosides or inhibition of their catabolism as a pharmacological approach for mitochondrial DNA depletion syndrome. *Hum. Mol. Genet.* **23**, 2459–2467 (2014).

84. Garone, C. *et al.* Deoxypyrimidine monophosphate bypass therapy for thymidine kinase 2 deficiency. *EMBO Mol. Med.* **6**, 1016–1027 (2014).

85. Lopez-Gomez, C. *et al.* Deoxycytidine and Deoxythymidine Treatment for Thymidine Kinase 2 Deficiency. *Ann. Neurol.* **81**, 641–652 (2017).

86. Viscomi, C. *et al.* In vivo correction of COX deficiency by activation of the AMPK/PGC-1α axis. *Cell Metab.* **14**, 80–90 (2011).

87. Cerutti, R. *et al.* NAD+-dependent activation of Sirt1 corrects the phenotype in a mouse model of mitochondrial disease. *Cell Metab.* **19**, 1042–1049 (2014).

88. Khan, N. A. *et al.* Effective treatment of mitochondrial myopathy by nicotinamide riboside, a vitamin B3. *EMBO Mol. Med.* **6**, 721–731 (2014).

89. Varanita, T. *et al.* The Opa1-dependent mitochondrial cristae remodeling pathway controls atrophic, apoptotic, and ischemic tissue damage. *Cell Metab.* **21**, 834–844 (2015).

90. Civiletto, G. *et al.* Opa1 overexpression ameliorates the phenotype of two mitochondrial disease mouse models. *Cell Metab.* **21**, 845–854 (2015).

91. Luna-Sanchez, M. *et al.* Opa1 Overexpression Protects from Early-Onset Mpv17−/−-Related Mouse Kidney Disease. *Mol. Ther.* **28**, 1918–1930 (2020).

92. Saxton, R. A. & Sabatini, D. M. mTOR Signaling in Growth, Metabolism, and Disease. *Cell* vol. 168 960–976 (2017).

93. Johnson, S. C. *et al.* MTOR inhibition alleviates mitochondrial disease in a mouse model of Leigh syndrome. *Science (80-.).* **342**, 1524–1528 (2013).

94. Wang, A., Mouser, J., Pitt, J., Promislow, D. & Kaeberlein, M. Rapamycin enhances survival in a Drosophila model of mitochondrial disease. *Oncotarget* **7**, 80131–80139 (2016).

95. Civiletto, G. *et al.* Rapamycin rescues mitochondrial myopathy via coordinated activation of autophagy and lysosomal biogenesis. *EMBO Mol. Med.* **10**, (2018).

96. Tiranti, V. *et al.* Loss of ETHE1, a mitochondrial dioxygenase, causes fatal sulfide toxicity in ethylmalonic encephalopathy. *Nat. Med.* **15**, 200–205 (2009).

97. Viscomi, C. *et al.* Combined treatment with oral metronidazole and N-acetylcysteine is effective in ethylmalonic encephalopathy. *Nat. Med.* **16**, 869–871 (2010).

98. Pereira, C. V. & Moraes, C. T. Current strategies towards therapeutic manipulation of mtDNA heteroplasmy. *Front. Biosci. - Landmark* **22**, 991–1010 (2017).

99. Tanaka, M. *et al.* Gene Therapy for Mitochondrial Disease by Delivering Restriction Endonuclease SmaI into Mitochondria. *J. Biomed. Sci.* **9**, 534–541 (2002).

100. Hashimoto, M. *et al.* MitoTALEN: A General Approach to Reduce Mutant mtDNA Loads and Restore Oxidative Phosphorylation Function in Mitochondrial Diseases. *Mol. Ther.* **23**, 1592–1599 (2015).

101. Bacman, S. R., Williams, S. L., Pinto, M., Peralta, S. & Moraes, C. T. Specific elimination of mutant mitochondrial genomes in patient-derived cells by mitoTALENs. *Nat. Med.* **19**, 1111–1113 (2013).

102. Gammage, P. A. & Minczuk, M. Enhanced manipulation of human mitochondrial DNA heteroplasmy in vitro using tunable mtZFN technology. in *Methods in Molecular Biology*

vol. 1867 43–56 (Humana Press Inc., 2018).

103. Gammage, P. A., Rorbach, J., Vincent, A. I., Rebar, E. J. & Minczuk, M. Mitochondrially targeted ZFNs for selective degradation of pathogenic mitochondrial genomes bearing large-scale deletions or point mutations. *EMBO Mol. Med.* **6**, 458–466 (2014).

104. Gammage, P. A. *et al.* Genome editing in mitochondria corrects a pathogenic mtDNA mutation in vivo. *Nature Medicine* vol. 24 (2018).

105. Silva-Pinheiro, P., Cerutti, R., Luna-Sanchez, M., Zeviani, M. & Viscomi, C. A Single Intravenous Injection of AAV-PHP.B-hNDUFS4 Ameliorates the Phenotype of Ndufs4−/− Mice. *Mol. Ther. - Methods Clin. Dev.* **17**, 1071–1078 (2020).

106. Guy, J. *et al.* Gene Therapy for Leber Hereditary Optic Neuropathy: Low- and Medium-Dose Visual Results. *Ophthalmology* **124**, 1621–1634 (2017).

107. Di Meo, I., Marchet, S., Lamperti, C., Zeviani, M. & Viscomi, C. AAV9-based gene therapy partially ameliorates the clinical phenotype of a mouse model of Leigh syndrome. *Gene Ther.* **24**, 661–667 (2017).

108. Cain, J. C. & Morton, R. Some minor constituents of liver oils. *Biochem. J.* **60**, 274–83 (1955).

109. Crane, F. L., Hatefi, Y., Lester, R. & Widmer, C. Isolation of a quinone from beed heart mitochondria. *Biochim Biophys Acta* **25**, 220–221 (1957).

110. Kagan, V. E. *et al.* Plasma membrane NADH-coenzyme Q0 reductase generates semiquinone radicals and recycles vitamin E homologue in a superoxide-dependent reaction. *FEBS Lett.* **428**, 43–6 (1998).

111. Navas, P., Villalba, J. M. & de Cabo, R. The importance of plasma membrane coenzyme Q in aging and stress responses. *Mitochondrion* **7**, (2007).

112. Alcázar-Fabra, M., Trevisson, E. & Brea-Calvo, G. Clinical syndromes associated with Coenzyme Q_{10} deficiency. *Essays Biochem.* **62**, 377–398 (2018).

113. Sohal, R. S. & Forster, M. J. Coenzyme Q, oxidative stress and aging. *Mitochondrion* **7**, S103-11 (2007).

114. Parrado, C. *et al.* Calorie restriction modifies ubiquinone and COQ transcripts levels in mouse tissues. *Free Radic. Biol. Med.* **50**, 1728–1736 (2011).

115. Lopez-Lluch, G., Rodríguez-Aguilera, J. C., Santos-Ocaña, C. & Navas, P. Is Coenzyme Q a key factor in aging? *Mech. Ageing Dev.* **131**, 225–235 (2010).

116. Varela-López, A., Giampieri, F., Battino, M. & Quiles, J. L. Coenzyme Q and its role in the dietary therapy against aging. *Molecules* **21**, 373 (2016).

117. Fernández-Ayala, D. J. M., Brea-Calvo, G., López-Lluch, G. & Navas, P. Coenzyme Q distribution in HL-60 human cells depends on the endomembrane system. *Biochim. Biophys. Acta - Biomembr.* **1713**, 129–137 (2005).

118. Kaurola, P., Sharma, V., Vonk, A., Vattulainen, I. & Róg, T. Distribution and dynamics of quinones in the lipid bilayer mimicking the inner membrane of mitochondria. *Biochim. Biophys. Acta - Biomembr.* **1858**, 2116–2122 (2016).

119. Quinn, P. J. Lipid-lipid interactions in bilayer membranes: Married couples and casual liaisons. *Progress in Lipid Research* vol. 51 179–198 (2012).

120. Bentinger, M., Tekle, M. & Dallner, G. Coenzyme Q – Biosynthesis and functions. *Biochem. Biophys. Res. Commun.* **396**, 74–79 (2010).

121. Zickermann, V. *et al.* Structural biology. Mechanistic insight from the crystal structure of mitochondrial complex I. *Science (80-.).* **347**, 44–49 (2015).

122. Goodsell, D. S., Autin, L. & Olson, A. J. Illustrate: Software for Biomolecular Illustration. *Structure* **27**, 1716-1720.e1 (2019).

123. Evans, D. R. & Guy, H. I. Mammalian pyrimidine biosynthesis: fresh insights into an ancient pathway. *J Biol Chem* **279**, 33035–33038 (2004).

124. Hey-Mogensen, M., Goncalves, R. L., Orr, A. L. & Brand, M. D. Production of superoxide/H2O2 by dihydroorotate dehydrogenase in rat skeletal muscle mitochondria. *Free Radic Biol Med* **72**, 149–155 (2014).

125. Rauchová, H., Battino, M., Fato, R., Lenaz, G. & Drahota, Z. Coenzyme Q-pool function in glycerol-3-phosphate oxidation in hamster brown adipose tissue mitochondria. *J. Bioenerg. Biomembr.* **24**, 235–41 (1992).

126. Mráček, T., Drahota, Z. & Houštěk, J. The function and the role of the mitochondrial glycerol-3-phosphate dehydrogenase in mammalian tissues. *Biochim. Biophys. Acta - Bioenerg.* **1827**, 401–410 (2013).

127. Watmough, N. J. & Frerman, F. E. The electron transfer flavoprotein: ubiquinone oxidoreductases. *Biochim Biophys Acta* **1797**, 1910–1916 (2010).

128. Blake, R. L., Hall, J. G. & Russell, E. S. Mitochondrial Proline Dehydrogenase Deficiency in Hyperprolinemic PRO / Re Mice : Genetic and Enzymatic Analyses. *Biochem Genet.* **14**, 739–757 (1976).

129. Summit, C. B. *et al.* Proline dehydrogenase 2 (PRODH2) is a hydroxyproline dehydrogenase (HYPDH) and molecular target for treating primary hyperoxaluria. *Biochem J* **466**, 273–281 (2015).

130. Hackfort, B. T. & Mishra, P. K. Emerging role of hydrogen sulfide-microRNA cross-talk in cardiovascular diseases. *Am. J. Physiol. Heart Circ. Physiol.* **310**, H802-12 (2016).

131. Ziosi, M. *et al.* Coenzyme Q deficiency causes impairment of the sulfide oxidation pathway. *EMBO Mol. Med.* **9**, 96–111 (2017).

132. Luna-Sánchez, M. *et al.* CoQ deficiency causes disruption of mitochondrial sulfide oxidation, a new pathomechanism associated with this syndrome. *EMBO Mol. Med.* **9**, (2017).

133. Quinzii, C. M. *et al.* The Role of Sulfide Oxidation Impairment in the Pathogenesis of Primary CoQ Deficiency. *Front. Physiol.* **8**, 525 (2017).

134. Murphy, M. P. How mitochondria produce reactive oxygen species. *Biochem J* **417**, 1–13 (2009).

135. Borgstahl, G. E. *et al.* The structure of human mitochondrial manganese superoxide dismutase reveals a novel tetrameric interface of two 4-helix bundles. *Cell* **71**, 107–118 (1992).

136. Han, D., Antunes, F., Canali, R., Rettori, D. & Cadenas, E. Voltage-dependent anion channels control the release of the superoxide anion from mitochondria to cytosol. *J Biol Chem* **278**, 5557–5563 (2003).

137. Genova, M. L. & Lenaz, G. Functional role of mitochondrial respiratory supercomplexes. *Biochim Biophys Acta* **1837**, 427–443 (2014).

138. Lagouge, M. & Larsson, N. G. The role of mitochondrial DNA mutations and free radicals in disease and ageing. *J Intern Med* **273**, 529–543 (2013).

139. Yee, C., Yang, W. & Hekimi, S. The intrinsic apoptosis pathway mediates the pro-longevity response to mitochondrial ROS in C. elegans. *Cell* **157**, 897–909 (2014).

140. Scialo, F., Mallikarjun, V., Stefanatos, R. & Sanz, A. Regulation of lifespan by the mitochondrial electron transport chain: reactive oxygen species-dependent and reactive

oxygen species-independent mechanisms. *Antioxid Redox Signal* **19**, 1953–1969 (2013).

141. Quinlan, C. L., Perevoshchikova, I. V, Hey-Mogensen, M., Orr, A. L. & Brand, M. D. Sites of reactive oxygen species generation by mitochondria oxidizing different substrates. *Redox Biol* **1**, 304–312 (2013).
142. Hirst, J. Mitochondrial complex I. *Annu. Rev. Biochem.* **82**, 551–75 (2013).
143. Hirst, J., King, M. S. & Pryde, K. R. The production of reactive oxygen species by complex I. *Biochem Soc Trans* **36**, 976–980 (2008).
144. Pryde, K. R. & Hirst, J. Superoxide is produced by the reduced flavin in mitochondrial complex I: a single, unified mechanism that applies during both forward and reverse electron transfer. *J Biol Chem* **286**, 18056–18065 (2011).
145. Allen, F. M. Mitochondrial Metabolism Elucidated by Rapid Fractionation from Tissue. *University of Cambridge* (2020). doi:https://doi.org/10.17863/CAM.49510.
146. Baker, M. A., Lane, D. J. R., Ly, J. D., De Pinto, V. & Lawen, A. VDAC1 Is a Transplasma Membrane NADH-Ferricyanide Reductase. *J. Biol. Chem.* **279**, 4811–4819 (2004).
147. Bersuker, K. *et al.* The CoQ oxidoreductase FSP1 acts parallel to GPX4 to inhibit ferroptosis. *Nature* (2019) doi:10.1038/s41586-019-1705-2.
148. Doll, S. *et al.* FSP1 is a glutathione-independent ferroptosis suppressor. *Nature* (2019) doi:10.1038/s41586-019-1707-0.
149. Hyun, D. H. Plasma membrane redox enzymes: new therapeutic targets for neurodegenerative diseases. *Archives of Pharmacal Research* vol. 42 436–445 (2019).
150. Gille, L. & Nohl, H. The existence of a lysosomal redox chain and the role of ubiquinone. *Arch. Biochem. Biophys.* **375**, 347–54 (2000).
151. Mukai, K. Free Radical Chemistry of Coenzyme Q. in *Coenzyme Q Molecular Mechanisms in Health and Disease* (ed. Kagan, V. E.; Guinn, P. J.) 43–61 (Taylor & Francis Group, 2001).
152. Forsmark-Andrée, P., Dallner, G. & Ernster, L. Endogenous ubiquinol prevents protein modification accompanying lipid peroxidation in beef heart submitochondrial particles. *Free Radic. Biol. Med.* **19**, 749–757 (1995).
153. Godic, A., Poljsak, B., Adamic, M. & Dahmane, R. The role of antioxidants in skin cancer prevention and treatment. *Oxid. Med. Cell. Longev.* **2014**, 860479 (2014).
154. Maroz, A., Anderson, R. F., Smith, R. A. J. & Murphy, M. P. Reactivity of ubiquinone and ubiquinol with superoxide and the hydroperoxyl radical: implications for in vivo antioxidant activity. *Free Radic. Biol. Med.* **46**, 105–109 (2009).
155. Bentinger, M., Brismar, K. & Dallner, G. The antioxidant role of coenzyme Q. *Mitochondrion* **7**, S41–S50 (2007).
156. Elmore, S. P., Qian, T., Grissom, S. F. & Lemasters, J. J. The mitochondrial permeability transition initiates autophagy in rat hepatocytes. *FASEB J.* **15**, 2286–7 (2001).
157. Walter, L., Miyoshi, H., Leverve, X., Bernardi, P. & Fontaine, E. Regulation of the mitochondrial permeability transition pore by ubiquinone analogs. A progress report. *Free Radic. Res.* **36**, 405–412 (2002).
158. Walter, L. *et al.* Three classes of ubiquinone analogs regulate the mitochondrial permeability transition pore through a common site. *J. Biol. Chem.* **275**, 29521–7 (2000).
159. Belliere, J. *et al.* Prerequisites for ubiquinone analogs to prevent mitochondrial permeability transition-induced cell death. *Journal of Bioenergetics and Biomembranes* vol. 44 207–212 (2012).
160. Fontaine, E., Ichas, F. & Bernardi, P. A Ubiquinone-binding Site Regulates the

Mitochondrial Permeability Transition Pore. *J. Biol. Chem.* **273**, 25734–25740 (1998).

161. Papucci, L. *et al.* Coenzyme q10 prevents apoptosis by inhibiting mitochondrial depolarization independently of its free radical scavenging property. *J. Biol. Chem.* **278**, 28220–8 (2003).
162. Busiello, R. A., Savarese, S. & Lombardi, A. Mitochondrial uncoupling proteins and energy metabolism. *Front. Physiol.* **6**, 36 (2015).
163. Chouchani, E. T., Kazak, L. & Spiegelman, B. M. New Advances in Adaptive Thermogenesis: UCP1 and Beyond. *Cell Metabolism* vol. 29 27–37 (2019).
164. Echtay, K. S., Winkler, E. & Klingenberg, M. Coenzyme Q is an obligatory cofactor for uncoupling protein function. *Nature* **408**, 609–13. (2000).
165. Acosta Lopez, M. J. *et al.* Vanillic Acid Restores Coenzyme Q Biosynthesis and ATP Production in Human Cells Lacking COQ6. *Oxid. Med. Cell. Longev.* **2019**, 1–11 (2019).
166. Ran, F. A. *et al.* Genome engineering using the CRISPR-Cas9 system. *Nat. Protoc.* **8**, 2281–308 (2013).
167. Chomyn, A. In vivo labeling and analysis of human mitochondrial translation products. *Methods Enzymol.* **264**, 197–211 (1996).
168. Fernández-Vizarra, E. *et al.* Isolation of mitochondria for biogenetical studies: An update. *Mitochondrion* **10**, 253–262 (2010).
169. Fernández-Silva, P., Acín-Pérez, R., Fernández-Vizarra, E., Pérez-Martos, A. & Enriquez, J. A. In Vivo and In Organello Analyses of Mitochondrial Translation. in *Methods in cell biology* vol. 80 571–588 (2007).
170. Sasarman, F. & Shoubridge, E. A. Radioactive Labeling of Mitochondrial Translation Products in Cultured Cells. in *Methods in Molecular Biology* vol. 837 207–217 (Methods Mol Biol, 2012).
171. Schindelin, J. *et al.* Fiji: an open-source platform for biological-image analysis. *Nat. Methods* **9**, 676–82 (2012).
172. Wittig, I., Braun, H. P. & Schägger, H. Blue native PAGE. *Nat. Protoc.* **1**, 418–428 (2006).
173. Schägger, H. Native electrophoresis for isolation of mitochondrial oxidative phosphorylation protein complexes. in *Methods in Enzymology* vol. 260 190–202 (Academic Press, 1995).
174. Nijtmans, L. G. J., Henderson, N. S. & Holt, I. J. Blue Native electrophoresis to study mitochondrial and other protein complexes. *Methods* **26**, 327–334 (2002).
175. Gilquin, B. *et al.* The AAA+ ATPase ATAD3A Controls Mitochondrial Dynamics at the Interface of the Inner and Outer Membranes. *Mol. Cell. Biol.* **30**, 1984–1996 (2010).
176. Reyes, A. *et al.* Actin and myosin contribute to mammalian mitochondrial DNA maintenance. *Nucleic Acids Res.* **39**, 5098–5108 (2011).
177. Rodríguez-Aguilera, J., Cortés, A., Fernández-Ayala, D. & Navas, P. Biochemical Assessment of Coenzyme Q10 Deficiency. *J. Clin. Med.* **6**, 27 (2017).
178. Bristow, T., Constantine, J., Harrison, M. & Cavoit, F. Performance optimisation of a new-generation orthogonal-acceleration quadrupole-time-of-flight mass spectrometer. *Rapid Commun. Mass Spectrom.* **22**, 1213–1222 (2008).
179. Robinet, P., Wang, Z., Hazen, S. L. & Smith, J. D. A simple and sensitive enzymatic method for cholesterol quantification in macrophages and foam cells. *J. Lipid Res.* **51**, 3364–3369 (2010).
180. Bugiani, M. *et al.* Clinical and molecular findings in children with complex I deficiency. *Biochim. Biophys. Acta - Bioenerg.* **1659**, 136–147 (2004).

181. García-Corzo, L. *et al.* Ubiquinol-10 ameliorates mitochondrial encephalopathy associated with CoQ deficiency. *Biochim. Biophys. Acta* **1842**, 893–901 (2014).

182. Ong, S.-E. *et al.* Stable isotope labeling by amino acids in cell culture, SILAC, as a simple and accurate approach to expression proteomics. *Mol. Cell. Proteomics* **1**, 376–86 (2002).

183. Ong, S.-E. & Mann, M. A practical recipe for stable isotope labeling by amino acids in cell culture (SILAC). *Nat. Protoc.* **1**, 2650–2660 (2006).

184. Ong, S.-E. & Mann, M. Stable Isotope Labeling by Amino Acids in Cell Culture for Quantitative Proteomics. in 37–52 (Humana Press, 2007). doi:10.1007/978-1-59745-255-7_3.

185. Meyer, T. S. & Lamberts, B. L. Use of coomassie brilliant blue R250 for the electrophoresis of microgram quantities of parotid saliva proteins on acrylamide-gel strips. *Biochim. Biophys. Acta - Gen. Subj.* **107**, 144–145 (1965).

186. Andrews, B., Carroll, J., Ding, S., Fearnley, I. M. & Walker, J. E. Assembly factors for the membrane arm of human complex I. *Proc. Natl. Acad. Sci.* **110**, 18934–18939 (2013).

187. Cox, J. & Mann, M. MaxQuant enables high peptide identification rates, individualized p.p.b.-range mass accuracies and proteome-wide protein quantification. *Nat. Biotechnol.* **26**, 1367–1372 (2008).

188. Tyanova, S. *et al.* The Perseus computational platform for comprehensive analysis of (prote)omics data. *Nature Methods* vol. 13 731–740 (2016).

189. Benjamini, Y. & Hochberg, Y. Controlling the False Discovery Rate: A Practical and Powerful Approach to Multiple Testing. *J. R. Stat. Soc. Ser. B* **57**, 289–300 (1995).

190. Oliveros, J. C. Venny. An interactive tool for comparing lists with Venn's diagrams. https://bioinfogp.cnb.csic.es/tools/venny/index.html. (2015).

191. Mi, H., Muruganujan, A., Ebert, D., Huang, X. & Thomas, P. D. PANTHER version 14: More genomes, a new PANTHER GO-slim and improvements in enrichment analysis tools. *Nucleic Acids Res.* **47**, D419–D426 (2019).

192. Carbon, S. *et al.* The Gene Ontology Resource: 20 years and still GOing strong. *Nucleic Acids Res.* **47**, D330–D338 (2019).

193. Ashburner, M. *et al.* Gene ontology: Tool for the unification of biology. *Nature Genetics* vol. 25 25–29 (2000).

194. Pfaffl, M. W. A new mathematical model for relative quantification in real-time RT-PCR. *Nucleic Acids Res.* **29**, e45 (2001).

195. Forzan, M. *et al.* Is CFTR 621+3 A>G a cystic fibrosis causing mutation? *J. Hum. Genet.* **55**, 23–26 (2010).

196. Thorvaldsdottir, H., Robinson, J. T. & Mesirov, J. P. Integrative Genomics Viewer (IGV): high-performance genomics data visualization and exploration. *Brief. Bioinform.* **14**, 178–192 (2013).

197. Rozen, S. & Skaletsky, H. Primer3 on the WWW for general users and for biologist programmers. *Methods Mol. Biol.* **132**, 365–386 (2000).

198. Koressaar, T. & Remm, M. Enhancements and modifications of primer design program Primer3. **23**, 1289–1291 (2007).

199. Novoradovsky, A. *et al.* Computational Principles of Primer Design for Site Directed Mutagenesis – TechConnect Briefs. *Technical Proceedings of 2005 NSTI Nanotechnology Conference and Trade Show* 532–535 https://briefs.techconnect.org/papers/computational-principles-of-primer-design-for-site-directed-mutagenesis/ (2005).

200. Pruitt, K. D., Tatusova, T. & Maglott, D. R. NCBI reference sequences (RefSeq): A curated non-redundant sequence database of genomes, transcripts and proteins. *Nucleic Acids Res.* **35**, D61–D65 (2007).

201. Bateman, A. *et al.* UniProt: The universal protein knowledgebase. *Nucleic Acids Res.* **45**, D158–D169 (2017).

202. Hall, T. BioEdit: a user-friendly biological sequence alignment editor and analysis program. *Nucl. Acids. Symp. Ser.* **41**, 95–98 (1999).

203. Larkin, M. A. *et al.* Clustal W and Clustal X version 2.0. *Bioinformatics* **23**, 2947–2948 (2007).

204. Pedersen, A. G. & Nielsen, H. Neural network prediction of translation initiation sites in eukaryotes: perspectives for EST and genome analysis. *Proc. Int. Conf. Intell. Syst. Mol. Biol.* **5**, 226–233 (1997).

205. Salamov, A. A., Nishikawa, T. & Swindells, M. B. Assessing protein coding region integrity in cDNA sequencing projects. *Bioinformatics* **14**, 384–390 (1998).

206. Gruber, A. R., Lorenz, R., Bernhart, S. H., Neuböck, R. & Hofacker, I. L. The Vienna RNA websuite. *Nucleic Acids Res.* **36**, W70–W74 (2008).

207. Drozdetskiy, A., Cole, C., Procter, J. & Barton, G. J. JPred4: A protein secondary structure prediction server. *Nucleic Acids Res.* **43**, W389–W394 (2015).

208. Smith, A. C. & Robinson, A. J. Mitominer v4.0: An updated database of mitochondrial localization evidence, phenotypes and diseases. *Nucleic Acids Res.* **47**, D1225–D1228 (2019).

209. Fukasawa, Y. *et al.* MitoFates: Improved prediction of mitochondrial targeting sequences and their cleavage sites. *Mol. Cell. Proteomics* **14**, 1113–1126 (2015).

210. Xue, Y. *et al.* GPS: a comprehensive www server for phosphorylation sites prediction. *Nucleic Acids Res.* **33**, W184–W187 (2005).

211. Gnad, F., Gunawardena, J. & Mann, M. PHOSIDA 2011: The posttranslational modification database. *Nucleic Acids Res.* **39**, 253–260 (2011).

212. Iakoucheva, L. M. *et al.* The importance of intrinsic disorder for protein phosphorylation. *Nucleic Acids Res.* **32**, 1037–1049 (2004).

213. Blom, N., Gammeltoft, S. & Brunak, S. Sequence and structure-based prediction of eukaryotic protein phosphorylation sites. *J. Mol. Biol.* **294**, 1351–1362 (1999).

214. Blom, N., Sicheritz-Pontén, T., Gupta, R., Gammeltoft, S. & Brunak, S. Prediction of post-translational glycosylation and phosphorylation of proteins from the amino acid sequence. *Proteomics* **4**, 1633–1649 (2004).

215. Wong, Y.-H. *et al.* KinasePhos 2.0: a web server for identifying protein kinase-specific phosphorylation sites based on sequences and coupling patterns. *Nucleic Acids Res.* **35**, W588–W594 (2007).

216. Hornbeck, P. V. *et al.* PhosphoSitePlus, 2014: Mutations, PTMs and recalibrations. *Nucleic Acids Res.* **43**, D512–D520 (2015).

217. Sim, N. L. *et al.* SIFT web server: Predicting effects of amino acid substitutions on proteins. *Nucleic Acids Res.* **40**, 452–457 (2012).

218. Adzhubei, I., Jordan, D. M. & Sunyaev, S. R. Predicting functional effect of human missense mutations using PolyPhen-2. *Curr. Protoc. Hum. Genet.* **0 7**, Unit7.20 (2013).

219. Leman, R. *et al.* Novel diagnostic tool for prediction of variant spliceogenicity derived from a set of 395 combined in silico/in vitro studies: An international collaborative effort. *Nucleic Acids Res.* **46**, 7913–7923 (2018).

220. Rentzsch, P., Witten, D., Cooper, G. M., Shendure, J. & Kircher, M. CADD: Predicting the deleteriousness of variants throughout the human genome. *Nucleic Acids Res.* **47**, D886–D894 (2019).

221. Schwede, T., Kopp, J., Guex, N. & Peitsch, M. C. SWISS-MODEL: An automated protein homology-modeling server. *Nucleic Acids Res.* **31**, 3381–3385 (2003).

222. Pettersen, E. F. *et al.* UCSF Chimera - A visualization system for exploratory research and analysis. *J. Comput. Chem.* **25**, 1605–1612 (2004).

223. Pei, J. & Grishin, N. V. AL2CO: Calculation of positional conservation in a protein sequence alignment. *Bioinformatics* **17**, 700–712 (2001).

224. Lohman, D. C. *et al.* An Isoprene Lipid-Binding Protein Promotes Eukaryotic Coenzyme Q Biosynthesis. *Mol. Cell* **0**, 1–12 (2019).

225. Quinzii, C. M. & Hirano, M. Primary and secondary CoQ10 deficiencies in humans. *BioFactors* **37**, 361–365 (2011).

226. Hughes, B. G., Harrison, P. M. & Hekimi, S. Estimating the occurrence of primary ubiquinone deficiency by analysis of large-scale sequencing data. *Sci. Rep.* **7**, 17744 (2017).

227. Horvath, R. *et al.* Adult-onset cerebellar ataxia due to mutations in CABC1/ADCK3. *J. Neurol. Neurosurg. Psychiatry* **83**, 174–178 (2012).

228. Barca, E. *et al.* Cerebellar ataxia and severe muscle CoQ 10 deficiency in a patient with a novel mutation in ADCK3. *Clin. Genet.* **90**, 156–160 (2016).

229. Atmaca, M. *et al.* Follow-up results of patients with ADCK4 mutations and the efficacy of CoQ10 treatment. *Pediatr. Nephrol.* **32**, 1369–1375 (2017).

230. Quinzii, C. M., Emmanuele, V. & Hirano, M. Clinical Presentations of Coenzyme Q 10 Deficiency Syndrome. *Mol Syndr.* **5**, 141–146 (2014).

231. Cao, Q. *et al.* [Coenzyme Q(10) treatment for one child with COQ6 gene mutation induced nephrotic syndrome and literature review]. *Zhonghua er ke za zhi = Chinese J. Pediatr.* **55**, 135–138 (2017).

232. Gigante, M. *et al.* Further phenotypic heterogeneity of CoQ10 deficiency associated with steroid resistant nephrotic syndrome and novel COQ2 and COQ6 variants. *Clin. Genet.* **92**, 224–226 (2017).

233. Heeringa, S. F. *et al.* COQ6 mutations in human patients produce nephrotic syndrome with sensorineural deafness. *J. Clin. Invest.* **121**, 2013–2024 (2011).

234. Koyun, M., Çomak, E. & Akman, S. CoenzymeQ10 therapy in two sisters with CoQ6 mutations with long-term follow-up. *Pediatr. Nephrol.* 1–2 (2018) doi:10.1007/s00467-018-4150-9.

235. Park, E. *et al.* COQ6 Mutations in Children With Steroid-Resistant Focal Segmental Glomerulosclerosis and Sensorineural Hearing Loss. *Am. J. Kidney Dis.* **70**, 139–144 (2017).

236. Yuruk Yildirim, Z. *et al.* Primary coenzyme Q10 Deficiency-6 (COQ10D6): Two siblings with variable expressivity of the renal phenotype. *Eur. J. Med. Genet.* (2019) doi:10.1016/j.ejmg.2019.01.011.

237. Park, E. *et al.* Genetic Study in Korean Pediatric Patients with Steroid-Resistant Nephrotic Syndrome or Focal Segmental Glomerulosclerosis. *J. Clin. Med.* **9**, 2013 (2020).

238. Wang, Y. *et al.* Pathogenicity of two COQ7 mutations and responses to 2,4-dihydroxybenzoate bypass treatment. *J. Cell. Mol. Med.* **21**, 2329–2343 (2017).

239. Freyer, C. *et al.* Rescue of primary ubiquinone deficiency due to a novel COQ7 defect

using 2,4-dihydroxybensoic acid. *J. Med. Genet.* **52**, 779–83 (2015).

240. Kwong, A. K.-Y. *et al.* A fatal case of COQ7 -associated primary coenzyme Q 10 deficiency. *JIMD Rep.* **47**, 23–29 (2019).
241. Mollet, J. *et al.* Prenyldiphosphate synthase, subunit 1 (PDSS1) and OH-benzoate polyprenyltransferase (COQ2) mutations in ubiquinone deficiency and oxidative phosphorylation disorders. *J. Clin. Invest.* **117**, 765–72 (2007).
242. Diomedi-Camassei, F. *et al.* COQ2 nephropathy: a newly described inherited mitochondriopathy with primary renal involvement. *J. Am. Soc. Nephrol.* **18**, 2773–80 (2007).
243. Zhang, H. *et al.* Steroid-resistant nephrotic syndrome caused by co-inheritance of mutations at NPHS1 and ADCK4 genes in two Chinese siblings. *Intractable Rare Dis. Res.* **6**, 299–303 (2017).
244. Bezdíčka, M. *et al.* Genetic diagnosis of steroid-resistant nephrotic syndrome in a longitudinal collection of Czech and Slovak patients: a high proportion of causative variants in NUP93. (2018) doi:10.1007/s00467-018-3950-2.
245. Sadowski, C. E. *et al.* A Single-Gene Cause in 29.5% of Cases of Steroid-Resistant Nephrotic Syndrome. *J. Am. Soc. Nephrol.* **26**, 1279–1289 (2015).
246. Smith, A. C. *et al.* A family segregating lethal neonatal coenzyme Q 10 deficiency caused by mutations in COQ9. (2018).
247. Olgac, A. *et al.* A rare case of primary coenzyme Q10 deficiency due to COQ9 mutation. *J. Pediatr. Endocrinol. Metab.* **33**, 165–170 (2020).
248. Duncan, A. J. *et al.* A nonsense mutation in COQ9 causes autosomal-recessive neonatal-onset primary coenzyme Q10 deficiency: a potentially treatable form of mitochondrial disease. *Am. J. Hum. Genet.* **84**, 558–66 (2009).
249. Dinwiddie, D. L. *et al.* Diagnosis of mitochondrial disorders by concomitant next-generation sequencing of the exome and mitochondrial genome. *Genomics* **102**, 148–156 (2013).
250. Yu, M. H. *et al.* Primary coenzyme Q10 deficiency-7: expanded phenotypic spectrum and a founder mutation in southern Chinese. *npj Genomic Med.* **4**, 18 (2019).
251. Brea-Calvo, G. *et al.* COQ4 Mutations Cause a Broad Spectrum of Mitochondrial Disorders Associated with CoQ10 Deficiency. *Am. J. Hum. Genet.* **96**, 309–317 (2015).
252. Chung, W. K. *et al.* Mutations in COQ4, an essential component of coenzyme Q biosynthesis, cause lethal neonatal mitochondrial encephalomyopathy. *J. Med. Genet.* **52**, 627–635 (2015).
253. Sacconi, S. *et al.* Coenzyme Q10 is frequently reduced in muscle of patients with mitochondrial myopathy. *Neuromuscul. Disord.* **20**, 44–48 (2010).
254. Trevisson, E., DiMauro, S., Navas, P. & Salviati, L. Coenzyme Q deficiency in muscle. *Curr. Opin. Neurol.* **24**, 449–456 (2011).
255. Salviati, L., Trevisson, E., Doimo, M. & Navas, P. *Primary Coenzyme Q10 Deficiency*. *GeneReviews®* (University of Washington, Seattle; 1993-2018, 2017).
256. Danhauser, K. *et al.* Fatal neonatal encephalopathy and lactic acidosis caused by a homozygous loss-of-function variant in COQ9. *Eur. J. Hum. Genet.* **24**, 450–454 (2016).
257. Eroglu, F. K. *et al.* Response to Early Coenzyme Q10 Supplementation Is not Sustained in CoQ10 Deficiency Caused by CoQ2 Mutation. *Pediatr. Neurol.* **88**, 71–74 (2018).
258. Li, G.-M. *et al.* Gene mutation analysis in 12 Chinese children with congenital nephrotic syndrome. (2018) doi:10.1186/s12882-018-1184-y.

259. Mancuso, M., McFarland, R., Klopstock, T., Hirano, M. & consortium on Trial Readiness in Mitochondrial Myopathies. International Workshop:: Outcome measures and clinical trial readiness in primary mitochondrial myopathies in children and adults. Consensus recommendations. 16-18 November 2016, Rome, Italy. *Neuromuscul. Disord.* **27**, 1126–1137 (2017).

260. Yubero, D.; Montero, R.; Amstrong, J.; Espinos, C.; Palau, F.; Santos-Ocaña, C.; Salviati, L.; Navas, P.; Artuch, R. Molecular diagnosis of coenzyme Q10 deficiency. *Expert Rev. Mol. Diagn.* **15**, 1049–1059 (2015).

261. Yubero, D., Allen, G., Artuch, R. & Montero, R. The Value of Coenzyme Q10 Determination in Mitochondrial Patients. *J. Clin. Med.* **6**, 37 (2017).

262. Starr, M. C. *et al.* COQ2 nephropathy: a treatable cause of nephrotic syndrome in children. *Pediatr. Nephrol.* **33**, 1257–1261 (2018).

263. Yubero, D. *et al.* Determination of urinary coenzyme Q 10 by HPLC with electrochemical detection: Reference values for a paediatric population. *BioFactors* **41**, 424–430 (2015).

264. Artuch, R. *et al.* Cerebellar ataxia with coenzyme Q10 deficiency: diagnosis and follow-up after coenzyme Q10 supplementation. *J. Neurol. Sci.* **246**, 153–8 (2006).

265. Quinzii, C. M. *et al.* Reactive oxygen species, oxidative stress, and cell death correlate with level of CoQ 10 deficiency. *FASEB J.* **24**, 3733–3743 (2010).

266. López-Martín, J. M. *et al.* Missense mutation of the COQ2 gene causes defects of bioenergetics and de novo pyrimidine synthesis. *Hum. Mol. Genet.* **16**, 1091–1097 (2007).

267. Jackson, M. R., Melideo, S. L. & Jorns, M. S. Human Sulfide:Quinone Oxidoreductase Catalyzes the First Step in Hydrogen Sulfide Metabolism and Produces a Sulfane Sulfur Metabolite. *Biochemistry* **51**, 6804–6815 (2012).

268. González-García, P. *et al.* Coenzyme Q10 modulates sulfide metabolism and links the mitochondrial respiratory chain to pathways associated to one carbon metabolism. *Hum. Mol. Genet.* **29**, 3296–3311 (2020).

269. Quinzii, C. M. & Lopez, L. C. Abnormalities of hydrogen sulfide and glutathione pathways in mitochondrial dysfunction. *J. Adv. Res.* **27**, 79–84 (2020).

270. Rodríguez-Hernández, Á. *et al.* Coenzyme Q deficiency triggers mitochondria degradation by mitophagy. *Autophagy* **5**, 19–32 (2009).

271. Peng, M. *et al.* Inhibiting cytosolic translation and autophagy improves health in mitochondrial disease. *Hum. Mol. Genet.* **24**, 4829–4847 (2015).

272. Fazakerley, D. J. *et al.* Mitochondrial CoQ deficiency is a common driver of mitochondrial oxidants and insulin resistance. *Elife* **7**, e32111 (2018).

273. Mignot, C. *et al.* Phenotypic variability in ARCA2 and identification of a core ataxic phenotype with slow progression. *Orphanet J. Rare Dis.* **8**, 173 (2013).

274. Galosi, S. *et al.* Dystonia-Ataxia with early handwriting deterioration in COQ8A mutation carriers: A case series and literature review. *Parkinsonism Relat. Disord.* **68**, 8–16 (2019).

275. Traschütz, A. *et al.* Clinico-Genetic, Imaging and Molecular Delineation of COQ8A-Ataxia: A Multicenter Study of 59 Patients. *Ann. Neurol.* **88**, 251–263 (2020).

276. Vazquez Fonseca, L. *et al.* Mutations in COQ8B (ADCK4) found in patients with steroid-resistant nephrotic syndrome alter COQ8B function. *Hum. Mutat.* **39**, 406–414 (2017).

277. Desbats, M. A. *et al.* The COQ2 genotype predicts the severity of Coenzyme Q10 deficiency. *Hum. Mol. Genet.* **25**, 4256–4265 (2016).

278. Luna-Sánchez, M. *et al.* The clinical heterogeneity of coenzyme Q10 deficiency results from genotypic differences in the Coq9 gene. *EMBO Mol. Med.* **7**, 670–87 (2015).

279. Garcia-Corzo, L. *et al.* Dysfunctional Coq9 protein causes predominant encephalomyopathy associated with CoQ deficiency. *Hum. Mol. Genet.* **22**, 1233–1248 (2013).

280. Bhagavan, H. N. & Chopra, R. K. Coenzyme Q10: Absorption, tissue uptake, metabolism and pharmacokinetics. *Free Radic. Res.* **40**, 445–453 (2006).

281. Zaki, N. M. Strategies for oral delivery and mitochondrial targeting of CoQ10. *Drug Deliv.* **23**, 1868–1881 (2016).

282. Stocker, R., Bowry, V. W. & Frei, B. Ubiquinol-10 protects human low density lipoprotein more efficiently against lipid peroxidation than does alpha-tocopherol. *Proc. Natl. Acad. Sci.* **88**, 1646–1650 (1991).

283. Mohr, D., Bowry, V. W. & Stocker, R. Dietary supplementation With coenzyme Q 10 results in increased levels of ubiquinol-10 within circulating lipoproteins and increased resistance of human low density lipoprotein to the initiation of lipid peroxidation. *Biochim. Biophys. Acta* **1126**, 247–254 (1992).

284. Potgieter, M., Pretorius, E. & Pepper, M. S. Primary and secondary coenzyme Q10 deficiency: The role of therapeutic supplementation. *Nutr. Rev.* **71**, 180–188 (2013).

285. Rötig, A. *et al.* Quinone-responsive multiple respiratory-chain dysfunction due to widespread coenzyme Q10deficiency. *Lancet* **356**, 391–395 (2000).

286. Montini, G., Malaventura, C. & Salviati, L. Early coenzyme Q10 supplementation in primary coenzyme Q10 deficiency. *N. Engl. J. Med.* **358**, 2849–50 (2008).

287. Saiki, R. *et al.* Coenzyme Q_{10} supplementation rescues renal disease in *Pdss2* $^{kd/kd}$ mice with mutations in prenyl diphosphate synthase subunit 2. *Am. J. Physiol. Physiol.* **295**, F1535–F1544 (2008).

288. Hathcock, J. N. & Shao, A. Risk assessment for coenzyme Q10 (Ubiquinone). *Regul. Toxicol. Pharmacol.* **45**, 282–288 (2006).

289. Pierrel, F. Impact of Chemical Analogs of 4-Hydroxybenzoic Acid on Coenzyme Q Biosynthesis: From Inhibition to Bypass of Coenzyme Q Deficiency. *Front. Physiol.* **8**, 4363389–436 (2017).

290. Desbats, M. A., Lunardi, G., Doimo, M., Trevisson, E. & Salviati, L. Genetic bases and clinical manifestations of Coenzyme Q10 (CoQ10) deficiency. *J. Inherit. Metab. Dis.* **38**, 145–156 (2015).

291. Yubero, D. *et al.* Secondary coenzyme Q 10 deficiencies in oxidative phosphorylation (OXPHOS) and non-OXPHOS disorders. *Mitochondrion* **30**, 51–58 (2016).

292. Gonzalez-Mariscal, I. *et al.* Regulation of coenzyme Q biosynthesis in yeast: a new complex in the block. *IUBMB Life* **66**, 63–70 (2014).

293. Montero, R. *et al.* Coenzyme Q10 deficiency in mitochondrial DNA depletion syndromes. *Mitochondrion* **13**, 337–341 (2013).

294. Kühl, I. *et al.* Transcriptomic and proteomic landscape of mitochondrial dysfunction reveals secondary coenzyme Q deficiency in mammals. *Elife* **6**, (2017).

295. Fernandez-Vizarra, E. *et al.* Impaired complex III assembly associated with BCS1L gene mutations in isolated mitochondrial encephalopathy. *Hum. Mol. Genet.* **16**, 1241–1252 (2007).

296. Bris, C. *et al.* Novel NDUFS4 gene mutation in an atypical late-onset mitochondrial form of multifocal dystonia . *Neurol. Genet.* **3**, e205 (2017).

297. Ortigoza-Escobar, J. D. *et al.* Ndufs4 related Leigh syndrome: A case report and review of the literature. *Mitochondrion* **28**, 73–78 (2016).

298. Talim, B. *et al.* Multisystem fatal infantile disease caused by a novel homozygous EARS2 mutation. *Brain* **136**, e228–e228 (2013).

299. Taskin, B. D. *et al.* Early-Onset Mild Type Leukoencephalopathy Caused by a Homozygous EARS2 Mutation. *J. Child Neurol.* **31**, 938–941 (2016).

300. Cotán, D. *et al.* Secondary coenzyme Q $_{10}$ deficiency triggers mitochondria degradation by mitophagy in MELAS fibroblasts. *FASEB J.* **25**, 2669–2687 (2011).

301. Buján, N. *et al.* Characterization of CoQ10 biosynthesis in fibroblasts of patients with primary and secondary CoQ10 deficiency. *J. Inherit. Metab. Dis.* **37**, 53–62 (2014).

302. Gempel, K. *et al.* The myopathic form of coenzyme Q10 deficiency is caused by mutations in the electron-transferring-flavoprotein dehydrogenase (ETFDH) gene. *Brain* **130**, 2037–2044 (2007).

303. Liang, W.-C. *et al.* ETFDH mutations, CoQ10 levels, and respiratory chain activities in patients with riboflavin-responsive multiple acyl-CoA dehydrogenase deficiency. *Neuromuscul. Disord.* **19**, 212–216 (2009).

304. Wen, B. *et al.* Increased muscle coenzyme Q10 in riboflavin responsive MADD with ETFDH gene mutations due to secondary mitochondrial proliferation. *Mol. Genet. Metab.* **109**, 154–160 (2013).

305. Date, H. *et al.* Early-onset ataxia with ocular motor apraxia and hypoalbuminemia is caused by mutations in a new HIT superfamily gene. *Nat. Genet.* **29**, 184–188 (2001).

306. Moreira, M.-C. *et al.* The gene mutated in ataxia-ocular apraxia 1 encodes the new HIT/Zn-finger protein aprataxin. *Nat. Genet.* **29**, 189–193 (2001).

307. Quinzii, C. M. *et al.* Coenzyme Q deficiency and cerebellar ataxia associated with an aprataxin mutation. *Neurology* **64**, 539–41 (2005).

308. Balreira, A. *et al.* ANO10 mutations cause ataxia and coenzyme Q(1)(0) deficiency. *J Neurol* **261**, 2192–2198 (2014).

309. Chamard, L., Sylvestre, G., Koenig, M. & Magnin, E. Executive and Attentional Disorders, Epilepsy and Porencephalic Cyst in Autosomal Recessive Cerebellar Ataxia Type 3 Due to ANO10 Mutation. *Eur. Neurol.* **75**, 186–190 (2016).

310. Nanetti, L. *et al.* ANO10 mutational screening in recessive ataxia: genetic findings and refinement of the clinical phenotype. *J. Neurol.* **266**, 378–385 (2019).

311. Yubero, D. *et al.* Association between coenzyme Q10and glucose transporter (GLUT1) deficiency. *BMC Pediatr.* **14**, 1–5 (2014).

312. Barca, E. *et al.* CoQ10 Deficiency Is Not a Common Finding in GLUT1 Deficiency Syndrome. in *JIMD Reports* vol. 29 47–52 (Springer, 2015).

313. Turunen, M., Olsson, J. & Dallner, G. Metabolism and function of Coenzyme Q. *Biochim. Biophys. Acta - Biomembr.* **1660**, 171–99 (2004).

314. Suárez-Rivero, J. M. *et al.* Intracellular cholesterol accumulation and coenzyme Q10 deficiency in Familial Hypercholesterolemia. *Biochim. Biophys. Acta - Mol. Basis Dis.* **1864**, 3697–3713 (2018).

315. Yen, H.-C., Yeh, W.-Y., Lee, S.-H., Feng, Y.-H. & Yang, S.-L. Characterization of human mitochondrial PDSS and COQ proteins and their roles in maintaining coenzyme Q10 levels and each other's stability. *Biochim. Biophys. Acta - Bioenerg.* **1861**, 148192 (2020).

316. Wang, Y. & Hekimi, S. The Complexity of Making Ubiquinone. *Trends Endocrinol. Metab.* **30**, 929–943 (2019).

317. Spinazzi, M. & De Strooper, B. PARL: The mitochondrial rhomboid protease. *Semin. Cell Dev. Biol.* **60**, 19–28 (2016).

318. Bottani, E. *et al.* TTC19 Plays a Husbandry Role on UQCRFS1 Turnover in the Biogenesis of Mitochondrial Respiratory Complex III. *Mol. Cell* **67**, 96-105.e4 (2017).

319. Spinazzi, M. *et al.* PARL deficiency in mouse causes Complex III defects, coenzyme Q depletion, and Leigh-like syndrome. *Proc. Natl. Acad. Sci. U. S. A.* **116**, 277–286 (2019).

320. Mourier, A. *et al.* Mitofusin 2 is required to maintain mitochondrial coenzyme Q levels. *J. Cell Biol.* **208**, 429–442 (2015).

321. Alcázar-Fabra, M., Rodríguez-Sánchez, F., Trevisson, E. & Brea-Calvo, G. Genotype-phenotype correlations in primary coenzyme Q deficiencies. *Free Radic Biol Med* **Under revi**, (2021).

322. Vasta, V., Merritt II, J. L., Saneto, R. P. & Hahn, S. H. Next-generation sequencing for mitochondrial diseases: a wide diagnostic spectrum. *Pediatr. Int.* **54**, 585–601 (2012).

323. Iványi, B. *et al.* Diffuse mesangial sclerosis in a PDSS2 mutation-induced coenzyme Q10 deficiency. *Pediatr. Nephrol.* **33**, 439–446 (2018).

324. López, L. C. *et al.* Leigh syndrome with nephropathy and CoQ10 deficiency due to decaprenyl diphosphate synthase subunit 2 (PDSS2) mutations. *Am. J. Hum. Genet.* **79**, 1125–9 (2006).

325. Rahman, S., Clarke, C. F. & Hirano, M. 176th ENMC International Workshop: Diagnosis and treatment of coenzyme Q10 deficiency. *Neuromuscul. Disord.* **22**, 76–86 (2012).

326. Malicdan, M. C. V. *et al.* A novel inborn error of the coenzyme Q10 biosynthesis pathway: cerebellar ataxia and static encephalomyopathy due to COQ5 C-methyltransferase deficiency. *Hum. Mutat.* **39**, 69–79 (2018).

327. Rahman, S., Hargreaves, I., Clayton, P. & Heales, S. Neonatal presentation of coenzyme Q10 deficiency. *J. Pediatr.* **139**, 456–8 (2001).

328. Desbats, M. A. *et al.* Primary coenzyme Q 10 deficiency presenting as fatal neonatal multiorgan failure. *Eur. J. Hum. Genet.* **23**, 1254–1258 (2015).

329. McCarthy, H. J. *et al.* Simultaneous sequencing of 24 genes associated with steroid-resistant nephrotic syndrome. *Clin. J. Am. Soc. Nephrol.* **8**, 637–648 (2013).

330. Wu, X., Wang, W., Liu, Y., Chen, W. & Zhao, L. A steroid-resistant nephrotic syndrome in an infant resulting from a consanguineous marriage with COQ2 and ARSB gene mutations: A case report. *BMC Med. Genet.* **20**, (2019).

331. Quinzii, C. *et al.* A mutation in para-hydroxybenzoate-polyprenyl transferase (COQ2) causes primary coenzyme Q10 deficiency. *Am. J. Hum. Genet.* **78**, 345–9 (2006).

332. Jakobs, B. S. *et al.* A novel mutation in COQ2 leading to fatal infantile multisystem disease. *J. Neurol. Sci.* **326**, 24–8 (2013).

333. Scalais, E. *et al.* Early myoclonic epilepsy, hypertrophic cardiomyopathy and subsequently a nephrotic syndrome in a patient with CoQ10 deficiency caused by mutations in para-hydroxybenzoate-polyprenyl transferase (COQ2). *Eur. J. Paediatr. Neurol.* **17**, 625–630 (2013).

334. Xu, K., Mao, X. Y., Yao, Y., Cheng, H. & Zhang, X. J. [Clinical analysis of one infantile nephrotic syndrome caused by COQ2 gene mutation and literature review]. *Zhonghua er ke za zhi = Chinese J. Pediatr.* **56**, 662–666 (2018).

335. Caglayan, A. O. *et al.* COQ4 Mutation Leads to Childhood-Onset Ataxia Improved by CoQ10 Administration. *The Cerebellum* **18**, 665–669 (2019).

336. Sondheimer, N. *et al.* Novel recessive mutations in COQ4 cause severe infantile cardiomyopathy and encephalopathy associated with CoQ 10 deficiency. *Mol. Genet. Metab. Reports* **12**, 23–27 (2017).

337. Helbig, K. L. *et al.* Diagnostic exome sequencing provides a molecular diagnosis for a significant proportion of patients with epilepsy. *Genet. Med.* **18**, 898–905 (2016).

338. Bosch, A. M. *et al.* Coenzyme Q10 deficiency due to a COQ4 gene defect causes childhood-onset spinocerebellar ataxia and stroke-like episodes. *Mol. Genet. Metab. Reports* **17**, 19–21 (2018).

339. Lu, M. *et al.* Clinical phenotype, in silico and biomedical analyses, and intervention for an East Asian population-specific c.370G>A (p.G124S) COQ4 mutation in a Chinese family with CoQ10 deficiency-associated Leigh syndrome. *J. Hum. Genet.* 1 (2019) doi:10.1038/s10038-019-0563-y.

340. Ling, T. *et al.* Clinical whole-exome sequencing reveals a common pathogenic variant in patients with CoQ10 deficiency: An underdiagnosed cause of mitochondriopathy. *Clin. Chim. Acta* **497**, 88–94 (2019).

341. Salviati, L. *et al.* Haploinsufficiency of COQ4 causes coenzyme Q10 deficiency. *J. Med. Genet.* **49**, 187–91 (2012).

342. Doimo, M. *et al.* Effect of vanillic acid on COQ6 mutants identified in patients with coenzyme Q10deficiency. *Biochim. Biophys. Acta - Mol. Basis Dis.* **1842**, 1–6 (2014).

343. Stańczyk, M., Bałasz-Chmielewska, I., Lipska-Ziętkiewicz, B. & Tkaczyk, M. CoQ10-related sustained remission of proteinuria in a child with COQ6 glomerulopathy-a case report. *Pediatr. Nephrol.* **33**, 2383–2387 (2018).

344. Gerards, M. *et al.* Nonsense mutations in CABC1/ADCK3 cause progressive cerebellar ataxia and atrophy. *Mitochondrion* **10**, 510–515 (2010).

345. Terracciano, A. *et al.* The use of muscle biopsy in the diagnosis of undefined ataxia with cerebellar atrophy in children. *Eur. J. Paediatr. Neurol.* **16**, 248–256 (2012).

346. Blumkin, L. *et al.* Heterozygous Mutations in the ADCK3 Gene in Siblings with Cerebellar Atrophy and Extreme Phenotypic Variability. *JIMD Rep.* **12**, 103–7 (2014).

347. Liu, Y. T. *et al.* Autosomal-recessive cerebellar ataxia caused by a novel ADCK3 mutation that elongates the protein:Clinical, genetic and biochemical characterisation. *J. Neurol. Neurosurg. Psychiatry* **85**, 493–498 (2014).

348. Malgireddy, K., Thompson, R. & Torres-Russotto, D. A novel CABC1/ADCK3 mutation in adult-onset cerebellar ataxia. *Park. Relat. Disord.* **33**, 151–152 (2016).

349. Hajjari, M. *et al.* Exome sequencing found a novel homozygous deletion in ADCK3 gene involved in autosomal recessive spinocerebellar ataxia. *Gene* (2019) doi:10.1016/J.GENE.2019.05.016.

350. Sun, M. *et al.* Targeted exome analysis identifies the genetic basis of disease in over 50% of patients with a wide range of ataxia-related phenotypes. *Genet. Med.* **21**, 195–206 (2019).

351. Schirinzi, T. *et al.* One-year outcome of coenzyme Q10 supplementation in ADCK3 ataxia (ARCA2). *Cerebellum & Ataxias* **6**, 15 (2019).

352. Chang, A. *et al.* ADCK3-related Coenzyme Q10 Deficiency: A Potentially Treatable Genetic Disease. *Mov. Disord. Clin. Pract.* **5**, 635–639 (2018).

353. Kaya Ozcora, G. D., Basak, N., Canpolat, M., Acer, H. & Kumandas, S. Coenzyme Q10 deficiency; A treatable autosomal recessive cerebellar ataxias. *Eur. J. Paediatr. Neurol.* **21**, e136 (2017).

354. Shalata, A. *et al.* Primary Coenzyme Q deficiency Due to Novel ADCK3 Variants, Studies in Fibroblasts and Review of Literature. *Neurochem. Res.* 1–13 (2019) doi:10.1007/s11064-019-02786-5.

355. Mutlu-Albayrak, H., Kırat, E. & Gürbüz, G. Childhood-onset autosomal recessive ataxias: a cross-sectional study from Turkey. *Neurogenetics* (2019) doi:10.1007/s10048-019-00597-y.

356. Lagier-Tourenne, C. *et al.* ADCK3, an ancestral kinase, is mutated in a form of recessive ataxia associated with coenzyme Q10 deficiency. *Am. J. Hum. Genet.* **82**, 661–72 (2008).

357. Mollet, J. *et al.* CABC1 Gene Mutations Cause Ubiquinone Deficiency with Cerebellar Ataxia and Seizures. *Am. J. Hum. Genet.* **82**, 623–630 (2008).

358. Pronicka, E. *et al.* New perspective in diagnostics of mitochondrial disorders: Two years' experience with whole-exome sequencing at a national paediatric centre. *J. Transl. Med.* **14**, 174 (2016).

359. Jacobsen, J. C. *et al.* Compound Heterozygous Inheritance of Mutations in Coenzyme Q8A Results in Autosomal Recessive Cerebellar Ataxia and Coenzyme Q10 Deficiency in a Female Sib-Pair. in *JIMD Reports* 31–36 (Springer, Berlin, Heidelberg, 2017). doi:10.1007/8904_2017_73.

360. Hikmat, O. *et al.* ADCK3 mutations with epilepsy, stroke-like episodes and ataxia: a POLG mimic? *Eur. J. Neurol.* **23**, 1188–1194 (2016).

361. Anheim, M. *et al.* Epidemiological, clinical, paraclinical and molecular study of a cohort of 102 patients affected with autosomal recessive progressive cerebellar ataxia from Alsace, Eastern France: Implications for clinical management. *Neurogenetics* **11**, 1–12 (2010).

362. Yang, J., Yang, Y. & Hu, Z. A novel ADCK4 mutation in a Chinese family with ADCK4-Associated glomerulopathy. *Biochem. Biophys. Res. Commun.* **506**, 444–449 (2018).

363. Ashraf, S. *et al.* ADCK4 mutations promote steroid-resistant nephrotic syndrome through CoQ10 biosynthesis disruption. *J. Clin. Invest.* **123**, 5179–89 (2013).

364. Korkmaz, E. *et al.* ADCK4-Associated Glomerulopathy Causes Adolescence-Onset FSGS. *J. Am. Soc. Nephrol.* **27**, 63–68 (2016).

365. Park, E. *et al.* Focal segmental glomerulosclerosis and medullary nephrocalcinosis in children with ADCK4 mutations. *Pediatr. Nephrol.* **32**, 1547–1554 (2017).

366. Feng, C. *et al.* Coenzyme Q10 supplementation therapy for 2 children with proteinuria renal disease and ADCK4 mutation. *Med. (United States)* **96**, e8880 (2017).

367. Lolin, K. *et al.* Early-onset of ADCK4 glomerulopathy with renal failure: a case report. *BMC Med. Genet.* **18**, 28 (2017).

368. Kakiuchi, T. *et al.* Association between Crohn's disease and AarF domain-containing kinase 4 glomerulopathy. *Clin. J. Gastroenterol.* **12**, 263–268 (2019).

369. Yang, Z. *et al.* [Mutation analysis of a family affected with isolated proteinuria]. *Zhonghua Yi Xue Yi Chuan Xue Za Zhi* **36**, 598–601 (2019).

370. Nair, P. *et al.* COQ8A and MED25 Mutations in a Child with Intellectual Disability, Microcephaly, Seizures, and Spastic Ataxia: Synergistic Effect of Digenic Variants? *Mol. Syndromol.* **9**, 319–323 (2018).

371. Bellman, M., Byrne, O. & Sege, R. Developmental assessment of children. *BMJ* **345**, 1–9 (2013).

372. Imai-Okazaki, A. *et al.* Cardiomyopathy in children with mitochondrial disease: Prognosis and genetic background. *Int. J. Cardiol.* (2019) doi:10.1016/J.IJCARD.2019.01.017.

373. Liu, J. L., Yee, C., Wang, Y. & Hekimi, S. A single biochemical activity underlies the pleiotropy of the aging-related protein CLK-1. *Sci. Rep.* **7**, 1–14 (2017).

374. Schalock, R. L., Borthwick-Duffy, S. A., Bradley, V. J., Buntinx, W. & Coulter, D. L.

Intellectual disability: definition, classification, and systems of supports. (American Association on Intellectual and Developmental Disabilities, 2010).

375. Salviati, L. *et al.* Infantile encephalomyopathy and nephropathy with CoQ10 deficiency: A CoQ10-responsive condition. *Neurology* **65**, 606–608 (2005).
376. Bezdíčka, M., Dluholucký, M., Cinek, O. & Zieg, J. Successful maintenance of partial remission in a child with COQ2 nephropathy by coenzyme Q10 treatment. *Nephrology* 1–2 (2019) doi:10.1111/nep.13600.
377. Song, X. *et al.* COQ8B nephropathy: Early detection and optimal treatment. *Mol. Genet. Genomic Med.* (2020) doi:10.1002/mgg3.1360.
378. Vázquez-Fonseca *et al.* ADCK2 Haploinsufficiency Reduces Mitochondrial Lipid Oxidation and Causes Myopathy Associated with CoQ Deficiency. *J. Clin. Med.* **8**, 1374 (2019).
379. Mitsui, J. *et al.* Mutations in COQ2 in Familial and Sporadic Multiple-System Atrophy. *N. Engl. J. Med.* **369**, 233–244 (2013).
380. Awad, A. M. *et al.* Coenzyme Q10 deficiencies: Pathways in yeast and humans. *Essays in Biochemistry* vol. 62 361–376 (2018).
381. Stefely, J. A. & Pagliarini, D. J. Biochemistry of Mitochondrial Coenzyme Q Biosynthesis. *Trends Biochem. Sci.* **42**, 824–843 (2017).
382. Katzeff, J. S., Phan, K., Purushothuman, S., Halliday, G. M. & Kim, W. S. Cross-examining candidate genes implicated in multiple system atrophy. *Acta neuropathologica communications* vol. 7 117 (2019).
383. Ogaki, K. *et al.* Analysis of COQ2 gene in multiple system atrophy. *Mol. Neurodegener.* **9**, 44 (2014).
384. Procopio, R. *et al.* Genetic mutation analysis of the COQ2 gene in Italian patients with multiple system atrophy. *Gene* vol. 716 (2019).
385. Stefely, J. A. *et al.* Mitochondrial ADCK3 Employs an Atypical Protein Kinase-like Fold to Enable Coenzyme Q Biosynthesis. *Mol. Cell* **57**, 83–94 (2015).
386. Barca, E. *et al.* Decreased Coenzyme Q10 levels in multiple system atrophy cerebellum. *J. Neuropathol. Exp. Neurol.* **75**, 663–672 (2016).
387. Zhai, S. B., Zhang, L., Sun, B. C., Zhang, Y. & Ma, Q. S. Early-onset COQ8B (ADCK4) glomerulopathy in a child with isolated proteinuria: A case report and literature review. *BMC Nephrology* vol. 21 (2020).
388. Herebian, D. *et al.* Detection of 6-demethoxyubiquinone in CoQ 10 deficiency disorders: Insights into enzyme interactions and identification of potential therapeutics. *Mol. Genet. Metab.* **121**, 216–223 (2017).
389. López, L. C., Luna-Sánchez, M., García-Corzo, L., Quinzii, C. M. & Hirano, M. Pathomechanisms in Coenzyme Q10-Deficient Human Fibroblasts. *Mol. Syndromol.* 163–169 (2014) doi:10.1159/000360494.
390. López, L. C. *et al.* Treatment of CoQ10 Deficient Fibroblasts with Ubiquinone, CoQ Analogs, and Vitamin C: Time- and Compound-Dependent Effects. *PLoS One* **5**, e11897 (2010).
391. Cerqua, C. *et al.* Vitamin K2 cannot substitute Coenzyme Q 10 as electron carrier in the mitochondrial respiratory chain of mammalian cells. *Sci. Rep.* **9**, (2019).
392. Santos-Ocaña, C. *et al.* Uptake of Exogenous Coenzyme Q and Transport to Mitochondria Is Required for bc 1 Complex Stability in Yeast coq Mutants. *J. Biol. Chem.* **277**, 10973–10981 (2002).
393. Falk, M. J. *et al.* Probucol ameliorates renal and metabolic sequelae of primary CoQ

deficiency in Pdss2 mutant mice. *EMBO Mol. Med.* **3**, 410–27 (2011).

394. Kleiner, G. *et al.* CoQ10 supplementation rescues nephrotic syndrome through normalization of H2S oxidation pathway. *Biochim. Biophys. Acta - Mol. Basis Dis.* **1864**, 3708–3722 (2018).

395. He, C. H., Xie, L. X., Allan, C. M., Tran, U. C. & Clarke, C. F. Coenzyme Q supplementation or over-expression of the yeast Coq8 putative kinase stabilizes multi-subunit Coq polypeptide complexes in yeast coq null mutants. *Biochim. Biophys. Acta* **1841**, 630–44 (2014).

396. Ozeir, M. *et al.* Coenzyme Q biosynthesis: Coq6 is required for the C5-hydroxylation reaction and substrate analogs rescue Coq6 deficiency. *Chem. Biol.* **18**, 1134–1142 (2011).

397. Xie, L. X. *et al.* Overexpression of the Coq8 Kinase in Saccharomyces cerevisiae coq Null Mutants Allows for Accumulation of Diagnostic Intermediates of the Coenzyme Q 6 Biosynthetic Pathway. *J. Biol. Chem.* **287**, 23571–23581 (2012).

398. Wang, Y., Oxer, D. & Hekimi, S. Mitochondrial function and lifespan of mice with controlled ubiquinone biosynthesis. *Nat Commun* **6**, 6393 (2015).

399. Hidalgo-Gutiérrez, A. *et al.* β-RA reduces DMQ/CoQ ratio and rescues the encephalopathic phenotype inCoq9 R239X mice. *EMBO Mol. Med.* **11**, (2019).

400. Widmeier, E. *et al.* Treatment with 2,4-Dihydroxybenzoic Acid Prevents FSGS Progression and Renal Fibrosis in Podocyte-Specific Coq6 Knockout Mice. *J. Am. Soc. Nephrol.* **30**, 393–405 (2019).

401. Widmeier, E. *et al.* ADCK4 Deficiency Destabilizes the Coenzyme Q Complex, Which Is Rescued by 2,4-Dihydroxybenzoic Acid Treatment. *J. Am. Soc. Nephrol.* **31**, 1191–1211 (2020).

402. Herebian, D. *et al.* 4-Hydroxybenzoic acid restores CoQ 10 biosynthesis in human COQ2 deficiency. *Ann. Clin. Transl. Neurol.* **4**, 902–908 (2017).

403. Licitra, F. & Puccio, H. An Overview of Current Mouse Models Recapitulating Coenzyme Q10 Deficiency Syndrome. *Mol. Syndromol.* 180–186 (2014) doi:10.1159/000362942.

404. Grant, J., Saldanha, J. W. & Gould, A. P. A Drosophila model for primary coenzyme Q deficiency and dietary rescue in the developing nervous system. *Dis. Model. Mech.* **3**, 799–806 (2010).

405. Fernández-Ayala, D. J. M., Jiménez-Gancedo, S., Guerra, I. & Navas, P. Invertebrate models for coenzyme q10 deficiency. *Mol. Syndromol.* **5**, 170–9 (2014).

406. Asencio, C., Rodríguez-Aguilera, J. C., Ruiz-Ferrer, M., Vela, J. & Navas, P. Silencing of ubiquinone biosynthesis genes extends life span in Caenorhabditis elegans. *FASEB J.* **17**, 1135–1137 (2003).

407. Gavilán, Án. *et al.* C. elegans knockouts in ubiquinone biosynthesis genes result in different phenotypes during larval development. *BioFactors* **25**, 21–29 (2005).

408. Wong, A., Boutis, P. & Hekimi, S. Mutations in the clk-1 gene of Caenorhabditis elegans affect developmental and behavioral timing. *Genetics* **139**, (1995).

409. Yang, Y.-Y. *et al.* The role of DMQ9 in the long-lived mutant clk-1. *Mech. Ageing Dev.* **132**, 331–339 (2011).

410. Asencio, C. *et al.* Differential expression pattern of coq-8 gene during development in Caenorhabditis elegans. *Gene Expr. Patterns* **6**, 433–439 (2006).

411. Kawamukai, M. Biosynthesis of coenzyme Q in eukaryotes. *Biosci. Biotechnol. Biochem.* **80**, 23–33 (2016).

412. Loiseau, L. *et al.* The ubiK protein is an accessory factor necessary for bacterial Ubiquinone (UQ) biosynthesis and forms a complex with the UQ biogenesis factor UbiJ. *J. Biol. Chem.* **292**, 11937–11950 (2017).

413. Hajj Chehade, M. *et al.* A Soluble Metabolon Synthesizes the Isoprenoid Lipid Ubiquinone. *Cell Chem. Biol.* **26**, 482-492.e7 (2019).

414. Tzagoloff, A. & Dieckmann, C. L. PET genes of Saccharomyces cerevisiae. *Microbiol. Rev.* **54**, 211–225 (1990).

415. Padilla, S. *et al.* Hydroxylation of demethoxy-Q6 constitutes a control point in yeast coenzyme Q6 biosynthesis. *Cell. Mol. Life Sci.* **66**, 173–186 (2009).

416. Berenguel Hernández, A. M. *et al.* Design of High-Throughput Screening of Natural Extracts to Identify Molecules Bypassing Primary Coenzyme Q Deficiency in Saccharomyces cerevisiae. *SLAS Discov. Adv. Sci. Drug Discov.* **25**, 299–309 (2020).

417. Lu, S. *et al.* Cerebellar defects in Pdss2 conditional knockout mice during embryonic development and in adulthood. *Neurobiol. Dis.* **45**, 219–233 (2012).

418. Peng, M. *et al.* Primary Coenzyme Q Deficiency in Pdss2 Mutant Mice Causes Isolated Renal Disease. *PLoS Genet.* **4**, e1000061 (2008).

419. Lapointe, J., Wang, Y., Bigras, E. & Hekimi, S. The submitochondrial distribution of ubiquinone affects respiration in long-lived Mclk1+/- mice. *J. Cell Biol.* **199**, 215–224 (2012).

420. Levavasseur, F. *et al.* Ubiquinone Is Necessary for Mouse Embryonic Development but Is Not Essential for Mitochondrial Respiration. *J. Biol. Chem.* **276**, 46160–46164 (2001).

421. Nakai, D. *et al.* Mouse homologue of coq7/clk-1, longevity gene in Caenorhabditis elegans, is essential for coenzyme Q synthesis, maintenance of mitochondrial integrity, and neurogenesis. *Biochem. Biophys. Res. Commun.* **289**, 463–471 (2001).

422. Liu, X. *et al.* Evolutionary conservation of the clk-1-dependent mechanism of longevity: Loss of mclk1 increases cellular fitness and lifespan in mice. *Genes Dev.* **19**, 2424–2434 (2005).

423. Murakami, S. & Johnson, T. E. A Genetic Pathway Conferring Life Extension and Resistance to UV Stress in Caenorhabditis elegans. *Genetics* **143**, (1996).

424. Stefely, J. A. *et al.* Cerebellar Ataxia and Coenzyme Q Deficiency through Loss of Unorthodox Kinase Activity. *Mol. Cell* **63**, 608–620 (2016).

425. Wang, Y. & Hekimi, S. Mitochondrial respiration without ubiquinone biosynthesis. *Hum. Mol. Genet.* **22**, 4768–4783 (2013).

426. Lyon, M. F. & Hulse, E. V. An inherited kidney disease of mice resembling human nephronophthisis. *J. Med. Genet.* **8**, 41–48 (1971).

427. Madaio, M. P. *et al.* Glomerular and tubular epithelial defects in kd/kd mice lead to progressive renal failure. *Am. J. Nephrol.* **25**, 604–610 (2005).

428. Peng, M. *et al.* Mutant prenyltransferase-like mitochondrial protein (PLMP) and mitochondrial abnormalities in kd/kd mice. *Kidney Int.* **66**, 20–28 (2004).

429. Takahashi, K. & Yamanaka, S. Induction of Pluripotent Stem Cells from Mouse Embryonic and Adult Fibroblast Cultures by Defined Factors. *Cell* **126**, 663–676 (2006).

430. Zahumenska, R. *et al.* Induced pluripotency: A powerful tool for in vitro modeling. *International Journal of Molecular Sciences* vol. 21 1–19 (2020).

431. Yahata, N., Boda, H. & Hata, R. Elimination of Mutant mtDNA by an Optimized mpTALEN Restores Differentiation Capacities of Heteroplasmic MELAS-iPSCs. *Mol. Ther. - Methods Clin. Dev.* **20**, 54–68 (2021).

432. Burbulla, L. F. *et al.* Modeling Brain Pathology of Niemann-Pick Disease Type C Using Patient-Derived Neurons. *Mov. Disord.* (2021) doi:10.1002/mds.28463.

433. García-López, M., Arenas, J. & Gallardo, M. E. Hereditary Optic Neuropathies: Induced Pluripotent Stem Cell-Based 2D/3D Approaches. *Genes (Basel).* **12**, 112 (2021).

434. Sercel, A. J., Carlson, N. M., Patananan, A. N. & Teitell, M. A. Mitochondrial DNA Dynamics in Reprogramming to Pluripotency. *Trends in Cell Biology* (2021) doi:10.1016/j.tcb.2020.12.009.

435. Romero-Moya, D., Castaño, J., Santos-Ocaña, C., Navas, P. & Menendez, P. Generation, genome edition and characterization of iPSC lines from a patient with coenzyme Q10 deficiency harboring a heterozygous mutation in COQ4 gene. *Stem Cell Res.* **24**, 144–147 (2017).

436. Romero-Moya, D. *et al.* Genetic Rescue of Mitochondrial and Skeletal Muscle Impairment in an Induced Pluripotent Stem Cells Model of Coenzyme Q<inf>10</inf>Deficiency. *Stem Cells* (2017) doi:10.1002/stem.2634.

437. Yen, H. C. *et al.* Disruption of the human COQ5-containing protein complex is associated with diminished coenzyme Q10 levels under two different conditions of mitochondrial energy deficiency. *Biochim. Biophys. Acta - Gen. Subj.* **1860**, 1864–1876 (2016).

438. Floyd, B. J. *et al.* Mitochondrial Protein Interaction Mapping Identifies Regulators of Respiratory Chain Function. *Mol. Cell* **63**, 621–632 (2016).

439. Graham, F. L., Smiley, J., Russell, W. C. & Nairn, R. Characteristics of a human cell line transformed by DNA from human adenovirus type 5. *J. Gen. Virol.* **36**, 59–72 (1977).

440. Antonicka, H. *et al.* A High-Density Human Mitochondrial Proximity Interaction Network. *Cell Metab.* **32**, 479-497.e9 (2020).

441. Kozak, M. Pushing the limits of the scanning mechanism for initiation of translation. *Gene* **299**, 1–34 (2002).

442. Kozak, M. Emerging links between initiation of translation and human diseases. *Mamm. Genome* **13**, 401–410 (2002).

443. Zhang, Y. *et al.* A Novel MLH1 Initiation Codon Mutation (c.3G>T) in a Large Chinese Lynch Syndrome Family with Different Onset Age and mRNA Expression Level. *Biomed Res. Int.* **2018**, 1–8 (2018).

444. Frank, McGrath, Poh-Fitzpatrick, Hawk & Christiano. Mutations in the translation initiation codon of the protoporphyrinogen oxidase gene underlie variegate porphyria. *Clin. Exp. Dermatol.* **24**, 296–301 (1999).

445. Wang, C. P. *et al.* Common genetic mutations in the start codon of the SDH subunit D gene among Chinese families with familial head and neck paragangliomas. *Oral Oncol.* **48**, 125–129 (2012).

446. Sargiannidou, I., Kim, G.-H., Kyriakoudi, S., Eun, B.-L. & Kleopa, K. A. A start codon CMT1X mutation associated with transient encephalomyelitis causes complete loss of Cx32. *Neurogenetics* **16**, 193–200 (2015).

447. Bertino, F. *et al.* Heme and sensory neuropathy. *Pain* **160**, 2766–2775 (2019).

448. Kuper, W. F. E. *et al.* The c.1A > C start codon mutation in CLN3 is associated with a protracted disease course . *JIMD Rep.* **52**, 23–27 (2020).

449. Navarro-Fernández, J. *et al.* Biochemical and cellular consequences of the antithrombin p.Met1? mutation identified in a severe thrombophilic family. *Oncotarget* **9**, 33202–33214 (2018).

450. Kazak, L. *et al.* Alternative translation initiation augments the human mitochondrial

proteome. *Nucleic Acids Res.* **41**, 2354–2369 (2013).

451. Monaghan, R. M. *et al.* A nuclear role for the respiratory enzyme CLK-1 in regulating mitochondrial stress responses and longevity. *Nat. Cell Biol.* **17**, 782–792 (2015).

452. Ivanov, I. P., Loughran, G., Sachs, M. S. & Atkins, J. F. Initiation context modulates autoregulation of eukaryotic translation initiation factor 1 (eIF1). *Proc. Natl. Acad. Sci. U. S. A.* **107**, 18056–18060 (2010).

453. Kearse, M. G. & Wilusz, J. E. Non-AUG translation: A new start for protein synthesis in eukaryotes. *Genes and Development* vol. 31 1717–1731 (2017).

454. Rodríguez-Hidalgo, M. *et al.* Reduction in the levels of CoQ biosynthetic proteins is related to an increase in lifespan without evidence of hepatic mitohormesis. *Sci. Rep.* **8**, (2018).

455. Anisimova, A. S., Alexandrov, A. I., Makarova, N. E., Gladyshev, V. N. & Dmitriev, S. E. Protein synthesis and quality control in aging. *Aging* vol. 10 4269–4288 (2018).

456. Padilla, S. *et al.* Demethoxy-Q, An Intermediate of Coenzyme Q Biosynthesis, Fails to Support Respiration in Saccharomyces cerevisiae and Lacks Antioxidant Activity. *J. Biol. Chem.* **279**, 25995–26004 (2004).

457. Stenmark, P. *et al.* A new member of the family of di-iron carboxylate proteins. Coq7 (clk-1), a membrane-bound hydroxylase involved in ubiquinone biosynthesis. *J. Biol. Chem.* **276**, 33297–33300 (2001).

458. Busso, C. *et al.* Coq7p relevant residues for protein activity and stability. *Biochimie* **119**, 92–102 (2015).

459. Emma, F., Montini, G., Parikh, S. M. & Salviati, L. Mitochondrial dysfunction in inherited renal disease and acute kidney injury. *Nat. Rev. Nephrol.* **12**, 267–280 (2016).

460. Hajj Chehade, M. *et al.* ubiI, a New Gene in Escherichia coli Coenzyme Q Biosynthesis, Is Involved in Aerobic C5-hydroxylation. *J. Biol. Chem.* **288**, 20085–20092 (2013).

461. Caminsky, N. G., Mucaki, E. J. & Rogan, P. K. Interpretation of mRNA splicing mutations in genetic disease: review of the literature and guidelines for information-theoretical analysis. *F1000Research* **3**, 282 (2014).

462. Zhao, S. Alternative splicing, RNA-seq and drug discovery. *Drug Discovery Today* vol. 24 1258–1267 (2019).

463. Mehmood, A. *et al.* Systematic evaluation of differential splicing tools for RNA-seq studies. *Brief. Bioinform.* **2019**, 1–14 (2019).

464. Belogrudov, G. I. *et al.* Yeast COQ4 Encodes a Mitochondrial Protein Required for Coenzyme Q Synthesis. *Arch. Biochem. Biophys.* **392**, 48–58 (2001).

465. Marbois, B. *et al.* Coq3 and Coq4 Define a Polypeptide Complex in Yeast Mitochondria for the Biosynthesis of Coenzyme Q. *J. Biol. Chem.* **280**, 20231–20238 (2005).

466. Marbois, B., Gin, P., Gulmezian, M. & Clarke, C. F. The yeast Coq4 polypeptide organizes a mitochondrial protein complex essential for coenzyme Q biosynthesis. *Biochim. Biophys. Acta - Mol. Cell Biol. Lipids* **1791**, 69–75 (2009).

467. Poon, W. W., Do, T. Q., Noelle Marbois, B. & Clarke, C. F. Sensitivity to treatment with polyunsaturated fatty acids is a general characteristic of the ubiquinone-deficient yeast coq mutants. *Mol. Aspects Med.* **18**, 121–127 (1997).

468. Johnson, A. *et al.* COQ9, a new gene required for the biosynthesis of coenzyme Q in Saccharomyces cerevisiae. *J. Biol. Chem.* **280**, 31397–31404 (2005).

469. Casarin, A. *et al.* Functional characterization of human COQ4, a gene required for Coenzyme Q10 biosynthesis. *Biochem. Biophys. Res. Commun.* **372**, 35–9 (2008).

470. Nguyen, T. P. T. *et al.* Molecular characterization of the human COQ5 C-methyltransferase in coenzyme Q10 biosynthesis. *Biochim. Biophys. Acta* **1841**, 1628–38 (2014).

471. Mojica, F. J. M., Díez-Villaseñor, C., García-Martínez, J. & Soria, E. Intervening sequences of regularly spaced prokaryotic repeats derive from foreign genetic elements. *J. Mol. Evol.* **60**, 174–182 (2005).

472. Jansen, R., Van Embden, J. D. A., Gaastra, W. & Schouls, L. M. Identification of genes that are associated with DNA repeats in prokaryotes. *Molecular Microbiology* vol. 43 1565–1575 (2002).

473. Wiedenheft, B. *et al.* Structural Basis for DNase Activity of a Conserved Protein Implicated in CRISPR-Mediated Genome Defense. *Structure* **17**, 904–912 (2009).

474. Charpentier, E. & Doudna, J. A. Rewriting a genome. *Nature* **495**, 50–51 (2013).

475. Cong, L. *et al.* Multiplex genome engineering using CRISPR/Cas systems. *Science* **339**, 819–23 (2013).

476. Bauer, D. E., Canver, M. C. & Orkin, S. H. Generation of Genomic Deletions in Mammalian Cell Lines via CRISPR/Cas9. *J. Vis. Exp.* e52118 (2014) doi:10.3791/52118.

477. Ran, F. A. *et al.* Double nicking by RNA-guided CRISPR cas9 for enhanced genome editing specificity. *Cell* **154**, 1380–1389 (2013).

478. Arroyo, J. D. *et al.* A Genome-wide CRISPR Death Screen Identifies Genes Essential for Oxidative Phosphorylation. *Cell Metab.* **24**, 875–885 (2016).

479. Antonicka, H. *et al.* A pseudouridine synthase module is essential for mitochondrial protein synthesis and cell viability. *EMBO Rep.* e201643391 (2016) doi:10.15252/embr.201643391.

480. Trinklein, N. D. *et al.* An abundance of bidirectional promoters in the human genome. *Genome Res.* **14**, 62–66 (2004).

481. Wang, G. *et al.* Identification of regulatory regions of bidirectional genes in cervical cancer. *BMC Med. Genomics* **6**, 1–9 (2013).

482. Yang, M. Q. & Elnitski, L. L. Diversity of core promoter elements comprising human bidirectional promoters. *BMC Genomics* **9**, 1–8 (2008).

483. El-Gebali, S. *et al.* The Pfam protein families database in 2019. *Nucleic Acids Res.* **47**, D427–D432 (2019).

484. Vargas, M. A. *et al.* Biochemical composition and fatty acid content of filamentous nitrogen-fixing cyanobacteria. *J. Phycol.* **34**, 812–817 (1998).

485. Rea, S. L., Graham, B. H., Nakamaru-Ogiso, E., Kar, A. & Falk, M. J. Bacteria, yeast, worms, and flies: exploiting simple model organisms to investigate human mitochondrial diseases. *Dev. Disabil. Res. Rev.* **16**, 200–18 (2010).

486. Reinders, J. *et al.* Profiling phosphoproteins of yeast mitochondria reveals a role of phosphorylation in assembly of the ATP synthase. *Mol. Cell. Proteomics* **6**, 1896–1906 (2007).

487. Acin-Perez, R., Gatti, D. L., Bai, Y. & Manfredi, G. Protein phosphorylation and prevention of cytochrome oxidase inhibition by ATP: Coupled mechanisms of energy metabolism regulation. *Cell Metab.* **13**, 712–719 (2011).

488. Gey, U., Czupalla, C., Hoflack, B., Rödel, G. & Krause-Buchholz, U. Yeast pyruvate dehydrogenase complex is regulated by a concerted activity of two kinases and two phosphatases. *J. Biol. Chem.* **283**, 9759–67 (2008).

489. Kato, M. *et al.* Structural basis for inactivation of the human pyruvate dehydrogenase

complex by phosphorylation: role of disordered phosphorylation loops. *Structure* **16**, 1849–59 (2008).

490. Tauche, A., Krause-Buchholz, U. & Rödel, G. Ubiquinone biosynthesis in Saccharomyces cerevisiae: The molecular organization of O-methylase Coq3p depends on Abc1p/Coq8p. *FEMS Yeast Res.* **8**, 1263–1275 (2008).
491. Xie, L. X. *et al.* Expression of the human atypical kinase ADCK3 rescues coenzyme Q biosynthesis and phosphorylation of Coq polypeptides in yeast coq8 mutants. *Biochim. Biophys. Acta* **1811**, 348–60 (2011).
492. Martín-Montalvo, A. *et al.* Respiratory-induced coenzyme Q biosynthesis is regulated by a phosphorylation cycle of Cat5p/Coq7p. *Biochem. J.* **440**, 107–14 (2011).
493. Martín-Montalvo, A. *et al.* The phosphatase Ptc7 induces coenzyme Q biosynthesis by activating the hydroxylase Coq7 in yeast. *J. Biol. Chem.* **288**, 28126–37 (2013).
494. Niemi, N. M. *et al.* Pptc7 is an essential phosphatase for promoting mammalian mitochondrial metabolism and biogenesis. *Nat. Commun.* **10**, (2019).
495. González-Mariscal, I. *et al.* The mitochondrial phosphatase PPTC7 orchestrates mitochondrial metabolism regulating coenzyme Q10 biosynthesis. *Biochim. Biophys. Acta - Bioenerg.* **1859**, 1235–1248 (2018).
496. Dunker, A. K. *et al.* Intrinsically disordered protein. *J. Mol. Graph. Model.* **19**, 26–59 (2001).
497. Zhou, H. *et al.* Toward a comprehensive characterization of a human cancer cell phosphoproteome. *J. Proteome Res.* **12**, 260–271 (2013).
498. Sacco, F. *et al.* Glucose-regulated and drug-perturbed phosphoproteome reveals molecular mechanisms controlling insulin secretion. *Nat. Commun.* **7**, (2016).
499. Lundby, A. *et al.* In vivo phosphoproteomics analysis reveals the cardiac targets of β-adrenergic receptor signaling. *Sci. Signal.* **6**, 1–14 (2013).
500. Huttlin, E. L. *et al.* A tissue-specific atlas of mouse protein phosphorylation and expression. *Cell* **143**, 1174–1189 (2010).
501. Lundby, A. *et al.* Quantitative maps of protein phosphorylation sites across 14 different rat organs and tissues. *Nat. Commun.* **3**, 810–876 (2012).
502. Filadi, R. *et al.* TOM70 Sustains Cell Bioenergetics by Promoting IP3R3-Mediated ER to Mitochondria Ca 2+ Transfer. *Curr. Biol.* **28**, 369-382.e6 (2018).
503. Luhr, M., Szalai, P. & Engedal, N. The Lactate Dehydrogenase Sequestration Assay — A Simple and Reliable Method to Determine Bulk Autophagic Sequestration Activity in Mammalian Cells. *J. Vis. Exp.* **2018**, 1–10 (2018).
504. Kalén, A., Norling, B., Appelkvist, E. L. & Dallner, G. Ubiquinone biosynthesis by the microsomal fraction from rat liver. *Biochim. Biophys. Acta - Gen. Subj.* **926**, 70–78 (1987).
505. Mugoni, V. *et al.* Ubiad1 Is an Antioxidant Enzyme that Regulates eNOS Activity by CoQ10 Synthesis. *Cell* **152**, 504–518 (2013).
506. Allan, C. M. *et al.* Identification of Coq11, a New Coenzyme Q Biosynthetic Protein in the CoQ-Synthome in Saccharomyces cerevisiae. *J. Biol. Chem.* **290**, 7517–7534 (2015).
507. Tsui, H. S. & Clarke, C. F. Ubiquinone Biosynthetic Complexes in Prokaryotes and Eukaryotes. *Cell Chem. Biol.* **26**, 465–467 (2019).
508. Clarke, C. F. New advances in coenzyme Q biosynthesis. *Protoplasma* **213**, 134–147 (2000).
509. Tohge, T., Watanabe, M., Hoefgen, R. & Fernie, A. R. Shikimate and Phenylalanine

Biosynthesis in the Green Lineage. *Front. Plant Sci.* **4**, 62 (2013).

510. Perli, T., Wronska, A. K., Ortiz-Merino, R. A., Pronk, J. T. & Daran, J. M. Vitamin requirements and biosynthesis in Saccharomyces cerevisiae. *Yeast* **37**, 283–304 (2020).
511. Siebert, M., Severin, K. & Heide, L. Formation of 4-hydroxybenzoate in Escherichia coli: Characterization of the ubiC gene and its encoded enzyme chorismate pyruvate-lyase. *Microbiology* **140**, 897–904 (1994).
512. Aussel, L. *et al.* Biosynthesis and physiology of coenzyme Q in bacteria. *Biochim. Biophys. Acta - Bioenerg.* **1837**, 1004–1011 (2014).
513. Payet, L.-A. *et al.* Mechanistic Details of Early Steps in Coenzyme Q Biosynthesis Pathway in Yeast. *Cell Chem. Biol.* **23**, 1241–1250 (2016).
514. Stefely, J. *et al.* Mitochondrial protein functions elucidated by multi-omic mass spectrometry profiling. *Nat. Biotechnol.* **34**, 1191–1197 (2016).
515. Xie, L. X. *et al.* Resveratrol and para-coumarate serve as ring precursors for coenzyme Q biosynthesis. *J. Lipid Res.* **56**, 909–919 (2015).
516. Fernández-del-Río, L. *et al.* Kaempferol increases levels of coenzyme Q in kidney cells and serves as a biosynthetic ring precursor. *Free Radic. Biol. Med.* **110**, 176–187 (2017).
517. Fernández-del-Río, L., Soubeyrand, E., Basset, G. J. & Clarke, C. F. Metabolism of the Flavonol Kaempferol in Kidney Cells Liberates the B-ring to Enter Coenzyme Q Biosynthesis. *Molecules* **25**, 2955 (2020).
518. Soubeyrand, E. *et al.* The peroxidative cleavage of kaempferol contributes to the biosynthesis of the benzenoid moiety of ubiquinone in plants. *Plant Cell* **30**, 2910–2921 (2018).
519. Marbois, B. *et al.* para -Aminobenzoic Acid Is a Precursor in Coenzyme Q 6 Biosynthesis in Saccharomyces cerevisiae. *J. Biol. Chem.* **285**, 27827–27838 (2010).
520. Pierrel, F. *et al.* Involvement of mitochondrial ferredoxin and para-aminobenzoic acid in yeast coenzyme Q biosynthesis. *Chem. Biol.* **17**, 449–59 (2010).
521. Roux, B. & Walsh, C. T. p-Aminobenzoate Synthesis in Escherichia coli : Kinetic and Mechanistic Characterization of the Amidotransferase PabA. *Biochemistry* **31**, 6904–6910 (1992).
522. Göbel, A., Rauner, M., Hofbauer, L. C. & Rachner, T. D. Cholesterol and beyond - The role of the mevalonate pathway in cancer biology. *Biochim. Biophys. Acta - Rev. Cancer* **1873**, 188351 (2020).
523. Goldstein, J. L. & Brown, M. S. Regulation of the mevalonate pathway. *Nature* **343**, 425–430 (1990).
524. Zhang, M., Luo, J., Ogiyama, Y., Saiki, R. & Kawamukai, M. Heteromer formation of a long-chain prenyl diphosphate synthase from fission yeast Dps1 and budding yeast Coq1*. *FEBS J.* **275**, 3653–3668 (2008).
525. Ashby, M. N. & Edwards, P. A. Elucidation of the deficiency in two yeast coenzyme Q mutants. Characterization of the structural gene encoding hexaprenyl pyrophosphate synthetase. *J. Biol. Chem.* **265**, 13157–64 (1990).
526. Saiki, R., Nagata, A., Kainou, T., Matsuda, H. & Kawamukai, M. Characterization of solanesyl and decaprenyl diphosphate synthases in mice and humans. *FEBS J.* **272**, 5606–5622 (2005).
527. Okada, K. *et al.* The ispB gene encoding octaprenyl diphosphate synthase is essential for growth of Escherichia coli. *J. Bacteriol.* **179**, 3058–3060 (1997).
528. Clizbe, D. B., Owens, M. L., Masuda, K. R., Shackelford, J. E. & Krisans, S. K. IDI2, a second

isopentenyl diphosphate isomerase in mammals. *J. Biol. Chem.* **282**, 6668–6676 (2007).

529. Hahn, F. M., Xuan, J. W., Chambers, A. F. & Poulter, C. D. Human isopentenyl diphosphate:dimethylallyl diphosphate isomerase: Overproduction, purification, and characterization. *Arch. Biochem. Biophys.* **332**, 30–34 (1996).

530. Kainou, T. *et al.* Dimer Formation of Octaprenyl-diphosphate Synthase (IspB) Is Essential for Chain Length Determination of Ubiquinone. *J. Biol. Chem.* **276**, 7876–7883 (2001).

531. Ashby, M. N., Kutsunai, S. Y., Ackerman, S., Tzagoloff, A. & Edwards, P. A. COQ2 is a candidate for the structural gene encoding para-hydroxybenzoate:polyprenyltransferase. *J. Biol. Chem.* **267**, 4128–36 (1992).

532. Forsgren, M. *et al.* Isolation and functional expression of human COQ2, a gene encoding a polyprenyl transferase involved in the synthesis of CoQ. *Biochem. J.* **382**, 519–26 (2004).

533. Wu, G., Williams, H. D., Gibson, F. & Poole, R. K. Mutants of Escherichia coli affected in respiration: The cloning and nucleotide sequence of ubiA, encoding the membrane-bound p-hydroxybenzoate:octaprenyltransferase. *J. Gen. Microbiol.* **139**, 1795–1805 (1993).

534. Clarke, C. F., Williams, W. & Teruya, J. H. Ubiquinone biosynthesis in Saccharomyces cerevisiae. Isolation and sequence of COQ3, the 3,4-dihydroxy-5-hexaprenylbenzoate methyltransferase gene. *J. Biol. Chem.* **266**, 16636–44 (1991).

535. Hsu, A. Y., Poon, W. W., Shepherd, J. A., Myles, D. C. & Clarke, C. F. Complementation of coq3 mutant yeast by mitochondrial targeting of the Escherichia coli UbiG polypeptide: evidence that UbiG catalyzes both O-methylation steps in ubiquinone biosynthesis. *Biochemistry* **35**, 9797–806 (1996).

536. Jonassen, T. & Clarke, C. F. Isolation and functional expression of human COQ3, a gene encoding a methyltransferase required for ubiquinone biosynthesis. *J. Biol. Chem.* **275**, 12381–7 (2000).

537. Poon, W. W. *et al.* Yeast and rat Coq3 and Escherichia coli UbiG polypeptides catalyze both O-methyltransferase steps in coenzyme Q biosynthesis. *J. Biol. Chem.* **274**, 21665–72 (1999).

538. Stroobant, P., Young, I. G. & Gibson, F. Mutants of Escherichia coli K-12 Blocked in the Final Reaction of Ubiquinone Biosynthesis: Characterization and Genetic Analysis. *J. Bacteriol.* **109**, (1972).

539. Barkovich, R. J. *et al.* Characterization of the COQ5 Gene from Saccharomyces cerevisiae. *Biochemistry* **272**, 9182–9188 (1997).

540. Lee, P. T., Hsu, A. Y., Ha, H. T. & Clarke, C. F. A C-methyltransferase involved in both ubiquinone and menaquinone biosynthesis: Isolation and identification of the Escherichia coli ubiE gene. *J. Bacteriol.* **179**, 1748–1754 (1997).

541. Gin, P. *et al.* The Saccharomyces cerevisiae COQ6 Gene Encodes a Mitochondrial Flavin-dependent Monooxygenase Required for Coenzyme Q Biosynthesis. *J. Biol. Chem.* **278**, 25308–25316 (2003).

542. Behan, R. K. & Lippard, S. J. The aging-associated enzyme CLK-1 is a member of the carboxylate-bridged diiron family of proteins. *Biochemistry* **49**, 9679–9681 (2010).

543. Lu, T. Te, Lee, S. J., Apfel, U. P. & Lippard, S. J. Aging-associated enzyme human clock-1: Substrate-mediated reduction of the diiron center for 5-demethoxyubiquinone hydroxylation. *Biochemistry* **52**, 2236–2244 (2013).

544. Tran, U. C. *et al.* Complementation of Saccharomyces cerevisiae coq7 Mutants by Mitochondrial Targeting of the Escherichia coli UbiF Polypeptide. *J. Biol. Chem.* **281**, 16401–16409 (2006).

545. Adachi, A. *et al.* Complementation of Escherichia coli ubiF mutation by Caenorhabditis elegans CLK-1, a product of the longevity gene of the nematode worm. *FEBS Lett.* **543**, 174–178 (2003).

546. Marbois, B. N. & Clarke, C. F. The COQ7 Gene Encodes a Protein in Saccharomyces cerevisiae Necessary for Ubiquinone Biosynthesis. *J. Biol. Chem.* **271**, 2995–3004 (1996).

547. Stenmark, P. *et al.* A New Member of the Family of Di-iron Carboxylate Proteins. *J. Biol. Chem.* **276**, 33297–33300 (2001).

548. Kwon, O., Kotsakis, A. & Meganathan, R. Ubiquinone (coenzyme Q) biosynthesis in Escherichia coli: identification of the ubiF gene. *FEMS Microbiol. Lett.* **186**, 157–161 (2000).

549. Marshall, S. A., Payne, K. A. P. & Leys, D. The UbiX-UbiD system: The biosynthesis and use of prenylated flavin (prFMN). *Arch. Biochem. Biophys.* **632**, 209–221 (2017).

550. Gulmezian, M., Hyman, K. R., Marbois, B. N., Clarke, C. F. & Javor, G. T. The role of UbiX in Escherichia coli coenzyme Q biosynthesis. *Arch. Biochem. Biophys.* **467**, 144–153 (2007).

551. Pelosi, L. *et al.* Evolution of Ubiquinone Biosynthesis: Multiple Proteobacterial Enzymes with Various Regioselectivities To Catalyze Three Contiguous Aromatic Hydroxylation Reactions. *mSystems* **1**, 1–16 (2016).

552. Young, I. G., Stroobant, P., Macdonald, C. G. & Gibson, F. Pathway for ubiquinone biosynthesis in Escherichia coli K-12: gene-enzyme relationships and intermediates. *J. Bacteriol.* **114**, 42–52 (1973).

553. Nakahigashi, K., Miyamoto, K., Nishimura, K. & Inokuchi, H. Isolation and characterization of a light-sensitive mutant of Escherichia coli K-12 with a mutation in a gene that is required for the biosynthesis of ubiquinone. *J. Bacteriol.* **174**, 7352–7359 (1992).

554. Zhu, Y. *et al.* Structural and biochemical studies reveal UbiG/Coq3 as a class of novel membrane-binding proteins. *Biochem. J.* **470**, 105–114 (2015).

555. Dai, Y. N. *et al.* Crystal structures and catalytic mechanism of the C-methyltransferase Coq5 provide insights into a key step of the yeast coenzyme Q synthesis pathway. *Acta Crystallogr. Sect. D Biol. Crystallogr.* **70**, 2085–2092 (2014).

556. Baba, S. W. *et al.* Yeast Coq5 C-methyltransferase is required for stability of other polypeptides involved in Coenzyme Q biosynthesis. *J. Biol. Chem.* **279**, 10052–9 (2004).

557. Ozeir, M. *et al.* Coq6 is responsible for the C4-deamination reaction in coenzyme Q biosynthesis in Saccharomyces cerevisiae. *J. Biol. Chem.* **290**, 24140–24151 (2015).

558. Rea, S. CLK-1/Coq7p is a DMQ mono-oxygenase and a new member of the di-iron carboxylate protein family. *FEBS Lett.* **509**, 389–394 (2001).

559. Jonassen, T. *et al.* Yeast clk-1 homologue (Coq7/Cat5) is a mitochondrial protein in coenzyme Q synthesis. *J. Biol. Chem.* **273**, 3351–3357 (1998).

560. Abby, S. S., Kazemzadeh, K., Vragniau, C., Pelosi, L. & Pierrel, F. Advances in bacterial pathways for the biosynthesis of ubiquinone. *Biochim. Biophys. Acta - Bioenerg.* **1861**, 148259 (2020).

561. Pelosi, L. *et al.* Ubiquinone Biosynthesis over the Entire O 2 Range: Characterization of a Conserved O 2 -Independent Pathway. *MBio* **10**, 1319–1338 (2019).

562. He, C. H. *et al.* Human COQ9 rescues a coq9 yeast mutant by enhancing Coenzyme Q biosynthesis from 4-hydroxybenzoic acid and stabilizing the CoQ-synthome. *Front. Physiol.* **8**, 1–10 (2017).

563. Hsieh, E. J. *et al.* Saccharomyces cerevisiae Coq9 polypeptide is a subunit of the

mitochondrial Coenzyme Q biosynthetic complex. *Arch. Biochem. Biophys.* **463**, 19–26 (2007).

564. Lohman, D. C. *et al.* Mitochondrial COQ9 is a lipid-binding protein that associates with COQ7 to enable coenzyme Q biosynthesis. *Proc. Natl. Acad. Sci.* **111**, E4697–E4705 (2014).
565. Allan, C. M. *et al.* A conserved START domain coenzyme Q-binding polypeptide is required for efficient Q biosynthesis, respiratory electron transport, and antioxidant function in Saccharomyces cerevisiae. *Biochim. Biophys. Acta - Mol. Cell Biol. Lipids* **1831**, 776–791 (2013).
566. Barros, M. H. *et al.* The Saccharomyces cerevisiae COQ10 Gene Encodes a START Domain Protein Required for Function of Coenzyme Q in Respiration. *J. Biol. Chem.* **280**, 42627–42635 (2005).
567. Cui, T.-Z. & Kawamukai, M. Coq10, a mitochondrial coenzyme Q binding protein, is required for proper respiration in Schizosaccharomyces pombe. *FEBS J.* **276**, 748–759 (2009).
568. Aussel, L. *et al.* UbiJ, a new gene required for aerobic growth and proliferation in macrophage, is involved in coenzyme q biosynthesis in Escherichia coli and Salmonella enterica serovar typhimurium. *J. Bacteriol.* **196**, 70–79 (2014).
569. Poon, W. W. *et al.* Identification of Escherichia coli ubiB, a gene required for the first monooxygenase step in ubiquinone biosynthesis. *J. Bacteriol.* **182**, 5139–5146 (2000).
570. Yoon, W., Hwang, S. H., Lee, S. H. & Chung, J. Drosophila ADCK1 is critical for maintaining mitochondrial structures and functions in the muscle. *PLoS Genet.* **15**, 1–25 (2019).
571. Kemmerer, Z. A. *et al.* UbiB proteins regulate cellular CoQ distribution. *bioRxiv* 2020.12.09.418202 (2020) doi:https://doi.org/10.1101/2020.12.09.418202.
572. Reidenbach, A. G. *et al.* Conserved Lipid and Small-Molecule Modulation of COQ8 Reveals Regulation of the Ancient Kinase-like UbiB Family. *Cell Chem. Biol.* **25**, 154-165.e11 (2018).
573. He, C. H. *et al.* Yeast Coq9 controls deamination of coenzyme Q intermediates that derive from para-aminobenzoic acid. *Biochim. Biophys. Acta* **1851**, 1227–39 (2015).
574. Tsui, H. S. *et al.* Human COQ10A and COQ10B are distinct lipid-binding START domain proteins required for coenzyme Q function. *J. Lipid Res.* **60**, jlr.M093534 (2019).
575. Zampol, M. A. *et al.* Over-expression of COQ10 in Saccharomyces cerevisiae inhibits mitochondrial respiration. *Biochem. Biophys. Res. Commun.* **402**, 82–87 (2010).
576. Murai, M. *et al.* Identification of the Binding Site of the Quinone-Head Group in Mitochondrial Coq10 by Photoaffinity Labeling. *Biochemistry* **53**, 3995–4003 (2014).
577. Fino, C. *et al.* PasT of Escherichia coli sustains antibiotic tolerance and aerobic respiration as a bacterial homolog of mitochondrial Coq10. *Microbiologyopen* **9**, (2020).
578. Bradley, M. C. *et al.* COQ11 deletion mitigates respiratory deficiency caused by mutations in the gene encoding the coenzyme Q chaperone protein Coq10. *J. Biol. Chem.* **295**, 6023–6042 (2020).
579. Bradley, M. C. *et al.* COQ11 deletion mitigates respiratory deficiency caused by mutations in the gene encoding the coenzyme Q chaperone protein Coq10. *J. Biol. Chem.* jbc.RA119.012420 (2020) doi:10.1074/jbc.RA119.012420.
580. Gin, P. & Clarke, C. F. Genetic Evidence for a Multi-subunit Complex in Coenzyme Q Biosynthesis in Yeast and the Role of the Coq1 Hexaprenyl Diphosphate Synthase. *J. Biol. Chem.* **280**, 2676–2681 (2005).

581. Hsu, A. Y., Do, T. Q., Lee, P. T. & Clarke, C. F. Genetic evidence for a multi-subunit complex in the O-methyltransferase steps of Coenzyme Q biosynthesis. *Biochim. Biophys. Acta* **1484**, 287–97 (2000).

582. Turunen, M., Olsson, J. & Dallner, G. Metabolism and function of coenzyme Q. *Biochim. Biophys. Acta* **1660**, 171–99 (2004).

583. Bentinger, M., Turunen, M., Zhang, X.-X., Yvonne Wan, Y.-J. & Dallner, G. Involvement of Retinoid X Receptor α in Coenzyme Q Metabolism. *J. Mol. Biol.* **326**, 795–803 (2003).

584. Brea-Calvo, G., Siendones, E., Sánchez-Alcázar, J. A., de Cabo, R. & Navas, P. Cell survival from chemotherapy depends on NF-kappaB transcriptional up-regulation of coenzyme Q biosynthesis. *PLoS One* **4**, e5301 (2009).

585. Brea-Calvo, G., Rodríguez-Hernández, Á., Fernández-Ayala, D. J. M., Navas, P. & Sánchez-Alcázar, J. A. Chemotherapy induces an increase in coenzyme Q10 levels in cancer cell lines. *Free Radic. Biol. Med.* **40**, 1293–1302 (2006).

586. Ortiz, T. *et al.* Amitriptyline down-regulates coenzyme Q10 biosynthesis in lung cancer cells. *Eur. J. Pharmacol.* **797**, 75–82 (2017).

587. Lapointe, C. P. *et al.* Multi-omics Reveal Specific Targets of the RNA-Binding Protein Puf3p and Its Orchestration of Mitochondrial Biogenesis. *Cell Syst.* **6**, 125-135.e6 (2018).

588. Cascajo, M. V *et al.* RNA-binding proteins regulate cell respiration and coenzyme Q biosynthesis by post-transcriptional regulation of COQ7. *RNA Biol.* **13**, 622–634 (2016).

589. Veling, M. T. *et al.* Multi-omic Mitoprotease Profiling Defines a Role for Oct1p in Coenzyme Q Production. *Mol. Cell* **68**, 970-977.e11 (2017).

590. Chen, Z. & Cole, P. A. Synthetic approaches to protein phosphorylation. *Curr. Opin. Chem. Biol.* **28**, 115–122 (2015).

591. Bukau, B. & Horwich, A. L. The Hsp70 and Hsp60 chaperone machines. *Cell* vol. 92 351–366 (1998).

592. Jebara, F., Weiss, C. & Azem, A. Hsp60 and Hsp70 Chaperones: Guardians of Mitochondrial Proteostasis. in *eLS* 1–9 (John Wiley & Sons, Ltd, 2017). doi:10.1002/9780470015902.a0027152.

593. Cavalier-Smith, T. Origin of mitochondria by intracellular enslavement of a photosynthetic purple bacterium. *Proceedings of the Royal Society B: Biological Sciences* vol. 273 1943–1952 (2006).

594. Allen, J. F. Why chloroplasts and mitochondria contain genomes. *Comparative and Functional Genomics* vol. 4 31–36 (2003).

595. Ott, M., Amunts, A. & Brown, A. Organization and Regulation of Mitochondrial Protein Synthesis. *Annu. Rev. Biochem.* **85**, 77–101 (2016).

596. Anderson, S. *et al.* Sequence and organization of the human mitochondrial genome. *Nature* **290**, 457–465 (1981).

597. Rantanen, A., Jansson, M., Oldfors, A. & Larsson, N. G. Downregulation of Tfam and mtDNA copy number during mammalian spermatogenesis. *Mamm. Genome* **12**, 787–792 (2001).

598. Kaneda, H. *et al.* Elimination of paternal mitochondrial DNA in intraspecific crosses during early mouse embryogenesis. *Proc. Natl. Acad. Sci. U. S. A.* **92**, 4542–4546 (1995).

599. Sutovsky, P. *et al.* Ubiquitin tag for sperm mitochondria. *Nature* **402**, 371–372 (1999).

600. Polovina, E. S., Parakatselaki, M. E. & Ladoukakis, E. D. Paternal leakage of mitochondrial DNA and maternal inheritance of heteroplasmy in Drosophila hybrids. *Sci. Rep.* **10**, 1–9 (2020).

601. Vissing, J. Paternal comeback in mitochondrial DNA inheritance. *Proceedings of the National Academy of Sciences of the United States of America* vol. 116 1475–1476 (2019).

602. Sato, K. & Sato, M. Multiple ways to prevent transmission of paternal mitochondrial DNA for maternal inheritance in animals. *Journal of Biochemistry* vol. 162 247–253 (2017).

603. Luo, S. *et al.* Biparental inheritance of mitochondrial DNA in humans. *Proc. Natl. Acad. Sci. U. S. A.* **115**, 13039–13044 (2018).

604. Ebert, K. M., Liem, H. & Hecht, N. B. Mitochondrial DNA in the mouse preimplantation embryo. *J. Reprod. Fertil.* **82**, 145–149 (1988).

605. Zhang, H., Burr, S. P. & Chinnery, P. F. The mitochondrial DNA genetic bottleneck: Inheritance and beyond. *Essays Biochem.* **62**, 225–234 (2018).

606. Stewart, J. B., Freyer, C., Elson, J. L. & Larsson, N.-G. Purifying selection of mtDNA and its implications for understanding evolution and mitochondrial disease. *Nat. Rev. Genet.* **9**, 657–662 (2008).

607. Stewart, J. B. & Larsson, N. G. Keeping mtDNA in Shape between Generations. *PLoS Genet.* **10**, (2014).

608. Legros, F., Malka, F., Frachon, P., Lombès, A. & Rojo, M. Organization and dynamics of human mitochondrial DNA. *J. Cell Sci.* **117**, 2653–2662 (2004).

609. Spelbrink, J. N. Functional organization of mammalian mitochondrial DNA in nucleoids: History, recent developments, and future challenges. *IUBMB Life* **62**, 19–32 (2010).

610. Rossignol, R. *et al.* Mitochondrial threshold effects. *Biochemical Journal* vol. 370 751–762 (2003).

611. Borst, P. Mitochondrial Nucleic Acids. *Annu. Rev. Biochem.* **41**, 333–376 (1972).

612. Falkenberg, M. Mitochondrial DNA replication in mammalian cells: Overview of the pathway. *Essays in Biochemistry* vol. 62 287–296 (2018).

613. Nicholls, T. J. & Minczuk, M. In D-loop: 40 years of mitochondrial 7S DNA. *Exp. Gerontol.* **56**, 175–181 (2014).

614. Di Re, M. *et al.* The accessory subunit of mitochondrial DNA polymerase γ determines the DNA content of mitochondrial nucleoids in human cultured cells. *Nucleic Acids Res.* **37**, 5701–5713 (2009).

615. Yasukawa, T. & Kang, D. An overview of mammalian mitochondrial DNA replication mechanisms. *Journal of Biochemistry* vol. 164 183–193 (2018).

616. Peter, B. & Falkenberg, M. TWINKLE and other human mitochondrial DNA helicases: Structure, function and disease. *Genes* vol. 11 (2020).

617. Nicholls, T. J. *et al.* Topoisomerase 3α Is Required for Decatenation and Segregation of Human mtDNA. *Mol. Cell* **69**, 9-23.e6 (2018).

618. Berk, A. J. & Clayton, D. A. Mechanism of mitochondrial DNA replication in mouse L-cells: Asynchronous replication of strands, segregation of circular daughter molecules, aspects of topology and turnover of an initiation sequence. *J. Mol. Biol.* **86**, 801–824 (1974).

619. Kühl, I. *et al.* POLRMT regulates the switch between replication primer formation and gene expression of mammalian mtDNA. *Sci. Adv.* **2**, (2016).

620. McKinney, E. A. & Oliveira, M. T. Replicating animal mitochondrial DNA. *Genet. Mol. Biol.* **36**, 308–15 (2013).

621. Reyes, A. *et al.* Mitochondrial DNA replication proceeds via a 'bootlace' mechanism involving the incorporation of processed transcripts. *Nucleic Acids Res.* **41**, 5837–5850 (2013).

622. D'Souza, A. R. & Minczuk, M. Mitochondrial transcription and translation: Overview. *Essays in Biochemistry* vol. 62 309–320 (2018).

623. Bouda, E., Stapon, A. & Garcia-Diaz, M. Mechanisms of mammalian mitochondrial transcription. *Protein Science* vol. 28 1594–1605 (2019).

624. Pearce, S., Nezich, C. L. & Spinazzola, A. Mitochondrial diseases: Translation matters. *Mol. Cell. Neurosci.* **55**, 1–12 (2013).

625. Antonicka, H. & Shoubridge, E. A. Mitochondrial RNA Granules Are Centers for Posttranscriptional RNA Processing and Ribosome Biogenesis. *Cell Rep.* **10**, 920–932 (2015).

626. Pearce, S. F. *et al.* Regulation of Mammalian Mitochondrial Gene Expression: Recent Advances. *Trends Biochem. Sci.* **42**, 625–639 (2017).

627. Ojala, D., Montoya, J. & Attardi, G. tRNA punctuation model of RNA processing in human mitochondria. *Nature* **290**, 470–474 (1981).

628. Rossmanith, W. Localization of human RNase Z isoforms: Dual nuclear/mitochondrial targeting of the ELAC2 gene product by alternative translation initiation. *PLoS One* **6**, 2–7 (2011).

629. Rossmanith, W. Of P and Z: Mitochondrial tRNA processing enzymes. *Biochimica et Biophysica Acta - Gene Regulatory Mechanisms* vol. 1819 1017–1026 (2012).

630. Mai, N., Chrzanowska-Lightowlers, Z. M. A. & Lightowlers, R. N. The process of mammalian mitochondrial protein synthesis. *Cell and Tissue Research* vol. 367 5–20 (2017).

631. Siira, S. J. *et al.* LRPPRC-mediated folding of the mitochondrial transcriptome. *Nat. Commun.* **8**, 1532 (2017).

632. Zaganelli, S. *et al.* The Pseudouridine Synthase RPUSD4 Is an Essential Component of Mitochondrial RNA Granules. *J. Biol. Chem.* **292**, 4519–4532 (2017).

633. Barrientos, A. Mitochondriolus: assembling mitoribosomes. *Oncotarget* **6**, 16800–16801 (2015).

634. Hällberg, B. M. & Larsson, N. G. Making proteins in the powerhouse. *Cell Metab.* **20**, 226–240 (2014).

635. Rath, S. *et al.* MitoCarta3.0: an updated mitochondrial proteome now with sub-organelle localization and pathway annotations. *Nucleic Acids Res.* (2020) doi:10.1093/nar/gkaa1011.

636. Ryan, M. T. & Hoogenraad, N. J. Mitochondrial-Nuclear Communications. *Annu. Rev. Biochem.* **76**, 701–722 (2007).

637. Couvillion, M. T., Soto, I. C., Shipkovenska, G. & Churchman, L. S. Synchronized mitochondrial and cytosolic translation programs. *Nature* **533**, 499–503 (2016).

638. Richter-Dennerlein, R. *et al.* Mitochondrial Protein Synthesis Adapts to Influx of Nuclear-Encoded Protein. *Cell* **167**, 471-483.e10 (2016).

639. Bonekamp, N. A. & Larsson, N.-G. SnapShot: Mitochondrial Nucleoid. *Cell* **172**, 388-388.e1 (2018).

640. Ježek, P., Špaček, T., Tauber, J. & Pavluch, V. Mitochondrial Nucleoids: Superresolution microscopy analysis. *Int. J. Biochem. Cell Biol.* **106**, 21–25 (2019).

641. Kukat, C. *et al.* Super-resolution microscopy reveals that mammalian mitochondrial nucleoids have a uniform size and frequently contain a single copy of mtDNA. *Proc. Natl. Acad. Sci.* **108**, 13534–13539 (2011).

642. Brown, T. A. *et al.* Superresolution Fluorescence Imaging of Mitochondrial Nucleoids

Reveals Their Spatial Range, Limits, and Membrane Interaction. *Mol. Cell. Biol.* **31**, 4994–5010 (2011).

643. Kukat, C. *et al.* Cross-strand binding of TFAM to a single mtDNA molecule forms the mitochondrial nucleoid. *Proc. Natl. Acad. Sci. U. S. A.* **112**, 11288–11293 (2015).

644. Bogenhagen, D. F., Rousseau, D. & Burke, S. The layered structure of human mitochondrial DNA nucleoids. *J. Biol. Chem.* **283**, 3665–3675 (2008).

645. Campbell, C. T., Kolesar, J. E. & Kaufman, B. A. Mitochondrial transcription factor A regulates mitochondrial transcription initiation, DNA packaging, and genome copy number. *Biochimica et Biophysica Acta - Gene Regulatory Mechanisms* vol. 1819 921–929 (2012).

646. Farge, G. *et al.* In Vitro-reconstituted nucleoids can block mitochondrial DNA replication and transcription. *Cell Rep.* **8**, 66–74 (2014).

647. Hensen, F., Cansiz, S., Gerhold, J. M. & Spelbrink, J. N. To be or not to be a nucleoid protein: A comparison of mass-spectrometry based approaches in the identification of potential mtDNA-nucleoid associated proteins. *Biochimie* **100**, 219–226 (2014).

648. Ban-Ishihara, R., Ishihara, T., Sasaki, N., Mihara, K. & Ishihara, N. Dynamics of nucleoid structure regulated by mitochondrial fission contributes to cristae reformation and release of cytochrome c. *Proc. Natl. Acad. Sci. U. S. A.* **110**, 11863–8 (2013).

649. Silva Ramos, E. *et al.* Mitochondrial fusion is required for regulation of mitochondrial DNA replication. *PLOS Genet.* **15**, e1008085 (2019).

650. Rajala, N., Gerhold, J. M., Martinsson, P., Klymov, A. & Spelbrink, J. N. Replication factors transiently associate with mtDNA at the mitochondrial inner membrane to facilitate replication. *Nucleic Acids Res.* **42**, 952–967 (2014).

651. Holt, I. J. *et al.* Mammalian mitochondrial nucleoids: Organizing an independently minded genome. *Mitochondrion* **7**, 311–321 (2007).

652. Gilkerson, R. *et al.* The Mitochondrial Nucleoid: Integrating Mitochondrial DNA into Cellular Homeostasis. *Cold Spring Harb. Perspect. Biol.* **5**, a011080–a011080 (2013).

653. Jing, J., Liu, G., Huang, Y. & Zhou, Y. A molecular toolbox for interrogation of membrane contact sites. *J. Physiol.* **598**, 1725–1739 (2020).

654. Nunnari, J. & Suomalainen, A. Mitochondria: In sickness and in health. *Cell* vol. 148 1145–1159 (2012).

655. Vance, J. E. MAM (mitochondria-associated membranes) in mammalian cells: Lipids and beyond. *Biochimica et Biophysica Acta - Molecular and Cell Biology of Lipids* vol. 1841 595–609 (2014).

656. Qin, J. *et al.* ER-mitochondria contacts promote mtDNA nucleoids active transportation via mitochondrial dynamic tubulation. *Nat. Commun.* **11**, (2020).

657. Petrungaro, C. & Kornmann, B. Lipid exchange at ER-mitochondria contact sites: a puzzle falling into place with quite a few pieces missing. *Curr. Opin. Cell Biol.* **57**, 71–76 (2019).

658. Giordano, F. Non-vesicular lipid trafficking at the endoplasmic reticulum–mitochondria interface. *Biochemical Society Transactions* vol. 46 437–452 (2018).

659. Acoba, M. G., Senoo, N. & Claypool, S. M. Phospholipid ebb and flow makes mitochondria go. *J. Cell Biol.* **219**, (2020).

660. Dimmer, K. S. & Rapaport, D. Mitochondrial contact sites as platforms for phospholipid exchange. *Biochim. Biophys. Acta - Mol. Cell Biol. Lipids* **1862**, 69–80 (2017).

661. Elustondo, P., Martin, L. A. & Karten, B. Mitochondrial cholesterol import. *Biochim. Biophys. Acta - Mol. Cell Biol. Lipids* **1862**, 90–101 (2017).

662. García-Ruiz, C., Ribas, V., Baulies, A. & Fernández-Checa, J. C. Mitochondrial cholesterol and the paradox in cell death. in *Handbook of Experimental Pharmacology* vol. 240 (Springer New York LLC, 2017).

663. Rone, M. B. *et al.* Identification of a Dynamic Mitochondrial Protein Complex Driving Cholesterol Import, Trafficking, and Metabolism to Steroid Hormones. *Mol. Endocrinol.* **26**, 1868–1882 (2012).

664. Cirigliano, A. *et al.* Ergosterol reduction impairs mitochondrial DNA maintenance in S. cerevisiae. *Biochim. Biophys. Acta - Mol. Cell Biol. Lipids* **1864**, 290–303 (2019).

665. Baudier, J. ATAD3 proteins: brokers of a mitochondria-endoplasmic reticulum connection in mammalian cells. *Biol. Rev.* **93**, 827–844 (2018).

666. Hubstenberger, A., Merle, N., Charton, R., Brandolin, G. & Rousseau, D. Topological analysis of ATAD3A insertion in purified human mitochondria. *J. Bioenerg. Biomembr.* **42**, 143–150 (2010).

667. Desai, R. *et al.* ATAD3 gene cluster deletions cause cerebellar dysfunction associated with altered mitochondrial DNA and cholesterol metabolism. *Brain* **140**, 1595–1610 (2017).

668. Cooper, H. M. *et al.* ATpase-deficient mitochondrial inner membrane protein ATAD3a disturbs mitochondrial dynamics in dominant hereditary spastic paraplegia. *Hum. Mol. Genet.* **26**, 1432–1443 (2017).

669. Gunning, A. C. *et al.* Recurrent De Novo NAHR Reciprocal Duplications in the ATAD3 Gene Cluster Cause a Neurogenetic Trait with Perturbed Cholesterol and Mitochondrial Metabolism. *Am. J. Hum. Genet.* **106**, 272–279 (2020).

670. Harel, T. *et al.* Recurrent De Novo and Biallelic Variation of ATAD3A, Encoding a Mitochondrial Membrane Protein, Results in Distinct Neurological Syndromes. *Am. J. Hum. Genet.* **99**, 831–845 (2016).

671. Peralta, S. *et al.* Novel ATAD3A recessive mutation associated to fatal cerebellar hypoplasia with multiorgan involvement and mitochondrial structural abnormalities. *Mol. Genet. Metab.* **128**, 452–462 (2019).

672. Madhoun, A. Al *et al.* Ketogenic diet attenuates cerebellar atrophy progression in a subject with a biallelic variant at the ATAD3A locus. *Appl. Clin. Genet.* **12**, 79–86 (2019).

673. Peralta, S. *et al.* ATAD3 controls mitochondrial cristae structure in mouse muscle, influencing mtDNA replication and cholesterol levels. *J. Cell Sci.* **131**, (2018).

674. Gomes, F., Tahara, E. B., Busso, C., Kowaltowski, A. J. & Barros, M. H. nde1 deletion improves mitochondrial DNA maintenance in Saccharomyces cerevisiae coenzyme Q mutants. *Biochem. J.* **449**, 595–603 (2013).

675. Liparulo, I. *et al.* Coenzyme Q biosynthesis inhibition induces HIF-1α stabilization and metabolic switch toward glycolysis. *FEBS J.* febs.15561 (2020) doi:10.1111/febs.15561.

676. Liu, S. *et al.* Role of UBIAD1 in Intracellular Cholesterol Metabolism and Vascular Cell Calcification. *PLoS One* **11**, e0149639 (2016).

677. Charman, M., Kennedy, B. E., Osborne, N. & Karten, B. MLN64 mediates egress of cholesterol from endosomes to mitochondria in the absence of functional Niemann-Pick Type C1 protein. *J. Lipid Res.* **51**, 1023–1034 (2010).

678. Szabadkai, G. *et al.* Chaperone-mediated coupling of endoplasmic reticulum and mitochondrial Ca2+ channels. *J. Cell Biol.* **175**, 901–911 (2006).

679. De Brito, O. M. & Scorrano, L. Mitofusin 2 tethers endoplasmic reticulum to mitochondria. *Nature* **456**, 605–610 (2008).

680. Filadi, R. *et al.* Mitofusin 2 ablation increases endoplasmic reticulum-mitochondria

coupling. *Proc. Natl. Acad. Sci. U. S. A.* **112**, E2174–E2181 (2015).

681. Salvador-Gallego, R., Hoyer, M. J. & Voeltz, G. K. SnapShot: Functions of Endoplasmic Reticulum Membrane Contact Sites. *Cell* **171**, 1224.e1-1224.e1 (2017).

682. Iwasawa, R., Mahul-Mellier, A. L., Datler, C., Pazarentzos, E. & Grimm, S. Fis1 and Bap31 bridge the mitochondria-ER interface to establish a platform for apoptosis induction. *EMBO J.* **30**, 556–568 (2011).

683. Wang, B., Nguyen, M., Chang, N. C. & Shore, G. C. Fis1, Bap31 and the kiss of death between mitochondria and endoplasmic reticulum. *EMBO J.* **30**, 451–452 (2011).

684. Wiseman, A. & Attardi, G. Reversible tenfod reduction in mitochondrial DNA content of human cells treated with ethidium bromide. *MGG Mol. Gen. Genet.* **167**, 51–63 (1978).

685. Alán, L., Špaček, T., Reguera Pajuelo, D., Jabůrek, M. & Ježek, P. Mitochondrial nucleoid clusters protect newly synthesized mtDNA during Doxorubicin- and Ethidium Bromide-induced mitochondrial stress. *Toxicol. Appl. Pharmacol.* **302**, 31–40 (2016).

686. Ylikallio, E., Tyynismaa, H., Tsutsui, H., Ide, T. & Suomalainen, A. High mitochondrial DNA copy number has detrimental effects in mice. *Hum. Mol. Genet.* **19**, 2695–2705 (2010).

687. Kasashima, K., Sumitani, M. & Endo, H. Human mitochondrial transcription factor A is required for the segregation of mitochondrial DNA in cultured cells. *Exp. Cell Res.* **317**, 210–220 (2011).

688. Kasashima, K., Sumitani, M. & Endo, H. Maintenance of mitochondrial genome distribution by mitochondrial AAA+ protein ClpX. *Exp. Cell Res.* **318**, 2335–2343 (2012).

689. Wang, Y. & Hekimi, S. Micellization of coenzyme Q by the fungicide caspofungin allows for safe intravenous administration to reach extreme supraphysiological concentrations. *Redox Biol.* **36**, 101680 (2020).

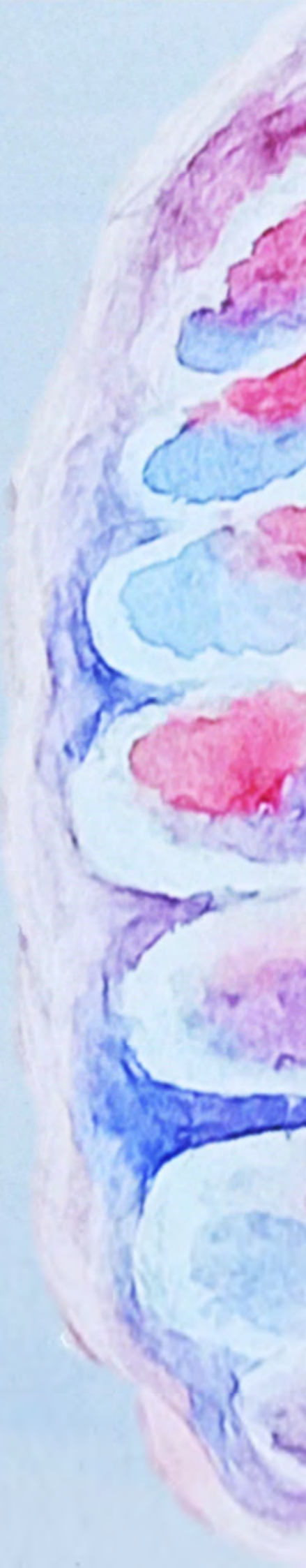

Universidad Pablo de Olavide

Dpto. Fisiología, Anatomía y Biología Celular